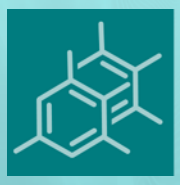

molecules

Volume 2

Antitumoral Properties of Natural Products

Edited by

Roberto Fabiani

Printed Edition of the Special Issue Published in *Molecules*

www.mdpi.com/journal/molecules

MDPI

Antitumoral Properties of Natural Products

Antitumoral Properties of Natural Products

Volume 2

Editor

Roberto Fabiani

MDPI • Basel • Beijing • Wuhan • Barcelona • Belgrade • Manchester • Tokyo • Cluj • Tianjin

Editor
Roberto Fabiani
Department of Chemistry, Biology and Biotechnology
University of Perugia
Italy

Editorial Office
MDPI
St. Alban-Anlage 66
4052 Basel, Switzerland

This is a reprint of articles from the Special Issue published online in the open access journal *Molecules* (ISSN 1420-3049) (available at: https://www.mdpi.com/journal/molecules/special_issues/molecules_APoNP).

For citation purposes, cite each article independently as indicated on the article page online and as indicated below:

LastName, A.A.; LastName, B.B.; LastName, C.C. Article Title. *Journal Name* **Year**, *Article Number*, Page Range.

Volume 2
ISBN 978-3-03943-114-4 (Hbk)
ISBN 978-3-03943-115-1 (PDF)

Volume 1-2
ISBN 978-3-03943-116-8 (Hbk)
ISBN 978-3-03943-117-5 (PDF)

Contents

About the Editor

Roberto Fabiani

Working Experience

1995–2002: Technician at the University of Perugia, Department of Cell and Molecular Biology.
2002–2010: Researcher at the Faculty of Sciences, Department of Medical-Surgical Specialties and Public Health, Section of Molecular Epidemiology and Environmental Hygiene -University of Perugia.
2010 to today: Associate Professor in the Scientific Sector (MED/42) General and Applied Hygiene, Department of Chemistry, Biology and Biotechnology – University of Perugia.

Education

1988 -Graduated summa cum laude in Biological Sciences at the University of Perugia.
1989–1990 Holder of a Fellowship for a Research on "Action mechanisms of some disinfectants" at the Department of Microbiology of the University of Perugia.
1991–1994 Holder of a 3 years Fellowship of the Italian "Ministero della Pubblica Istruzione/ Ricerca Scientifica" at the Department of Clinical Chemistry of the University of Uppsala, Sweden.
1994 Ph.D. in Medical Science at the Department of Clinical Chemistry of the University of Uppsala, Sweden.
1997 Holder of a Fellowship of the Italian "CNR" at the Federal Centre for Nutrition, Institute of Nutritional Physiology, Karlsruhe, Germany.
1999 Holder of a Fellowship of the Italian "CNR" at the Federal Centre for Nutrition, Institute of Nutritional Physiology, Karlsruhe, Germany.

Research Interest

The scientific activity of Dr. Roberto Fabiani has been mainly devoted to investigate the relationships between nutrition and cancer. He has studied the cancer risk associated to the consumption of some foods and cellular effects induced by possible risk and protective factors on the carcinogenesis process. He has been interested to study the oxidative DNA damage induced and/or prevented by different environmental pollutants and their metabolites, intestinal substances such as bile acids and short chain fatty acids, and natural compounds present in the different foods, in particular from Mediterranean diet. In addition, he was involved in the study of chemopreventive activities of secoiridoid phenolic compounds isolated from extra virgin olive oil on different cell systems both in vitro and in vivo. Major attention has been paid to the effects these compounds on proliferation, cell cycle, differentiation and apoptosis of tumor cells, and to the molecular mechanisms involved.

molecules

MDPI

Article

Liposomal Taro Lectin Nanocapsules Control Human Glioblastoma and Mammary Adenocarcinoma Cell Proliferation

Anna C. N. T. F. Corrêa [1], Mauricio A. Vericimo [2], Andriy Dashevskiy [3], Patricia R. Pereira [1] and Vania M. F. Paschoalin [1,*]

[1] Chemistry Institute, Universidade Federal do Rio de Janeiro, Rio de Janeiro 21941-909, Brazil; annac.correa@hotmail.com (A.C.N.T.F.C.); biopatbr@gmail.com (P.R.P.)
[2] Immunobiology Department, Universidade Federal Fluminense, Niterói 24020-150, Brazil; vericimo@vm.uff.br
[3] Pharmaceutical Technology Department, Freie Universität Berlin, 12169 Berlin, Germany; dashevsk@zedat.fu-berlin.de
* Correspondence: paschv@iq.ufrj.br; Tel.: +55-21-3938-7362; Fax: +55-21-3938-7266

Academic Editor: Roberto Fabiani
Received: 22 December 2018; Accepted: 23 January 2019; Published: 29 January 2019

Abstract: The search for natural anticancer agents and nanocarrier uses are a part of the current strategies to overcome the side effects caused by chemotherapeutics. Liposomal nanocapsules loaded with purified tarin, a potential immunomodulatory and antitumoral lectin found in taro corms, were produced. Liposomes were composed by 1,2-dioleoyl-sn-glycerol-3-phosphoethanolamine, cholesterylhemisuccinate, and 1,2-distearoyl-sn-glycero-3-phosphoethanolamine-*N*-[folate(polyethylene glycol)-2000 prepared by thin-film hydration. Small unilamellar vesicles were achieved by sonication and extrusion. Scanning electron microscopy evidenced round-shaped nanocapsules presenting a smooth surface, 150 nm diameter and polydispersity index <0.2, estimated by dynamic light scattering. Tarin entrapment rates were over 80% and leakage of ~3% under 40 days of storage at 4 °C. Entrapped tarin exhibited an 83% release after 6 h at pH 4.6–7.4 and 36 °C. Both free and encapsulated tarin exhibited no in vitro toxicity against healthy mice bone marrow and L929 cells but stimulated the production of fibroblast-like and large round-shaped cells. Encapsulated tarin resulted in inhibition of human glioblastoma (U-87 MG) and breast adenocarcinoma (MDA-MB-231) proliferation, with an IC_{50} of 39.36 and 71.38 μg/mL, respectively. The effectiveness of encapsulated tarin was similar to conventional chemotherapy drugs, such as cisplatin and temozolide. Tarin liposomal nanocapsules exhibited superior pharmacological activity compared to free tarin as a potential chemotherapy adjuvant.

Keywords: *Colocasia esculenta*; food bioactive; tarin; stable nanocapsules; entrapment efficiency; no-toxicity; preclinical tests; antitumoral activity; chemotherapeutic adjuvant

1. Introduction

Cancer is among the leading causes of death worldwide, defined by the exacerbated proliferation of normal cells into tumor cells due to a multistage process that usually involves mutation [1]. Due to the high number of new cancer diagnoses every year, over 4700 every day in the USA alone, many studies, including breast cancer and glioblastoma proliferation control research, are being developed in order to search for the best strategy to improve patient quality of life and life expectancy [2].

Breast cancer is the second main cause of death by cancer in women, second only to lung cancer. The American Cancer Society estimated that about 266,120 new cases of invasive breast cancer in women would be diagnosed in 2018, and that about 40,920 women would die from this disease [3].

Most women with breast cancer require surgical intervention to remove the tumor and, may, before or after, undergo radiotherapy or chemotherapy to control or avoid metastasis. Anthracyclines, such as doxorubicin (Adriamycin) and epirubicin (Ellence), taxanes, like paclitaxel (taxol) and docetaxel (taxotere), 5-fluorouracil (5-FU), cyclophosphamide (cytoxan), and carboplatin (paraplatin) are the most common drugs applied in as a two or three-combination for breast cancer treatment [4]. On the other hand, glioblastoma affects the central nervous system and represents 81% of malignant brain tumors, with a low average survival estimate of five years in 5% of all cases [5]. Temozolomide has been the most common FDA-approved glioma treatment for over 20 years [6]. However, like other chemotherapeutics, temozolomide reduces the number of circulating leukocytes, making the patient more susceptible to infections, and also leads to other side effects, such as vomiting, nausea, and alopecia. A combination therapy has been suggested to improve survival rates [7].

Throughout the years, several strategies have been used to overcome or minimize side effects, including the search for natural anticancer agents, which are extensively associated to lower toxicity, due to their favorable body absorption and metabolism compared to conventional synthetic drugs [8]. Additionally, progress in cancer therapeutics has led to the development of nanosystems, including liposomes, to increase intracellular drug concentrations in cancerous cells while minimizing toxicity to normal cells [9], a non-specific characteristic of conventional treatments. Current therapies have focused on the use of biodegradable nanoparticles to encapsulate pharmacologically active compounds that can later be released into the bloodstream or the desired local target, and have been explored as a way to protect active molecules from enzymatic degradation and increase their bioavailability.

Tarin has been purified and fully characterized as a lectin naturally found in taro corms (*Colocasia esculenta)* [10–13]. Studies on tarin biological activities have revealed that this lectin exhibits both in vitro and in vivo immunomodulatory potential, as well as promising anticancer and antimetastatic properties [10,14–17]. Although much is known about the encapsulation of bioactive compounds in liposomes and tarin bioactivities, no study has been carried out on tarin encapsulation in nanoliposomes. Tarin encapsulation into liposomes could potentiate the pharmacological properties of this molecule, as well as therapeutic treatment results, reducing the necessary dose of new compounds, decreasing side effects or undesirable interactions and allowing tarin to remain longer in the blood stream [18,19].

In this context, tarin liposomal nanocapsules were produced and characterized and the immunomodulatory and antitumoral potentials of the bioactive lectin nanocapsules were evaluated in order to apply this newly designed composite as a future chemotherapeutic adjuvant.

2. Results

2.1. Liposomal Tarin Encapsulation and Characterization

Liposomal tarin nanocapsules were prepared by an extrusion technique based on two distinct previously reported methods, reaching encapsulation efficiencies of 29% and 68%, respectively [20,21]. Scanning electron microscopy (SEM) and dynamic light scattering (DLS) analyses revealed the presence of smooth-surfaced round-shaped vesicles, with an average size of ~150 nm and polydispersity index (PdI) of 0.168 on the first day, confirming successful liposomal nanocapsule production (Figure 1 and Table 1).

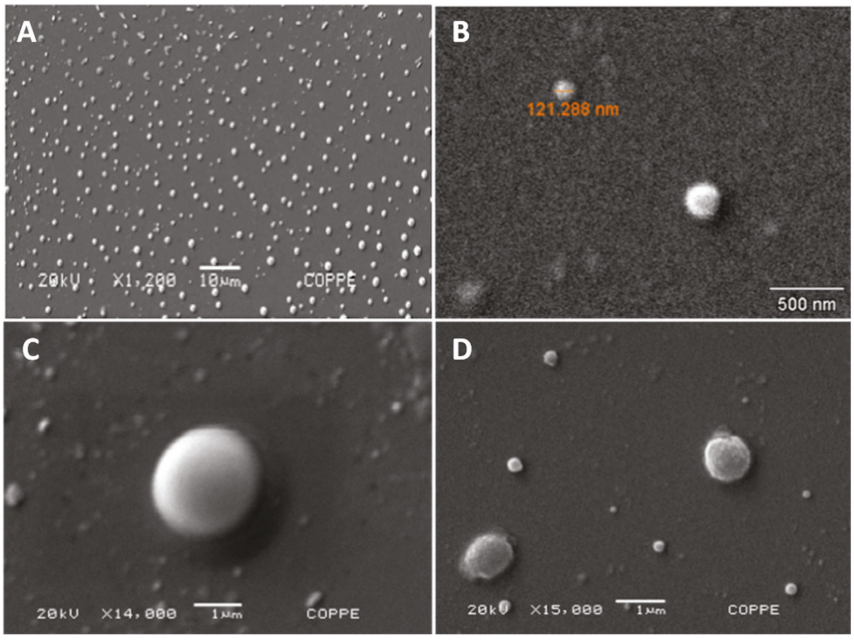

Figure 1. Morphological characterization of liposomal tarin nanocapsules. A scanning electron microscope was used to record DOPE, PEG, and CHEMS nanocapsules (formulation A1). Photographs show liposomes at 20 kV and magnification of 1200× (**A**); 45,000× (**B**); 14,000× (**C**) and 15,000× (**D**).

Table 1. Stability of liposomal tarin nanocapsules.

Membrane Pore Size	Storage Time Intervals at 4 °C (days)	Size Distribution (nm)	Average Size (nm)	Polydispersity Index (PdI)	Peak (nm)	Entrapment Efficiency
0.2 µm	1	50.75–396.1	154.6	0.168	93.55 ± 38.75	0.83
	10	43.82–396.1	155.0	0.191	78.74 ± 35.19	
	90	50.75–396.1	149.8	0.163	88.21 ± 35.69	
	120	43.82–396.1	149.2	0.192	84.65 ± 34.57	
	150	50.75–396.1	151.3	0.191	39.64 ± 22.36	
	180	58.77–396.1	149.9	0.135	99.12 ± 36.50	

The stability of the liposomal nanocapsules (A1 formulation) under storage at 4 °C for 180 days, obtained through 0.2 µm pore membrane extrusion, was evaluated by DLS. Entrapment efficiency was determined by the ratio between the amount of unencapsulated tarin and initial tarin load [22].

In order to optimize liposomal tarin encapsulation, a formulation based on the dos Santos Ferreira et al. [21] methodology was modified regarding liposome composition, sonication, tarin entrapment time, initial tarin load, and organic solvent (Figure S1). Liposomes prepared from DOPE (1,2-dioleoyl-sn-glycerol-3-phosphoethanolamine) as the fundamental component plus CHEMS and DSPE-PEG (2000), presented diameters ranging from 120 nm to 163.2 nm, and PdI close to 0.2 for the A1, A2, B1, and B2 formulations (Figure 2A,B). Nanocapsules size and polydispersity index were not significantly affected during 40 days of storage at 4 °C. On the other hand, formulation C prepared without DSPE-PEG (2000) exhibited a fluctuating PdI between 0.6 and 0.4 and diameter size (Z-average) ranging from 238.8 nm to around 170 nm when comparing day 0 to successive days (Figure 2A,B and Figure S1).

The type of organic solvent, sonication time (1 or 10 min), initial tarin load (1 mg/mL or 2 mg/mL) and exposure time for tarin entrapment did not affect the size or homogeneity of any of the formulations (Figure 2A,B and Figure S1).

Tarin leakage assays monitored for 40 days at 4 °C storage indicate that liposome formulations with the highest tarin leakage were those prepared using methanol, namely B1 and B2 formulations, which presented 14.5 and 12.3% leakages, respectively, compared to the chloroform formulations, which exhibited less than 7% tarin leakage profiles (Figure 2C). Based on physical analyses, formulations A1 and A2 presented the most promising features and less leakage, of under 1.5% and 3.3%, respectively, combined with size stability and homogeneity during 40 days of storage at 4 °C (Figure 2A–C). Since sonication time did not lead to significant differences, formulation A1 was adopted in order to produce stable vesicles for the subsequent studies.

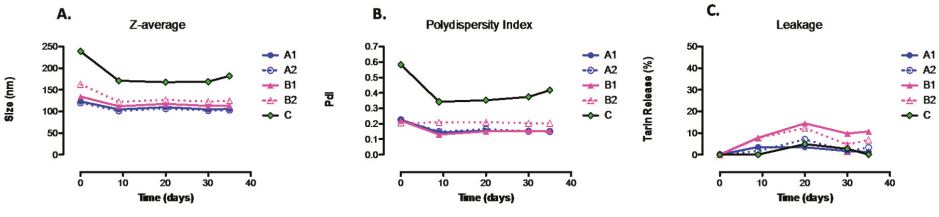

Figure 2. Physicochemical characterization and stability evaluation of liposomal of tarin formulations. The Z-average (**A**), polydispersity index (**B**) and leakage (**C**) of liposome preparations storage at 4 °C were monitored for 40 days. A1, A2, B1, B2, and C represent distinct liposomal encapsulation formulations, presented in Figure S1.

The stability of formulation A1 was monitored by a size distribution evaluation, Z-average and PdI during 180 days of storage at 4 °C. An extrusion membrane porosity of 0.2 μm produced liposomal nanocapsules with average size of around 150 nm and PdI from 0.135 to 0.192, which did not significantly vary during the storage period (Table 1). Tarin entrapment efficiency into liposomal nanocapsules was very high, reaching 83%. In other independent experiments, entrapment efficiency was even higher, reaching >90% and once again, PEG exhibited an important role in liposome formulation since liposomes produced without PEG exhibited less efficient tarin entrapment (79% tarin encapsulation—data not shown).

Taken together, the optimized outlined protocol for tarin encapsulation in nanoliposomes should follow the steps described for the A1 formulation and extrusion should be performed through 0.2 μm pore membranes to proceed to the in vitro and in vivo tarin liposomal nanocapsule bioactivity assays.

2.2. Release Control under Physiological Conditions

To evaluate the performance of the liposomes formulated with DOPE, PEG, and CHEMS, dissolved in chloroform and extruded through a 0.2 μm membrane (A1 formulation), a kinetic release assay was carried out for 6 h, mimicking human body pH conditions (4.6, 5.6, 6.6, and 7.4). The liposomes produced herein were capable of releasing entrapped tarin in a controlled manner, in both acidic and neutral environments. The time necessary to release half the tarin loads at pH 4.6 and 6.6 was reached in 2.3 h, occurring between 4 and 5 h for pH 5.6 and, for pH 7.4, around 4 h. After 6 h, almost 80% of the tarin had been released at all pHs of interest (Figure 3).

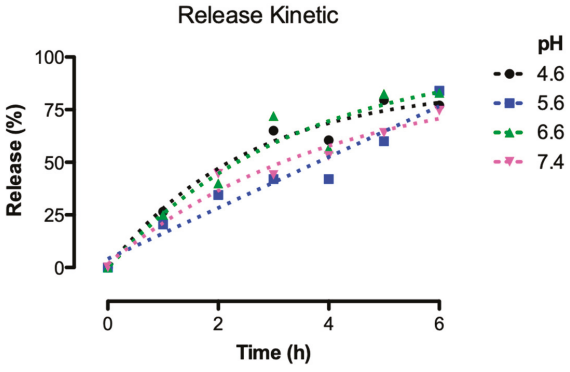

Figure 3. Release profile of encapsulated tarin exposed to pH 4.6, 5.6, 6.6, and 7.4, mimicking human body traits and cellular compartments. Tarin liposomal nanocapsules (A1 formulation) prepared through 0.2 μm pore extrusion membrane were maintained at 36 °C for 6 h. Tarin release was measured hourly, as described by Peterson [23].

2.3. In Vitro Pre-Clinical Tests

2.3.1. Toxicological Screening and Morphological Modifications of Healthy Mice Cells Treated with Free or Encapsulated Tarin

The viabilities of mice bone marrow and fibroblast L929 cells cultivated in the presence of increasing free or encapsulated tarin (A1 formulation) concentrations ranging from 0.78125 to 100 μg/mL were not affected. Instead, free tarin exhibited a proliferative effect, enhancing the number of bone marrow cells with tarin at 50 or 100 μg/mL. When encapsulated tarin was tested, no dose-dependent cytotoxicity was observed for both lineage cells, reinforcing the potential applicability of liposomal tarin nanocapsules for future studies in murine models (Figure 4).

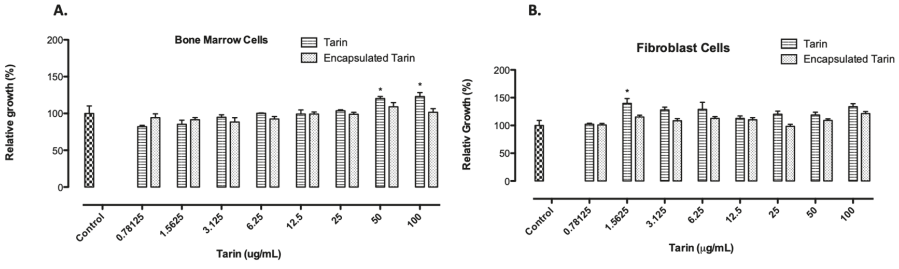

Figure 4. Toxicological effects of free or encapsulated tarin on healthy mice cells. (**A**) bone marrow and (**B**) fibroblast L929 cell line. Viability of cells exposed to increasing doses of free or encapsulated tarin for 24 h was determined using resazurin as indicator. Cultures with no tarin addition were used as control. * $p < 0.05$ compared to control.

The morphological characteristics of bone marrow cells cultured with free or encapsulated tarin (20 μg/mL) were monitored during 14 days, revealing several differences, such as alterations in cell density between control wells and between cells treated with free or encapsulated tarin (Figure 5A–I). On the fifth day, control wells displayed a considerably higher number of cells (Figure 5A–C). However, after 14 days, the cell-occupied area (61.5%) was enhanced after tarin treatment, in both free (96.8%) and encapsulated (94%) form (Figure 5D–F). The percentage of elongated cells was also increased when treated by tarin (95.5% free-tarin; 90.9% encapsulated tarin) while the percentage of occupied

area remained the same and was reduced in the controls (35.6%) (control versus tarin and control versus encapsulated tarin) (Figure 5D–F).

Control cells were smaller and presented homogeneous and similar morphological characteristics, with no significant variability within the cell population (Figure 5A,D,G). However, after 14 days of treatment, tarin in its free form (Figure 5E,H) led to a high number of fibroblast-like cells, while a significant amount of large round cells was detected in wells containing encapsulated tarin, with the suggestive appearance of stromal and progenitor cells, respectively (Figure 5F,I).

Cytosmears of cultured cells revealed the presence of numerous spherical cells with prominent surface ruffles, blebs and reniform nucleus, characteristic of monocytes. Granules and numerous vesicles were also evidenced at or near the cell surface, reinforcing the hypothesis that cells exposed to tarin treatment for five days may be monocytes [24]. Multilobed nucleus cells, characteristic of neutrophils, were detected after exposure to tarin for five days (Figure 5A–C).

Cytoplasm vesicles were apparently larger and more numerous in cells cultivated with encapsulated tarin when compared to free tarin or control cells (Figure 5A–C) after exposure to tarin for five days.

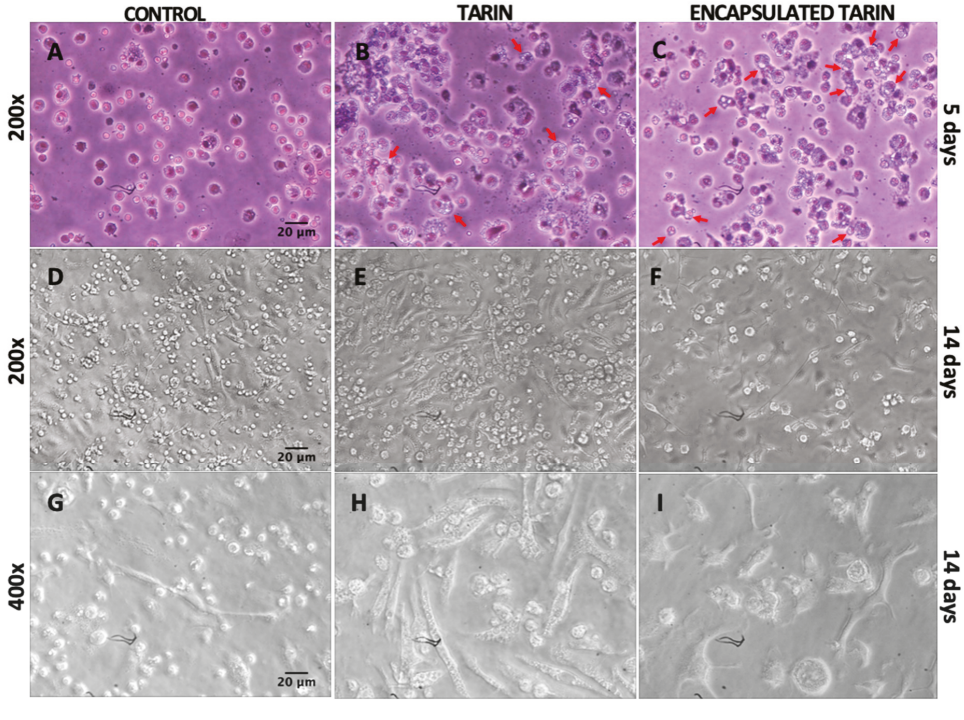

Figure 5. Morphological characteristics of mice bone marrow cells treated with free and encapsulated tarin. Bone marrow cells were harvested from cultures after 5 (**A**–**C**) or directly observed from cultures after 14 days (**D**–**I**). Five-day culture cells were subjected to cytospin and stained with Grunwald-Giemsa. Red arrows indicate the presence of vesicles inside the cytoplasm. Photographs were recorded at 200× and 400× magnifications.

2.3.2. In Vitro Antitumoral Activity of Free and Encapsulated Tarin

The antitumoral activity of free and encapsulated tarin in comparison with empty liposomes was tested against human glioblastoma U-87 MG and human breast adenocarcinoma MDA-MB-231 cell lines. Tumoral cells were cultivated in the presence of increasing concentrations of free and encapsulated tarin ranging from 0.78125 to 50 μg/mL for 24 h (Figure 6A,B).

Both lineage cells were dose-dependently inhibited by encapsulated tarin, exhibiting an IC_{50} of 39.36 μg/mL and 71.38 μg/mL for glioblastoma and breast cancer cells, respectively. Glioblastoma cells were 65% and 35% susceptible to encapsulated tarin at 50 and 25 μg/mL, respectively (Figure 6A). Similarly, using the same doses of encapsulated tarin, breast cancer cells were 41% and 35% inhibited when compared to the control group. In contrast, free tarin did not affect tumoral cell growth at either dose after 24 h of exposure (Figure 6B).

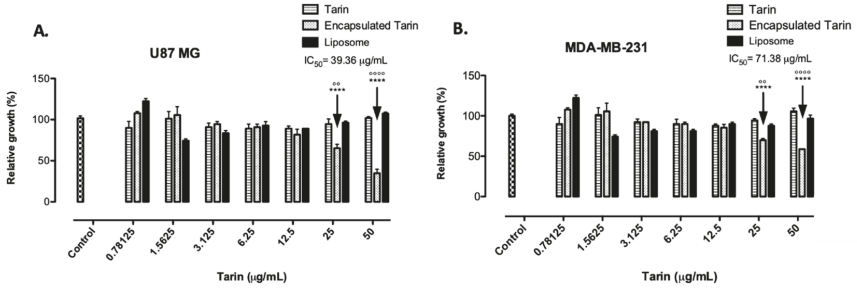

Figure 6. Toxicological effects of free or encapsulated tarin on human tumoral cells. Viability of human (**A**) glioblastoma U-87 MG cell line and (**B**) adenocarcinoma MDA-MB-231 cell line. Non-treated wells, filled with cells and medium, were used as control. To unify the units represented in x axis, tarin concentrations were chosen as reference. Liposome and encapsulated tarin groups are at the same liposome concentration differing only by the presence of tarin. **** $p < 0.0001$ compared to control; °° $p < 0.01$ and °°°° $p < 0.0001$ compared to free tarin.

3. Discussion

Liposome encapsulation of bioactive agents has been proven a successful drug-carrier system due to certain important features, such as biocompatibility with cellular membranes and the ability to incorporate hydrophobic or hydrophilic molecules and enhance therapeutic indices. The use of liposome-encapsulated products has been previously established for different purposes, including drug, biomolecule, and gene delivery [25,26]. Since a drug delivery system can be restricted by physical and chemical instabilities, the preparation of liposomal formulations is a critical step that requires special attention in order to achieve optimal efficiency.

Herein, liposomes preparation was performed according to two distinct protocols, in order to select the most efficient one [20,21]. Both methodologies were adapted to produce nanoliposomal vesicles composed of DOPE (18:1), a neutrally charged phospholipid as the main liposome component, followed by CHEMS, a cholesterol component which fluidizes the membrane, providing additional stability by minimizing bilayer permeability and contributing with cohesive strength [27,28], and PEG, which reduces macrophage recognition, preventing liposomes from a quick clearance from the blood stream, and able to retain tarin for an extended period of time during circulation with no significant loss [29]. Stable liposomes were successfully produced, presenting a typical round shape, ideal size, and polydispersity index as evidenced by DLS analysis (Figure 1). The modified dos Santos Ferreira et al. [21] protocol was used, a higher entrapment efficiency was achieved and this formulation, identified herein as A1, was used as the standard protocol and was further modified, leading to four additional formulations (A1, A2, B1, B2, and C) (Figure S1). The Z average, PdI and capability to hold entrapped tarin for each formulation were monitored for 40 days, in order to select

the best liposomal preparation (Figure 2A–C). Formulation A1 was produced without PEG, using two different organic solvents for lipid solubilization, chloroform [21], and methanol [20], as well as different sonication times, initial tarin loads and exposure times for tarin entrapment. The PEG coating was shown to be essential to control nanoparticle size, entrapment efficiency, homogeneity, and stability (Figure 2A–C). Changing solvents, replacing methanol by chloroform, which could be less harmful to the environment, did not lead to remarkable differences in size, homogeneity or entrapment efficiency. However, this change affected stability, leading to higher tarin leakage during the 40-day experiment (Figure 2C). Variations in sonication, exposure time for tarin entrapment, and initial tarin load did not affect physical liposome characteristics.

Both phospholipid hydrolysis and oxidation led to instability resulting in increased leakage rates of the encapsulated agent or vesicle aggregation, which leads to increased size [30,31]. Vesicle aggregation may have occurred in C formulations, since these presented the highest variations in size and PdI throughout the 40 days of storage at 4 °C. Aggregation may be occurred due to the lack of PEG in formulation C. Thus, this formulation was discarded (Figure 2A,B). Encapsulated tarin leakage was also investigated, in order to choose the formulation able to improve liposome-mediated drug delivery, since leakage can decrease the amount of the drug available for delivery, thus defeating the ability for efficient drug entrapment [32]. The most significant difference observed in leakage rates was detected in liposomes whose lipids were dissolved in methanol in comparison to those dissolved in chloroform (Figure 2C). Taking into account all liposomal nanocapsule features, the A1 formulation exhibited the ideal composition and matched the constraints to ensure therapeutic efficacy, and was, thus, chosen for subsequent assays.

Nanoparticles displaying diameters of about 100 nm are able to permeate the endothelial layer of blood vessels, reaching the bloodstream, followed by target tissues, and should be capable to deliver tarin to tissues [33,34]. Their spherical shape and smooth surface, confirmed by scanning electron microscopy, decreases hemodynamic forces, allowing them to easily circulate inside the vessels [35]. Different-sized nanocapsules were observed and evidenced by scanning electron microscope images and DLS measurements (Figure 1 and Table 1), corroborating previous results, since liposome production usually displays polydispersity in vesicle diameters, and the ability to finely adjust their geometry and size may be critical for the development of efficient carriers [35].

A controlled tarin release was achieved in a certain pH range, which is significantly advantageous, since liposomes could then be applied for several purposes, as release of encapsulated material could occur, leading to different traits and/or intracellular compartments (Figure 3). The release of tarin at pH 7.4 indicates that it can circulate in the bloodstream or be absorbed by any target tissue, release at pH 6.6 would allow tarin to reach the interstitium of a tumoral mass, and at pH 5.6 or 4.6 the liposome could be phagocyted and released at any stage from the endosome to the lysosome [36]. Although a preference for a specific pH was not clearly demonstrated, after 6 h the half-time releases differed considerably between the different assayed pH. Thus, controlled tarin release might be promoted by a combination effect of temperature and pH, since tarin nanocapsules stored at 4 °C exhibited no significant leakage for 180 days. Based on these observations, further experiments are still necessary to establish the releasing mechanism of tarin nanocapsules.

Liposomal tarin nanocapsule toxicity testing is an essential step for the development of a new potential chemotherapeutic adjuvant to guarantee minimal injury risks for healthy tissues. Free or encapsulated tarin was not toxic to healthy mice bone marrow and L929 fibroblast cells at all assessed doses (0.78125–100 μg/mL) (Figure 4). Thus, at the dosage range tested herein, liposomal tarin nanocapsules could be safely applied both in vitro and in vivo for further experimental evaluations, with the potential to increase their therapeutic efficiency while being protected from cellular proteolytic systems. A proliferative effect for both cell types cultured for 24 h was observed in some free tarin doses, indicating a quicker effect when compared to the encapsulated form. Tarin nanocapsules seems to require an additional time to promote a similar effect, since they were shown to release lectin in constant, but low, doses. This observation was corroborated by the optical microscopy analysis,

which revealed the presence of fibroblast-like and/or large rounded cells, characteristics of stromal and progenitor cells, in mice bone marrow cell cultures treated with free or encapsulated tarin after 14 days of culture. Moreover, cytospin slides of the cultured cells evidenced the presence of cells displaying morphological granulocyte and monocyte characteristics after five days of tarin treatment. Merida et al. [17] demonstrated that tarin was able to maintain hematopoietic progenitors and promote granulocyte repopulation (GR1 + cells) in in vitro mice bone marrow cell culture, corroborating the observations described herein and indicating that encapsulated tarin may present a similar potential to stimulate hematopoiesis. However, further studies using cell molecular markers should be performed to determine the immunomodulatory potential of liposomal tarin nanocapsules.

Additionally, several vesicles were observed in the cytoplasm of mice bone marrow cells treated with liposomal tarin nanocapsules, indicating high intracellular activity and constant production of molecules by the endoplasmic reticulum, evidenced by intracellular vesicle formation (Figure 5C). This observation corroborates the hypothesis considered by Merida et al. [17], who states that free tarin may activate transcriptional factors in these cells and stimulate molecule production, such as cytokines or growth factors, which could trigger the multiplication or differentiation of progenitor cells in the bone marrow environment. Although evidence indicates encapsulated tarin immunomodulatory activities, additional studies must be performed in order to establish its mechanism of action and identify the affected bone marrow cell population.

Considering the lack of toxicity to healthy cells associated to an immunostimulatory effect, liposomal tarin nanocapsules exhibited promising results inhibiting the proliferation of human glioblastoma and mammary adenocarcinoma cell lines. These cancer cells lines presented sensitivity to encapsulated tarin comparable to usual chemotherapeutic drug effects. Concerning glioblastoma, the determined IC_{50} for encapsulated tarin (39.36 μg/mL) was equivalent to 65% of cisplatin (29 μg/mL) and 82.2% of temozolide (33.40 μg/mL) inhibition growth effects (Table 2) [37,38]. On the other hand, breast adenocarcinoma cells displayed a less favorable panorama when compared to literature results. Liposomal tarin nanocapsules inhibited breast cancer cell proliferation, displaying an IC_{50} of 71.38 μg/mL, while doxorubicin and cisplatin exhibited IC_{50} of 0.50 and 2.30 μg/mL, respectively [39,40] (Table 2). It should be considered that conventional chemotherapeutic drugs are highly cytotoxic to healthy cells since their effective dose against tumoral cells is usually close to the cytotoxic doses for healthy cells, meaning they display a low selective index, the ratio between the CC_{50} (the concentration required to cause 50% cytotoxicity) and IC_{50} (the concentration required to cause 50% inhibition). In this study, the CC_{50} value for healthy mice cells was unable to be determined, as no cytotoxic effect was observed up to 100 μg of tarin. It is possible that encapsulated tarin presents a higher selective index compared to doxorubicin or cisplatin. These tarin nanocapsule properties would ensure a safer application of this composite at effective doses with minimal adverse effects to healthy tissues. On the other hand, exposure time should also be considered, since antitumoral activity was evaluated after only 24 h. To answer this question, further cytotoxicity experiments should be performed with mice healthy cells using higher tarin doses and longer exposure tarin times in order to determine the selective index.

Table 2. Single-dose cytotoxicity of conventional drugs and encapsulated tarin to human tumoral cells after 24 h exposure.

Tumoral Cell Lines	Antitumoral Molecules	IC_{50} (μg/mL)	Reference
U-87 MG	Cisplatin	29.00	[35]
	Temozolomide	33.40	[36]
	Tarin liposomal nanocapsules	39.36	Present study
MDA-MB-231	Cisplatin	2.30	[37]
	Doxorubicin	0.50	[38]
	Tarin liposomal nanocapsules	71.38	Present study

Interestingly, free tarin failed to exhibit cytotoxicity to the assessed cancer cell lines, since tumoral cells were 100% resistant to the free form of tarin (Figure 6A,B). It is known that the taro lectin recognizes and binds to high mannose *N*-glycans that are a part of the Lewis Y/CD174, H2/CD173, and CA125 antigens, commonly found in human cancer cells [11,16]. Additionally, free tarin has been reported to exhibit a modest response to antitumoral cells, including the murine mammary tumor cell line 66.1 [14,15]. Although a direct comparison cannot be carried out because Kundu et al. [15] did not specify the tarin concentration used in antitumoral assays, it is possible that the free tarin concentrations used herein were not enough to exert the antitumoral effect but that nanoencapsulation of tarin in liposomes may contribute to promote tarin internalization, enhancing intracellular concentrations, triggering stronger antitumoral activity, and potentiating the inhibition mechanism. However, tarin molecular mechanisms on cancer cells has not been evaluated. Further studies should be carried out to determine if tarin could act on cancer cell surfaces through specific carbohydrate-binding, as hypothesized in a previous study, or if the lectin could be internalized, both in its free and encapsulated form [16]. A combination of both mechanisms should also be considered.

In addition, according to Merida et al. [17], when tarin was administered combined with cyclophosphamide (CY), a currently applied breast cancer drug, a protective effect against CY cytotoxicity was observed, decreasing the frequency of micronucleated erythrocytes and also displaying immunostimulatory potential Thus, even if tarin encapsulation does not contribute to pharmacological effects comparable to doxorubicin and cisplatin in breast cancer cells (MDA-MD-231) proliferation, it could minimize cyclophosphamide cytotoxicity and protect progenitor hematopoietic cells, allowing for faster recovery.

Due to the successful and non-toxic tarin-liposome encapsulation and its activity against human tumoral cells, tarin may be considered a promising pharmacological agent if the methodologies used for tarin obtainment and encapsulation are reproductive and the yield compatible with scale-up the drug preparation. Considering a standard procedure, 100 g of taro corms—smaller than a tennis ball can yield about 300 mg of purified tarin which, after liposomal encapsulation could result in liposomal tarin nanocapsules sufficient to be used in 3000 in vivo murine model assays or 12,000 in vitro culture cell lineage assays. In addition, the fact that taro is cropped throughout the entire year in tropical or subtropical zones, which include large South America, Africa, and Asia areas, located between the Tropics of Cancer and Capricorn, should also be considered. Taro is consumed as a supplementary carbohydrate source in these areas and its extract has been used by indigenous populations for medicinal purposes since ancient times.

Although further pre-clinical trials may be performed, the results reported herein have encouraged us to invest in the development of liposomal tarin nanocapsules to be tested as an adjuvant candidate presenting immunomodulatory and antitumoral activities in a tumor-bearing murine model considering a classical chemotherapy regimen.

4. Material and Methods

4.1. Tarin Purification

Colocasia esculenta corms were purchased at a local market in the Niterói municipality (22°52′51″ S, 43°6′15″ W), Southeastern Brazil. The crude taro extract was obtained according to Roy et al. [41], with modifications, and fractionated using the affinity chromatography resin Cibacron Blue 3G-A (Sigma-Aldrich Co, St. Louis, MO, USA), as described by Pereira et al. [10]. In order to reduce interferences in subsequent in vitro and in vivo experiments, the Tris-HCl present in the purified fraction containing tarin was removed by dialysis (Fisherbrand, Pittsburgh, PA, USA) against water at 8 °C for 18 h under constant stirring and lyophilized (Labconco, Kansas, MO, USA) for storage. Protein quantification in the crude extract was performed by the Peterson [23] method, using bovine serum albumin (BSA) as standard.

4.2. Liposomal Nanocapsules Preparation

Liposomes were obtained by modifying the protocols described by dos Santos Ferreira et al. [21] and Andrade et al. [20]. Liposomes were prepared by dissolving the lipid components DOPE (1,2-dioleoyl-sn-glycerol-3-phosphoethanolamine) (Lipoid GMBH, Luidwigshafen, Germany), MPEG 2000-DSPE 1,2-distearoyl-sn-glycero-3-phosphoethanolamine-*N*-[amino(polyethylene glycol)-2000] (ammonium salt) (Lipoid GMBH) and CHEMS (cholesterylhemisuccinate) (Sigma-Aldrich Co) (5.7:3.8:0.5 μmol of lipids) in a chloroform solution under constant stirring at 150 rpm for 15 min. The organic solution was then removed by evaporation under reduced pressure for 25 min at 40 ± 1 °C and constant stirring at 120 rpm. The dry lipid film was rehydrated to reach a 0.01 M concentration in an aqueous phase consisting of 0.3 M ammonium sulfate (pH 7.4) containing tarin at 1 mg/mL, followed by incubation for 12 h at 4 °C. Then, the suspension was maintained under magnetic stirring for 40 min and the large unilamellar vesicles formed were sonicated for 1 min, followed by a 12-cycle extrusion through a polycarbonate 0.2 μm pore membrane. Unencapsulated and encapsulated tarin were recovered by ultracentrifugation carried out at 150,000× *g* at 4 °C for 90 min using an Optima L-90k ultracentrifuge (Beckman Coulter, Brea, CA, USA). The pellet containing encapsulated tarin was suspended in a HEPES buffered saline solution (HBS) at pH 7.4 and the supernatant containing unencapsulated tarin was quantified by Peterson's method [23] to avoid lipid interference. Entrapment efficiency was determined by the ratio between the amount of unencapsulated tarin and the original amount of tarin used in the encapsulation assay [22].

The liposome preparation protocol was subjected to some variations in order to optimize stability and entrapment efficiency conditions. Different organic solvents, sonication times, initial tarin loads, and times for tarin entrapment were tested (Figure S1).

4.3. Morphological Liposome Characterization

Liposome characterization was performed according to Murtey and Ramasamy [42]. Liposomes were attached to microscope slide coverslips, previously coated with poly-L-lysine, and fixed in 4% glutaraldehyde prepared in 0.1 M phosphate buffer pH 7.2, at 4 °C for 48 h. The coverslips were then washed three times for 5 min with the same phosphate buffer. Fixed samples were then dehydrated as follows: 35% ethanol 1× for 15 min, 50% ethanol 1× for 15min, 75% ethanol 1× for 15 min, 95% ethanol 2× for 15 min and absolute ethanol 3× for 20 min. Subsequently, samples were chemically dried by immersion in 1–2 mL of hexamethyldisilazane (HMDS) for 10 min, twice, and left in a desiccator at room temperature overnight. Dried samples were then mounted on a sample stub with a double-sided sticky tape, sputtered with gold and visualized using a JEOL JSM-6460LV scanning electron microscope (SEM) (JEOL, Peabody, MA, USA) at 20kV.

4.4. Encapsulated Tarin Stability Determination

Size distribution and the polidispersity index (PdI) of liposomal tarin nanocapsules stored at 4 °C for 180 days were assessed by dynamic light scattering (DLS) (Zetasizer Malvern Panalytical, Almelo, NLD).

Nanocapsule tarin leakage was quantified by Peterson's method [23] during 40 days of storage at 4 °C.

4.5. Kinetic Release of Encapsulated Tarin

The influence of time, temperature and pH on tarin release was determined according to the protocol described by Deniz et al. [43]. A liposome suspension containing tarin was diluted (1:10) in phosphate buffered saline at pH 4.6, 5.6, 6.6, and 7.4., followed by incubation at 36 °C under constant gentle agitation. Aliquots (100 μL) were collected at 0, 1, 2, 3, 4, 5 and 6 h to determine the amount of released tarin, applying Peterson's method [23].

4.6. Pre-Clinical In Vitro Tests

4.6.1. Animals

Adult isogenic male C57Bl/6 mice (aged 10–16 weeks) were provided and maintained at the Animal Center Laboratory (NAL), belonging to the Universidade Federal Fluminense (UFF), Rio de Janeiro, Brazil.

The research protocol was approved by the Universidade Federal Fluminense Ethics Committee in Animal Use (CEUA), under No. 821/2016.

4.6.2. Tarin Cytotoxicity on Healthy Bone Marrow and Fibroblasts Cells

Tarin cytotoxicity was assessed by the median inhibitory dose, capable of killing 50% of cultured cells. Healthy mouse bone marrow and L929 cell lines (Sigma-Aldrich Co) were seeded in 96-well polystyrene microplates at a concentration of 5×10^5 cells/well and 1.5×10^5 cells/well, respectively, in 100 μL of RPMI-1640 media (Sigma-Aldrich Co), supplemented with 10% fetal calf serum (FCS), 2 mM L-glutamin, 5×10^5 M2-mercaptoethanol, and incubated at 37 °C in a humidified atmosphere containing 5% CO_2. After 24 h incubation, the time required for cell adherence to the plate, different free or encapsulated tarin concentrations (from 0.78125 to 100 μg/mL) and empty liposomes were added to a final volume of 100 μL. The positive controls comprised cells cultivated in culture media, while 12.5% sodium azide (25 μL) was added to the negative control wells. Cells were incubated for an additional 24 h and cell viability was assessed by the colorimetric assay using resazurin as the indicator. A 20 μL aliquot of resarzurin 125 μg/mL was added to each well, followed by 4 h of incubation. Fluorescence intensity was determined using a SpectraMax Microplate Reader M4 (Molecular Devices, Sunnyvale, CA, USA) at 530 nm (excitation filter), 570 nm (cutoff), and 586 nm (emission filter) wavelengths.

4.6.3. Morphology of Bone Marrow Cells Treated with Free and Encapsulated Tarin

Cells were cultured (2×10^6 cells/mL) in RPMI-1640 media (Sigma-Aldrich Co), supplemented with 10% fetal calf serum (FCS), 2 mM L-glutamin, 5×10^{-5} M 2-mercaptoethanol and 20 μg/mL gentamicin, in the presence or absence of 20 μg/mL tarin, at 37 °C in a humidified atmosphere containing 5% CO_2, for 14 days. Media were replaced every five days. Cell samples were collected on days 0, 5, and 14, and transferred to glass slides by centrifugation (284× *g* for 10 min at room temperature) using a Cytopro 7620 centrifuge (WESCOR Inc, Logan, UT, USA). Cells were analyzed after staining by the May–Grunwald–Giemsa method under an optical microscope (Olympus BX41, Shinjuku, Tokyo, Japan) [44]. Photomicrographs of the cultures were acquired under an inverted-phase microscope Zeiss Telaval 31 (Carl Zeiss Co., Oberkochen, Germany) and occupied area was determined using the ImageJ software (version, version 2, Wayne Rasband, Bethesda, MD, USA) [45].

4.6.4. Evaluation of Antitumoral Tarin Activity

The viabilities of the human cancer cell lines MDA-MB-231 (ATCC® HTB-26™) (breast adenocarcinoma) and U-87 MG (ATCC ® HTB-14™) (glioblastoma) were determined by the redox resazurin method described in Section 4.6.2. Cells (1.5×10^5 cells/well) were seeded in 25 cm^2 culture bottles, containing Dulbecco's modified Eagle medium (Nutrient Mixture F-12 - DMEM/F-12) (Sigma-Aldrich Co), supplemented with 10% fetal calf serum (FCS), 2 mM L-glutamin, 5×10^5 M2-mercaptoethanol. Culture bottles were incubated at 37 °C in a 95% humidified atmosphere containing 5% CO_2 until a semiconfluent monolayer was achieved.

Cells from the semiconfluent monolayer were detached from the culture bottles with soft movements after the addition of 2 mL of a solution containing 1 mL 20% trypsin, 0.5 mL 10% ethylenediaminetetraacetic acid (EDTA), and 3.5 mL PBS. Cell suspensions were then centrifuged at 200× *g* for 7 min and pelleted cells were suspended in DMEM medium followed by cell counting using an optical microscope in a Neubauer hemocytometer (Laboroptik, Lancing, England, UK).

Cancer cells at 5×10^5 cells per well, at a final volume of 100 μL, were cultivated in 96-well culture microplates containing DMEM medium and the cytotoxicity evaluation procedure was performed as described previously.

The units displayed in the *x*-axis were standardized per tarin concentration (Figure 6). For this purpose, empty liposomes and encapsulated tarin were prepared using the same parameters, composition, and amount of components. The final preparation was suspended in equal volumes (3 mL) and the serial dilution of encapsulated and empty liposomes was prepared using a similar initial volume (100 μL) to ensure that both samples presented the same liposome concentration, differing only in the presence of tarin. Based on this, liposome concentration was similar in both preparations with and without tarin.

4.7. Statistical Analyses

The results were compared through an analysis of variance (ANOVA) followed by multiple comparisons by Tukey's method. The GraphPad Prism software (version 7, GraphPad, San Diego, CA, USA) was used.

5. Conclusions

The methodology described herein allowed for the reproducible production of spherical, smooth-surfaced, and nanomeric (<0.2 nm) liposomal capsules that exhibit high tarin entrapment efficiencies and low leakage rates under storage conditions. Liposomal tarin nanocapsules exhibited no toxicity to healthy mice bone marrow and L929 cells and inhibited the proliferation of MDA-MB-231 and, to a higher extent, U-87 MG cell lines, indicating an improvement of the pharmacological ability of encapsulated tarin compared to its free form. Healthy mice bone marrow cells treated with free and encapsulated tarin also indicates a possible immunomodulatory effect, which could be useful to boost the host immune system. Liposomal tarin nanocapsules seem to be a promising anti-cancer candidate, obtained from a food matrix and exhibiting two of the most valuable characteristics for any anticancer drug, namely anti-tumor efficacy and low toxicity to healthy cells, enabling it as a putative composite to be associated as an adjuvant to traditional chemotherapy.

Supplementary Materials: The following are available online, Figure S1: Preparation of liposomal tarin nanocapsules using different formulations and procedure.

Author Contributions: Conceptualization, A.C.N.T.F.C., M.A.V., and P.R.P.; Data curation, A.C.N.T.F.C., M.A.V., and P.R.P.; Formal analysis, A.C.N.T.F.C.; Funding acquisition, V.M.F.P.; Methodology, A.D.; Project administration, V.M.F.P.; Resources, A.D., P.R.P., and V.M.F.P.; Supervision, M.A.V., A.D., P.R.P., and V.M.F.P.; Writing—original draft, A.C.N.T.F.C.; Writing—review and editing, A.C.N.T.F.C., P.R.P., and V.M.F.P.

Funding: This study was financed in part by the Coordenação de Aperfeiçoamento de Pessoal de Nível Superior—Brasil (CAPES)—Finance Code 001 (grant No. 1627392); by Fundação Carlos Chagas Filho de Amparo à Pesquisa do Estado do Rio de Janeiro (FAPERJ) (grant No. E-26/202.815/2018; E-26/202.815/2018; E-26/203.039/2015 and E-26/202.860/2016) and by Conselho Nacional de Desenvolvimento Científico e Tecnológico (CNPq) (grant No. 406601/2018-6).

Acknowledgments: The authors are thankful to the facilities from COPPE/UFRJ, Electronic Microscopy Laboratory and Multiuser Materials Characterization Laboratory; to Dr. Jeniffer Lowe, professor at the Universidade Federal do Rio de Janeiro—UFRJ, Brazil, for the instructions and possibility to work with the Ultracentrifuge; to Dr Alexandre Guedes Torres, professor at the Universidade Federal do Rio de Janeiro—UFRJ, Brazil, for the use of the rotary evaporator and to Professor Roland Bodmeier from the Freie Universität—Berlin—who have helped with resources, provided new methodologies, and supervised ACNTF during the three-month Erasmus$^+$ fellowship in Germany.

Conflicts of Interest: The authors declare no conflict of interest.

References

1. World Health Organization. *World health statistics 2018: Monitoring Health for the SDGs, Sustainable Development Goals*; World Health Organization: Geneva, Switzerland, 2018.
2. Siegel, R.L.; Miller, K.D.; Jemal, A. Cancer statistics, 2018. *CA Cancer J. Clin.* **2018**, *68*, 7–30. [CrossRef]
3. American Cancer Society. About Breast Cancer. Available online: https://www.cancer.org/content/dam/CRC/PDF/Public/8577.00.pdf (accessed on 3 September 2018).
4. American Cancer Society. Chemotherapy for Breast Cancer. Available online: https://www.cancer.org/cancer/breast-cancer/treatment/chemotherapy-for-breast-cancer.html (accessed on 3 September 2018).
5. Ostrom, Q.T.; Gittleman, H.; Liao, P.; Rouse, C.; Chen, Y.; Dowling, J.; Wolinsky, Y.; Kruchko, C.; Barnholtz-Sloan, J. CBTRUS statistical report: Primary brain and central nervous system tumors diagnosed in the United States in 2007–2011. *Neuro Oncol.* **2014**, *16*, iv1–iv63. [CrossRef]
6. Agarwala, S.S.; Kirkwood, J.M. Temozolomide, a novel alkylating agent with activity in the central nervous system, may improve the treatment of advanced metastatic melanoma. *Oncologist* **2000**, *5*, 144–151. [CrossRef] [PubMed]
7. Sharma, P.; Allison, J.P. The future of immune checkpoint therapy. *Science* **2015**, *348*, 56–61. [CrossRef] [PubMed]
8. Du, J.; Tang, X.L. Natural products against cancer: A comprehensive bibliometric study of the research projects, publications, patents and drugs. *J. Cancer Res. Ther.* **2014**, *10*, 27. [PubMed]
9. Wang, X.; Wang, Y.; Chen, Z.G.; Shin, D.M. Advances of cancer therapy by nanotechnology. *Cancer Res. Treat* **2009**, *41*, 1–11. [CrossRef] [PubMed]
10. Pereira, P.R.; Del Aguila, E.M.; Vericimo, M.A.; Zingali, R.B.; Paschoalin, V.M.F.; Silva, J.T. Purification and characterization of the lectin from taro (*Colocasia esculenta*) and its effect on mouse splenocyte proliferation in vitro and in vivo. *Prot. J.* **2014**, *33*, 92–99. [CrossRef]
11. Pereira, P.R.; Winter, H.C.; Verícimo, M.A.; Meagher, J.L.; Stuckey, J.A.; Goldstein, I.J.; Paschoalin, V.M.; Silva, J.T. Structural analysis and binding properties of isoforms of tarin, the GNA-related lectin from *Colocasia esculenta*. *BBA Proteins Proteom.* **2015**, *1854*, 20–30. [CrossRef]
12. Pereira, P.R.; Silva, J.T.; Verícimo, M.A.; Paschoalin, V.M.; Teixeira, G.A. Crude extract from taro (*Colocasia esculenta*) as a natural source of bioactive proteins able to stimulate haematopoietic cells in two murine models. *J. Funct. Foods* **2015**, *18*, 333–343. [CrossRef]
13. Pereira, P.R.; Meagher, J.L.; Winter, H.C.; Goldstein, I.J.; Paschoalin, V.M.; Silva, J.T.; Stuckey, J.A. High-resolution crystal structures of *Colocasia esculenta* tarin lectin. *Glycobiology* **2016**, *27*, 50–56. [CrossRef]
14. Sang Chan, Y.; Ho Wong, J.; Bun Ng, T. A cytokine-inducing hemagglutinin from small taros. *Protein Peptide Lett.* **2010**, *17*, 823–830. [CrossRef]
15. Kundu, N.; Campbell, P.; Hampton, B.; Lin, C.-Y.; Ma, X.; Ambulos, N.; Zhao, X.F.; Goloubeva, O.; Holt, D.; Fulton, A.M. Antimetastatic activity isolated from *Colocasia esculenta* (taro). *Anticancer Drugs* **2012**, *23*, 200. [CrossRef] [PubMed]
16. Pereira, P.R.; Corrêa, A.C.N.T.F.; Vericimo, M.A.; Paschoalin, V.M.F. Tarin, a Potential Immunomodulator and COX-Inhibitor Lectin Found in Taro (*Colocasia esculenta*). *Compr. Rev. Food Sci. Food Saf.* **2018**. [CrossRef]
17. Merida, L.A.; Mattos, E.B.; Corrêa, A.C.; Pereira, P.R.; Paschoalin, V.M.; Pinho, M.F.; Vericimo, M.A. Tarin stimulates granulocyte growth in bone marrow cell cultures and minimizes immunosuppression by cyclo-phosphamide in mice. *PLoS ONE* **2018**, *13*, e0206240. [CrossRef]
18. Santos, N.C.; Castanho, M.A. Liposomes: Has the magic bullet hit the target? *Quim. Nova* **2002**, *25*, 1181–1185. [CrossRef]
19. Papachristos, A.; Pippa, N.; Ioannidis, K.; Sivolapenko, G.; Demetzos, C. Liposomal forms of anticancer agents beyond anthracyclines: Present and future perspectives. *J. Liposome Res.* **2015**, *25*, 166–173. [CrossRef] [PubMed]
20. Andrade, C.A.; Correia, M.T.; Coelho, L.C.; Nascimento, S.C.; Santos-Magalhães, N.S. Antitumor activity of *Cratylia mollis* lectin encapsulated into liposomes. *Int. J. Pharm.* **2004**, *278*, 435–445. [CrossRef]
21. dos Santos Ferreira, D.; Faria, S.D.; de Araújo Lopes, S.C.; Teixeira, C.S.; Malachias, A.; Magalhães-Paniago, R.; de Souza Filho, J.D.; Oliveira, B.L.d.J.P.; Guimarães, A.R.; Caravan, P. Development of a bone-targeted pH-sensitive liposomal formulation containing doxorubicin: Physicochemical characterization, cytotoxicity, and biodistribution evaluation in a mouse model of bone metastasis. *Int. J. Nanomed.* **2016**, *11*, 3737.

22. Mukthavaram, R.; Jiang, P.; Saklecha, R.; Simberg, D.; Bharati, I.S.; Nomura, N.; Chao, Y.; Pastorino, S.; Pingle, S.C.; Fogal, V. High-efficiency liposomal encapsulation of a tyrosine kinase inhibitor leads to improved in vivo toxicity and tumor response profile. *Int. J. Nanomed.* **2013**, *8*, 3991.
23. Peterson, G.L. A simplification of the protein assay method of Lowry et al. which is more generally applicable. *Anal. Biochem.* **1977**, *83*, 346–356. [CrossRef]
24. Douglas, S.; Tuluc, F. Morphology of Monocytes and Macrophages. In *Williams Hematology, 8e*; The McGraw-Hill Companies: New York, NY, USA, 2010; Chapter 67.
25. Bulbake, U.; Doppalapudi, S.; Kommineni, N.; Khan, W. Liposomal formulations in clinical use: An updated review. *Pharmaceutics* **2017**, *9*, 12. [CrossRef] [PubMed]
26. Bozzuto, G.; Molinari, A. Liposomes as nanomedical devices. *Int. J. Nanomed.* **2015**, *10*, 975. [CrossRef] [PubMed]
27. Coelho, J.F.; Ferreira, P.C.; Alves, P.; Cordeiro, R.; Fonseca, A.C.; Góis, J.R.; Gil, M.H. Drug delivery systems: Advanced technologies potentially applicable in personalized treatments. *EPMA J.* **2010**, *1*, 164–209. [CrossRef]
28. Mahmud, M.; Piwoni, A.; Filiczak, N.; Janicka, M.; Gubernator, J. Long-circulating curcumin-loaded liposome formulations with high incorporation efficiency, stability and anticancer activity towards pancreatic adenocarcinoma cell lines in vitro. *PLoS ONE* **2016**, *11*, e0167787. [CrossRef] [PubMed]
29. Woodle, M.; Collins, L.; Sponsler, E.; Kossovsky, N.; Papahadjopoulos, D.; Martin, F. Sterically stabilized liposomes. Reduction in electrophoretic mobility but not electrostatic surface potential. *Biophys. J.* **1992**, *61*, 902–910. [CrossRef]
30. Sharma, U.S.; Sharma, A.; Chau, R.I.; Straubinger, R.M. Liposome-mediated therapy of intracranial brain tumors in a rat model. *Pharm. Res.* **1997**, *14*, 992–998. [CrossRef]
31. Nakhla, T.; Marek, M.; Kovalcik, T. Issues associated with large-scale production of liposomal formulations. *Drug Deliv. Technol.* **2002**, *2*.
32. Comiskey, S.J.; Heath, T.D. Leakage and delivery of liposome-encapsulated methotrexate-γ-aspartate in a chemically defined medium. *Biochim. Biophys Acta Biomembr.* **1990**, *1024*, 307–317. [CrossRef]
33. Tabata, Y.; Ikada, Y. Phagocytosis of polymer microspheres by macrophages. In *New Polymer Materials*; Springer: Berlin, Germany, 1990; pp. 107–141.
34. Stolnik, S.; Illum, L.; Davis, S. Long circulating microparticulate drug carriers. *Adv. Drug Deliv. Rev.* **1995**, *16*, 195–214. [CrossRef]
35. Caldorera-Moore, M.; Guimard, N.; Shi, L.; Roy, K. Designer nanoparticles: Incorporating size, shape and triggered release into nanoscale drug carriers. *Expert Opin. Drug Deliv.* **2010**, *7*, 479–495. [CrossRef]
36. Ferreira, D.d.S.; Lopes, S.C.d.A.; Franco, M.S.; Oliveira, M.C. pH-sensitive liposomes for drug delivery in cancer treatment. *Ther. Deliv.* **2013**, *4*, 1099–1123. [CrossRef] [PubMed]
37. Thakor, F.K.; Wan, K.-W.; Welsby, P.J.; Welsby, G. Pharmacological effects of asiatic acid in glioblastoma cells under hypoxia. *Mol. Cell. Biochem.* **2017**, *430*, 179–190. [CrossRef] [PubMed]
38. Baer, J.; Freeman, A.; Newlands, E.; Watson, A.; Rafferty, J.; Margison, G. Depletion of O 6-alkylguanine-DNA alkyltransferase correlates with potentiation of temozolomide and CCNU toxicity in human tumour cells. *Br. J. Cancer* **1993**, *67*, 1299. [CrossRef]
39. Yin, L.L.; Wen, X.M.; Lai, Q.H.; Li, J.; Wang, X.W. Lenalidomide improvement of cisplatin antitumor efficacy on triple-negative breast cancer cells in vitro. *Oncol. Lett.* **2018**, *15*, 6469–6474. [CrossRef] [PubMed]
40. Pilco-Ferreto, N.; Calaf, G.M. Influence of doxorubicin on apoptosis and oxidative stress in breast cancer cell lines. *Int. J. Oncol.* **2016**, *49*, 753–762. [CrossRef]
41. Roy, A.; Banerjee, S.; Majumder, P.; Das, S. Efficiency of mannose-binding plant lectins in controlling a homopteran insect, the red cotton bug. *J. Agric. Food Chem.* **2002**, *50*, 6775–6779. [CrossRef]
42. Murtey, M.D.; Ramasamy, P. Sample Preparations for Scanning Electron Microscopy–Life Sciences. In *Modern Electron Microscopy in Physical and Life Sciences*; InTech: London, UK, 2016.
43. Deniz, A.; Sade, A.; Severcan, F.; Keskin, D.; Tezcaner, A.; Banerjee, S. Celecoxib-loaded liposomes: Effect of cholesterol on encapsulation and in vitro release characteristics. *Biosci. Rep.* **2010**, *30*, 365–373. [CrossRef] [PubMed]

44. Iwama, A.; Oguro, H.; Negishi, M.; Kato, Y.; Morita, Y.; Tsukui, H.; Ema, H.; Kamijo, T.; Katoh-Fukui, Y.; Koseki, H. Enhanced self-renewal of hematopoietic stem cells mediated by the polycomb gene product Bmi-1. *Immunity* **2004**, *21*, 843–851. [CrossRef]
45. Schindelin, J.; Rueden, C.T.; Hiner, M.C.; Eliceiri, K.W. The ImageJ ecosystem: An open platform for biomedical image analysis. *Mol. Reprod. Dev.* **2015**, *82*, 518–529. [CrossRef]

Sample Availability: Samples of the compounds are not available from the authors.

molecules

MDPI

Article

Phenolic Compounds of *Catalpa speciosa*, *Taxus cuspidata*, and *Magnolia acuminata* have Antioxidant and Anticancer Activity

Hosam O. Elansary [1,2,3,*], Agnieszka Szopa [4], Paweł Kubica [4], Fahed A. Al-Mana [1], Eman A. Mahmoud [5], Tarek K. Ali Zin El-Abedin [6], Mohamed A. Mattar [6] and Halina Ekiert [4]

1 Plant production Department, College of Food and Agriculture Sciences, King Saud University, Riyadh 11451, Saudi Arabia; falmana@ksu.edu.sa
2 Floriculture, Ornamental Horticulture and Garden Design, Faculty of Agriculture, Alexandria University, Alexandria 00203, Egypt
3 Department of Geography, Environmental Management and Energy Studies, University of Johannesburg, Auckland Park Kingsway Campus (APK) Campus, Johannesburg 2006, South Africa
4 Department of Pharmaceutical Botany, Medical College, Jagiellonian University, ul. Medyczna 9, 30-688 Kraków, Poland; a.szopa@uj.edu.pl (A.S.); p.kubica@uj.edu.pl (P.K.); mfekiert@cyf-kr.edu.pl (H.E.)
5 Department of Food Industries, Faculty of Agriculture, Damietta University, Damietta 34511, Egypt; emanmail2005@yahoo.com
6 Department of Agricultural Engineering, College of Food and Agriculture Sciences, King Saud University, Riyadh 11451, Saudi Arabia; tkamalzein@ksu.edu.sa (T.K.A.Z.E.-A.); mmattar@ksu.edu.sa (M.A.M.)
* Correspondence: helansary@ksu.edu.sa; Tel.: +966-571586389

Received: 6 January 2019; Accepted: 22 January 2019; Published: 23 January 2019

Abstract: Tree bark represents an important source of medicinal compounds that may be useful for cancer therapy. In the current study, high-performance liquid chromatography with diode-array detection (HPLC-DAD) was used to determine the profile of the phenolic compounds of *Catalpa speciosa*, *Taxus cuspidata*, and *Magnolia acuminata* bark extracts. The antioxidant and anticancer bioactivities against different cancer cell lines were investigated. *M. acuminata* exerted significantly higher antioxidant activities in the diphenyl picrylhydrazine and β-carotene-linoleic acid assays than the other species. In *C. speciosa*, novel profiles of phenolic acids (ferulic acid was the predominant compound) and catechin were detected. In *T. cuspidata*, six phenolic acids were detected; the predominant compounds were hydroxycaffeic acid and protocatechuic acid. In *M. acuminata*, two phenolic acids and three catechins were detected; catechin was the predominant compound. The three species exerted clear anticancer activity against MCF-7, HeLa, Jurkat, T24, and HT-29 cells, with the strongest activity found in the extracts from *M. acuminata*. No antiproliferative activity against normal cells was found. Flow cytometry revealed greater accumulation of necrotic and early/late apoptotic cells in various treated cancer cells than in untreated control cells, and protocatechuic acid induced a similar accumulation of necrotic cells to that of the bark extracts. Caspase-3 and -7 activity was increased in cancer cells treated with different bark extracts; the highest activity was found in the *M. acuminata* treatment. Our results suggested that the treatment of cancer cells with bark extracts of *M. acuminata*, *C. speciosa*, and *T. cuspidata*, and protocatechuic acid induced apoptosis, suggesting an association between anticancer activities and individual phenolic compounds.

Keywords: *Catalpa speciosa*; *Taxus cuspidata*; *Magnolia acuminata*; phenols; antioxidants; anticancer

1. Introduction

Tree bark is used widely in folklore medicine to treat ailments and control the progress of many diseases and injuries, such as arthritis, gonorrhea, rheumatism, dysentery, malaria, inflammation, wounds, ulcers, and constipation [1–3]. Recent investigations found that tree bark may contain antioxidant and anticancer phenolic compounds [2,4–6]. However, the current knowledge of the pharmaceutical properties of tree bark is limited.

Catalpa belongs to Bignoniaceae and the genus contains several species, including *Catalpa speciosa*, which are distributed throughout North America and some parts of Europe [7]. Leaf extracts from other *Catalpa* species, including *C. ovata, C. fargesii*, *C. bignonioides*, and *C. bungei* are known to have antioxidant activity [8,9] and high phenolic composition. No pharmaceutical studies of *C. speciosa* have been conducted.

Magnolia species, which belong to Magnoliaceae, contain several species, including *M. officinalis, M. obovata*, and *M. biondii,* which have been used in folklore medicine for thousands of years in Asia [10]. Moreover, *Magnoliae officinalis cortex* is listed in the newest European Pharmacopoeia 9.0 as an official pharmaceutical raw plant material in Europe [11]. The dried parts of the magnolia are used to control diarrhea, abdominal swelling, or constipation, and cough [12]. The analyses of the bark and/or seeds of *M. officinalis, M. obovata*, and *M. biondii* revealed the availability of specific bioactive compounds, such as magnolol, honokiol, and obovatol, which have potent anticancer and antioxidant activities [4,6]. Other species, such as *M. acuminata*, have attracted little attention.

Taxus belongs to Taxaceae and contains approximately 13 species distributed throughout Asia, Europe, and North America [13]. The leaves and bark of some species. such as *Taxus wallichiana*, are used in the traditional Ayurveda and Unani medicines for the control of fever, cough, and cold, and exert anticancer activities [5]. The bark of *Taxus baccata* is a well-known pharmaceutical raw material that contains paclitaxel, a known anticancer compound [11]. *T. cuspidata* bark extract showed anticancer activities due to the presence of paclitaxel and other lignans in the roots [14,15]. However, no studies revealed the detailed phenolic and catechin profiles of this species.

The current study explores the phenolic, catechin, and flavonoid content of *C. speciosa*, *T. cuspidata,* and *M. acuminata* using HPLC-DAD method. The antioxidant, antiproliferative, apoptotic, and caspase-3/7 activities have been explored using several cancer cell lines.

2. Results

2.1. Targeted Profiling of Catechins and Phenols

2.1.1. *C. speciosa*

In *C. speciosa* methanolic bark extract, seven phenolic acids (caffeic acid, p-coumaric acid, ferulic acid, gallic acid, p-hydroxybenzoic acid, protocatechuic acid, and vanillic acid) were found out of the 22 screened (Table 1 and Supplementary files). Ferulic acid was the predominant compound (22.7 ± 0.18 mg 100 g^{-1} DW); other phenolic acids were detected in lower quantities. The content of p-hydroxybenzoic acid and vanillic acid was approximately 6 mg 100 g^{-1} DW, the content of caffeic acid, p-coumaric acid, and protocatechuic acid was approximately 3 mg 100 g^{-1} DW, and gallic acid was present at the lowest concentration (ca. 1.6 mg 100 g^{-1} DW). A low amount of catechin (ca. 1.2 mg 100 g^{-1} DW) was detected out of the five analyzed catechin derivatives (Table 2). No flavonoids were detected.

Table 1. The phenolic acid compositions of *Catalpa speciosa*, *Taxus cuspidata*, and *Magnolia acuminnata* outer bark extracts.

Species	Chemical Compound	Amount [mg 100g^{-1}] D.W.
Catalpa speciosa	Caffeic acid	3.04 ± 0.45
	p-Coumaric acid	3.28 ± 0.44
	Ferulic acid	22.7 ± 0.18
	Gallic acid	1.57 ± 0.04
	p-Hydroxybenzoic acid	6.42 ± 0.03
	Protocatechuic acid	3.22 ± 0.02
	Vanillic acid	5.77 ± 0.22

Table 1. *Cont.*

Species	Chemical Compound	Amount [mg 100g^{-1}] D.W.
Taxus cuspidata	Caffeic acid	3.05 ± 0.01
	Chlorogenic acid	8.30 ± 0.22
	Gallic acid	2.04 ± 0.07
	p-Hydroxybenzoic acid	2.42 ± 0.16
	Hydroxycaffeic acid	23.98 ± 1.3
	Protocatechuic acid	20.97 ± 0.56
Magnolia acuminnata	Ellagic acid	0.43 ± 0.08
	Protocatechuic acid	15.31 ± 1.19

Table 2. The catechin derivatives compositions of *Catalpa speciosa* and *Magnolia acuminnata* outer bark extracts.

Species	Chemical Compound	Amount [mg 100g^{-1}] D.W.
Catalpa speciosa	Catechin	1.19 ± 0.05
Magnolia acuminnata	Catechin	85.47 ± 1.30
	Epicatechin	22.78 ± 0.53
	Epigallocatechin gallate	14.22 ± 0.95

2.1.2. *T. cuspidata*

In *T. cuspidata* bark extracts, caffeic acid, chlorogenic acid, gallic acid, p-hydroxybenzoic acid, hydroxycaffeic acid, and protocatechuic acid were identified (Table 1 and Supplementary files). The predominant compounds were protocatechuic acid (ca. 21 mg 100 g^{-1} DW) and hydroxycaffeic acid (ca. 24 mg 100 g^{-1} DW). In the extracts, no flavonoids or catechins were found.

2.1.3. *M. acuminata*

In the *M. acuminata* bark extracts, protocatechuic acid (ca. 15 mg 100 g^{-1} DW) was the dominant phenolic acid (Table 1 and Supplementary files). A low composition of ellagic acid (less than 0.5 mg 100 g^{-1} DW) was also identified. However, catechins and catechin derivatives, epicatechin, and epigallocatechin gallate, were found in the extracts (Table 2). Catechin was the main compound (ca. 85.5 mg 100 g^{-1} DW), followed by epicatechin (ca. 23 mg 100 g^{-1} DW) (Table 2). No flavonoids were detected by using the HPLC-DAD method.

2.2. Antioxidant Activities

Bark extracts showed antioxidant activity as found in Table 3. *M. acuminata* exhibited the highest antioxidant activities in the diphenyl picryl hydrazyl (DPPH) (IC_{50}, 3.1 μg mL^{-1}) and β-carotene-linoleic acid (IC_{50}, 3.6 μg mL^{-1}) assays compared to other species. *T. cuspidata* exhibited higher antioxidant activities than *C. speciosa*. *M. acuminata* antioxidant power was comparable with those of the standard antioxidant (BHT).

Table 3. Diphenyl picryl hydrazyl (DPPH) and *β*-carotene-linoleic acid of *Catalpa speciosa*, *Taxus cuspidata*, *Magnolia acuminnata* outer bark extracts.

Plant/Standard	DPPH Free Radical Scavenging Activity (IC50, μg mL^{-1})	β-Carotene-Linoleic Acid Assay (IC50, μg mL^{-1})
Catalpa speciosa	4.4 ± 0.1a	5.1 ± 0.1a
Taxus cuspidata	4.2 ± 0.1b	4.8 ± 0.1b
Magnolia acuminnata	3.1 ± 0.1c	3.6 ± 0.1c
BHT	2.9 ± 0.1c	3.2 ± 0.1c

2.3. Antiproliferative Activities

The bark extracts exhibited antiproliferative activities against different cancer cell lines, as shown in Table 4. Anticancer activity against MCF-7, HeLa, Jurkat, T24, and HT-29 cells was noted. The strongest anticancer bioactivity was found in *M. acuminata* (IC_{50}, 16.20–152.8 μg/mL). Further, no extract exerted antiproliferative activity against normal HEK-293 cells. Specific catechins and phenolics found in the bark extracts, including protocatechuic acid, catechin, ferulic acid, and hydroxycaffeic acid, exhibited notable antiproliferative activity against most cancer cells.

Table 4. In vitro antiproliferative activity (IC_{50} (μg/mL)) of *Catalpa speciosa*, *Taxus cuspidata*, *Magnolia acuminnata* outer bark extracts on cancer cell lines.

Plant/Standard	HeLa	MCF-7	Jurkat	T24	HT-29	HEK-293
Catalpa speciosa	58.3 ± 1.7	41.19 ± 1.6	41.4 ± 1.1	249.5 ± 2.9	111.5 ± 2.9	>400
Taxus cuspidata	54.5 ± 1.9	39.51 ± 0.9	37.3 ± 0.5	220.1 ± 2.9	102.2 ± 3.1	>400
Magnolia acuminnata	28.4 ± 1.3	16.20 ± 1.1	25.1 ± 1.1	152.8 ± 2.9	89.2 ± 2.5	>400
Catechin	36.48 ± 1.2	17.64 ± 1.8	38.16 ± 0.7	183.28 ± 4.3	96.16 ± 1.5	>400
Protocatechuic acid	39.10 ± 2.3	18.97 ± 2.1	47.35 ± 2.1	176.35 ± 2.1	95.35 ± 3.3	>400
Ferulic acid	51.73 ± 3.5	43.85 ± 1.3	39.11 ± 2.3	227.26 ± 5.1	126.26 ± 4.4	>400
Hydroxycaffeic acid	65.31 ± 2.4	58.11 ± 0.9	63.09 ± 1.4	176.12 ± 3.6	113.15 ± 2.9	>400
Vinblastine sulfate	2.7 ± 0.06	-	0.1 ± 0.09	65.7 ± 2.1	21.0 ± 0.1	50.1± 2.3
Vincristine	8.5 ± 0.1	4.63 ± 1.8	0.4 ± 0.05	89.8 ± 2.5	47.3 ± 0.2	78.3 ± 1.6
Taxol	-	0.09 ± 0.009	-	-	-	-

2.4. Apoptotic Cell Population

Flow cytometry revealed the extent of apoptosis in different cell lines subjected to the (50% Inhibition concentration) IC_{50} of bark extracts (Figures 1 and 2). The results showed a greater accumulation of necrotic cells, and early and late apoptotic cells in treated cancer cells than in control cells in various cancer cell lines. Treatment with protocatechuic acid showed similar accumulation of necrotic cells as treatment with the bark extracts of the three species. The bioactivity of the extracts and protocatechuic acid was sustained after 48 h.

2.5. Detection of Caspase-3/7 Activity

The effects of bark extracts on caspase-3/7 activity were investigated in HeLa, MCF-7, Jurkat, HT-29, and T24 cells (Figure 3). The results showed that greater caspase 3/7 activity occurred after *M. acuminata*, *T. cuspidata*, and *C. speciosa* treatment in all cancer cell lines than in the untreated control cells. *M. acuminata* resulted in a higher activity of caspase 3/7 than the other treatments.

2.6. Western Blotting Analyses of Caspases-3 and Caspase-7

Western blotting of caspase-3 and caspase-7 activation by bark extracts was tested as shown in Figure 4. Bark extracts increased the activation of caspase-3 and caspase-7 in all cancer cells, except in MCF-7 which was deficient for caspase-3. Further, high proteolytic cleavage of the nuclear enzyme poly (adenosine diphosphate ribose) polymerase/PARP (caspase substrates) was found in all treatments compared to control. This increased cleavage is required for the activation of key apoptosis executioners (caspase-3 and caspase-7).

3. Discussion

This is the first report to document detailed phenolic and catechin profiles of *C. speciosa* bark extract. The phenolic acid profile of *C. speciosa* bark was relatively unique (compared to other species) and contained ferulic acid (as the dominant compound), caffeic acid, p-coumaric acid, gallic acid, p-hydroxybenzoic acid, protocatechuic acid, and vanillic acid. Previous investigations into *C. ovata*, *C. fargesii*, and *C. bungei* leaves [8] have revealed only flavonoids such as luteolin and apigenin. *C. bignonioides* flowers and leaves had high phenolic contents [9]. The current investigation was

the first to identify several phenolics in the *T. cuspidata* bark extract. Previously detected paclitaxel, a diterpenoid with anticancer activity, in the *T. cuspidata* bark extract [14]. In addition, several lignans were isolated from other parts of this species [15]. In different species (*Taxus wallichiana* Zucc.), the leaves and bark were found to contain paclitaxel and exhibit potent anticancer activities [5].

In *M. acuminata* bark, two phenolic acids (ellagic acid and protocatechuic acid) and three catechins (catechin, epicatechin, and epigallocatechin gallate) were found. Catechin was the predominant compound, followed by epicatechin; neither had been previously isolated from *M. acuminata.* Previous investigations described other phenols in *M. officinalis* stem bark; these phenols included magnolianone and its derivatives, which exerted antioxidant activities [4,16], and magnoloside, a phenylethanoid glycoside [6].

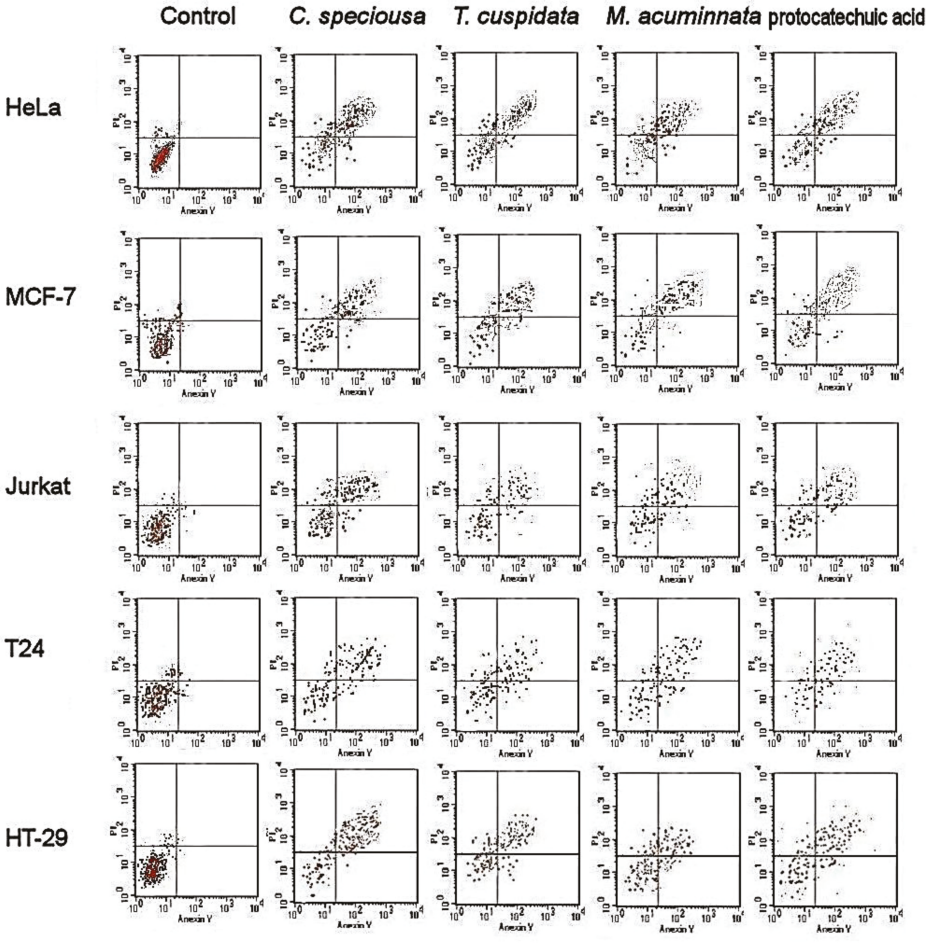

Figure 1. Cellular apoptosis induced in cancer cells at 24 h following treatment with bark extracts and catechin. Lower left, viable cells; upper left, necrotic cells; lower right, early apoptotic cells; and upper right, late apoptotic cells.

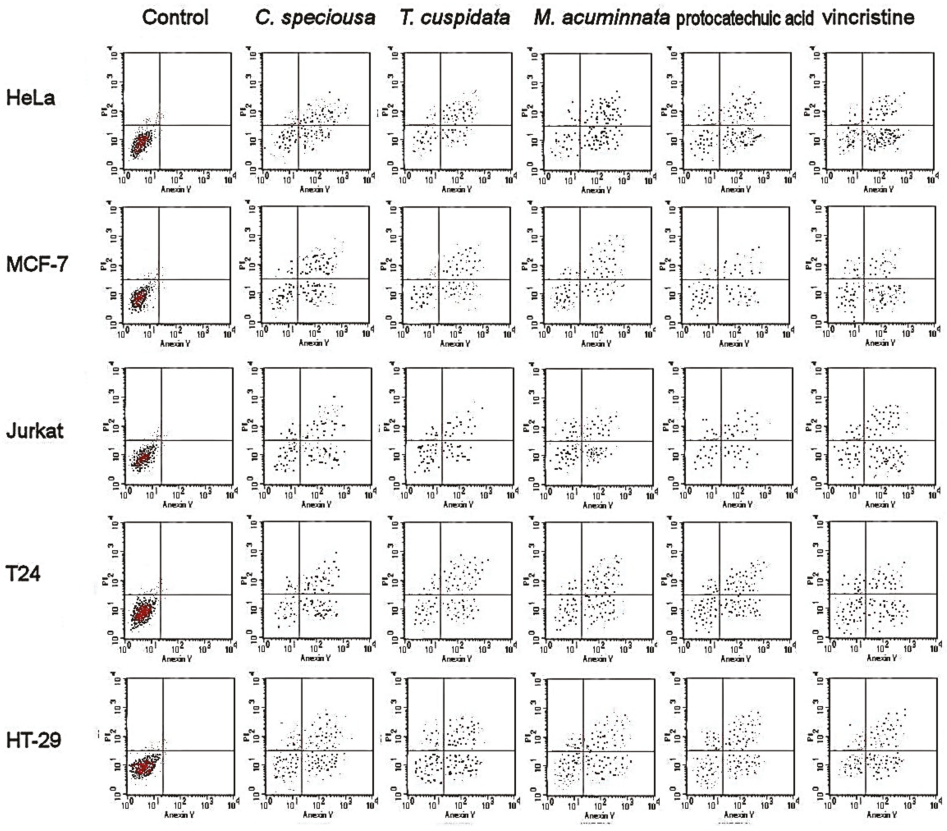

Figure 2. Cellular apoptosis induced in cancer cells at 48 h following treatment with bark extracts and catechin. Lower left, viable cells; upper left, necrotic cells; lower right, early apoptotic cells; and upper right, late apoptotic cells.

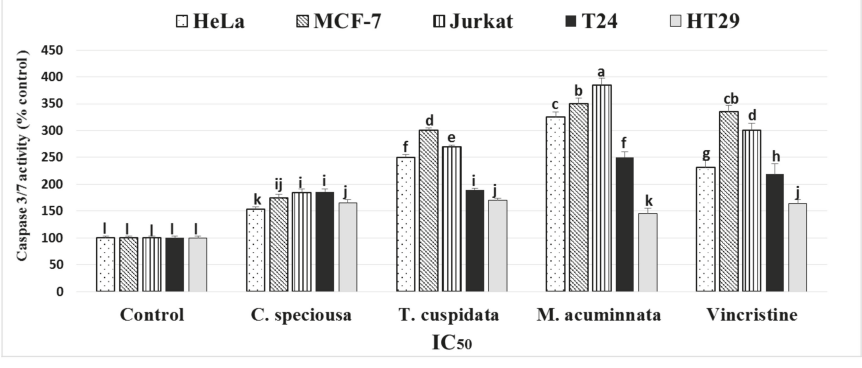

Figure 3. Enzyme activity of caspase 3/7 following treatment of different cancer cells with *C. speciousa*, *T. cuspidate*, and *M. acuminnata* bark extracts (IC_{50}). The activity was expressed as a percentage (%) of untreated cells.

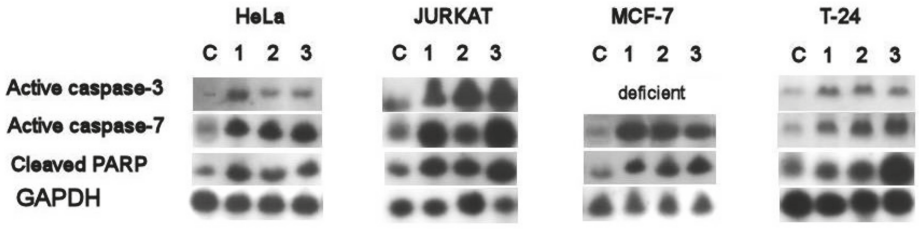

Figure 4. Western blot analysis of active caspase-3, caspase-7 and cleaved PARP using bark extracts (IC_{50}) of *C. speciousa* (1), *T. cuspidata* (2), and *M. acuminnata* (3).

The antioxidant activity assays showed that *M. acuminata* bark extract had the highest antioxidant activity. This high antioxidant activity was mainly attributable to the high concentration of catechin (85.47 ± 1.30 mg 100 g^{-1}) and catechin derivatives in the bark extracts. Catechin is strongly associated with the overall antioxidant activities in various species [17,18]. The barks of other species, such as *Magnolia officinalis*, were shown to have antioxidant activities [19], which were attributed to the glycosides and flavonoids in another study [20]. Studied on other species, such as *Magnolia grandiflora*, it revealed antioxidant effect in the flower extract [21] and comparable activity in the leaf extract [22]. *T. cuspidata* exerted stronger antioxidant activities than *C. speciosa*. A study on *T. cuspidata* bark revealed polyphenols that might have antioxidant effects, including lignans and catechins [23]; the authors found catechin and epicatechin, although we did not detect these types of catechins in the current study. In *C. speciosa*, we found a moderate antioxidant effect for the bark. Previous investigations revealed the antioxidant effect of the leaves of *C. ovata, C. fargesii*, and *C. bungei* [8], as well as in the inflorescence and leaves of *C. bignonioides* [9]. These antioxidant activities were attributed to the high total phenolic content [9] or the presence of flavonoids such as luteolin and apigenin [8]. In our study, this antioxidant bioactivity of *C. speciosa* bark extract was attributed to specific phenolic contents, including ferulic acid (22.7 ± 0.18 mg 100 g^{-1}), which are known to be strong antioxidants [24].

Anticancer activities against the MCF-7, HeLa, Jurkat, T24, and HT-29 cells were found; the highest activities were exhibited by *M. acuminata*. The main components detected in *M. acuminata* were catechins, which were relatively abundant, including catechin, epicatechin, protocatechuic acid, and epigallocatechin gallate; the observed effects were related to these components of the bark. Protocatechuic acid (PCA, 3,4-dihydroxybenzoic acid) has been correlated to anticancer activities against different cancer cells, as found in this investigation, and is a relatively strong antioxidant [25,26]. Catechins are strongly associated with anticancer effects, such as reports of green tea catechins [27] and the synergistic effects with other treatments [28]. Epicatechin is also associated with the anticancer activity and the induction of apoptosis [29], especially epicatechin oligomers [30]. In addition, it is believed that epicatechin and epigallocatechin in green tea have anticancer and apoptosis-inducing activities [31]. Other species of *Magnolia* also have anticancer activities [32].

The anticancer bioactivity of *C. speciosa* is correlated with its major phenolic compartments, including ferulic acid, p-hydroxybenzoic acid, vanillic acid, and caffeic acid. Ferulic acid suppresses the metastasis in breast cancer cells by regulating the reversal of epithelial-mesenchymal transition [33] and inducing the cell cycle arrest in the cells of cervical cancer [34]. In our study, ferulic acid was the major phenol found in the bark extract (22.7 ± 0.18 mg 100 g^{-1}) and is greatly associated with anticancer activity. We found that *C. speciosa* bark extracts have potential antioxidant and anticancer activities against MCF-7 breast cancer, which may be attributable to phenolic acid compounds such as protocatechuic acid and p-hydroxybenzoic acid. These compounds were found to have the power to control MCF-7 breast and PC-3 prostate cancers [35].

T. cuspidata showed antiproliferative activities against Jurkat, MCF-7, and HeLa cancer cells and these activities were directly associated with the major phenolic and catechin components, including hydroxycaffeic acid (23.98 ± 1.3 mg 100 g^{-1}), chlorogenic acid (8.3 ± 0.22 mg 100 g^{-1}),

protocatechuic acid (20.97 ± 0.56 mg 100 g^{-1}), and gallic acid (2.04 ± 0.07 mg 100 g^{-1}). These phenolic and catechin compounds were shown to have antiproliferative effects against different cancer cells [35,36]. In addition to our results that the bark extracts had clear antiproliferative activities against specific cancer cell types, it was previously reported that twigs and needles of the same plant exert anticancer activities against human cancer [37].

The results of flow cytometry showed an accumulation of necrotic cells and early and late apoptotic cells in various cancer cells subjected to bark extracts compared with the untreated control cells. The apoptotic activities of *M. acuminata* are strongly connected with the catechin composition, as similar effects to those of catechin were found. This conclusion was strongly supported by the apoptosis induction described before for catechins such as epicatechin [29], epicatechin oligomers [30], epicatechin, and epigallocatechin [31]. The flower extract of *M. grandiflora* showed an apoptotic effect in lymphocytic leukemia cells [38]. There was a high accumulation of early and late apoptotic cells after following bark extracts and catechin treatment. In *C. speciosa*, ferulic acid was suggested to be the cornerstone of the apoptosis-inducing activities as it was associated with the death of osteosarcoma cells through the promotion of caspase-3 and apoptosis [39]. In another study, ferulic acid induced cell cycle arrest in cervical cancer cells [34]. In *T. cuspidata*, the apoptotic activities observed in this study agreed with a previous investigation into the needle and twig extracts of the same species [37]. The authors reported HeLa cells apoptosis in HeLa cells and low toxicity in normal cells and G(2)/M cell cycle arrest. The major phenolic acid in *T. cuspidata* is protocatechuic acid which showed apoptosis and slow metastasis in cancer cells [40].

Caspase-3 and -7 enzymes function as mediators of apoptosis through DNA fragmentation and apoptotic chromatin condensation, which lead to cell death [41,42]. We found increased activities of these enzymes in bark extract-treated cancer cells except in MCF-7 which was deficient for caspase-3 only [43,44]. The western plotting of these enzymes confirmed the antiproliferative and apoptotic activities of the three bark extracts as found in in the extracts of other plants [45]. Previous investigations into the use of ferulic acid to control cancer cells revealed that this compound promoted the apoptosis pathway through the activation of caspase-3 [39]. This was the case for *C. speciosa*, in which ferulic acid was the major phenol found in the bark extracts studied. *C. speciosa* might be a potential new natural source of ferulic acid. The highest activities of caspase-3/7 were found after *M. acuminata* treatment and this activity may be associated with the important catechins in this bark, such as epigallocatechin gallate and epicatechin, and the phenolic acid, protocatechuic acid. Epigallocatechin gallate was one of the major catechins found in *M. acuminata* bark in this study and was strongly related to the increased activities of caspase-3 in green tea catechins [46]. Protocatechuic acid was shown to increase caspase-3 activities [40]; however, another study reported contrasting results [25]. Epicatechin is strongly related to caspase-3 activity in several studies [47,48]. *T. cuspidata* showed some degree of caspase-3/7 activation, which may be attributable to several phenolic compounds found in the bark extract that stimulate the activity of caspase-3, such as chlorogenic acid [49] and gallic acid [50].

4. Materials and Methods

4.1. Plant Material

Catalpa speciosa (Bignoniaceae), *Taxus cuspidata* Siebold & Zucc.(Taxaceae), and *Magnolia acuminata* L. (Magnoliaceae) outer bark was obtained from identified plants at the Arboretum of University of Guelph, Ontario, Canada. The samples were identified by Hosam Elansary and a voucher was deposited at the University of Guelph and Alexandria University (Hosam000980-2018).

4.2. Sample Preparation and Cell Cultures

Fresh bark (0.25 g) was dried at 35 °C until a constant weight was obtained. The samples were ground and then dissolved in 3 mL methanol (99%) for 1 h in the dark at 25 °C. Bark solutions

were centrifuged for 5 min at 10,000 rpm (7000 × *g*) and the supernatant was obtained (~2.7 mL). The samples were passed through a 0.45 μm polytetrafluroethylene (PTFE) nylon filter and then stored at −80 °C. Analytical grade chemicals (Sigma Aldrich, Germany) were used in the bioassays. The cancer cell lines, including cervical adenocarcinoma (HeLa), breast adenocarcinoma (MCF-7), T-cell lymphoblast like (Jurkat), urinary bladder carcinoma (T24), and colon adenocarcinoma (HT-29), were obtained from the American Type Culture Collection (ATCC).

4.3. Analyses of Phenolic Compounds

C. speciosa, *T. cuspidata*, and *M. acuminata* bark samples were dried by lyophilization (Labconco, Kansas City, MO, USA) and powdered. Bark samples were extracted (0.5 g) as described before [51]. Validated chromatographic analyses were performed using the HPLC [52,53]. A Purospher® RP-18e analytical column (4 × 250 mm, 5 mL; Merck, Berlin, Germany) was used in the HPLC-DAD (Merck-Hitachi, Tokyo, Japan) equipment. A gradient program was used with a flow rate of 1 mL/min, a detection wavelength of 254 nm, and an injection volume of 10 μL [51,54,55]. UV-DAD spectra and t_r values were used for the quantification of the compounds alongside the phenolic, catechin, and flavonoid standards. These included benzoic acid and related derivatives: Ellagic, gallic, 3,4-dihydroxyphenylacetic, protocatechuic, gentisic, p-hydroxybenzoic, salicylic, vanillic, and syringic acids. In addition to cinnamic acid and the related derivatives, such as caffeic, coumaric, ferulic, *o*-coumaric, *m*-coumaric, *p*-hydrocaffeic, isoferulic, sinapic acids, and depsides (chlorogenic, rosmarinic, and neochlorogenic acids). The catechins included catechin, epicatechin, epigallocatechin gallate, epicatechin gallate, and epigallocatechin. The flavonoid standards included aglycones (kaempferol, myricetin, quercetin luteolin, and rhamnetin) and glycosides (apigetrin, cynaroside, robinin, hyperoside, isoquercetin, quercitrin, rutin, trifolin, and vitexin). The standards were obtained from Sigma-Aldrich (Berlin, Germany).

4.4. Antioxidant Activity

The DPPH and β-carotene-linoleic acid assays were used in the Faculty of Food and Agricultural Sciences, King Saud University to determine the antioxidant activities of bark extract [56]. For the DPPH assay, the samples were incubated for 30 min and the absorbance of the samples at 517 nm was measured. In the β-carotene-linoleic acid assay, the absorbance of the samples at 470 nm was measured. The concentration of the sample required to scavenge 50% of the DPPH/β-carotene-linoleic acid solutions, the IC_{50} (μg/mL) was determined by plotting the inhibition percentage against extract concentration. A standard antioxidant (butylated hydroxytoluene, BHT) was used as a positive control and the inhibition by the concentration of each sample was compared with that of the BHT and blank. The antioxidant activities were repeated twice in duplicates.

4.5. Antiproliferative Activity

The antiproliferative activity of bark extracts was examined in different cancer cells lines (HeLa, MCF-7, Jurkat, HT-29, and T24) and in normal cells (HEK-293) by using a modified 3-(4,5-dimethylthiazol-2-yl)-2,5-diphenyltetrazolium bromide (MTT) method [57]. The cells were grown in 75 cm^2 flasks in MEM supplemented with 10% FBS, 17.8 mM $NaHCO_3$, 0.1 mM non-essential amino acids, and 1 mM sodium pyruvate. They were seeded into 96-well plates at a density of 4×10^{-4} per well, left to stand in 270 μL of medium, and incubated in an atmosphere of 37 °C and 5% CO_2. Sterilin-filtered leaf extracts were added to the culture media in microtiter plates. Five doses of bark extracts were used at final concentrations of 50, 100, 200, 300, and 400 μg/mL in culture medium. Untreated cells were considered used as negative controls and vinblastine sulfate and taxol treatment were used as the positive controls. After incubation of the culture medium for 2 days at 37 °C and 5% CO_2, phosphate buffer saline (PBS) washes were performed to remove extract traces and the medium supplied was 12 mM MTT dissolved in PBS. Subsequently, 0.04 N HCl dissolved in isopropanol was mixed in each well, left to stand for 40 min, and the absorbance at 570 nm was determined by using a

microplate reader (Thermo Fisher Scientific, Waltham, Massachusetts, USA). The percentage inhibition of antiproliferation activity was calculated in triplicate [58]:

% Inhibition = (Abs.570 nm control—Abs.570 nm sample)/Abs.570 nm control × 100. Subsequently, IC_{50} values were obtained by plotting the percentage of cell viability against the extract concentration and expressed in μg/mL.

4.6. Apoptotic Cell Population

Flow cytometry (FAC Scan, Becton Dickinson, Iowa, USA) was used to measure the apoptotic cell population [59]. Different types of cancer cells were cultured (37 °C, 5% CO_2) in 6-well plates and treated for 24/48 h with the IC_{50} of bark extract, as determined from the MTT assay, and catechin and untreated samples were considered as the control. The cells were detached by using trypsin (0.25%) in Hank's balanced salt solution (Thermo Fisher Scientific, Berlin, Germany). For staining the cells, the Annexin V apoptosis detection kit (Sigma, St. Louis, MO, USA) was used. Briefly, the cells were incubated in the dark at 37 °C for 15 min and washed with cold PBS, and the apoptotic populations were shown by the flow cytometer in quadrants: Lower left (viable cells), upper left (necrotic cells), lower right (early apoptotic cells), and upper right (late apoptotic cells).

4.7. Caspase-Glo 3/7 Assay

The effect of different bark extracts on caspase-3/7 activity using different cancer cell lines was detected by the Caspase-Glo 3/7 Assay kit (Promega, Berlin, Germany). The cancer cell lines were cultured in Roswell Park Memorial Institute (RPMI) growth medium (Sigma-Aldrich, St. Louis, MO, USA) in 96-well plates in the presence of the IC_{50} of the extracts, catechin, or DMSO (solvent control) for 24 h. Caspase-Glo 3/7 reagent (100 μL) was added to each well, mixed, and then incubated at room temperature for 1 h. The luminescence was of each well was detected by using an Infinite M2000 Pro™ (Tecan). The activity of caspase-3/7 was expressed as a percentage (%) of the untreated samples.

4.8. Western Blotting of Caspase-3 and Caspase-7

Cancer cells were treated with bark extracts (IC_{50}) for 24 h then harvested, washed with PBS, lysed in protease-inhibitor cocktail buffer (Roche Diagnostic, Bern, Switzerland). The supernatant was collected by centrifugation (2500 ×g for 15 min), then the protein was extracted and the concentration was determined by the bicinchoninic acid protein assay kit (Sigma-Aldrich, Berlin, Germany). Sample proteins (60–80) μg were separated by SDS-PAGE (10%) then blotted on a Polyvinylidene difluoride (PVDF) membrane. Blocking of proteins was achieved by treating the membrane with 5% skimmed milk + 1XTBS + 0.1% Tween 20 for 60 min. The membrane was treated with caspase-3 (#9661), Caspase-7 primary antibodies (#9492), poly (adenosine diphosphate ribose) polymerase (PARP) (#9542), and GAPDH (internal control, #sc-32233) (1:1,000; Cell Signaling Technology, Danvers, MA, USA) at 4 °C overnight. The membrane was washed then incubated with anti-rabbit (cat. no. sc-2030)/ anti-mouse (cat. no. sc-2005) secondary antibody (1:2,000; Santa Cruz Biotechnology, Inc. Dallas, Texas, USA). The bands were detected by ECL reagent and GE Healthcare Bio-Sciences AB Image Quant LAS 4000 (GE Healthcare, Berlin, Germany). The results shown are representative of three independent experiments.

4.9. Statistical Analyses

The least significant difference (LSD) was computed by using SPSS software (version 22.0, IBM, New York, USA). The quantitative results of the chromatographic analyses are expressed in (mg 100 g^{-1} DW) as the mean ± SD of three series of experiments.

5. Conclusions

M. acuminata showed significantly higher antioxidant activities than the other species tested and standard antioxidants. In *C. speciosa,* seven phenolic acids (ferulic acid, caffeic acid, p-hydroxybenzoic acid, p-coumaric acid, gallic acid, protocatechuic acid, and vanillic acid) and catechin were detected by using HPLC-DAD analysis. In *T. cuspidata*, five phenolics were detected and the dominant compound was hydroxycaffeic acid. In *M. acuminata*, two phenolic acids (ellagic acid and protocatechuic acid) and three catechins (catechin, epicatechin, and epigallocatechin gallate) were detected; catechin was the predominant compound. The extracts exerted clear anticancer activities against MCF-7, HeLa, Jurkat, T24, and HT-29 cells. The strongest anticancer activity was exerted by the extract of *M. acuminata*. Further, no antiproliferative activities in normal cells were observed. Flow cytometry showed a greater accumulation of necrotic cells and early and late apoptotic cells in various cancer cell lines treated with the extracts compared with the untreated control cells. Protocatechuic acid resulted in similar accumulation of necrotic cells as the bark extracts of the three species. Increased caspase-3/7 activities were observed in cancer cells treated with different bark extracts and the highest activity was induced by *M. acuminata* treatment. In conclusion, our results indicate the induction of apoptosis after the treatment of cancer cells with bark extracts of *M. acuminata, C. speciosa, T. cuspidata*, and protocatechuic acid, and suggest the association between anticancer activities and the individual phenolic constituents.

Supplementary Materials: The following are available online at http://www.mdpi.com/1420-3049/24/3/412/s1, Figure S1: The representative HPLC-UV chromatogram (λ = 254 nm) of *Magnolia acuminnata* bark extract; 1 - protocatechuic acid (tR = 6.3 min), 2 – catechin (tR = 8.8 min), 3 - elgaic acid (tR = 12.2 min), 4 - epigallocatechin gallate (tR = 14.8 min), 5 – epicatechin (tR = 19.2 min), Figure S2: The representative HPLC-UV chromatogram (λ = 254 nm) of Taxus cuspidate bark extract; 1 - gallic acid (tR = 3.2 min), 2 - protocatechuic acid (tR = 6.3 min), 3 - chlorogenic acid (tR=9.2 min), 4 - p-hydroxybensoic acid (tR = 11.8 min), 5 - caffeic acid (tR = 15.2 min), 6 - hydroxycaffeic acid (tR = 15.8 min), Figure S3: The representative HPLC-UV chromatogram (λ = 254 nm) of Catalpa speciosa bark extract; 1 - gallic acid (tR = 3.2 min), 2 - protocatechuic acid (tR = 6.3 min), 3 – catechin (tR = 8.8 min), 4- p-hydroxybensoic acid (tR = 11.8 min), 5 - vanillic acid (tR = 12 min), 6 -caffeic acid (tR = 15.2 min), 7 - p-coumaric acid(tR = 26 min), 8 - ferulic acid(tR = 34.4 min).

Author Contributions: H.E., A.S., P.K., F.A., E.M., M.M., T K., and H.E. participated in conducting experiments, writing and approving the final manuscript.

Funding: Funding was approved by the Deanship of Scientific Research at King Saud University through research group no. (RG - 1440-12).

Acknowledgments: We acknowledge the funding of this work from the Deanship of Scientific Research at King Saud University through research group no. (RG - 1440-12).

Conflicts of Interest: The authors declare no conflict of interest.

References

1. Grace, O.M.; Prendergast, H.D.V.; Jager, A.K.; van Staden, J. Bark medicines used in traditional healthcare in KwaZulu-Natal, South Africa: An inventory. *S. Afr. J. Bot.* **2003**, *69*, 301–363. [CrossRef]
2. Bello, I.; Shehu, M.W.; Musa, M.; Asmawi, M.Z.; Mahmud, R. Kigelia africana (Lam.) Benth. (Sausage tree): Phytochemistry and pharmacological review of a quintessential African traditional medicinal plant. *J. Ethnopharmacol.* **2016**, *189*, 253–276. [CrossRef] [PubMed]
3. Vermeulen, W.J.; Geldenhuys, C.J.; Esler, K.J. Response of Ocotea bullata, Curtisia dentata and Rapanea melanophloeos to medicinal bark stripping in the southern Cape, South Africa: Implications for sustainable use. *South. For.* **2012**, *74*, 183–193. [CrossRef]
4. Chuang, D.Y.; Chan, M.H.; Zong, Y.; Sheng, W.; He, Y.; Jiang, J.H.; Simonyi, A.; Gu, Z.; Fritsche, K.L.; Cui, J.; et al. *Magnolia polyphenols* attenuate oxidative and inflammatory responses in neurons and microglial cells. *J. Neuroinflamm.* **2013**, *10*, 15. [CrossRef]
5. Juyal, D.; Thawani, V.; Thaledi, S.; Joshi, M. Ethnomedical properties of Taxus wallichiana zucc. (Himalayan yew). *J. Tradit. Complement. Med.* **2014**, *4*, 159–161. [CrossRef] [PubMed]
6. Yu, S.X.; Yan, R.Y.; Liang, R.X.; Wang, W.; Yang, B. Bioactive polar compounds from stem bark of *Magnolia officinalis*. *Fitoterapia* **2012**, *83*, 356–361. [CrossRef]

7. Hemmings, E.T.; Core, E.L. Archeological Evidence for Range Extension of the Catawba Tree (*Catalpa speciosa* Warder) in West Virginia. *Castanea* **1976**, *41*, 9–11.
8. Xu, H.; Hu, G.; Dong, J.; Wei, Q.; Shao, H.; Lei, M. Antioxidative Activities and Active Compounds of Extracts from Catalpa Plant Leaves. *Sci. World J.* **2014**, *2014*, 857982. [CrossRef]
9. Dvorska, M.; Zemlicka, M.; Muselik, J.; Karafiatova, J.; Suchy, V. Antioxidant activity of *Catalpa bignonioides*. *Fitoterapia* **2007**, *78*, 437–439. [CrossRef]
10. Lee, Y.J.; Lee, Y.M.; Lee, C.K.; Jung, J.K.; Han, S.B.; Hong, J.T. Therapeutic applications of compounds in the Magnolia family. *Pharmacol. Ther.* **2011**, *130*, 157–176. [CrossRef]
11. European Directorate for the Quality of Medicines and Healthcare. *European Pharmacopoeia 9.0*; Council of Europe: Strasbourg, France, 2017.
12. Park, J.; Lee, J.; Jung, E.S.; Park, Y.; Kim, K.; Park, B.; Jung, K.S.; Park, E.; Kim, J.; Park, D. In vitro antibacterial and anti-inflammatory effects of honokiol and magnolol against *Propionibacterium* sp. *Eur. J. Pharmacol.* **2004**, *496*, 189–195. [CrossRef] [PubMed]
13. Farjon, A. World Checklist and Bibliography of Conifers. In *World Checklists and Bibliographies*, *3*, 2nd ed.; Royal Botanic Gardens, Kew: Kew, UK, 2001; p. 300.
14. Kawamura, F.; Kikuchi, Y.; Ohira, T.; Yatagai, M. Accelerated solvent extraction of paclitaxel and related compounds from the bark of *Taxus cuspidata*. *J. Nat. Prod.* **1999**, *62*, 244–247. [CrossRef]
15. Kawamura, F.; Kikuchi, Y.; Ohira, T.; Yatagai, M. Phenolic constituents of *Taxus cuspidata* I: Lignans from the roots. *J. Wood Sci.* **2000**, *46*, 167–171. [CrossRef]
16. Shen, C.C.; Ni, C.L.; Shen, Y.C.; Huang, Y.L.; Kuo, C.H.; Wu, T.S.; Chen, C.C. Phenolic constituents from the stem bark of *Magnolia officinalis*. *J. Nat. Prod.* **2009**, *72*, 168–171. [CrossRef] [PubMed]
17. Grzesik, M.; Naparlo, K.; Bartosz, G.; Sadowska-Bartosz, I. Antioxidant properties of catechins: Comparison with other antioxidants. *Food Chem.* **2018**, *241*, 480–492. [CrossRef]
18. Kerio, L.C.; Wachira, F.N.; Wanyoko, J.K.; Rotich, M.K. Total polyphenols, catechin profiles and antioxidant activity of tea products from purple leaf coloured tea cultivars. *Food Chem.* **2013**, *136*, 1405–1413. [CrossRef] [PubMed]
19. Oh, S.; Gadde, U.D.; Bravo, D.; Lillehoj, E.P.; Lillehoj, H.S. Growth-Promoting and Antioxidant Effects of Magnolia Bark Extract in Chickens Uninfected or Co-Infected with Clostridium perfringens and Eimeria maxima as an Experimental Model of Necrotic Enteritis. *Curr. Dev. Nutr.* **2018**, *2*, nzy009. [CrossRef] [PubMed]
20. Zhang, M.; Cheng, S.; Liang, Y.; Mu, Y.; Yan, H.; Liu, Q.; Geng, Y.; Wang, X.; Zhao, H. Rapid purification of antioxidants from *Magnolia officinalis* by semi-prep-HPLC with a two-step separation strategy guided by on-line HPLC-radical scavenging detection. *J. Chromatogr. B* **2018**, *1100–1101*, 140–147. [CrossRef]
21. Huang, H.C.; Hsieh, W.Y.; Niu, Y.L.; Chang, T.M. Inhibition of melanogenesis and antioxidant properties of *Magnolia grandiflora* L. flower extract. *BMC Complement. Altern. Med.* **2012**, *12*, 72. [CrossRef] [PubMed]
22. Zhang, D.; Dong, W.; Zhang, D.; Jin, L.; Zhang, D.; Zhang, J.; Tao, S. Screening of Natural Antioxidants and Application In the Course of Perry Brewing. *Energy Procedia* **2012**, *17*, 1811–1816. [CrossRef]
23. Veselova, M.V.; Fedoreev, S.A.; Vasilevskaya, N.A.; Denisenko, V.A.; Gerasimenko, A.V. From leaf to flower: Revisiting Goethe's concepts on the "metamorphosis" of plants. *Pharm. Chem. J.* **2007**, *41*, 88–93. [CrossRef]
24. Kikuzaki, H.; Hisamoto, M.; Hirose, K.; Akiyama, K.; Taniguchi, H. Antioxidant properties of ferulic acid and its related compounds. *J. Agric. Food Chem.* **2002**, *50*, 2161–2168. [CrossRef] [PubMed]
25. Semaming, Y.; Pannengpetch, P.; Chattipakorn, S.C.; Chattipakorn, N. Pharmacological Properties of Protocatechuic Acid and Its Potential Roles as Complementary Medicine. *Evid.-Based Complement. Altern.* **2015**, *2015*, 593902. [CrossRef] [PubMed]
26. Xi, X.J.; Hu, S.Q.; Zhou, Z.X.; Liu, X.R.; Tang, J.B.; Shen, Y.Q. Dendrimers with the protocatechuic acid building block for anticancer drug delivery. *J. Mater. Chem. B* **2016**, *4*, 5236–5245. [CrossRef]
27. Yu, Y.; Deng, Y.; Lu, B.M.; Liu, Y.X.; Li, J.; Bao, J.K. Green tea catechins: A fresh flavor to anticancer therapy. *Apoptosis* **2014**, *19*, 1–18. [CrossRef] [PubMed]
28. Manikandan, R.; Beulaja, M.; Arulvasu, C.; Sellamuthu, S.; Dinesh, D.; Prabhu, D.; Babu, G.; Vaseeharan, B.; Prabhu, N.M. Synergistic anticancer activity of curcumin and catechin: An in vitro study using human cancer cell lines. *Microsc. Res. Tech.* **2012**, *75*, 112–116. [CrossRef]
29. Abdulkhaleq, L.A.; Assi, M.A.; Noor, M.H.M.; Abdullah, R.; Saad, M.Z.; Taufiq-Yap, Y.H. Therapeutic uses of epicatechin in diabetes and cancer. *Vet. World* **2017**, *10*, 869–872. [CrossRef]

30. Takanashi, K.; Suda, M.; Matsumoto, K.; Toda, C.I.K.; Toda, K.; Kawaguchi, K.; Senga, S.; Kobayashi, N.; Ichikawa, M.; Katoh, M.; et al. Epicatechin oligomers longer than trimers have anti-cancer activities, but not the catechin counterparts. *Sci. Rep.* **2017**, *7*, 7791. [CrossRef]
31. Azam, S.; Hadi, N.; Khan, N.U.; Hadi, S.M. Prooxidant property of green tea polyphenols epicatechin and epigallocatechin-3-gallate: Implications for anticancer properties. *Toxicol. In Vitro* **2004**, *18*, 555–561. [CrossRef]
32. Arora, S.; Singh, S.; Piazza, G.A.; Contreras, C.M.; Panyam, J.; Singh, A.P. Honokiol: A Novel Natural Agent for Cancer Prevention and Therapy. *Curr. Mol. Med.* **2012**, *12*, 1244–1252. [CrossRef]
33. Zhang, X.; Lin, D.; Jiang, R.; Li, H.; Wan, J.; Li, H. Ferulic acid exerts antitumor activity and inhibits metastasis in breast cancer cells by regulating epithelial to mesenchymal transition. *Oncol. Rep.* **2016**, *36*, 271–278. [CrossRef]
34. Gao, J.; Yu, H.; Guo, W.; Kong, Y.; Gu, L.; Li, Q.; Yang, S.; Zhang, Y.; Wang, Y. The anticancer effects of ferulic acid is associated with induction of cell cycle arrest and autophagy in cervical cancer cells. *Cancer Cell Int.* **2018**, *18*, 102–102. [CrossRef] [PubMed]
35. Spilioti, E.; Jaakkola, M.; Tolonen, T.; Lipponen, M.; Virtanen, V.; Chinou, I.; Kassi, E.; Karabournioti, S.; Moutsatsou, P. Phenolic acid composition, antiatherogenic and anticancer potential of honeys derived from various regions in Greece. *PLoS ONE* **2014**, *9*, e94860. [CrossRef]
36. Elansary, H.O.; Szopa, A.; Kubica, P.; Ekiert, H.; Ali, H.M.; Elshikh, M.S.; Abdel-Salam, E.M.; El-Esawi, M.; El-Ansary, D.O. Bioactivities of Traditional Medicinal Plants in Alexandria. *Evid.-Based Complement. Altern. Med.* **2018**, *2018*, 1463579. [CrossRef]
37. Shang, W.; Qiao, J.; Gu, C.; Yin, W.; Du, J.; Wang, W.; Zhu, M.; Han, M.; Lu, W. Anticancer activity of an extract from needles and twigs of *Taxus cuspidata* and its synergistic effect as a cocktail with 5-fluorouracil. *BMC Complement. Altern. Med.* **2011**, *11*, 123. [CrossRef] [PubMed]
38. Marin, G.H.; Mansilla, E. Apoptosis induced by Magnolia Grandi fl ora extract in chlorambucil-resistant B-chronic lymphocytic leukemia cells. *J. Cancer Res. Ther.* **2010**, *6*, 463–465. [CrossRef] [PubMed]
39. Zhang, X.D.; Wu, Q.; Yang, S.H. Ferulic acid promoting apoptosis in human osteosarcoma cell lines. *Pak. J. Med. Sci.* **2017**, *33*, 127–131. [CrossRef]
40. Yin, M.C.; Lin, C.C.; Wu, H.C.; Tsao, S.M.; Hsu, C.K. Apoptotic effects of protocatechuic acid in human breast, lung, liver, cervix, and prostate cancer cells: Potential mechanisms of action. *J. Agric. Food Chem.* **2009**, *57*, 6468–6473. [CrossRef]
41. Alvarado-Sansininea, J.J.; Sanchez-Sanchez, L.; Lopez-Munoz, H.; Escobar, M.L.; Flores-Guzman, F.; Tavera-Hernandez, R.; Jimenez-Estrada, M. Quercetagetin and Patuletin: Antiproliferative, Necrotic and Apoptotic Activity in Tumor Cell Lines. *Molecules* **2018**, *23*, 2579. [CrossRef]
42. Bell, R.A.V.; Megeney, L.A. Evolution of caspase-mediated cell death and differentiation: Twins separated at birth. *Cell Death Differ.* **2017**, *24*, 1359–1368. [CrossRef]
43. Turner, C.; Devitt, A.; Parker, K.; MacFarlane, M.; Giuliano, M.; Cohen, G.M.; Gregory, C.D. Macrophage-mediated clearance of cells undergoing caspase-3-independent death. *Cell Death Differ.* **2003**, *10*, 302–312. [CrossRef] [PubMed]
44. Kagawa, S.; Gu, J.; Honda, T.; McDonnell, T.J.; Swisher, S.G.; Roth, J.A.; Fang, B. Deficiency of Caspase-3 in MCF7 Cells Blocks Bax-mediated Nuclear Fragmentation but not Cell Death. *Clin. Cancer Res.* **2001**, *7*, 1474–1480.
45. Sung, M.H.; Kwon, O.K.; Oh, S.R.; Lee, J.; Park, S.H.; Han, S.B.; Ahn, K.S. Azorella compacta methanolic extract induces apoptosis via activation of mitogen-activated protein kinase. *Mol. Med. Rep.* **2015**, *12*, 6821–6828. [CrossRef]
46. Wu, B.T.; Hung, P.F.; Chen, H.C.; Huang, R.N.; Chang, H.H.; Kao, Y.H. The apoptotic effect of green tea (-)-epigallocatechin gallate on 3T3-L1 preadipocytes depends on the Cdk2 pathway. *J. Agric. Food Chem* **2005**, *53*, 5695–5701. [CrossRef]
47. Spencer, J.P.; Schroeter, H.; Kuhnle, G.; Srai, S.K.; Tyrrell, R.M.; Hahn, U.; Rice-Evans, C. Epicatechin and its in vivo metabolite, 3′-O-methyl epicatechin, protect human fibroblasts from oxidative-stress-induced cell death involving caspase-3 activation. *Biochem. J.* **2001**, *354*, 493–500. [CrossRef] [PubMed]
48. Elbaz, H.A.; Lee, I.; Antwih, D.A.; Liu, J.; Huttemann, M.; Zielske, S.P. Epicatechin stimulates mitochondrial activity and selectively sensitizes cancer cells to radiation. *PLoS ONE* **2014**, *9*, e88322. [CrossRef]
49. Yang, J.S.; Liu, C.W.; Ma, Y.S.; Weng, S.W.; Tang, N.Y.; Wu, S.H.; Ji, B.C.; Ma, C.Y.; Ko, Y.C.; Funayama, S.; et al. Chlorogenic acid induces apoptotic cell death in U937 leukemia cells through caspase- and mitochondria-dependent pathways. *In Vivo* **2012**, *26*, 971–978.

50. Ji, B.C.; Hsu, W.H.; Yang, J.S.; Hsia, T.C.; Lu, C.C.; Chiang, J.H.; Yang, J.L.; Lin, C.H.; Lin, J.J.; Suen, L.J.; et al. Gallic acid induces apoptosis via caspase-3 and mitochondrion-dependent pathways in vitro and suppresses lung xenograft tumor growth in vivo. *J. Agric. Food Chem.* **2009**, *57*, 7596–7604. [CrossRef] [PubMed]
51. Szopa, A.; Kokotkiewicz, A.; Kubica, P.; Banaszczak, P.; Wojtanowska-Krosniak, A.; Krosniak, M.; Marzec-Wroblewska, U.; Badura, A.; Zagrodzki, P.; Bucinski, A.; et al. Comparative analysis of different groups of phenolic compounds in fruit and leaf extracts of *Aronia* sp.: A-melanocarpa, A-arbutifolia, and A. xprunifolia and their antioxidant activities. *Eur. Food Res. Technol.* **2017**, *243*, 1645–1657. [CrossRef]
52. Ellnain-Wojtaszek, M.; Zgorka, G. High-performance liquid chromatography and thin-layer chromatography of phenolic acids from *Ginkgo biloba* L-leaves collected within vegetative period. *J. Liq. Chromatogr. Relat. Technol.* **1999**, *22*, 1457–1471. [CrossRef]
53. Sulkowska-Ziaja, K.; Maslanka, A.; Szewczyk, A.; Muszynska, B. Physiologically Active Compounds in Four Species of Phellinus. *Nat. Prod. Commun.* **2017**, *12*, 363–366. [PubMed]
54. Szopa, A.; Kokotkiewicz, A.; Bednarz, M.; Luczkiewicz, M.; Ekiert, H. Studies on the accumulation of phenolic acids and flavonoids in different in vitro culture systems of Schisandra chinensis (Turcz.) Baill. using a DAD-HPLC method. *Phytochem. Lett.* **2017**, *20*, 462–469. [CrossRef]
55. Szopa, A.; Ekiert, H.; Szewczyk, A.; Fugas, E. Production of bioactive phenolic acids and furanocoumarins in in vitro cultures of Ruta graveolens L. and Ruta graveolens ssp. divaricata (Tenore) Gams. under different light conditions. *Plant Cell Tissue Org.* **2012**, *110*, 329–336. [CrossRef]
56. Elansary, H.O.; Salem, M.Z.M.; Ashmawy, N.A.; Yessoufou, K.; El-Settawy, A.A.A. In vitro antibacterial, antifungal and antioxidant activities of Eucalyptus spp. leaf extracts related to phenolic composition. *Nat. Prod. Res.* **2017**, *31*, 2927–2930. [CrossRef]
57. Mosmann, T. Rapid colorimetric assay for cellular growth and survival: Application to proliferation and cytotoxicity assays. *J. Immunol. Methods* **1983**, *65*, 55–63. [CrossRef]
58. Parry, J.; Su, L.; Moore, J.; Cheng, Z.; Luther, M.; Rao, J.N.; Wang, J.Y.; Yu, L.L. Chemical compositions, antioxidant capacities, and antiproliferative activities of selected fruit seed flours. *J. Agric. Food Chem.* **2006**, *54*, 3773–3778. [CrossRef]
59. Komina, A.; Palkina, N.; Aksenenko, M.; Tsyrenzhapova, S.; Ruksha, T. Antiproliferative and Pro-Apoptotic Effects of MiR-4286 Inhibition in Melanoma Cells. *PLoS ONE* **2016**, *11*, e0168229. [CrossRef]

Sample Availability: Not available.

molecules

MDPI

Article

Evaluating Antitumor and Antioxidant Activities of Yellow *Monascus* Pigments from *Monascus ruber* Fermentation

Hailing Tan [1,2], Ziyi Xing [3], Gong Chen [4], Xiaofei Tian [1,*] and Zhenqiang Wu [1,*]

1 School of Biology and Biological Engineering, South China University of Technology, Guangzhou 510006, China; callingmeling@163.com
2 Pan Asia (Jiangmen) Institute of Biological Engineering and Health, Jiangmen 529080, China
3 The Key Laboratory of Pathobiology, Ministry of Education, The College of Basic Medical Sciences, Jilin University, Changchun 130021, China; xingzy17@mails.jlu.edu.cn
4 School of Environmental Ecology and Biological Engineering, Wuhan Institute of Technology, Wuhan 430205, China; chengong@wit.edu.cn
* Correspondence: xtien@scut.edu.cn (X.T.); btzhqwu@scut.edu.cn (Z.W.); Tel./Fax: +86-20-3938-0636 (X.T.); +86-20-3938-0663 (Z.W.)

Academic Editor: Roberto Fabiani
Received: 23 November 2018; Accepted: 4 December 2018; Published: 7 December 2018

Abstract: Yellow *Monascus* pigments can be of two kinds: Natural and reduced, in which natural yellow *Monascus* pigments (NYMPs) attract widespread attention for their bioactivities. In this study, the antioxidative and antibreast cancer effects of the water-soluble NYMPs fermented by *Monascus ruber* CGMCC 10910 were evaluated. Results showed that water-soluble NYMPs had a significantly improved antioxidative activities compared to the reduced yellow *Monascus* pigments (RYMPs) that were chemically derived from orange or red *Monascus* pigments. Furthermore, NYMPs exhibited a concentration-dependent inhibition activity on MCF-7 cell growth ($p < 0.001$). After a 48-h incubation, a 26.52% inhibition yield was determined with 32 μg/mL of NYMPs. NYMPs also significantly inhibited the migration and invasion of MCF-7 cells. Mechanisms of the activities were associated with a down-regulation of the expression of matrix metalloproteinases and vascular endothelial growth factor. Rather than being alternatively used as natural colorants or antioxidants, this work suggested that NYMPs could be selected as potential functional additives in further test of breast cancer prevention and adjuvant therapy.

Keywords: natural yellow *Monascus* pigments; water-soluble; antioxidation; migration; invasion; MCF-7 cells

1. Introduction

Monascus metabolites are popular bioactive candidates for the development of functional foods. *Monascus*-fermented pigments have shown bioactivities of antioxidation [1,2] and anticancer [3]. Natural yellow *Monascus* pigments (NYMPs) have attracted great attention due to their beneficial effects for human healthcare [1,2,4]. Alcohol-soluble NYMPs, such as ankaflavin [5], monascin [6], monascuspiloin [7], monapurpyridine A [8], and monaphilones A [9], are reported with remarkable anticancer activities. Ho et al. [10] found that ankaflavin, synergized with Monacolin K, inhibited proliferation and induced apoptosis in mouse lung cancer LCC cells. Additionally, Shi et al. [11] reported that the monascin increased the survival of *Caenorhabditis elegans* under juglone-induced oxidative stress and attenuated endogenous levels of reactive oxygen species. Although NYMPs possess promising biological activities, the hydrophobic property of most NYMPs limits their further application in the food industry. As an important food coloration additive, water-soluble NYMPs are chemically derived from the hydrophobic orange *Monascus* pigments.

It was reported that some water-soluble NYMPs could be produced through fermentation with *Monascus ruber* CGMCC 10910 [12], which have a great potential to be used as additives in functional food and healthcare products. However, the knowledge of the biological activities of water-soluble NYMPs needs to be further expanded.

Breast cancer is one of the leading causes of mortality among women worldwide [13]. The current clinical treatments of breast cancer usually come with serious adverse effects [14]. Therefore, it is necessary to develop effective antitumor agents with reduced side effects to treat breast cancer. Drugs from natural resources have shown possible anticancer effects, with mechanisms of inhibiting angiogenesis [15], decreasing cell growth and proliferation, apoptosis [16], and preventing oxidation [17].

Several lines of evidence have established that antioxidation attenuates free radical-induced oncogene mutation and prevents carcinogenesis [18]. What is more, the inhibition ability of matrix metalloproteinases (MMPs) is important for the prevention of cell invasion [19]. For breast cancer cells, the vascular endothelial growth factor (VEGF) acts as the survival factor which possesses the ability to promote cancer growth [20,21]. Reducing the expressions of MMPs and VEGF is one of the promising approaches in cancer therapy.

In this work, the antioxidative effects of water-soluble NYMPs from *M. ruber* CGMCC 10910 were studied. The antitumor activity of the NYMPs was determined by exploring their effects on cell migration and invasion of the MCF-7 cell line. In the meantime, the possible underlying mechanisms in vitro models were also investigated.

2. Results and Discussion

2.1. Antioxidant Activities of Water-Soluble NYMPs

Previous work has verified that water-soluble NYMPs could be produced by the *M. ruber* CGMCC 10910 without citrinin [12]. The main extracellular pigments were mixtures of four components, including Y1, Y2, Y3, and Y4, with molecular weights of 250, 254, 402, and 358 Da., respectively. Huang et al. [22] reported that the chemical characteristics of Y1, Y2, Y3, and Y4, in which Y3 and Y4 had strong yellow fluorescence at UV of 365 nm and Y1 was the Azanigerone E ($C_{13}H_{14}O_5$), a known natural pigment.

The antioxidant activities of water-soluble NYMPs were assessed by DPPH and $ABTS^+$ (2,2′-azino-bis(3-ethylbenzothiazoline-6-sulfonic acid)) scavenging assays. Butylated hydroxytoluene (BHT) was used as a positive control. DPPH scavenging occurred by the reduction of DPPH radical in the presence of a proton-donating substance. The DPPH radical scavenging activities were promoted along with increased NYMP concentrations (Table 1). When the concentration of 1 mg/mL was tested, the DPPH scavenging ratio by the NYMPs was 86.33%, which was close to that of the BHT but 2.63 times that of the reduced yellow *Monascus* pigments (RYMPs) with a ratio of only 32.84%. Compared to the RYMPs, the NYMPs had a more effective DPPH scavenging activity, since the calculated IC_{50} of NYMPs and RYMPs were 0.23 mg/mL and 2.77 mg/mL, respectively.

Table 1. DPPH radical scavenging activity of yellow *Monascus* pigments.

Samples (mg/mL)	0.025	0.075	0.100	0.500	1.000
RYMPs [b]	[d] 3.59 ± 0.14	6.57 ± 0.75	8.91 ± 0.19	20.75 ± 0.13	32.84 ± 1.02
NYMPs [a]	9.54 ± 0.23	21.23 ± 1.37	26.74 ± 0.36	69.03 ± 0.92	86.33 ± 1.50
BHT [c]	14.25 ± 1.45	37.48 ± 2.63	47.07 ± 2.40	94.42 ± 0.17	95.14 ± 0.58

[a] NYMPs represents natural yellow *Monascus* pigments. [b] RYMPs represents reduced yellow *Monascus* pigments. [c] BHT represents butylated hydroxytoluene. [d] Each value represents averages of three replicates ± standard deviation.

The $ABTS^+$ scavenging assay was generally used for evaluating the antioxidant activities of hydrophilic compounds. The $ABTS^+$ radical scavenging ratio by 0.25 mg/mL NYMPs was equivalent

to that of the BHT (Table 2). The IC_{50} of the NYMPs was 0.035 mg/mL, which was far lower than 0.176 mg/mL of the RYMP. This indicated that the *Monascus*-fermented NYMPs possessed significantly improved antioxidative activities than the chemically-derived RYMPs.

Table 2. [e] $ABTS^+$ radical scavenging activity of yellow *Monascus* pigments.

Samples (mg/mL)	0.025	0.050	0.075	0.100	0.250
RYMPs [b]	[d] 13.95 ± 0.94	25.33 ± 0.32	38.00 ± 0.86	45.77 ± 0.33	84.92 ± 1.77
NYMPs [a]	38.00 ± 1.71	60.67 ± 1.00	81.92 ± 0.33	87.03 ± 0.11	99.95 ± 0.09
BHT [c]	94.42 ± 2.48	99.70 ± 0.38	99.45 ± 0.31	99.76 ± 0.28	98.61 ± 0.10

[a] NYMPs represents natural yellow *Monascus* pigments. [b] RYMPs represents reduced yellow *Monascus* pigments. [c] BHT represents butylated hydroxytoluene. [d] Each value represents averages of three replicates ± standard deviation. [e] ABTS represents 2,2′-azino-bis(3-ethylbenzothiazoline-6-sulfonic acid).

Srianta et al. [23] reported that a higher *Monascus* pigment content had higher antioxidant activities. Similarly, the antioxidant activities of NYMPs applied corresponded to the intensity of the pigments in this work. To our knowledge, the antioxidant activities of *Monascus*-fermented substrate were generally contributed by the water-soluble *Monascus* pigments [24,25]. The advantage of water-soluble NYMP products showed a considerable application prospect in the food industry.

2.2. Cytotoxicity of Water-Soluble NYMPs on MCF-7 Cells

Water-soluble yellow *Monascus* pigments have attracted much attention thanks to their low toxicity as well as improved antioxidative activity, which could potentially be used to prevent carcinogenesis in human body. Ankaflavin was found to be toxic to human cancer cell lines Hep G2 and A549, while it displayed no significant toxicity to normal MRC-5 and WI-38 cells [26].

The toxicity of fermented NYMPs (0–128 μg/mL) on cell viability was determined by the microculture tetrazolium (MTT) assay. It was found that NYMPs exhibited no significant toxicity to MCF-7 cells. As shown in Figure 1, cell viability was not significantly affected by NYMPs after a 24-h treatment, which indicated that the NYMPs were not toxic to MCF-7 cells. The result was consistent with the yellow *Monascus* pigment, Monascusone A, which exhibited no cytotoxicity against breast cancer [27].

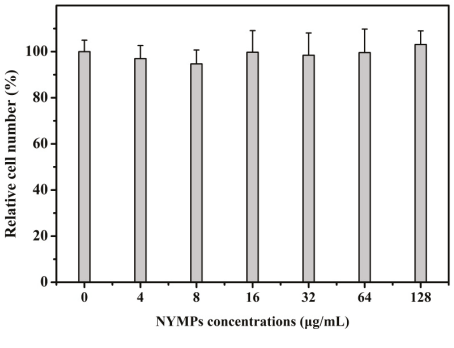

Figure 1. Cytotoxicity of water-soluble NYMPs on human breast cancer MCF-7 cells under different concentrations. Each value represents the mean ± standard deviation (n = 3).

Several studies showed that *Monascus* metabolites had antiproliferative activities in various cancers [28]. Hsu et al. [29] investigated four new azaphilones with yellow fluorescence, which exhibited antiproliferative activities against human laryngeal carcinoma (HEp-2) and human colon adenocarcinoma (WiDr). Chang et al. [27] reported that the extract of *Monascus purpureus* CWT715 significantly inhibited the proliferation of SK-Hep-1 cells at 100 μg/mL. Park et al. [30] found that RYRG extracts had antiproliferative effects against HepG2 human liver cancer cells, HT-29 human

colon cancer cells, and B16F10 murine melanoma cells. Figure 2 shows that the proliferation of MCF-7 cells is inhibited by NYMPs in a concentration-dependent way by 23.56% ($p < 0.001$) and 26.52% ($p < 0.001$) at 32 μg/mL in a 24-h and 48-h incubation, respectively. The results suggested the existence of antiproliferative activity of the water-soluble NYMPs. As Huang et al. [22] reported, the Y3 and Y4 components had strong yellow fluorescence in the NYMPs. We speculated that Y3 and Y4 might be the active ingredients in the NYMPs.

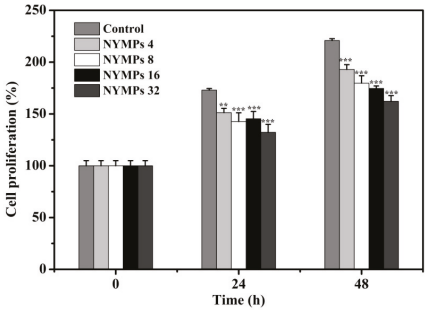

Figure 2. Effects of water-soluble NYMPs on cell proliferation of human breast cancer MCF-7 cells. Cells were incubated with NYMPs for 24 and 48 h. NYMPs 4, NYMPs 8, NYMPs 16, and NYMPs 32 represents 4, 8, 16, and 32 μg/mL, respectively. Each value represents the mean ± standard deviation ($n = 3$). * $p < 0.05$, ** $p < 0.01$ and *** $p < 0.001$ indicated statistically significant differences versus control group.

Figure 3 shows that NYMPs have significantly inhibited the cell invasion of MCF-7 cells at a 24-h incubation, with 31.01% ($p < 0.01$) inhibition yield at a concentration of 40 μg/mL. Similar to those on cell invasion in the Transwell assays, NYMPs had a 32.58% ($p < 0.01$) inhibition on cell migration at a concentration of 40 μg/mL (Figure 4). In the wound healing assay, the reduction of the transferred area indicated that the migration inhibition yield of MCF-7 cells by NYMPs (40 μg/mL) was 40.44% ($p < 0.01$) (Figure 5). The results suggested that NYMPs inhibited the migration and invasion of MCF-7 cells.

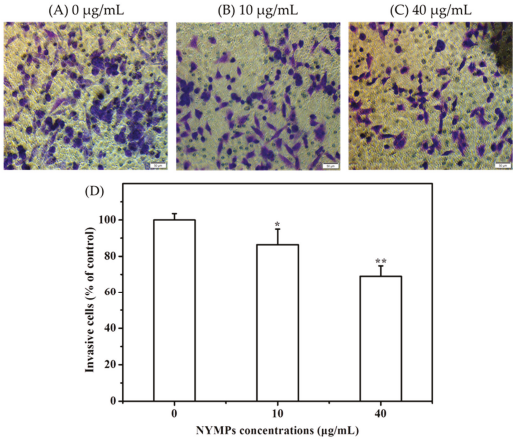

Figure 3. Effects of NYMPs on cell invasion of human breast cancer MCF-7 cells (Magnification× 200). (**A**) Images of cells treated without NYMPs. (**B**) Image of cells treated with 10 μg/mL NYMPs. (**C**) Image of cells treated with 40 μg/mL NYMPs. (**D**) Invasion ability. Each value represents the mean ± standard deviation ($n = 3$). * $p < 0.05$ and ** $p < 0.01$ indicated statistically significant differences versus control group.

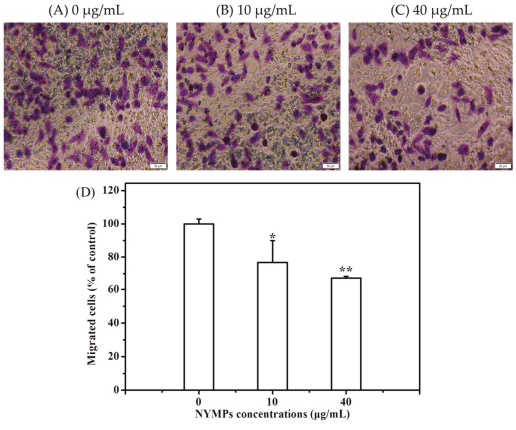

Figure 4. Effects of NYMPs on cell migration of human breast cancer MCF-7 cells (Magnification× 200). (**A**) Image of cells treated without NYMPs. (**B**) Image of cells treated with 10 μg/mL NYMPs. (**C**) Image of cells treated with 40 μg/mL NYMPs. (**D**) Invasion ability. Each value represents the mean ± standard deviation ($n = 3$). * $p < 0.05$ and ** $p < 0.01$ indicated statistically significant differences versus control group.

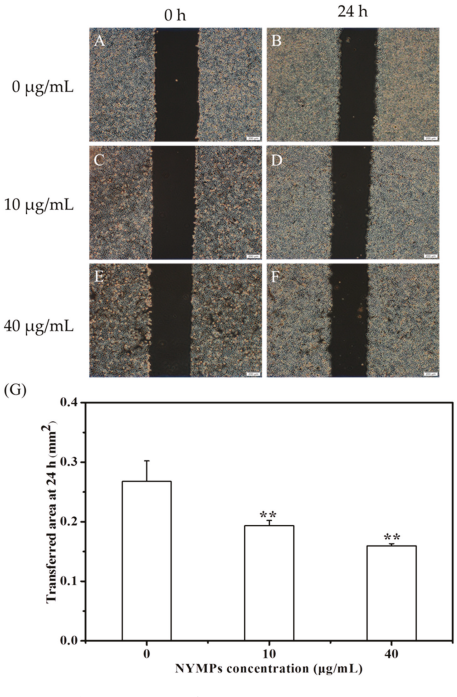

Figure 5. Effects of NYMPs on cell migration of human breast cancer MCF-7 cells (Magnification× 40). (**A**,**B**) Images of cells treated without NYMPs. (**C**,**D**) Images of cells treated with 10 μg/mL NYMPs. (**E**,**F**) Images of cells treated with 40 μg/mL of NYMPs. (**G**) Migrated ability. Each value represents the mean ± standard deviation ($n = 3$). ** $p < 0.01$ indicated statistically significant differences versus control group.

2.3. Regulating Effect of Water-Soluble NYMPs on the Expression of MMP-2, MMP-9, and VEGF

MMPs were required for extravasation out of the vessel, leading to the movement of cancer cells to the target tissue, which could work as pivotal targets for suppressing breast cancer invasion and metastasis [31]. Known as key enzymes in the degradation of type IV collagen, MMP-2 [32] and MMP-9 [33] were overexpressed in breast cancer cells among all of the MMPs [34]. The inhibition of MMP-2 and MMP-9 expressions was a critical step in the prevention of cancer metastasis. To examine the possible antimetastatic mechanisms of NYMPs, the expression of MMP-2 and MMP-9 in the culture media of MCF-7 cells was determined by Western blotting assay. The NYMPs significantly suppressed the expression of MMP-2 by 23.42% ($p < 0.01$), and slightly decreased the activities of MMP-9 by 7.53% at a concentration of 40 μg/mL (Figure 6). The results indicated that the possible antimetastatic mechanism of NYMPs was through the inhibition of the expression of MMP-2 protein.

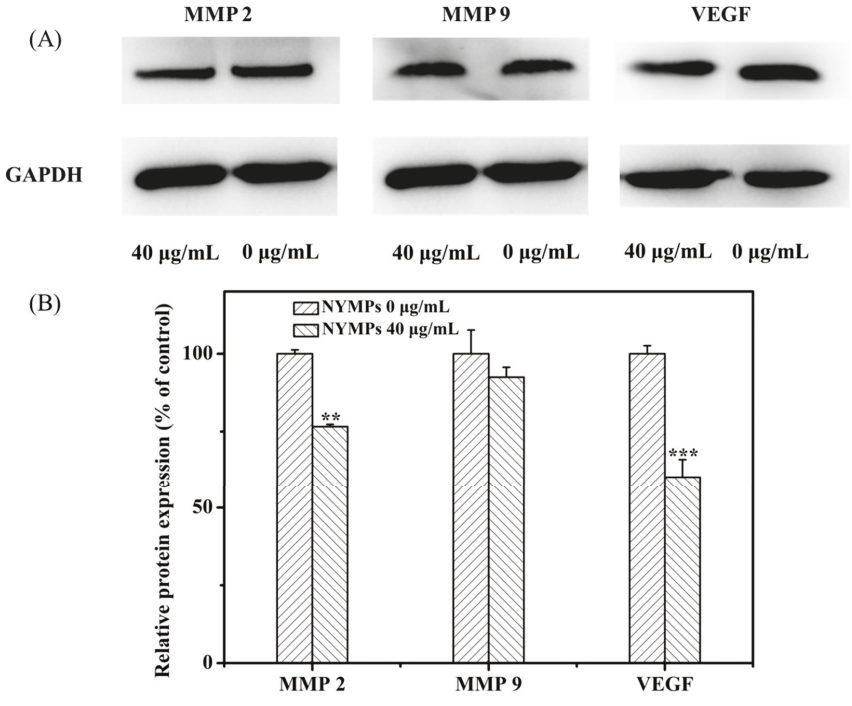

Figure 6. Effects of NYMPs on protein expression level of MMP-2, MMP-9, and VEGF. (**A**) Expression of MMP-2, MMP-9, and VEGF, GAPDH (Glyceraldehyde-3-phosphate dehydrogenase) as loading control; (**B**) Densitometric analyses of (A). Each value represents the mean ± standard deviation ($n = 3$). ** $p < 0.01$, *** $p < 0.001$ indicated statistically significant differences versus control group.

Monascin and ankaflavin targeted the network of pathogenic inflammatory mediators, which contributed in tumor angiogenesis and metastasis. A significant reduction in the VEGF level was reported as a marker of angiogenesis in the free yellow-*Monascus*-pigment-treated mice group compared to the positive control group [35]. Water-soluble NYMPs significantly suppressed the expression of VEGF by 39.72% ($p < 0.001$) at a concentration of 40 μg/mL (Figure 6). This implied that NYMPs at least in part contributed to an anticancer effect directly by regulating VEGF protein expression.

3. Materials and Methods

3.1. Microorganisms and Chemicals

The *M. ruber* 10910 strain preserved in the China General Microbiological Culture Collection Center (CGMCC, Beijing, China) was cultivated on potato dextrose agar (PDA) medium at 30 °C for 7 days before use.

DPPH was purchased from Shanghai Macklin Biochemical Co., Ltd. (Shanghai, China). $ABTS^+$ and BHT were obtained from Aladdin Industrial Corporation (Shanghai, China). All chemical reagents were purchased from ZhiYuan Reagent Co., Ltd. (Tianjin, China) in analytical grade. RYMPs samples prepared by chemical derivation from red *Monascus* pigment were purchased from Tianyi Biotechnology Co., Ltd. (Dongguan, Guangdong, China).

3.2. Monascus Pigment Fermentation

The method for *Monascus* pigment fermentation was according to the approach reported by Wang et al. [12]. A total of 5–6 loops of single colonies (10 mm diameter) were scraped off from the culture plate and inoculated in a 250 mL flask with 50 mL seed medium and incubated at 30 °C for 25 h in a rotary shaker (Labwit Scientific, Shanghai, China) at 180 rpm. For fermentation, 2 mL seed culture was transferred to a 250 mL Erlenmeyer flask containing 25 mL fermentation culture medium and incubated at 30 °C for 9 days on a shaker in 180 rpm. The preparation of seed and fermentation culture media is referred to in our previous work [22].

3.3. Isolation of Water-Soluble NYMPs

The fermented broth was filtered through a mixed cellulose esters membrane (0.8 mm, Xiya purification equipment Co. Ltd., Shanghai, China). According to Wu et al. [36], with minor modifications, a column (30 × 6 cm, 1.98 L) with 150 g adsorption resin (DA-201C, Zhengzhou Qinshi Technology Co., Ltd., Henan, China), was employed for isolation and purification of the NYMPs from the filtrated broth. A 60% (v/v) ethanol solution was used as the eluent with a flow rate of 1 mL/min. After eluting for 90 min, the aqueous ethanol solution was submitted to vacuum-evaporation and freeze-dried. The solid was dispersed in distilled water and centrifuged at 8000× g for 20 min. The supernatant was collected as the NYMPs solution.

3.4. Antioxidant Activity Determination

The antioxidant activities of the yellow *Monascus* pigments were determined by the activities of DPPH radical scavenging and ABTS radical cation ($ABTS^+$) scavenging evaluated. According to the method reported by Wang et al. [37], with minor modifications, 50 μL NYMPs solution at concentrations of 25, 75, 100, 500, and 1000 μg/mL were mixed with 200 μL DPPH methanol solution (600 μmol/L). The mixture was kept in the dark at room temperature for 60 min. Absorbance at 517 nm (A_{517}) was measured using a SpectraMax Gemini microtiter plate reader (Molecular Devices, Sunnyvale, CA, USA) with Softmax Pro 3.0 software (Molecular Devices, Sunnyvale, CA, USA). BHT was used as a positive control. The sample concentration achieving a 50% DPPH free radical scavenging activity was defined as the IC_{50} value. The efficiency for DPPH free radical scavenging was calculated according to Equation (1):

$$\text{DPPH radical scavenging activity } (\%) = 1 - \frac{A_S}{A_0} \times 100 \quad (1)$$

where A_0 is the A_{517} of the DPPH solution and As is the A_{517} of the mixture after reaction.

The freshly prepared $ABTS^+$ solution was prepared by oxidation of 7 mmol/L ABTS with 2.45 mmol/L potassium persulfate [37]. A 50 μL sample solution at concentrations of 25, 50, 75, 100, and 250 μg/mL was thoroughly mixed with 200 μL of $ABTS^+$ solution and kept at room temperature

for 60 min in the dark. The absorbance at 734 nm (A_{734}) was measured. BHT was used as a positive control. The $ABTS^+$ scavenging activity was calculated by Equation (2):

$$ABTS^+ \text{radical scavenging activity } (\%) = \left(1 - \frac{A_2}{A_1}\right) \times 100 \quad (2)$$

where A_1 is the A_{734} of the $ABTS^+$ solution and A_2 is the A_{734} of the mixture after reaction.

3.5. MCF-7 Cell Line and Culture

Human breast cancer cells MCF-7 were obtained from the key laboratory of pathobiology, Ministry of Education, Jilin University (Changchun, Jilin, China), and routinely cultured in H–DMEM (High Glucose- Dulbecco's Modified Eagle Medium) containing 10% (*v*/*v*) fetal bovine serum (FBS), 0.37% (*w*/*v*) $NaHCO_3$, penicillin (100 unit/mL), and streptomycin (100 unit/mL) in a humidified incubator (Thermo Fisher Scientific, Waltham, MA, USA) under 5% CO_2 and 95% air at 37 °C.

3.6. Measurement of Cytotoxicity and Inhibition Activity in Cell Proliferation

The cytotoxic effects of the various concentrations of NYMPs on MCF-7 cells were determined by MTT assay [19]. Cells (4×10^3 per well) were seeded in triplicate onto a sterile 96-well plate (Corning, Corning, NY, USA) containing 100 μL medium in each well. After a 24-h incubation, the medium was replaced with 100 μL fresh FBS-free medium which contained NYMPs at concentrations of 0, 2, 4, 8, 16, 32, 64, and 128 μg/mL. The plate was incubated for 24 h and then the media were discarded. Afterwards, the cells were stained with 100 μL of MTT solution at 37 °C for 4 h. Thereafter, the supernatant was aspirated, and 150 μL of DMSO was added to dissolve the formazan. The optical density at 570 nm (OD_{570}) was determined.

The inhibition activities of NYMPs toward MCF-7 cells proliferation were quantified using the MTT assay as described above, with minor modifications. Briefly, 4×10^3 MCF-7 cells were plated in each well of the 96-well plate and incubated at 37 °C in 5% CO_2 for 24 h. Then, the cells were treated with various doses of NYMPs at 37 °C in 5% CO_2 for 24 h and 48 h. (Medium: H-DMEM with 10% FBS). The remaining cells on the bottom of wells were quantified. The percentage of inhibition was calculated using Equation (3):

$$\text{Growth inhibition } (\%) = \left(1 - \frac{OD_{test}}{OD_{control}}\right) \times 100 \quad (3)$$

where $OD_{control}$ is the OD_{570} in the control wells (cells incubated with vehicle only) and OD_{test} is the OD_{570} of the cells exposed to NYMPs.

3.7. Transwell Assay

Cell migration was assayed according to the methods of Justus et al. [38], with some modifications. MCF-7 cells were suspended in 200 μL DMEM (serum free supplemented with NYMPs), placed in the upper transwell chambers, and 600 μL medium with 20% FBS was added into the lower chamber. Before the determination of cell migration and cell invasion, the number of cells was adjusted to an equal number (2×10^5 cells/mL) in the Transwell assays to avoid interference by cell numbers. After 24 h of incubation at 37 °C, the cells on the upper surface of the filter were completely wiped away with a cotton swab. The cells on the lower surface of the filter were fixed in 4% paraformaldehyde, stained with crystal violet, and then counted under a microscope (Olympus Corporation, Tokyo, Japan). For each replicate, the tumor cells in 10 randomly-selected fields were determined, and the counts were averaged.

3.8. Wound-Healing Assay

Cells were seeded in 2×10^5 cells/mL and grown to 80–90% confluence in a 6-well plate at 37 °C. The monolayers were scratched with a 200 μL sterile pipette tip, washed twice with PBS, and then replaced with complete DMEM. MCF-7 cells were treated with NYMPs (0, 10, and 40 μg/mL) and incubated for 24 h. Cell migration into the wound area was photographed under an inverted microscope (Olympus Corporation, Tokyo, Japan). Migrated cells across the blue lines were calculated in 3 random fields from each triplicate treatment.

3.9. Invasion Assay

Cell invasion was analyzed using Transwell assays [38], with some modifications. The upper chambers were coated with 60 μL Matrigel (dilution 1:6) in cold DMEM and 4×10^4 cells were then seeded in the upper chamber of each well in serum-free medium containing NYMPs. Additionally, 600 μL DMEM media supplemented with 20% FBS was added to the lower chamber. The cells were incubated for 24 h. The conditions and methods of staining and counting were similar with the migration assay.

3.10. Western Blotting

Total cellular proteins extracted from cells were assayed using a BCA (Bicinchoninic acid) kit (Beyotime Institute of Biotechnology, Beijing, China). Equal amounts of protein were subjected to sodium dodecyl sulfate polyacrylamide gel electrophoresis and then electrophoretically transferred to polyvinylidene fluoride membranes. Membranes were blocked with 5% nonfat dry milk in tris buffered saline (TBS) with 0.1% Tween-20 for 1 h and incubated with anti-MMP 2 (abcam, Cambridge, UK, ab92536, 1:1000), anti-MMP 9 (abcam, ab76003, 1:1000), anti-VEGFA (Wanleibio, Shenyang, China, WL0009b, 1:1000,) and anti-GAPDH (Glyceraldehyde-3-phosphate dehydrogenase) (CST, Danvers, MA, USA, #2118, 1:1000) antibodies at 4 °C overnight. The protein blots were then visualized with a use of the streptavidin–HRP ELC (HRP: Horseradish Peroxidase; ELC: Electrochemiluminescence) assay (Beyotime Institute of Biotechnology, Beijing, China). Image-Pro Plus 6.0 (Media Cybernetics, Rockville, MD, USA) was used for the quantification of the data from western blot.

3.11. Statistical Analysis

All data were expressed as the mean ± standard deviations (SD) from at least triplicate independent runs. Statistical analysis was performed with SPSS Statistics 17 (SPSS Inc., Chicago, IL, USA). Statistical differences were analyzed using t-tests and one-way analysis of variance (ANOVA). A value of $p < 0.05$ was considered as significant difference.

4. Conclusions

Water-soluble NYMPs exhibited the capacity of antioxidation and inhibited the migration and invasion of breast cancer MCF-7 cells with no cell cytotoxicity. The antitumor effect is possibly associated with the down-regulation of MMP-2 and VEGF protein expression. Cell line studies suggest that the fermented water-soluble NYMPs could be selected as potential functional additives in further tests of breast cancer prevention and adjuvant therapy.

Author Contributions: H.T. and Z.W. conceived and designed the experiments. H.T. and Z.X. performed the experiments. H.T. analyzed the date and wrote the paper. G.C., X.T. and Z.W. revised the paper.

Funding: This research was funded by the Major Project on synergy innovation at the Enterprise University Institute of Guangzhou, China, grant number 201604046011.

Acknowledgments: The work was supported by the Major Project on synergy innovation at the Enterprise University Institute of Guangzhou, China (201604046011).

Conflicts of Interest: The authors declared no conflict of interest.

References

1. Chen, G.; Wu, Z.-Q. Production and biological activities of yellow pigments from *Monascus* fungi. *World J. Microbiol. Biotechnol.* **2016**, *32*, 136–144. [CrossRef] [PubMed]
2. Patakova, P. *Monascus* secondary metabolites: Production and biological activity. *J. Ind. Microbiol. Biotechnol.* **2013**, *40*, 169–181. [CrossRef] [PubMed]
3. Zheng, Y.; Zhang, Y.; Chen, D.; Chen, H.; Lin, L.; Zheng, C.; Guo, Y. *Monascus* pigment Rubropunctatin: A potential dual agent for cancer chemotherapy and phototherapy. *J. Agric. Food Chem.* **2016**, *64*, 2541–2548. [CrossRef] [PubMed]
4. Hsu, W.-H.; Pan, T.-M. *Monascus purpureus*-fermented products and oral cancer: A review. *Appl. Microbiol. Biotechnol.* **2012**, *93*, 1831–1842. [CrossRef] [PubMed]
5. Su, N.-W.; Lin, Y.-L.; Lee, M.-H.; Ho, C.-Y. Ankaflavin from *Monascus*-fermented red rice exhibits selective cytotoxic effect and induces cell death on Hep G2 cells. *J. Agric. Food Chem.* **2005**, *53*, 1949–1954. [CrossRef] [PubMed]
6. Akihisa, T.; Tokuda, H.; Ukiya, M.; Kiyota, A.; Yasukawa, K.; Sakamoto, N.; Kimura, Y.; Suzuki, T.; Takayasu, J.; Nishino, H. Anti-tumor-initiating effects of Monascin, an azaphilonoid pigment from the extract of *Monascus pilosus* fermented rice (red-mold rice). *Chem. Biodivers.* **2005**, *2*, 1305–1309. [CrossRef] [PubMed]
7. Camphausen, K.; Chiu, H.-W.; Fang, W.-H.; Chen, Y.-L.; Wu, M.-D.; Yuan, G.-F.; Ho, S.-Y.; Wang, Y.-J. Monascuspiloin enhances the radiation sensitivity of human prostate cancer cells by stimulating endoplasmic reticulum stress and inducing autophagy. *PLoS ONE* **2012**, *7*, e40462. [CrossRef]
8. Hsu, L.-C.; Hsu, Y.-W.; Liang, Y.-H.; Liaw, C.-C.; Kuo, Y.-H.; Pan, T.-M. Induction of apoptosis in human breast adenocarcinoma cells MCF-7 by monapurpyridine A, a new azaphilone derivative from *Monascus purpureus* NTU 568. *Molecules* **2012**, *17*, 664–673. [CrossRef]
9. Hsu, Y.-W.; Hsu, L.-C.; Chang, C.-L.; Liang, Y.-H.; Kuo, Y.-H.; Pan, T.-M. New anti-inflammatory and anti-proliferative constituents from fermented red mold rice *Monascus purpureus* NTU 568. *Molecules* **2010**, *15*, 7815–7824. [CrossRef]
10. Ho, B.-Y.; Pan, T.-M. The *Monascus* metabolite monacolin K reduces tumor progression and metastasis of Lewis lung carcinoma cells. *J. Agric. Food Chem.* **2009**, *57*, 8258–8265. [CrossRef]
11. Shi, Y.-C.; Pan, T.-M.; Liao, V.-H. Monascin from *Monascus*-fermented products reduces oxidative stress and amyloid-beta toxicity via DAF-16/FOXO in caenorhabditis elegans. *J. Agric. Food Chem.* **2016**, *64*, 7114–7120. [CrossRef] [PubMed]
12. Wang, M.; Huang, T.; Chen, G.; Wu, Z.-Q. Production of water-soluble yellow pigments via high glucose stress fermentation of *Monascus ruber* CGMCC 10910. *Appl. Microbiol. Biotechnol.* **2017**, *101*, 3121–3130. [CrossRef] [PubMed]
13. Barchuk, A.; Bespalov, A.; Huhtala, H.; Chimed, T.; Laricheva, I.; Belyaev, A.; Bray, F.; Anttila, A.; Auvinen, A. Breast and cervical cancer incidence and mortality trends in Russia 1980–2013. *Cancer Epidemiol.* **2018**, *55*, 73–80. [CrossRef] [PubMed]
14. Fletcher, C.; Wilson, C.; Hutchinson, A.D.; Grunfeld, E.A. The relationship between anticipated response and subsequent experience of cancer treatment-related side effects: A meta-analysis comparing effects before and after treatment exposure. *Cancer Treat. Rev.* **2018**, *68*, 86–93. [CrossRef] [PubMed]
15. Agarwal, A.; Kasinathan, A.; Ganesan, R.; Balasubramanian, A.; Bhaskaran, J.; Suresh, S.; Srinivasan, R.; Aravind, K.B.; Sivalingam, N. Curcumin induces apoptosis and cell cycle arrest via the activation of reactive oxygen species–independent mitochondrial apoptotic pathway in Smad4 and p53 mutated colon adenocarcinoma HT29 cells. *Nutr. Res.* **2018**, *51*, 67–81. [CrossRef] [PubMed]
16. García, E.R.; Gutierrez, E.A.; Melo, F.C.S.A.D.; Novaes, R.D.; Gonçalves, R.V. Flavonoids effects on hepatocellular carcinoma in murine models: A systematic review. *Evid. Based Complement. Altern. Med.* **2018**, 1–23. [CrossRef] [PubMed]
17. Russo, M.; Spagnuolo, C.; Russo, G.L.; Skalicka-Wozniak, K.; Daglia, M.; Sobarzo-Sanchez, E.; Nabavi, S.F.; Nabavi, S.M. Nrf2 targeting by sulforaphane: A potential therapy for cancer treatment. *Crit. Rev. Food Sci.* **2018**, *58*, 1391–1405. [CrossRef]
18. Chikara, S.; Nagaprashantha, L.D.; Singhal, J.; Horne, D.; Awasthi, S.; Singhal, S.S. Oxidative stress and dietary phytochemicals: Role in cancer chemoprevention and treatment. *Cancer Lett.* **2018**, *413*, 122–134. [CrossRef]

19. Huang, G.-J.; Yang, C.-M.; Chang, Y.-S.; Amagaya, S.; Wang, H.-C.; Hou, W.-C.; Huang, S.-S.; Hu, M.-L. Hispolon suppresses SK-Hep1 human hepatoma cell metastasis by inhibiting matrix metalloproteinase-2/9 and urokinase-plasminogen activator through the PI3K/Akt and ERK signaling pathways. *J. Agric. Food Chem.* **2010**, *58*, 9468–9475. [CrossRef]
20. Fujii, T.; Yajima, R.; Tatsuki, H.; Oosone, K.; Kuwano, H. Anticancer effect of rapamycin on MCF-7 via downregulation of VEGF expression. *Vitr. Cell Dev. Biol. Anim.* **2016**, *52*, 45–48. [CrossRef]
21. Barr, M.P.; Bouchier-Hayes, D.J.; Harmey, J.H. Vascular endothelial growth factor is an autocrine survival factor for breast tumour cells under hypoxia. *Int. J. Oncol.* **2008**, *32*, 41–48. [CrossRef] [PubMed]
22. Huang, T.; Tan, H.-L.; Chen, G.; Wang, L.; Wu, Z.-Q. Rising temperature stimulates the biosynthesis of water-soluble fluorescent yellow pigments and gene expression in *Monascus ruber* CGMCC10910. *AMB Express.* **2017**, *7*, 134. [CrossRef] [PubMed]
23. Srianta, I.; Zubaidah, E.; Estiasih, T.; Iuchi, Y.; Harijono, H.; Yamada, M. Antioxidant activity of pigments derived from *Monascus purpureus*-fermented rice, corn, and sorghum. *Int. Food Res. J.* **2017**, *24*, 1186–1191. [CrossRef]
24. Huang, Q.; Zhang, H.; Xue, D. Enhancement of antioxidant activity of Radix Puerariae and red yeast rice by mixed fermentation with *Monascus purpureus*. *Food Chem.* **2017**, *226*, 89–94. [CrossRef] [PubMed]
25. Jongrungruangchok, S.; Kittakoop, P.; Yongsmith, B.; Bavovada, R.; Tanasupawat, S.; Lartpornmatulee, N.; Thebtaranonth, Y. Azaphilone pigments from a yellow mutant of the fungus *Monascus kaoliang*. *Phytochemistry* **2004**, *65*, 2569–2575. [CrossRef]
26. Hsu, Y.-W.; Hsu, L.-C.; Liang, Y.-H.; Kuo, Y.-H.; Pan, T.-M. Monaphilones A–C, three new antiproliferative azaphilone derivatives from *Monascus purpureus* NTU 568. *J. Agric. Food Chem.* **2010**, *58*, 8211–8216. [CrossRef]
27. Chang, W.-T.; Chuang, C.-H.; Lee, W.-J.; Huang, C.-S. Extract of *Monascus purpureus* CWT715 fermented from sorghum liquor biowaste inhibits migration and invasion of SK-Hep-1 human hepatocarcinoma cells. *Molecules* **2016**, *21*, 1691. [CrossRef]
28. Zheng, Y.-Q.; Xin, Y.-W.; Shi, X.-N.; Guo, Y.-H. Anti-cancer effect of rubropunctatin against human gastric carcinoma cells BGC-823. *Appl. Microbiol. Biot.* **2010**, *88*, 1169–1177. [CrossRef]
29. Hsu, Y.-W.; Hsu, L.-C.; Liang, Y.-H.; Kuo, Y.-H.; Pan, T.-M. New bioactive orange pigments with yellow fluorescence from *Monascus*-fermented dioscorea. *J. Agric. Food Chem.* **2011**, *59*, 4512–4518. [CrossRef]
30. Park, H.-J.; Kim, I.-S. Antioxidant activities and anticancer effects of red yeast rice grown in the medium containing garlic. *Food Sci. Biotechnol.* **2011**, *20*, 297–302. [CrossRef]
31. Gialeli, C.; Theocharis, A.D.; Karamanos, N.K. Roles of matrix metalloproteinases in cancer progression and their pharmacological targeting. *FEBS J.* **2011**, *278*, 16–27. [CrossRef] [PubMed]
32. Duffy, M.J.; Maguire, T.M.; Hill, A.; McDermott, E.; O'Higgins, N. Metalloproteinases: Role in breast carcinogenesis, invasion and metastasis. *Breast Cancer Res.* **2000**, *2*, 252–257. [CrossRef] [PubMed]
33. Kim, H.S.; Kim, H.J.; Park, K.G.; Kim, Y.N.; Kwon, T.K.; Park, J.Y.; Lee, K.U.; Kim, J.G.; Lee, I.K. alpha-Lipoic acid inhibits matrix metalloproteinase-9 expression by inhibiting NF-kappa B transcriptional activity. *Exp. Mol. Med.* **2007**, *39*, 106–113. [CrossRef] [PubMed]
34. Jezierska, A.; Motyl, T. Matrix metalloproteinase-2 involvement in breast cancer progression: A mini-review. *Med. Sci. Monit.* **2009**, *15*, 32–40. [CrossRef]
35. El-Far, S.W.; Helmy, M.W.; Khattab, S.N.; Bekhit, A.A.; Hussein, A.A.; Elzoghby, A.O. Phytosomal bilayer-enveloped casein micelles for codelivery of monascus yellow pigments and resveratrol to breast cancer. *Nanomedicine* **2018**, *13*, 481–499. [CrossRef]
36. Wu, Z.-Q.; Wang, M.-H.; Tang, R.; Chen, G. Adsorption and separation of *Monascus* yellow pigments in *Monascus* fermentation broth. *Mod. Food Sci. Technol.* **2017**, *33*, 150–157. [CrossRef]

37. Wang, L.; Wu, Y.-N.; Huang, T.; Shi, K.; Wu, Z.-Q. Chemical compositions, antioxidant and antimicrobial activities of essential oils of *Psidium guajava* L. Leaves from different geographic regions in China. *Chem. Biodivers.* **2017**, *14*, e1700114. [CrossRef]
38. Justus, C.R.; Leffler, N.; Ruiz-Echevarria, M.; Yang, L.V. In vitro Cell Migration and Invasion Assays. *J. Vis. Exp.* **2014**, 1–8. [CrossRef]

Sample Availability: Samples of natural yellow *Monascus* pigments and reduced yellow *Monascus* pigments are not available from the authors.

molecules

MDPI

Article

FAK and S6K1 Inhibitor, Neferine, Dually Induces Autophagy and Apoptosis in Human Neuroblastoma Cells

Dinh-Chuong Pham [1,†], Yu-Chuan Chang [2,†], Shian-Ren Lin [2], Yuh-Ming Fuh [2], May-Jywan Tsai [3] and Ching-Feng Weng [2,*]

1 Faculty of Applied Sciences, Ton Duc Thang University, Ho Chi Minh City 700000, Vietnam; phamdinhchuong@tdtu.edu.vn
2 Department of Life Science and Institute of Biotechnology, National Dong Hwa University, Shoufeng, Hualien 97401, Taiwan; kevin7699402@hotmail.com (Y.-C.C.); mecurry@gmail.com (S.-R.L.); ming56564542@yahoo.com.tw (Y.-M.F.)
3 Neural Regeneration Laboratory, Taipei Veterans General Hospital, Taipei 11260, Taiwan; mjtsai2@vghtpe.gov.tw
* Correspondence: cfweng@gms.ndhu.edu.tw; Tel.: +886-3-890-3637
† These authors contributed equally to this work.

Academic Editor: Marco Guerrini
Received: 4 November 2018; Accepted: 25 November 2018; Published: 28 November 2018

Abstract: Human neuroblastoma cancer is the most typical extracranial solid tumor. Yet, new remedial treatment therapies are demanded to overcome its sluggish survival rate. Neferine, isolated from the lotus embryos, inhibits the proliferation of various cancer cells. This study aimed to evaluate the anti-cancer activity of neferine in IMR32 human neuroblastoma cells and to expose the concealable molecular mechanisms. IMR32 cells were treated with different concentrations of neferine, followed by 3-(4,5-dimethylthiazol-2-yl)-2,5-diphenyltetrazolium bromide (MTT) assay to assess cell viability. In an effort to determine the molecular mechanisms in neferine-incubated IMR32 cells, cell cycle arrest, cell migration, and focal adhesion kinase (FAK), the 70-kDa ribosomal S6 kinase 1 (S6K1), poly (ADP-ribose) polymerase (PARP), caspase-3, Beclin-1, and microtubule-associated protein 1A/1B-light chain 3 (LC3) protein expressions were investigated. Neferine strongly disrupted the neuroblastoma cell growth via induction of G2/M phase arrest. Furthermore, neferine provoked autophagy and apoptosis in IMR32 cells, confirmed by p-FAK, and p-S6K1 reduction, LC3-II accumulation, Beclin-1 overexpression, and cleaved caspase-3/PARP improvement. Finally, neferine markedly retarded cell migration of neuroblastoma cancer cells. As a result, our findings for the first time showed an explicit anti-cancer effect of neferine in IMR32 cells, suggesting that neferine might be a potential candidate against human neuroblastoma cells to improve clinical outcomes with further in vivo investigation.

Keywords: neferine; FAK/S6K1; autophagy; apoptosis; human neuroblastoma cells

1. Introduction

Neuroblastoma (NB) is the most common malignant nervous system tumor in babies and the third-most common cancer in children, accounting for ~8% of childhood cancers and 15% of all pediatric cancer deaths [1]. Even though some newborns can recuperate spontaneously, many of those damaged have poor prognosis and aggressive tendency of metastasis [2]. Ongoing treatment used in the administration of neuroblastoma includes surgery, chemotherapy, radiotherapy, and biotherapy. In spite of rigorous multi-combining therapy, the overall survival rates are less than 40% of the cases [3]. Some chemo drugs, like cyclophosphamide, doxorubicin, and etoposide show low

potency with numerous side effects because the low penetrations of blood brain barrier (BBB) resulted in low bioavailability. It has been shown that neuroblastoma gets resistance to cytotoxic drugs due to stable genetic alterations occurring during treatment [4]. Therefore, effective and safe drugs are high-priority required.

Nature is the best supplier of natural drugs where more than 600 approved anti-cancer products were isolated [5]. Neferine is a prime bisbenzylisoquinoline alkaloid, obtained from the green seed embryos of the lotus *Nelumbo nucifera* [6]. Previous works have proved that neferine effectively inhibits the proliferation of multidrug-resistant cancer cells [7], induces autophagy in lung cancer cells [8], regulates apoptosis in HSC-T6 cells [9], and enhances the anti-tumor activity of chemo drugs like cisplatin [10], and doxorubicin [11]. Recently, our research group has shown that neferine is a novel dual inhibitor of focal adhesion kinase (FAK) and the 70-kDa ribosomal S6 kinase 1 (S6K1) via molecular docking [12]. FAK and S6K1 proteins are the important candidate targets against which anticancer treatments could be developed. Although neferine is tested on various types of cancer, no particular study has been described its activity on human neuroblastoma tumor cells. In this study, human neuroblastoma tumor cells-IMR32 cells were treated with various concentrations of neferine, followed by MTT assay to measure cell viability. In an effort was further to investigate the molecular mechanisms of neferine-incubated IMR32 cells through cell cycle arrest, cell migration, and FAK, S6K1, PARP, caspase-3, Beclin-1, and LC3 protein expressions. Temozolomide, a clinical reagent of brain tumors, which can induce autophagy or apoptosis signaling pathways in malignant glioma cells [13–15], was used as a positive control of anti-cancer activity in this study. Herein, this is first evidenced that neferine induces autophagy and apoptosis in IMR32 human neuroblastoma cells through down-regulation of FAK and S6K1 pathways.

2. Results

2.1. Neferine Suppresses Cell Proliferation in Human Neuroblastoma Cells

In order to determine the cytotoxicity effects of neferine on IMR32 human neuroblastoma cell line, the cells were cultured and treated with various concentrations of neferine or temozolomide (TMZ), respectively for 24 h (Figure 1), followed by using MTT assay to analyze the cell viability. As expected, neferine significantly induced IMR32 cell death in a dose-dependent manner with IC50 (the half maximal inhibitory concentration) at 10 μM for 24 h ($p < 0.001$, Figure 1A). However, IMR32 cells were much less susceptible to TMZ, exhibiting an IC50 at 191 μM for 24 h ($p < 0.001$, Figure 1B). Next, we determined the cytotoxic effects of neferine on normal human astrocytes in comparison with TMZ. As shown in Figure 1C, neferine treatment exhibited much less cytotoxicity (<10%, $p < 0.001$) at dose 30 μM for 24 h incubation in normal astrocytes. The cytotoxicity of neferine for the normal cells showed much lower levels than for the neuroblastoma cells tested under the same conditions. TMZ treatment induced higher levels of cytotoxicity (<25%, $p < 0.001$) at dose 400 μM for 24 h incubation in normal human astrocytes (Figure 1D). These results indicate that neferine induces tumor cell-specific proliferation-inhibiting activity at low concentrations.

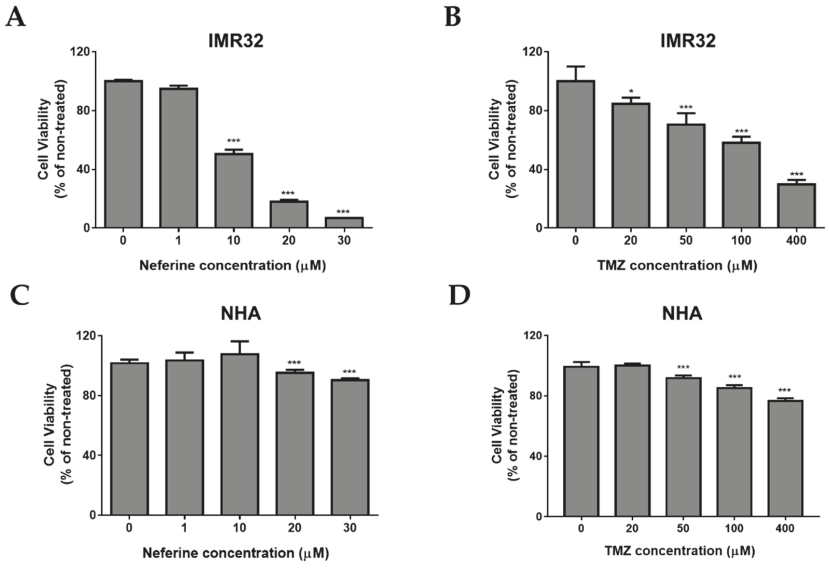

Figure 1. Neferine suppresses cell proliferation in human neuroblastoma cells. (**A**,**B**) IMR32 cells were treated with 1, 10, 20, and 30 μM of neferine or 20, 50, 100, and 400 μM of TMZ for 24 h; (**C**,**D**) Normal human astrocytes (NHA) were exposed to the indicated doses of neferine and TMZ for 24 h. Cell viability was analyzed by MTT assay, and the surviving cells were determined and presented as a percentage of the non-treated cells. Data are presented as mean ± standard deviation (SD) in three independent experiments. * $p < 0.05$, *** $p < 0.001$ as compared with the non-treated control.

2.2. Neferine Induces G2/M Cell Cycle Arrest in Human Neuroblastoma Cells

To check if the cell growth inhibition is related to cell cycle arrest, we measured the role of neferine in the cell cycle distribution. IMR32 cells were treated with the indicated concentrations of neferine or TMZ for 24 h, and then analyzed using PI method. As shown in Figure 2, the percentage of IMR32 cells incubated with 30 μM neferine (Figure 2A,C) or 400 μM TMZ (Figure 2B,D) at G1/S phase was strongly decreased from 70.9% and 79.7% to 51.4% and 58.7%, respectively ($p < 0.01$), while the proportion of neuroblastoma cells at G2/M phase was strikingly increased from 17.3% and 14.6% to 33.9% and 35.95%, respectively ($p < 0.001$). Therefore, the data manifested that low-dose neferine caused G2/M cell cycle arrest in IMR32 neuroblastoma cells after 24 h treatment.

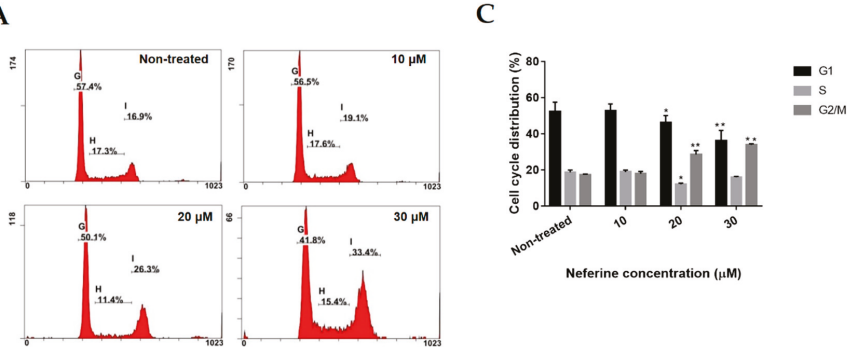

Figure 2. *Cont.*

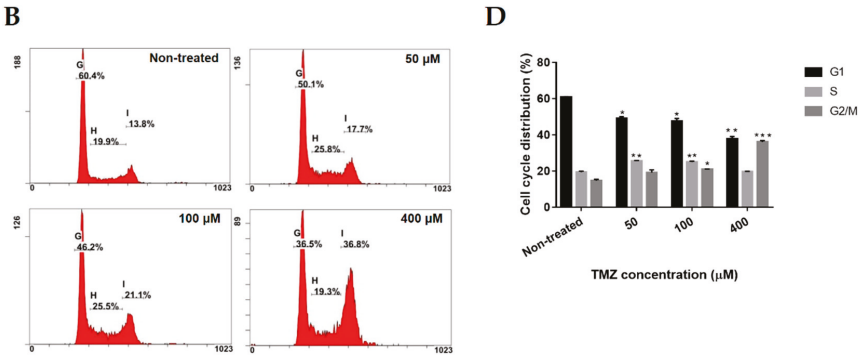

Figure 2. Neferine induces G2/M cell cycle arrest in human neuroblastoma cells. (**A**,**B**) IMR32 cells were cultured at the described concentrations of neferine (**A**) or TMZ (**B**) for 24 h, and then flow cytometry analysis was used to determine the cell cycle distributions; (**C**,**D**) The quantification of cell cycle arrest in neferine-treated or TMZ-treated IMR32 cells was shown. Data are expressed as mean ± SD in three independent experiments. * $p < 0.05$, ** $p < 0.01$, *** $p < 0.001$ as compared with the non-treated control.

2.3. Neferine Inhibits p-FAK and p-S6K1 Protein Levels in Human Neuroblastoma Cells

FAK and S6K1 are well-known targets for anti-cancer therapy because of their key roles in cell proliferation, cell viability, and cell migration [16,17]. To determine the effects of neferine on FAK, p-FAK, S6K1, and p-S6K1 proteins, IMR32 cells were incubated with different concentrations of neferine or TMZ, respectively for 24 h, and Western blot analysis was used to measure protein levels. In IMR32 cells treated with 30 μM neferine, the protein levels of p-FAK and p-S6K1 were significantly reduced by approximately 3.2-fold and 2.1-fold than those in non-treated control, respectively ($p < 0.01$, Figure 3A,C). In keeping with the detection acquired in the IMR32-incubated neferine, treatment of IMR32 cells with 400 μM TMZ also inhibited the p-FAK and p-S6K1 protein expression levels by 2-fold and 1.5-fold than those in non-treated control, respectively ($p < 0.01$, Figure 3B,D). The protein levels of FAK and S6K1 were not significantly different in neferine or TMZ-treated cells compared with non-treated control. Thus, the results revealed that neuroblastoma cell proliferation was obstructed by the loss of p-FAK and p-S6K1 proteins under neferine treatment.

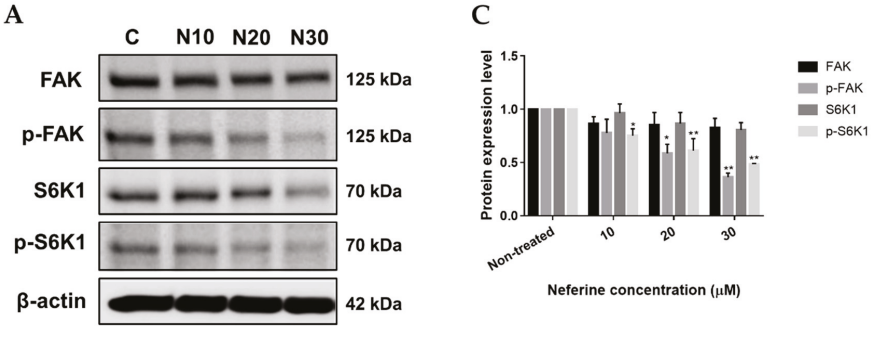

Figure 3. *Cont.*

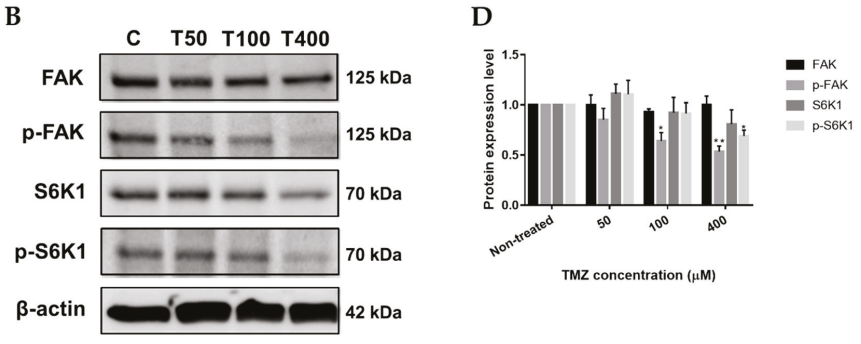

Figure 3. Neferine inhibits FAK, p-FAK, S6K1, and p-S6K1 protein levels in human neuroblastoma cells. (**A**,**B**) IMR32 cells were incubated with the desired concentrations of neferine (**A**) or TMZ (**B**) for 24 h. Then, all cells were harvested and lysed for Western blot analysis; (**C**,**D**) Changes in the levels of FAK, p-FAK, S6K1, and p-S6K1 proteins after being normalized to the levels of beta actin were presented. Data are shown as mean ± SD of three independent experiments. * $p < 0.05$, ** $p < 0.01$ as compared with the non-treated control.

2.4. Neferine triggers autophagy in human neuroblastoma cells

Autophagy is the natural, catabolic procedure forming autophagosomes, the double-membrane vesicles, to uptake cytoplasmic content, which is degraded and recycled by fusion of the autophagosomes and the lysosomes [18]. Augmentation of autophagy-dependent cell death from abnormal cells is one of the perfect choices among anti-cancer therapies [8]. To check whether neferine could induce autophagy in neuroblastoma cells or not, IMR32 cells were treated with various concentrations of neferine or TMZ, respectively for 24 h, followed by Western blot analysis. Microtubule-associated protein 1A/1B light chain 3-II (LC3-II) and Beclin-1 are the valid autophagosomal markers to reflect autophagic cell death and autophagy formation [19,20]. Beclin-1 expression and LC3-II conversion were found to be strongly induced by neferine incubation in a dose-dependent manner, especially with 2-fold and 2.4-fold higher than those of non-treated control, respectively ($p < 0.01$, Figure 4A,C) at 30 μM neferine for 24 h. TMZ showed similar induction on Beclin-1 and LC3-II formation, although to a lesser extent than that of neferine ($p < 0.05$, Figure 4B,D). Taken together, the data conveyed that neferine could trigger autophagy in human neuroblastoma cells.

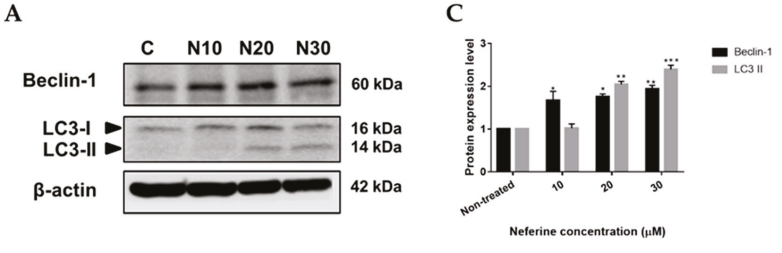

Figure 4. *Cont.*

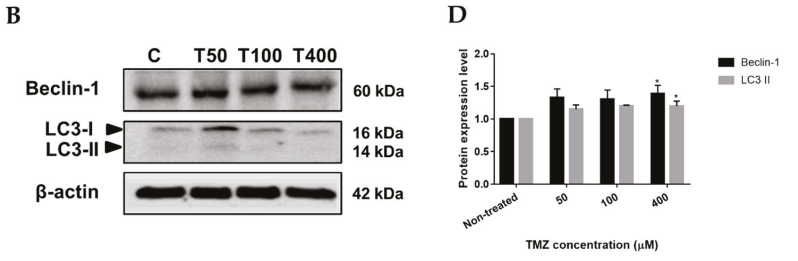

Figure 4. Neferine triggers autophagy in human neuroblastoma cells. (**A**,**B**) IMR32 cells were exposed to the indicated concentrations of neferine (**A**) or TMZ (**B**) for 24 h. Then, autophagy-related proteins, including Beclin-1 and LC3, were assessed using Western blot analysis; (**C**,**D**) Changes in the levels of Beclin-1, LC3-I, and LC3-II after being normalized to the levels of beta actin were shown. The data are expressed as mean ± SD in three independent experiments. * $p < 0.05$, ** $p < 0.01$, *** $p < 0.001$ as compared with the non-treated control.

2.5. Neferine Induces Apoptosis in Human Neuroblastoma Cells

Apoptosis is a typical and crucial mode of programmed cell death, which involves the elimination of cells by two well-established mechanisms, the intrinsic and extrinsic pathways [21]. Cell death by anti-cancer drugs are closely related to pivotal molecular mechanisms of apoptosis. As a consequence, if apoptosis correlated with the growth inhibition of human neuroblastoma cells by neferine was further investigated. It is remarkable that caspase-3 and PARP cleavage are known apoptotic markers. The Western blot outcome showed that cleaved Caspase-3 and PARP were greatly elevated by neferine ($p < 0.01$, Figure 5A,C) or TMZ ($p < 0.05$, Figure 5B,D) culture in a dose-dependent manner. Hence, the results proved that IMR32 neuroblastoma cell suppression was associated with apoptosis caused by neferine administration.

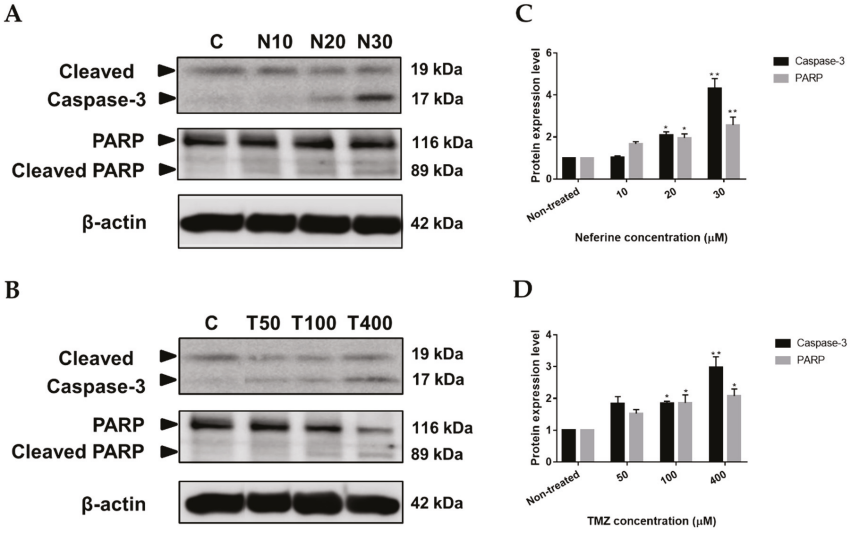

Figure 5. Neferine induces apoptosis in human neuroblastoma cells. (**A**,**B**) IMR32 cells were incubated at the described concentrations of neferine (**A**) or TMZ (**B**) for 24 h. Then, apoptosis-related proteins, including cleaved Caspase-3 and PARP, were determined using Western blot analysis; (**C**,**D**) Changes in the levels of cleaved Caspase-3 and PARP after being normalized to the levels of beta actin were displayed. Data are shown as mean ± SD in three independent experiments. * $p < 0.05$, ** $p < 0.01$ as compared with the non-treated control.

2.6. Neferine Inhibits Migration in Human Neuroblastoma Cells

Tumor metastasis is a significant factor which gives rise to cancer-related mortalities. The expanding migration assists cancer cells in underlining tumor invasion [22]. For that reason, inhibiting cancer cell migration could be prospective target for chemotherapy. Therefore, the potential anti-migration effect of neferine or TMZ on IMR32 cells was carried out through a wound healing assay. As supposed, neferine (Figure 6A) and TMZ (Figure 6B) remarkably suppressed neuroblastoma cell motility in time- and dose-dependent manners when compared with that of the non-treated control ($p < 0.01$). The wound areas of 30 μM neferine and 400 μM TMZ treatments were 85.4% and 67.5%, respectively (Figure 6C,D). These results demonstrated that neferine displayed a better migration inhibition activity than TMZ on human neuroblastoma cells.

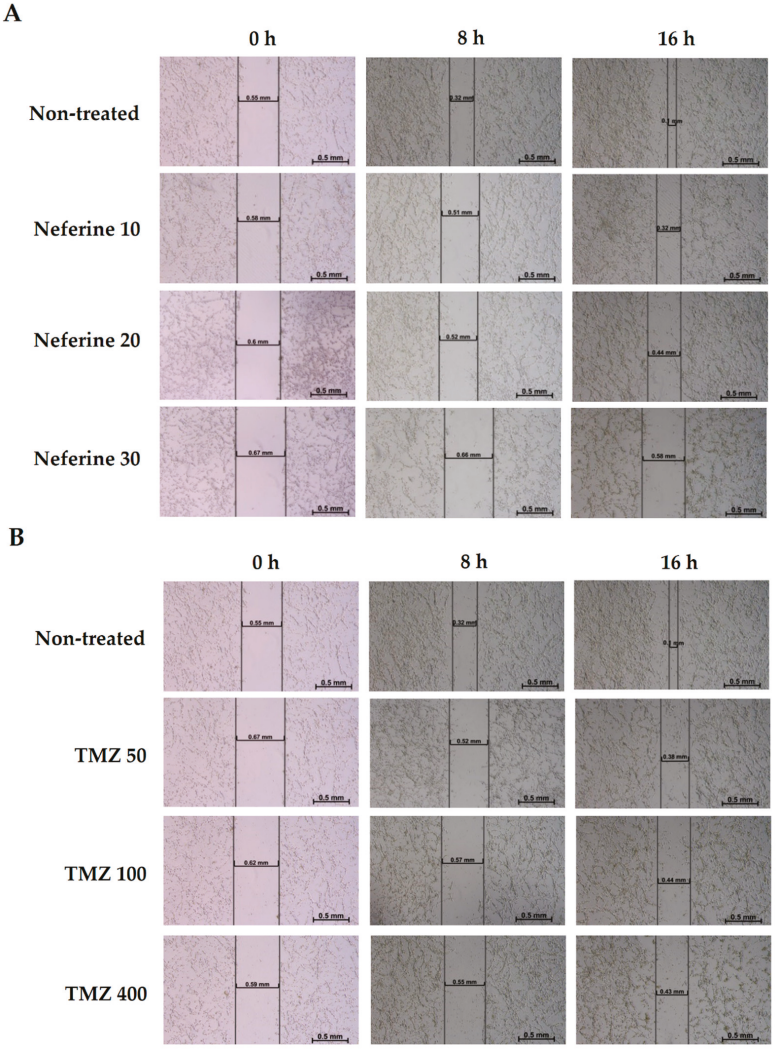

Figure 6. *Cont.*

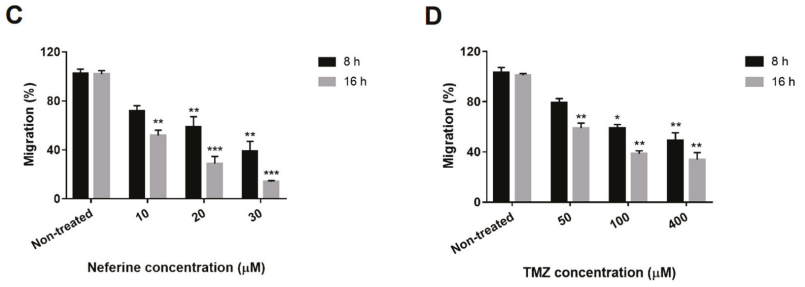

Figure 6. Neferine inhibits migration in human neuroblastoma cells. (**A**,**B**) IMR32 cell monolayer was scratched and treated with neferine (**A**) or TMZ (**B**) in time-dependent manner for wound-healing migration assay. Images were accessed by inverted microscope; (**C**,**D**) The quantification of cell migration in wound healing assay after treatment with neferine (**C**) or TMZ (**D**) were measured. Data are shown as percentages of the recovered scratch area relative to non-treated control. Results are presented as mean ± SD in three independent experiments. * $p < 0.05$, ** $p < 0.01$, and *** $p < 0.001$ as compared with the non-treated control.

3. Discussion

In this decade, numerous common foods provide potential benefits for the anti-cancer remedy, such as soy beans, green tea, and red wine [23,24]. *Nelumbo nucifera*, known as lotus, is spread all over the world and all the segments of lotus plant are consumable. Evidence has proved that the green seed embryos of lotus plant are important for pharmaceutical. Neferine is a bis-benzylisoquinoline alkaloid, which is isolated from seed embryos of lotus plant, has been shown for its inhibitory effects on the proliferation of liver cancer cells, lung cancer cells, and osteosarcoma cells [8,25,26]. Because of the great potentials for treating different types of cancer, neferine was a potential candidate in this study to further unveil its anti-cancer capacity. To the best of our knowledge, this is the first report to investigate neferine activity in human neuroblastoma cells. Here, we discovered that neferine could retard cell growth, induce G2/M cell cycle arrest, decrease FAK, p-FAK, S6K1, and p-S6K1 protein levels, cause autophagy and apoptosis, and block tumor cell migration in human IMR32 neuroblastoma cells.

Cell cycle arrest plays an important role to maintain genome stability because it allows cells with DNA damage to repair of mutations [27]. Decay of cell cycle arrest leads to cancer progression [28]. Up till now, many natural compounds were reported to possess malignant growth inhibition activity by blocking the cell cycle [29–31]. Importantly, cell cycle arrest at G2/M phase might be the key to cause the cancer cell death [32,33]. The results showed that neferine strongly retarded IMR32 cell proliferation in dose-dependent fashion ($p < 0.001$, Figure 1) and this reduction in cell growth arose from G2/M cell cycle arrest. After 24 h of neferine treatment, the G2/M cell population was dramatically increased at the expense of a decreased G1/S cell population of IMR32 neuroblastoma cells ($p < 0.01$, Figure 2).

Focal adhesion kinase (FAK), a 125 kDa non-receptor protein tyrosine kinase, has been shown to be important for survival signaling, motility, and metastasis and is overexpressed in a number of tumors [34]. FAK has been implicated in the control of cell proliferation where it is thought to mediate signals from growth factor receptors and integrins to regulate cell cycle progression [35]. It has been shown that FAK regulates proliferation of cancer cells [36] and the silencing of FAK inhibits cell proliferation in gastric cancer and lung cancer [37,38]. In addition, the 70-kDa Ribosomal S6 kinase 1 (S6K1), a 70 kDa Ser/Thr protein kinase, has been shown to control the cell proliferation [39]. In recent years, S6K1 was found to be overexpressed in brain tumors [40], breast tumors [41], and S6K1 protein expression has been according to the poor prognosis of those cancers. Thus, the targeting of FAK together with S6K1 may give a powerful approach for the treatment of cancer patients. Our previous study showed that some natural compounds, such as neferine, antroquinonol D, and curcumin could

bind to FAK and S6K1 demonstrated by molecular docking method, and then inhibit C6 rat glioma cell proliferation [12]. Furthermore, our results revealed that neferine combined with cisplatin could down regulate the expression of Bcl-2, up regulate the expression of Bax, Bad, Bak, release of cytochrome c, p53 levels, activate cleavage forms of caspase-9, caspase-3, and PARP, and reduce the protein levels of FAK and VEGF [42]. In the present study, we proved that neferine treatment dramatically decreased the protein levels of p-FAK and p-S6K1 in IMR32 human neuroblastoma cells. The protein expression levels of p-FAK and p-S6K1 in 30 μM of neferine were much lower than those in 400 μM of TMZ administration ($p < 0.01$, Figure 3).

Autophagy is type II programmed cell death which responses to various anti-cancer therapies in many kinds of tumors [43]. The fusion between autophagosome and lysosome leading to the degradation of targeted cytoplasmic constituents is a key mechanism of autophagy [44]. Beclin-1 and microtubule-associated protein 1A/1B light chain 3 (LC3) play the crucial roles in autophagy pathway. LC3-II, known as autophagosomal marker, increases from the conjugation between LC3-I and phosphatidyl ethanolamine when autophagic cell death is activated [45,46]. Besides, overexpression of Beclin-1, the mammalian ortholog of yeast Atg6, results in the elevation of autophagic cell death [47,48]. In this study, neferine induced autophagy in dose-dependent manner, which the enhancement of LC3-I/LC3-II and Beclin-1 ($p < 0.01$, Figure 4). Our data are congenial with the previous findings of Cheng and colleagues, 2017 who showed that FAK was a novel negative regulator of Beclin1-mediated autophagy [49].

Apoptosis is a highly regulated process which leads to cellular morphological changes and cell death. Induction of apoptosis is a useful vehicle of targeted treatment in cancer [50]. Execution phase regarded as the terminal pathway of apoptosis, can activate the prosecution caspases, such as caspase-3, caspase-6 to cleave distinct substrates including cytokeratins, PARP to undergo apoptosis [51]. Therefore, cleaved caspase-3 and cleaved PARP are recognized as markers of apoptosis [52]. Previous researches also indicated that FAK depletion enhanced susceptibility to DOX-induced myocyte apoptosis and cardiac dysfunction [53,54]. We found that caspase-3 and PARP were remarkably cleaved with an increased concentration of neferine administration ($p < 0.01$, Figure 5).

It is notable that cancers lack angiogenesis standing reposefully. Suppressing angiogenesis might play a role in anti-cancer therapy to inhibit tumor progression and diminish the threat of metastasis [55]. Our results showed that neferine crucially reduced migration in IMR32 human neuroblastoma cells ($p < 0.01$, Figure 6). In this study, TMZ as a positive control could arrest the cell cycle of IMR32 cells at G2/M phase, increase the levels of apoptotic proteins, cleaved caspase-3 and cleaved PARP, as well as the levels of autophagy-related proteins, Beclin-1 and LC3-II, and retard IMR32 cell migration. As compared with the reference drug TMZ, neferine as a potent anti-brain tumor through the causes of apoptosis and autophagy as TMZ is demonstrated and further supported the first evidence for the suppression of FAK and S6K1 proteins as an inhibitor.

4. Materials and Methods

4.1. Chemicals and Antibodies

Neferine was isolated according to the previous method [6]. Temozolomide was obtained from Orion Corporation (New Jersey, USA). The primary antibodies of FAK, p-FAK, S6K, p-S6K, Beclin-1, LC3, Cleaved Caspase-3, and PARP were purchased from Cell Signaling (Danvers, MA, USA). The antibody for β-actin was obtained from Sigma (Kawasaki, Japan), the anti-mouse and anti-rabbit IgG horseradish peroxidase-conjugated secondary antibodies were purchased from GE Healthcare (Chicago, IL, USA).

4.2. Cell Culture

IMR32 human neuroblastoma cell line was provided by Dr. May-Jywan Tsai (Neural Regeneration Laboratory, Taipei Veterans General Hospital, Taipei, Taiwan). IMR32 cells were maintained in DMEM

(low glucose, pH 7.4) supplemented with 10% fetal bovine serum (FBS, Gibco, MA, USA), 2 mM L-glutamine, 1% NEAA, and 1% antibiotics (100 U/mL of penicillin and 100 μg/mL of streptomycin) at 37 °C in a humidified atmosphere of 5% CO_2. Normal human astrocytes from human fetal cortex were obtained from Lonza (Walkersville, MD, USA) and cultured according to manufacturer's instructions.

4.3. MTT Assay

The 3-(4, 5-dimethylthiazol-2-yl)-2,5-diphenyltetrazolium bromide (MTT, Invitrogen, Waltham, MA, USA), a colorimetric-based assay was performed to analyze the viable cells. IMR32 cells and normal human astrocytes were seeded at 2×10^4 cells per well in 96-well plate in 5% CO_2 at 37 °C. Cells were treated with 1, 10, 20, and 30 μM of neferine or 20, 50, 100, and 400 μM of TMZ for 24 h, and then 20 μL/well MTT (25 μg/mL) solution was added into the wells and further incubated for additional 3 h. The medium was removed, and formazan was solubilized by the addition of 100 μL/well dimethyl sulfoxide (DMSO, Sigma, MO, USA), and OD value was measured at 570 nm using a microplate reader (ELISA reader, Thermo Labsystems, Waltham, MA, USA). The percentage of viable cells was determined from a comparison with untreated control.

4.4. Cell Cycle Analysis

IMR32 cells (ATCC® CCL-127™, Manassas, VA, USA) were seeded at 3×10^5 cells per well in 6-well plate. Cells were treated with 10, 20, and 30 μM of neferine or 50, 100, and 400 μM of TMZ for 24 h. Cells were harvested and fixed with ice cold 70% ethanol at −20 °C overnight and washed with cold PBS twice, and then incubated in 1 mL (v/v) staining solution (20 μg/mL propidium iodide (PI), 0.1% Triton X-100, and 0.2 mg/mL RNase) at 37 °C for 30 min. Then cell were analyzed by using flow cytometer (CytomicsTM FC500, Beckman, Fullerton, CA, USA). For each experiment, 10,000 cells were counted and data were analyzed.

4.5. Western Blot Analysis

IMR32 cells were seeded at 5×10^5 cells per well in 6-well plate, and then incubated with 10, 20, and 30 μM of neferine or 50, 100, and 400 μM of TMZ for 24 h. After incubation, the medium was removed and the cells were washed with PBS, then cells were collected and lysed with RIPA buffer at 4 °C for 30 min and centrifuged at 12,000 × g for 30 min. The supernatant was collected and quantified by Bradford protein assay (Bio-Rad, Hercules, CA, USA). Protein samples (28 μg) were loaded into the well and separated with sodium dodecyl sulfate polyacrylamide gel electrophoresis (SDS-PAGE), then the gel was transferred to the PVDF membrane (Perkin Elmer Life Sciences, Boston, MA, USA). The blots were blocked with 10% non-fat milk in TBS/T (20 mM Tris-Base, 137 mM NaCl at pH 7.4 and 0.05% Tween-20) at room temperature (RT) for 30 min and then blots were incubated with the appropriate primary antibody at 4 °C overnight. The blots were washed 3 times with TBS/T, and then incubated with horseradish peroxidase (HRP)-conjugated secondary antibodies at RT for 1 h. After blots exposed to ECL reagents (PerkinElmer Life Sciences), the proteins bands were visualized and the protein expression was analyzed by Luminescent image analyzer (LAS)-3000 (Fujifilm, Minato, Tokyo, Japan).

4.6. Wound Healing Assay

For measuring the migration rate, IMR32 cells were seeded 3×10^5 cells per well in 6-well plate. After cells reached 70–80% confluent, a 10 μL pipette tip was used to make a straight scratch for simulating a wound and then cells were treated with 10, 20, and 30 μM of neferine or 50, 100, and 400 μM of TMZ for various time points. Wound closure was monitored and photographed at 0, 8, and 16 h by ZEISS inverted microscope connected with Canon 700D camera.

4.7. Statistical Analysis

All the data were expressed as mean ± standard deviation (SD) of three independent experiments. Statistical comparisons of multiple variables were made by one-way analysis of variance (ANOVA) and the Tukey test. p value of <0.05 was considered to be statistically significant differences (* $p < 0.05$, ** $p < 0.01$, *** $p < 0.001$).

5. Conclusions

Together, this study demonstrates for the first time that neferine has therapeutic prospect for targeting IMR32 human neuroblastoma cells through the best fit in the binding pocket of FAK and S6K1 proteins, and caused decrease the level of these two proteins. Furthermore, neferine showed a potential effect on cell viability, induced the autophagy and apoptosis, and inhibited the cell motility of IMR32 cells. When these head-to-head comparative quality studies of drugs approved by FDA, and new drug candidate are taken into consideration, neferine could be a promising anti-brain tumor drug as clinical reagent temozolomide.

Author Contributions: D.-C.P. and Y.-C.C. were responsible for the experimental design, conducted the experiments, analyzed the data and wrote the manuscript. S.-R.L., Y.-M.F. and M.-J.T. analyzed the data and provided critical feedbacks. C.-F.W. contributed in the experimental design, analyzed the data, and provided critical feedbacks for the manuscript.

Funding: This study was supported by a grant from Ministry of Science and Technology, grant number 107-2320-B-259-003 (C.-F.W.).

Acknowledgments: The authors would like to acknowledge Chin-Piao Chen (Department of Chemistry, NDHU, Hualien, Taiwan) for research support.

Conflicts of Interest: The authors declare no conflict of interest.

References

1. Maris, J.M.; Hogarty, M.D.; Bagatell, R.; Cohn, S.L. Neuroblastoma. *Lancet* **2007**, *369*, 2106–2120. [CrossRef]
2. Weinstein, J.L.; Katzenstein, H.M.; Cohn, S.L. Advances in the diagnosis and treatment of neuroblastoma. *Oncologist* **2003**, *8*, 278–292. [CrossRef] [PubMed]
3. Matthay, K.K.; Villablanca, J.G.; Seeger, R.C.; Stram, D.O.; Harris, R.E.; Ramsay, N.K.; Swift, P.; Shimada, H.; Black, C.T.; Brodeur, G.M.; et al. Treatment of high-risk neuroblastoma with intensive chemotherapy, radiotherapy, autologous bone marrow transplantation, and 13-*cis*-retinoic acid. Children's Cancer Group. *New Engl. J. Med.* **1999**, *341*, 1165–1173. [CrossRef] [PubMed]
4. Keshelava, N.; Seeger, R.C.; Reynolds, C.P. Drug resistance in human neuroblastoma cell lines correlates with clinical therapy. *Eur. J. Cancer* **1997**, *33*, 2002–2006. [CrossRef]
5. Rayan, A.; Raiyn, J.; Falah, M. Nature is the best source of anticancer drugs: Indexing natural products for their anticancer bioactivity. *PLoS ONE* **2017**, *12*, e0187925. [CrossRef] [PubMed]
6. Wu, S.; Sun, C.; Cao, X.; Zhou, H.; Hong, Z.; Pan, Y. Preparative counter-current chromatography isolation of liensinine and its analogues from embryo of the seed of *Nelumbo nucifera* GAERTN. using upright coil planet centrifuge with four multilayer coils connected in series. *J. Chromatogr. A* **2004**, *1041*, 153–162. [CrossRef] [PubMed]
7. Kadioglu, O.; Law, B.Y.K.; Mok, S.W.F.; Xu, S.W.; Efferth, T.; Wong, V.K.W. Mode of action analyses of neferine, a bisbenzylisoquinoline alkaloid of lotus (*Nelumbo nucifera*) against multidrug-resistant tumor cells. *Front. Pharmacol.* **2017**, *8*, 238. [CrossRef] [PubMed]
8. Poornima, P.; Weng, C.F.; Padma, V.V. Neferine from *Nelumbo nucifera* induces autophagy through the inhibition of PI3K/Akt/mTOR pathway and ROS hyper generation in A549 cells. *Food Chem.* **2013**, *141*, 3598–3605. [CrossRef] [PubMed]
9. Ding, H.; Shi, J.H.; Wang, Y.; Guo, J.; Zhao, J.H.; Dong, L. Neferine inhibits cultured hepatic stellate cell activation and facilitates apoptosis A possible molecular mechanism. *Eur. J. Pharmacol.* **2011**, *650*, 163–169. [CrossRef] [PubMed]

10. Selvi, S.K.; Vinoth, A.; Varadharajan, T.; Weng, C.F.; Padma, V.V. Neferine augments therapeutic efficacy of cisplatin through ROS-mediated non-canonical autophagy in human lung adenocarcinoma (A549 cells). *Food Chem. Toxicol.* **2017**, *103*, 28–40. [CrossRef] [PubMed]
11. Poornima, P.; Kumar, V.B.; Weng, C.F.; Padma, V.V. Doxorubicin induced apoptosis was potentiated by neferine in human lung adenocarcima, A549 cells. *Food Chem. Toxicol.* **2014**, *68*, 87–98. [CrossRef] [PubMed]
12. Thiyagarajan, V.; Lin, S.H.; Chang, Y.C.; Weng, C.F. Identification of novel FAK and S6K1 dual inhibitors from natural compounds via ADMET screening and molecular docking. *Biomed. Pharmacother.* **2016**, *80*, 52–62. [CrossRef] [PubMed]
13. Scicchitano, B.M.; Sorrentino, S.; Proietti, G.; Lama, G.; Dobrowolny, G.; Catizone, A.; Binda, E.; Larocca, L.M.; Sica, G. Levetiracetam enhances the temozolomide effect on glioblastoma stem cell proliferation and apoptosis. *Cancer Cell Int.* **2018**, *18*, 136. [CrossRef] [PubMed]
14. Wurstle, S.; Schneider, F.; Ringel, F.; Gempt, J.; Lammer, F.; Delbridge, C.; Wu, W.; Schlegel, J. Temozolomide induces autophagy in primary and established glioblastoma cells in an EGFR independent manner. *Oncol. Lett.* **2017**, *14*, 322–328. [CrossRef] [PubMed]
15. Tomicic, M.T.; Meise, R.; Aasland, D.; Berte, N.; Kitzinger, R.; Kramer, O.H.; Kaina, B.; Christmann, M. Apoptosis induced by temozolomide and nimustine in glioblastoma cells is supported by JNK/c-Jun-mediated induction of the BH3-only protein BIM. *Oncotarget* **2015**, *6*, 33755–33768. [CrossRef] [PubMed]
16. Parsons, J.T.; Martin, K.H.; Slack, J.K.; Taylor, J.M.; Weed, S.A. Focal adhesion kinase: A regulator of focal adhesion dynamics and cell movement. *Oncogene* **2000**, *19*, 5606–5613. [CrossRef] [PubMed]
17. Pullen, N.; Thomas, G. The modular phosphorylation and activation of p70s6k. *FEBS Lett.* **1997**, *410*, 78–82. [CrossRef]
18. Xie, Z.; Klionsky, D.J. Autophagosome formation: Core machinery and adaptations. *Nat. Cell Biol.* **2007**, *9*, 1102–1109. [CrossRef] [PubMed]
19. Kang, R.; Zeh, H.J.; Lotze, M.T.; Tang, D. The Beclin 1 network regulates autophagy and apoptosis. *Cell Death Differ.* **2011**, *18*, 571–580. [CrossRef] [PubMed]
20. Tanida, I.; Ueno, T.; Kominami, E. LC3 and Autophagy. *Methods in Mol. Biol.* **2008**, *445*, 77–88.
21. Elmore, S. Apoptosis: A review of programmed cell death. *Toxicol. Pathol.* **2007**, *35*, 495–516. [CrossRef] [PubMed]
22. Friedl, P.; Wolf, K. Plasticity of cell migration: A multiscale tuning model. *J. Cell Biol.* **2010**, *188*, 11–19. [CrossRef] [PubMed]
23. Kang, J.; Badger, T.M.; Ronis, M.J.; Wu, X. Non-isoflavone phytochemicals in soy and their health effects. *J. Agric. Food Chem.* **2010**, *58*, 8119–8133. [CrossRef] [PubMed]
24. Lambert, J.D.; Sang, S.; Hong, J.; Yang, C.S. Anticancer and anti-inflammatory effects of cysteine metabolites of the green tea polyphenol, (-)-epigallocatechin-3-gallate. *J. Agric. Food Chem.* **2010**, *58*, 10016–10019. [CrossRef] [PubMed]
25. Poornima, P.; Quency, R.S.; Padma, V.V. Neferine induces reactive oxygen species mediated intrinsic pathway of apoptosis in HepG2 cells. *Food Chem.* **2013**, *136*, 659–667. [CrossRef] [PubMed]
26. Zhang, X.; Liu, Z.; Xu, B.; Sun, Z.; Gong, Y.; Shao, C. Neferine, an alkaloid ingredient in lotus seed embryo, inhibits proliferation of human osteosarcoma cells by promoting p38 MAPK-mediated p21 stabilization. *Eur. J. Pharmacol.* **2012**, *677*, 47–54. [CrossRef] [PubMed]
27. Senderowicz, A.M.; Sausville, E.A. Preclinical and clinical development of cyclin-dependent kinase modulators. *J. Natl. Cancer Inst.* **2000**, *92*, 376–387. [CrossRef] [PubMed]
28. Simmons Kovacs, L.A.; Orlando, D.A.; Haase, S.B. Transcription networks and cyclin/CDKs: The yin and yang of cell cycle oscillators. *Cell Cycle* **2008**, *7*, 2626–2629. [CrossRef] [PubMed]
29. Gloria, N.F.; Soares, N.; Brand, C.; Oliveira, F.L.; Borojevic, R.; Teodoro, A.J. Lycopene and beta-carotene induce cell-cycle arrest and apoptosis in human breast cancer cell lines. *Anticancer Res.* **2014**, *34*, 1377–1386. [PubMed]
30. Huang, W.S.; Kuo, Y.H.; Kuo, H.C.; Hsieh, M.C.; Huang, C.Y.; Lee, K.C.; Lee, K.F.; Shen, C.H.; Tung, S.Y.; Teng, C.C. CIL-102-Induced Cell Cycle Arrest and Apoptosis in Colorectal Cancer Cells via Upregulation of p21 and GADD45. *PLoS ONE* **2017**, *12*, e0168989. [CrossRef] [PubMed]

31. Ji, L.; Zhong, B.; Jiang, X.; Mao, F.; Liu, G.; Song, B.; Wang, C.Y.; Jiao, Y.; Wang, J.P.; Xu, Z.B.; et al. Actein induces autophagy and apoptosis in human bladder cancer by potentiating ROS/JNK and inhibiting AKT pathways. *Oncotarget* **2017**, *8*, 112498–112515. [CrossRef] [PubMed]
32. Shin, S.Y.; Yong, Y.; Kim, C.G.; Lee, Y.H.; Lim, Y. Deoxypodophyllotoxin induces G2/M cell cycle arrest and apoptosis in HeLa cells. *Cancer Lett.* **2010**, *287*, 231–239. [CrossRef] [PubMed]
33. Zhang, L.; Zheng, Y.; Deng, H.; Liang, L.; Peng, J. Aloperine induces G2/M phase cell cycle arrest and apoptosis in HCT116 human colon cancer cells. *Int. J. Mol. Med.* **2014**, *33*, 1613–1620. [CrossRef] [PubMed]
34. Golubovskaya, V.M.; Cance, W.G. Focal adhesion kinase and p53 signaling in cancer cells. *Int. Rev. Cytol.* **2007**, *263*, 103–153. [PubMed]
35. Zhao, J.H.; Bian, Z.C.; Yee, K.; Chen, B.P.C.; Chien, S.; Guan, J.L. Identification of transcription factor KLF8 as a downstream target of focal adhesion kinase in its regulation of cyclin D1 and cell cycle progression. *Mol. Cell* **2003**, *11*, 1503–1515. [CrossRef]
36. Ding, Q.; Grammer, J.R.; Nelson, M.A.; Guan, J.L.; Stewart, J.E., Jr.; Gladson, C.L. p27Kip1 and cyclin D1 are necessary for focal adhesion kinase regulation of cell cycle progression in glioblastoma cells propagated in vitro and in vivo in the scid mouse brain. *J. Biol. Chem.* **2005**, *280*, 6802–6815. [CrossRef] [PubMed]
37. Feng, R.; Yang, S. Effects of combining erlotinib and RNA-interfered downregulation of focal adhesion kinase expression on gastric cancer. *J. Int. Med. Res.* **2016**, *44*, 855–864. [CrossRef] [PubMed]
38. Shi, R.; Wang, Q.; Ouyang, Y.; Wang, Q.; Xiong, X. Picfeltarraenin IA inhibits lipopolysaccharide-induced inflammatory cytokine production by the nuclear factor-kappaB pathway in human pulmonary epithelial A549 cells. *Oncol. Lett.* **2016**, *11*, 1195–1200. [CrossRef] [PubMed]
39. Woo, M.S.; Ohta, Y.; Rabinovitz, I.; Stossel, T.P.; Blenis, J. Ribosomal S6 kinase (RSK) regulates phosphorylation of filamin a on an important regulatory site. *Mol. Cell. Biol.* **2004**, *24*, 3025–3035. [CrossRef] [PubMed]
40. Ismail, H.M. Overexpression of s6 kinase 1 in brain tumours is associated with induction of hypoxia-responsive genes and predicts patients' survival. *J. Oncol.* **2012**, *2012*, 416927. [CrossRef] [PubMed]
41. Sinclair, C.S.; Rowley, M.; Naderi, A.; Couch, F.J. The 17q23 amplicon and breast cancer. *Breast Cancer Res. Treat.* **2003**, *78*, 313–322. [CrossRef] [PubMed]
42. Sivalingam, K.S.; Paramasivan, P.; Weng, C.F.; Viswanadha, V.P. Neferine Potentiates the Antitumor Effect of Cisplatin in Human Lung Adenocarcinoma Cells Via a Mitochondria-Mediated Apoptosis Pathway. *J. Cell. Biochem.* **2017**, *118*, 2865–2876. [CrossRef] [PubMed]
43. Liu, Y.L.; Yang, P.M.; Shun, C.T.; Wu, M.S.; Weng, J.R.; Chen, C.C. Autophagy potentiates the anti-cancer effects of the histone deacetylase inhibitors in hepatocellular carcinoma. *Autophagy* **2010**, *6*, 1057–1065. [CrossRef] [PubMed]
44. Mizushima, N.; Yoshimori, T.; Ohsumi, Y. The role of Atg proteins in autophagosome formation. *Ann. Rev. Cell Dev. Biol.* **2011**, *27*, 107–132. [CrossRef] [PubMed]
45. Cao, Q.H.; Liu, F.; Yang, Z.L.; Fu, X.H.; Yang, Z.H.; Liu, Q.; Wang, L.; Wan, X.B.; Fan, X.J. Prognostic value of autophagy related proteins ULK1, Beclin 1, ATG3, ATG5, ATG7, ATG9, ATG10, ATG12, LC3B and p62/SQSTM1 in gastric cancer. *Am. J. Transl. Res.* **2016**, *8*, 3831–3847. [PubMed]
46. Li, W.L.; Xiong, L.X.; Shi, X.Y.; Xiao, L.; Qi, G.Y.; Meng, C. IKKbeta/NFkappaBp65 activated by interleukin-13 targets the autophagy-related genes LC3B and beclin 1 in fibroblasts co-cultured with breast cancer cells. *Exp. Ther. Med.* **2016**, *11*, 1259–1264. [CrossRef] [PubMed]
47. Shin, J.Y.; Hong, S.H.; Kang, B.; Minai-Tehrani, A.; Cho, M.H. Overexpression of beclin1 induced autophagy and apoptosis in lungs of K-rasLA1 mice. *Lung Cancer* **2013**, *81*, 362–370. [CrossRef] [PubMed]
48. Nascimento-Ferreira, I.; Santos-Ferreira, T.; Sousa-Ferreira, L.; Auregan, G.; Onofre, I.; Alves, S.; Dufour, N.; Colomer Gould, V.F.; Koeppen, A.; Deglon, N.; et al. Overexpression of the autophagic beclin-1 protein clears mutant ataxin-3 and alleviates Machado-Joseph disease. *Brain* **2011**, *134*, 1400–1415. [CrossRef] [PubMed]
49. Cheng, Z.; Zhu, Q.; Dee, R.; Opheim, Z.; Mack, C.P.; Cyr, D.M.; Taylor, J.M. Focal Adhesion Kinase-mediated Phosphorylation of Beclin1 Protein Suppresses Cardiomyocyte Autophagy and Initiates Hypertrophic Growth. *J. Biol. Chem.* **2017**, *292*, 2065–2079. [CrossRef] [PubMed]
50. Philchenkov, A.; Zavelevich, M.; Kroczak, T.J.; Los, M. Caspases and cancer: Mechanisms of inactivation and new treatment modalities. *Exp. Oncol.* **2004**, *26*, 82–97. [PubMed]
51. Slee, E.A.; Adrain, C.; Martin, S.J. Executioner caspase-3, -6, and -7 perform distinct, non-redundant roles during the demolition phase of apoptosis. *J. Biol. Chem.* **2001**, *276*, 7320–7326. [CrossRef] [PubMed]

52. Yang, Y.; Zhao, S.; Song, J. Caspase-dependent apoptosis and -independent poly(ADP-ribose) polymerase cleavage induced by transforming growth factor beta1. *Int. J. Biochem. Cell Biol.* **2004**, *36*, 223–234. [CrossRef]
53. Cheng, Z.; DiMichele, L.A.; Rojas, M.; Vaziri, C.; Mack, C.P.; Taylor, J.M. Focal adhesion kinase antagonizes doxorubicin cardiotoxicity via p21(Cip1.). *J. Mol. Cell. Cardiol.* **2014**, *67*, 1–11. [CrossRef] [PubMed]
54. Cheng, Z.; DiMichele, L.A.; Hakim, Z.S.; Rojas, M.; Mack, C.P.; Taylor, J.M. Targeted focal adhesion kinase activation in cardiomyocytes protects the heart from ischemia/reperfusion injury. *Arterioscler. Thromb. Vasc. Biol.* **2012**, *32*, 924–933. [CrossRef] [PubMed]
55. Thomas, S.A.; Thamkachy, R.; Ashokan, B.; Komalam, R.J.; Sreerekha, K.V.; Bharathan, A.; Santhoshkumar, T.R.; Rajasekharan, K.N.; Sengupta, S. Diaminothiazoles inhibit angiogenesis efficiently by suppressing Akt phosphorylation. *J. Pharmacol. Exp. Ther.* **2012**, *341*, 718–724. [CrossRef] [PubMed]

Sample Availability: Samples of the compounds neferine and temozolomide are not available from the authors.

molecules

MDPI

Article

Tumidulin, a Lichen Secondary Metabolite, Decreases the Stemness Potential of Colorectal Cancer Cells

Yi Yang [1,2,3], Suresh R. Bhosle [1], Young Hyun Yu [1], So-Yeon Park [1], Rui Zhou [1], İsa Taş [1,2], Chathurika D. B. Gamage [1,2], Kyung Keun Kim [3], Iris Pereira [4], Jae-Seoun Hur [2,*], Hyung-Ho Ha [1,*] and Hangun Kim [1,*]

[1] College of Pharmacy, Sunchon National University, 255 Jungang-ro, Sunchon, Jeonnam 57922, Korea; yangyi_520@hotmail.com (Y.Y.); bhoslesuresh1005@gmail.com (S.R.B.); chmyyh@gmail.com (Y.H.Y.); sinbu17@naver.com (S.-Y.P.); zhourui274@hotmail.com (R.Z.); mr.isatas@gmail.com (İ.T.); chathurika.gamage@gmail.com (C.D.B.G.)

[2] Korean Lichen Res. Institute, Sunchon National University, 255 Jungang-ro, Sunchon, Jeonnam 57922, Korea

[3] Medical Research Center for Gene Regulation, Brain Korea 21 Project, Chonnam National University Medical School, 160 Baekseo-ro, Dong-gu, Gwangju 61469, Korea; kimkk@chonnam.ac.kr

[4] Institute of Biological Sciences, Universidad de Talca, Talca 747-721, Chile; ipereira@utalca.cl

* Correspondence: jshur1@sunchon.ac.kr (J.-S.H.); hhha@sunchon.ac.kr (H.-H.H.); hangunkim@sunchon.ac.kr (H.K.); Tel.: +82-61-750-3383 (J.-S.H.); +82-61-750-3754 (H.-H.H.); +82-61-750-3761 (H.K.)

Academic Editor: Roberto Fabiani

Received: 9 October 2018; Accepted: 12 November 2018; Published: 14 November 2018

Abstract: Lichens produce various unique chemicals that are used in the pharmaceutical industry. To screen for novel lichen secondary metabolites that inhibit the stemness potential of colorectal cancer cells, we tested acetone extracts of 11 lichen samples collected in Chile. Tumidulin, isolated from *Niebla* sp., reduced spheroid formation in CSC221, DLD1, and HT29 cells. In addition, mRNA expressions and protein levels of cancer stem markers aldehyde dehydrogenase-1 (ALDH1), cluster of differentiation 133 (CD133), CD44, Lgr5, and Musashi-1 were reduced after tumidulin treatment. Tumidulin decreased the transcriptional activity of the glioma-associated oncogene homolog zinc finger protein (Gli) promoter in reporter assays, and western blotting confirmed decreased Gli1, Gli2, and Smoothened (SMO) protein levels. Moreover, the tumidulin activity was not observed in the presence of Gli and SMO inhibitors. Together, these results demonstrate for the first time that tumidulin is a potent inhibitor of colorectal cancer cell stemness.

Keywords: lichen; secondary metabolites; tumidulin; stemness potential; colorectal cancer cells; oncogene; transcriptional regulation

1. Introduction

Colorectal cancer (CRC) is one of the most commonly diagnosed cancers worldwide [1], and its high mortality rate has made it a priority in clinical cancer therapy [2]. Large numbers of CRC patients present with metastatic disease [3], and the 5-year survival rate is only 12.5% [3]. Furthermore, resistance to chemotherapy occurs in 90% of patients with metastatic cancer, and this is believed to be the main reason for treatment failure, despite the development of numerous therapeutic agents targeting CRC in the past decade [4]. Mounting evidence indicates that cancer stem cells (CSCs) contribute to chemotherapy resistance [5–7], and recent studies suggest that the efficiency of chemotherapy could be improved by exploiting the therapeutic opportunities provided by the molecular properties of CSCs. Cluster of differentiation (CD) 133 [8,9], CD44 [10], and leucine-rich repeat-containing G-protein coupled receptor 5 (LGR5) [11] are colorectal CSC markers related to

proliferation, invasion, metastasis, and chemoresistance, and aldehyde dehydrogenase (ALDH) activity has been linked to the mechanism of chemoresistance in CSCs [12]. Therefore, it is important to seek new therapeutic strategies targeting CSC-like properties.

The extensive chemical diversity of lichen secondary metabolites makes them a powerful natural resource for candidate pharmaceutical reagents. In a previous study, we described the wide pharmaceutical application of lichen bioresources in anti-cancer chemotherapy reagent screening [13–16]. However, no attempt has been made to screen anti-cancer activity based on CSC-like traits, which has the potential to identify more efficient chemotherapeutic agents. Therefore, in the present work, we examined the inhibitory activity of 11 lichen species from Chile against the stemness potential of CRC cells, and investigated the possible molecular mechanisms underlying this inhibitory activity to identify novel compounds that could lower the chemoresistance of target therapeutic drugs.

2. Results

2.1. Acetone Extracts of Lichens Collected in Chile Inhibit CRC Cell Stemness

The self-renewing ability of cancer stem cells (CSCs) can result in resistance to targeted therapies. To identify inhibitory substances among lichen secondary metabolites, Gli luciferase activity was tested against 11 acetone extracts of Chilean lichen thalli for in the NIH 3T3 cell line in which a Gli reporter gene was stably incorporated. For this, 5 μg/mL concentration of extracts was tested as cytotoxicity was not observed at this concentration (Figure S1). As shown in Figure 1a, *Niebla* sp. (1) and *Niebla* sp. (4) both inhibited Gli-luc activity at a concentration of 5 μg/mL. To further check whether the above lichen extracts possessed inhibitory activity against the spheroid formation ability of CSC221 cells (human colorectal adenocarcinoma-enriched cancer stem cells [17]), spheroid formation assays were performed using ultra-low attachment 24-well plates with serum-free medium. As shown in Figure 1b, the number of spheroids in cells treated with acetone extracts was lower than in dimethyl sulfoxide (DMSO)-treated controls, and quantitative analysis revealed that the differences were significant (Figure 1c). These results showed that acetone extracts of *Niebla* sp. (1) and *Niebla* sp. (4) exhibited inhibitory activity against colorectal cancer (CRC) cell stemness.

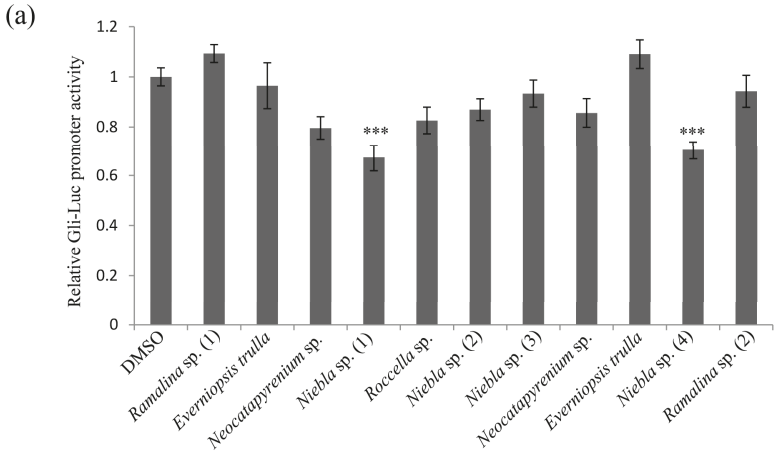

Figure 1. *Cont.*

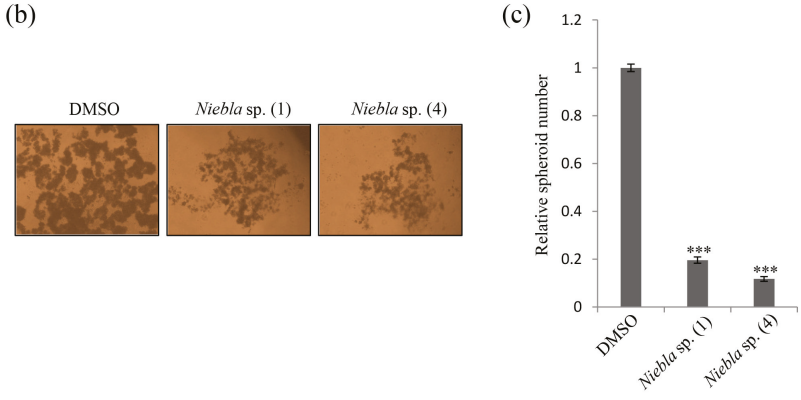

Figure 1. Acetone extracts of lichens collected in Chile decrease CSC221 cell stemness. (**a**) Quantitative analysis of Gli-luc reporter assays of NIH 3T3 cells (stably incorporating Gli-dependent firefly luciferase and constitutive Renilla luciferase reporters) treated with 5 μg/mL acetone extracts of *Ramalina* sp. (1), *Everniopsis trulla*, *Neocatapyrenium* sp., *Niebla* sp. (1), *Roccella* sp., *Niebla* sp. (2), *Niebla* sp. (3), *Neocatapyrenium* sp., *Everniopsis trulla*, *Niebla* sp. (4), and *Ramalina* sp. (2) for 48 h. (**b**) Representative images of spheroid formation of CSC221 cells treated with extracts of *Niebla* sp. (1) or *Niebla* sp. (4) for 14 days. (**c**) Quantitative analysis of the number of spheroids following each treatment. Quantitative data were obtained from three independent experiments ($n = 3$). Data represent mean ± standard error of the mean (SEM), and analysis was performed by one-way ANOVA. *** $p < 0.001$ compared with dimethyl sulfoxide (DMSO)-treated CSC221 cells.

2.2. Tumidulin, A Lichen Secondary Metabolite from Niebla sp., Inhibits CRC Cell Stemness

The chemical compounds isolated from *Niebla* sp. (1; CH130494) and *Niebla* sp. (4; CH130414) were almost identical according to the results of thin layer chromatography (TLC) (Figure S2); hence *Niebla* sp. (1) was chosen for subsequent research. To investigate the active compounds possessing inhibitory activity against CRC cell stemness, an acetone extract of *Niebla* sp. (1) was analyzed by high-performance liquid chromatography (HPLC) (Figure 2a), and the three main fractions were collected and tested in Gli-luc reporter assays using NIH 3T3 cell lines. The fraction II decreased Gli-luc activity in a dose-dependent manner comparable to crude extract (Figure 2b). This active fraction was therefore used for purification and structural identification of active components. The active, purified fraction was confirmed as tumidulin (molecular weight = 401.192 g/mol, purity > 99%) by liquid chromatography-mass spectrometry (LC-MS) and nuclear magnetic resonance (NMR) analyses (Figure 2c; Figures S3–S7 in File S1). The 3-(4,5-dimethylthiazol-2-yl)-2,5-diphenyltetrazolium bromide (MTT) assay revealed that cell viability was not significantly affected by tumidulin on CSC221 cells at less than 5 μg/mL (= 12.5 μM) concentration (Figure 2d). These results indicate that tumidulin is the active compound responsible for the inhibitory activity against CRC cell stemness in the *Niebla* sp. (1) acetone extract.

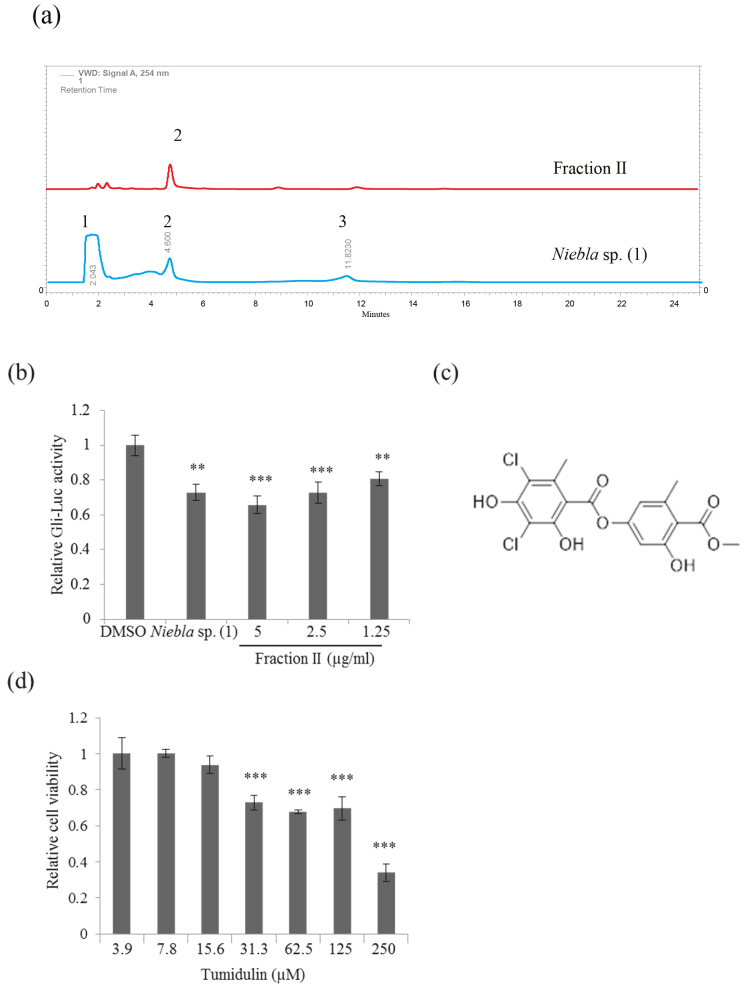

Figure 2. Tumidulin is an active lichen secondary metabolite from *Niebla* sp. (1) that inhibits CSC221 cell stemness. (**a**) High-performance liquid chromatography (HPLC) analysis of the inhibitory activity of stemness in CSC221 cells by crude and active *Niebla* sp. (1) fractions using a methanol:water:phosphoric acid (80:20:1, *v*/*v*/*v*) solvent system. (**b**) Quantitative analysis of reporter assays of NIH 3T3 cells treated with a 5 µg/mL acetone extract of *Niebla* sp. and various concentrations of the active (tumidulin) fraction for 48 h. (**c**) Chemical structure of tumidulin. (**d**) Relative viability of CSC221 cells treated with tumidulin for 48 h by MTT assay. Quantitative data were obtained from three independent experiments ($n = 3$). Data represent mean ± SEM, and analysis was performed by one-way ANOVA. ** $p < 0.01$ and *** $p < 0.001$ compared with DMSO-treated CSC 221 cells.

2.3. Tumidulin Inhibits Spheroid Formation in CRC Cells

To further confirm the CRC cell stemness inhibitory activity of tumidulin, the reduction in cancer stemness by acetone crude extracts of *Niebla* sp. (1) and tumidulin was evaluated by measuring spheroid formation in various CRC cell lines. As shown in Figure 3a, the number of spheroids following treatment with a 5 µg/mL crude extract of *Niebla* sp. (1) and various concentrations of tumidulin was significantly less than in DMSO-treated control cells for all CRC cell lines tested, including CSC221,

DLD1, and HT29 cells. However, their profiles at the same concentrations exhibited some differences. Tumidulin did not inhibit spheroid formation in CSC221 cells at 1.25 μg/mL (= 3.1 μM), but it did decrease the spheroid number in the other two CRC cell lines (DLD1 and HT29). Quantitative analysis confirmed that tumidulin inhibited spheroid formation in a dose-dependent manner for all three CRC cells ($EC_{50\ CSC221}$ = 2.609 μg/mL = 6.523 μM; $EC_{50\ DLD1}$ = 1.926 μg/mL = 4.815 μM; $EC_{50\ HT29}$ = 1.944 μg/mL = 4.860 μM) (Figure 3b,c). It should be noted that cell viability was not significantly affected by acetone extracts of *Niebla* sp. (1) and tumidulin on tested CRC cells at 12.5 μM (= 5 μg/mL) concentration (Figure S8), suggesting that cell death or blockade of cell proliferation is not involved in these effects. Taken together, these results indicate that tumidulin decreased the stemness of CRC cells.

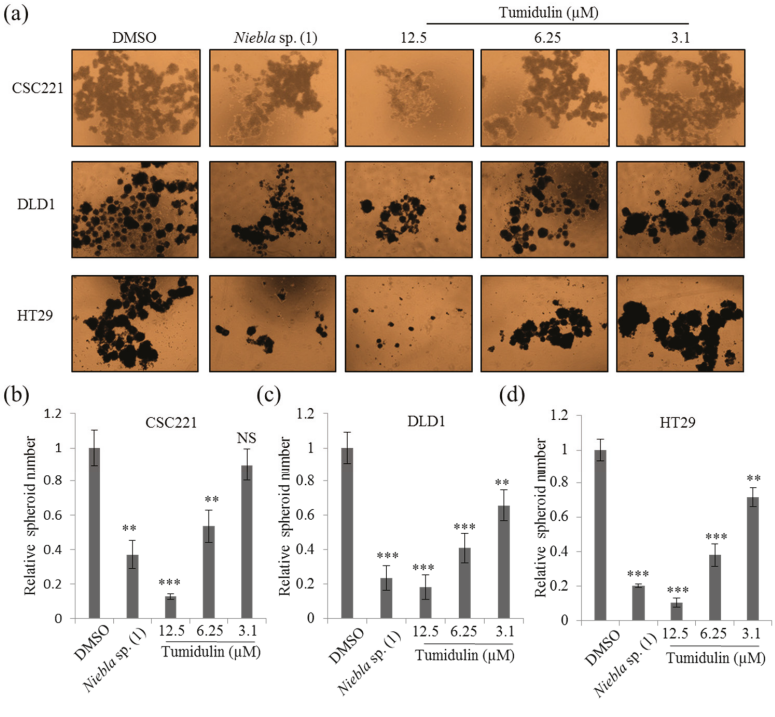

Figure 3. Effects of crude acetone extracts of *Niebla* sp. (1) and tumidulin on spheroid formation of colorectal cancer (CRC) cells. CRC cells were treated with crude extracts of *Niebla* sp. (1) and various concentrations of tumidulin. After 14 days incubation, spheroid formation of CRC cells was calculated as described in the Materials and Methods. (**a**) Representative images of spheroid formation of CSC221, DLD1, and HT29 cells following treatment with crude extracts of *Niebla* sp. (1) and the purified tumidulin fraction at the indicated concentrations. (**b**–**d**) Quantitative spheroid assay data following treatment of CSC221 (**b**), DLD1 (**c**), and HT29 (**d**) cells with crude extracts of *Niebla* sp. (1) and the purified tumidulin fraction. Quantitative data were obtained from three independent experiments (n = 3). Data represent mean ± SEM, and analysis was performed by one-way ANOVA. ** $p < 0.01$; *** $p < 0.001$; NS: no significant difference compared with DMSO-treated CRC cells.

2.4. Tumidulin Decreases Cancer Stem Markers

ALDH1, CD133, CD44, Lgr5, and Msi-1 are markers for the acquisition of cancer stemness. Since tumidulin inhibited spheroid formation in CRC cells (Figure 3), we hypothesized that the expression of CSC markers could be downregulated at compound concentrations at which spheroid formation was reduced. To investigate whether tumidulin affected the expression of cancer stemness

markers in CRC cells, mRNA expressions and protein levels of ALDH1, CD133, CD44, Lgr5, and Msi-1 were measured by qRT-PCR and western blotting, respectively. As shown in Figure 4a,b, the inhibitory activity of tumidulin was similar to that of the crude acetone extract of *Niebla* sp. (1), and it reduced mRNA expressions and protein levels of all five cancer stem markers at concentrations of 2.5 and 5 μg/mL (= 6.25 and 12.5 μM).

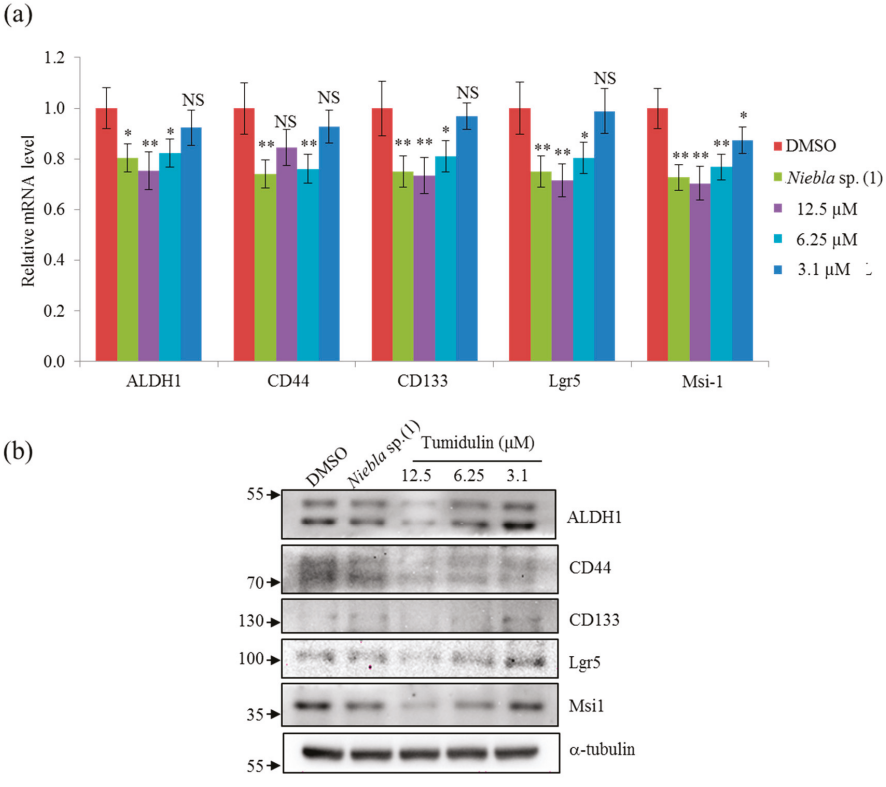

Figure 4. Effects of crude extracts of *Niebla* sp. (1) and tumidulin on cancer stemness-related gene expression and protein level. CSC221 cells were treated with 5 μg/mL acetone extracts of *Niebla* sp. (1) or various concentrations of tumidulin for 48 h. (**a**) Quantitative analysis of mRNA expression levels of cancer stem markers aldehyde dehydrigebase-1 (ALDH1), cluster of differentiation 133 (CD133), CD44, Lgr5, and Musashi-1. Data represent mean ± SEM, and analysis was performed by one-way ANOVA. * $p < 0.05$; ** $p < 0.01$; NS: no significant difference compared with DMSO-treated CSC221 cells. (**b**) Representative immunoblots are shown with the indicated antibodies.

2.5. Tumidulin Reduces Gli and SMO Protein Levels

To identify target signaling pathways involved in the inhibition of cancer stemness by tumidulin, reporter assays were performed using the HEK293T cell line transfected with Gli-luc, TOPFLASH-luc, and Hes-1-luc genes conjugated with firefly plasmids. Based on the relative values calculated with Renilla luciferase as an internal control, only Gli-luc activity was downregulated significantly by tumidulin treatment in a dose-dependent manner (Figure 5a–c). Since Gli is the main transcription factor in the sonic hedgehog (SHH) signaling pathway, this pathway is likely involved in the reduction of CRC stemness by tumidulin treatment. These results suggest that tumidulin might decrease CRC cancer stemness by downregulating the expression of CSC markers and inhibiting Gli transcription.

To confirm the involvement of the SHH signaling pathway in the CRC stemness reduction activity of tumidulin, Gli1/2, and smoothened (SMO) protein levels were measured. As shown in Figure 5d,f, both Gli1 and Gli2 protein levels were significantly downregulated by tumidulin at a concentration of 2.5 or 5 μg/mL (= 6.25 or 12.5 μM) in the CSC221 cell line. The Gli2 protein was decreased to a greater extent than Gli1 based on the quantification results shown in Figure 5f. Furthermore, SMO protein levels were also reduced by tumidulin treatment at 2.5 or 5 μg/mL (= 6.25 or 12.5 μM) (Figure 5e,g). These Gli proteins are the terminal effectors of SHH signaling, and SMO is a transcriptional regulator that acts upstream of the canonical hedgehog (Hh) pathway [18]. Together, these results suggest that tumidulin inhibits the Hh signaling pathway by suppressing Gli and SMO.

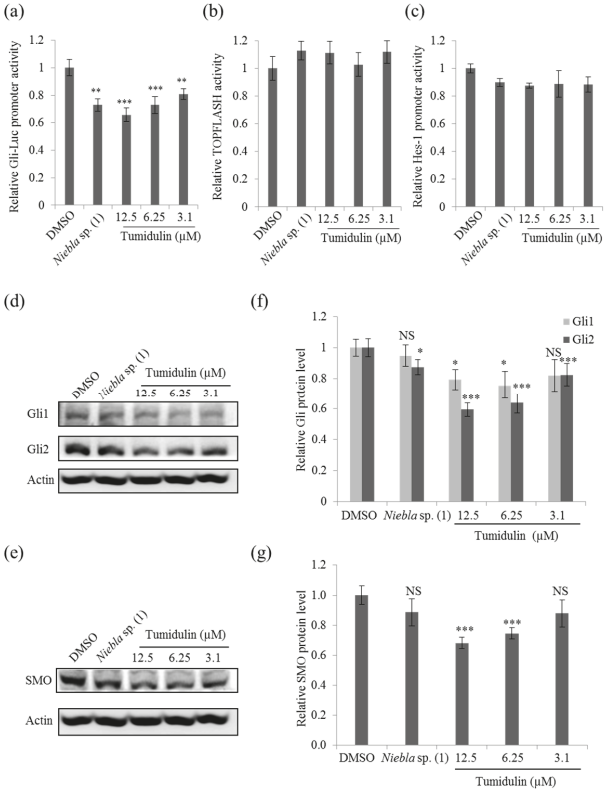

Figure 5. Effects of crude acetone extracts of *Niebla* sp. (1) and tumidulin on transcription factor activity and the expression of proteins related to cancer stemness. (**a**–**c**) Relative activities of promoters related to Hedgehog, Wnt, and Notch signaling pathways. HEK293T cells were co-transfected with the pRL-TK (Renilla) plasmid and the pGli-luc (**a**), pTOPFLASH (**b**), and pHES-luc (**c**) reporter plasmids (firefly). After 12 h, transfected cells were treated with crude extracts of *Niebla* sp. (1) or various concentrations of tumidulin and incubated for an additional 48 h. The relative firefly luciferase activity of treated vs. control groups is shown. Quantitative data were obtained from at least two independent experiments. (**d**–**g**) CSC221 cells were treated with 5 μg/mL *Niebla* sp. (1) or various concentrations of tumidulin. After incubation for 48 h, cells were lysed and total protein was subjected to immunoblot analyses with the indicated antibodies. (**d**,**e**) Representative immunoblots of Gli1/2 (**d**) and SMO (**e**). (**f**,**g**) Relative protein levels of Gli1/2 (**f**) and SMO (**g**) compared with the untreated group. Data represent the mean ± SEM, and analysis was performed by one-way ANOVA. * $p < 0.05$; ** $p < 0.01$; *** $p < 0.001$; NS: no significant difference compared with DMSO-treated CSC221 cells.

2.6. Tumidulin Activity on Reducing ALDH1 Expression is Gli and SMO Dependent

To confirm the involvement of the Gli and SMO in the CRC stemness reduction activity of tumidulin, the mRNA expression level of ALDH1 were measured in the presence of Gli and SMO inhibitors [18]. As shown in Figure 6, Gli inhibitor (GANT61) and SMO inhibitor (GDC-0449) treatment decreased the mRNA expression of ALDH1, and GANT61 which targets downstream of pathway reduced the mRNA expression more than those of GDC-0449. In the presence of these inhibitors, tumidulin did not further decrease the ALDH1 expression, suggesting that the activity of tumidulin is dependent on Gli and SMO (Figure 6). Given the extent of reduction in ALDH1 expression (Figure 4), tumidulin seems to act upstream of the pathway. mTOR inhibition by rapamycin has been reported to decreased pancreatic cancer stem cell population [19]. However, treatment of rapamycin did not affect the ALDH1 expression in CSC221 cells, and tumidulin decreased the ALDH1 expression in the presence of rapamycin (Figure 6), suggesting that the activity of tumidulin is independent on mTOR pathway. Together, these results showed that the lichen secondary metabolite tumidulin decreases CRC cell stemness by inhibiting the Hh signaling pathway, and has great potential for therapeutics development.

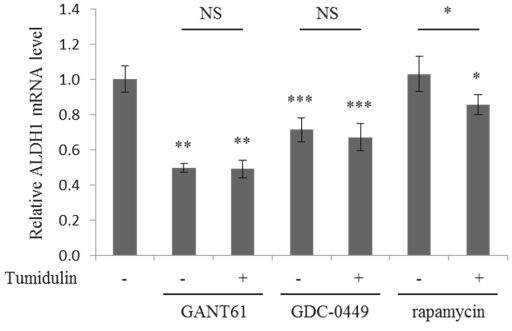

Figure 6. Effects of tumidulin on mRNA expression levels of ALDH1 in the presence of Gli, SMO, and mTOR inhibitors. CSC221 cells were treated with 5 μg/mL GANT61 (Gli inhibitor), GDC-0449 (SMO inhibitor), and rapamycin (mTOR inhibitor) together with or without 12.5 μM tumidulin for 48 h. Quantitative analysis of mRNA expression level of ALDH1 were presented as mean ± SEM, (*n* = 3). Analysis was performed by one-way ANOVA. * $p < 0.05$; ** $p < 0.01$; *** $p < 0.001$; NS: no significant difference compared with DMSO-treated CSC221 cells or between indicated groups.

3. Discussion

Numerous novel chemicals isolated from lichens display anti-cancer activity and show great potential for pharmaceutical usage. In the present study, the active chemical compound tumidulin was isolated from the lichen *Niebla* sp. from Chile, and found to exhibit inhibitory activity against CRC cell stemness. Tumidulin, also known as methyl 3,5-dichlorolecanorate, was first discovered in *Ramalina ceruchis* var. *tumidula* [20,21]. However, surprisingly, this compound could not be found in the type specimen, and as previously reported, many specimens of *Vermilacinia* were erroneously claimed to contain methyl 3,5-dichlorolecanorate [22]. In the present work, we isolated tumidulin from the lichen *Niebla* sp., and found that (1) this lichen secondary metabolite displays inhibitory activity against CRC stemness, (2) mRNA levels of several cancer stem markers including ALDH1, CD133, CD44, Lgr5, and Musashi-1 are downregulated by tumidulin treatment, and (3) the Hh signaling pathway is involved in the suppression of Gli and SMO protein levels by tumidulin treatment. These results indicate that tumidulin inhibits CRC stemness and has great pharmaceutical potential.

Since tumidulin was confirmed to decrease CRC cell stemness, several major signaling pathways related to this phenomenon, including Gli-mediated Hh, β-catenin-mediated Wnt, and Hes-1-mediated Notch signaling, were investigated using reporter assays. The Gli, TOPFLASH, and Hes-1 promoters

were tested using firefly luciferase gene-conjugated plasmid transfection, and only Gli-luc activity was downregulated by tumidulin treatment, suggesting that Hh signaling may be involved in the inhibition of CRC stemness by tumidulin treatment. The Hh signaling pathway is a major regulator of cell differentiation, cell proliferation, and tissue polarity, and aberrant activation of the Hh signaling pathway is involved in various types of human cancers [18]. The gene encoding Gli was the first Hh signaling pathway gene found to be upregulated in human glioblastoma and derivative cell lines [23]. In the present study, Gli1/2 and SMO protein levels were downregulated following tumidulin treatment, which further confirmed that tumidulin decreases CRC cell stemness via suppression of the Hh signaling pathway. However, our results cannot determine whether other signaling pathways are involved in the downregulation of Gli protein expression, since Gli can be activated via both Hh-dependent and Hh-independent signaling pathways [18]. Thus, the exact molecular mechanisms require further investigation.

Together, the results of the present study suggest that tumidulin has great potential for development of a CRC cell stemness inhibitor, and further demonstrate the wide application of lichen bioresources for pharmaceutical reagent screening.

4. Materials and Method

4.1. Preparation of Lichen Extracts

Thalli of lichens were collected in 2013 during field trips in the National Park of Torres Del Paine, Patagonia, Chile, organized by Dr. Pereira from Talca University, Talca, Chile. The permit to collect lichen specimens from this location was issued by the Administration of the National Forestry Corporation (CONAF) of Punta Arenas, and the Administration of the National Park Torres del Paine, Magallanes Region and Chilean Antarctic, which is part of the National System of Protected Wild Areas of the State of Chile. Field studies did not involve any endangered or protected species. Duplicate samples have been deposited at the Korean Lichen and Allied Bioresource Center (KOLABIC) in the Korean Lichen Res. Institute (KoLRI), Sunchon National University, Korea. The dried thalli of the lichens were extracted with acetone then filtered and dried in rotary vacuum evaporator at 45 °C (Heidolph Instruments GmBH & CO, Schwabach, Germany). The dry extracts were dissolved in dimethyl sulfoxide (DMSO, Sigma-Aldrich, St. Louis, MO, USA) for further experiment use.

4.2. High-Performance Liquid Chromatography (HPLC) Analysis of Lichen Material

Acetone extracts of lichen thalli at a concentration of 5 mg/mL were subjected to high-performance liquid chromatography (HPLC) analysis using an Agilent 1260 instrument (Agilent Technology, Santa Clara, CA, USA) equipped with a YMC-Pack ODS reversed-phase column A (150 × 4.6 mm internal diameter) containing fully end-capped C18 material (particle size = 5 µm, pore size = 12 nm). Elution was performed at a flow rate of 1 mL/min with a solvent system of methanol:water:phosphoric acid (80:20:1, $v/v/v$) at a column temperature of 40 °C. Separation was monitored using an Agilent 1260 Infinity II Variable Wavelength Detector (1260 VWD; Agilent Technology) over a range of 190–800 nm. Observed peaks were detected at 254 nm. The sample injection volume was 50 µL. Salazinic acid (t_R = 2.27 ± 0.2 min) isolated from the lichen *Lobaria pulmonaria* was used as a standard, and voucher specimens were deposited in the herbarium of KOLABIC at the KoLRI, Sunchon National University, Korea.

4.3. Separation and Identification of Tumidulin

Niebla sp. (1; CL130494) extract was separated by HPLC as described above, and the fraction identified as tumidulin was collected. The supernatant was dried and weighed after centrifugation, and the HPLC assay was performed to confirm that the purified sample yielded a single peak. The structure of tumidulin was then confirmed by liquid chromatography-mass spectrometry (LC-MS, Shimadzu

Corporation, Kyoto, Japan; Figure S2) and nuclear magnetic resonance (NMR, JEOL Ltd., Tokyo, Japan) analysis (Figures S3 and S4 in File S1).

4.4. Cell Culture and Reagents

The human colon cancer cell lines CSC221 (human colorectal adenocarcinoma-enriched CSCs [17]), DLD1, HT29 (CRC cells), and HEK293T (human embryonic kidney cells) were used in this study. Cells were cultured in Dulbecco's modified Eagle's medium (DMEM) supplemented with 10% fetal bovine serum and 1% penicillin-streptomycin solution under a humidified 5% CO_2 atmosphere at 37 °C in an incubator. GDC-0449 (Vismodegib, A10258) was purchased from AdooQ Bioscience (Irvine, CA, USA). GANT61 (G9048) and rapamycin (R8781) were purchased from Sigma-Aldrich.

4.5. Reporter Assay

HEK293T cells were transfected with Gli-luc, TOPFLASH-luc, and Hes-1-conjugated firefly plasmid, together with Renilla-luc (pRL-TK) plasmid, using X-treme GENE 9 DNA transfection reagent (Roche, Werk Penzberg, Germany). At 12 h after transfection, cells were treated with crude *Niebla* sp. acetone extract, tumidulin, or 0.01% DMSO and incubated for 48 h at 37 °C under 5% CO_2. Normalized luciferase activity was obtained against Renilla activity to determine the transfection efficiency using a Dual-Luciferase reporter assay system (Promega, Madison, WI, USA).

4.6. Spheroid Assay

Cells were trypsinized then rinsed with N2-supplemented DMEM/F12 (Invitrogen, Carlsbad, CA, USA) having human recombinant epidermal growth factor (hrEGF; 20 ng/mL; Biovision, Atlanta, GA, USA) and human basic fibroblast growth factor (hbFGF; 10 ng/mL; Invitrogen) and then seeded at a density of 1×10^4 cells/well in ultra-low attachment 24-well plates (Corning Inc., Corning, NY, USA). After 14 days of culture, spheres were quantitated by inverted phase contrast microscopy (Nikon, Kawasaki, Japan). The IMT iSolution software (IMT iSolution Inc., Northampton, NJ, USA) was used to measure the pixel intensity of the sphere area from random microscope views in each plate. To measure the percentage area of spheres, normalization of the number of pixels in the sphere area was done by multiplying the given pixels by the pixel squares. Data are presented as the average of three independent experiments.

4.7. MTT Assay

Cells were seeded at a density of 2.5×10^3 cells/well in 96-well plates, grown overnight, and then treated with the lichen acetone extracts or pure active fraction for 48 h. All the tested samples were dissolved in DMSO and diluted with DMEM to obtain indicated concentrations. The 3-(4,5-dimethylthiazol-2-yl)-2,5-diphenyltetrazolium bromide (MTT) was added and maintained for 4 h once treatment was completed. DMSO was added after removing the medium. Absorbance at 540 nm was determined using a microplate reader with Gen 5 (2.03.1) software (BioTek, Winooski, VT, USA).

4.8. Western Blotting

Cells treated with DMSO, *Niebla* sp. (1), or tumidulin for 48 h were washed twice with ice-cold phosphate-buffered saline (PBS) and lysed in lysis buffer [24]. Antibodies against ALDH1, CD44, CD133, Lgr5, Msi1, and α-tubulin were used as previously described [17]. Antibodies against Gli1 (sc-20687; SANTA CRUZ, Dallas, TX, USA), Gli2 (sc-271786; SANTA CRUZ), Smoothened (SMO; ab72130; Abcam, Cambridge, MA, USA), and β-Actin (sc-47778; SANTA CRUZ) were detected with horseradish peroxidase-conjugated secondary antibody (Thermo Fisher Scientific, Waltham, MA, USA) using an Immobilon Western Chemiluminescent HRP Substrate Kit (Merck Millipore, Billerica, MA, USA) and luminescence imaging on an Image Quant LAS 4000 mini. Bands were

measured using Multi-Gauge 3.0 software, and the relative density was calculated based on the density of the β-actin bands in each sample. Values are expressed as arbitrary densitometric units corresponding to signal intensity.

4.9. Quantitative Reverse-Transcription PCR (qRT-PCR)

All quantitative reverse-transcription PCR (qRT-PCR) assays were performed as previously described [25]. Briefly, RNA (1 mg) isolated from CSC221 cells treated with DMSO, *Niebla* sp. (1), or tumidulin for 48 h using RNAiso Plus (TaKaRa, Otsu, Shiga 520-2193, Japan) was converted to cDNA using a M-MLV Reverse Transcriptase Kit (Invitrogen) and SYBR green (Enzynomics, Seoul, Korea). Primers used for qRT-PCR were as follows: ALDH1 (forward) 5′-tgttagctcatgccgacttg-3′ and (reverse) 5′-ttcttagcccgctcaacact-3′; Msi-1 (forward) 5′-accaagagatccaggggttt-3′ and (reverse) 5′-tcgttcgagtcacc atcttg-3′; Lgr5 (forward) 5′-ctcttcctcaaaccgtctgc-3′ and (reverse) 5′-gatcggaggctaagcaactg-3′; CD44 (forward) 5′-tgccgctttgcaggtgtat-3′ and (reverse) 5′-ggcctccgtccgagaga-3′; CD133 (forward) 5′-ggacccattggcattctc-3′ and (reverse) 5′-caggacacagcatagaataatc-3′; GAPDH (forward) 5′-atcaccatcttc caggagcga-3′ and (reverse) 5′-agttgtcatggatgaccttggc-3′. All reactions and analyses were performed using CFX (Bio-Rad, Hercules, CA, USA).

4.10. Statistical Analysis

All experiments were assayed in triplicate ($n = 3$). Results are reported as mean ± standard error of the mean (SEM). All statistical analyses were performed using the SPSS version 17 (IBM, Chicago, IL, USA). Treatment effects were determined using one-way ANOVA post-hoc analysis. The level of significance was set at $p < 0.05$.

5. Conclusions

In summary, tumidulin was isolated from Chilean lichen *Niebla* sp. (1; CH130494). Tumidulin exhibited significant inhibitory activity on spheroid formation in CRC cells and decreased the expression of CSC markers in CRC cells. The inhibitory activity of tumidulin against colorectal cancer stemness is through regulation of Hedgehog signaling pathways.

Supplementary Materials: The following are available online.

Author Contributions: Y.Y., S.R.B., S.-Y.P., R.Z., İ.T., and C.D.B.G. performed the experiments. K.K.K. reviewed the study proposal and served as scientific advisor. I.P. and J.-S.H. provided the materials. H.-H.H. provided analysis tools for chemical purification of lichen extract and identification of tumidulin. Y.Y. and H.K. analyzed the data and wrote the manuscript. H.K. conceived and designed the experiments. All authors read and approved the final manuscript.

Funding: This work was supported by National Res. Foundation of Korea grants (NRF-2016R1C1B2007494, NRF-2015R1A4A1041219 to HK; and NRF-2018M3A9A8023762 to KKK; NRF-2018R1D1A1B07042608 to YY) funded by the Korea government (MSIP). This work was also supported by a grant from the Forest Science & Technology Projects (Project No. 2017024A00-1720-BA01 to JSH) funded by the Korea Forest Service.

Conflicts of Interest: The authors declare no conflict of interest.

References

1. Bhandari, A.; Woodhouse, M.; Gupta, S. Colorectal cancer is a leading cause of cancer incidence and mortality among adults younger than 50 years in the USA: A SEER-based analysis with comparison to other young-onset cancers. *J. Investig. Med.* **2017**, *65*, 311–315. [CrossRef] [PubMed]
2. Favoriti, P.; Carbone, G.; Greco, M.; Pirozzi, F.; Pirozzi, R.E.M.; Corcione, F. Worldwide burden of colorectal cancer: A review. *Updates Surg.* **2016**, *68*, 7–11. [CrossRef] [PubMed]
3. Siegel, R.; Ma, J.; Zou, Z.; Jemal, A. Cancer statistics, 2014. *CA Cancer J. Clin.* **2014**, *64*, 9–29. [CrossRef] [PubMed]
4. Longley, D.; Johnston, P. Molecular mechanisms of drug resistance. *J. Pathol.* **2005**, *205*, 275–292. [CrossRef] [PubMed]

5. Vidal, S.J.; Rodriguez-Bravo, V.; Galsky, M.; Cordon-Cardo, C.; Domingo-Domenech, J. Targeting cancer stem cells to suppress acquired chemotherapy resistance. *Oncogene* **2014**, *33*, 4451. [CrossRef] [PubMed]
6. Dylla, S.J.; Beviglia, L.; Park, I.-K.; Chartier, C.; Raval, J.; Ngan, L.; Pickell, K.; Aguilar, J.; Lazetic, S.; Smith-Berdan, S. Colorectal cancer stem cells are enriched in xenogeneic tumors following chemotherapy. *PLoS ONE* **2008**, *3*, e2428. [CrossRef]
7. Mertins, S.D. Cancer stem cells: A systems biology view of their role in prognosis and therapy. *Anti-Cancer Drugs* **2014**, *25*, 353. [CrossRef] [PubMed]
8. Elsaba, T.M.; Martinez-Pomares, L.; Robins, A.R.; Crook, S.; Seth, R.; Jackson, D.; McCart, A.; Silver, A.R.; Tomlinson, I.P.; Ilyas, M. The stem cell marker CD133 associates with enhanced colony formation and cell motility in colorectal cancer. *PLoS ONE* **2010**, *5*, e10714. [CrossRef] [PubMed]
9. Zhang, S.S.; Han, Z.P.; Jing, Y.Y.; Tao, S.F.; Li, T.J.; Wang, H.; Wang, Y.; Li, R.; Yang, Y.; Zhao, X.; et al. CD133(+)CXCR4(+) colon cancer cells exhibit metastatic potential and predict poor prognosis of patients. *BMC Med.* **2012**, *10*, 85. [CrossRef] [PubMed]
10. Wang, C.; Xie, J.; Guo, J.; Manning, H.C.; Gore, J.C.; Guo, N. Evaluation of CD44 and CD133 as cancer stem cell markers for colorectal cancer. *Oncol. Rep.* **2012**, *28*, 1301–1308. [CrossRef] [PubMed]
11. Hirsch, D.; Barker, N.; McNeil, N.; Hu, Y.; Camps, J.; McKinnon, K.; Clevers, H.; Ried, T.; Gaiser, T. LGR5 positivity defines stem-like cells in colorectal cancer. *Carcinogenesis* **2013**, *35*, 849–858. [CrossRef] [PubMed]
12. Abdullah, L.N.; Chow, E.K.-H. Mechanisms of chemoresistance in cancer stem cells. *Clin. Transl. Med.* **2013**, *2*, 3. [CrossRef] [PubMed]
13. Yang, Y.; Park, S.-Y.; Nguyen, T.T.; Yu, Y.H.; Van Nguyen, T.; Sun, E.G.; Udeni, J.; Jeong, M.-H.; Pereira, I.; Moon, C. Lichen secondary metabolite, physciosporin, inhibits lung cancer cell motility. *PLoS ONE* **2015**, *10*, e0137889. [CrossRef] [PubMed]
14. Yang, Y.; Nguyen, T.T.; Jeong, M.-H.; Crişan, F.; Yu, Y.H.; Ha, H.-H.; Choi, K.H.; Jeong, H.G.; Jeong, T.C.; Lee, K.Y. Inhibitory Activity of (+)-Usnic Acid against Non-Small Cell Lung Cancer Cell Motility. *PLoS ONE* **2016**, *11*, e0146575. [CrossRef] [PubMed]
15. Zhou, R.; Yang, Y.; Park, S.Y.; Nguyen, T.T.; Seo, Y.W.; Lee, K.H.; Lee, J.H.; Kim, K.K.; Hur, J.S.; Kim, H. The lichen secondary metabolite atranorin suppresses lung cancer cell motility and tumorigenesis. *Sci. Rep.* **2017**, *7*, 8136. [CrossRef] [PubMed]
16. Yang, Y.; Bae, W.K.; Nam, S.-J.; Jeong, M.-H.; Zhou, R.; Park, S.-Y.; Taş, İ.; Hwang, Y.-H.; Park, M.-S.; Chung, I.J. Acetonic extracts of the endolichenic fungus EL002332 isolated from Endocarpon pusillum exhibits anticancer activity in human gastric cancer cells. *Phytomedicine* **2018**, *40*, 106–115. [CrossRef] [PubMed]
17. Cho, Y.C.; Nguyen, T.T.; Park, S.Y.; Kim, K.; Kim, H.S.; Jeong, H.G.; Kim, K.K.; Kim, H. Bromopropane Compounds Increase the Stemness of Colorectal Cancer Cells. *Int. J. Mol. Sci.* **2017**, *18*, 1888. [CrossRef] [PubMed]
18. Rimkus, T.K.; Carpenter, R.L.; Qasem, S.; Chan, M.; Lo, H.W. Targeting the Sonic Hedgehog Signaling Pathway: Review of Smoothened and GLI Inhibitors. *Cancers* **2016**, *8*, 22. [CrossRef] [PubMed]
19. Miyazaki, Y.; Matsubara, S.; Ding, Q.; Tsukasa, K.; Yoshimitsu, M.; Kosai, K.; Takao, S. Efficient elimination of pancreatic cancer stem cells by hedgehog/GLI inhibitor GANT61 in combination with mTOR inhibition. *Mol. Cancer* **2016**, *15*, 49. [CrossRef] [PubMed]
20. Huneck, S. Flechteninhaltsstoffe, XXIV. Die Struktur von Tumidulin, einem neuen chlorhaltigen Depsid. *Chem. Ber.* **1966**, *99*, 1106–1110. [CrossRef]
21. Huneck, S.; Follmann, G. Über die Inhaltsstoffe von Ramalina ceruchis (ACH.) DE NOT. var tumidula (TAYL.) NYL. *Z. Naturforschung B* **1965**, *20*, 611–612. [CrossRef]
22. Spjut, R.W. *Niebla and Vermilacinia (Ramalinaceae) from California and Baja California*; BRIT Press: Fort Worth, TX, USA, 1996.
23. Kinzler, K.W.; Bigner, S.H.; Bigner, D.D.; Trent, J.M.; Law, M.L.; O'Brien, S.J.; Wong, A.J.; Vogelstein, B. Identification of an amplified, highly expressed gene in a human glioma. *Science* **1987**, *236*, 70–73. [CrossRef] [PubMed]

24. Kim, H.; Ki, H.; Park, H.S.; Kim, K. Presenilin-1 D257A and D385A mutants fail to cleave Notch in their endoproteolyzed forms, but only presenilin-1 D385A mutant can restore its gamma-secretase activity with the compensatory overexpression of normal C-terminal fragment. *J. Biol. Chem.* **2005**, *280*, 22462. [CrossRef] [PubMed]
25. Yang, Y.; Zhou, R.; Park, S.-Y.; Back, K.; Bae, W.K.; Kim, K.K.; Kim, H. 2-Hydroxymelatonin, a Predominant Hydroxylated Melatonin Metabolite in Plants, Shows Antitumor Activity against Human Colorectal Cancer Cells. *Molecules* **2017**, *22*, 453. [CrossRef] [PubMed]

Sample Availability: Samples of the compounds are available from the authors.

molecules

MDPI

Article

Quercetagetin and Patuletin: Antiproliferative, Necrotic and Apoptotic Activity in Tumor Cell Lines

Jesús J. Alvarado-Sansininea [1], Luis Sánchez-Sánchez [2], Hugo López-Muñoz [2], María L. Escobar [3], Fernando Flores-Guzmán [2], Rosario Tavera-Hernández [1] and Manuel Jiménez-Estrada [1,*]

[1] Laboratorio 2-10, Departamento de Productos Naturales, Instituto de Química, Universidad Nacional Autónoma de México, 04510 Ciudad de México, Mexico; javier33@comunidad.unam.mx (J.J.A.-S.); rosario.tavera@gmail.com (R.T.-H.)

[2] Laboratorio 6, 2do piso, UMIEZ, Facultad de Estudios Superiores Zaragoza, Universidad Nacional Autónoma de México, 09230 Ciudad de México, Mexico; luisss@unam.mx (L.S.-S.); hugolm@comunidad.unam.mx (H.L.-M.); molekulare@yahoo.com.mx (F.F.-G.)

[3] Laboratorio de Microscopía Electrónica, Departamento de Biología Celular, Facultad de Ciencias, Universidad Nacional Autónoma de México, 04510 Ciudad de México, Mexico; escobarluisa@ciencias.unam.mx

* Correspondence: manueljemex@gmail.com; Tel.: +52-(55)-56-22-44-30

Received: 22 August 2018; Accepted: 4 October 2018; Published: 9 October 2018

Abstract: Quercetagetin and patuletin were extracted by the same method from two different *Tagetes* species that have multiple uses in folk medicine in Mexico and around the globe, one of which is as an anticancer agent. Their biological activity (IC_{50} and necrotic, apoptotic and selective activities of these flavonols) was evaluated and compared to that of quercetin, examining specifically the effects of C6 substitution among quercetin, quercetagetin and patuletin. We find that the presence of a methoxyl group in C6 enhances their potency.

Keywords: necrotic; apoptosis; quercetin; quercetagetin; patuletin

1. Introduction

Cancer is one of the most severe public health problems worldwide. The urgent need to obtain new drugs to treat it arises from the fact that conventional treatments cause many side effects that negatively impact patients' quality of life. This has fostered the use of plant extracts and their metabolites as sources of active compounds [1]. Plants are still widely-used for medicinal purposes by the indigenous peoples in Mexico, and the biological activity of many plant derivatives has been evaluated and shown to have medicinal importance [2]. The genus *Tagetes* belongs to the family Asteraceae. It is highly-esteemed as an ornamental plant, and in some parts of the world is has ritual-cultural importance [3]. Several species of *Tagetes* are found in Mexico, some known commonly as Cempasuchil or Cempoalxochitl [4]. Two representative species are *Tagetes erecta* and *Tagetes patula* [5], both of which have important therapeutic potential due to their antiparasitic, antimalarial, anti-inflammatory, antitumorogenic and antiviral effects [6].

Tagetes flowers contain different classes of natural products [7], including terpenes, carotenoids and flavonoids, which are known to have pharmacological effects [8]. Differences in their molecular structures may be responsible for their different pharmacological properties [9]. Specifically, the genus *Tagetes* has many kinds of flavonoids [10]. Of these, quercetagetin and patuletin present distinct inhibitory activity [11]. In the present study, we implemented a method to obtain quercetagetin and patuletin from *Tagetes erecta* and *Tagetes patula*, respectively [12,13], and performed a structure-activity relationship (SAR) study [14], focused on their anticancer properties by comparing them to quercetin [15].

Flavonoids are polyphenolic compounds with a C_6-C_3-C_6 phenylbenzopyrone structure (Figure 1a) and they exhibit great structural diversity due to their various hydroxylation, methoxylation, glycosylation and acylation patterns [16]. The basic structure of the flavonoid nucleus has different substitution patterns in the A, B and C rings that result in various subgroups, one of which are the flavonols, which possess a 3-hydroxyflavone structure (Figure 1b). Examples of this type of flavonoid are the compounds quercetin, myricetin and kaempferol [17]. Flavonoids display diverse biological activities, including chemopreventive and chemotherapeutic effects on cancer. The following mechanisms of action have been reported: carcinogen inactivation, antiproliferation, cell-cycle arrest, induction of apoptosis, inhibition of angiogenic processes, modulation of multi-drug resistance, and antioxidative activity [18,19].

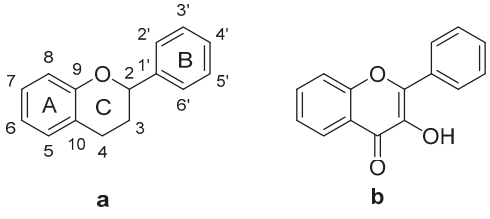

Figure 1. (**a**) Base structure of flavonoids; (**b**) Structure of flavonols.

Some structure-activity relationship studies have been conducted, and they indicate that the presence of the C2=C3 double bond and the hydroxylation pattern of flavonoids influence tumor proliferation modulation [20]. In this regard, research has shown that hydroxylated flavonoids possess stronger inhibitory activity on cancer cells than permethoxylated flavonoids, and that C3-hydroxylation is important for this activity. Apigenin, for example, which lacks a 3-OH group, presents lower antiproliferative activity than kaempferol [21]. The catechol group in ring B enhances anticancer activity [22]. There are few studies of substituents at C6 in relation to anticancer activity, but flavonols like quercetin, quercetagetin and patuletin all have the aforementioned structural characteristics that seem to be important for antiproliferative activity. The only difference among these compounds is the C6 group substituent, as quercetin has a C6-H, quercetagetin has a C6-OH, and patuletin has a C6-OMe (Figure 2). Given this background, the present study was designed to contribute to the study of the role of C6 substitution in ring A in the cytotoxic activity of flavonols like quercetin, quercetagetin and patuletin. The fact that some cancer cells show resistance to certain kinds of cell death can pose a problem for treatment success, so identifying and characterizing molecules that induce apoptosis or necrosis [23] will allow us to add new strategies to existing therapeutic approaches.

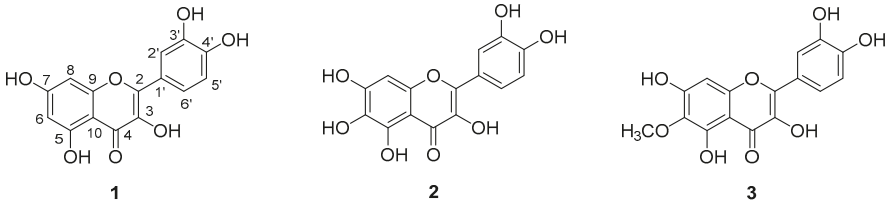

Figure 2. Structures of (**1**) quercetin, (**2**) quercetagetin and (**3**) patuletin.

2. Results

In the present study, quercetagetin (**2**) and patuletin (**3**) were isolated by the same method from different species of *Tagetes* plants. Upon comparing the structure of isolated compound **2** and quercetin, we found that they share a basic flavonol structure type and that the only difference is the substituent

group at the ring-A C6 position (Figure 2). These structures were confirmed by 1D and 2D NMR experiments that assigned the quercetagetin hydrogen and carbon positions.

2.1. Identification of Compounds **2** *and* **3**

Compound **2** was isolated as a yellow powder. The structure was elucidated and the compound identified as quercetagetin by 700 MHz 1D and 2D NMR experiments in DMSO-d_6. The ^{1}H-NMR spectrum displayed six hydroxyl proton signals and four aromatic proton signals at δ_H 7.66 (1H, d, J = 2.2 Hz, H-2′), 7.53 (1H, dd, J = 8.5, 2.2 Hz, H-6′), 6.88 (1H, d, J = 8.5 Hz, H-5′) and 6.49 (1H, s, H-8). This assignment disagrees with a previously reported one [13] because the HSQC experiment showed correlations between the protons mentioned above with the aromatic carbons at δ_c 115.05 (C-2′), 119.91 (C-6′), 115.03 (C-5′) and 93.22 (C-8). Additionally, the ^{13}C-NMR spectrum showed 15 signals corresponding to the base structure of flavonols and a signal at δ_c 175.84 corresponding to a carbonyl group (C-4). The other carbon atom assignments were made with the support of HMBC experiments (see Supplementary Material) and the corresponding correlations are shown in Figure 3. Complete assignments are listed in Table 1.

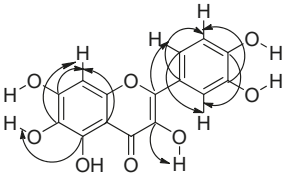

Figure 3. HMBC correlations of quercetagetin.

Table 1. ^{1}H and ^{13}C-NMR data of quercetagetin (**2**) and patuletin (**3**) (ppm).

2 [a]			**3**				
				Measured [b]		**Literature** [c]	
Position	**δ_c (J in Hz)**	**δ_H (J in Hz)**	**Position**	**δ_c (J in Hz)**	**δ_H (J in Hz)**	**δ_c (J in Hz)**	**δ_H (J in Hz)**
4	175.84		4	177.58		177.86	
5	153.58		9	158.46 [d]		158.76 [d]	
7	148.81		5	153.61 [d]		153.89 [d]	
4′	147.57		7	153.00 [d]		153.28 [d]	
2	146.64		4′	148.82		149.10	
6	145.88		2	148.28		148.56	
3′	145.04		3′	146.22		146.51	
3	135.32		3	136.96		137.25	
9	128.53		6	132.17		132.47	
1′	122.21		1′	124.14		124.43	
6′	119.91	7.53 (dd, J = 8.5, 2.2)	6′	121.72	7.64 dd (J = 8.5, 2.2)	122.02	7.65 dd (J = 8.4, 2.2)
5′	115.59	6.88 (d, J = 8.5)	2′	116.22	7.74 d (J = 2.2)	116.52	7.76 (J = 2.2)
2′	115.03	7.66 (d, J = 2.2)	5′	116.02	6.89 d (J = 8.5)	116.31	6.92 d (J = 8.5)
10	103.31		10	104.95		105.25	
8	93.22	6.49 (s)	8	94.70	6.50 s	95.00	6.52 s
			OCH_3	60.97	3.89 s	61.27	3.92 s
C5-OH		12.25 (s)					
C6-OH		10.48 (s)					
C3′-OH		9.55 (s)					
C4′-OH		9.28 (s)					
C3-OH		9.19 (s)					
C7-OH		8.65 (s)					

[a] 700 MHz, DMSO-d_6; [b] 700 MHz, CD_3OD; [c] 400 MHz, CD_3OD; [d] these values may be interchangeable.

The molecular formula of **2** was verified by HR-DART-MS as $C_{15}H_{11}O_8$ by an $[M + H]^+$ ion peak at m/z 319.04553, indicating the molecular formula was $C_{15}H_{10}O_8$. Compound **3** was isolated as a yellow powder and identified as patuletin. The HR-DART-MS of **3** showed a ion peak at m/z 333.6114 $[M + H]^+$ (calcd. for $C_{16}H_{13}O_8$: 333.06104) indicating the molecular formula was $C_{16}H_{12}O_8$. The structure was elucidated by 1D and 2D NMR experiments carried out at 700 MHz in CD_3OD,

and compared with the structure reported in [11] the displacements were very similar, however, the values of the quaternary carbons at δ_c 158.46, 153.61 and 153.00 could be interchangeable due to their proximity and the last two only correlate with the proton H-8 (δ_H 6.50). The ^{1}H-NMR spectrum displayed four aromatic protons signals at δ_H 7.74 (1H, d, J = 2.2 Hz, H-5′), 7.64 (1H, dd, J = 8.5, 2.2 Hz, H-6′), 6.89 (1H, d, J = 8.5 Hz, H-2′) and 6.50 (1H, s, H-8), methyl connected to an oxygen protons were displayed at δ_H 3.88 (OCH_3, s, 3H). The assignments of the carbons and protons of patuletin in comparison with NMR literature data are given in Table 1.

2.2. Antiproliferative Activity

To determine the concentration of flavonols required to inhibit the proliferation of CaSki, MDA-MB-231 and SK-Lu-1 by half (IC_{50}), 7500 cells were cultured for 24 h with 6, 12, 25, 50 and 100 µg/mL of quercetin, quercetagetin or patuletin. After 24 h, the number of cells was evaluated using crystal violet staining (Figure 4, Table 2).

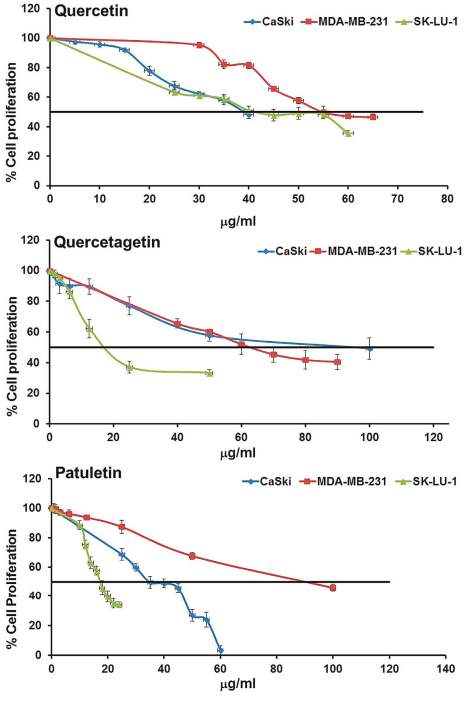

Figure 4. Dose-response curves of the antiproliferative effect of quercetin, quercetagetin and patuletin.

Table 2. Antiproliferative activity of the quercetin, quercetagetin and patuletin compounds in tumor cell lines [1].

Compound/Cell line	CaSki	MDA-MB-231	SK-LU-1
Quercetin	39 (129)	55 (129)	39 (181)
Quercetagetin	88 (276)	60 (188)	19 (59)
Patuletin	37 (111)	86 (258)	18 (54.17)

[1] IC_{50} µg/mL (µM).

Results showed a dose-dependent proliferation inhibition (Table 2). The IC_{50} values calculated were between 37 and 88 μg/mL (Table 2). It is interesting to note that the three cell lines showed different susceptibilities. The IC_{50} values of the three compounds for the SK-Lu-1 cell line suggest that they could be more effective for this particular type of cancer.

2.3. Necrotic Activity in Tumor Cells

The necrotic activity of quercetin, quercetagetin and patuletin was evaluated to determine whether they induce necrosis (Figure 5). CaSki, MDA-MB-231 and SK-Lu-1 cultures were exposed to the compounds at the aforementioned IC_{50} values, and the amount of LDH released into the culture supernatant after treatment was used as a measure of the loss of plasma-membrane integrity. In addition, the three cancer cell lines were treated with Triton X-100 in independent experiments, and the LDH released was adjusted to 100% to serve as a positive control. Our results show that quercetin and patuletin do not manifest necrotic cell death activity, as evidenced by the fact that the cellular decrease observed in the treated cultures was not a consequence of a necrotic process. This finding suggests that some other type of cell death, distinct from necrosis, was responsible for the decrease in the number of cells. In contrast, the amount of LDH released in the cells treated with quercetagetin did indicate significant necrotic activity (15–30%), suggesting that part of the decrease in the number of cells using this compound was due to a necrotic process. As a result, we would suggest that the structure of quercetagetin, which has a hydroxyl group in C6, could be important for this compound's necrotic activity. It is important to mention that there are no existing reports of necrotic activity in relation to any of these three molecules.

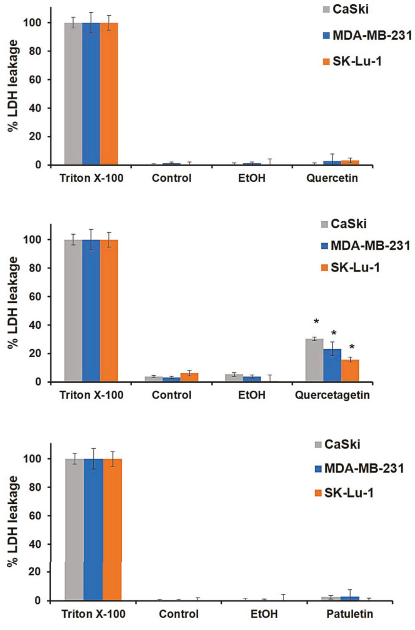

Figure 5. LDH activity induced by quercetin, quercetagetin and patuletin on CaSki, MDA-MB-231 and SK-Lu-1 cultures. In each case, 7500 cells/well were seeded in 96-well tissue culture plates. After 24 h, the medium was removed, and the cells were stimulated with the IC_{50} values for quercetin, quercetagetin and patuletin, or EtOH (10 μL/mL). The amount of lactate dehydrogenase (LDH) released into the culture supernatant was measured after 24 h of treatment. Experimental data are presented as mean ± S.D. for three independent experiments with three repetitions. * $p < 0.05$ versus EtOH (ANOVA followed by a Tukey's test).

2.4. Apoptotic Bodies under DAPI Staining

Apoptosis is characterized by morphological changes and chromatin condensation that produce smaller, more compact nuclei and/or the formation of apoptotic bodies. Our CaSki, MDA-MB-231 and SK-Lu-1 cell cultures were stimulated with quercetin, quercetagetin and patuletin to evaluate morphological changes, chromatin condensation and the formation of apoptotic bodies. The latter were identified by staining with fluorochrome 4,6-diamidino-2-phenylindole (DAPI) and epifluorescence microscopy observation (Figures 6–8).

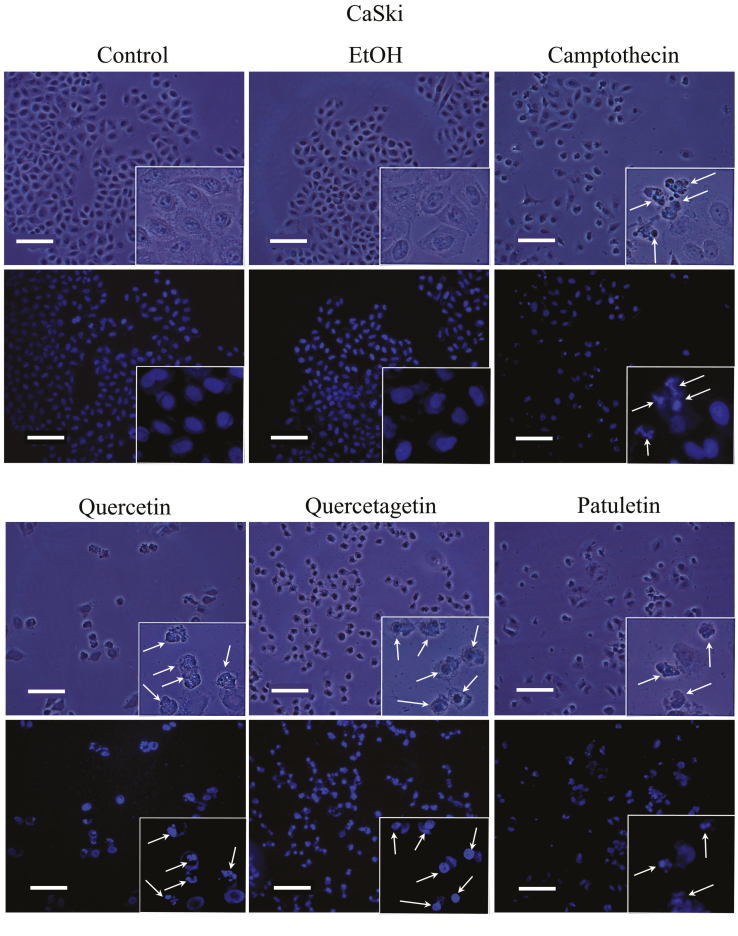

Figure 6. Morphology and DAPI staining. CaSki cell cultures were exposed to quercetin, quercetagetin and patuletin at the aforementioned IC_{50} values. Camptothecin was used as a positive control for apoptosis. The phase-contrast images evidenced cellular shapes under the different experimental conditions. The control and EtOH cells had extended cytoplasm with chromatin distributed in the nuclear space, as shown by the fluorescent distribution of DAPI. After treatment, both the cytoplasm and nucleus were contracted, and several apoptotic bodies were visible (arrows), Scale bars 100 microns.

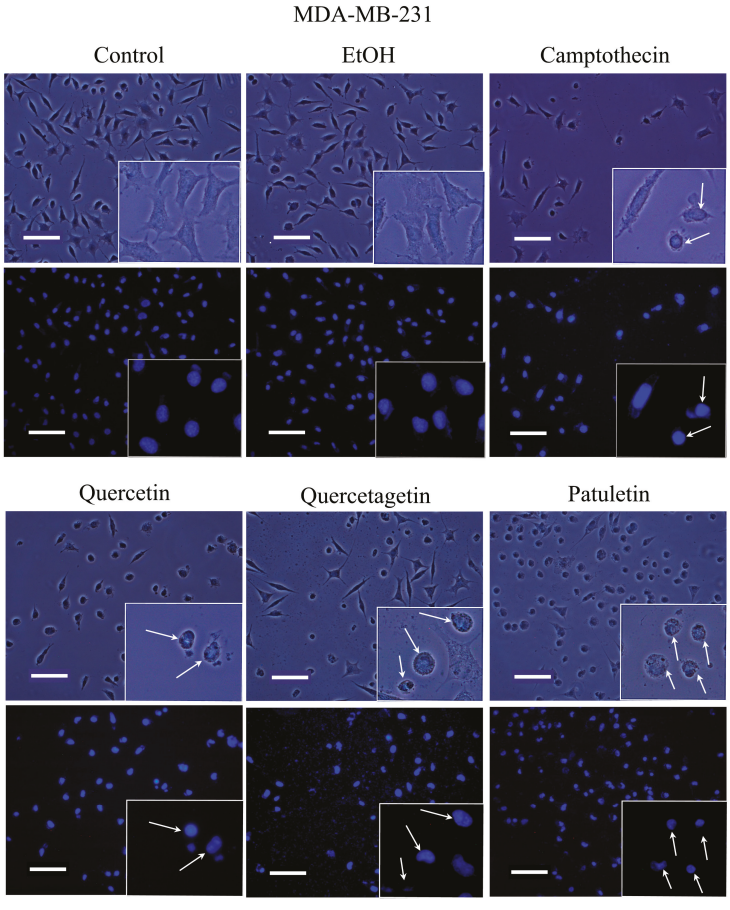

Figure 7. Morphology and DAPI staining. MDA-MB-231 cell cultures were exposed to quercetin, quercetagetin and patuletin at the aforementioned IC_{50} values. Camptothecin was used as a positive control for apoptosis. The phase-contrast images evidenced cellular shapes under the different experimental conditions. The control and EtOH cells had extended cytoplasm with chromatin distributed in the nuclear space, as shown by the fluorescent distribution of DAPI. After treatment, both the cytoplasm and nucleus were contracted, and several apoptotic bodies were visible (arrows), Scale bars 100 microns.

Observations under phase-contrast illumination revealed that the morphology of the control and vehicle cells was conserved, with a polyhedral shape and extended cytoplasm. In these conditions, chromatin is distributed throughout the nucleoplasm (see DAPI staining). After treatment with quercetin, quercetagetin or patuletin, the morphology of the cells was clearly altered, as they showed shrinkage, evidenced by the loss of the polyhedral form. Compact nuclei and apoptotic bodies were also visible, suggesting the presence of the apoptotic process in the CaSki (Figure 6), MDA-MB-231 (Figure 7), and SK-Lu-1 (Figure 8), cells. Despite these results, it is still necessary to detect the activation of effector caspases such as active caspase-3, to establish that a caspase-dependent apoptotic process has been activated. Thus, more conclusive experiments were performed, as described below.

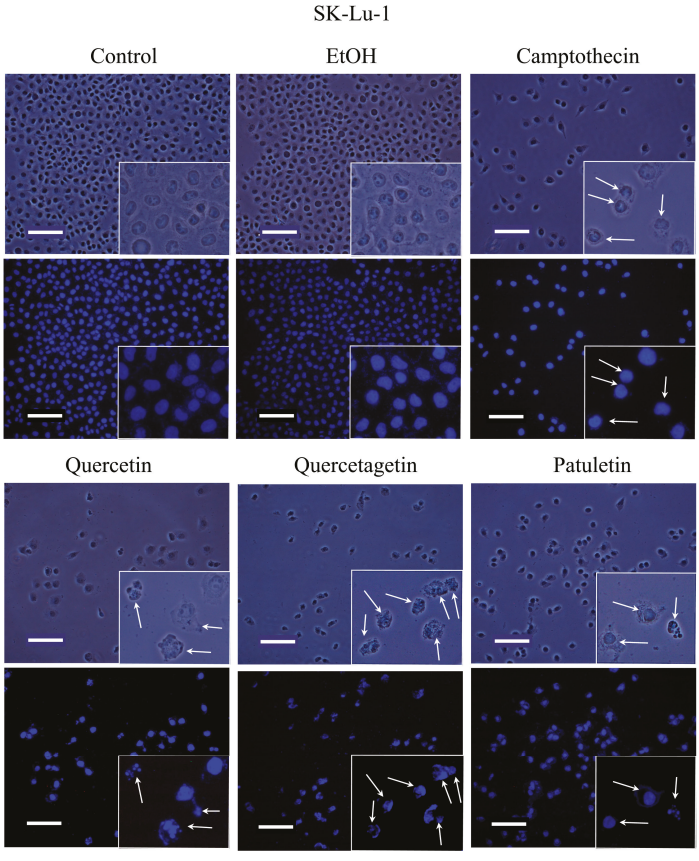

Figure 8. Morphology and DAPI staining. view of SK-Lu-1 cultures, were exposed to quercetin, quercetagetin and patuletin at the aforementioned IC_{50} values. Camptothecin was used as a positive control for apoptosis. The phase-contrast images evidence cellular shapes under the different experimental conditions. The control and EtOH cells had extended cytoplasm with chromatin distributed in the nuclear space, as shown by the fluorescent distribution of DAPI. After treatment, both the cytoplasm and nucleus were contracted, and several apoptotic bodies were visible (arrows), Scale bars 100 microns.

Detection of Active Caspase-3, Active Caspase-8, Active Caspase-9 and PARP

The caspases are a family of cysteine proteases that function as crucial mediators of apoptosis. Poly (ADP-ribose) polymerases (PARPs) are a family of related enzymes that play an important role in DNA repair. PARP is a cleavage that occurs during increased levels of active caspase-3, which is likely the most well-understood of the mammalian caspases in terms of its specificity and role in apoptosis. Caspase-3 is also required for some typical hallmarks of apoptosis and is indispensable for apoptotic chromatin condensation and DNA fragmentation. Likewise, it is essential for certain processes associated with the formation of apoptotic bodies. The apoptosis process can be conducted in two classic signaling pathways: one extrinsic, the other intrinsic.

The extrinsic pathway is mediated by caspase-8, while caspase-9 is determinant in the intrinsic pathway. In this study, we identified active caspase-3 and PARP by means of western blots to determine the presence of the apoptotic process. In addition, we immunodetected active caspase-3, active caspase-8 and active caspase-9 to evaluate the presence of these enzymes in the three cell lines

treated with quercetin, quercetagetin and patuletin. Finally, all of these caspases were evaluated using flow cytometry to obtain quantitative results.

Results show that the expression of active caspase-3 and PARP proteins occurred in all three cell lines treated with quercetin, quercetagetin and patuletin (Figure 9). This confirms the participation of the apoptotic process during elimination of cells treated with the compounds used in this study. The quantitative evaluation of active caspase-3 by cytometry (Figure 10) showed that the number of cells positive to active caspase-3 had different percentages: SK-Lu-1 cells presented greater susceptibility to quercetin and quercetagetin, since these presented a higher percentage of positive cells compared to the other two cell types (Table 3). Conversely, MDA-MB-231 proved to be more sensitive to patuletin (Table 3). Our morphological and biochemical results evidence the presence of apoptosis during elimination of the cancer cells treated with quercetin, quercetagetin and patuletin.

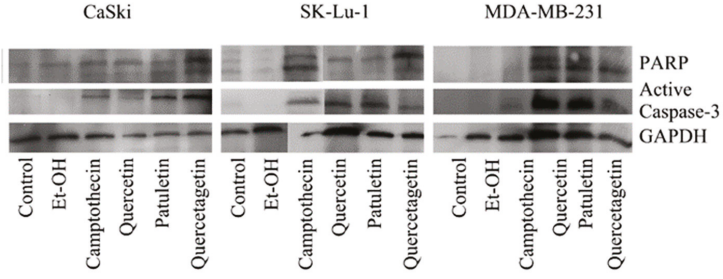

Figure 9. Expression of active caspase-3 and PARP in CaSki, MDA-MB-231 and SK-Lu-1 cell cultures exposed to quercetin, quercetagetin and patuletin at the aforementioned IC_{50} values.

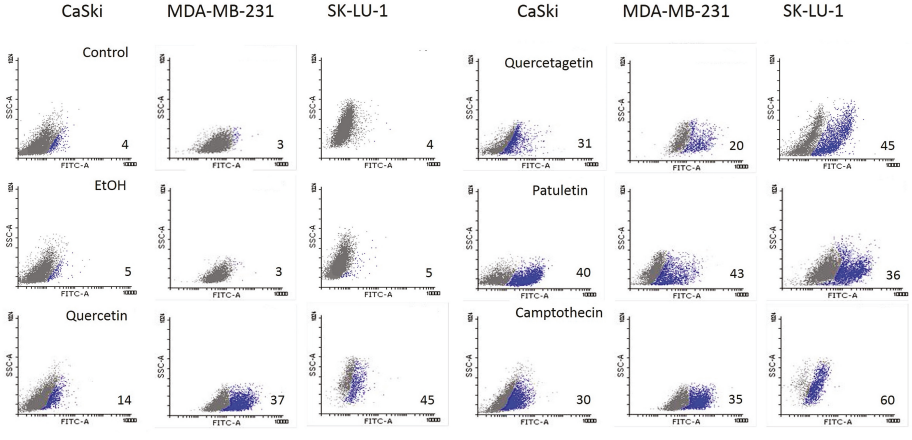

Figure 10. Detection of active caspase-3 in CaSki, MDA-MB-231 and SK-Lu-1 cell cultures exposed to quercetin, quercetagetin and patuletin at the aforementioned IC_{50} values. Cells were analyzed by FACS from Cell Quest; numbers indicate the percentages of caspase-3 activity.

Table 3. Percentage of positive cells to active caspase-3 in cultures of CaSki, MDA-MB-231 and SK-Lu-1 cells treated with IC_{50} values of quercetin, quercetagetin and patuletin.

	CaSki	MDA-MB-231	SK-LU-1
		Quercetin	
Control	4	3	4
EtOH	5	3	5
Quercetin	14	37	45
Camptothecin	30	35	60
		Quercetagetin	
Control	4	4	4
EtOH	6	5	5
Quercetagetin	31	20	45
Camptothecin	50	25	50
		Patuletin	
Control	3	5	3
EtOH	4	5	5
Patuletin	40	43	36
Camptothecin	65	32	43

Active caspase-9 and active caspase-8 were also present in the treated cancer cells, though the numbers of cells positive to caspase-9 detection were significantly higher than those that were positive to caspase-8 (Figure 11). This finding suggests that quercetin, quercetagetin and patuletin induce the apoptotic process through the intrinsic apoptotic pathway (see Supplementary Material).

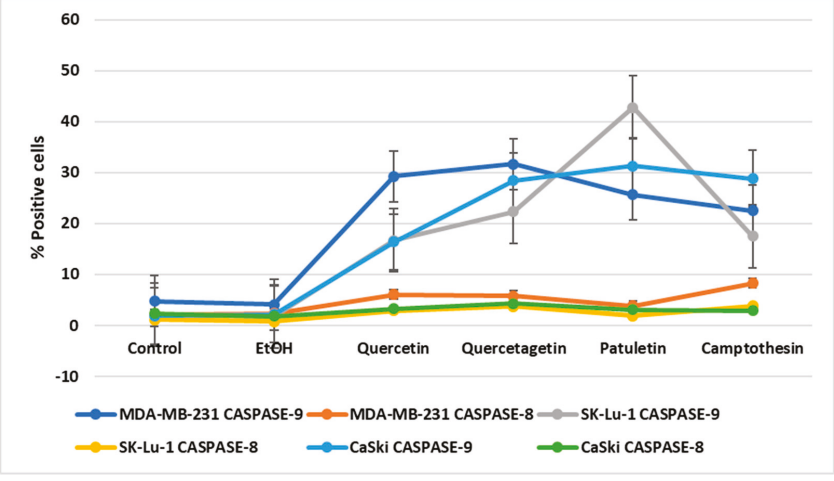

Figure 11. Percentage of positive cells to active caspase-8 and caspase-9 treated with quercetin, quercetagetin, and patuletin.

2.5. Effect of Quercetin, Quercetagetin and Patuletin on Non-Tumor Cells

The main compounds currently used in chemotherapy present problems in terms of their selective activity on malignant cells and because they produce undesirable side effects. We thus considered it crucial to determine the selectivity of the compounds tested in the present work, and to evaluate their antiproliferative activity in non-tumor cells in order to reach conclusions concerning their potential anticancer activity. Our research has demonstrated the anti-proliferative activity of quercetin, quercetagetin and patuletin in CaSki, MDA-MB-231, and SK-Lu-1 tumor cells; however, their effect

on non-tumor cells has not yet been determined. To test the selectivity of the compounds evaluated, we used lymphocytic cells. A sample of an enriched lymphocyte population (ELP) from peripheral blood was treated with the three compounds to assess the proliferation of this cellular fraction. ELPs from a normal blood donor were induced for three cycles of proliferation by phyto-hemagglutinin and labeled with 5(6)-carboxyfluorescein diacetate *N*-succinimidyl ester (CFSE). These cells were treated with quercetin, quercetagetin and patuletin after 48 h of culture (second proliferation cycle) and then cultured for another 72 h. The cells were harvested, and their proliferative potential was analyzed by flow cytometry.

To evaluate the anti-proliferative potential of the flavonoids on lymphocytes, cells were cultured at the IC_{50} concentration values for 24 h and then labeled with 5(6)-carboxyfluorescein diacetate *N*-succinimidyl ester (CSFE). Fluorescence was measured using a cytometer. A culture without flavonoids was used as a positive control, while eluents were used as negative controls. Normal lymphocytes were induced for two cycles of proliferation by phyto-hemagglutinin (Figure 12). Quercetin, quercetagetin and patuletin all produced significant proliferation at the concentration employed.

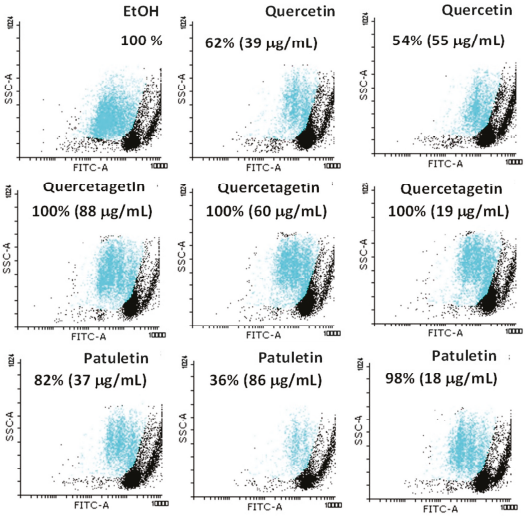

Figure 12. Evaluation of the anti-proliferative effect of quercetin, quercetagetin and patuletin in lymphocytes. The compounds showed no evidence of any anti-proliferative effect on normal cells.

Cells treated only with the vehicle only were used as an experimental control (EtOH). They showed 100% proliferation (Figure 12); however, when the lymphocytes were treated at the aforementioned IC_{50} values of the compounds their behavior differed, as the proliferative potential of lymphocytes was negatively-affected by treatment with 86 µg/mL of patuletin. The treatment with quercetin affected all the cells evaluated in a proportion of approximately 50%. In contrast, quercetagetin did not affect the proliferation activity of the lymphocytes.

2.6. Necrotic Effect of Quercetin, Quercetagetin and Patuletin in Non-Tumor Cells

To determine the necrotic effect of different flavonoids on normal cells, human lymphocytes were induced to proliferate by phytohemagglutinin for 72 h, and the amount of LDH released into the media was measured. The percentage of LDH released after treating the lymphocytes with quercetin, quercetagetin and patuletin was below 8%. Upon comparing this percentage to the amount released by the tumor cells, it was determined that the necrotic effect inside non-tumor cells was not

significant. Our results show that treatment with the compounds evaluated—quercetin, quercetagetin and patuletin—did not cause any necrotic effect in the lymphocytes. This result is suggestive of a selective effect of quercetin, quercetagetin and patuletin in non-tumor cells (Figure 13).

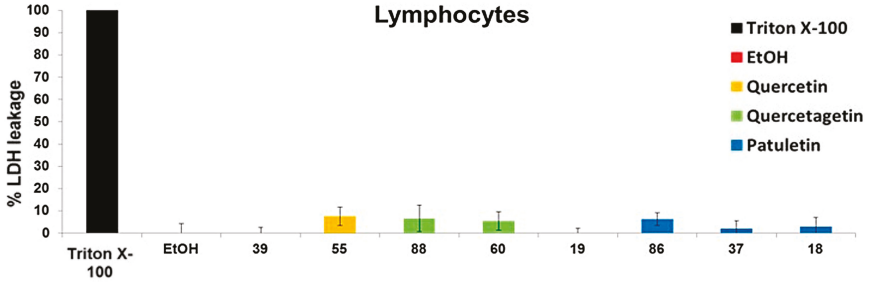

Figure 13. Evaluation of necrosis by quercetin, quercetagetin and patuletin on normal cell lymphocytes. The medium was removed, and the cells were stimulated to the level of IC_{50} values for quercetin, quercetagetin and patuletin, as well as with EtOH (10 µL/mL). After 24 h, the amount of lactate dehydrogenase (LDH) released from the culture supernatant was evaluated. Experimental data are presented as mean ± S.D. for three independent experiments with three repetitions.

3. Discussion

Cancer is still considered the most detrimental disease for humans. Extensive research suggests that quercetin may be an antiproliferative agent [24] and that it interacts with DNA [25], causes tumor regression [26] and apoptosis [27]. For this reason, it is important to broaden our knowledge of other compounds derived from natural products, since it is well-known that changes in the general structure of flavonoids function to enhance many biological activities [28]. In terms of their structure, however, the flavonoids quercetin, quercetagetin and patuletin differ only in their substitution patterns in C6, as quercetin has a hydrogen atom, quercetagetin has a hydroxyl group, and patuletin has a methoxy group, at this position. Additionally, all three compounds have a catechol, C2–C3 unsaturation and 3-hydroxyl groups, which have been reported to participate in various biological activities [29]. Biological activity has been attributed to phytochemicals obtained from species of *Tagetes* worldwide [30], including cytotoxic and antiproliferative action [31]. However, before the present study, no one knew if quercetagetin and patuletin molecules were capable of inducing apoptosis and/or necrosis, or if they would also affect normal cells at the same time and in the same models when compared to quercetin [32–35]. Our study presents interesting evidence which demonstrates that quercetin, quercetagetin and patuletin do indeed have anti-proliferative activity. Moreover, it appears likely that the change in C6 of the flavonoid skeleton of quercetagetin and patuletin could be a potentiator of anti-proliferative activity in SK-Lu-1 cells, as evidenced by comparing the IC_{50}'s used in the treatments described.

Our results also show that quercetin and patuletin do not produce a necrotic effect. Quercetagetin was present only in tumor cell lines. These findings suggest that cell elimination is not achieved through necrotic cell death; rather, treating these cancer cell lines with flavonoids evidenced the presence of apoptosis, distinguished by the classic morphological changes of cytoplasmic and nuclear compaction. The presence of active caspase-3, caspase-8, caspase-9 and cleaved PARP in the treated cells lends additional support to this statement. We could speculate that the substitution of the –OH group for the methoxyl group in C6 between quercetagetin and patuletin [21] accounts for this. What has been ascertained is that quercetin is capable of inducing apoptosis [36]. Our work shows that quercetin, quercetagetin and patuletin all cause significant nuclear fragmentation and have a great capacity to induce caspase-3 activation, sometimes even greater than camptothecin, a well-known inducer of apoptosis [37].

Our results clearly show that quercetin, quercetagetin and patuletin all have good cytotoxic activity against different cancer cell lines, and that they achieve cell elimination through the ordered cell-death process called apoptosis. In addition, the results indicate that these compounds induce the intrinsic apoptotic pathway. Also, quercetin and quercetagetin evidenced a selective pro-apoptotic activity against the SK-Lu-1 lung cancer cell line. In this regard, it is important to emphasize that the occurrence of side effects during current chemotherapy treatments are related to the necrotic activity caused by the compound(s) applied.

In addition to demonstrating the pro-apoptotic action exerted by quercetin, quercetagetin and patuletin inside tumor cells, we were also able to determine that these compounds show a selective effect on non-tumor cells, since when normal lymphocytes were treated with the doses applied to the cancer cell lines, the necrotic effect measured was not statistically-significant. Finally, and contrary to their effect on tumor cells, the compounds evaluated herein exhibited a non-antiproliferative effect inside non-tumor cells, relevant data that could be used in other investigations [38] with flavonoids [39]. All these results allow us to propose these flavonoids and modifications in substitution patterns in C6 as options that have selective activity against cancer cells but do not damage normal cells, indicating that they may have future utilization in cancer treatment or other biological activities.

4. Materials and Methods

4.1. Instrumentation

Melting points were determined using a Fisher Scientific (Pittsburg, PA, USA) apparatus. NMR spectra were recorded on an Advance III 700 MHz spectrometer (Bruker, Billerica, MA, USA) with the residual solvent peak as reference. HR-MS-DART data were obtained by an AccuTOF JMS-T100LC mass spectrometry system (Jeol Ltd., Tokyo, Japan). HPLC-UV analysis were run by an Agilent 1200 Series Binary SL system (Agilent, Carpinteria, CA, USA) equipped with a 2996 UV-Vis diode array detector (Waters Corporation, Milford, MA, USA). The samples were dissolved in methanol and analyzed on a Luna 3 μm C18 (100 × 2.0 mm, 100 Å) column (Phenomenex, Torrance, CA, USA); the mobile phase was composed by water (A) and methanol (B). The elution was performed in gradient conditions, starting from 20 to 100 of B in 30 min; the rate flow was 0.2 mL/min and the UV detection was fixed at 254 nm. The separation of quercetagetin and patuletin were carry out by reverse-phase thin layer chromatography plates (20 × 10 cm, 0.25 mm) (Macherel-Nagel, Düren, Germany). The extract was obtained concentrating in under vacuum using a rotary evaporator (R-100, Büchi, Meierseggstrasse, Switzerland). Quercetin was purchased from Sigma-Aldrich (Sigma, St. Louis, MO, USA).

4.2. Plant Materials

Flowers of *Tagetes erecta* and *Tagetes patula* were collected from October–November in Puebla and the State of Mexico; Mexico. Two prepared herbarium specimens were authenticated and deposited in the National Herbarium of Mexico (MEXU), under folio numbers 1409057 and 1409058 respectively.

4.3. Extraction and Isolation

Quercetagetin and patuletin were isolated from *Tagetes erecta* and *Tagetes patula* flowers respectively. Once the flowers were cut, we separated the ligules from the receptacles, then, 500 g of each flower were subjected to a static maceration at room temperature in ethanol (1L) for 24 h, the solution was filtered, and ethanol was concentrated in vacuum using a rotary evaporator to give a residue (10 g). The separation of extracts (100 mg) was performed utilizing reverse-phase thin layer chromatography plates (20 × 10 cm, 0.25 mm) eluting with ethyl acetate/methanol/water 7.8:1.2:1.0. This separation conditions were utilized for each extract to afford quercetagetin (70 mg) and patuletin (30 mg).

4.4. Compound Characterization

Quercetagetin (**2**). Yellow solid; m.p. 255–260 °C; ^{1}H-NMR (700 MHz, DMSO-d_6) and ^{13}C-NMR (176 MHz, DMSO) see Table 1. HR-DART-MS (positive ion mode) m/z 319.04553 $[M + H]^+$ (Calcd. for $C_{15}H_{11}O_8$: 319.04539); HPLC-UV area peak = 95.17%, retention time = 16.454 min; UV (CH_3OH) λ_{max} 258.0, 361.7 nm.

Patuletin (**3**). Yellow solid, 260–263 °C. ^{1}H-NMR (700 MHz, Methanol-d_4) and ^{13}C-NMR (175 MHz, Methanol-d_4) see Table 1. HR-DART-MS (positive ion mode) m/z 333.06114 $[M + H]^+$ (Calcd. for $C_{16}H_{13}O_8$: 333.06104); HPLC-UV area peak = 89.47%, retention time = 19.865 min; UV (CH_3OH) λ_{max} 256.8, 367.1 nm.

4.5. Cell Culture

The following cell lines were purchased from the American Type Culture Collection (ATCC Rockville, MD, USA): CaSki, (cervical cancer), MDA-MB-231 (breast cancer), and SK-Lu-1 (lung cancer). They were cultured in RPMI-1640 medium (GIBCO, Invitrogen Corp., Grand Island, NY, USA) containing 5% Newborn Calf Serum (NCS, GIBCO, Invitrogen Corp., Grand Island, NY, USA) with red phenol supplemented by benzylpenicillin. All cultures were stored in a humidified atmosphere with 5% CO_2 at 37 °C. All cell-based assays were performed using cells in the exponential growth phase.

4.6. Cell Proliferation Assay

Assays were performed by seeding 7500 cells/well in 96-well tissue cultured plates in a volume of 100 µL of RPMI-1640 medium supplemented with 5% NCS per well. Cells were allowed to grow for 24 h in the culture medium prior to exposure to the compounds. Also, 1% of vehicle (EtOH) was added to the control cells. Antiproliferative activity (IC_{50}) was determined after 24 h by crystal violet staining [40]. Cellular density was determined by measuring absorbance at 590 nm on an Enzyme-linked ImmunoSorbent Assay (ELISA) plate reader (Tecan, Seestrasse, MÄ, Switzerland).

4.7. Determination of LDH

Necrotic activity was determined by means of the LDH Cytotoxicity Assay Kit (BioVision, Milpitas, CA, USA). following the manufacturer's instructions. LDH oxidizes lactate to pyruvate, which then reacts with the tetrazolium salt 2-(4-iodophenyl)-3-(4-nitrophenyl)-5-phenyltetrazolium (INT) to produce formazan. The increase in the amount of formazan generated in the culture supernatant directly correlates to the increase in the number of lysed cells. Formazan dye is water-soluble and can be detected with a spectrophotometer at 500 nm [41].

4.8. Observation of Morphological Characteristics of Apoptotic Cells by Fluorescence Microscopy

Cells were cultured in glass coverslips and treated with the IC_{50} of quercetin, quercetagetin and patuletin for 24 h. They were then fixed in 2% paraformaldehyde in PBS at pH 7.2 for 20 min. After rinsing in the same buffer, they were stained with 4,6-diamidino-2-phenylindole (DAPI) and evaluated under an Eclipse E600 microscope (Nikon, Melville, NY, USA). Images were recorded with a DXM1200F digital camera (Nikon, Melville, NY, USA).

4.9. CFSE-Labeling Assay

Heparinized blood samples were obtained from healthy human volunteers. Peripheral blood mononuclear cells (PBMCs) were isolated using standard Hypaque (Sigma-Aldrich, St. Louis, MO, USA) gradient density centrifugation. The PBMCs were washed twice with RPMI 1640 medium (GIBCO) containing 10% NCS, penicillin (100 U/mL), and streptomycin (100 U/mL). The lymphocyte population was further enriched (ELP) by eliminating adherent cells (i.e., the cells were incubated at 37 °C, 5% CO_2 for 1 h, and non-adherent cells were harvested). The ELPs were re-suspended in RPMI-1640 medium at a concentration of 1×10^6 cells/mL and 5(6)-carboxyfluorescein diacetate

N-succinimidyl ester (CFSE) (Sigma-Aldrich) was added to the cell suspension to a final concentration of 12 μM, and then incubated for 15 min at room temperature in the dark. Labeling was completed by adding the same volume of NCS during 5 min at room temperature to quench the free CFSE. The labeled cells were washed five times with sterile PBS containing 10% NCS, counted, and then re-suspended in RPMI-1640 medium at 1×10^6 cells/mL [42]. Unstimulated, phytohaemagglutinin (PHA)-stimulated, or treated, cells were plated at 2×10^5 cells/mL in 96-well, flat-bottomed cell culture plates, and five replicate samples for each treated amount were prepared. Cells were incubated in a 5% CO_2 incubator at 37 °C for 72 h. Cultured cells were harvested, washed twice with PBS, fixed with 1% formaldehyde, and then analyzed by flow cytometry to acquire a minimum of 20,000 events from each sample. Data analysis was performed using CellQuest software (Becton–Dickinson, Franklin Lakes, NJ, USA).

4.10. Immunolocalization of Active Caspase-3, Active Caspase 8 and Active Caspase-9 by Flow Cytometry

The CaSki, MDA-MB-231 and SK-Lu-1 cells were seeded at 105 cells/mL in 60-mm tissue culture plates and allowed to grow for 24 h in culture medium before being treated with their respective IC_{50}. Cells were harvested with versene solution. For active caspase-3, caspase-8 and caspase-9 immunodetection, the cells were fixed and permeabilized in 50% methanol in PBS, washed in PBS, incubated with primary antibody anti-active-caspase-3 (Novous Biologicals, Littleton, CO, USA), anti-active-caspase-8 (Novous Biologicals, Littleton, CO, USA) or anti-active-caspase-9 (Novous Biologicals, Littleton, CO, USA), and then diluted in PBS (1:500) for 18 h. Next, the cells were washed and incubated with the secondary goat anti-rabbit antibody with FITC (SIGMA, St. Louis, MO, USA), and then diluted to 1:200 in PBS for 2 h. The samples were analyzed by flow cytometry, acquiring a minimum of 20,000 events from each sample. Data analysis was performed using CellQuest software (Becton–Dickinson, Franklin Lakes, NJ, USA) [43].

4.11. Western Blot Analysis

Protein expression levels were evaluated using western blot assays. The CaSki, MDA-MB-231 and SK-Lu-1 cells were seeded at 105 cells/mL in 60-mm tissue culture plates and allowed to grow for 24 h in culture medium before being treated with their respective IC_{50}. Cells were harvested with versene solution. Next, the cells were incubated for 15 min in lysis buffer (50 mMTris–Cl, pH 7.5; 150 mM NaCl, 0.1% SDS, 1 mM PMSF, 0.5% sodium deoxycholate, and 1% Nonidet P-40), supplemented with the complete protease inhibitor cocktail (Roche, Mannheim, Germany). Total proteins were measured by the Qubit system using the Qubit 3 Fluorometer (Thermo Fisher Scientific, Waltham, MA, USA), as follows: 100 μg of total proteins were loaded onto a 12% SDS-PAGE gel before being transferred to polyvinylidene fluoride (PVDF) membranes, which were blotted using the SNAP i.d.® 2.0 Protein Detection System. Briefly: membranes were incubated in blocking buffer, then incubated with anti-active caspase-3 and anti-PARP antibodies at a dilution of 1:5000. After that, the proteins were tagged by incubation with peroxidase-conjugated secondary antibody (Jackson, Newmarket, UK) at 1:10,000 in blocking buffer. Using Horse Radish Peroxidase (HRP) as the substrate (Immobilon Western, Millipore Co., Darmstadt, Germany.), specific labeling was detected by chemiluminescence. Amersham Biosciences Hyperfilm (Amersham Biosciences, Corston, UK) was exposed to the membranes to detect chemiluminescence.

4.12. Statistical Analysis

Means and standard deviations (SD) were calculated using Excel (Microsoft Office, 2016 Version, Redmond, WA, USA). Statistical analysis of differences was carried out by analysis of variance (ANOVA) using SPSS 10.0 for Windows (Microsoft, Redmond, WA, USA). A p value < 0.05 (Student's t test) was considered significant. In all cases, the data represent three independent experiments performed in triplicate.

5. Conclusions

Our conclusion, therefore, is that quercetin quercetagetin and patuletin all demonstrate antiproliferative activity in a dose-dependent manner, with only quercetagetin showing significant necrotic activity. All three compounds induced the intrinsic apoptotic route, but none of them affected the proliferation of normal cells. These results suggest that the presence of a methoxyl group in C6 enhances the potency of flavonols. In future studies, structural modifications will be made as we continue to conduct research on this type of biological activity in an effort to improve our understanding of these compounds and how they could be incorporated into applications to combat different types of cancer in the future.

Supplementary Materials: The following are available online. Figure S1: ^{1}H-NMR spectrum of quercetagetin (**2**), Figure S2: ^{13}C-NMR spectrum of quercetagetin (**2**), Figure S3: HSQC spectrum of quercetagetin (**2**), Figure S4: HMBC spectrum of quercetagetin (**2**), Figure S5: HR-DART-MS positive ion mode spectrum of patuletin (**3**), Figure S6: HR-DART-MS positive ion mode spectrum of quercetagetin (**2**), Figure S7: Detection of active caspase-8 in CaSki, MDA-MB-231 and SK-Lu-1 cell cultures exposed to quercetin, quercetagetin and patuletin at the aforementioned IC_{50} values, Figure S8: Detection of active caspase-9 in CaSki, MDA-MB-231 and SK-Lu-1 cell cultures exposed to quercetin, quercetagetin and patuletin at the aforementioned IC_{50} values.

Author Contributions: J.J.A.-S. designed the study and performed the research. M.J.-E. and L.S.-S. were involved in the study design, organization, and resourcing and wrote the paper together with all other author. M.L.E. designed and performed microscopy assays. R.T.-H. designed and performed the chemical analysis. H.L.-M. and F.F.-G. designed and performed Flow Cytometry and LDH assays. All authors read and approved the final manuscript.

Funding: This research was funded by SEP-CONACYT, Investigacion Cientifica Basica: 253979 and 255881; DGAPA, PAPIIT IG 200418, PAPIIT IN216718, IN220916 and IN225117; Fernando Flores Guzman acknowledge a postdoctoral fellowship from DGAPA/UNAM and Jesus Javier Alvarado Sansininea received fellowship from CONACYT, 440947.

Acknowledgments: Jesus Javier Alvarado Sansininea is a doctoral student from Posgrado en Ciencias Biologicas. The authors are grateful to, Instituto de Química, UNAM; Beatriz Quiroz Garcia, Isabel Chavez Uribe, Luis Velazco Ibarra and Francisco Javier Perez Lopez for technical assistance; Paul C. Kersey Johnson for reviewing the English word usage and grammar and Evaristo Javier, the *Tagetes* plantation owner.

Conflicts of Interest: The authors declare no conflict of interest.

References

1. Newman, D.J.; Cragg, G.M. Natural products as sources of new drugs from 1981 to 2014. *J. Nat. Prod.* **2016**, *79*, 629–661. [CrossRef] [PubMed]
2. Alonso-Castro, A.J.; Villarreal, M.L.; Salazar-Olivo, L.A.; Gomez-Sanchez, M.; Dominguez, F.; Garcia-Carranca, A. Mexican medicinal plants used for cancer treatment: Pharmacological, phytochemical and ethnobotanical studies. *J. Ethnopharmacol.* **2011**, *133*, 945–972. [CrossRef] [PubMed]
3. Neher, R.T. The ethnobotany of *Tagetes*. *Econ. Bot.* **1968**, *22*, 317–325. [CrossRef]
4. Vasudevan, P.; Kashyap, S.; Sharma, S. *Tagetes*: A multipurpose plant. *Bioresour. Technol.* **1997**, *62*, 29–35. [CrossRef]
5. Martínez, R.; Diaz, B.; Vásquez, L.; Compagnone, R.S.; Tillett, S.; Canelón, D.J.; Torrico, F.; Suárez, A.I. Chemical composition of essential oils and toxicological evaluation of *Tagetes erecta* and *Tagetes patula* from Venezuela. *J. Essent. Oil Bear. Plants* **2009**, *12*, 476–481. [CrossRef]
6. Priyanka, D.; Shalini, T.; Navneet, V.K. A brief study on Marigold (*Tagetes* species): A review. *Int. Res. J. Pharm.* **2013**, *4*, 43–48.
7. Devika, R.; Justin Koilpillai, Y. Phytochemical screening studies of bioactive compounds of *Tagetes erecta*. *Int. J. Pharm. BioSci.* **2012**, *3*, 596–602.
8. Xu, L.; Chen, J.; Qi, H.; Shi, Y. Phytochemicals and their biological activities of plants in *Tagetes* L. *Chin. Herb. Med.* **2012**, *4*, 103–117. [CrossRef]
9. Wang, T.; Li, Q.; Bi, K. Bioactive flavonoids in medicinal plants: Structure, activity and biological fate. *Asian J. Pharm. Sci.* **2018**, *13*, 12–23. [CrossRef]
10. Singh, P.; Krishna, A.; Kumar, V.; Krishna, S.; Singh, K.; Gupta, M.; Singh, S. Chemistry and biology of industrial crop *Tagetes* species: A review. *J. Essent. Oil Res.* **2016**, *28*, 1–14. [CrossRef]

11. Abdel-Wahhab, M.A.; Said, A.; Huefner, A. NMR and radical scavenging activities of patuletin from *Urtica urens*. Against aflatoxin B_1. *Pharm. Biol.* **2005**, *43*, 515–525. [CrossRef]
12. Gong, Y.; Liu, X.; He, W.-H.; Xu, H.-G.; Yuan, F.; Gao, Y.-X. Investigation into the antioxidant activity and chemical composition of alcoholic extracts from defatted marigold (*Tagetes erecta* L.) residue. *Fitoterapia* **2012**, *83*, 481–489. [CrossRef] [PubMed]
13. Gutiérrez-Venegas, G.; Jiménez-Estrada, M.; Maldonado, S. The effect of flavonoids on transduction mechanisms in lipopolysaccharide-treated human gingival fibroblasts. *Int. Immunopharmacol.* **2007**, *7*, 1199–1210. [CrossRef] [PubMed]
14. Tu, B.; Liu, Z.-J.; Chen, Z.-F.; Ouyang, Y.; Hu, Y.-J. Understanding the structure–activity relationship between quercetin and naringenin: In vitro. *RSC Adv.* **2015**, *5*, 106171–106181. [CrossRef]
15. Flavonoids: Recent Advances as Anticancer Drugs. Available online: http://www.eurekaselect.com/85957/article (accessed on 16 August 2018).
16. Flavonoids in Health and Disease. Available online: https://www.crcpress.com/Flavonoids-in-Health-and-Disease-Second-Edition/Rice-Evans-Packer/p/book/9780824742348 (accessed on 27 September 2018).
17. Aherne, S.A.; O'Brien, N.M. Dietary flavonols: Chemistry, food content, and metabolism. *Nutrition* **2002**, *18*, 75–81. [CrossRef]
18. Ren, W.; Qiao, Z.; Wang, H.; Zhu, L.; Zhang, L. Flavonoids: Promising anticancer agents. *Med. Res. Rev.* **2003**, *23*, 519–534. [CrossRef] [PubMed]
19. López-Lázaro, M. Flavonoids as anticancer agents: Structure-activity relationship study. *Curr. Med. Chem. Anticancer Agents* **2002**, *2*, 691–714. [CrossRef] [PubMed]
20. Ravishankar, D.; Rajora, A.K.; Greco, F.; Osborn, H.M.I. Flavonoids as prospective compounds for anti-cancer therapy. *Int. J. Biochem. Cell Biol.* **2013**, *45*, 2821–2831. [CrossRef] [PubMed]
21. Chidambara Murthy, K.N.; Kim, J.; Vikram, A.; Patil, B.S. Differential inhibition of human colon cancer cells by structurally similar flavonoids of citrus. *Food Chem.* **2012**, *132*, 27–34. [CrossRef] [PubMed]
22. Kothandan, G.; Gadhe, C.G.; Madhavan, T.; Choi, C.H.; Cho, S.J. Docking and 3D-QSAR (quantitative structure activity relationship) studies of flavones, the potent inhibitors of p-glycoprotein targeting the nucleotide binding domain. *Eur. J. Med. Chem.* **2011**, *46*, 4078–4088. [CrossRef] [PubMed]
23. Fink, S.L.; Cookson, B.T. Apoptosis, pyroptosis, and necrosis: Mechanistic description of dead and dying eukaryotic cells. *Infect. Immun.* **2005**, *73*, 1907–1916. [CrossRef] [PubMed]
24. Amrutha, K.; Nanjan, P.; Shaji, S.K.; Sunilkumar, D.; Subhalakshmi, K.; Rajakrishna, L.; Banerji, A. Discovery of lesser known flavones as inhibitors of NF-κB signaling in MDA-MB-231 breast cancer cells—A SAR study. *Bioorg. Med. Chem. Lett.* **2014**, *24*, 4735–4742. [CrossRef] [PubMed]
25. Yang, L.; Liu, Y.; Wang, M.; Qian, Y.; Dong, X.; Gu, H.; Wang, H.; Guo, S.; Hisamitsu, T. Quercetin-induced apoptosis of HT-29 colon cancer cells via inhibition of the Akt-CSN6-Myc signaling axis. *Mol. Med. Rep.* **2016**, *14*, 4559–4566. [CrossRef] [PubMed]
26. Maurya, A.K.; Vinayak, M. Anticarcinogenic action of quercetin by downregulation of phosphatidylinositol 3-kinase (PI3K) and protein kinase C (PKC) via induction of p53 in hepatocellular carcinoma (HepG2) cell line. *Mol. Med. Rep.* **2015**, *42*, 1419–1429. [CrossRef] [PubMed]
27. Srivastava, S.; Somasagara, R.R.; Hegde, M.; Nishana, M.; Tadi, S.K.; Srivastava, M.; Choudhary, B.; Raghavan, S.C. Quercetin, a natural flavonoid interacts with DNA, arrests cell cycle and causes tumor regression by activating mitochondrial pathway of apoptosis. *Sci. Rep.* **2016**, *6*, 24049. [CrossRef] [PubMed]
28. Chemistry and Biological Activities of Flavonoids: An Overview. Available online: https://www.hindawi.com/journals/tswj/2013/162750/ (accessed on 17 August 2018).
29. Bate-Smith, E.C. Quercetagetin and patuletin in *Eriocaulon*. *Phytochemistry* **1969**, *8*, 1035–1037. [CrossRef]
30. Kaisoon, O.; Konczak, I.; Siriamornpun, S. Potential health enhancing properties of edible flowers from Thailand. *Food Res. Int.* **2012**, *46*, 563–571. [CrossRef]
31. Vallisuta, O.; Nukoolkarn, V.; Mitrevej, A.; Sarisuta, N.; Leelapornpisid, P.; Phrutivorapongkul, A.; Sinchaipanid, N. In vitro studies on the cytotoxicity, and elastase and tyrosinase inhibitory activities of marigold (*Tagetes erecta* L.) flower extracts. *Exp. Ther. Med.* **2014**, *7*, 246–250. [CrossRef] [PubMed]
32. Zhu, W.; Lv, C.; Wang, J.; Gao, Q.; Zhu, H.; Wen, H. Patuletin induces apoptosis of human breast cancer SK-BR-3 cell line via inhibiting fatty acid synthase gene expression and activity. *Oncol. Lett.* **2017**, *14*, 7449–7454. [CrossRef] [PubMed]

33. Holder, S.; Zemskova, M.; Zhang, C.; Tabrizizad, M.; Bremer, R.; Neidigh, J.W.; Lilly, M.B. Characterization of a potent and selective small-molecule inhibitor of the PIM1 kinase. *Mol. Cancer Ther.* **2007**, *6*, 163–172. [CrossRef] [PubMed]
34. Kang, G.-J.; Han, S.-C.; Ock, J.-W.; Kang, H.-K.; Yoo, E.-S. Anti-inflammatory effect of quercetagetin, an active component of immature citrus unshiu, in HaCaT human keratinocytes. *Biomol. Ther.* **2013**, *21*, 138–145. [CrossRef] [PubMed]
35. Kobayakawa, J.; Sato-Nishimori, F.; Moriyasu, M.; Matsukawa, Y. G2-M arrest and antimitotic activity mediated by casticin, a flavonoid isolated from Viticis Fructus (*Vitex rotundifolia* Linne fil.). *Cancer Lett.* **2004**, *208*, 59–64. [CrossRef] [PubMed]
36. Lee, J.H.; Lee, H.-B.; Jung, G.O.; Oh, J.T.; Park, D.E.; Chae, K.M. Effect of quercetin on apoptosis of PANC-1 cells. *J. Korean Surg. Soc.* **2013**, *85*, 249–260. [CrossRef] [PubMed]
37. Zeng, C.-W.; Zhang, X.-J.; Lin, K.-Y.; Ye, H.; Feng, S.-Y.; Zhang, H.; Chen, Y.-Q. Camptothecin induces apoptosis in cancer cells via MicroRNA-125b-mediated mitochondrial pathways. *Mol. Pharmacol.* **2012**, *81*, 578–586. [CrossRef] [PubMed]
38. Mazhar, M.; Faizi, S.; Gul, A.; Kabir, N.; Simjee, S.U. Effects of naturally occurring flavonoids on ferroportin expression in the spleen in iron deficiency anemia in vivo. *RSC Adv.* **2017**, *7*, 23238–23245. [CrossRef]
39. Periasamy, R.; Kalal, I.G.; Krishnaswamy, R.; Viswanadha, V. Quercetin protects human peripheral blood mononuclear cells from OTA-induced oxidative stress, genotoxicity, and inflammation. *Environ. Toxicol.* **2016**, *31*, 855–865. [CrossRef] [PubMed]
40. Kueng, W.; Silber, E.; Eppenberger, U. Quantification of cells cultured on 96-well plates. *Anal. Biochem.* **1989**, *182*, 16–19. [CrossRef]
41. Fotakis, G.; Timbrell, J.A. In vitro cytotoxicity assays: Comparison of LDH, neutral red, MTT and protein assay in hepatoma cell lines following exposure to cadmium chloride. *Toxicol. Lett.* **2006**, *160*, 171–177. [CrossRef] [PubMed]
42. Quah, B.J.C.; Parish, C.R. The use of carboxyfluorescein diacetate succinimidyl ester (CFSE) to monitor lymphocyte proliferation. *J. Vis. Exp.* **2010**, *2259*. [CrossRef] [PubMed]
43. Tuschl, H.; Schwab, C.E. Flow cytometric methods used as screening tests for basal toxicity of chemicals. *Toxicol. In Vitro* **2004**, *18*, 483–491. [CrossRef] [PubMed]

Sample Availability: Samples of the compounds quercetin, quercetagetin and patuletin are available from the authors.

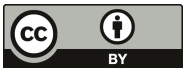

molecules

MDPI

Article

Ethylenediamine Derived Carboxamides of Betulinic and Ursolic Acid as Potential Cytotoxic Agents

Michael Kahnt [1], Lucie Fischer (née Heller) [1], Ahmed Al-Harrasi [2] and René Csuk [1,*]

[1] Division of Organic Chemistry, Martin-Luther-University Halle-Wittenberg, Kurt-Mothes-Str. 2, D-06120 Halle (Saale), Germany; michael.kahnt@chemie.uni-halle.de (M.K.); lucie.heller@chemie.uni-halle.de (L.F.)

[2] Chair of Oman's Medicinal Plants and Marine Natural Products, University of Nizwa, P.O. Box 33, Birkat Al-Mauz, Nizwa 611, Oman; aharrasi@unizwa.edu.om

* Correspondence: rene.csuk@chemie.uni-halle.de; Tel.: +49-345-55-25660

Received: 11 September 2018; Accepted: 3 October 2018; Published: 8 October 2018

Abstract: Two easily accessible, natural occurring triterpenoids, betulinic and ursolic acid, were used as starting materials for the synthesis of novel cytotoxic agents. A set of 28 ethylenediamine-spacered carboxamides was prepared holding an additional substituent connected to the ethylenediamine group. The compounds were screened in SRB assays to evaluate their cytotoxic activity employing several human tumor cell lines. Betulinic acid-derived carboxamides **17**–**30** showed significantly higher cytotoxicity than their ursolic acid analogs **3**–**16**. In particular, compounds **25** and **26** were highly cytotoxic, as indicated by EC_{50} values lower than 1 μM.

Keywords: ursolic acid; betulinic acid; cytotoxicity; triterpenoids

1. Introduction

During the last decade, significant progress has been made in the therapy of cancer, with several major breakthroughs recorded in recent years. Two examples illustrate today's medical advances in fighting cancer: In August 2017, the first adoptive cell immunotherapy (chimeric antigen receptor T-cell therapy) and the first gene therapy (tisagenlecleucel) were officially approved by the FDA [1]. However, the battle against cancer is far from being won, as the prognosis for many types of cancer remains poor. Despite the promising therapeutic benefits of immuno- or gene therapy, chemotherapy nonetheless remains a key means of cancer treatment. Therefore, research is and should still be focused on the development of new bioactive drugs applicable to chemotherapy.

Many natural products show a wide range of pharmacological properties, including antiviral, antimalarial, anti-inflammatory and antitumor activities. Thus, they are considered as ideal lead structures for the development of new bioactive substances. Triterpenes are a class of pharmacologically interesting natural products that also exhibit cytotoxic properties among several other biological activities [2]. Our own work in recent years has been focused on modifications of naturally occurring triterpenes, such as ursolic, oleanolic, glycyrrhetinic, betulinic, boswellic, platanic and maslinic acid, in which cytotoxic agents were synthesized for their cancer-fighting properties.

The objective of this work was to improve the cytotoxic properties of the two triterpenoids, ursolic (**UA**) and betulinic acid (**BA**), by structural modification at the C-28 carbonyl moiety. Many modifications of UA and BA have been reported [3–5], and the cytotoxicity of these analogs was determined. As a result, two major features seem important for obtaining compounds of high cytotoxicity: First, an intact carbonyl group at C-28 has to be present; reduction or removal of this moiety led to compounds of low cytotoxicity. Second, previous findings [6–11] reported an increased cytotoxicity for amino-substituted triterpenes, regardless of the position of this moiety. Hence, we introduced an amino function into the skeleton of the triterpene, and carboxamides with α,ω-diamines, such as ethylenediamine, were prepared. Furthermore, ethylenediamine-spacered carboxamides of

oleanolic (**OA**) or platanic acid (**PA**) have previously been shown to be highly cytotoxic for human tumor cell lines [10,12]. Ursolic and betulinic acid were chosen as starting compounds: they are easily accessible and structurally related to **OA** and **PA**, respectively (Figure 1).

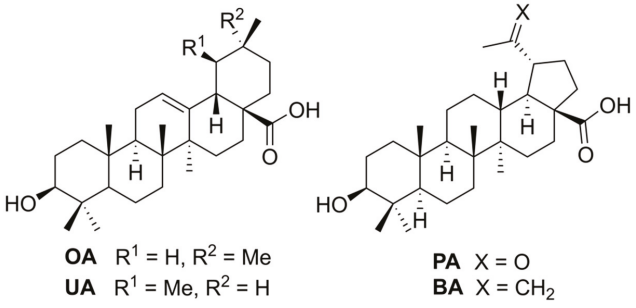

Figure 1. Structures of oleanolic (**OA**), ursolic (**UA**), platanic (**PA**) and betulinic acid (**BA**).

2. Results and Discussion

2.1. Chemistry

Acetylation of betulinic (**BA**) and ursolic acid (**UA**) yielded acetates **1** and **2**. The carboxamides **3**–**30** were prepared in two steps (Scheme 1). Thus, the acetates **1** and **2** were treated with oxalyl chloride in dry dichloromethane in the presence of a catalytic amount of *N*,*N*-dimethylformamide to yield the corresponding acyl chlorides, which were used without further purification. Subsequent treatment of the crude acyl chlorides with various amines in dry dichloromethane provided carboxamides **3**–**9** and **17**–**23**. Their deacetylation yielded compounds **10**–**16** and **24**–**30**, respectively.

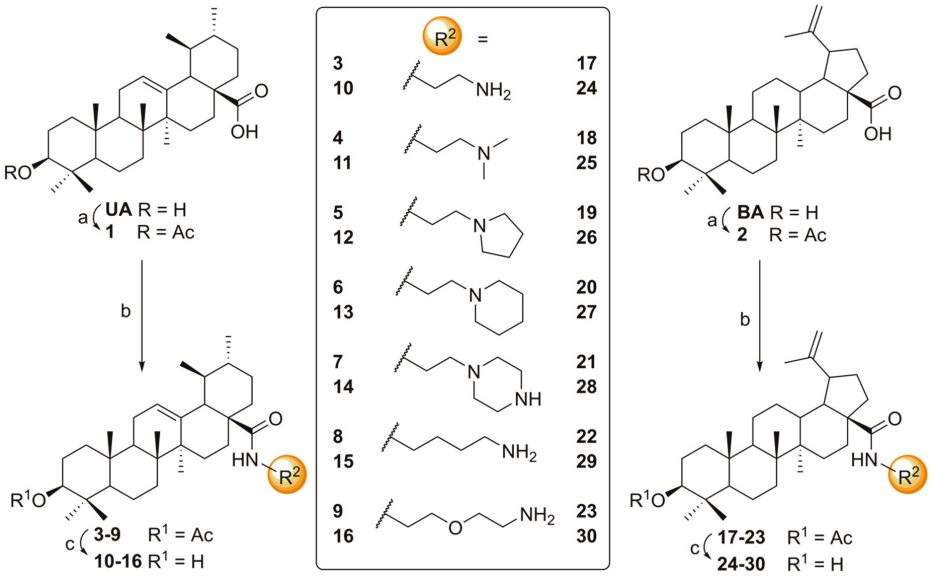

Scheme 1. Synthesis of ursolic and betulinic carboxamides **3**–**30**: (**a**) Ac_2O, NEt_3, DCM, 25 °C, 2 days, yielding **1** (96%) and **2** (93%); (**b**) oxalyl chloride, DCM, DMF, 0–25 °C, 1 h, then amine, 25 °C, 2 h, yielding **3**–**9** and **17**–**23**; (**c**) MeOH/KOH, 25 °C, 2–3 days, yielding **10**–**16** and **24**–**30**.

2.2. Biology

The cytotoxicity of ursolic and betulinic carboxamides **3**–**30** was determined in sulforhodamine B (SRB) assays [13]. The results of this screening are compiled in Table 1.

Table 1. Cytotoxicity of compounds **3**–**30**, betulinic acid (**BA**), ursolic acid (**UA**), and doxorubicin hydrochloride (**DRC**): EC_{50} values from SRB assays after 96 h of treatment are given in μM (n.d. not detected); the values are averaged from three independent experiments each performed in triplicate; confidence interval CI = 95%.

	518A2	A2780	HT29	MCF-7	8505C	NIH 3T3
BA	9.4 ± 0.70	8.8 ± 0.90	14.4 ± 2.3	10.2 ± 1.2	n.d.	13.1 ± 1.1
UA	14.7 ± 0.1	11.7 ± 0.6	10.6 ± 0.7	12.7 ± 0.1	13.5 ± 1.5	18.7 ± 1.6
3	2.7 ± 0.10	2.3 ± 0.10	1.8 ± 0.10	2.0 ± 0.10	4.1 ± 0.40	2.6 ± 0.30
4	5.3 ± 0.40	3.6 ± 0.40	3.4 ± 0.30	3.3 ± 0.70	8.3 ± 0.70	3.7 ± 0.20
5	4.5 ± 0.20	3.1 ± 0.20	2.1 ± 0.20	2.9 ± 0.70	4.3 ± 0.20	3.3 ± 0.30
6	12.2 ± 0.30	6.5 ± 0.50	4.2 ± 0.50	6.0 ± 0.90	15.5 ± 2.7	7.2 ± 1.20
7	3.2 ± 0.10	2.4 ±0.10	1.8 ± 0.20	2.7 ± 0.30	5.4 ± 0.40	2.2 ± 0.10
8	2.7 ± 0.10	2.6 ± 0.10	1.7 ± 0.10	1.7 ± 0.10	3.2 ± 0.01	1.3 ± 0.20
9	3.5 ± 0.60	3.4 ± 0.50	1.6 ± 0.10	2.3 ± 0.40	5.8 ± 0.40	3.1 ± 0.40
10	3.7 ± 0.50	3.3 ± 0.10	2.0 ± 0.10	3.2 ± 0.30	3.7 ± 0.40	3.9 ± 0.10
11	6.6 ± 0.30	4.3 ± 0.50	3.0 ± 0.20	4.2 ± 0.90	7.3 ± 0.20	6.7 ± 1.30
12	5.5 ± 0.10	3.3 ± 0.30	2.6 ± 0.30	3.5 ± 1.00	5.7 ± 0.20	6.2 ± 0.40
13	12.6 ± 0.20	7.6 ± 0.60	8.4 ± 0.70	11.1 ± 1.40	11.1 ± 0.30	3.5 ± 0.60
14	7.0 ± 0.40	4.9 ± 0.40	2.8 ± 0.40	4.4 ± 0.10	7.8 ± 0.50	6.6 ± 0.60
15	9.3 ± 0.10	5.4 ± 1.40	2.1 ± 0.30	5.5 ± 1.10	10.8 ± 1.20	5.6 ± 0.30
16	9.9 ± 0.20	6.5 ± 1.40	3.1 ± 0.30	6.3 ± 0.60	10.6 ± 1.10	7.5 ± 0.80
17	1.6 ± 0.10	1.4 ± 0.20	1.0 ± 0.30	1.3 ± 0.06	2.5 ± 0.03	1.4 ± 0.10
18	1.3 ± 0.10	1.1 ± 0.05	0.3 ± 0.02	1.0 ± 0.30	1.4 ± 0.15	1.0 ± 0.40
19	1.5 ± 0.10	1.4 ± 0.09	0.5 ± 0.08	1.2 ± 0.20	1.6 ± 0.09	1.2 ± 0.07
20	3.1 ± 0.30	1.6 ± 0.20	0.8 ± 0.10	1.5 ± 0.50	3.0 ± 0.36	1.2 ± 0.20
21	2.5 ± 0.70	1.5 ± 0.06	0.6 ± 0.30	1.9 ± 0.10	1.1 ± 0.09	1.0 ± 0.05
22	1.0 ± 0.03	1.1 ± 0.03	0.6 ± 0.05	0.8 ± 0.04	1.4 ± 0.05	0.6 ± 0.04
23	1.9 ± 0.01	1.5 ± 0.10	0.4 ± 0.10	1.4 ± 0.20	2.2 ± 0.81	1.0 ± 0.10
24	0.4 ± 0.01	0.4 ± 0.03	0.4 ± 0.02	0.4 ± 0.02	0.4 ± 0.07	0.4 ± 0.02
25	0.3 ± 0.16	0.2 ± 0.01	0.3 ± 0.05	0.3 ± 0.07	0.4 ± 0.04	0.3 ± 0.09
26	0.4 ± 0.06	0.3 ± 0.10	0.4 ± 0.02	0.2 ± 0.05	0.5 ± 0.06	0.4 ± 0.02
27	0.5 ± 0.10	0.4 ± 0.10	0.4 ± 0.03	0.4 ± 0.01	0.8 ± 0.09	0.4 ± 0.01
28	0.9 ± 0.21	0.8 ± 0.04	0.8 ± 0.18	0.3 ± 0.02	0.85 ± 0.17	0.8 ± 0.22
29	0.4 ± 0.06	0.6 ± 0.10	0.4 ± 0.10	0.6 ± 0.10	0.8 ± 0.26	0.5 ± 0.10
30	0.5 ± 0.04	0.5 ± 0.04	0.5 ± 0.07	0.4 ± 0.20	0.2 ± 0.01	0.4 ± 0.07
DRC	0.2 ± 0.05	0.01 ± 0.01	0.9 ± 0.2	1.1 ± 0.3	1.1 ± 0.4	0.06 ± 0.03

Ursolic acid-derived amides **3**–**16** were found cytotoxic; their EC_{50} values were between 15 μM and 1 μM. For HT29 tumor cells and compound **9**, the most potent ursolic acid derivative, an EC_{50} value of 1.6 μM ± 0.10 μM was observed. Variation of the alkyl substituents at the terminal amino group of the ethylenediamine spacer (as in compounds **3**–**6** or **10**–**13**) did not influence the cytotoxic properties at all. Exceptions, however, are the compounds **6** and **13**: their EC_{50} values are significantly higher as compared to other ursolic carboxamides. For ethylenediamine-spacered carboxamides, substitution at position 3 with an acetyl group did not affect EC_{50} values. Close inspection of the results, however, revealed a small influence of the acetyl moiety at position C-3. Thus, 3-*O*-acetyl-derivatives **6**–**9** show significantly lower EC_{50} values than their deacetylated analogues **13**–**16** (Figure 2).

Betulinic acid-derived carboxamides **17**–**30** were more cytotoxic than their corresponding ursolic acid derived analogs (**3**–**16**), showing EC_{50} values ranging between 5 μM and 0.2 μM. This is particularly evident for compounds **13** and **27** or **16** and **30** (Figure 2). The most active compounds, however, **25** and **26,** showed EC_{50} values of 0.2 μM ± 0.01 μM (**25**) and 0.3 μM ± 0.1 μM (**26**) for A2780 tumor cells. Compared to the known chemotherapeutic agent doxorubicin hydrochloride (**DRC**,

EC_{50} = 0.01 ± 0.01 μM), the activities of **25** and **26** are reduced by factors of 20 and 30, respectively. With respect to the MCF-7 human tumor cell line, however, **25** (EC_{50} = 0.3 μM ± 0.07 μM) and **26** (EC_{50} = 0.2 μM ± 0.05 μM) are even more cytotoxic than the reference compound (**DRC**, EC_{50} = 1.1 ± 0.3 μM). Calculations using the SwissTargetPrediction suggest that **25** and **26** may be possible inhibitors of tyrosine phosphates [14].

Moreover, substituents exerted similar influence for betulinic acid as well as for ursolic acid-derived carboxamides. The presence of extra substituents at the ethylenediamine spacer also had no influence onto the cytotoxicity of the compounds. However, differences between 3-*O*-acetyl-derivatives **17**–**23** and deacetylated analogs **24**–**30** were observed. Interestingly, a different trend becomes visible for most of the compounds as compared to the carboxamides from ursolic acid. Thereby, compounds holding an acetyl moiety at position 3 are significantly less cytotoxic than the corresponding 3-hydroxy-derivatives. This trend is illustrated in Figure 2 for compounds **20** and **27** and **23** and **30**, respectively.

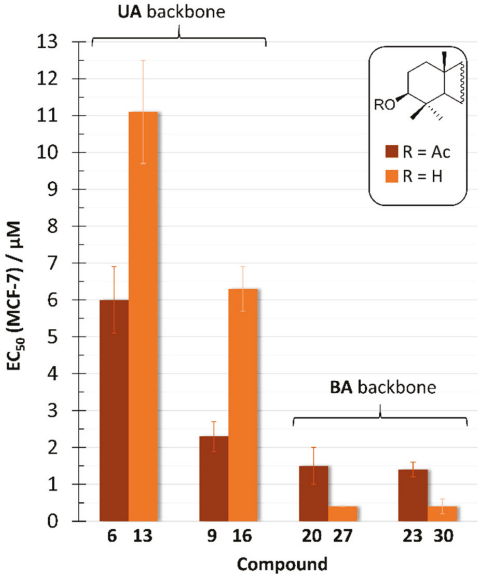

Figure 2. Comparison of EC_{50} values of selected ursolic and betulinic carboxamides for MCF-7 tumor cells.

In addition to EC_{50} values, the selectivity (which is defined as selectivity index (SI); SI = EC_{50} (NIH 3T3)/EC_{50} (tumor cell line)) is an important parameter to characterize a compound's cytotoxic activity. Therefore, the SI of each substance with respect to the individual tumor cell lines was determined (Table 2). Unfortunately, for most of the compounds, selectivity towards cancerous cells is quite poor, as indicated by SI factors close to 1. Some compounds even showed reverse selectivity behavior (SI < 1). Selectivity trends are best seen by close inspection of the SI factors for HT29 tumor cells. For ursolic acid derivatives **3**–**16**, selectivity towards HT29 cells is increased by removing the 3-*O*-acetyl moiety. The most selective ursolic acid derivative is compound **15,** with an SI of 2.67 for HT29 cells. Its acetylated analogue **8** only shows an SI of 0.76 for the same cancerous cell line. Similar to the trends observed for EC_{50} values, a different trend with regard to selectivity becomes visible for betulinic carboxamides **17**–**30** as compared to ursolic analogs. Removal of the 3-*O*-acetyl moiety seems to result in a loss of selectivity. The highest selectivity was observed for compound **18** with SI = 3.33 (NIH 3T3/HT29). Hence it is three times more cytotoxic towards HT29 tumor cells than towards nonmalignant mouse fibroblasts. Thus, its selectivity is only slightly smaller than that of the known chemotherapeutic agent doxorubicin hydrochloride (**DRC**), which shows an SI of 6 towards A2780 tumor cells. Interestingly,

compound **25**, the deacetylated analog of **18**, shows no selectivity for HT29 tumor cells at all (SI = 1.00). For the two most active compounds **25** and **26**, decreased selectivity was observed. SI factors are close to 1 for most of the cancerous cell lines. However, both compounds are slightly selective towards A2780 tumor cells (**25**: SI = 1.5; **26**: SI = 1.33) and in case of compound **26**, selectivity for MCF-7 tumor cells was also observed (SI = 2.00).

Table 2. Selectivity of compounds **3**–**30**, betulinic acid (**BA**), ursolic acid (**UA**) and doxorubicin hydrochloride (**DRC**): Selectivity index (SI) is defined as: SI = EC_{50} (NIH 3T3)/EC_{50} (tumor cell line).

	(518A2)	A2780	HT29	MCF-7	8505C
BA	1.39	1.49	0.91	1.28	-
UA	1.27	1.59	1.76	1.47	1.39
3	0.96	1.13	1.44	1.30	0.63
4	0.70	1.03	1.09	1.12	0.45
5	0.73	1.06	1.57	1.14	0.77
6	0.59	1.11	1.71	1.20	0.46
7	0.69	0.92	1.22	0.81	0.41
8	0.48	0.50	0.76	0.76	0.41
9	0.89	0.91	1.93	1.35	0.53
10	1.05	1.18	1.95	1.22	1.05
11	1.02	1.56	2.23	1.60	0.92
12	1.13	1.88	2.38	1.77	1.09
13	0.28	0.46	0.42	0.32	0.32
14	0.94	1.35	2.36	1.50	0.85
15	0.60	1.04	2.67	1.02	0.52
16	0.76	1.15	2.42	1.19	0.71
17	0.88	1.00	1.40	1.08	0.56
18	0.77	0.91	3.33	1.00	0.71
19	0.80	0.86	2.40	1.00	0.75
20	0.39	0.75	1.50	0.80	0.40
21	0.40	0.67	1.67	0.53	0.91
22	0.60	0.55	1.00	0.75	0.43
23	0.53	0.67	2.50	0.71	0.45
24	1.00	1.00	1.00	1.00	1.00
25	1.00	1.50	1.00	1.00	0.75
26	1.00	1.33	1.00	2.00	0.80
27	0.80	1.00	1.00	1.00	0.50
28	0.89	1.00	1.00	2.67	0.94
29	1.25	0.83	1.25	0.83	0.63
30	0.80	0.80	0.80	1.00	2.00
DRC	0.30	6.00	0.07	0.05	0.05

Extended biological investigations were performed for compounds **25** and **26** using dye exclusion acridine orange (AO)/propidium iodide (PI) assays by treating MCF-7 or A2780 tumor cells with **25** and **26**, respectively for 24 h (Figure 3). Fluorescence microscopic images of MCF-7 cells treated with compound **25** showed, in addition to many vital cells, both apoptotic (membrane blebbing, marked by white arrows in Figure 3) and necrotic cells (red staining). After treatment of MCF-7 cells with **26,** intact cell membranes (green staining) were observed. Close inspection revealed the presence of protrusions in the plasma membrane (blebbing) of some cells, which can be considered a feature of apoptosis. A2780 human tumor cells treated with **25** (1 μM) or **26** (1 μM) showed both green colored cells as well as late-stage apoptotic cells recognizable by orange stained nuclei. For both compounds, membrane blebbing of some cells could also be observed. These observations can be regarded as indications of apoptosis. This parallels previous findings for related oleanolic [12] and platanic carboxamides [10], whose cytotoxicity mechanisms were investigated using Annexin V-FITC/PI assays and cell cycle evaluation, and which showed them to trigger cell death by apoptosis.

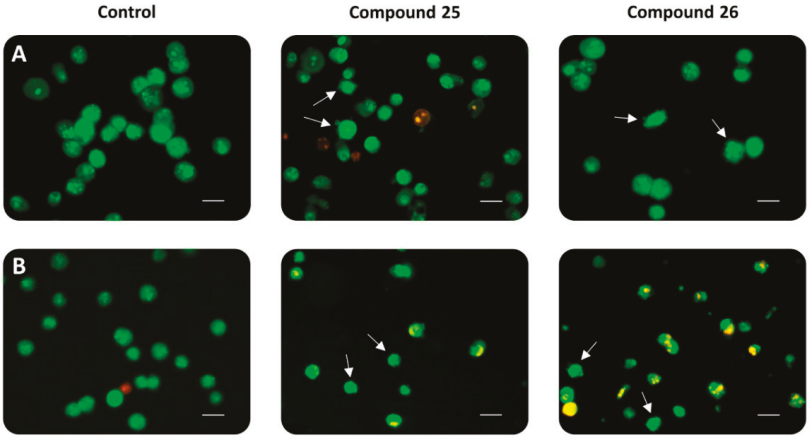

Figure 3. Fluorescence microscopic images: (**A**) treatment of MCF-7 cells with **25** (1 μM) and **26** (0.75 μM) for 24 h; (**B**) treatment of A2780 cells with **25** (1 μM) and **26** (1 μM) for 24 h; scale bar = 10 μm, AO and PI were used.

3. Materials and Methods

3.1. General

NMR spectra were recorded using the Varian spectrometers Gemini 2000 or Unity 500 (δ given in ppm, *J* in Hz; typical experiments: APT, H-H-COSY, HMBC, HSQC, NOESY), MS spectra were recorded on a Finnigan MAT LCQ 7000 (electrospray, voltage 4.1 kV, sheath gas nitrogen) instrument. The optical rotations were measured on a Perkin-Elmer polarimeter at 20 °C; TLC was performed on silica gel (Merck 5554, detection with cerium molybdate reagent); melting points are uncorrected (Leica hot stage microscope), and elemental analyses were performed on a Foss-Heraeus Vario EL (CHNS) unit. IR spectra were recorded on a Perkin Elmer FT-IR spectrometer Spectrum 1000. The solvents were dried according to usual procedures. The purity of the compounds was determined by HPLC and found to be >96%. Ursolic (**UA**) and betulinic acids (**BA**) were obtained from betulinines (Stříbrná Skalice, Czech Republic) in bulk quantities. Fluorescence microscopic images were recorded on an Axioskop 20 with an AxioCam MR3 (Carl Zeiss AG, Oberkochen, Germany).

3.2. Biology

3.2.1. Cell Lines and Culture Conditions

The cell lines used were human cancer cell lines: 518A2 (melanoma), A2780 (ovarian carcinoma), HT29 (colon adenocarcinoma), MCF-7 (breast adenocarcinoma), 8505C (thyroid carcinoma) and non-malignant mouse fibroblasts NIH 3T3. Cultures were maintained as monolayers in RPMI 1640 medium with L-glutamine (Capricorn Scientific GmbH, Ebsdorfergrund, Germany) supplemented with 10% heat inactivated fetal bovineserum (Sigma-Aldrich Chemie GmbH, Steinheim, Germany) and penicillin/streptomycin (Capricorn Scientific GmbH, Ebsdorfergrund, Germany) at 37 °C in a humidified atmosphere with 5% CO_2.

3.2.2. Cytotoxic Assay (SRB)

The cytotoxicity of the compounds was evaluated using the sulforhodamine-B (Kiton-Red S, ABCR) micro culture colorimetric assay. Cells were seeded into 96-well plates on day 0 at appropriate cell densities to prevent confluence of the cells during the period of experiment. After 24 h, the cells were treated with 6 different concentrations (1, 3, 7, 12, 20 and 30 μM) minimum. The final

concentration of DMSO/DMF never exceeded 0.5%, which was non-toxic to the cells. After a 96 h treatment, the supernatant medium from the 96-well plates was discarded, the cells were fixed with 10% trichloroacetic acid (TCA) and allowed to rest at 4 °C. After 24 h fixation, the cells were washed in a strip washer and dyed with SRB solution (100 μL, 0.4% in 1% acetic acid) for about 20 min. After dying, the plates were washed four times with 1% acetic acid to remove the excess of the dye and allowed to air-dry overnight. Tris base solution (200 μL, 10 mM) was added to each well and absorbance was measured at λ = 570 nm using a 96-well plate reader (Tecan Spectra, Crailsheim, Germany). The EC_{50} values were averaged from three independent experiments performed each in triplicate calculated from semi logarithmic dose response curves applying a non-linear 4P Hills-slope equation (GraphPad Prism5; variables top and bottom were set to 100 and 0, respectively).

3.2.3. AO/PI Dye Exclusion Test

Morphological characteristics of cell death were analyzed employing an AO/PI assay using human cancer cell lines A2780 and MCF-7. Approximately 8×10^5 cells were seeded in cell culture flasks (25 cm^2), and the cells were allowed to grow for 24 h. After removing the used medium, fresh medium was reloaded (or a blank new medium was used as a control). After 24 h, the content of the flask was collected and centrifuged (1200 rpm, 4 °C), and the pellet was gently suspended in phosphate-buffered saline (PBS (*w*/*w*), 1 mL) and centrifuged again. The PBS was removed, and the pellet gently suspended in PBS (50 μL) again. The analysis of the cells was performed using a fluorescence microscope after having mixed the cell suspension (10 μL) with a solution of AO/PI (1 μg/mL, 10 μL).

4. Experimental

*4.1. General Procedure A for the Acetylation of Triterpenoic Acids (***1**–**2***)*

To a solution of **UA** or **BA** (5 g, 11 mmol) in dry DCM (150 mL) was added triethylamine (4.6 mL, 33 mmol), acetic anhydride (3.1 mL, 33 mmol) and DMAP (cat.). After stirring for 2 days at 25 °C, a saturated solution of NH_3 in MeOH was added (3 mL), and the mixture was stirred for another 30 min. Dilution with DCM and subsequent aqueous work-up provided crude 3-*O*-acetyl-UA or 3-*O*-acetyl-BA. Recrystallization from EtOH yielded pure acetates **1** (5.3 g, 96%) and **2** (5.1 g, 93%) both as colorless solids, whose analytical and spectroscopic data were in full agreement with data from the literature.

*4.2. General Procedure B for the Synthesis of Triterpenoic Amides (***3**–**9**, **17**–**23***)*

Compounds **1** or **2** (0.8 mmol) were each dissolved in dry DCM (15 mL), cooled to 0 °C, and oxalyl chloride (3.2 mmol) and dry DMF (3 drops) were added. After warming to 25 °C, the mixture was stirred for 1 h. The solvent was removed under reduced pressure, re-evaporated with dry THF (4 × 15 mL), and the residue was immediately resolved in dry DCM (10 mL). This mixture was then added dropwise to a solution of the amine (2.4 mmol) in dry DCM (5 mL) and stirred at 25 °C for 2 h. After usual aqueous work-up, the solvent was removed under reduced pressure, and the crude product was subjected to column chromatography (silica gel, chloroform/methanol mixtures). Compounds **3**–**9** and **17**–**23** were each obtained as colorless solids.

*4.3. General Procedure C for Deacetylation of Triterpenoic Amides (***10**–**16**, **24**–**30***)*

To a solution of acetylated amides **3**–**9** or **17**–**23** (0.33 mmol) in methanol (10 mL) was added a solution of potassium hydroxide (1.65 mmol) in methanol (2 mL). The mixture was stirred at 25 °C for 2 or 3 days. After completion of the reaction (as indicated by TLC), aq. HCl was added until pH = 7. After usual work-up, the solvent was removed under reduced pressure, and the residue was subjected to column chromatography (silica gel, chloroform/methanol mixtures) yielding compounds **10**–**16** and **24**–**30** each as colorless solids.

(3β)-3-Acetyloxy-urs-12-en-28-oic acid (**1**). Compound **1** was prepared according to general procedure A from ursolic acid. Yield: 96%; m.p. 287–290 °C (lit.: 289–290 °C [15]).

(3β)-3-Acetyloxy-lup-20(29)en-28-oic acid (**2**). Compound **2** was prepared according to general procedure A from betulinic acid. Yield: 93%; m.p. 281–284 °C (lit.: 280-282 °C [16]).

(3β)-N-(2-Aminoethyl)-3-acetyloxy-urs-12-en-28-amide (**3**). Compound **3** was prepared from **1** according to general procedure B using ethylenediamine. Column chromatography (SiO_2, $CHCl_3$/MeOH 9:1) gave **3** (yield: 80%); m.p. 202–205 °C (lit.: 140–142 °C [17]); $[\delta]_D$ = +39.4° (*c* 0.355, $CHCl_3$); R_f = 0.48 ($CHCl_3$/MeOH 9:1); IR (KBr): ν = 3413*br s*, 2948*s*, 1735*s*, 1633*s*, 1526*s*, 1456*s*, 1370*s*, 1247*s*, 1174*w*, 1147*w*, 1092*w*, 1028*s*, 1006*m*, 986*m*, 755*m* cm^{-1}; ^{1}H-NMR (500 MHz, $CDCl_3$): δ = 6.88 (*t*, *J* = 5.3 Hz, 1H, NH), 5.34 (*t*, *J* = 3.3 Hz, 1H, 12-H), 4.49 (*dd*, *J* = 10.0, 5.9 Hz, 1H, 3-H), 3.62–3.54 (*m*, 1H, 31-H_a), 3.38–3.30 (*m*, 1H, 31-H_b), 3.13–3.01 (*m*, 2H, 32-H_a, 32-H_b), 2.09–2.04 (*m*, 1H, 18-H), 2.04 (*s*, 3H, Ac), 2.03–1.87 (*m*, 3H, 16-H_a, 11-H_a, 11-H_b), 1.82–1.22 (*m*, 15H, 22-H_a, 16-H_b, 1-H_a, 15-H_a, 2-H_a, 2-H_b, 9-H, 22-H_b, 6-H_a, 21-H_a, 7-H_a, 19-H, 6-H_b, 7-H_b, 21-H_b), 1.08 (*s*, 3H, 27-H), 1.07–0.95 (*m*, 3H, 1-H_b, 15-H_b, 20-H), 0.96–0.92 (*m*, 4H, 25-H, 20-H), 0.89–0.85 (*m*, 6H, 23-H, 29-H), 0.85 (*s*, 3H, 24-H), 0.84–0.80 (*m*, 1H, 5-H), 0.74 (*s*, 3H, 26-H) ppm; ^{13}C-NMR (126 MHz, $CDCl_3$): δ = 180.2 (C-28), 171.1 (Ac), 139.3 (C-13), 126.0 (C-12), 81.0 (C-3), 55.4 (C-5), 53.1 (C-18), 47.9 (C-17), 47.6 (C-9), 42.4 (C-14), 40.6 (C-32), 39.8 (C-19), 39.7 (C-8), 39.0 (C-20), 38.7 (C-31), 38.5 (C-1), 37.8 (C-4), 37.4 (C-22), 37.0 (C-10), 32.8 (C-7), 31.0 (C-21), 28.2 (C-23), 28.0 (C-15), 24.8 (C-16), 23.7 (C-2), 23.5 (C-11), 23.5 (C-27), 21.4 (Ac), 21.3 (C-30), 18.3 (C-6), 17.4 (C-29), 17.2 (C-26), 16.9 (C-24), 15.7 (C-25) ppm; MS (ESI, MeOH): *m*/*z* = 541 (100 %, $[M + H]^+$); analysis calcd for $C_{34}H_{56}N_2O_3$ (540.83): C 75.51, H 10.44, N 5.18; found: C 75.32, H 10.61, N 5.01.

*(3β)-N-[2-(Dimethylamino)ethyl]-3-acetyloxy-urs-12-en-28-*amide (**4**). Compound **4** was prepared from **1** according to general procedure B using *N*,*N*-dimethylethylenediamine. Column chromatography (SiO_2, $CHCl_3$/MeOH 95:5) gave **4** (yield: 88%); m.p. 121–124 °C; $[\alpha]_D$ = +44.9° (*c* 0.300, $CHCl_3$); R_f = 0.49 ($CHCl_3$/MeOH 9:1); IR (KBr): ν = 3422*br m*, 2937*m*, 1734*m*, 1636*m*, 1522*w*, 1457*m*, 1384*s*, 1247*m*, 1028*m* cm^{-1}; ^{1}H-NMR (500 MHz, $CDCl_3$): δ = 6.68 (*t*, *J* = 5.0 Hz, 1H, NH), 5.33 (*t*, *J* = 3.4 Hz, 1H, 12-H), 4.48 (*dd*, *J* = 10.5, 5.6 Hz, 1H, 3-H), 3.62–3.52 (*m*, 1H, 31-H_a), 3.29–3.21 (*m*, 1H, 31-H_b), 2.83 (*t*, *J* = 5.3 Hz, 2H, 32-H), 2.58 (*s*, 6H, 33-H, 33′-H), 2.03 (*s*, 3H, Ac), 2.02–1.86 (*m*, 4H, 16-H_a, 18-H, 11-H_a, 11-H_b), 1.83–1.76 (*m*, 1H, 22-H_a), 1.73–1.67 (*m*, 1H, 16-H_b), 1.67–1.57 (*m*, 4H, 1-H_a, 15-H_a, 2-H_a, 2-H_b), 1.57–1.26 (*m*, 9H, 9-H, 6-H_a, 7-H_a, 21-H_a, 22-H_b, 19-H, 6-H_b, 21-H_b, 7-H_b), 1.07 (*s*, 3H, 27-H), 1.06–0.94 (*m*, 3H, 1-H_b, 15-H_b, 20-H), 0.93 (*d*, *J* = 6.1 Hz, 3H, 30-H), 0.93 (*s*, 3H, 25-H), 0.87 (*d*, *J* = 6.5 Hz, 3H, 29-H), 0.85 (*s*, 3H, 23-H), 0.84 (*s*, 3H, 24-H), 0.83–0.80 (*m*, 1H, 5-H), 0.75 (*s*, 3H, 26-H) ppm; ^{13}C-NMR (126 MHz, $CDCl_3$): δ = 179.1 (C-28), 171.1 (Ac), 139.2 (C-13), 126.0 (C-12), 81.0 (C-3), 57.7 (C-32), 55.4 (C-5), 53.4 (C-18), 47.9 (C-17), 47.6 (C-9), 44.6 (C-33, C-33′), 42.4 (C-14), 39.8 (C-19), 39.7 (C-8), 39.0 (C-20), 38.4 (C-1), 37.8 (C-4), 37.4 (C-22), 37.0 (C-10), 35.9 (C-31), 32.8 (C-7), 31.0 (C-21), 28.2 (C-23), 28.0 (C-15), 24.8 (C-16), 23.7 (C-2), 23.5 (C-11), 23.4 (C-27), 21.4 (Ac), 21.3 (C-30), 18.3 (C-6), 17.3 (C-29), 17.1 (C-26), 16.9 (C-24), 15.7 (C-25) ppm; MS (ESI, MeOH): *m*/*z* = 569 (100%, $[M + H]^+$); analysis calcd for $C_{36}H_{60}N_2O_3$ (568.89): C 76.01, H 10.63, N 4.92; found: C 75.87, H 10.84, N 4.69.

(3β)-N-(2-Pyrrolidin-1-ylethyl)-3-acetyloxy-urs-12-en-28-amide (**5**). Compound **5** was prepared from **1** according to general procedure B using 1-(2-aminoethyl)-pyrrolidine. Column chromatography (SiO_2, $CHCl_3$/MeOH 95:5) gave **5** (yield: 92%). m.p. 156–159 °C; $[\alpha]_D$ = +45.9° (*c* 0.355, $CHCl_3$); R_f = 0.44 ($CHCl_3$/MeOH 9:1); IR (KBr): ν = 3404*br s*, 2948*s*, 1734*s*, 1651*s*, 1526*s*, 1456*s*, 1371*s*, 1246*s*, 1146*w*, 1091*m*, 1027*s*, 1006*m*, 985*m*, 753*m* cm^{-1}; ^{1}H-NMR (500 MHz, $CDCl_3$): δ = 6.90 (*dd*, *J* = 11.5, 5.6 Hz, 1H, NH), 5.36 (*dd*, *J* = 7.1, 3.6 Hz, 1H, 12-H), 4.47 (*dd*, *J* = 10.5, 5.3 Hz, 1H, 3-H), 3.89–3.82 (*m*, 1H, 31-H_a), 3.82–3.73 (*m*, 2H, 33-H_a, 33′-H_a) 3.41–3.32 (*m*, 1H, 31-H_b), 3.30–3.21 (*m*, 2H, 32-H), 2.93–2.83 (*m*, 2H, 33-H_b, 33′-H_b), 2.23–2.06 (*m*, 4H, 34-H, 34′-H), 2.02 (*s*, 3H, Ac), 2.01–1.95 (*m*, 2H, 16-H_a, 18-H), 1.95–1.90 (*m*, 2H, 11-H_a, 11-H_b), 1.76–1.56 (*m*, 6H, 22-H_a, 16-H_b, 1-H_a, 15-H_a, 2-H_a, 2-H_b), 1.55–1.41 (*m*, 5H, 9-H, 6-H_a, 22-H_b, 7-H_a, 21-H_a), 1.41–1.21 (*m*, 4H, 19-H, 6-H_b, 7-H_b, 21-H_b), 1.06 (*s*, 3H, 27-H), 1.10–0.94 (*m*, 3H, 1-H_b, 15-H_b, 20-H), 0.92 (*s*, 3H, 25-H), 0.91 (*d*, *J* = 6.1 Hz, 3H, 30-H), 0.86 (*d*, *J* = 6.5 Hz, 3H, 29-H),

0.84 (*s*, 3H, 23-H), 0.83 (*s*, 3H, 24-H), 0.82–0.78 (*m*, 1H, 5-H), 0.71 (*s*, 3H, 26-H) ppm; ^{13}C-NMR (126 MHz, $CDCl_3$): δ = 179.8 (C-28), 171.1 (Ac), 138.9 (C-13), 126.0 (C-12), 80.9 (C-3), 55.3 (C-5), 55.0 (C-32), 54.8 (C-33, C-33′), 52.9 (C-18), 47.9 (C-17), 47.5 (C-9), 42.3 (C-14), 39.7 (C-19), 39.7 (C-8), 38.8 (C-20), 38.4 (C-1), 37.8 (C-4), 37.4 (C-22), 37.0 (C-10), 36.2 (C-31), 32.8 (C-7), 30.9 (C-21), 28.2 (C-23), 27.9 (C-15), 24.7 (C-16), 23.6 (C-2), 23.5 (C-27), 23.4 (C-11), 23.3 (C-34, C-34′), 21.4 (Ac), 21.3 (C-30), 18.3 (C-6), 17.2 (C-29), 17.1 (C-26), 16.8 (C-24), 15.6 (C-25) ppm; MS (ESI, MeOH): *m*/*z* = 595 (100%, $[M + H]^+$); analysis calcd for $C_{38}H_{62}N_2O_3$ (594.93): C 76.72, H 10.50, N 4.71; found: C 76.60, H 10.72, N 4.59.

*(3β)-N-(2-Piperidin-1-ylethyl)-3-acetyloxy-urs-12-en-28-*amide (**6**). Compound **6** was prepared from **1** according to general procedure B using 1-(2-aminoethyl)-piperidine. Column chromatography (SiO_2, $CHCl_3$/MeOH 95:5) gave **6** (yield: 83%); m.p. 124–127 °C; $[\alpha]_D$ = +34.6° (*c* 0.365, $CHCl_3$); R_f = 0.26 ($CHCl_3$/MeOH 95:5); IR (KBr): ν = 3424*br s*, 2936*s*, 2872*m*, 2854*m*, 1736*s*, 1638*s*, 1508*m*, 1456*m*, 1370*m*, 1246*s*, 1154*w*, 1128*w*, 1092*w*, 1028*m* cm^{-1}; ^{1}H-NMR (400 MHz, $CDCl_3$): δ = 6.56–6.51 (*m*, 1H, NH), 5.30 (*t*, *J* = 3.6 Hz, 1H, 12-H), 4.49 (*dd*, *J* = 10.4, 5.8 Hz, 1H, 3-H), 3.41–3.29 (*m*, 1H, 31-H_a), 3.24–3.12 (*m*, 1H, 31-H_b), 2.49–2.27 (*m*, 6H, 32-H, 33-H, 33′-H), 2.03 (*s*, 3H, Ac), 2.01–1.80 (*m*, 5H, 16-H_a, 11-H_a, 11-H_b, 18, 22-H_a), 1.78–1.22 (*m*, 20H, 16-H_b, 15-H_a, 1-H_a, 2-H_a, 2-H_b, 34-H, 34′-H, 9-H, 6-H_a, 21-H_a, 7-H_a, 35-H, 22-H_b, 19-H, 6-H_b, 21-H_b, 7-H_b), 1.08 (*s*, 3H, 27-H), 1.14–0.96 (*m*, 3H, 1-H_b, 15-H_b, 20-H), 0.95–0.93 (*m*, 3H, 30-H), 0.93 (*s*, 3H, 25-H), 0.88 (*d*, *J* = 6.5 Hz, 3H, 29-H), 0.86 (*s*, 3H, 23-H), 0.85 (*s*, 3H, 24-H), 0.84–0.79 (*m*, 1H, 5-H), 0.77 (*s*, 3H, 26-H) ppm; ^{13}C-NMR (101 MHz, $CDCl_3$): δ = 178.0 (C-28), 171.1 (Ac), 139.5 (C-13), 125.6 (C-12), 81.0 (C-3), 57.2 (C-32), 55.4 (C-5), 54.5 (C-33, C-33′), 54.0 (C-18), 47.9 (C-17), 47.6 (C-9), 42.5 (C-14), 39.9 (C-19), 39.7 (C-8), 39.2 (C-20), 38.4 (C-1), 37.8 (C-4), 37.5 (C-22), 37.0 (C-10), 36.0 (C-31), 32.9 (C-7), 31.1 (C-21), 28.2 (C-23), 28.0 (C-15), 26.2 (C-34, C-34′), 24.9 (C-16), 24.5 (C-35), 23.7 (C-2), 23.5 (C-11), 23.4 (C-27), 21.4 (Ac), 21.4 (C-30), 18.3 (C-6), 17.5 (C-29), 17.1 (C-26), 16.9 (C-24), 15.7 (C-25) ppm; MS (ESI, MeOH): *m*/*z* = 609 (100%, $[M + H]^+$); analysis calcd for $C_{39}H_{64}N_2O_3$ (608.95): C 76.92, H 10.59, N 4.60; found: C 76.77, H 10.79, N 4.41.

(3β)-N-(2-Piperazin-1-ylethyl)-3-acetyloxy-urs-12-en-28-amide (**7**). Compound **7** was prepared from **1** according to general procedure B using 1-(2-aminoethyl)-piperazine. Column chromatography (SiO_2, $CHCl_3$/MeOH 9:1) gave **7** (yield: 82%); m.p. 145–147 °C (lit.: 147–150 °C [18]); $[a]_D$ = +35.9° (*c* 0.365, $CHCl_3$); R_f = 0.29 ($CHCl_3$/MeOH 9:1); IR (KBr): ν = 3441*s*, 2947*m*, 1734*m*, 1636*m*, 1458*w*, 1370*w*, 1247*m*, 1027*w* cm^{-1}; ^{1}H-NMR (400 MHz, $CDCl_3$): δ = 6.42 (*t*, *J* = 4.6 Hz, 1H, N*H*), 5.30 (*t*, *J* = 3.6 Hz, 1H, 12-H), 4.49 (*dd*, *J* = 10.4, 5.3 Hz, 1H, 3-H), 3.42–3.32 (*m*, 1H, 31-H_a), 3.23–3.13 (*m*, 1H, 31-H_b), 2.93 (*t*, *J* = 4.9 Hz, 4H, 34-H, 34′-H), 2.49–2.37 (*m*, 6H, 32-H, 33-H, 33′-H), 2.04 (*s*, 3H, Ac), 2.02–1.80 (*m*, 5H, 16-H_a, 11-H_a, 11-H_b, 22-H_a, 18-H), 1.80–1.22 (*m*, 14H, 16-H_b, 15-H_a, 1-H_a, 2-H_a, 2-H_b, 9-H, 6-H_a, 21-H_a, 7-H_a, 22-H_b, 19-H, 6-H_b, 21-H_b, 7-H_b), 1.08 (*s*, 3H, 27-H), 1.07–0.94 (*m*, 3H, 1-H_b, 15-H_b, 20-H), 0.96–0.94 (*m*, 3H, 30-H), 0.93 (*s*, 3H, 25-H), 0.88 (*d*, *J* = 6.5 Hz, 3H, 29-H), 0.86 (*s*, 3H, 23-H), 0.85 (*s*, 3H, 24-H), 0.84–0.78 (*m*, 1H, 5-H), 0.77 (*s*, 3H, 26-H) ppm; ^{13}C-NMR (101 MHz, $CDCl_3$): δ = 178.0 (C-28), 171.1 (Ac), 139.7 (C-13), 125.5 (C-12), 81.0 (C-3), 57.1 (C-32), 55.4 (C-5), 54.1 (C-18), 53.9 (C-33), 47.9 (C-17), 47.6 (C-9), 46.1 (C-34), 42.6 (C-14), 39.9 (C-19), 39.7 (C-8), 39.3 (C-20), 38.4 (C-1), 37.8 (C-4), 37.5 (C-22), 37.0 (C-10), 35.8 (C-31), 32.8 (C-7), 31.1 (C-21), 28.2 (C-23), 28.0 (C-15), 25.0 (C-16), 23.7 (C-2), 23.6 (C-11), 23.4 (C-27), 21.4 (Ac), 21.3 (C-30), 18.3 (C-6), 17.5 (C-29), 17.1 (C-26), 16.9 (C-24), 15.7 (C-25) ppm; MS (ESI, MeOH): *m*/*z* = 610 (100 %, $[M + H]^+$); analysis calcd for $C_{38}H_{63}N_3O_3$ (609.94): C 74.83, H 10.41, N 6.89; found: C 74.57, H 10.69, N 6.64.

(3β)-N-(4-Aminobutyl)-3-acetyloxy-urs-12-en-28-amide (**8**). Compound **8** was prepared from **1** according to general procedure B using 1,4-diaminobutane. Column chromatography (SiO_2, $CHCl_3$/MeOH/NH_4OH 90:10:1) gave **8** (yield: 79%); m.p. 117–120 °C; $[\alpha]_D$ = +33.7° (*c* 0.305, $CHCl_3$); R_f = 0.34 ($CHCl_3$/MeOH/NH_4OH 90:10:1); IR (KBr): ν = 3440*s*, 2928*m*, 1736*w*, 1636*m*, 1522*w*, 1458*w*, 1370*w*, 1246*m*, 1028*w* cm^{-1}; ^{1}H-NMR (400 MHz, $CDCl_3$): δ = 6.03 (*t*, *J* = 5.5 Hz, 1H, NH), 5.30 (*t*, *J* = 3.6 Hz, 1H, 12-H), 4.53–4.46 (*dd*, *J* = 9.7, 6.2 Hz, 1H, 3-H), 3.41–3.30 (*m*, 1H, 31-H_a), 3.05–2.94 (*m*, 1H, 31-H_b), 2.78 (*t*, *J* = 6.2 Hz, 2H, 32-H_a, 32-H_b), 2.04 (*s*, 3H, Ac), 2.02–1.90 (*m*, 3H, 11-H_a, 11-H_b, 16-H_a), 1.90–1.80 (*m*, 2H, 18-H, 22-H_a), 1.76–1.20 (*m*, 18H, 16-H_b, 15-H_a, 1-H_a, 2-H_a, 2-H_b, 9-H, 6-H_a, 34-H_a,

34-H_b, 33-H_a, 33-H_b, 21-H_a, 7-H_a, 19-H, 22-H_b, 6-H_b, 21-H_b, 7-H_b), 1.09 (*s*, 3H, 27-H), 1.14–1.01 (*m*, 2H, 1-H_b, 15-H_b), 0.95 (*s*, 7H, 25-H, 30-H, 20-H), 0.89–0.86 (*m*, 3H, 29-H), 0.86 (*s*, 3H, 23-H), 0.85 (*s*, 3H, 24-H), 0.84–0.80 (*m*, 1H, 5-H), 0.77 (*s*, 3H, 26-H) ppm; ^{13}C-NMR (101 MHz, $CDCl_3$): δ = 178.2 (C-28), 171.1 (Ac), 140.2 (C-13), 125.6 (C-12), 81.0 (C-3), 55.4 (C-5), 54.1 (C-18), 47.8 (C-17), 47.6 (C-9), 42.7 (C-14), 41.8 (C-32), 39.9 (C-19), 39.7 (C-8), 39.4 (C-31), 39.3 (C-20), 38.5 (C-1), 37.8 (C-4), 37.4 (C-22), 37.0 (C-10), 32.8 (C-7), 31.2 (C-21), 30.8 (C-33), 28.2 (C-23), 28.0 (C-15), 26.9 (C-34), 25.0 (C-16), 23.7 (C-2), 23.6 (C-11), 23.4 (C-27), 21.5 (Ac), 21.4 (C-30), 18.3 (C-6), 17.4 (C-29), 17.1 (C-26), 16.9 (C-24), 15.7 (C-25) ppm; MS (ESI, MeOH): *m*/*z* = 569 (100%, $[M + H]^+$); analysis calcd for $C_{36}H_{60}N_2O_3$ (568.89): C 76.01, H 10.63, N 4.92; found: C 75.84, H 10.91, N 4.63.

(3β)-N-[2-(2-Aminoethoxy)ethyl]-3-acetyloxy-urs-12-en-28-amide (**9**). Compound **9** was prepared from **1** according to general procedure B using 2,2′-oxybis(ethylamine). Column chromatography (SiO_2, $CHCl_3$/MeOH/NH_4OH 90:10:0.1) gave **9** (yield: 78%); m.p. 91–94 °C; $[\alpha]_D$ = +18.3° (*c* 0.310, $CHCl_3$); R_f = 0.39 ($CHCl_3$/MeOH 9:1); IR (KBr): ν = 3424*br s*, 2927*s*, 2871*s*, 1735*s*, 1640*s*, 1529*m*, 1455*m*, 1370*m*, 1247*s*, 1120*m*, 1027*m* cm^{-1}; ^{1}H-NMR (500 MHz, $CDCl_3$): δ = 6.29 (*t*, *J* = 5.0 Hz, 1H, NH), 5.28 (*t*, *J* = 3.6 Hz, 1H, 12-H), 4.48 (*dd*, *J* = 10.9, 5.3 Hz, 1H, 3-H), 3.57–3.44 (*m*, 5H, 31-H_a, 32-H, 33-H), 3.30–3.22 (*m*, 1H, 31-H_b), 2.87 (*t*, J = 5.3 Hz, 2H, 34-H), 2.03 (*s*, 3H, Ac), 2.01–1.81 (*m*, 5H, 16-H_a, 11-H_a, 11-H_b, 18-H, 22-H_a), 1.78–1.22 (*m*, 14H, 16-H_b, 15-H_a, 1-H_a, 2-H_a, 2-H_b, 9-H, 6-H_a, 21-H_a, 7-H_a, 22-H_b, 19-H, 6-H_b, 21-H_b, 7-H_b), 1.08 (*s*, 3H, 27-H), 1.12–1.00 (*m*, 2H, 1-H_b, 15-H_b), 0.99–0.90 (*m*, 4H, 30-H, 20-H), 0.93 (*s*, 3H, 25-H), 0.86 (*d*, *J* = 6.6 Hz, 3H, 29-H), 0.85 (*s*, 3H, 23-H), 0.84 (*s*, 3H, 24-H), 0.83–0.80 (*m*, 1H, 5-H), 0.78 (*s*, 3H, 26-H) ppm; ^{13}C-NMR (126 MHz, $CDCl_3$): δ = 178.3 (C-28), 171.1 (Ac), 139.8 (C-13), 125.7 (C-12), 81.0 (C-3), 73.2 (C-33), 69.6 (C-32), 55.4 (C-5), 53.9 (C-18), 47.9 (C-17), 47.6 (C-9), 42.6 (C-14), 42.0 (C-34), 39.9 (C-19), 39.7 (C-8), 39.3 (C-31), 39.2 (C-20), 38.4 (C-1), 37.8 (C-4), 37.3 (C-22), 37.0 (C-10), 32.8 (C-7), 31.0 (C-21), 28.2 (C-23), 28.0 (C-15), 25.0 (C-16), 23.7 (C-2), 23.6 (C-11), 23.4 (C-27), 21.4 (Ac), 21.4 (C-30), 18.3 (C-6), 17.4 (C-29), 17.0 (C-26), 16.8 (C-24), 15.7 (C-25) ppm; MS (ESI, MeOH): *m*/*z* = 585 (100 %, $[M + H]^+$); analysis calcd for $C_{36}H_{60}N_2O_4$ (584.89): C 73.93, H 10.34, N 4.79; found: C 73.77, H 10.51, N 4.56.

(3β)-N-(2-Aminoethyl)-3-hydroxy-urs-12-en-28-amide (**10**). Compound **10** was prepared from **3** according to general procedure C. Column chromatography (SiO_2, $CHCl_3$/MeOH/NH_4OH 90:10:0.1) gave **10** (yield: 85%); m.p. 139–142 °C (lit.: 145–147 °C [17]); $[\alpha]_D$ = +38.6° (*c* 0.300, $CHCl_3$); R_f = 0.34 ($CHCl_3$/MeOH 9:1); IR (KBr): ν = 3425*br s*, 2926*s*, 1638*m*, 1529*m*, 1454*m*, 1386*w*, 1092*w*, 1046*m*, 755*m* cm^{-1}; ^{1}H-NMR (400 MHz, $CDCl_3$): δ = 6.36 (*t*, *J* = 5.4 Hz, 1H, N*H*), 5.33 (*t*, *J* = 3.4 Hz, 1H, 12-H), 3.46–3.36 (*m*, 1H, 31-H_a), 3.21 (*dd*, *J* = 11.1, 4.7 Hz, 1H, 3-H), 3.13–3.02 (*m*, 1H, 31-H_b), 2.82 (*t*, *J* = 5.9 Hz, 2H, 32-H_a, 32-H_b), 2.05–1.82 (*m*, 5H, 16-H_a, 11-H_a, 11-H_b, 18-H, 22-H_a), 1.77–1.23 (*m*, 14H, 16-H_b, 15-H_a, 1-H_a, 2-H_a, 2-H_b, 9-H, 6-H_a, 21-H_a, 7-H_a, 22-H_b, 19-H, 6-H_b, 21-H_b, 7-H_b), 1.09 (*s*, 3H, 27-H), 1.07–0.99 (*m*, 2H, 15-H_b, 1-H_b), 0.98 (*s*, 3H, 23-H), 0.96–0.93 (*m*, 4H, 20-H, 30-H), 0.91 (*s*, 3H, 25-H), 0.87 (*d*, *J* = 6.5 Hz, 3H, 29-H), 0.78 (*s*, 6H, 24-H, 26-H), 0.74–0.69 (*m*, 1H, 5-H) ppm; ^{13}C-NMR (101 MHz, $CDCl_3$): *δ* = 178.8 (C-28), 139.7 (C-13), 125.9 (C-12), 79.1 (C-3), 55.3 (C-5), 53.9 (C-18), 48.0 (C-17), 47.7 (C-9), 42.6 (C-14), 41.8 (C-31), 41.3 (C-32), 39.9 (C-19), 39.7 (C-8), 39.2 (C-20), 38.9 (C-4), 38.8 (C-1), 37.5 (C-22), 37.1 (C-10), 32.9 (C-7), 31.1 (C-21), 28.3 (C-23), 28.0 (C-15), 27.4 (C-2), 25.0 (C-16), 23.6 (C-11), 23.4 (C-27), 21.4 (C-30), 18.4 (C-6), 17.4 (C-29), 17.1 (C-26), 15.8 (C-24), 15.7 (C-25) ppm; MS (ESI, MeOH): *m*/*z* = 499 (100 %, $[M + H]^+$); analysis calcd for $C_{32}H_{54}N_2O_2$ (498.80): C 77.06, H 10.91, N 5.62; found: C 76.92, H 11.08, N 5.40.

(3β)-N-[2-(Dimethylamino)ethyl]-3-hydroxy-urs-12-en-28-amide (**11**). Compound **11** was prepared from **4** according to general procedure C. Column chromatography (SiO_2, $CHCl_3$/MeOH 95:5) gave **11** (yield: 86%). m.p. 270–273 °C (decomp.); $[\alpha]_D$ = +38.5° (*c* 0.375, $CHCl_3$); R_f = 0.44 ($CHCl_3$/MeOH 9:1); IR (KBr): ν = 3402*br s*, 2924*s*, 2868*s*, 2684*m*, 1658*s*, 1518*m*, 1460*s*, 1386*m*, 1212*w*, 1138*w*, 1046*m*, 1028*m*, 994*m* cm^{-1}; ^{1}H-NMR (500 MHz, $CDCl_3$): δ = 7.18 (*dd*, *J* = 5.6, 5.6 Hz, 1H, NH), 5.41 (*t*, *J* = 3.6 Hz, 1H, 12-H), 3.78–3.68 (*m*, 1H, 31-H_a), 3.59–3.49 (*m*, 1H, 31-H_b), 3.21 (*dd*, *J* = 11.0, 4.7 Hz, 1H, 3-H), 3.18–3.13 (*m*, 2H, 32-H), 2.84 (*s*, 6H, 33-H, 33′-H), 2.20 (*d*, *J* = 10.5 Hz, 1H, 18-H), 2.03 (*ddd*, *J* = 13.7, 13.7, 4.2 Hz, 1H,

16-H_a), 1.96–1.91 (*m*, 2H, 11-H_a, 11-H_b), 1.81–1.26 (*m*, 15H, 22-H_a, 16-H_b, 15-H_a, 1-H_a, 2-H_a, 2-H_b, 6-H_a, 9-H, 22-H_b, 7-H_a, 21-H_a, 19-H, 6-H_b, 7-H_b, 21-H_b), 1.08 (*s*, 3H, 27-H), 1.07–0.96 (*m*, 3H, 15-H_b, 20-H, 1-H_b), 0.98 (*s*, 3H, 23-H), 0.93 (*d*, *J* = 6.5 Hz, 3H, 30-H), 0.90 (*s*, 3H, 25-H), 0.88 (*d*, *J* = 6.5 Hz, 3H, 29-H), 0.77 (*s*, 3H, 24-H), 0.73 (*s*, 3H, 26-H), 0.72–0.69 (*m*, 1H, 5-H) ppm; ^{13}C-NMR (126 MHz, $CDCl_3$): δ = 179.6 (C-28), 138.8 (C-13), 126.2 (C-12), 79.1 (C-3), 58.2 (C-32), 55.3 (C-5), 52.7 (C-18), 48.0 (C-17), 47.7 (C-9), 44.2 (C-33), 43.9 (C-33′), 42.3 (C-14), 39.7 (C-8), 39.7 (C-19), 38.9 (C-1), 38.8 (C-20), 38.7 (C-4), 37.4 (C-22), 37.1 (C-10), 35.1 (C-31), 32.9 (C-7), 31.0 (C-21), 28.3 (C-23), 28.0 (C-15), 27.4 (C-2), 24.6 (C-16), 23.6 (C-27), 23.5 (C-11), 21.3 (C-30), 18.4 (C-6), 17.2 (C-29), 17.2 (C-26), 15.8 (C-24), 15.6 (C-25) ppm; MS (ESI, MeOH): *m*/*z* = 527 (100%, $[M + H]^+$); analysis calcd for $C_{34}H_{58}N_2O_2$ (526.85): C 77.51, H 11.10, N 5.32; found: C 77.37, H 11.25, N 5.17.

(3β)-N-(2-Pyrrolidin-1-ylethyl)-3-hydroxy-urs-12-en-28-amide (**12**). Compound **12** was prepared from **5** according to general procedure C. Column chromatography (SiO_2, $CHCl_3$/MeOH 95:5) gave **12** (yield: 84%); m.p. 263–266 °C (decomp.); $[\alpha]_D$ = +39.8° (*c* 0.445, MeOH); R_f = 0.40 ($CHCl_3$/MeOH 9:1); IR (KBr): ν = 3420*br s*, 2926*s*, 2670*s*, 2616*m*, 2488*m*, 2360*s*, 2342*m*, 1636*m*, 1526*m*, 1456*m*, 1386*m*, 1278*w*, 1244*w*, 1092*w*, 1046*m*, 998*m*, 668*m* cm^{-1}; ^{1}H-NMR (500 MHz, $CDCl_3$): δ = 7.06 (*t*, *J* = 5.5 Hz, 1H, NH), 5.40 (*t*, *J* = 3.5 Hz, 1H, 12-H), 3.89–3.77 (*m*, 2H, 33-H_a, 33′-H_a), 3.76–3.66 (*m*, 1H, 31-H_a), 3.61–3.51 (*m*, 1H, 31-H_b), 3.27–3.14 (*m*, 3H, 3-H, 32-H), 2.89–2.77 (*m*, 2H, 33-H_b, 33′-H_b), 2.26–2.17 (*m*, 2H, 34-H_a, 34′-H_a), 2.14 (*d*, *J* = 11.0 Hz, 1H, 18-H), 2.12–1.97 (*m*, 3H, 34-H_b, 34′-H_b, 16-H_a), 1.94 (*dd*, *J* = 8.8, 3.4 Hz, 2H, 11-H_a, 11-H_b), 1.81–1.22 (*m*, 15H, 22-H_a, 16-H_b, 15-H_a, 1-H_a, 2-H_a, 2-H_b, 6-H_a, 9-H, 22-H_b, 7-H_a, 21-H_a, 19-H, 6-H_b, 21-H_b, 7-H_b), 1.08 (*s*, 3H, 27-H), 1.07–0.96 (*m*, 3H, 15-H_b, 20-H, 1-H_b), 0.98 (*s*, 3H, 23-H), 0.94 (*d*, *J* = 6.3 Hz, 3H, 30-H), 0.91 (*s*, 3H, 25-H), 0.88 (*d*, *J* = 6.4 Hz, 3H, 29-H), 0.78 (*s*, 3H, 24-H), 0.73 (*s*, 3H, 26-H), 0.73–0.69 (*m*, 1H, 5-H) ppm; ^{13}C-NMR (126 MHz, $CDCl_3$): δ = 179.6 (C-28), 138.9 (C-13), 126.2 (C-12), 79.2 (C-3), 55.4 (C-32), 55.3 (C-5), 54.9 (C-33), 54.6 (C-33′), 52.9 (C-18), 47.9 (C-17), 47.7 (C-9), 42.4 (C-14), 39.8 (C-19), 39.7 (C-8), 38.9 (C-1), 38.9 (C-20), 38.7 (C-4), 37.4 (C-22), 37.1 (C-10), 36.1 (C-31), 32.9 (C-7), 31.0 (C-21), 28.3 (C-23), 28.0 (C-15), 27.4 (C-2), 24.7 (C-16), 23.6 (C-27), 23.5 (C-34, C-34′), 23.4 (C-11), 21.4 (C-30), 18.5 (C-6), 17.3 (C-29), 17.2 (C-26), 15.8 (C-24), 15.6 (C-25) ppm; MS (ESI, MeOH): *m*/*z* = 553 (100%, $[M + H]^+$); analysis calcd for $C_{36}H_{60}N_2O_2$ (552.89): C 78.21, H 10.94, N 5.07; found: C78.02, H 11.09, N 4.83.

(3β)-N-(2-Piperidin-1-ylethyl)-3-hydroxy-urs-12-en-28-amide (**13**). Compound **13** was prepared from **6** according to general procedure C. Column chromatography (SiO_2, $CHCl_3$/MeOH 95:5) gave **13** (yield: 93%); m.p. 120–124 °C; $[\alpha]_D$ = +40.5° (*c* 0.350, $CHCl_3$); R_f = 0.23 ($CHCl_3$/MeOH 95:5); IR (KBr): ν = 3416*br s*, 2934*s*, 2870*m*, 2854*m*, 1636*s*, 1512*m*, 1456*m*, 1378*m*, 1358*w*, 1304*w*, 1272*w*, 1256*w*, 1156*w*, 1130*w*, 1092*w*, 1046*m*, 998*m*, 754*m* cm^{-1}; ^{1}H-NMR (400 MHz, $CDCl_3$): δ = 6.62–6.54 (*m*, 1H, NH), 5.31 (*t*, J = 3.6 Hz, 1H, 12-H), 3.42–3.32 (*m*, 1H, 31-H_a), 3.25–3.16 (*m*, 2H, 3-H, 31-H_b), 2.50–2.35 (*m*, 6H, 32-H, 33-H, 33′-H), 2.02–1.80 (*m*, 5H, 16-H_a, 11-H_a, 11-H_b, 18-H, 22-H_a), 1.78–1.20 (*m*, 20H, 16-H_b, 15-H_a, 1-H_a, 34-H, 34′-H, 35-H, 9-H, 6-H_a, 21-H_a, 7-H_a, 2-H_a, 2-H_b, 22-H_b, 19-H, 6-H_b, 21-H_b, 7-H_b), 1.08 (*s*, 3H, 27-H), 1.07–0.97 (*m*, 3H, 15-H_b, 1-H_b, 20-H), 0.98 (*s*, 3H, 23-H), 0.96–0.93 (*m*, 3H, 30-H), 0.91 (*s*, 3H, 25-H), 0.87 (*d*, J = 6.4 Hz, 3H, 29-H), 0.77 (*s*, 6H, 24-H, 26-H), 0.74–0.69 (*m*, 1H, 5-H) ppm; ^{13}C-NMR (101 MHz, $CDCl_3$): *δ* = 178.0 (C-28), 139.4 (C-13), 125.8 (C-12), 79.1 (C-3), 57.2 (C-32), 55.3 (C-5), 54.4 (C-33, C-33′), 53.9 (C-18), 47.7 (C-17), 47.7 (C-9), 42.5 (C-14), 39.9 (C-19), 39.7 (C-8), 39.2 (C-20), 38.9 (C-1), 38.8 (C-4), 37.5 (C-22), 37.1 (C-10), 35.9 (C-31), 32.9 (C-7), 31.1 (C-21), 28.3 (C-23), 28.0 (C-15), 27.3 (C-35), 26.0 (C-34, C-34′), 24.9 (C-16), 24.4 (C-2), 23.5 (C-11), 23.4 (C-27), 21.4 (C-30), 18.4 (C-6), 17.4 (C-29), 17.1 (C-26), 15.8 (C-24), 15.6 (C-25) ppm; MS (ESI, MeOH): *m*/*z* = 567 (100%, $[M + H]^+$); analysis calcd for $C_{37}H_{62}N_2O_2$ (566.92): C 78.39, H 11.02, N 4.94; found: C 78.11, H 11.19, N 4.80.

(3β)-N-(2-Piperazin-1-ylethyl)-3-hydroxy-urs-12-en-28-amide (**14**). Compound **14** was prepared from **7** according to general procedure C. Column chromatography (SiO_2, $CHCl_3$/MeOH 9:1) gave **14** (yield: 88%); m.p. 214–217 °C (lit.: 217–220 °C [18]); $[\alpha]_D$ = +32.2° (*c* 0.335, $CHCl_3$); R_f = 0.20 ($CHCl_3$/MeOH 9:1); IR (KBr): ν = 3420*br s*, 2928*s*, 2870*m*, 2496*w*, 1630*s*, 1528*m*, 1458*m*, 1384*s*, 1178*w*, 1138*w*, 1092*w*, 1046*m*, 1030*m*, 998*m* cm^{-1}; ^{1}H-NMR (400 MHz, CD_3OD): *δ* = 5.37 (*t*, *J* = 3.6 Hz, 1H, 12-H), 3.42–3.31 (*m*,

1H, 31-H_a), 3.28–3.18 (*m*, 2H, 31-H_b, 3-H), 3.16 (*t*, *J* = 5.0 Hz, 4H, 34-H, 34'-H), 2.77–2.61 (*m*, 4H, 33-H, 33'-H), 2.54 (*t*, *J* = 6.6 Hz, 2H, 32-H), 2.17–1.89 (*m*, 4H, 18-H, 16-H_a, 11-H_a, 11-H_b), 1.86–1.30 (*m*, 15H, 15-H_a, 22-H_a, 16-H_b, 1-H_a, 2-H_a, 2-H_b, 9-H, 6-H_a, 7-H_a, 22-H_b, 21-H_a, 19-H, 6-H_b, 21-H_b, 7-H_b), 1.16 (*s*, 3H, 27-H), 1.15–1.02 (*m*, 3H, 15-H_b, 1-H_b, 20-H), 1.02–0.97 (*m*, 3H, 30-H), 1.01 (*s*, 3H, 23-H), 0.99 (*s*, 3H, 25-H), 0.95 (*d*, *J* = 6.4 Hz, 3H, 29-H), 0.84 (*s*, 3H, 26-H), 0.81 (*s*, 3H, 24-H), 0.80–0.76 (*m*, 1H, 5-H) ppm; ^{13}C-NMR (101 MHz, CD_3OD): δ = 180.3 (C-28), 140.1 (C-13), 127.0 (C-12), 79.6 (C-3), 57.8 (C-32), 56.7 (C-5), 54.3 (C-18), 51.8 (C-33, C-33'), 49.0 (C-17), 48.9 (C-9), 45.3 (C-34, C-34'), 43.4 (C-14), 40.9 (C-8), 40.9 (C-19), 40.3 (C-20), 39.9 (C-1), 39.8 (C-4), 38.8 (C-22), 38.1 (C-10), 37.4 (C-31), 34.1 (C-7), 31.9 (C-21), 29.0 (C-15), 28.8 (C-23), 27.9 (C-2), 25.3 (C-16), 24.5 (C-11), 24.0 (C-27), 21.6 (C-30), 19.4 (C-6), 18.0 (C-26), 17.7 (C-29), 16.4 (C-24), 16.1 (C-25) ppm; MS (ESI, MeOH): *m*/*z* = 568 (100%, $[M + H]^+$); analysis calcd for $C_{36}H_{61}N_3O_2$ (567.90): C 76.14, H 10.83, N 7.40; found: C 75.84, H 11.03, N 7.25.

(3β)-N-(4-Aminobutyl)-3-hydroxy-urs-12-en-28-amide (**15**). Compound **15** was prepared from **8** according to general procedure C. Column chromatography (SiO_2, $CHCl_3$/MeOH 9:1) gave **15** (yield: 87%); m.p. 177–180 °C; $[\alpha]_D$ = +42.2° (*c* 0.315, DMSO); R_f = 0.33 ($CHCl_3$/MeOH 88:12); IR (KBr): ν = 3424*br m*, 2927*m*, 1629*w*, 1534*w*, 1384*s*, 1029*w* cm^{-1}; ^{1}H-NMR (400 MHz, DMSO-d_6): δ = 7.79–7.54 (*m*, 2H, NH_2), 7.17 (*t*, *J* = 5.7 Hz, 1H, NH), 5.19 (*t*, *J* = 3.6 Hz, 1H, 12-H), 4.28 (*s*, 1H, OH), 3.07–2.90 (*m*, 3H, 3-H, 31-H), 2.76 (*t*, *J* = 7.4 Hz, 2H, 32-H), 2.15 (*d*, *J* = 10.9 Hz, 1H, 18-H), 1.97–1.65 (*m*, 4H, 16-H_a, 11-H_a, 11-H_b, 15-H_a), 1.65–1.17 (*m*, 18H, 16-H_b, 22-H_a, 1-H_a, 34-H_a, 34-H_b, 6-H_a, 9-H, 2-H_a, 2-H_b, 7-H_a, 22-H_b, 21-H_a, 33-H_a, 33-H_b, 19-H, 6-H_b, 21-H_b, 7-H_b), 1.03 (s, 3H, 27-H), 0.95–0.88 (*m*, 6H, 15-H_b, 1-H_b, 30-H, 20-H), 0.89 (*s*, 3H, 23-H), 0.85 (*s*, 3H, 25-H), 0.82 (*d*, *J* = 6.4 Hz, 3H, 29-H), 0.67 (*s*, 6H, 24-H, 26-H), 0.67–0.64 (*m*, 1H, 5-H) ppm; ^{13}C-NMR (101 MHz, DMSO-d_6): δ = 176.2 (C-28), 138.4 (C-13), 124.5 (C-12), 76.8 (C-3), 54.8 (C-5), 51.9 (C-18), 47.0 (C-9), 46.5 (C-17), 41.6 (C-14), 39.1 (C-8), 38.8 (C-19), 38.7 (C-32), 38.5 (C-20), 38.4 (C-4), 38.2 (C-1), 38.0 (C-31), 37.1 (C-22), 36.5 (C-10), 32.7 (C-7), 30.4 (C-21), 28.3 (C-23), 27.4 (C-15), 27.0 (C-2), 26.0 (C-33), 24.6 (C-34), 23.5 (C-16), 23.3 (C-27), 22.9 (C-11), 21.1 (C-30), 18.0 (C-6), 17.1 (C-29), 16.8 (C-26), 16.1 (C-24), 15.2 (C-25) ppm; MS (ESI, MeOH): *m*/*z* = 527 (100 %, $[M + H]^+$), 1053 (18 %, $[2M + H]^+$); analysis calcd for $C_{34}H_{58}N_2O_2$ (526.85): C 77.51, H 11.10, N 5.32; found: C 77.39, H 11.30, N 5.16.

(3β)-N-[2-(2-Aminoethoxy)ethyl]-3-acetyloxy-urs-12-en-28-amide (**16**). Compound **16** was prepared from **9** according to general procedure C. Column chromatography (SiO_2, $CHCl_3$/MeOH 9:1) gave **16** (yield: 86%). m.p. 126–129 °C; $[\alpha]_D$ = +34.3° (*c* 0.305, $CHCl_3$); R_f = 0.20 ($CHCl_3$/MeOH 9:1); IR (KBr): ν = 3426*br s*, 2926*s*, 2870*m*, 1636*m*, 1534*m*, 1534*m*, 1456*w*, 1384*w*, 1118*w*, 1044*w*, 1030*w* cm^{-1}; ^{1}H-NMR (500 MHz, CD_3OD): δ = 5.33 (*t*, *J* = 3.7 Hz, 1H, 12-H), 3.62 (*dd*, *J* = 5.7, 4.7 Hz, 2H, 33-H), 3.52 (*t*, *J* = 5.9 Hz, 2H, 32-H), 3.44–3.37 (*m*, 1H, 31-H_a), 3.34–3.24 (*m*, 1H, 31-H_b), 3.16 (*dd*, *J* = 11.3, 4.7 Hz, 1H, 3-H), 3.03 (*dd*, *J* = 5.7, 4.6 Hz, 2H, 34-H), 2.16–1.91 (*m*, 4H, 18-H, 16-H_a, 11-H_a, 11-H_b), 1.84–1.27 (*m*, 15H, 15-H_a, 22-H_a, 1-H_a, 16-H_b, 2-H_a, 2-H_b, 9-H, 6-H_a, 7-H_a, 22-H_b, 21-H_a, 19-H, 6-H_b, 21-H_b, 7-H_b), 1.13 (*s*, 3H, 27-H), 1.11–0.98 (*m*, 3H, 15-H_b, 1-H_b, 20-H), 0.98–0.95 (*m*, 3H, 30-H), 0.98 (*s*, 3H, 23-H), 0.96 (*s*, 3H, 25-H), 0.91 (*d*, *J* = 6.4 Hz, 3H, 29-H), 0.81 (*s*, 3H, 26-H), 0.78 (*s*, 3H, 24-H), 0.77–0.73 (*m*, 1H, 5-H) ppm; ^{13}C-NMR (126 MHz, CD_3OD): δ = 180.6 (C-28), 140.0 (C-13), 127.1 (C-12), 79.6 (C-3), 70.8 (C-32), 68.9 (C-33), 56.7 (C-5), 54.2 (C-18), 49.2 (C-17), 48.9 (C-9), 43.3 (C-14), 40.9 (C-8), 40.9 (C-34), 40.8 (C-19), 40.3 (C-20), 40.2 (C-31), 40.0 (C-1), 39.8 (C-4), 38.8 (C-22), 38.1 (C-10), 34.2 (C-7), 31.9 (C-21), 29.0 (C-15), 28.8 (C-23), 27.9 (C-2), 25.3 (C-16), 24.4 (C-11), 24.0 (C-27), 21.6 (C-30), 19.4 (C-6), 17.9 (C-29), 17.7 (C-26), 16.4 (C-24), 16.1 (C-25) ppm; MS (ESI, MeOH): *m*/*z* = 543 (100%, $[M + H]^+$); analysis calcd for $C_{34}H_{58}N_2O_3$ (542.85): C 75.23, H 10.77, N 5.16; found: C 75.02, H 10.98, N 5.02.

(3β)-N-(2-Aminoethyl)-3-acetyloxy-lup-20(29)-en-28-amide (**17**). Compound **17** was prepared from **2** according to general procedure B using ethylenediamine. Column chromatography (SiO_2, $CHCl_3$/MeOH 9:1) gave **17** (yield: 83%); m.p. 152–154 °C; $[\alpha]_D$ = +8.4° (*c* 0.330, $CHCl_3$); R_f = 0.38 ($CHCl_3$/MeOH 9:1); IR (KBr): ν = 3442*br s*, 2946*s*, 1734*m*, 1638*m*, 1522*m*, 1452*m*, 1376*m*, 1248*s*, 1030*m* cm^{-1}; ^{1}H-NMR (400 MHz, $CDCl_3$): δ = 6.39 (*t*, *J* = 5.5 Hz, 1H, N*H*), 4.73–4.70 (*m*, 1H, 29-H_a), 4.60–4.57 (*m*, 1H, 29-H_b), 4.45 (*dd*, *J* = 10.0, 6.2 Hz, 1H, 3-H), 3.40–3.33 (*m*, 2H, 31-H), 3.09 (*ddd*, *J* = 11.0, 11.0, 4.0

Hz, 1H, 19-H), 2.90 (*t*, *J* = 5.9 Hz, 2H, 32-H), 2.42 (*ddd*, *J* = 12.7, 12.7, 3.4 Hz, 1H, 13-H), 2.03 (*s*, 3H, Ac), 2.01–1.68 (*m*, 4H, 16-H_a, 21-H_a, 22-H_a,12-H_a), 1.67 (*s*, 3H, 30-H_a), 1.66–1.07 (*m*, 16H, 22-H_b, 2-H_a, 2-H_b, 18-H, 16-H_b, 15-H_a, 6-H_a, 1-H_a, 11-H_a, 6-H_b, 21-H_b, 7-H_a, 7-H_b, 9-H, 11-H_b, 15-H_b), 1.05–0.88 (*m*, 2H, 12-H_b, 1-H_b), 0.95 (*s*, 3H, 27-H), 0.92 (*s*, 3H, 26-H), 0.83 (*s*, 6H, 25-H, 23-H), 0.82 (*s*, 3H, 24-H), 0.80–0.74 (*m*, 1H, 5-H) ppm; ^{13}C-NMR (101 MHz, $CDCl_3$): δ = 177.2 (C-28), 171.1 (Ac), 150.9 (C-20), 109.6 (C-29), 81.1 (C-3), 55.9 (C-17), 55.6 (C-5), 50.7 (C-9), 50.3 (C-18), 47.0 (C-19), 42.6 (C-14), 41.5 (C-32), 40.9 (C-8), 40.8 (C-31), 38.6 (C-1, C-22), 37.9 (C-4), 37.9 (C-13), 37.3 (C-10), 34.5 (C-7), 33.8 (C-16), 31.1 (C-21), 29.6 (C-15), 28.1 (C-23), 25.7 (C-12), 23.8 (C-2), 21.5 (Ac), 21.1 (C-11), 19.6 (C-30), 18.3 (C-6), 16.6 (C-24), 16.4 (C-25), 16.3 (C-26), 14.8 (C-27) ppm; MS (ESI, MeOH): *m*/*z* = 541 (100 %, $[M + H]^+$); analysis calcd for $C_{34}H_{56}N_2O_3$ (540.83): C 75.51, H 10.44, N 5.18; found: C 75.35, H 10.67, N 5.02.

(3β)-N-[2-(Dimethylamino)ethyl]-3-acetyloxy-lup-20(29)-en-28-amide (**18**). Compound **18** was prepared from **2** according to general procedure B using *N*,*N*-dimethylethylenediamine. Column chromatography (SiO_2, $CHCl_3$/MeOH 95:5) gave **18** (yield: 94%); m.p. 108–110 °C; $[\alpha]_D$ = +16.4° (*c* 0.320, $CHCl_3$); R_f = 0.51 ($CHCl_3$/MeOH 9:1); IR (KBr): ν = 3420*br s*, 2945*s*, 2869*m*, 1736*s*, 1641*m*, 1456*s*, 1375*m*, 1246*s*, 1195*w*, 1029*m*, 979*m* cm^{-1}; ^{1}H-NMR (500 MHz, $CDCl_3$): δ = 6.24 (*t*, *J* = 4.7 Hz, 1H, NH), 4.74–4.72 (*m*, 1H, 29-H_a), 4.60–4.58 (*m*, 1H, 29-H_b), 4.46 (*dd*, *J* = 10.4, 5.9 Hz, 1H, 3-H), 3.40–3.24 (*m*, 2H, 31-H), 3.11 (*ddd*, *J* = 11.0, 11.0, 4.2 Hz, 1H, 19-H), 2.47–2.38 (*m*, 3H, 32-H + 13-H), 2.26 (*s*, 6H, 33-H, 33′-H), 2.03 (*s*, 3H, Ac), 2.03–1.89 (*m*, 2H, 16-H_a, 21-H_a), 1.80–1.74 (m, 1H, 22-H_a), 1.73–1.63 (*m*, 2H, 12-H_a, 22-H_b), 1.68 (*s*, 3H, 30-H), 1.63–1.11 (*m*, 15H, 2-H_a, 2-H_b, 18-H, 16-H_b, 15-H_a, 6-H_a, 11-H_a, 1-H_a, 6-H_b, 7-H_a, 7-H_b, 21-H_b, 9-H, 11-H_b, 15-H_b), 1.05–0.94 (*m*, 2H, 12-H_b, 1-H_b), 0.96 (*s*, 3H, 27-H), 0.94 (*s*, 3H, 26-H), 0.83 (*s*, 6H, 23-H, 25-H), 0.82 (*s*, 3H, 24-H), 0.80–0.76 (*m*, 1H, 5-H) ppm; ^{13}C-NMR (126 MHz, $CDCl_3$): δ = 176.5 (C-28), 171.1 (Ac), 151.2 (C-20), 109.5 (C-29), 81.1 (C-3), 58.3 (C-32), 55.9 (C-17), 55.6 (C-5), 50.7 (C-9), 50.2 (C-18), 47.1 (C-19), 45.3 (C-33, C-33′), 42.7 (C-14), 40.9 (C-8), 38.6 (C-22), 38.6 (C-1), 38.0 (C-13), 38.0 (C-4), 37.3 (C-10), 36.6 (C-31), 34.5 (C-7), 33.8 (C-16), 31.1 (C-21), 29.6 (C-15), 28.1 (C-23), 25.8 (C-12), 23.9 (C-2), 21.5 (Ac), 21.1 (C-11), 19.6 (C-30), 18.4 (C-6), 16.6 (C-24), 16.4 (C-25), 16.3 (C-26), 14.8 (C-27) ppm; MS (ESI, MeOH): *m*/*z* = 569 (100%, $[M + H]^+$); analysis calcd for $C_{26}H_{60}N_2O_3$ (568.89): C 76.01, H 10.63, N 4.92; found: C 75.77, H 10.84, N 4.63.

(3β)-N-(2-Pyrrolidin-1-ylethyl)-3-acetyloxy-lup-20(29)-en-28-amide (**19**). Compound **19** was prepared from **2** according to general procedure B using 1-(2-aminoethyl)-pyrrolidine. Column chromatography (SiO_2, $CHCl_3$/MeOH 95:5) gave **19** (yield: 86%); m.p. 143–145 °C; $[\alpha]_D$ = +11.7° (*c* 0.330, $CHCl_3$); R_f = 0.53 ($CHCl_3$/MeOH 9:1); IR (KBr): ν =3422*br m*, 2946*s*, 1734*m*, 1640*m*, 1451*m*, 1384*s*, 1247*s*, 1029*m*, 979*m* cm^{-1}; ^{1}H-NMR (400 MHz, $CDCl_3$): δ = 7.23 (*t*, *J* = 5.5 Hz, 1H, NH), 4.72–4.70 (*m*, 1H, 29-H_a), 4.58–4.56 (*m*, 1H, 29-H_b), 4.44 (*dd*, *J* = 10.8, 5.5 Hz, 1H, 3-H), 3.68–3.56 (*m*, 2H, 31-H), 3.47–3.27 (*m*, 4H, 33-H, 33′-H), 3.24 (*t*, *J* = 6.1 Hz, 2H, 32-H), 3.05 (*ddd*, *J* = 10.9, 10.9, 4.2 Hz, 1H, 19-H), 2.39 (*ddd*, *J* = 12.8, 12.8, 3.5 Hz, 1H, 13-H), 2.13–2.04 (*m*, 5H, 34-H, 34′-H, 16-H_a), 2.02 (*s*, 3H, Ac), 1.89–1.76 (*m*, 2H, 21-H_a, 22-H_a), 1.66 (*s*, 3H, 30-H), 1.71–1.11 (*m*, 17H, 12-H_a, 1-H_a, 2-H_a, 2-H_b, 18-H, 16-H_b, 6-H_a, 22-H_b, 11-H_a, 21-H_b, 7-H_a, 7-H_b, 15-H_a, 6-H_b, 9-H, 11-H_b, 15-H_b), 1.03–0.91 (*m*, 2H, 12-H_b, 1-H_b), 0.93 (*s*, 3H, 27-H), 0.89 (*s*, 3H, 26-H), 0.82 (*s*, 6H, 23-H, 25-H), 0.81 (*s*, 3H, 24-H), 0.78–0.75 (*m*, 1H, 5-H) ppm; ^{13}C-NMR (101 MHz, $CDCl_3$): δ = 177.8 (C-28), 171.1 (Ac), 151.0 (C-20), 109.6 (C-29), 81.1 (C-3), 55.9 (C-17), 55.6 (C-5), 55.5 (C-32), 54.8 (C-33, C-33′), 50.6 (C-9), 50.3 (C-18), 47.0 (C-19), 42.6 (C-14), 40.9 (C-8), 38.5 (C-1), 38.2 (C-22), 37.9 (C-13), 37.9 (C-4), 37.3 (C-10), 36.3 (C-31), 34.5 (C-7), 33.2 (C-16), 31.0 (C-21), 29.6 (C-15), 28.1 (C-23), 25.7 (C-12), 23.8 (C-2), 23.4 (C-34, C-34′), 21.4 (Ac), 21.1 (C-11), 19.5 (C-30), 18.3 (C-6), 16.6 (C-24), 16.3 (C-25), 16.3 (C-26), 14.7 (C-27) ppm; MS (ESI, MeOH): *m*/*z* = 595 (100%, $[M + H]^+$); analysis calcd for $C_{38}H_{62}N_2O_3$ (594.93): C 76.72, H 10.50, N 4.71; found: C 76.50, H 10.74, N 4.51.

(3β)-N-(2-Piperidin-1-ylethyl)-3-acetyloxy-lup-20(29)-en-28-amide (**20**). Compound **20** was prepared from **2** according to general procedure B using 1-(2-aminoethyl)-piperidine. Column chromatography (SiO_2, $CHCl_3$/MeOH 95:5) gave **20** (yield: 81%); m.p. 124–127 °C; $[\alpha]_D$ = +14.1° (*c* 0.340, $CHCl_3$); R_f = 0.25 ($CHCl_3$/MeOH 95:5); IR (KBr): ν = 3424*br s*, 2942*s*, 2968*m*, 1736*s*, 1638*s*, 1508*m*, 1452*m*, 1376*m*, 1246*s*, 1154*w*, 1128*w*, 1028*m* cm^{-1}; ^{1}H-NMR (400 MHz, $CDCl_3$): δ = 6.52–6.39 (*m*, 1H, NH), 4.75–4.70 (*m*, 1H,

29-H_a), 4.61–4.56 (*m*, 1H, 29-H_b), 4.46 (*dd*, *J* = 9.8, 6.5 Hz, 1H, 3-H), 3.41–3.25 (*m*, 2H, 31-H_a, 31-H_b), 3.08 (*ddd*, *J* = 11.1, 10.9, 3.9 Hz, 1H, 19-H), 2.53–2.40 (*m*, 6H, 32-H, 33-H, 33′-H), 2.35 (*ddd*, *J* = 12.4, 12.3, 3.6 Hz, 1H, 13-H), 2.03 (*s*, 3H, Ac), 2.12–1.89 (*m*, 2H, 16-H_a, 21-H_a), 1.83–1.74 (*m*, 1H, 22-H_a), 1.68 (*s*, 3H, 30-H), 1.72–1.54 (*m*, 9H, 12-H_a, 1-H_a, 2-H_a, 2-H_b, 18-H, 34-H, 34′-H), 1.55–1.15 (*m*, 13H, 16-H_b, 15-H_a, 6-H_a, 35-H, 11-H_a, 22-H_b, 21-H_b, 6-H_b, 7-H_a, 7-H_b, 9-H, 11-H_b), 1.15–1.09 (*m*, 1H, 15-H_b), 1.08–0.93 (*m*, 2H, 12-H_b, 1-H_b), 0.96 (*s*, 3H, 27-H), 0.92 (*s*, 3H, 26-H), 0.83 (*s*, 6H, 25-H, 23-H), 0.82 (*s*, 3H, 24-H), 0.80–0.74 (*m*, 1H, 5-H) ppm; ^{13}C-NMR (101 MHz, $CDCl_3$): δ = 176.3 (C-28), 171.1 (Ac), 151.1 (C-20), 109.5 (C-29), 81.1 (C-3), 57.1 (C-32), 56.0 (C-17), 55.6 (C-5), 54.3 (C-33, C-33′), 50.6 (C-9), 50.0 (C-18), 47.2 (C-19), 42.7 (C-14), 40.9 (C-8), 38.5 (C-1), 38.5 (C-22), 38.1 (C-13), 37.9 (C-4), 37.3 (C-10), 35.7 (C-31), 34.5 (C-7), 33.8 (C-16), 31.1 (C-21), 29.6 (C-15), 28.1 (C-23), 26.1 (C-34, C-34′), 25.8 (C-12), 24.4 (C-35), 23.8 (C-2), 21.4 (Ac), 21.1 (C-11), 19.6 (C-30), 18.4 (C-6), 16.6 (C-24), 16.4 (C-25), 16.3 (C-26), 14.8 (C-27) ppm; MS (ESI, MeOH): *m*/*z* = 609 (100%, $[M + H]^+$); analysis calcd for $C_{39}H_{64}N_2O_3$ (608.95): C 76.92, H 10.59, N 4.60; found:

(3β)-N-(2-Piperazin-1-ylethyl)-3-acetyloxy-lup-20(29)-en-28-amide (**21**). Compound **21** was prepared from **2** according to general procedure B using 1-(2-aminoethyl)-piperazine. Column chromatography (SiO_2, $CHCl_3$/MeOH/NH_4OH 90:11:0.5) gave **21** (yield: 84%); m.p. 107–110 °C; $[\alpha]_D$ = +13.7° (*c* 0.335, $CHCl_3$); R_f = 0.44 ($CHCl_3$/MeOH/NH_4OH 90:10:1);IR (KBr): ν = 3422*br s*, 2944*s*, 2870*m*, 1734*s*, 1638*s*, 1522*m*, 1452*m*, 1374*m*, 1318*w*, 1248*s*, cm^{-1}; 1194*w*, 1138*w*, 1028*m* cm^{-1}; ^{1}H-NMR (400 MHz, $CDCl_3$): δ = 6.22 (*t*, *J* = 4.8 Hz, 1H, NH), 4.75–4.70 (*m*, 1H, 29-H_a), 4.61–4.58 (*m*, 1H, 29-H_b), 4.46 (*dd*, *J* = 9.7, 6.5 Hz, 1H, 3-H), 3.41–3.23 (*m*, 2H, 31-H), 3.08 (*ddd*, *J* = 11.1, 11.1, 3.8 Hz, 1H, 19-H), 2.92 (*t*, *J* = 4.9 Hz, 4H, 34-H, 34′-H), 2.55–2.41 (*m*, 6H, 32-H, 33-H, 33′-H), 2.36 (*ddd*, *J* = 12.4, 12.4, 3.6 Hz, 1H, 13-H), 2.03 (s, 3H, Ac), 2.05–1.89 (*m*, 2H, 16-H_a, 21-H_a), 1.68 (*s*, 3H, 30-H), 1.81–1.53 (*m*, 6H, 22-H_a, 12-H_a, 1-H_a, 18-H, 2-H_a, 2-H_b), 1.52–1.19 (*m*, 11H, 16-H_b, 15-H_a, 6-H_a, 11-H_a, 22-H_b, 6-H_b, 21-H_b, 7-H_a, 7-H_b, 9-H, 11-H_b), 1.20–0.90 (*m*, 3H, 15-H_b, 12-H_b, 1-H_b), 0.96 (*s*, 3H, 27-H), 0.91 (*s*, 3H, 26-H), 0.83 (*s*, 6H, 23-H, 25-H), 0.82 (*s*, 3H, 24-H), 0.80–0.74 (*m*, 1H, 5-H) ppm; ^{13}C-NMR (101 MHz, $CDCl_3$): δ = 176.3 (C-28), 171.1 (Ac), 151.0 (C-20), 109.6 (C-29), 81.1 (C-3), 57.1 (C-32), 56.0 (C-17), 55.6 (C-5), 53.7 (C-33, C-33′), 50.6 (C-9), 50.0 (C-18), 47.2 (C-19), 46.1 (C-34, C-34′), 42.7 (C-14), 40.9 (C-8), 38.5 (C-1, C-22), 38.1 (C-13), 37.9 (C-4), 37.3 (C-10), 35.6 (C-31), 34.5 (C-7), 33.8 (C-16), 31.1 (C-21), 29.6 (C-15), 28.1 (C-23), 25.7 (C-12), 23.8 (C-2), 21.5 (Ac), 21.1 (C-11), 19.6 (C-30), 18.3 (C-6), 16.6 (C-24), 16.4 (C-25), 16.3 (C-26), 14.8 (C-27) ppm; MS (ESI, MeOH): *m*/*z* = 610 (100%, $[M + H]^+$); analysis calcd for $C_{38}H_{63}N_3O_3$ (609.94): C 74.83, H 10.41, N 6.89; found: C 74.65, H 10.69, N 6.64.

(3β)-N-(4-Aminobutyl)-3-acetyloxy-lup-20(29)-en-28-amide (**22**). Compound **22** was prepared from **2** according to general procedure B using 1,4-diaminobutane. Column chromatography (SiO_2, $CHCl_3$/MeOH/NH_4OH 90:11:0.5) gave **22** (yield: 84%); m.p. 133–135 °C; $[\alpha]_D$ = +7.4° (*c* 0.350, $CHCl_3$); R_f = 0.33 ($CHCl_3$/MeOH/NH_4OH 90:10:1); IR (KBr): ν = 3422*br s*, 2944*s*, 2868*m*, 1736*s*, 1638*s*, 1522*m*, 1452*m*, 1374*m*, 1248*s*, 1028*m*, 980*m*, 754*m* cm^{-1}; ^{1}H-NMR (400 MHz, $CDCl_3$): δ = 5.94 (*t*, *J* = 5.8 Hz, 1H, NH), 4.75–4.69 (*m*, 1H, 29-H_a), 4.61–4.55 (*m*, 1H, 29-H_b), 4.45 (*dd*, *J* = 8.7, 7.6 Hz, 1H, 3-H), 3.35–3.15 (*m*, 2H, 31-H_a, 31-H_b), 3.11 (*ddd*, *J* = 11.0, 4.0 Hz, 4.0 Hz, 1H, 19-H), 2.84–2.73 (*m*, 2H, 32-H_a, 32-H_b), 2.45 (*ddd*, *J* = 12.4, 3.6 Hz, 3.6 Hz, 1H, 13-H), 2.03 (*s*, 3H, Ac), 2.00–1.80 (*m*, 2H, 21-H_a, 16-H_a), 1.67 (*s*, 3H, 30-H), 1.77–1.18 (*m*, 21H, 22-H_a, 12-H_a, 1-H_a, 2-H_a, 2-H_b, 34-H_a, 34-H_b, 18-H, 33-H_a, 33-H_b, 16-H_b, 6-H_a, 15-H_a, 11-H_a, 22-H_b, 6-H_b, 21-H_b, 7-H_a, 7-H_b, 11-H_b, 9-H), 1.16–1.08 (*m*, 1H, 15-H_b), 1.04–0.90 (*m*, 2H, 12-H_b, 1-H_b), 0.95 (*s*, 3H, 27-H), 0.92 (*s*, 3H, 26-H), 0.84 (*s*, 3H, 25-H), 0.83 (*s*, 3H, 23-H), 0.82 (*s*, 3H, 24-H), 0.80–0.74 (*m*, 1H, 5-H) ppm; ^{13}C-NMR (101 MHz, $CDCl_3$): δ = 176.4 (C-28), 171.1 (Ac), 151.1 (C-20), 109.5 (C-29), 81.1 (C-3), 55.8 (C-17), 55.6 (C-5), 50.7 (C-9), 50.3 (C-18), 46.9 (C-19), 42.6 (C-14), 41.4 (C-32), 40.9 (C-8), 39.1 (C-31), 38.6 (C-22), 38.5 (C-1), 38.0 (C-4), 37.9 (C-13), 37.3 (C-10), 34.5 (C-7), 33.9 (C-16), 31.1 (C-21), 29.9 (C-33), 29.6 (C-15), 28.1 (C-23), 27.3 (C-34), 25.8 (C-12), 23.9 (C-2), 21.5 (Ac), 21.1 (C-11), 19.6 (C-30), 18.3 (C-6), 16.6 (C-24), 16.4 (C-25), 16.3 (C-26), 14.8 (C-27) ppm; MS (ESI, MeOH): *m*/*z* = 569 (100%, $[M + H]^+$); analysis calcd for $C_{36}H_{60}N_2O_3$ (568.89): C 76.01, H 10.63, N 4.92; found: C75.81, H 10.77, N 4.75.

(3β)-N-[2-(2-Aminoethoxy)ethyl]-3-acetyloxy-lup-20(29)-en-28-amide (**23**). Compound **23** was prepared from **2** according to general procedure B using 2,2′-oxybis(ethylamine). Column chromatography (SiO_2, $CHCl_3$/MeOH 9:1) gave **23** (yield: 81%); m.p. 109–112 °C; $[\alpha]_D$ = +38.4° (*c* 0.325, $CHCl_3$); R_f = 0.58 ($CHCl_3$/MeOH/NH_4OH 90:10:1); IR (KBr): ν = 3448*br s*, 2944*m*, 1734*m*, 1637*m*, 1527*w*, 1375w, 1248*m*, 1029*w* cm^{-1}; ^{1}H-NMR (500 MHz, $CDCl_3$): δ = 6.09 (*t*, *J* = 5.4 Hz, 1H, NH), 4.74–4.70 (*m*, 1H, 29-H_a), 4.60–4.56 (*m*, 1H, 29-H_b), 4.46 (*dd*, *J* = 10.6, 5.8 Hz, 1H, 3-H), 3.58–3.44 (*m*, 5H, 32-H, 33-H, 31-H_a), 3.43–3.35 (*m*, 1H, 31-H_b), 3.10 (*ddd*, *J* = 11.1, 11.0, 4.2 Hz, 1H, 19-H), 2.88 (*t*, *J* = 5.2 Hz, 2H, 34-H), 2.43 (*ddd*, *J* = 12.9, 11.5, 3.7 Hz, 1H, 13-H), 2.03 (*s*, 3H, Ac), 2.00–1.88 (*m*, 2H, 16-H_a, 21-H_a), 1.78–1.72 (*m*, 1H, 22-H_a), 1.67 (*s*, 3H, 30-H), 1.72–1.17 (*m*, 16H, 12-H_a, 1-H_a, 2-H_a, 2-H_b, 18-H, 16-H_b, 6-H_a, 15-H_a, 22-H_b, 11-H_a, 6-H_b, 21-H_b, 7-H_a, 7-H_b, 9-H, 11-H_b), 1.16–1.09 (*m*, 1H, 15-H_b), 1.05–0.95 (*m*, 2H, 12-H_b, 1-H_b), 0.95 (*s*, 3H, 27-H), 0.93 (*s*, 3H, 26-H), 0.83 (*s*, 3H, 25-H), 0.83 (*s*, 3H, 23-H), 0.82 (*s*, 3H, 24-H), 0.80–0.74 (*m*, 1H, 5-H) ppm; ^{13}C-NMR (126 MHz, $CDCl_3$): δ = 176.4 (C-28), 171.1 (Ac), 151.0 (C-20), 109.5 (C-29), 81.1 (C-3), 72.8 (C-33), 70.1 (C-32), 55.9 (C-17), 55.6 (C-5), 50.7 (C-9), 50.2 (C-18), 47.0 (C-19), 42.6 (C-14), 41.8 (C-34), 40.9 (C-8), 39.1 (C-31), 38.6 (C-1), 38.5 (C-22), 37.9 (C-4), 37.9 (C-13), 37.3 (C-10), 34.5 (C-7), 33.9 (C-16), 31.0 (C-21), 29.5 (C-15), 28.1 (C-23), 25.7 (C-12), 23.9 (C-2), 21.4 (Ac), 21.1 (C-11), 19.6 (C-30), 18.4 (C-6), 16.6 (C-24), 16.3 (C-25), 16.3 (C-26), 14.8 (C-27) ppm; MS (ESI, MeOH): *m*/*z* = 585 (100 %, $[M + H]^+$), 607 (47 %, $[M + Na]^+$); analysis calcd for $C_{36}H_{60}N_2O_4$ (584.89): C 73.93, H 10.34, N 4.79; found: C 73.69, H 10.54, N 4.56.

(3β)-N-(2-Aminoethyl)-3-hydroxy-lup-20(29)-en-28-amide (**24**). Compound **24** was prepared from **17** according to general procedure C. Column chromatography (SiO_2, $CHCl_3$/MeOH 9:1) gave **24** (yield: 86%); m.p. 218–220 °C; $[\alpha]_D$ = +4.5° (*c* 0.300, DMSO); R_f = 0.28 ($CHCl_3$/MeOH 9:1);IR (KBr): ν = 3424*br s*, 2941*m*, 1636*m*, 1449*m*, 1044*m*, 879*w* cm^{-1}; ^{1}H-NMR (400 MHz, DMSO-d_6): δ = 7.53 (*t*, *J* = 5.5 Hz, 1H, NH), 4.67–4.63 (*m*, 1H, 29-H_a), 4.54–4.51 (*m*, 1H, 29-H_b), 3.15–2.92 (*m*, 4H, 32-H_a, 19-H, 32-H_b, 3-H), 2.60–2.51 (*m*, 3H, 13-H, 31-H_a, 31-H_b), 2.16–2.09 (*m*, 1H, 16-H_a), 1.82–1.65 (*m*, 2H, 22-H_a, 21-H_a), 1.62 (*s*, 3H, 30-H), 1.61–0.92 (*m*, 17H, 12-H_a, 1-H_a, 2-H_a, 2-H_b, 6-H_a, 18-H, 16-H_b, 11-H_a, 22-H_b, 15-H_a, 6-H_b, 7-H_a, 7-H_b, 21-H_b, 9-H, 11-H_b, 15-H_b), 0.92–0.78 (*m*, 2H, 12-H_b, 1-H_b), 0.91 (*s*, 3H, 27-H), 0.87 (*s*, 3H, 23-H), 0.84 (*s*, 3H, 26-H), 0.76 (*s*, 3H, 25-H), 0.65 (*s*, 3H, 24-H), 0.64–0.60 (*m*, 1H, 5-H) ppm; ^{13}C-NMR (101 MHz, DMSO-d_6): δ = 175.6 (C-28), 150.9 (C-20), 109.1 (C-29), 76.8 (C-3), 54.9 (C-5), 54.9 (C-17), 50.1 (C-9), 49.7 (C-18), 46.2 (C-19), 41.9 (C-14), 41.8 (C-32), 41.4 (C-31), 40.3 (C-8), 38.5 (C-4), 38.3 (C-1), 37.7 (C-22), 36.7 (C-10), 36.6 (C-13), 34.0 (C-7), 32.4 (C-16), 30.3 (C-21), 28.9 (C-15), 28.1 (C-23), 27.1 (C-2), 25.2 (C-12), 20.6 (C-11), 19.0 (C-30), 17.9 (C-6), 15.9 (C-25), 15.8 (C-26), 15.7 (C-24), 14.3 (C-27) ppm; MS (ESI, MeOH): *m*/*z* = 499 (100 %, $[M + H]^+$); analysis calcd for $C_{32}H_{54}N_2O_2$ (498.80): C 77.06, H 10.91, N 5.62; found: C 76.81, H 11.07, N 5.55.

(3β)-N-[2-(Dimethylamino)ethyl]-3-hydroxy-lup-20(29)-en-28-amide (**25**). Compound **25** was prepared from **18** according to general procedure C. Column chromatography (SiO_2, $CHCl_3$/MeOH 95:5) gave **25** (yield: 89%); m.p. 118–120 °C; $[\alpha]_D$ = −4.4° (*c* 0.330, MeOH); R_f = 0.43 ($CHCl_3$/MeOH 9:1); IR (KBr): ν = 3408*br s*, 2944*s*, 2866*s*, 1638*s*, 1528*m*, 1464*s*, 1376*m*, 1246*m*, 1194*m*, 1044*m*, 880*m* cm^{-1}; ^{1}H-NMR (500 MHz, $CDCl_3$): δ = 6.26 (*t*, *J* = 4.9 Hz, 1H, NH), 4.73–4.71 (*m*, 1H, 29-H_a), 4.58–4.56 (*m*, 1H, 29-H_b), 3.37–3.22 (*m*, 2H, 31-H), 3.16 (*dd*, *J* = 11.0, 5.2 Hz, 1H, 3-H), 3.10 (*ddd*, *J* = 11.1, 11.1, 4.2 Hz, 1H, 19-H), 2.46–2.37 (*m*, 3H, 13-H, 32-H), 2.22 (*s*, 6H, 33-H, 33′-H), 2.06–1.89 (*m*, 2H, 16-H_a, 21-H_a), 1.79–1.72 (*m*, 1H, 22-H_a), 1.67 (*s*, 3H, 30-H), 1.72– 1.16 (*m*, 16H, 12-H_a, 1-H_a, 2-H_a, 2-H_b, 18-H, 6-H_a, 16-H_b, 15-H_a, 11-H_a, 22-H_b, 6-H_b, 7-H_a, 7-H_b, 21-H_b, 9-H, 11-H_b), 1.15–1.10 (*m*, 1H, 15-H_b), 1.04–0.96 (*m*, 1H, 12-H_b), 0.95 (*s*, 3H, 27-H), 0.95 (*s*, 3H, 23-H), 0.93 (*s*, 3H, 26-H), 0.91–0.81 (*m*, 1H, 1-H_b), 0.80 (*s*, 3H, 25-H), 0.74 (*s*, 3H, 24-H), 0.69–0.64 (*m*, 1H, 5-H) ppm; ^{13}C-NMR (126 MHz, $CDCl_3$): δ = 176.4 (C-28), 151.2 (C-20), 109.4 (C-29), 79.1 (C-3), 58.3 (C-32), 55.9 (C-17), 55.5 (C-5), 50.8 (C-9), 50.2 (C-18), 47.0 (C-19), 45.3 (C-33, C-33′), 42.6 (C-14), 40.9 (C-8), 39.0 (C-4), 38.9 (C-1), 38.6 (C-22), 38.0 (C-13), 37.4 (C-10), 36.7 (C-31), 34.6 (C-7), 33.8 (C-16), 31.1 (C-21), 29.6 (C-15), 28.1 (C-23), 27.6 (C-2), 25.8 (C-12), 21.1 (C-11), 19.6 (C-30), 18.5 (C-6), 16.3 (C-26), 16.2 (C-25), 15.5 (C-24), 14.8 (C-27) ppm; MS (ESI, MeOH): *m*/*z* = 527 (100%, $[M + H]^+$); analysis calcd for $C_{34}H_{58}N_2O_2$ (526.85): C 77.51, H 11.10, N 5.32; found: C 77.40, H 11.22, N 5.18.

(3β)-N-(2-Pyrrolidin-1-ylethyl)-3-hydroxy-lup-20(29)-en-28-amide (**26**). Compound **26** was prepared from **19** according to general procedure C. Column chromatography (SiO_2, $CHCl_3$/MeOH 95:5) gave **26** (yield: 80%); m.p. 253–256 °C (decomp.); $[\alpha]_D = -14.7°$ (*c* 0.320, MeOH); $R_f = 0.40$ ($CHCl_3$/MeOH 9:1); IR (KBr): ν = 3426*br s*, 2942*s*, 2866*s*, 2696*m*, 2620*m*, 2500*m*, 1638*s*, 1544*m*, 1450*m*, 1376*m*, 1246*w*, 1196*w*, 1046*m*, 880*m* cm^{-1}; ^{1}H-NMR (500 MHz, $CDCl_3$): δ = 7.54 (*t*, *J* = 5.7 Hz, 1H, NH), 4.73–4.71 (*m*, 1H, 29-H_a), 4.59–4.57 (*m*, 1H, 29-H_b), 3.91–3.79 (*m*, 2H, 33-H_a, 33′-H_a), 3.78–3.61 (*m*, 2H, 31-H), 3.24–3.15 (*m*, 3H, 32-H, 3-H), 3.07 (*ddd*, *J* = 10.9, 10.9, 4.2 Hz, 1H, 19-H), 2.89–2.78 (*m*, 2H, 33-H_b, 33′-H_b), 2.42 (*ddd*, J = 12.6, 12.6, 3.6 Hz, 1H, 13-H), 2.31–2.18 (*m*, 3H, 16-H_a, 34-H_a, 34′-H_a), 2.15–2.05 (*m*, 2H, 34-H_b, 34′-H_b), 1.96–1.78 (*m*, 2H, 22-H_a, 21-H_a), 1.67 (*s*, 3H, 30-H), 1.73–1.14 (*m*, 17H, 12-H_a, 1-H_a, 2-H_a, 2-H_b, 18-H, 16-H_b, 6-H_a, 22-H_b, 11-H_a, 6-H_b, 21-H_b, 7-H_a, 7-H_b, 15-H_a, 9-H, 11-H_b, 15-H_b), 1.01–0.92 (*m*, 1H, 12-H_b), 0.96 (*s*, 6H, 23-H, 27-H), 0.91 (*s*, 3H, 26-H), 0.89–0.81 (*m*, 1H, 1-H_b), 0.81 (*s*, 3H, 25-H), 0.75 (*s*, 3H, 24-H), 0.70–0.65 (*m*, 1H, 5-H) ppm; ^{13}C-NMR (126 MHz, $CDCl_3$): δ = 177.9 (C-28), 151.1 (C-20), 109.5 (C-29), 79.1 (C-3), 56.6 (C-32), 56.1 (C-17), 55.5 (C-5), 54.8 (C-33, C-33′), 50.8 (C-9), 50.4 (C-18), 47.0 (C-19), 42.6 (C-14), 40.9 (C-8), 39.0 (C-4), 38.9 (C-1), 38.2 (C-22), 37.9 (C-13), 37.4 (C-10), 35.7 (C-31), 34.6 (C-7), 33.2 (C-16), 31.1 (C-21), 29.7 (C-15), 28.1 (C-23), 27.6 (C-2), 25.8 (C-12), 23.5 (C34, C-34′), 21.1 (C-11), 19.6 (C-30), 18.5 (C-6), 16.4 (C-26), 16.3 (C-25), 15.5 (C-24), 14.8 (C-27) ppm; MS (ESI, MeOH): *m*/*z* = 553 (100%, $[M + H]^+$); analysis calcd for $C_{36}H_{60}N_2O_2$ (552.89): C 78.21, H 10.94, N 5.07; found: C 78.00, H 11-09, N 4.81.

(3β)-N-(2-Piperidin-1-ylethyl)-3-hydroxy-lup-20(29)-en-28-amide (**27**). Compound **27** was prepared from **20** according to general procedure C. Column chromatography (SiO_2, $CHCl_3$/MeOH 95:5) gave **27** (yield: 83%); m.p. 141–144 °C (decomp.); $[\alpha]_D = +4.9°$ (*c* 0.315, $CHCl_3$); $R_f = 0.21$ ($CHCl_3$/MeOH 95:5); IR (KBr): ν = 3424*br s*, 2940*s*, 2866*m*, 2364*w*, 1638*s*, 1508*m*, 1452*m*, 1376*m*, 1248*w*, 1194*w*, 1128*w*, 1046*m* cm^{-1}; ^{1}H-NMR (400 MHz, $CDCl_3$): δ = 6.78–6.57 (*m*, 1H, NH), 4.76–4.69 (*m*, 1H, 29-H_a), 4.61–4.56 (*m*, 1H, 29-H_b), 3.48–3.31 (*m*, 2H, 31-H), 3.17 (*dd*, *J* = 11.1, 5.0 Hz, 1H, 3-H), 3.08 (*ddd*, *J* = 11.0, 10.8, 3.9 Hz, 1H, 19-H), 2.65–2.46 (*m*, 6H, 32-H, 33-H, 33′-H), 2.37 (*ddd*, *J* = 12.4, 12.3, 3.6 Hz, 1H, 13-H), 2.15–2.08 (*m*, 1H, 16-H_a), 2.00–1.88 (*m*, 1H, 21-H_a), 1.85–1.76 (*m*, 1H, 22-H_a), 1.68 (*s*, 3H, 30-H), 1.73–1.08 (*m*, 23H, 12-H_a, 35-H, 1-H_a, 18-H, 34-H, 34′-H, 6-H_a, 2-H_a, 2-H_b, 16-H_b, 15-H_a, 11-H_a, 22-H_b, 21-H_b, 6-H_b, 7-H_a, 7-H_b, 9-H, 11-H_b, 15-H_b), 1.08–0.95 (*m*, 1H, 12-H_b), 0.96 (*s*, 3H, 27-H), 0.95 (*s*, 3H, 23-H), 0.91 (*s*, 3H, 26-H), 0.91–0.82 (*m*, 1H, 1-H_b), 0.80 (*s*, 3H, 25-H), 0.74 (*s*, 3H, 24-H), 0.70–0.63 (*m*, 1H, 5-H) ppm; ^{13}C-NMR (101 MHz, $CDCl_3$): δ = 176.6 (C-28), 151.1 (C-20), 109.5 (C-29), 79.1 (C-3), 57.3 (C-32), 56.1 (C-17), 55.5 (C-5), 54.3 (C-33, C-33′), 50.7 (C-9), 50.1 (C-18), 47.1 (C-19), 42.7 (C-14), 40.9 (C-8), 39.0 (C-4), 38.9 (C-1), 38.4 (C-22), 38.1 (C-13), 37.4 (C-10), 35.5 (C-31), 34.6 (C-7), 33.6 (C-16), 31.1 (C-21), 29.6 (C-15), 28.1 (C-23), 27.6 (C-34, C-34′), 25.8 (C-12), 25.5 (C-35), 24.0 (C-2), 21.1 (C-11), 19.6 (C-30), 18.5 (C-6), 16.3 (C-26), 16.2 (C-25), 15.5 (C-24), 14.8 (C-27) ppm; MS (ESI, MeOH): *m*/*z* = 567 (100%, $[M + H]^+$); analysis calcd for $C_{37}H_{62}N_2O_2$ (566.92): C 78.39, H 11.02, N 4.94; found: C 78.16, H 11.20, N 4.71.

(3β)-N-(2-Piperazin-1-ylethyl)-3-hydroxy-lup-20(29)-en-28-amide (**28**). Compound **28** was prepared from **21** according to general procedure C. Column chromatography (SiO_2, $CHCl_3$/MeOH/NH_4OH 90:10:0.5) gave **28** (yield: 90%); m.p. 146–148 °C (decomp.); $[\alpha]_D = +6.5°$ (*c* 0.380, $CHCl_3$); R_f = 0.30 ($CHCl_3$/MeOH/NH_4OH 90:10:1); IR (KBr): ν = 3422*br s*, 3072*w*, 2942*s*, 2868*m*, 1638*s*, 1510*m*, 1452*m*, 1376*m*, 1320*w*, 1248*w*, 1194*w*, 1138*w*, 1046*w*, 754*m* cm^{-1}; ^{1}H-NMR (400 MHz, $CDCl_3$): δ = 6.19 (*t*, *J* = 4.9 Hz, 1H, NH), 4.77–4.70 (*m*, 1H, 29-H_a), 4.63–4.55 (*m*, 1H, 29-H_b), 3.42–3.28 (*m*, 2H, 31-H), 3.17 (*dd*, *J* = 11.1, 5.0 Hz, 1H, 3-H), 3.09 (*ddd*, *J* = 10.8, 10.3, 3.7 Hz, 1H, 19-H), 2.97 (*t*, *J* = 4.9 Hz, 4H, 34-H, 34′-H), 2.58–2.42 (*m*, 6H, 32-H, 33-H, 33′-H), 2.37 (*ddd*, *J* = 12.4, 12.3, 3.7 Hz, 1H, 13-H), 2.06–1.89 (*m*, 2H, 16-H_a, 21-H_a), 1.68 (*s*, 3H, 30-H), 1.81–1.08 (*m*, 18H, 22-H_a, 12-H_a, 1-H_a, 18-H, 2-H_a, 2-H_b, 6-H_a, 16-H_b, 15-H_a, 11-H_a, 22-H_b, 6-H_b, 21-H_b, 7-H_a, 7-H_b, 9-H, 11-H_b, 15-H_b), 1.07–0.95 (*m*, 1H, 12-H_b), 0.97 (*s*, 3H, 27-H), 0.95 (*s*, 3H, 23-H), 0.92 (*s*, 3H, 26-H), 0.96–0.83 (*m*, 1H, 1-H_b), 0.80 (*s*, 3H, 25-H), 0.75 (*s*, 3H, 24-H), 0.70–0.64 (*m*, 1H, 5-H) ppm; ^{13}C-NMR (101 MHz, $CDCl_3$): δ = 176.3 (C-28), 151.0 (C-20), 109.6 (C-29), 79.1 (C-3), 57.1 (C-32), 56.0 (C-17), 55.5 (C-5), 53.6 (C-33, C-33′), 50.7 (C-9), 50.1 (C-18), 47.2 (C-19), 46.0 (C-34, C-34′), 42.7 (C-14), 40.9 (C-8), 39.0 (C-4), 38.9 (C-1), 38.5 (C-22), 38.1 (C-13), 37.4

(C-10), 35.6 (C-31), 34.6 (C-7), 33.9 (C-16), 31.1 (C-21), 29.6 (C-15), 28.2 (C-23), 27.6 (C-2), 25.8 (C-12), 21.1 (C-11), 19.6 (C-30), 18.5 (C-6), 16.4 (C-26), 16.3 (C-25), 15.5 (C-24), 14.8 (C-27) ppm; MS (ESI, MeOH): m/z = 568 (100%, $[M + H]^+$); analysis calcd for $C_{36}H_{61}N_3O_2$ (567.90): C 76.14, H 10.83, N 7.40; found: C 75.96, H 11.01, N 7.27.

(3β)-N-(4-Aminobutyl)-3-hydroxy-lup-20(29)-en-28-amide (**29**). Compound **29** was prepared from **22** according to general procedure C. Column chromatography (SiO_2, $CHCl_3$/MeOH 9:1) gave **29** (yield: 85%); m.p. 130–133 °C; $[\alpha]_D$ = +4.8° (*c* 0.380, DMSO); R_f = 0.31 ($CHCl_3$/MeOH 88:12);IR (KBr): ν = 3448*br s*, 2941*s*, 2867*m*, 1636*m*, 1534*m*, 1452*m*, 1384*w*, 1195*w*, 1045*w* cm^{-1}; ^{1}H-NMR (400 MHz, DMSO-d_6): δ = 7.55 (*t*, *J* = 5.8 Hz, 1H, NH), 4.67–4.62 (*m*, 1H, 29-H_a), 4.55–4.50 (*m*, 1H, 29-H_b), 3.12–2.88 (*m*, 4H, 31-H_a, 19-H, 3-H, 31-H_b), 2.61–2.51 (*m*, 3H, 13-H, 32-H_a, 32-H_b), 2.18–2.09 (*m*, 1H, 16-H_a), 1.81–1.64 (*m*, 2H, 22-H_a, 21-H_a), 1.62 (*s*, 3H, 30-H), 1.61–1.51 (*m*, 2H, 1-H_a, 12-H_a), 1.49–0.98 (*m*, 19H, 2-H_a, 2-H_b, 6-H_a, 18-H, 34-H_a, 34-H_b, 11-H_a, 16-H_b, 15a, 22-H_b, 6-H_b, 33-H_a, 33-H_b, 7-H_a, 7-H_b, 9-H, 21-H_b, 11-H_b, 15-H_b), 0.97–0.78 (*m*, 2H, 1-H_b, 12-H_b), 0.90 (*s*, 3H, 27-H), 0.86 (*s*, 3H, 23-H), 0.84 (*s*, 3H, 26-H), 0.76 (*s*, 3H, 25-H), 0.65 (*s*, 3H, 24-H), 0.64–0.59 (*m*, 1H, 5-H) ppm; ^{13}C-NMR (101 MHz, DMSO-d_6): δ = 175.2 (C-28), 150.9 (C-20), 109.1 (C-29), 76.8 (C-3), 55.0 (C-5), 54.8 (C-17), 50.1 (C-9), 49.7 (C-18), 46.1 (C-19), 41.9 (C-14), 41.2 (C-32), 40.3 (C-8), 38.5 (C-4), 38.3 (C-31), 38.2 (C-1), 37.7 (C-22), 36.7 (C-10), 36.6 (C-13), 34.0 (C-7), 32.4 (C-16), 30.4 (C-21, C33), 28.9 (C-15), 28.1 (C-23), 27.2 (C-2), 26.7 (C-34), 25.2 (C-12), 20.6 (C-11), 19.0 (C-30), 18.0 (C-6), 16.0 (C-25), 15.8 (C-26), 15.7 (C-24), 14.3 (C-27) ppm; MS (ESI, MeOH): m/z = 527 (100 %, $[M + H]^+$), 1053 (22 %, $[2M + H]^+$); analysis calcd for $C_{34}H_{58}N_2O_2$ (526.45): C 77.51, H 11.10, N 5.32; found: C 77.38, H 11.30, N 5.13.

(3β)-N-[2-(2-Aminoethoxy)ethyl]-3-hydroxy-lup-20(29)-en-28-amide (**30**). Compound **30** was prepared from **23** according to general procedure C. Column chromatography (SiO_2, $CHCl_3$/MeOH 9:1) gave **30** (yield: 91%); m.p. 182–183 °C; $[\alpha]_D$ = −1.1° (*c* 0.315, MeOH); R_f = 0.45 ($CHCl_3$/MeOH/NH_4OH 90:10:1); IR (KBr): ν = 3424*br s*, 2942*s*, 2868*m*, 1636*s*, 1534*m*, 1450*w*, 1384*w*, 1318*w*, 1278*w*, 1248*w*, 1196*w*, 1108*m*, 1044*m* cm^{-1}; ^{1}H-NMR (500 MHz, CD_3OD): δ = 4.72–4.68 (*m*, 1H, 29-H_a), 4.61–4.57 (*m*, 1H, 29-H_b), 3.70–3.63 (*m*, 2H, 33-H), 3.57–3.51 (*m*, 2H, 32-H), 3.47–3.31 (*m*, 2H, 31-H), 3.15–3.05 (*m*, 4H, 3-H, 19-H, 34-H), 2.56 (*ddd*, *J* = 12.8, 12.4, 3.6 Hz, 1H, 13-H), 2.12 (*ddd*, *J* = 13.1, 3.3, 3.2 Hz, 1H, 16-H_a), 1.93–1.78 (*m*, 2H, 21-H_a, 22-H_a), 1.69 (*s*, 3H, 30-H), 1.76–1.63 (*m*, 2H, 12-H_a, 1-H_a), 1.65–1.10 (*m*, 15H, 2-H_a, 2-H_b, 18-H, 16-H_b, 6-H_a, 15-H_a, 22-H_b, 11-H_a, 6-H_b, 7-H_a, 7-H_b, 21-H_b, 9-H, 11-H_b, 15-H_b), 1.09–0.96 (*m*, 1H, 12-H_b), 1.00 (*s*, 3H, 27-H), 0.97 (*s*, 3H, 26-H), 0.95 (*s*, 3H, 23-H), 0.95–0.88 (*m*, 1H, 1-H_b), 0.86 (*s*, 3H, 25-H), 0.75 (*s*, 3H, 24-H), 0.73–0.69 (*m*, 1H, 5-H) ppm; ^{13}C-NMR (126 MHz, CD_3OD): δ = 179.6 (C-28), 152.3 (C-20), 110.0 (C-29), 79.6 (C-3), 71.4 (C-32), 67.8 (C-33), 57.1 (C-17), 56.9 (C-5), 52.1 (C-9), 51.4 (C-18), 48.2 (C-19), 43.5 (C-14), 42.0 (C-8), 40.7 (C-34), 40.1 (C-1), 39.9 (C-4), 39.7 (C-31), 39.3 (C-22), 39.0 (C-13), 38.3 (C-10), 35.6 (C-7), 34.1 (C-16), 31.9 (C-21), 30.6 (C-15), 28.6 (C-23), 28.0 (C-2), 27.0 (C-12), 22.2 (C-11), 19.6 (C-30), 19.5 (C-6), 16.9 (C-24), 16.8 (C-25), 16.1 (C-26), 15.1 (C-27) ppm; MS (ESI, MeOH): m/z = 543 (100 %, $[M + H]^+$), 1085 (10 %, $[2M + H]^+$); analysis calcd for $C_{34}H_{58}N_2O_3$ (542.58): C 75.23, H 10.77, N 5.16; found: C 75.11, H 10.94, N 4.97.

5. Conclusions

A set of 28 ursolic and betulinic carboxamides was prepared and screened for their cytotoxic activity using SRB assays. This screening revealed the compounds derived from betulinic acid to be more potent than those from ursolic acid. In particular, betulinic carboxamides **24**–**30** showed remarkable cytotoxicity, as indicated by EC_{50} values lower than 1 μM. The most potent compounds of this study are (*3β*)-*N*-[2-(dimethylamino)ethyl]-3-hydroxy-lup-20(29)-en-28-amide (**25**, EC_{50} = 0.2 μM ± 0.01 μM for A2780 tumor cells; SI = 1.50) and (*3β*)-*N*-(2-pyrrolidin-1-ylethyl)-3-hydroxy-lup-20(29)-en-28-amide (**26**, EC_{50} = 0.2 μM ± 0.05 μM for MCF-7 tumor cells; SI = 2.00). Compound **18** showed the highest selectivity for HT29 tumor cells (EC_{50} = 0.3 ± 0.02 μM; SI = 3.33). Further structural modifications showed that the replacement of the 3-*O*-acetyl moiety has an impact on the cytotoxicity and on the selectivity, respectively. Compounds **25** and **26** were selected for extended biological testing

employing MCF-7 and A2780 human tumor cell lines. Fluorescence microscopic images revealed both of the compounds to show characteristics of apoptosis.

Supplementary Materials: Supplementary data related to this article can be found at http://www.mdpi.com/1420-3049/23/10/2558/s1.

Author Contributions: M.K. and R.C. conceived and designed the experiments; M.K. performed the experiments; L.F. performed the biological assays and experiments; M.K., L.F., A.A.-H. and R.C. analyzed the data and wrote the paper.

Funding: We acknowledge the financial support of the Open Access Publications Fund of the Martin-Luther-University Halle-Wittenberg.

Acknowledgments: We'd like to thank R. Kluge for measuring the ESI-MS spectra and Dieter Ströhl and his team for the NMR spectra. Thanks are also due to Jana Wiese and Vivienne Simon for measuring the IR spectra and optical rotations. The cell lines were kindly provided by Thomas Müller (Dept. of Haematology/Oncology, Martin-Luther University Halle-Wittenberg).

Conflicts of Interest: The authors declare no conflict of interest.

References

1. Heymach, J.; Krilov, L.; Alberg, A.; Baxter, N.; Chang, S.M.; Corcoran, R.B.; Dale, W.; DeMichele, A.; Diefenbach, C.S.M.; Dreicer, R.; et al. Clinical cancer advances 2018: Annual report on progress against cancer from the american society of clinical oncology. *J. Clin. Oncol.* **2018**, *36*, 1020–1044. [CrossRef] [PubMed]
2. Laszczyk, M.N. Pentacyclic triterpenes of the lupane, oleanane and ursane group as tools in cancer therapy. *Planta Medica* **2009**, *75*, 1549–1560. [CrossRef] [PubMed]
3. Chen, H.; Gao, Y.; Wang, A.; Zhou, X.; Zheng, Y.; Zhou, J. Evolution in medicinal chemistry of ursolic acid derivatives as anticancer agents. *Eur. J. Med. Chem.* **2015**, *92*, 648–655. [CrossRef] [PubMed]
4. Csuk, R. Betulinic acid and its derivatives: A patent review (2008–2013). *Expert Opin. Ther. Pat.* **2014**, *24*, 913–923. [CrossRef] [PubMed]
5. Tripathi, L.; Kumar, P.; Singh, R. A review on extraction, synthesis and anticancer activity of betulinic acid. *Curr. Bioact. Compd.* **2009**, *5*, 160–168. [CrossRef]
6. Csuk, R.; Schwarz, S.; Siewert, B.; Kluge, R.; Ströhl, D. Synthesis and antitumor activity of ring a modified glycyrrhetinic acid derivatives. *Eur. J. Med. Chem.* **2011**, *46*, 5356–5369. [CrossRef] [PubMed]
7. Heller, L.; Sommerwerk, S.; Tzschöckell, F.; Wiemann, J.; Schwarz, S.; Siewert, B.; Al-Harrasi, A.; Csuk, R. First occurrence of a furano-glycyrrhetinoate and its cytotoxicity. *Arch. Pharm.* **2015**, *348*, 889–896. [CrossRef] [PubMed]
8. Ma, C.-M.; Wu, X.-H.; Hattori, M.; Wang, X.-J.; Kano, Y. Hcv protease inhibitory, cytotoxic and apoptosis-inducing effects of oleanolic acid derivatives. *J. Pharm. Pharm. Sci.* **2009**, *12*, 243–248. [CrossRef] [PubMed]
9. Ma, C.-M.; Cai, S.-Q.; Cui, J.-R.; Wang, R.-Q.; Tu, P.-F.; Hattori, M.; Daneshtalab, M. The cytotoxic activity of ursolic acid derivatives. *Eur. J. Med. Chem.* **2005**, *40*, 582–589. [CrossRef] [PubMed]
10. Kahnt, M.; Heller, L.; Grabandt, P.; Al-Harrasi, A.; Csuk, R. Platanic acid: A new scaffold for the synthesis of cytotoxic agents. *Eur. J. Med. Chem.* **2018**, *143*, 259–265. [CrossRef] [PubMed]
11. Kahnt, M.; Heller, L.; Al-Harrasi, A.; Schäfer, R.; Kluge, R.; Wagner, C.; Otgonbayar, C.; Csuk, R. Platanic acid-derived methyl 20-amino-30-norlupan-28-oates are potent cytotoxic agents acting by apoptosis. *Med. Chem. Res.* **2018**, *27*, 1757–1769. [CrossRef]
12. Heller, L.; Knorrscheidt, A.; Flemming, F.; Wiemann, J.; Sommerwerk, S.; Pavel, I.Z.; Al-Harrasi, A.; Csuk, R. Synthesis and proapoptotic activity of oleanolic acid derived amides. *Bioorg. Chem.* **2016**, *68*, 137–151. [CrossRef] [PubMed]
13. Skehan, P.; Storeng, R.; Scudiero, D.; Monks, A.; McMahon, J.; Vistica, D.; Warren, J.T.; Bokesch, H.; Kenney, S.; Boyd, M.R. New colorimetric cytotoxicity assay for anticancer-drug screening. *J. Natl. Cancer Inst.* **1990**, *82*, 1107–1112. [CrossRef] [PubMed]
14. Swiss Institute of Bioinformatics—SwissAMDE. Available online: www.swissadme.ch (accessed on 21 September 2018).
15. Deng, S.L.; Baglin, I.; Nour, M.; Cavé, C. Synthesis of phosphonodipeptide conjugates of ursolic acid and their homologs. *Heteroat. Chem.* **2008**, *19*, 55–65. [CrossRef]

16. Petrenko, N.; Elantseva, N.; Petukhova, V.; Shakirov, M.; Shul'ts, E.; Tolstikov, G. Synthesis of betulonic acid derivatives containing amino-acid fragments. *Chem. Nat. Compd.* **2002**, *38*, 331–339. [CrossRef]
17. Bai, K.-K.; Yu, Z.; Chen, F.-L.; Li, F.; Li, W.-Y.; Guo, Y.-H. Synthesis and evaluation of ursolic acid derivatives as potent cytotoxic agents. *Bioorg. Med. Chem. Lett.* **2012**, *22*, 2488–2493. [CrossRef] [PubMed]
18. Yang, X.; Li, Y.; Jiang, W.; Ou, M.; Chen, Y.; Xu, Y.; Wu, Q.; Zheng, Q.; Wu, F.; Wang, L. Synthesis and biological evaluation of novel ursolic acid derivatives as potential anticancer prodrugs. *Chem. Biol. Drug Des.* **2015**, *86*, 1397–1404. [CrossRef] [PubMed]

Sample Availability: Samples of all compounds are available from the authors.

molecules

MDPI

Article

Ganoderma tsugae Inhibits the SREBP-1/AR Axis Leading to Suppression of Cell Growth and Activation of Apoptosis in Prostate Cancer Cells

Shih-Yin Huang [1], Guan-Jhong Huang [2], Hsi-Chin Wu [3], Ming-Ching Kao [4,5,6] and Wen-Chin Huang [1,*]

1 Graduate Institute of Biomedical Sciences, School of Medicine, China Medical University, Taichung 40402, Taiwan; nerissana777@gmail.com
2 School of Chinese Pharmaceutical Sciences and Chinese Medicine Resources, College of Chinese Medicine, China Medical University, Taichung 40402, Taiwan; gjhuang@mail.cmu.edu.tw
3 Department of Urology, China Medical University Hospital, Taichung 40402, Taiwan; wuhc@mail.cmuh.org.tw
4 Department of Biological Science and Technology, College of Biopharmaceutical and Food Sciences, China Medical University, Taichung 40402, Taiwan; mckao@mail.cmu.edu.tw
5 Research Center for Chinese Herbal Medicine, China Medical University, Taichung 40402, Taiwan
6 Chinese Medicine Research Center, China Medical University, Taichung 40402, Taiwan
* Correspondence: huangwc@mail.cmu.edu.tw; Tel.: +886-4-2205-2121 (ext. 7721)

Received: 12 September 2018; Accepted: 3 October 2018; Published: 5 October 2018

Abstract: Recent research suggests that the activation of lipid biosynthesis (lipogenesis) is linked with prostate cancer (PCa) malignancy. Sterol regulatory element-binding protein-1 (SREBP-1) is a key transcriptional regulator controlling lipogenesis. Moreover, androgen receptor (AR) has been well defined to play an important role in lethal PCa aggressiveness from androgen-responsive to castration-resistant status. In this study, we showed that the quality-assured *Ganoderma tsugae* ethanol extract (GTEE), a Chinese natural and herbal product, significantly inhibited expression of SREBP-1 and its downstream genes associated with lipogenesis in PCa cells. Through inhibiting SREBP-1, GTEE reduced the levels of intracellular fatty acids and lipids in PCa cells. Importantly, GTEE also downregulated the expression of AR and prostate-specific antigen (PSA) in both androgen-responsive and castration-resistant PCa cells. By blocking the SREBP-1/AR axis, GTEE suppressed cell growth and progressive behaviors, as well as activating the caspase-dependent apoptotic pathway in PCa cells. These data provide a new molecular basis of GTEE for the development of a potential therapeutic approach to treat PCa malignancy.

Keywords: AR; *Ganoderma tsugae*; lipogenesis; prostate cancer; SREBP-1

1. Introduction

Cancer progression is the underlying cause of death in prostate cancer (PCa) patients. One of the main clinical challenges is that PCa progresses from androgen-responsive to androgen-refractory/castration-resistant prostate cancer (CRPC), which is incurable. Androgen receptor (AR), a master androgenic hormone-activated transcription factor, plays a key role in the regulation of PCa growth, survival, and deadly CRPC progression [1,2]. Androgen deprivation therapy (ADT), blocking the androgen/AR signaling pathway, is a first-line therapy in clinical intervention in PCa patients. However, most PCa patients who receive ADT suffer severe adverse effects and eventually relapse with lethal CRPC progression. Therefore, there is an urgent need to develop novel and effective treatments to prevent and cure this fatal aggressiveness.

Sterol regulatory element-binding proteins (SREBPs; SREBP-1 and SREBP-2) mainly control the expression of genes associated with lipogenesis, cholesterogenesis, and lipid/cholesterol homeostasis [3,4]. SREBPs would be able to interact with sterol regulatory element (SRE) *cis*-acting elements that are found in the promoter regions of genes encoding enzymes for the de novo biosynthesis of fatty acids, lipids, and cholesterol [3,5,6]. Specifically, SREBP-1 transcriptionally activates genes that are involved in lipogenesis, such as fatty acid synthase (FASN; a rate-limiting enzyme and a check point for lipogenesis), whereas SREBP-2 mediates cholesterol biosynthesis through the regulation of HMG CoA reductase (HMGCR; a rate-limiting enzyme and a check point for cholesterogenesis) [3,5,6]. We previously reported that SREBP-1 induced PCa cell growth and progression through the concerted activation of the metabolic and signaling networks involving lipogenesis, AR, and oxidative stress [7]. In addition, SREBP-1 regulated AR expression through transcriptionally activation in PCa cells [7,8]. Importantly, overexpression of SREBP-1 protein was associated with aggressive pathological features and CRPC progression in PCa patients [7,9]. These findings provide a rationale for targeting SREBP-1 and its regulated downstream axis as an attractive therapeutic approach to eliminating PCa aggressiveness.

Traditional Chinese medicine is a healing and herbal system, which has been established a medical foundation for a long history. *Ganoderma tsugae* (GT), a Chinese herbal product, is a restricted species of *Lingzhi* that is cultivated in Taiwan, and it has been shown to exhibit antioxidant activity, and it is applied to treat cardiovascular and allergic diseases [10,11]. Our laboratory previously demonstrated that an ethanol extract of GT (GTEE) displayed anti-proliferative effects on human cancer cells [12–15]. However, the clinical benefits and the molecular basis of GTEE in PCa malignancy remain unknown.

The aim of this study is to reveal and evaluate the molecular mechanisms and the therapeutic efficacy of a Chinese herbal medicine, GTEE, in PCa cells, including LNCaP (androgen-responsive) and C4-2 (castration-resistant) cells. GTEE inhibited the expression of SREBP-1 and FASN in LNCaP and C4-2 cells. By inhibiting genes associated with lipogenesis, GTEE reduced the amounts of intracellular fatty acid and lipid accumulation in PCa cells. Furthermore, GTEE decreased the expression of AR and prostate-specific antigen (PSA), an AR downstream target gene, in both LNCaP and C4-2 cells. GTEE also suppressed cell growth and aggressive behaviors, as well as inducing the caspase-dependent apoptotic pathway in PCa cells. Taken together, these results provide an innovative molecular basis of GTEE in PCa cells, and targeting the SREBP-1/AR axis by GTEE could be a promising approach for the treatment of malignant PCa.

2. Results

2.1. GTEE Inhibits the Expression of SREBP-1 and Its Downstream Associated Genes in PCa Cells

To investigate whether GTEE inhibits SREBP-1/lipogenesis and the AR axis in PCa cells, which play important roles in PCa development, survival, and progression [7,8,16,17], we performed quantitative Reverse Transcription-Polymerase Chain Reaction (qRT-PCR) and Western blot analyses to determine the expression of genes that are associated with SREBPs and AR. As shown in Figure 1A, GTEE decreased the mRNA expression of SREBP-1 and FASN in both LNCaP and C4-2 cells. However, GTEE did not significantly change the expression of SREBP-2 and HMGCR in PCa cells, which mainly controlled cholesterogenesis. We also examined whether GTEE affected AR and PSA expression in these AR-positive PCa cells, because we previously reported that SREBP-1 transcriptionally regulated AR expression [7,8]. By inhibiting SREBP-1 expression, GTEE decreased the mRNA expression of AR and its downstream target genes, PSA, in LNCaP and C4-2 cells (Figure 1A). Fitting with the effects of GTEE on mRNA expression, the protein levels of SREBP-1, FASN, and AR, but not SREBP-2 were also decreased by GTEE in LNCaP and C4-2 cells (Figure 1B). Collectively, the data of qRT-PCR and Western blot analyses suggest that GTEE inhibited the expression of SREBP-1 and its downstream associated genes, including FASN and AR, in PCa cells.

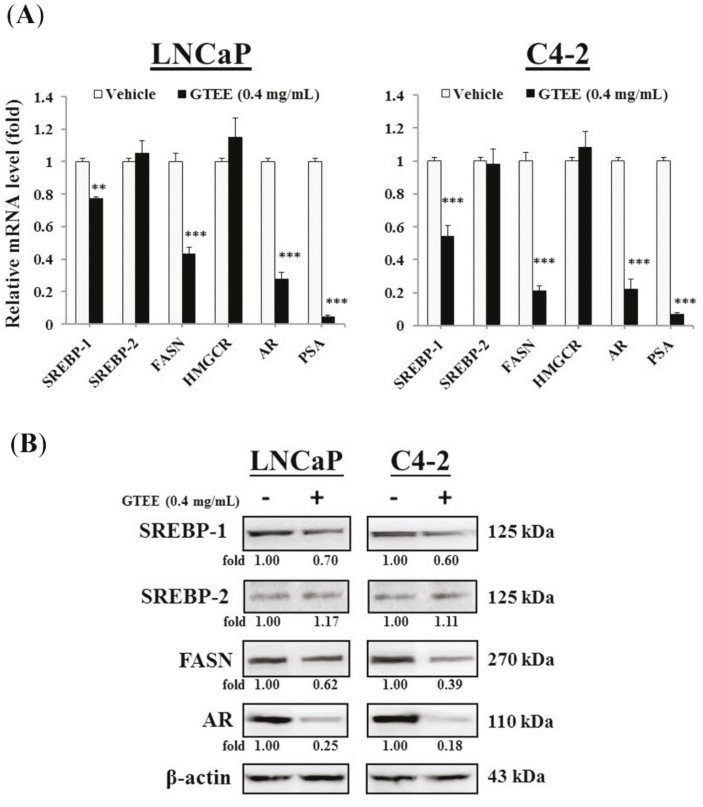

Figure 1. *Ganoderma tsugae* ethanol extract (GTEE) inhibits the expression of SREBP-1 and its downstream related genes in prostate cancer (PCa) cells. (**A**) GTEE significantly inhibited the mRNA expression of SREBP-1, FASN, AR, and PSA but not SREBP-2 and HMGCR in both LNCaP and C4-2 PCa cells determined by quantitative Reverse Transcription-Polymerase Chain Reaction (qRT-PCR) analysis. The relative mRNA level (fold) was assigned as 1.0 in vehicle-treated cells. Data were normalized to β-actin and represented as the mean ± SD of three independent duplicate experiments. ** $p < 0.01$, *** $p < 0.001$. (**B**) GTEE suppressed the protein levels of SREBP-1, FASN, and AR, but not SREBP-2 in LNCaP, and C4-2 cells assayed by Western blot analysis. β-actin was used as a loading control. The protein bands were scanned and quantified using ImageJ software. The relative level (fold) of protein expression with the vehicle treatment and normalized to β-actin was assigned as 1.00.

2.2. GTEE Reduces the Levels of Intracellular Fatty Acid and Lipid Accumulation in PCa Cells

Because GTEE inhibited the expression of key genes (SREBP-1 and FASN) linked with lipogenesis, we subsequently performed quantification and staining assays to determine the changes of the intracellular fatty acid and lipid levels in PCa cells caused by GTEE. As shown in Figure 2A, the amounts of intracellular fatty acids were significantly decreased in GTEE-treated LNCaP and C4-2 cells in a dose-dependent pattern compared to a vehicle group. Furthermore, the lipid droplet accumulation was determined by the Oil Red O staining and quantification. The lipid droplet levels of GTEE-treated LNCaP and C4-2 cells were also decreased in comparison with vehicle-treated cells (Figure 2B). The results of lipogenesis assays indicate that GTEE led to a decrease in the levels of intracellular fatty acid and lipid accumulation in LNCaP and C4-2 cells through the inhibition of SREBP-1 and FASN (Figure 1).

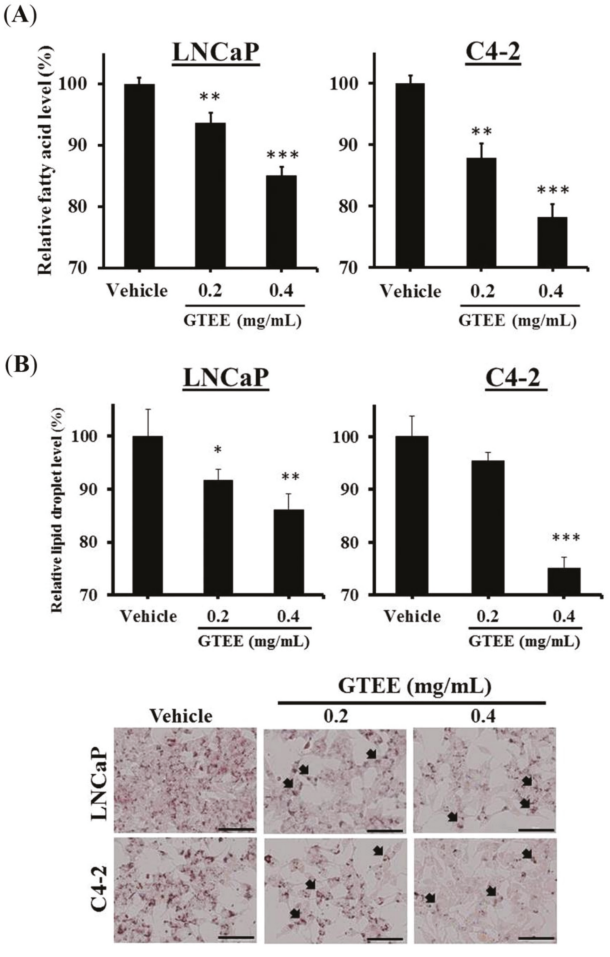

Figure 2. GTEE reduces the amounts of intracellular fatty acid and lipid accumulation in PCa cells. (**A**) LNCaP and C4-2 cells were treated with vehicle (0.3% ethanol) or GTEE (0.2 or 0.4 mg/mL) for 24 h. The levels of intracellular fatty acid were determined by a fatty acid quantification kit. The relative fatty acid level (%) was assigned as 100% in vehicle-treated PCa cells. Data were shown as the mean ± SD of three independent experiments. ** $p < 0.01$, *** $p < 0.001$. (**B**) GTEE decreased the amounts of lipid droplet accumulation assayed by the Oil Red O staining in LNCaP and C4-2 cells at 24 h. The relative lipid droplet level (%) was assigned as 100% in vehicle-treated cells. Data were shown as the mean ± SD of three independent experiments. * $p < 0.05$, ** $p < 0.01$, *** $p < 0.001$. The arrowheads indicate lipid droplets in PCa cells (bottom panel). Scale bars = 100 μm.

2.3. GTEE Suppresses the Cell Growth and In Vitro Progression of PCa Cells

To assess the potential for biological consequences elicited by GTEE (Figures 1 and 2), LNCaP and C4-2 cells were treated with various concentrations of GTEE followed by functional analyses, including cell growth and in vitro migration and invasion assays. We first determined the growth of PCa cells using a MTS assay. As shown in Figure 3A,B, GTEE suppressed the growth of LNCaP and C4-2 cells at varying concentrations (0.2, 0.4, 0.6, 0.8 and 1.0 mg/mL) and at varying times (24, 48 and 72 h). The half maximal inhibitory concentrations (IC_{50}) of GTEE for LNCaP and C4-2 cells were 0.746 and 0.735 mg/mL (48 h), respectively.

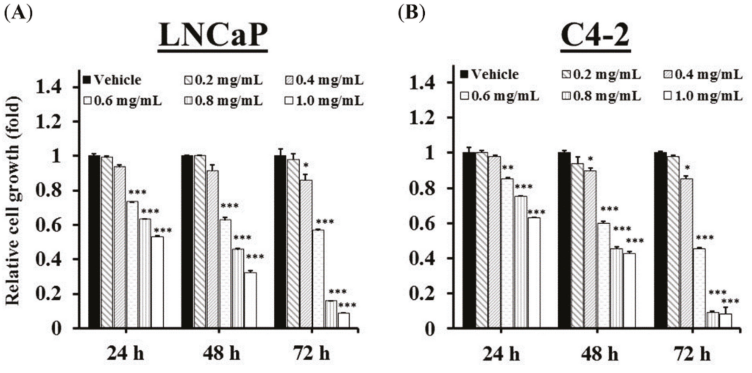

Figure 3. GTEE suppresses the cell growth of PCa cells. (**A**) LNCaP and (**B**) C4-2 cells were treated with vehicle (0.3% ethanol) or GTEE (0.2, 0.4, 0.6, 0.8 or 1.0 mg/mL) for 24, 48 and 72 h. Cell growth was determined by MTS assay. The relative cell growth (fold) was assigned as 1.0 in vehicle-treated cells at each time point. Data were shown as the mean ± SD of three independent experiments. * $p < 0.05$, ** $p < 0.01$, *** $p < 0.001$.

Next, the effects of GTEE on the migratory and invasive potentials of PCa cells were determined. A wound healing method was used to evaluate the migratory ability. As shown in Figure 4A, GTEE treatment led to a significant inhibition of wound closure in both LNCaP and C4-2 cells. Besides, the Boyden chamber method was also used to determine migration and invasion in PCa cells that were affected by GTEE. GTEE (0.1, 0.2 and 0.4 mg/mL) significantly decreased the capabilities of migration and invasion of LNCaP and C4-2 cells in a concentration-dependent pattern (Figure 4B and Figure S1). These biofunctional results suggest that GTEE suppressed cell growth and in vitro progression in LNCaP and C4-2 cells.

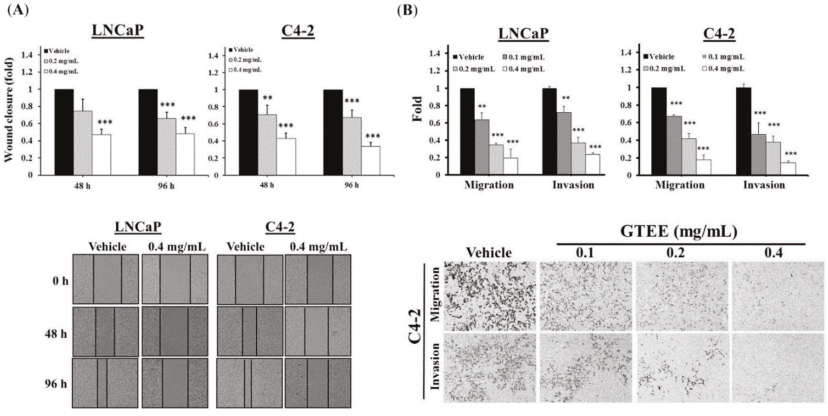

Figure 4. GTEE inhibits the in vitro progression of PCa cells. (**A**) LNCaP and C4-2 cells were treated with vehicle (0.3% ethanol) or GTEE (0.2 or 0.4 mg/mL). Wound closure was determined by migratory distance at 48 and 96 h. Data were shown as the mean ± SD of three independent experiments. ** $p < 0.01$, *** $p < 0.001$ (top panel). Representative images of wound closure in LNCaP and C4-2 cells treated with vehicle or GTEE (0.4 mg/mL) were shown (bottom panel). (**B**) The migration and invasion of LNCaP and C4-2 cells treated with vehicle (0.3% ethanol) or GTEE (0.1, 0.2 or 0.4 mg/mL) were performed by the Boyden chamber method. Data represented the mean ± SD of three separate experiments. ** $p < 0.01$, *** $p < 0.001$ (top panel). Representative images of the migration and invasion of C4-2 cells treated with vehicle or GTEE were shown (bottom panel).

2.4. GTEE Induces Apoptosis through the Caspase-Dependent Pathway in PCa Cells

We observed that many attached LNCaP and C4-2 cells on cultured dishes were floating/dying during treatment with high concentrations of GTEE, such as 0.8 or 1.2 mg/mL. Therefore, we next determined apoptotic death in PCa cells caused by GTEE. Flow cytometry-based annexin V-FITC staining analysis, caspase enzymatic activity assay, and Western blot analysis of caspase and PARP proteins were conducted to evaluate whether GTEE induced the caspase-dependent apoptotic pathway in PCa cells. The results of Annexin V-FITC staining analysis showed that GTEE increased the percentages of apoptotic cells in LNCaP and C4-2 cells with a concentration-dependent manner after 24 h treatment (Figure 5A). Subsequently, the caspase-3/7 enzymatic activity and the expression of caspase-3 and PARP proteins were examined. As shown in Figure 5B, GTEE significantly increased the caspase-3/7 activity in LNCaP and C4-2 cells in a dose-dependent pattern (0.8 and 1.2 mg/mL). Moreover, the results of Western blot analysis showed that GTEE greatly decreased the expression of full length (F)-caspase-3 (35 kDa) as well as increased the expression of cleaved (C)-caspase 3 (17 kDa) and C-PARP (89 kDa) in both LNCaP and C4-2 cells (Figure 5C). Collectively, these data suggest that GTEE induces the caspase-dependent apoptotic death in PCa cells.

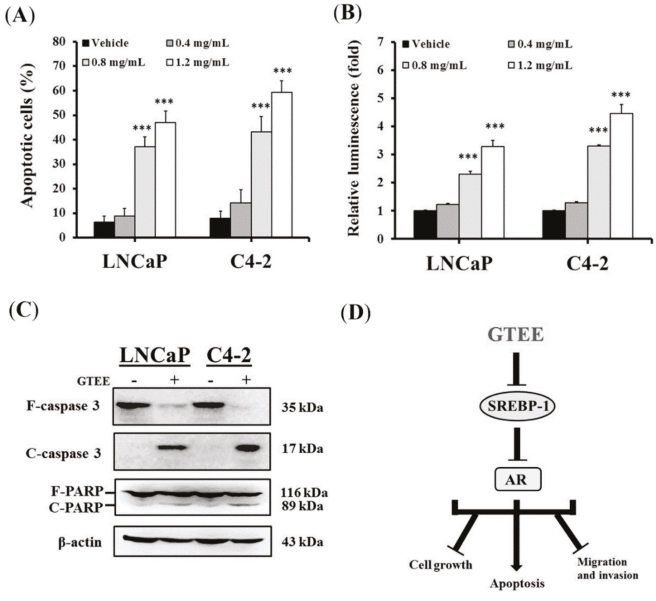

Figure 5. GTEE induces apoptosis through the caspase-dependent pathway in PCa cells. (**A**) After 24 h treatment with the vehicle (0.3% ethanol) or GTEE (0.4, 0.8 or 1.2 mg/mL), apoptotic cells (%) of LNCaP and C4-2 were determined by Annexin V-FITC staining analysis using flow cytometry. Data represented the mean ± SD of triplicate experiments. *** $p < 0.001$. (**B**) GTEE increased the caspase-3/7 activity in LNCaP and C4-2 cells with a dose-dependent manner. Luminescence of the caspase-3/7 activity was measured by an enzymatic activity assay. The relative luminescence (fold) was assigned as 1 in vehicle-treated cells. Results were shown as the mean ± SD of three independent experiments. *** $p < 0.001$. (**C**) Western blot analysis of caspase-3 and PARP proteins in PCa cells treated with vehicle (0.3% ethanol) or GTEE (1.2 mg/mL) for 20 h. GTEE greatly decreased full length (F)-caspase-3 as well as increased cleaved (C)-caspase-3 and C-PARP in LNCaP and C4-2 cells. β-actin was used as a loading control. (**D**) A schematic model of GTEE blocked the SREBP-1/AR axis to further suppress cell growth, migration, and invasion, and induce apoptosis in PCa cells was proposed.

3. Discussion

Activation of lipogenesis in cancer cells has been shown to be triggered by increased needs for the components of cell lipid bilayer membranes, and promotion of the signaling transduction mediated by cell membranes during uncontrolled cell division, growth, and tumor aggressiveness [18–20]. Overexpression of a master transcription regulator for lipogenesis, SREBP-1, was associated with aggressive pathologic features, including CRPC progression, and poor clinical outcomes in human PCa [7]. Therefore, targeting aberrant de novo fatty acid/lipid biosynthesis linked to SREBP-1 represents a new and attractive therapeutic strategy to treat PCa malignancy. In this study, we first discovered that GTEE would be able to suppress the genotypes (Figure 1) and phenotypes (Figure 2) of lipogenesis in both LNCaP (androgen-responsive) and C4-2 (castration-resistant) cells. Through the inhibition of SREBP-1 and FASN genes (Figure 1), determined by qPCR and Western blot analyses, GTEE decreased the levels of intracellular fatty acid and lipid accumulation (Figure 2) in PCa cells. Intriguingly, FASN has been reported to be a metabolic oncogene [21] and it is involved in PCa progression [9,22]. Furthermore, GTEE significantly suppressed cell growth, migration, and invasion in PCa cells. Indeed, it has been demonstrated that silencing of SREBP-1 caused a decrease in SREBP-1 downstream lipogenic genes, including FASN, inhibition of cell growth and aggressive behaviors, and induction of programmed death in PCa [23], endometrial [24], and ovarian [25] cancer cells. Moreover, the ablation of SREBP-1 expression led to induced endoplasmic reticulum stress, reactive oxygen species (ROS) accumulation, and apoptosis in glioblastoma and breast cancer cells [26]. Consistent with our previous findings [7], SREBP-1 was associated with oxidative stress and ROS production in PCa cells. Although we demonstrated that GTEE interrupted the SREBP-1-regulated metabolic pathway and suppressed PCa cell growth and progression in the present study, the molecular mechanism by which GTEE inhibits SREBP-1 expression in PCa cells remains unclear. In order to determine the molecular basis, an additional experiment was performed using a promoter-luciferase reporter vector of SREBP-1. As shown in Figure S2, GTEE significantly decreased the promoter-luciferase activity of SREBP-1 in LNCaP and C4-2 cells. Based on the results of qPCR, Western blotting (Figure 1) and the promoter reporter assays, GTEE blocking SREBP-1 in PCa cells is mediated through transcriptional regulation.

AR is referred to as one of the most significant protein factors for PCa, even in lethal CRPC aggressiveness, and it is still the primary focus of new drug design. Up-regulation of AR expression and activity has been well defined to promote PCa development, survival, and CRPC progression [1,2,27]. The therapeutic strategies of PCa treatment have been developed to target AR via a blockade of AR nuclear translocation [27,28], silencing of AR gene expression [8,29,30], including the full length or splice variants of AR, or interruption of the interaction between AR and its co-factors, as well as their downstream functions [27,28,31]. In this study, we revealed that GTEE significantly inhibited the expression of AR mRNA and protein in LNCaP and C4-2 cells. The molecular basis of AR expression inhibited by GTEE could be due to down-regulation of SREBP-1, because we previously demonstrated that SREBP-1 transcriptionally activated AR expression through binding of a SREBP-1 *cis*-acting element located in the 5′ flanking AR promoter region [8]. Besides, GTEE also reduced PSA expression in LNCaP and C4-2 cells. PSA is one of the downstream target genes of AR and it has been well used to diagnose PCa disease [32,33] as a clinically important serum biomarker for PCa. Taken together, through the inhibition of SREBP-1, GTEE impaired AR and PSA expression in PCa cells. This could be exploited for a better therapeutic application by co-targeting aberrant lipogenesis and the AR/PSA signaling pathway using GTEE in PCa.

GTEE also displayed the induction of apoptosis in PCa cells. Apoptosis is a biological process of programmed cell death that occurs in embryonic development, normal cell turnover, and cancer cell treatment. Many anti-cancer drugs have been reported to show efficacy on the induction of the apoptotic pathway in tumor cells [13,23,34]. Caspase-3 is a major factor that converges the mitochondrial-regulated and the death receptor-regulated apoptotic pathways in cells [35]. Upon the activation of caspase-3 enzymatic activity, the downstream substrates are cleaved, including PARP, and this leads to apoptotic cell death. Our data showed that GTEE-induced apoptosis through

activation of caspase-3/7 enzymatic activity in PCa cells in a dose-dependent pattern (Figure 5B). Besides, GTEE increased protein expression of cleaved-caspase 3 and cleaved-PARP in LNCaP and C4-2 cells (Figure 5C). The activation of apoptosis-associated proteins by GTEE is responsible for the concomitant execution phase of programmed cell death in PCa cells. These findings suggest that GTEE would be able to kill PCa cells via the caspase-dependent pathway. Additionally, GTEE displayed no obvious cytotoxicity in a mouse model bearing human ovarian tumors [12]. This result implicates that GTEE may not affect normal cells in vivo, and it could be considered as a low toxic/safe therapeutic agent. Previous studies showed that several triterpenes isolated from *Ganoderma lucidum* inhibited cell proliferation and induced apoptosis in PCa cells [36,37]. We are currently attempting to purify and identify the ingredient(s) from GTEE, which exerts the apoptotic functions through blockade of the SREBP-1/AR axis in PCa cells. Potentially, the functional factors in GTEE or in the *Ganoderma* family will be applied as attractive new medicines for PCa treatment.

In conclusion, these results demonstrated for the first time that: (1) GTEE, a traditional Chinese medicine, inhibited the expression of SREBP-1, FASN, and AR in both androgen-responsive and castration-resistant PCa cells; (2) GTEE decreased the amounts of intracellular fatty acid and lipid in PCa cells; and 3) blockade of the SREBP-1/AR axis by GTEE resulted in significant inhibition of cell growth, migration and invasion, as well as induction of apoptosis via the caspase-associated pathway in PCa cells (Figure 5D). An additional study will be warranted to evaluate the anti-cancer efficacy of GTEE in animal models bearing PCa tumors in the near future. Taken together, the data support the possibility that GTEE, a natural and herbal product, can be developed as an effective pharmacologic strategy for the treatment of PCa malignancy.

4. Materials and Methods

4.1. PCa Cell Lines and Cell Culture

PCa cell lines, LNCaP (androgen-responsive) and C4-2 (androgen-independent /castration-resistant) cells, were kindly provided by Dr. Leland W.K. Chung (Cedars-Sinai Medical Center, Los Angeles, CA, USA) [38]. LNCaP and C4-2 cells were cultured in RPMI 1640 medium (Thermo Fisher Scientific/GIBCO, Waltham, MA, USA) supplemented with 10% fetal bovine serum (Thermo Fisher Scientific/HyClone), 100 U/mL penicillin, and 100 μg/mL streptomycin in a humidified 37 °C incubator with 5% CO_2.

4.2. Preparation of GTEE

GT was provided by the Luo-Gui-Ying Fungi Agriculture Farm, Taoyuan, Taiwan. The powder of the GT fruiting body (30 g) was soaked in ethanol (3000 mL) and shaken for 24 h on a rotating shaker. After centrifugation, the supernatant was filtered through a filter paper (Whatman No.1, Cat. No. 1001-110) and the residues were extracted by ethanol twice, as mentioned above. The filtrates were harvested and subjected to concentration under reduced pressure to produce a brown gel-like GT extract (GTEE). Subsequently, GTEE was prepared as a stock solution with ethanol solvent (200 mg/mL) and stored at −80 °C until use. Furthermore, the quality control of GTEE was assessed and validated using both bioresponse fingerprint (PhytomicsQC platform) [39] as well as chemical fingerprint (HPLC and ESI-MS) [13] analyses, as described previously.

4.3. Quantitative Reverse Transcription-Polymerase Chain Reaction (qRT-PCR)

Total RNAs from PCa cells treated with GTEE or vehicle (0.3% ethanol) were isolated by RNeasy mini Kit (Qiagen, Valencia, CA, USA) and converted into cDNA using a SuperScript III First-Strand Synthesis Kit (Thermo Fisher Scientific/Life Technologies). Quantitative polymerase chain reaction was performed using the SYBR Green PCR Master mix and an ABI 7500 Fast Real-Time PCR System (Applied Biosystems, Grand Island, NY, USA). Data were normalized to β-actin as an internal reference and represented as the average ratio of triplicates. The oligonucleotide primer sets for qPCR, including SREBP-1, SREBP-2, FASN, HMGCR, AR, PSA, and β-actin were listed in Table S1.

4.4. Western Blot Analysis

The cell lysates were prepared from PCa cells treated with GTEE or vehicle (0.3% ethanol) using PRO-PREP Protein Extraction Solution (iNtRON technology, South Korea) with protease inhibitors added. The protein concentrations of the cell lysates were assayed using a Pierce™ BCA Protein Assay Kit (Thermo Fisher Scientific). For Western blotting, 50 μg of protein extract was loaded into the sodium dodecyl sulfate polyacrylamide gel electrophoresis (SDS-PAGE) gel and transferred onto polyvinylidene difluoride (PVDF) membranes. After blocking by 5% non-fat milk in PBST (PBS with Tween-20) buffer for 1 h at room temperature, PVDF membranes were incubated with primary antibodies for overnight at 4 °C, followed by incubation with a horseradish peroxidase (HRP)-conjugated secondary antibody. The reactive signals were visualized using an Enhanced Chemiluminescence Kit (Amersham Biosciences, Arlington Heights, IL, USA). Subsequently, the reactive protein bands were scanned and quantified using ImageJ software. Primary antibodies were used as follows: anti-SREBP-1, anti-FASN, anti-AR (Santa Cruz Biotechnology, Dallas, TX, USA), anti-SREBP-2 (Abcam, Cambridge, MA, USA), anti-caspase 3 (Novus Biologicals, Littleton, CO, USA), anti-PARP (GeneTex, Irvine, CA, USA), and anti-β-actin (Millipore, Burlington, MA, USA).

4.5. The Fatty Acid Level and Lipid Droplet Accumulation Analyses

The levels of fatty acids in PCa cells were determined by a Fatty Acid Quantification Kit (MBL International Corporation, Woburn, MA, USA) according to the manufacturer's instructions. Lipid droplet accumulation was assayed by an Oil Red O staining method as previously described [7,23]. Oil Red O staining images were examined and recorded by a phase contrast microscope. For quantification, Oil Red O retained in cells were extracted by 100% isopropanol and optical absorbance at 500 nm was measured, normalized by the total cell numbers.

4.6. Cell Growth and In Vitro Progression Assays

For cell growth assay [34], LNCaP and C4-2 cells were plated on 96-well plates (10,000 cells/well) and treated with various concentrations of GTEE or vehicle (0.3% ethanol). Cell growth was assayed by MTS assay (Promega Corp. Madison, WI, USA) according to the manufacturer's instructions. In vitro cell migration or invasion [17,23] was determined by Boyden chambers pre-coated with nothing (for migration assay) or with growth factor-depleted Matrigel matrix (BD Bioscience, San Jose, CA, USA; for invasion assay). PCa cells (8×10^4 cells/well) were seeded into the inside of the pre-coated upper chambers and treated with GTEE or vehicle (0.3% ethanol). After incubation for 48 h, a crystal violet staining method was used to measure the numbers of migrated or invading cells affected by GTEE. Additionally, a wound healing assay was performed as previously described [13].

4.7. Flow Cytometric Analysis

For analysis of apoptosis [34], PCa cells treated with GTEE or vehicle (0.3% ethanol) were stained using an Annexin V-FITC Apoptosis Detection Kit I (BD Biosciences) according to the manufacturer's instructions. The amounts (%) of apoptotic cells were determined by flow cytometry and analyzed by the FACS Express v2.0 software.

4.8. Statistical Analysis

All data were analyzed at least three individual experiments by using a two-tailed unpaired Student's *t* test for comparison of independent means. *P* values of less than 0.05 were considered to be statistically significant.

Supplementary Materials: The following materials are available online. Figure S1: Representative images of the migration and invasion of LNCaP cells treated with vehicle or GTEE. Figure S2: The promoter-luciferase reporter activity of SREBP-1 was inhibited by GTEE in PCa cells. Table S1: The oligonucleotide primer sets for qPCR.

Author Contributions: M.C.K. and W.C.H. designed the study. S.Y.H. and G.J.H. conducted the experiments. S.Y.H., H.C.W., and W.C.H. compiled and analyzed the data. M.C.K. and W.C.H. discussed and drafted the manuscript. All authors have reviewed the manuscript.

Funding: This study was supported by grants from the Ministry of Science and Technology of Taiwan (MOST 106-2320-B-039-058) (W.C.H.) and (MOST 107-2320-B-039-011) (M.C.K.); China Medical University, Taiwan (CMU106-S-43) (W.C.H.); and the "Chinese Medicine Research Center, China Medical University" from The Featured Areas Research Center Program within the framework of the Higher Education Sprout Project by the Ministry of Education in Taiwan (CHM106-10 and CMRC-CHM-10) (M.C.K.)

Conflicts of Interest: The authors declare no conflict of interest.

References

1. Lonergan, P.E.; Tindall, D.J. Androgen receptor signaling in prostate cancer development and progression. *J. Carcinog.* **2011**, *10*, 20. [PubMed]
2. Heinlein, C.A.; Chang, C. Androgen receptor in prostate cancer. *Endocr. Rev.* **2004**, *25*, 276–308. [CrossRef] [PubMed]
3. Shimano, H. Sterol regulatory element-binding proteins (SREBPs): Transcriptional regulators of lipid synthetic genes. *Prog. Lipid Res.* **2001**, *40*, 439–452. [CrossRef]
4. Brown, M.S.; Goldstein, J.L. The SREBP pathway: Regulation of cholesterol metabolism by proteolysis of a membrane-bound transcription factor. *Cell* **1997**, *89*, 331–340. [CrossRef]
5. Swinnen, J.V.; Heemers, H.; Deboel, L.; Foufelle, F.; Heyns, W.; Verhoeven, G. Stimulation of tumor-associated fatty acid synthase expression by growth factor activation of the sterol regulatory element-binding protein pathway. *Oncogene* **2000**, *19*, 5173–5181. [CrossRef] [PubMed]
6. Horton, J.D.; Shimomura, I.; Brown, M.S.; Hammer, R.E.; Goldstein, J.L.; Shimano, H. Activation of cholesterol synthesis in preference to fatty acid synthesis in liver and adipose tissue of transgenic mice overproducing sterol regulatory element-binding protein-2. *J. Clin. Invest.* **1998**, *101*, 2331–2339. [CrossRef] [PubMed]
7. Huang, W.C.; Li, X.; Liu, J.; Lin, J.T.; Chung, L.W. Activation of androgen receptor, lipogenesis and oxidative stress converged by SREBP-1 is responsible for regulating growth and progression of prostate cancer cells. *Mol. Cancer Res.* **2012**, *10*, 133–142. [CrossRef] [PubMed]
8. Huang, W.C.; Zhau, H.E.; Chung, L.W. Androgen receptor survival signaling is blocked by anti-beta2-microglobulin monoclonal antibody via a MAPK/lipogenic pathway in human prostate cancer cells. *J. Biol. Chem.* **2010**, *285*, 7947–7956. [CrossRef] [PubMed]
9. Ettinger, S.L.; Sobel, R.; Whitmore, T.G.; Akbari, M.; Bradley, D.R.; Gleave, M.E.; Nelson, C.C. Dysregulation of sterol response element-binding proteins and downstream effectors in prostate cancer during progression to androgen independence. *Cancer Res.* **2004**, *64*, 2212–2221. [CrossRef] [PubMed]
10. Kuok, Q.Y.; Yeh, C.Y.; Su, B.C.; Hsu, P.L.; Ni, H.; Liu, M.Y.; Mo, F.E. The triterpenoids of Ganoderma tsugae prevent stress-induced myocardial injury in mice. *Mol. Nutr. Food Res.* **2013**, *57*, 1892–1896. [PubMed]
11. Chen, M.L.; Hsieh, C.C.; Chiang, B.L.; Lin, B.F. Triterpenoids and Polysaccharide Fractions of Ganoderma tsugae Exert Different Effects on Antiallergic Activities. *Evid. Based Complement. Alternat. Med.* **2015**, *2015*, 754836. [PubMed]
12. Kuo, H.P.; Hsu, S.C.; Ou, C.C.; Li, J.W.; Tseng, H.H.; Chuang, T.C.; Liu, J.Y.; Chen, S.J.; Su, M.H.; Cheng, Y.C.; et al. Ganoderma tsugae Extract Inhibits Growth of HER2-Overexpressing Cancer Cells via Modulation of HER2/PI3K/Akt Signaling Pathway. *Evid. Based Complement. Alternat. Med.* **2013**, *2013*, 219472. [CrossRef] [PubMed]
13. Yu, Y.H.; Kuo, H.P.; Hsieh, H.H.; Li, J.W.; Hsu, W.H.; Chen, S.J.; Su, M.H.; Liu, S.H.; Cheng, Y.C.; Chen, C.Y.; et al. Ganoderma tsugae Induces S Phase Arrest and Apoptosis in Doxorubicin-Resistant Lung Adenocarcinoma H23/0.3 Cells via Modulation of the PI3K/Akt Signaling Pathway. *Evid. Based Complement. Alternat. Med.* **2012**, *2012*, 371286. [CrossRef] [PubMed]
14. Hsu, S.C.; Ou, C.C.; Chuang, T.C.; Li, J.W.; Lee, Y.J.; Wang, V.; Liu, J.Y.; Chen, C.S.; Lin, S.C.; Kao, M.C. Ganoderma tsugae extract inhibits expression of epidermal growth factor receptor and angiogenesis in human epidermoid carcinoma cells: In vitro and in vivo. *Cancer Lett.* **2009**, *281*, 108–116. [CrossRef] [PubMed]

15. Hsu, S.C.; Ou, C.C.; Li, J.W.; Chuang, T.C.; Kuo, H.P.; Liu, J.Y.; Chen, C.S.; Lin, S.C.; Su, C.H.; Kao, M.C. Ganoderma tsugae extracts inhibit colorectal cancer cell growth via G(2)/M cell cycle arrest. *J. Ethnopharmacol.* **2008**, *120*, 394–401. [CrossRef] [PubMed]
16. Li, X.; Wu, J.B.; Li, Q.; Shigemura, K.; Chung, L.W.; Huang, W.C. SREBP-2 promotes stem cell-like properties and metastasis by transcriptional activation of c-Myc in prostate cancer. *Oncotarget* **2016**, *7*, 12869–12884. [CrossRef] [PubMed]
17. Li, X.; Chen, Y.T.; Josson, S.; Mukhopadhyay, N.K.; Kim, J.; Freeman, M.R.; Huang, W.C. MicroRNA-185 and 342 inhibit tumorigenicity and induce apoptosis through blockade of the SREBP metabolic pathway in prostate cancer cells. *PLoS ONE* **2013**, *8*, e70987. [CrossRef] [PubMed]
18. Yamashita, T.; Honda, M.; Takatori, H.; Nishino, R.; Minato, H.; Takamura, H.; Ohta, T.; Kaneko, S. Activation of lipogenic pathway correlates with cell proliferation and poor prognosis in hepatocellular carcinoma. *J. Hepatol.* **2009**, *50*, 100–110. [CrossRef] [PubMed]
19. Swinnen, J.V.; Brusselmans, K.; Verhoeven, G. Increased lipogenesis in cancer cells: New players, novel targets. *Curr. Opin. Clin. Nutr. Metab. Care* **2006**, *9*, 358–365. [CrossRef] [PubMed]
20. Freeman, M.R.; Cinar, B.; Lu, M.L. Membrane rafts as potential sites of nongenomic hormonal signaling in prostate cancer. *Trends Endocrinol. Metab.* **2005**, *16*, 273–279. [CrossRef] [PubMed]
21. Menendez, J.A.; Decker, J.P.; Lupu, R. In support of fatty acid synthase (FAS) as a metabolic oncogene: Extracellular acidosis acts in an epigenetic fashion activating FAS gene expression in cancer cells. *J. Cell Biochem.* **2005**, *94*, 1–4. [CrossRef] [PubMed]
22. Swinnen, J.V.; Heemers, H.; van de Sande, T.; de Schrijver, E.; Brusselmans, K.; Heyns, W.; Verhoeven, G. Androgens, lipogenesis and prostate cancer. *J. Steroid Biochem. Mol. Biol.* **2004**, *92*, 273–279. [CrossRef] [PubMed]
23. Li, X.; Chen, Y.T.; Hu, P.; Huang, W.C. Fatostatin displays high antitumor activity in prostate cancer by blocking SREBP-regulated metabolic pathways and androgen receptor signaling. *Mol. Cancer Ther.* **2014**, *13*, 855–866. [CrossRef] [PubMed]
24. Lin, L.; Zheng, X.; Qiu, C.; Dongol, S.; Lv, Q.; Jiang, J.; Kong, B.; Wang, C. SIRT1 promotes endometrial tumor growth by targeting SREBP1 and lipogenesis. *Oncol. Rep.* **2014**, *32*, 2831–2835. [CrossRef] [PubMed]
25. Nie, L.Y.; Lu, Q.T.; Li, W.H.; Yang, N.; Dongol, S.; Zhang, X.; Jiang, J. Sterol regulatory element-binding protein 1 is required for ovarian tumor growth. *Oncol. Rep.* **2013**, *30*, 1346–1354. [CrossRef] [PubMed]
26. Griffiths, B.; Lewis, C.A.; Bensaad, K.; Ros, S.; Zhang, Q.; Ferber, E.C.; Konisti, S.; Peck, B.; Miess, H.; East, P.; et al. Sterol regulatory element binding protein-dependent regulation of lipid synthesis supports cell survival and tumor growth. *Cancer Metab.* **2013**, *1*, 3. [CrossRef] [PubMed]
27. Taplin, M.E. Androgen receptor: Role and novel therapeutic prospects in prostate cancer. *Expert Rev. Anticancer Ther.* **2008**, *8*, 1495–1508. [CrossRef] [PubMed]
28. Chang, C.Y.; McDonnell, D.P. Androgen receptor-cofactor interactions as targets for new drug discovery. *Trends Pharmacol. Sci.* **2005**, *26*, 225–228. [CrossRef] [PubMed]
29. Boudadi, K.; Antonarakis, E.S. Resistance to Novel Antiandrogen Therapies in Metastatic Castration-Resistant Prostate Cancer. *Clin. Med. Insights Oncol.* **2016**, *10*, 1–9. [CrossRef] [PubMed]
30. Huang, W.C.; Havel, J.J.; Zhau, H.E.; Qian, W.P.; Lue, H.W.; Chu, C.Y.; Nomura, T.; Chung, L.W. b2-Microglobulin Signaling Blockade Inhibited Androgen Receptor Axis and Caused Apoptosis in Human Prostate Cancer Cells. *Clin. Cancer Res.* **2008**, *14*, 5341–5347. [CrossRef] [PubMed]
31. Shiota, M.; Yokomizo, A.; Fujimoto, N.; Naito, S. Androgen receptor cofactors in prostate cancer: Potential therapeutic targets of castration-resistant prostate cancer. *Curr. Cancer Drug Targets.* **2011**, *11*, 870–881. [CrossRef] [PubMed]
32. Lange, P.H.; Brawer, M.K. Serum prostate-specific antigen: Its use in diagnosis and management of prostate cancer. *Urology* **1989**, *33*, 13–17. [CrossRef]
33. Kim, J.; Coetzee, G.A. Prostate specific antigen gene regulation by androgen receptor. *J. Cell Biochem.* **2004**, *93*, 233–241. [CrossRef] [PubMed]
34. Li, X.; Wu, J.B.; Chung, L.W.; Huang, W.C. Anti-cancer efficacy of SREBP inhibitor, alone or in combination with docetaxel, in prostate cancer harboring p53 mutations. *Oncotarget* **2015**, *38*, 41018–41032. [CrossRef] [PubMed]
35. Porter, A.G.; Janicke, R.U. Emerging roles of caspase-3 in apoptosis. *Cell Death Differ.* **1999**, *6*, 99–104. [CrossRef] [PubMed]

36. Qu, L.; Li, S.; Zhuo, Y.; Chen, J.; Qin, X.; Guo, G. Anticancer effect of triterpenes from Ganoderma lucidum in human prostate cancer cells. *Oncol. Lett.* **2017**, *14*, 7467–7472. [PubMed]
37. Kladar, N.V.; Gavaric, N.S.; Bozin, B.N. Ganoderma: Insights into anticancer effects. *Eur. J. Cancer Prev.* **2016**, *25*, 462–471. [CrossRef] [PubMed]
38. Thalmann, G.N.; Sikes, R.A.; Wu, T.T.; Degeorges, A.; Chang, S.M.; Ozen, M.; Pathak, S.; Chung, L.W. LNCaP progression model of human prostate cancer: Androgen-independence and osseous metastasis. *Prostate* **2000**, *44*, 91–103. [CrossRef]
39. Tilton, R.; Paiva, A.A.; Guan, J.Q.; Marathe, R.; Jiang, Z.; van Eyndhoven, W.; Bjoraker, J.; Prusoff, Z.; Wang, H.; Liu, S.H.; et al. A comprehensive platform for quality control of botanical drugs (PhytomicsQC): A case study of Huangqin Tang (HQT) and PHY906. *Chin. Med.* **2010**, *5*, 30. [CrossRef] [PubMed]

Sample Availability: Samples of the compounds are not available.

molecules

MDPI

Article

Structural Characterization of Polysaccharides from *Dendrobium officinale* and Their Effects on Apoptosis of HeLa Cell Line

Wenxia Yu [1,†], Zhiyao Ren [1,†], Xiaofeng Zhang [1], Shangping Xing [1], Shengchang Tao [1], Chenxing Liu [1], Gang Wei [1,*], Yuan Yuan [2,*] and Zhouxi Lei [3,*]

[1] School of Pharmaceutical Sciences, Guangzhou University of Chinese Medicine, No. 232 Wai Huan Dong Road, Higher education mega center, Panyu District, Guangzhou 511400, China; yuwenxia3486@outlook.com (W.Y.); r._what@163.com (Z.R.); 15521076223@163.com (X.Z.); shaopingxing@gmail.com (S.X.); taoshengchang@hotmail.com (S.T.); liuchenxingstar@126.com (C.L.)

[2] National Resource Center for Chinese Materia Medica, China Academy of Chinese Medical Sciences, Beijing 100000, China

[3] Guangdong Institute of Traditional Chinese Medicine, Guangzhou 510000, China

* Correspondence: weigang@gzucm.edu.cn (G.W.); y_yuan0732@163.com (Y.Y.); leizhouxi@gdtcm.org.cn (Z.L.); Tel.: +86-020-39358519 (G.W.); +86-010-64087649 (Y.Y.); +86-020-15017576198 (Z.L.)

† These authors contributed equally to this paper.

Academic Editor: Roberto Fabiani

Received: 4 September 2018; Accepted: 25 September 2018; Published: 27 September 2018

Abstract: *Dendrobium officinale* is a widely used medicinal plant in China with numerous bio-activities. However, the main structure and anti-tumor activity of the polysaccharides from this plant have not been investigated. In this study, we elucidated the main structure of polysaccharides purified with DEAE and Sephadex G-25 from *Dendrobium officinale* grown under different planting conditions. In addition, the anti-tumor activity was tested via MTT assays. The results showed that the polysaccharides of *Dendrobium officinale* grown under different conditions were almost the same, with slight differences in the branched chain; both polysaccharide fractions consisted of (1→4)-linked mannose and (1→4)-linked glucose, with an O-acetyl group in the mannose. After degradation, the polysaccharide fractions from wild plants showed significant anti-proliferation activity in HeLa cells. The fractions F1 and F3 induced apoptosis by up-regulating the expression of ERK, JNK, and p38. We concluded that polysaccharides from *Dendrobium officinale* planted in the wild exhibit significant anti-tumor effects only after being degraded to smaller molecular weight species. The planting mode is a significant factor in the pharmacological activity of *Dendrobium officinale*. We advise that the planting conditions for *Dendrobium officinale* should be changed.

Keywords: *Dendrobium officinale*; structure elucidation; anti-tumor activity; plantation mode

1. Introduction

Dendrobium officinale is a medicinal plant that has been widely used in China for thousands of years. As the medicinal materials market has grown, the demand for the medicinal plant *Dendrobium officinale* has increased dramatically [1]. Since the wild resource is limited, researchers have developed a series of greenhouse cultivation methods to improve productivity. However, the metabolic components in plants are influenced greatly by the environment. Plants planted in the greenhouse are different from those grown in the wild. Based on our observation, the external properties of this medicinal plant planted in the wild and cultivated in the greenhouse are different. However, no studies have reported pharmacological differences between these two planting modes. Modern pharmacological

studies have revealed that the stem extract of *Dendrobium officinale* exhibits significant bio-activities, including anti-inflammatory [2], anti-oxidant [3], anti-tumor [4], salivary secretion promoting [5], and immunomodulatory [6] activities. A study of the bio-active ingredients in *Dendrobium officinale* showed that several types of active compounds were present in this medicinal plant, including alkaloids, flavonoids, phenanthrenes, and polysaccharides [1]. Polysaccharides are the main component and account for 20% to 40% of the total compounds [7]. In recent years, several studies on the structure of polysaccharides as well as the bio-activities of *Dendrobium* species have been reported [8–18]. However, a literature investigation showed that a study of the anti-tumor activities of the polysaccharides in *Dendrobium officinale* was still missing. No papers have reported the structure and anti-tumor activity differences in polysaccharides from *Dendrobium officinale* grown under different conditions. In this study, we compared the structure differences in polysaccharides from *Dendrobium officinale* grown under two different conditions, and their anti-tumor properties were also investigated.

2. Results

2.1. Elution Graph of the Purified Polysaccharide Fractions (PPFs)

After deproteinization with Sevag reagents, the crude polysaccharides were purified with a DEAE column and a Sephadex G-25 column. The elution graph is shown in Figure 1. All the tubes with polysaccharides were collected and concentrated. According to the elution graph of the Sephadex G-25 column, the PPFs from the two sources of *Dendrobium officinale* were divided into two groups: the first group was named DWDOP and the second, FWDOP. The DWDOP represented PPFs from *Dendrobium officinale* planted in the greenhouse, whereas the FWDOP represented PPFs from plants grown in the wild. Each group obtained three polysaccharide fractions; these purified polysaccharide fractions were named DWDOP1, DWDOP2, and DWOPD3 and FWDOP1, FWDOP2, and FWDOP3, respectively. From the graph, DWDOP1 and FWDOP1 were the two major purified polysaccharide fractions. Therefore, DWDOP1 and FWDOP1 were further analyzed for structural elucidation.

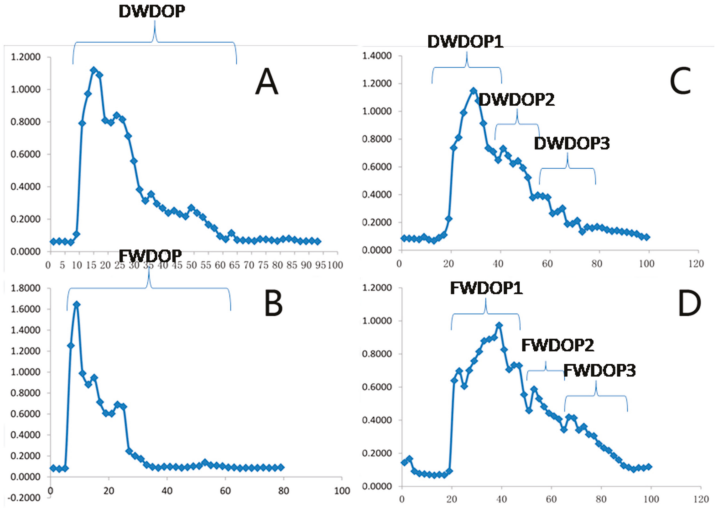

Figure 1. The (**A**,**B**) DEAE and (**C**,**D**) Sephadex G-25 elution graphs of DWDOP and FWDOP.

2.2. Molecular Weight and Monosaccharide Composition of the PPFs

From the HPLC graph of the monosaccharide analysis, all six PPFs consisted of mannose and glucose. The mannose content in all PPFs was higher than the glucose content. The mannose/glucose ratio in DWDOP1, DWDOP2, and DWDOP3 and FWDOP1, FWDOP2, and FWDOP3 was 6.76, 6.09,

and 4.50 and 7.46, 6.85, and 6.84, respectively. The monosaccharide analysis graph is shown in Figure 2. The molecular weight of the PPFs was determined by high performance gel permeation chromatography (HPGPC) using a series of dextran standard references. The exact molecular weight of the dextran standard and the retention time in HPGPC were used for establishing a standard curve. The equation of the standard curve calculated using the dextran standards is shown below:

$$Y = -1.9145X + 27.106 \quad (1)$$

$$R^2 = 0.9929 \quad (2)$$

The molecular weight of the four pure polysaccharide fractions, specifically, FWDOP1, FWDOP2, DWDOP1, and DWDOP2, was 1,341,061 Da, 540,216 Da, 1,415,641 Da, and 1,320,256 Da. Both DWDOP3 and FWDOP3 were not pure fractions.

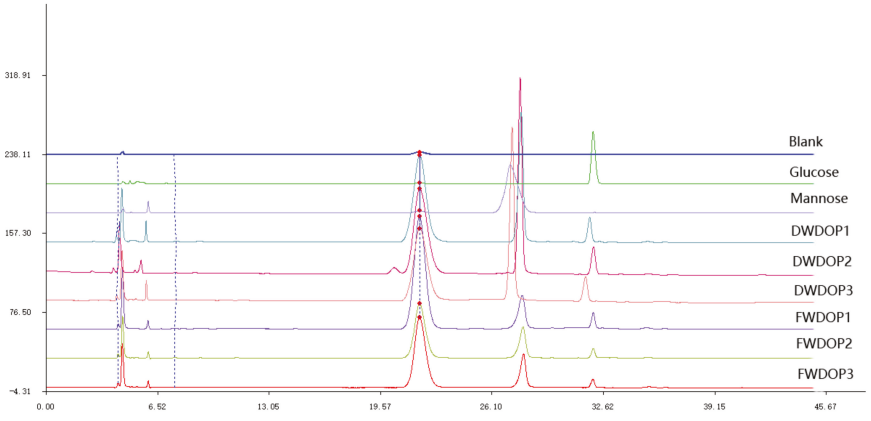

Figure 2. The HPLC of blank control solution, glucose standard solution, mannose standard solution and pure polysaccharides fractions DWDOP1, DWDOP2, DWDOP3, FWDOP1, FWDOP2, FWDOP3.

2.3. Structure of DWDOP1 and FWDOP1

The structure of DWDOP1 and FWDOP1 was elucidated through 1D and 2D-NMR analysis. The ^{1}H-NMR signals for DWDOP1 and FWDOP1 were almost the same; DWDOP1 signals were observed at δ5.43, 5.10, 4.89, 4.42, 4.11, 4.04, 3.98, 3.95, 3.91, 3.85, 3.83, 3.74, 3.70, 3.56, 3.48, 3.28, 2.11, 2.08, and 1.84. FWDOP1 signals were located at δ5.44, 5.10, 5.02, 4.43, 4.05, 3.98, 3.96, 3.92, 3.88, 3.86, 3.83, 3.74, 3.69, 3.67, 3.56, 3.49, 3.27, 2.11, 2.08, and 1.85. From the ^{1}H-NMR signals, a signal at 5.43 or 5.44 is observed in the spectrum of both polysaccharides. This signal is unique and represents the hydrogen in the skeleton of a sugar connected to an acetoxy group. In addition, the signals from 1.84 to 2.11 should be assigned to the hydrogen of the methyl of the acetoxy group. It can be speculated that both DWDOP1 and FWDOP1 contain an acetoxy group. The ^{13}C-NMR signals for DWDOP1 and FWDOP1 were also almost the same. For DWDOP1, signals in the^{13}C-NMR spectrum were located at δ102.48, 100.12, 78.45, 76.51, 75.00, 73.84, 72.76, 71.40, 69.92, 60.47, 23.04, and 20.52. The FWDOP1 ^{13}C-NMR spectrum showed signals at δ102.48, 100.11, 78.43, 76.49, 75.00, 73.86, 72.74, 71.40, 69.93, 60.45, 23.17, and 20.53. From these spectra, 102.48 should be assigned to the carbon at the 2 position of the mannose connected with the acetoxy group. The signals from 20.52 to 23.17 should be assigned to the methyl carbon of the acetoxy group. The 1D-NMR spectra are shown in Figure 3.

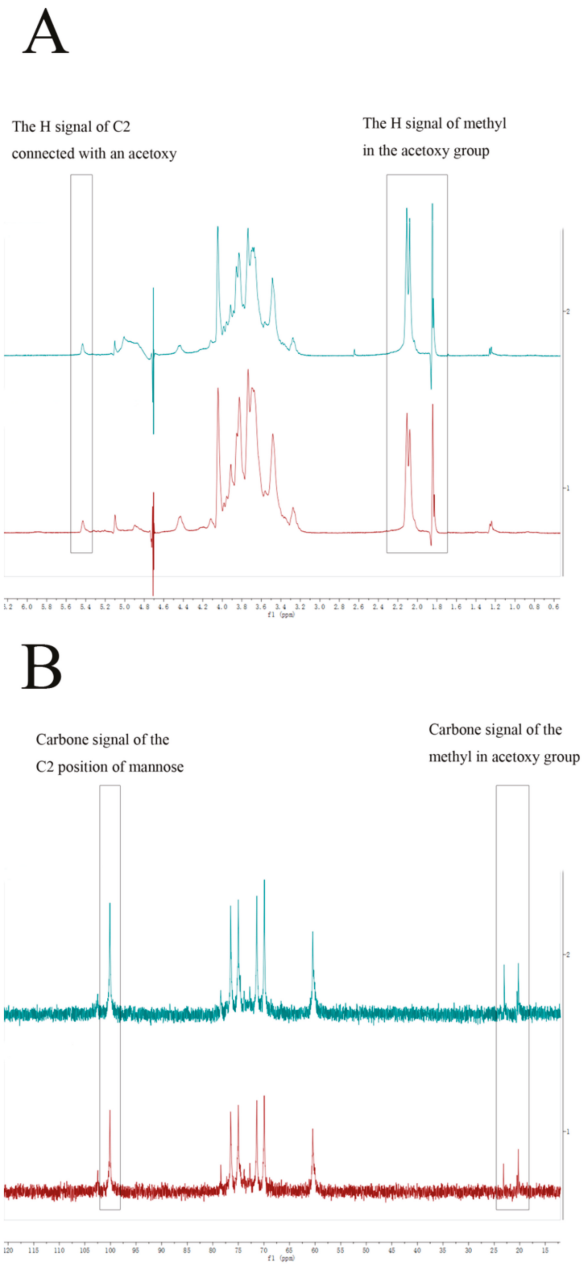

Figure 3. The (**A**) ^{1}H-NMR spectra of DWDOP1 and FWDOP1; the (**B**) ^{13}C spectra of DWDOP1 and FWDOP1.

Apart from 1D-NMR spectroscopy, 2D-NMR spectroscopy (^{1}H-^{1}H COSY, TOSY, ^{13}C-^{1}H HSQC, and ^{13}C-^{1}H HMBC) was also applied. From the 1D and 2D-NMR spectra, we can speculate on the structure of the DWDOP1 and FWDOP1 compounds. The annotation of the 2D-NMR signals is shown in Figure 4. The attribution of the NMR signals was based on published papers and structural

elucidation experience [19–22]. First, we characterized the structure of DWDOP1. From the HSQC signals, we found the (71.46, 5.43) signal, which should be attributed to C_2 of 2-acetoxy-(1→4)-linked mannose. The signals (102.46, 4.44) and (100.10, 4.68) should be attributed to coupling between the anomer carbon and hydrogen in (1→4)-linked glucose and (1→4)-linked mannose, respectively. From the COSY signals, we found the signals (4.43, 3.28), (3.23, 3.43) and (3.48, 3.74). The signal at δ4.43 represents the anomer hydrogen of (1→4)-linked glucose. Therefore, δ3.28 can be attributed to the C_2 hydrogen of β-(1→4)-linked glucose. The δ3.28 and δ3.23, δ3.43, and δ3.48 signals were the same signals and were correlated with each other. Therefore, we can speculate that the δ3.43 signal represents the C_3 hydrogen of (1→4)-linked glucose, whereas δ3.74 can be attributed to the C_4 hydrogen of (1→4)-linked glucose. From the HSQC spectrum, we found the signal (76.49, 3.74). The signal 76.49 should be attributed to the C4 carbon of (1→4)-linked glucose. Searching the HMBC spectrum, we found the signal (100.04, 3.72); the signal 100.04 is the same as the 100.10 signal of the anomer carbon of (1→4)-linked mannose. Therefore, we can confirm that C4 of (1→4)-linked glucose is connected to C1 of (1→4)-linked mannose. In the COSY signals, a (4.73, 4.05) correlation was observed; the signal δ4.73 was close to the δ4.68 signal, and thus, δ4.73 should be attributed to the anomer hydrogen of (1→4)-linked mannose, and δ4.05 should be attributed to the C2 hydrogen of (1→4)-linked mannose. The signal (4.04, 4.43) was the coupling signal between the C2 hydrogen and C3 hydrogen of (1→4)-linked mannose, and the signal (4.43, 3.28) was the coupling signal of the C3 and C4 hydrogen signal. Therefore, we can confirm that the signal δ3.28 is the signal of the C4 hydrogen in (1→4)-linked mannose. From the HSQC spectrum, we found the signal (72.79, 3.27) and can confirm that 72.29 represents the C4 carbon of (1→4)-linked mannose. From the HMBC spectrum, we found the signal (3.27, 102.42). We had previously confirmed that 3.27 should be attributed to the C4 hydrogen and 102.42 should be attributed to the anomer carbon of (1→4)-linked glucose. From here, we can confirm that C1 of (1→4)-linked glucose is connected with C4 of the (1→4)-linked mannose. The connection of (1→4)-linked glucose and (1→4)-linked mannose constructs the skeleton of the DWDOP1 compound. From the 1D-NMR spectra, we confirmed that 5.42 represented the 2-acetoxy-(1→4)-linked mannose hydrogen. In the TOSY spectrum, we confirmed that 3.91, 3.76, and 3.53 indicated the hydrogen of C3, C4, and C5, and that 4.83 is the anomer hydrogen signal. In the HMBC spectrum, we found the signal (100.04, 3.72). This signal may also be attributed to (1→4)-linked mannose connected with 2-acetoxy-(1→4)-linked mannose. In the HMBC spectrum, we found the signals (4.66, 76.20) and (4.66, 69.74). The former signal should be attributed to the coupling signal of the anomer hydrogen of (1→4)-linked mannose and the C4 carbon of (1→4)-linked glucose. The latter indicated that the anomer hydrogen of mannose was coupled with another carbon. In the HSQC spectrum, the signals (69.93, 4.04) and (69.58, 3.43) were observed. The signals 4.04 and 3.43 were from the C2 and C3 position hydrogen of (1→4)-linked mannose and (1→4)-linked glucose. Therefore, we speculated that the signal (4.66, 69.74) in the HMBC spectrum was the coupling signal of the anomer hydrogen of (1→4)-linked mannose and the C2 carbon of (1→4)-linked mannose or the C3 carbon of (1→4)-linked glucose. In the HSQC spectrum, we also found the signals (93.58, 5.10) and (99.03, 4.87). The (99.03, 4.87) signal should be attributed to the anomer of the terminal glucose, and (93.58, 5.10) may be the C2 hydrogen signal of (1, 2→4)-linked mannose. Here, we can speculate that the skeleton of the polysaccharides in DWDOP1 mainly consisted of (1→4)-linked mannose connected with (1→4)-linked glucose. The chemical shifts of all atoms are shown in Figure 5. The complete NMR figures of all polysaccharides can be reached in the supplemental data.

The structure of the FWDOP1 polysaccharide was almost the same as that of the DWDOP1 polysaccharide, mainly consisting of (1→4)-linked mannose and (1→4)-linked glucose, 2-acetoxy-(1→4)-linked mannose. The primary difference between these two polysaccharides was based on the three characterized signals in the HSQC spectra, namely, (90.52, 4.06), (88.40, 4.03), and (80.70, 4.69). The carbon signals from 80 to 88 were the characteristic signals of the furan configuration of sugar [23]. The hydrogen signal 4.03 should be attributed to the C2 hydrogen of mannose, whereas 4.69 should be attributed to the anomer hydrogen of mannose. Therefore, we speculated that a mannofuranose was present in FWDOP1.

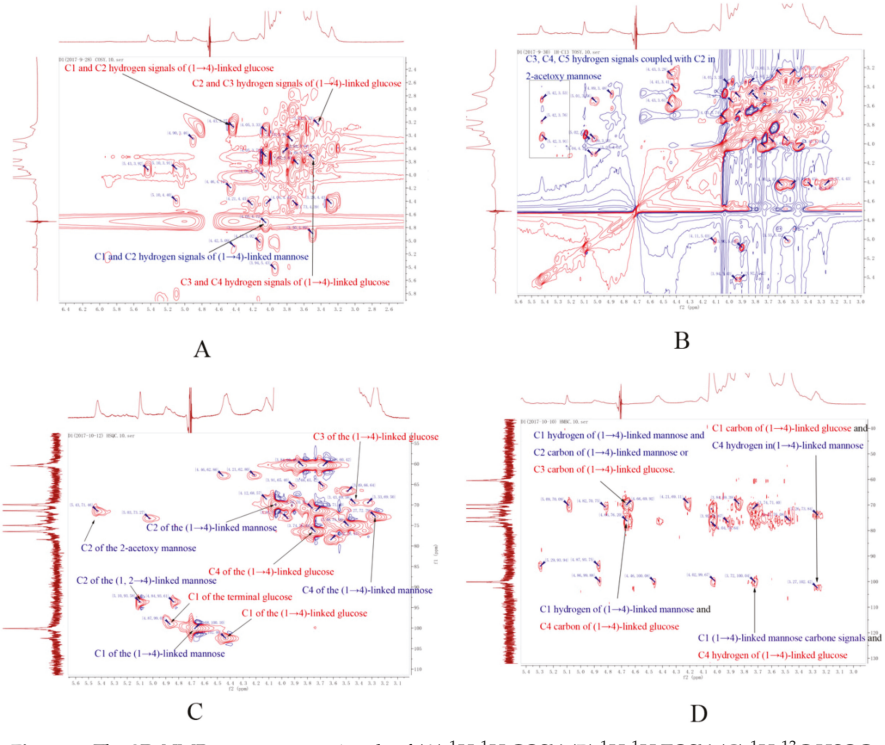

Figure 4. The 2D-NMR spectroscopy signals of (**A**) ^{1}H-^{1}H COSY, (**B**) ^{1}H-^{1}H TOSY, (**C**) ^{1}H-^{13}C HSQC, and (**D**) ^{1}H-^{13}C HMBC.

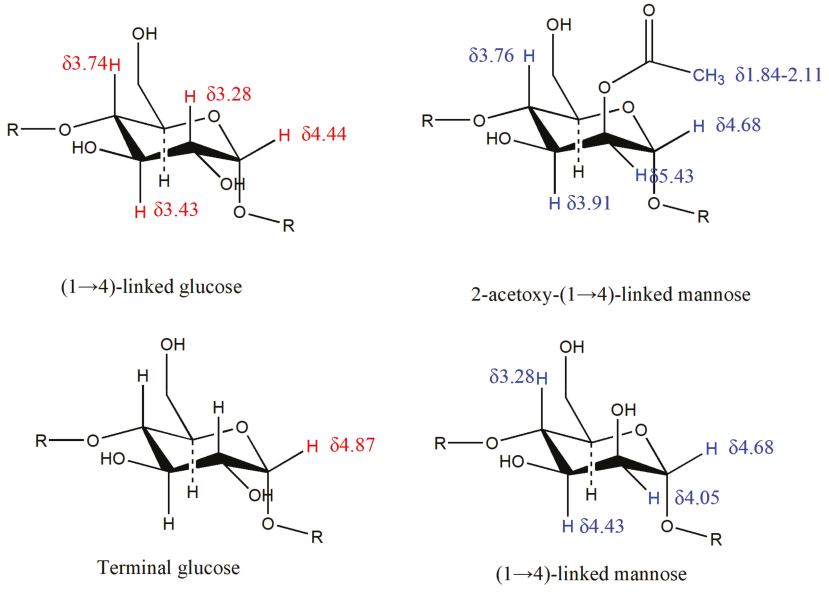

Figure 5. The attributed chemical shifts of all atoms.

Based on the molecular weight and the monosaccharide composition of DPFs after degradation, a DPF series was obtained. The degraded DPFs from *Dendrobium officinale* planted in a greenhouse were named D1–D6. The degraded DPFs from the plants planted in the wild were named F1–F6. The molecular weight of the DPFs was calculated with a standard curve constructed using a series of standard references: T5, T11, T80, T273, and T667. The standard curve used was the same as the one described in the previous section. After calculation, the molecular weight of D1 to D6 was 119,374 Da, 83,162 Da, 60,532 Da, 44,532 Da, 40,313 Da, and 21,818 Da. The molecular weight of F1 to F6 was 86,993 Da, 75,819 Da, 62,872 Da, 57,798 Da, 24,188 Da, and 29,904 Da. From the HPLC spectra, the monosaccharide composition of the DPFs was different. All DPFs consisted of mannose and glucose, and the ratio of mannose and glucose in D1 to D6 was 5.4, 5.7, 5.8, 5.7, 5.4, and 5.0, whereas the ratio in F1 to F6 was 8.0, 8.2, 6.6, 8.5, 6.2, and 6.5. The graph of HPLC was shown in Figure 6. From the results, the mannose content in F1 to F6 was larger than the content in D1 to D6.

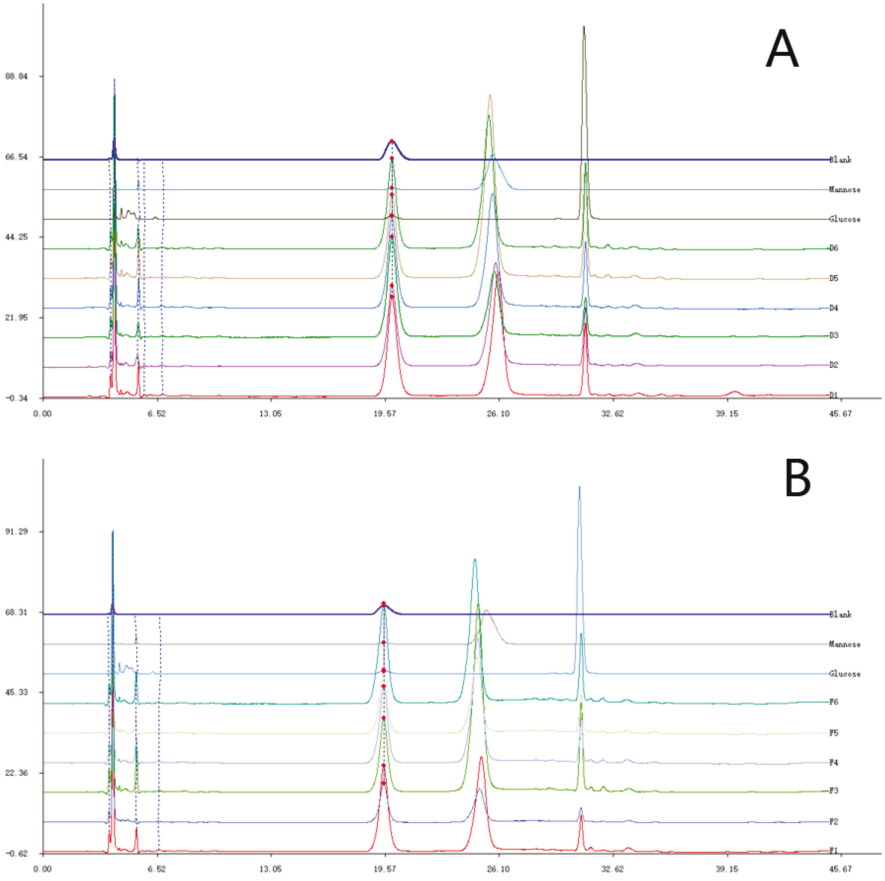

Figure 6. Monosaccharide analysis of (**A**) D1–D6 and (**B**) F1–F6.

2.4. Effects of the DPFs on HeLa Cell Proliferation

In this study, we applied MTT assays to detect the anti-proliferation activity of the CP and DPFs. From the graph, the CP from *Dendrobium officinale* planted in a green house or planted in the wild showed no significant activity on HeLa cells after treatment for 24 h. After treatment for 24 h at the highest concentration (400 μg/mL), the anti-proliferation activity of D1–D6 was 7.9%, 9.2%, 16.3%,

17.4%, 20.0% and 29.8%. D1–D6 exhibited no significant anti-proliferation activity in HeLa cells. The anti-proliferation activity of F1–F6 was 42.5%, 2.2%, 43.0%, 36.8%, 28.2%, and 35.9%. The DPFs F1 and F3 were the most effective. The anti-proliferation activity of F1 and F3 at concentrations ranging from 25 μg/mL to 400 μg/mL was 24.4%, 22.5%, 24.4%, 35.6%, and 42.5% and 15.2%, 21.7%, 27.0%, 31.6%, and 43.0%, respectively. The DPFs F1 and F3 exhibited significant anti-proliferation activity in a dose-dependent manner. We proceeded to further study the anti-proliferation activity of F1–F6. The activity of both F1 and F3 was high. When the concentration was 400 μg/mL, the anti-proliferation rate induced by F1 and F3 was 48.3% and 48%, respectively. For the other four DPFs (i.e., F2, F4, F5, and F6), the rate was 21.5%, 27.6%, 17.5%, and 25.2%, respectively. The graph of inhibition rate was shown in Figure 7.

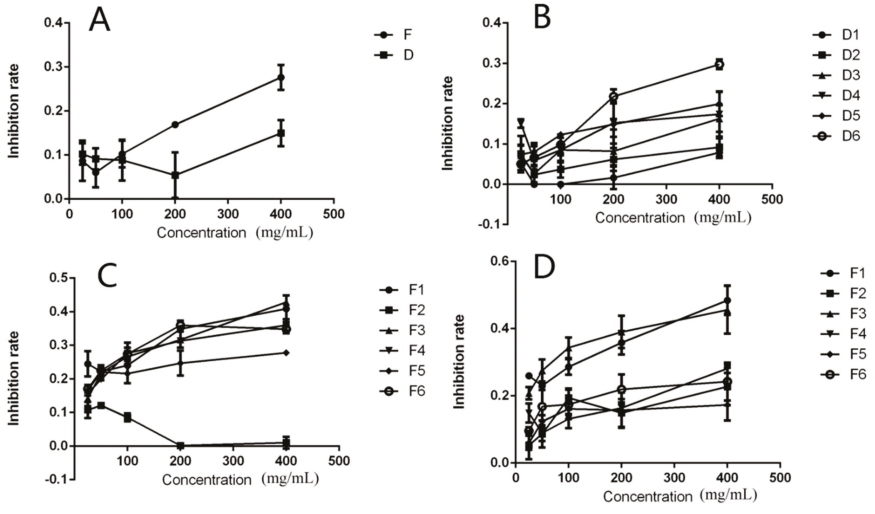

Figure 7. The anti-proliferation effects of (**A**) crude polysaccharides, (**B**) D1–D6, and (**C**) F1–F6 on HeLa cells after treatment for 24 h and (**D**) 48 h.

2.5. Apoptosis Rate of HeLa Cells after Treatment with F1 and F3 for 24 h and 48 h

The apoptosis rate induced by the DPFs F1 and F3 was tested using flow cytometry. After treatment with F1 and F3 for 24 h at a concentration of 400 μg/mL, the necrosis rate and percentage of HeLa cells in early and late phase apoptosis was 3.5%, 6.9%, and 1.3% and 2.4%, 9.9%, and 3.0%, respectively, which is statistically higher than in the control group treated with PBS. If the duration time was increased to 48 h with the same concentration of 400 μg/mL, the necrosis rate and percentage of HeLa cells in early phase and late phase apoptosis was 2.4%, 16.5%, and 7.2% and 12.3%, 16.3%, and 23.7%, respectively. The graph of flow cytometry was shown in Figure 8. The apoptosis rate of cells treated with F1 and F3 was significantly higher than that of control group cells. The results demonstrated that the DPFs F1 and F3 can induce apoptosis in HeLa cells.

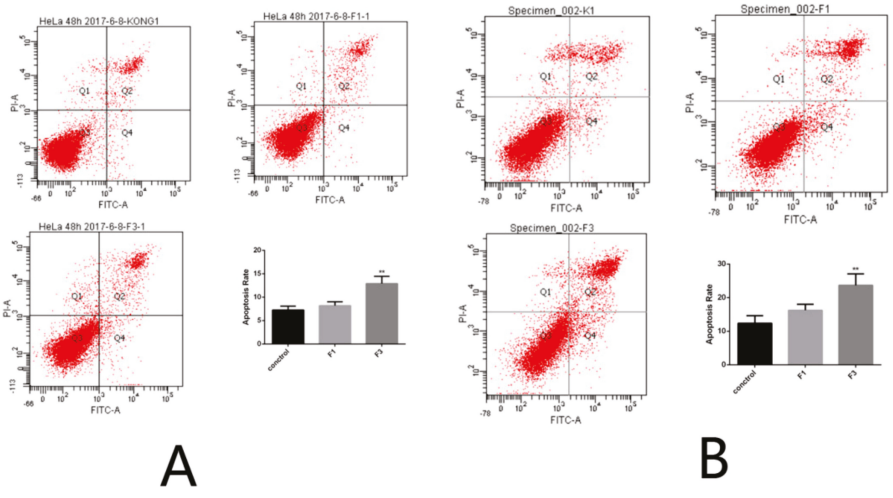

Figure 8. The apoptosis rate of HeLa cells after treatment with F1 and F3 for (**A**) 24 h and (**B**) 48 h.

2.6. Morphology Changes in HeLa Cells after Treatment with F1 and F3 for 24 h and 48 h

The morphology changes in HeLa cells after treatment with F1 and F3 at a concentration of 400 μg/mL for 24 and 48 h was observed. As it was shown in Figure 9 of the microscopy images of cell morphology, no fluorescent dots were present in the control group of HeLa cells. However, in the F1- and F3-treated groups, some blue fluorescence was observed, which was caused by leakage of cellular content. In addition, after treatment for 48 h, the amount of blue fluorescence increased. As the treatment duration was increased, the morphology changes in the HeLa cells were exacerbated.

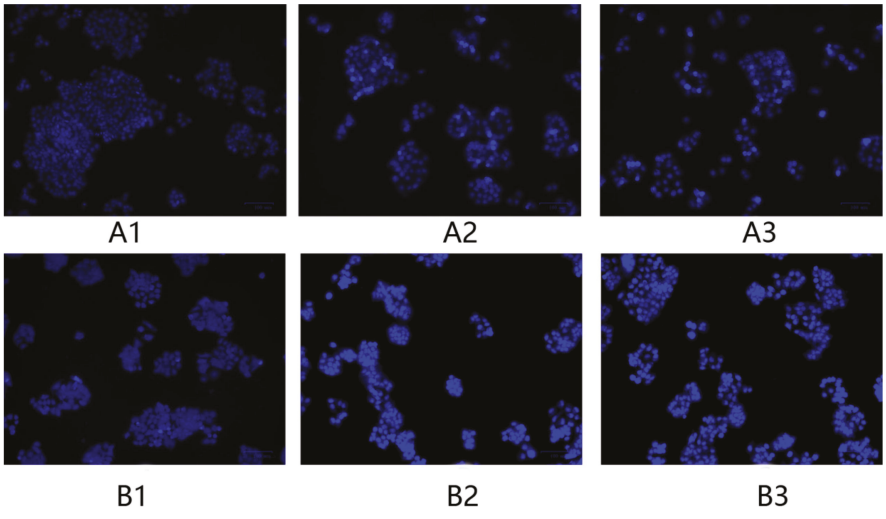

Figure 9. The morphology changes in HeLa cells in the (**A1**,**B1**) control group, (**A2**,**B2**) F1 treatment group, and (**A3**,**B3**) F3 treatment group after treatment for (**A**) 24 h and (**B**) 48 h.

2.7. Relative Expression of Apoptosis Genes and Proteins

In this study, the relative expression level of five apoptosis-related genes, namely, Bcl-2, ERK, JNK, NF-κB, and p38, were tested. In the F1 and F3 group, the expression level of four of the five

apoptosis-related genes in HeLa cells after treatment with 400 μg/mL F1 and F3 for 48 h showed no significant differences compared with the control group. However, the expression level of p38 in the F3 group was significantly higher than in the control group. F3 up-regulated the expression of the p38 gene in HeLa cells. In the positive drug group, three apoptosis-related genes, Bcl-2, NF-κB and p38, showed significant differences compared with the control group. The positive drug 5-FU can down-regulate the expression level of Bcl-2 and up-regulate the expression level of NF-κB and p38. The graph of relative expression of all tested genes was shown in Figure 10. Apart from the apoptosis-related genes, we also applied western blotting to test the expression of the apoptosis-related proteins JNK, ERK, and p38. From the graph of the western-blot results, and after treatment with F1 and F3, the protein expression of JNK, ERK, and p38 was significantly up-regulated compared with the control group. The graph of relative expression of tested protein was shown in Figure 11A, and the graph of Western-blot was shown in Figure 11B.

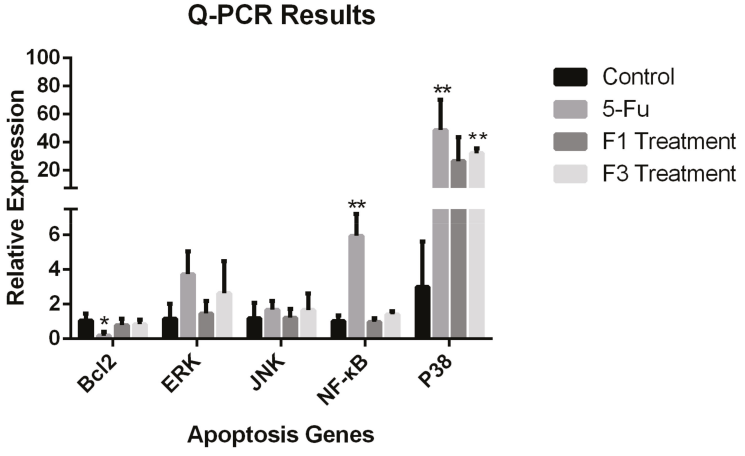

Figure 10. The relative expression level of apoptosis-related genes. (comparing with control group, * $p \leq 0.05$; ** $p \leq 0.01$).

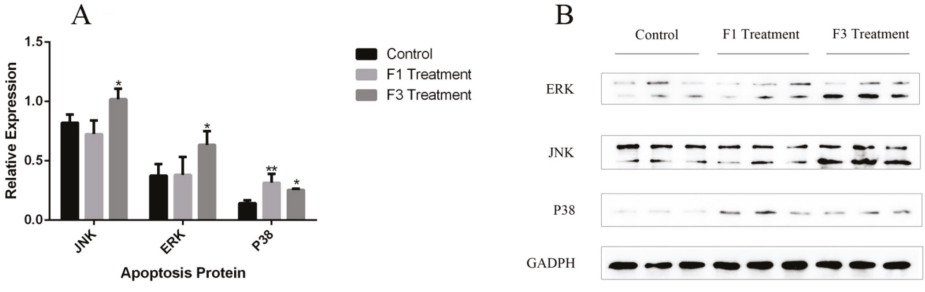

Figure 11. The relative expression level of apoptosis-related proteins (**A**) (comparing with control group, * $p \leq 0.05$; ** $p \leq 0.01$); (**B**) The graph of Westen-blot.

3. Discussion

The plant *Dendrobium officinale* has been used for thousands of years in China as a folk medicine. In recent decades, scientists have found that the polysaccharides in this plant exhibit fine bio-activities, including anti-tumor, immunomodulatory, hypoglycemic, anti-inflammatory, and antioxidant activities. However, no studies have examined the structure of polysaccharides from *Dendrobium officinale* grown under different conditions or their anti-tumor activities. The results of this study have shown that

the skeleton of the polysaccharides from wild-grown and greenhouse-grown *Dendrobium officinale* was the same and consisted of (1→4)-linked mannose and (1→4)-linked glucose. Differences were found in the mannose and glucose ratio, as well as in the side chains. The polysaccharides from wild plants may consist of the furan configuration of sugar, whereas this configuration was not present in the *Dendrobium officinale* planted in a greenhouse. The crude polysaccharides from both wild and greenhouse-grown plants exhibited no significant activities in HeLa cells. Through literature investigation, we found that molecular weight is a critical factor that influences the bio-activities of polysaccharides. Degradation by oxidative reagents can increase the activity of polysaccharides. In this study, the polysaccharides from wild plants exhibited certain anti-tumor activities in HeLa cells after degradation. It was obvious that molecular weight played an important role in anti-tumor activities. In addition, after degradation, the polysaccharide fractions from wild plants exhibited certain anti-tumor activity [24–29]. However, the activity of the polysaccharide fractions from greenhouse plants was still not significant. In addition, through monosaccharide analysis, we found that the mannose-related content in polysaccharide fractions from wild plants was significantly higher than in fractions from the greenhouse plants. Therefore, we speculated that the activity of polysaccharides from *Dendrobium officinale* was related to molecular weight as well as monosaccharide composition. We also speculated that the anti-tumor activities may be related to the furan configuration. In this study, we thoroughly investigated the anti-tumor mechanism of the degraded polysaccharide fractions. We found that the degraded polysaccharide fractions induced apoptosis in HeLa cells through the p38/MAPK signaling pathway. We believe that when people drink the water extract of *Dendrobium officinale*, the polysaccharide is degraded by the gastrointestinal tract before being absorbed into the blood. The degradation process in this study can be considered to mimic the gastrointestinal digestion process. Polysaccharides with a smaller molecular weight will be present after absorption. In this study, we compared the anti-tumor activities of polysaccharides from *Dendrobium officinale* grown under two different conditions and found that the anti-tumor effect of wild plants was significant. We therefore advise that the planting mode of *Dendrobium officinale* should be improved. Even though greenhouse cultivation can increase the production of this medicinal plant, simulating wild plant conditions is a better approach.

4. Methods and Reagents

4.1. Materials and Reagents

The *Dendrobium officinale* plants used in this study were divided into two groups, those planted in the greenhouse and those planted in the wild. All plants were collected from Shaoguan City, Guangdong Province. After authentication by Gang Wei, professor at Guangdong University of Chinese Medicine, the plants were identified as *Dendrobium officinale*.

The reagents used in the extraction, purification, and degradation are listed below. The DEAE column, Sephadex G-25 column, and PMP were purchased from Macklin (Macklin, Shanghai, China). T-series dextran was purchased from Sigma (Sigma-Aldrich, St. Louis, MO, USA). The reagents used in the in vitro experiments were Minimum Eagles' Medium (MEM) (KeyGene, Jiangsu, China), Phosphate Buffer Saline (PBS) (KeyGene), fetal bovine serum, trypsin (KeyGene), a cell apoptosis kit array kit (KeyGene), 5-FU (Sigma-Aldrich), a Hoechst 33258 kit (KeyGene), Trizol (KeyGene), a cDNA synthesis kit (KeyGene), a qPCR reagent kit (abm Inc., New York, NY, USA), a protein extraction kit (KeyGene), an SDS-PAGE kit (KeyGene), an ECL kit (KeyGene), a BCA protein detection kit (KeyGene), a protein marker (KeyGene), a loading buffer (KeyGene), as well as GADPH (ABclonal, Wuhan, China), goat anti-mouse (ABclonal), and IgG antibodies (ABclonal). The HeLa cell line used in this study was purchased from iCell (iCell Bioscience Inc., Shanghai, China).

4.2. Extraction of Dendrobium Officinale Polysaccharides

The stem of *Dendrobium officinale* was dried in an oven and crushed into powder before the experiments. Then, 50 g of the powder was weighed, 500 mL of petroleum ether was added to remove

the lipids, and 500 mL of 80% ethanol was added to remove low polarity substances. The polysaccharide was extracted using 1500 mL of distilled water. The extract was precipitated with 80% ethanol to obtain the polysaccharides. The Sevag method was applied to remove protein in the polysaccharides to obtain crude polysaccharide (CP).

4.3. Purification of Polysaccharides

The crude polysaccharide (CP) was re-dissolved in distilled water and purified with DEAE and Sephadex G-25 columns to obtain the purified polysaccharide fraction (PPF). The elution phase for the DEAE column was distilled water, the flow speed was 1 mL/min, and 100 tubes of the elution phase were collected. The elution phase for the Sephadex G-25 column was 0.2 M NaCl, the flow speed was set at 0.5 mL/min, and 100 tubes of the elution phase were collected. The polysaccharide content in the elution phase was tested using phenol-sulfuric acid.

4.4. Oxidative Degradation of Crude Polysaccharides

The crude polysaccharide (CP) was re-dissolved in distilled water, a series of reagents were applied for degradation to obtain the degraded polysaccharide fractions (DPFs). The reagents used in this experiment were vitamin C, H_2O_2, $FeCl_2{\cdot}4H_2O$, and distilled water. Each of the final volumes of the degradation system was 50 mL. The degradation process was carried out in the dark, at room temperature (25 °C), and the duration time was 60 min. The ratios of these reagents used in the experiment are shown in Table 1.

Table 1. The condition of degradation method.

Order	Vitamin C (mL)	H_2O_2 (mL)	$FeCl_2{\cdot}4H_2O$ (mL)	CP	Water (mL)
1	0.5	0.05	0.05	30	19.4
2	1	0.1	0.1	30	18.8
3	2	0.2	0.2	30	17.6
4	4	0.4	0.4	30	15.2
5	5	0.5	0.5	30	14
6	6	0.6	0.6	30	12.6

4.5. Detection of the Molecular Weight of PPF and DPF

An adequate amount of the PPF and DPF was weighed and dissolved in distilled water to a fixed concentration of 5 mg/mL to obtain sample solutions. T-series dextran was weighed precisely and dissolved in distilled water to obtain standard solutions. High Performance Gel Permeation Chromatography (HPGPC) was used in this study. The samples and the T-series dextran standards (MW: 667, 273, 147, 80, 11, and 5 kDa) were analyzed on an Agilent 1100 series HPLC system (Palo Alto, CA, USA) equipped with an RI-101SHODEX RID detector (Tosoh, Tokyo, Japan). The molecular weight of the samples was determined using a standard curve established with the standard solution.

4.6. Detection of Monosaccharide Composition and Ratio of PPF and DPF

An adequate amount of the PPF and DPF was weighed and dissolved in distilled water to a fixed concentration of 1 mg/mL to obtain sample solutions. The standard solutions were prepared with glucose and mannose standard references using the same preparation method used for the sample solution. The blank control solution was also prepared with the same method without adding any substance. The experiment to detect the monosaccharide composition and ratio was performed as follows. First, the solution was hydrolyzed with HCl in an oven at 110 °C. Then, the pH value of the solution was adjusted to 7 with NaOH. PMP was added to the solution to react. The reaction was then subjected to monosaccharide detection using HPLC. The HPLC analysis was performed on an HPLC system (Shimadzu, Kyoto, Japan) with an XDB-C18 analytical column (4.6 × 150 mm, 5 μm, Agilent ZORBAX). The mobile phase was 0.05 M aqueous KH_2PO_4 (solvent A) and acetonitrile (solvent B).

4.7. NMR Spectrometer Analysis of PPFs

An amount of 30 mg PPF was weighed precisely and deuterium-exchanged by freeze drying three time from 99% D2O to obtain the sample solution. A 0.5 mL portion of the sample solution was transferred to a 5 mm tube. NMR spectra were recorded in 25 °C on a Bruker NMR spectrometer (Avance III HD 400 MHz Digital NMR Spectrometer, Bruker, Karlsruhe, Germany).

4.8. MTT Assay of HeLa Cells Treated with CP and DPF

The CP and DPF were dissolved in PBS at a fixed concentration of 4 mg/mL. The DPF solutions were filtered through 0.22-μm microporous filter membranes to avoid contamination. HeLa cells were cultured in MEM with 10% fetal bovine serum. The cells were transferred to a 96-well plate during exponential growth. After being cultured for 24 h, the cells were treated with DPFs in a concentration series for 24 h and 48 h. MTT was then added and incubated with the cells for 4 h. MTT was removed, and 100 μL of DMSO was added to each well. The absorption at 490 nm was tested using a microplate reader (BX51, Olympus Optical Co. Ltd., Tokyo, Japan).

4.9. Detection of the Apoptosis Rate of HeLa Cells

The apoptosis rate of HeLa cells was tested by Annexin V-FITC/PI staining. The HeLa cells were seeded in 6-well plates during exponential growth and cultured for 24 h before being treated with DPFs. The cells were collected using EDT-free trypsin and washed with PBS three times. Then, the cells were re-suspended in 500 μL of binding buffer with 5 μL of Annexin V-FITC, PI was added into the cell suspension, and the cells were incubated in the dark at room temperature for 10 min. The apoptosis rate of the cells was tested using flow cytometry (Attune® Acoustic Focusing Cytometer, Thermo Fisher Co. Ltd., Waltham, MA, USA).

4.10. Morphological Observation of HeLa Cells

The morphology of the HeLa cells was observed with a fluorescence microscope after staining with Hoechst 33258, according to the following procedure. The HeLa cells were seeded in 6-well plates during exponential growth. The cells were cultured for 24 h before being treated with DPFs and incubated for 48 h. The upper MEM was removed, and the cells were washed with PBS three times. Then, 4% paraformaldehyde was added for fixation and incubated with the cells at 4 °C for 10 min. The 4% paraformaldehyde was removed, and the cells were washed three times with PBS. Hoechst 33258 (500 μL) was added to each well and incubated with the cells in dark conditions for 10 min. The Hoechst 33258 was removed, and the cells were washed two times with PBS. The morphology of the HeLa cells was observed using a fluorescence microscope (BX51, Olympus Optical Co. Ltd.).

4.11. Q-PCR Assay of the Expression of Apoptosis-Related Genes

After treatment with DPFs and incubation for 48 h, RNA was extracted from the cells using an RNA extraction kit reagent. The concentration and quality of the extracted RNA was tested using a nucleic acid analyzer. Before proceeding to Q-PCR detection, cDNA was synthesized from the extracted RNA using cDNA synthesis kit reagents. The expression level of the apoptosis-related genes NF-κB, Bcl-2, p38, ERK, and JNK was determined by Q-PCR equipment (CFX96 Touch™ Real-Time PCR Detection System, Bio-rad Laboratories, Inc., Hercules, CA, USA).

4.12. Western-Blotting Assay of MAPK Protein

After treatment with DPFs and incubation for 48 h, protein was extracted from the cells using lysing reagents. A BCA protein quantitative method was used to quantify the concentration of each protein sample. Then, the protein was separated by SDS-PAGE. The gel was selected after comparison with the protein marker, and the protein was transferred to a membrane. A blocking reagent was

used to bind the protein before incubation with primary and secondary antibodies. The protein bands were developed using an ECL kit. The bands were recorded using a chemiluminescence analyzer (ChemiDoc™ MP system, Bio-rad Laboratories, Inc.), and the gray value was counted.

Supplementary Materials: The following are available online.

Author Contributions: Conceptualization, G.W., Y.Y., and Z.L.; Methodology, W.Y. and Z.R.; Formal Analysis, X.Z.; Pharmacology Experiments, S.X. and S.T.; Resources, C.L.

Funding: This project was supported by the Special Foundation of 2015 and 2017 High Level University Construction (No. 2050205, A1-AFD018171Z11024), and the Key project at the central government level—the ability establishment of sustainable use for valuable Chinese medicine resources (No. 2060302).

Conflicts of Interest: All authors declare no conflict of interest.

References

1. Ng, T.B.; Liu, J.; Wong, J.H.; Ye, X.; Wing Sze, S.C.; Tong, Y.; Zhang, K.Y. Review of research on *Dendrobium*, a prized folk medicine. *Appl. Microbiol. Biotechnol.* **2012**, *93*, 1795–1803. [CrossRef] [PubMed]
2. Cai, H.L.; Huang, X.J.; Nie, S.P.; Xie, M.Y.; Phillips, G.O.; Cui, S.W. Study on *Dendrobium officinale* O-acetyl-glucomannan (Dendronan®): Part III–Immunomodulatory activity in vitro. *Bioact. Carbohydr. Diet. Fibre* **2015**, *5*, 99–105. [CrossRef]
3. Huang, X.J.; Nie, S.P.; Cai, H.L.; Zhang, G.Y.; Cui, S.W.; Xie, M.Y.; Phillips, G.O. Study on *Dendrobium officinale* O-acetyl-glucomannan (Dendronan®): Part VI. Protective effects against oxidative stress in immunosuppressed mice. *Food Res. Int.* **2015**, *72*, 168–173. [CrossRef]
4. Xiang, L.; Stephen Sze, C.W.; Ng, T.B.; Tong, Y.; Shaw, P.C.; Sydney Tang, C.W.; Kalin Zhang, Y.B. Polysaccharides of *Dendrobium officinale* inhibit TNF-α-induced apoptosis in A-253 cell line. *Inflamm. Res.* **2013**, *62*, 313–324. [CrossRef] [PubMed]
5. Lin, X.; Liu, J.; Chung, W.; Sze, S.C.; Li, H.; Lao, L.; Zhang, Y. Polysaccharides of *Dendrobium officinale* induce aquaporin 5 translocation by activating M3 muscarinic receptors. *Planta Med.* **2015**, *81*, 130–137. [CrossRef] [PubMed]
6. Xia, L.; Liu, X.; Guo, H.; Zhang, H.; Zhu, J.; Ren, F. Partial characterization and immunomodulatory activity of polysaccharides from the stem of *Dendrobium officinale* (*Tiepishihu*) in vitro. *J. Funct. Foods* **2012**, *4*, 294–301. [CrossRef]
7. Xing, X.; Cui, S.W.; Nie, S.; Phillips, G.O.; Douglas Goff, H.; Wang, Q. A review of isolation process, structural characteristics, and bioactivities of water-soluble polysaccharides from *Dendrobium* plants. *Bioact. Carbohydr. Diet. Fibre* **2013**, *1*, 131–147. [CrossRef]
8. Hsieh, Y.S.; Chien, C.; Liao, S.K.; Liao, S.F.; Hung, W.T.; Yang, W.B.; Lin, C.C.; Cheng, T.J.; Chang, C.C.; Fang, J.M.; et al. Structure and bioactivity of the polysaccharides in medicinal plant *Dendrobium huoshanense*. *Bioorg. Med. Chem.* **2008**, *16*, 6054–6068. [CrossRef] [PubMed]
9. Li, Q.; Xie, Y.; Su, J.; Ye, Q.; Jia, Z. Isolation and structural characterization of a neutral polysaccharide from the stems of *Dendrobium densiflorum*. *Int. J. Biol. Macromol.* **2012**, *50*, 1207–1211. [CrossRef] [PubMed]
10. Li, X.L.; Xiao, J.J.; Zha, X.Q.; Pan, L.H.; Asghar, M.N.; Luo, J.P. Structural identification and sulfated modification of an antiglycation *Dendrobium huoshanense* polysaccharide. *Carbohydr. Polym.* **2014**, *106*, 247–254. [CrossRef] [PubMed]
11. Luo, A.; He, X.; Zhou, S.; Fan, Y.; Luo, A.; Chun, Z. Purification, composition analysis and antioxidant activity of the polysaccharides from *Dendrobium nobile* Lindl. *Carbohydr. Polym.* **2010**, *79*, 1014–1019. [CrossRef]
12. Sun, Y.D.; Wang, Z.H.; Ye, Q.S. Composition analysis and anti-proliferation activity of polysaccharides from *Dendrobium chrysotoxum*. *Int. J. Biol. Macromol.* **2013**, *62*, 291–295. [CrossRef] [PubMed]
13. Tian, C.C.; Zha, X.Q.; Pan, L.H.; Luo, J.P. Structural characterization and antioxidant activity of a low-molecular polysaccharide from *Dendrobium huoshanense*. *Fitoterapia* **2013**, *91*, 247–255. [CrossRef] [PubMed]
14. Wang, J.H.; Luo, J.P.; Zha, X.Q. Structural features of a pectic polysaccharide from the stems of *Dendrobium nobile* Lindl. *Carbohydr. Polym.* **2010**, *81*, 1–7. [CrossRef]
15. Xu, J.; Li, S.L.; Yue, R.Q.; Ko, C.H.; Hu, J.M.; Liu, J.; Ho, H.M.; Yi, T.; Zhao, Z.Z.; Zhou, J.; et al. A novel and rapid HPGPC-based strategy for quality control of saccharide-dominant herbal materials: *Dendrobium officinale*, a case study. *Anal. Bioanal. Chem.* **2014**, *406*, 6409–6417. [CrossRef] [PubMed]

16. Yang, B.; Prasad, K.N.; Jiang, Y. Structure identification of a polysaccharide purified from litchi (*Litchi chinensis Sonn.*) pulp. *Carbohydr. Polym.* **2016**, *137*, 570–575. [CrossRef] [PubMed]
17. Zha, X.Q.; Lu, C.Q.; Cui, S.H.; Pan, L.H.; Zhang, H.L.; Wang, J.H.; Luo, J.P. Structural identification and immunostimulating activity of a *Laminaria japonica* polysaccharide. *Int. J. Biol. Macromol.* **2015**, *78*, 429–438. [CrossRef] [PubMed]
18. Zha, X.Q.; Luo, J.P.; Luo, S.Z.; Jiang, S.T. Structure identification of a new immunostimulating polysaccharide from the stems of *Dendrobium huoshanense*. *Carbohydr. Polym.* **2007**, *69*, 86–93. [CrossRef]
19. Hua, Y.F.; Zhang, M.; Fu, C.X.; Chen, Z.H.; Chan, G.Y. Structural characterization of a 2-*O*-acetylglucomannan from *Dendrobium officinale* stem. *Carbohydr. Res.* **2004**, *339*, 2219–2224. [CrossRef] [PubMed]
20. Xing, X.; Cui, S.W.; Nie, S.; Phillips, G.O.; Goff, H.D.; Wang, Q. Study on *Dendrobium officinale* O-acetyl-glucomannan (Dendronan®): Part I. Extraction, purification, and partial structural characterization. *Bioact. Carbohydr. Diet. Fibre* **2014**, *4*, 74–83. [CrossRef]
21. Xing, X.; Cui, S.W.; Nie, S.; Phillips, G.O.; Goff, H.D.; Wang, Q. Study on *Dendrobium officinale* O-acetyl-glucomannan (Dendronan®): Part II. Fine structures of O-acetylated residues. *Carbohydr. Polym.* **2015**, *117*, 422–433. [CrossRef] [PubMed]
22. He, T.B.; Huang, Y.P.; Yang, L.; Liu, T.T.; Gong, W.Y.; Wang, X.J.; Sheng, J.; Hu, J.M. Structural characterization and immunomodulating activity of polysaccharide from *Dendrobium officinale*. *Int. J. Biol. Macromol.* **2016**, *83*, 34–41. [CrossRef] [PubMed]
23. Smoum, R.; Rubinstein, A.; Srebnik, M. Combined ^{1}H, ^{13}C and ^{11}B-NMR and mass spectral assignments of boronate complexes of D-(+)-glucose, D-(+)-mannose, methyl-α-D-glucopyranoside, methyl-β-D-galactopyranoside and methyl-α-D-mannopyranoside. *Magn. Reson. Chem.* **2003**, *41*, 1015–1020. [CrossRef]
24. Sheng, J.; Sun, Y. Antioxidant properties of different molecular weight polysaccharides from *Athyrium multidentatum* (Doll.) Ching. *Carbohydr. Polym.* **2014**, *108*, 41–45. [CrossRef] [PubMed]
25. Sun, L.; Wang, L.; Zhou, Y. Immunomodulation and antitumor activities of different-molecular-weight polysaccharides from *Porphyridium cruentum*. *Carbohydr. Polym.* **2012**, *87*, 1206–1210. [CrossRef]
26. Sun, Y.; Yang, B.; Wu, Y.; Liu, Y.; Gu, X.; Zhang, H.; Wang, C.; Cao, H.; Huang, L.; Wang, Z. Structural characterization and antioxidant activities of κ-carrageenan oligosaccharides degraded by different methods. *Food Chem.* **2015**, *178*, 311–318. [CrossRef] [PubMed]
27. Yu, L.; Xue, C.; Chang, Y.; Hu, Y.; Xu, X.; Ge, L.; Liu, G. Structure and rheological characteristics of fucoidan from sea cucumber *Apostichopus japonicus*. *Food Chem.* **2015**, *180*, 71–76. [CrossRef] [PubMed]
28. Zhang, Z.; Wang, X.; Zhao, M.; Qi, H. Free-radical degradation by Fe^{2+}/Vc/H_2O_2 and antioxidant activity of polysaccharide from *Tremella fuciformis*. *Carbohydr. Polym.* **2014**, *112*, 578–582. [CrossRef] [PubMed]
29. Zhao, T.; Zhang, Q.; Qi, H.; Zhang, H.; Niu, X.; Xu, Z.; Li, Z. Degradation of porphyran from *Porphyra haitanensis* and the antioxidant activities of the degraded porphyrans with different molecular weight. *Int. J. Biol. Macromol.* **2006**, *38*, 45–50. [CrossRef] [PubMed]

Sample Availability: The sample of plant *Dendrobium officinale* is available from the corresponding author Gang Wei and Zhouxi Lei.

molecules

MDPI

Article

Microbial Synthesis of Non-Natural Anthraquinone Glucosides Displaying Superior Antiproliferative Properties

Trang Thi Huyen Nguyen [1,†], Ramesh Prasad Pandey [1,2,†], Prakash Parajuli [1], Jang Mi Han [1], Hye Jin Jung [1,2], Yong Il Park [3] and Jae Kyung Sohng [1,2,*]

1 Department of Life Science and Biochemical Engineering, Sun Moon University, 70 Sunmoon-ro 221, Tangjeong-myeon, Asan-si, Chungnam 31460, Korea; nguyenhuyentrang0512@gmail.com (T.T.H.N.); ramesh.pandey25@gmail.com (R.P.P.); parajuli1985@gmail.com (P.P.); gkswkdal200@naver.com (J.M.H.); poka96@sunmoon.ac.kr (H.J.J.)

2 Department of BT-Convergent Pharmaceutical Engineering, Sun Moon University, 70 Sunmoon-ro 221, Tangjeong-myeon, Asan-si, Chungnam 31460, Korea

3 Department of Biotechnology, The Catholic University of Korea, Bucheon, Gyeonggi-do 14662, Korea; yongil382@catholic.ac.kr

* Correspondence: sohng@sunmoon.ac.kr; Tel: +82-(41)-530-2246; Fax: +82-(41)-530-8229

† These authors contributed equally to this work.

Received: 17 July 2018; Accepted: 21 August 2018; Published: 28 August 2018

Abstract: Anthraquinones, naturally occurring bioactive compounds, have been reported to exhibit various biological activities, including anti-inflammatory, antiviral, antimicrobial, and anticancer effects. In this study, we biotransformed three selected anthraquinones into their novel *O*-glucoside derivatives, expressing a versatile glycosyltransferase (YjiC) from *Bacillus licheniformis* DSM 13 in *Escherichia coli*. Anthraflavic acid, alizarin, and 2-amino-3-hydroxyanthraquinone were exogenously fed to recombinant *E. coli* as substrate for biotransformation. The products anthraflavic acid-*O*-glucoside, alizarin 2-*O*-*β*-D-glucoside, and 2-amino-3-*O*-glucosyl anthraquinone produced in the culture broths were characterized by various chromatographic and spectroscopic analyses. The comparative anti-proliferative assay against various cancer cells (gastric cancer-AGS, uterine cervical cancer-HeLa, and liver cancer-HepG2) were remarkable, since the synthesized glucoside compounds showed more than 60% of cell growth inhibition at concentrations ranging from ~50 μM to 100 μM. Importantly, one of the synthesized glucoside derivatives, alizarin 2-*O*-glucoside inhibited more than 90% of cell growth in all the cancer cell lines tested.

Keywords: anti-cancer agents; anthraquinones; glycosyltransferase

1. Introduction

Anthraquinones are naturally occurring phenolic compounds based on the 9,10-anthraquinone skeleton. They are widely available from plants, microbes, fungi, and lichens [1]. Anthraquinones have various biological benefits [2,3]. Anthraquinones of the *Rubiaceae* family exhibit interesting in vivo biological activities such as antimicrobial [4], antifungal [5], hypotensive and analgesic [6], anti-malarial [7], anti-oxidant [8], antileukemic, and mutagenic functions [9]. Several anthraquinones are widely used in the treatment of cancer. They display cytotoxic activities through interaction with DNA, preferentially at guanine/cytosine-rich sites [10]. Emodin was studied as an agent that could reduce the impact of type 2 diabetes [11] and could inhibit human cytomegalovirus development [12]. Aloe emodin has strong stimulant-laxative action [13] and is found in the gel, soap or leaves of *Aloe vera* and the rhizome of rhubarb (*Rheum rhaponticum*). Chrysazin (known as Dantron) is mainly used in palliative care to counteract the constipating effects of opioids [14]. Quinizarin is an inexpensive

dye used to color gasoline and heating oil [15]. It is also used as an intermediate for the synthesis of indanthrene- and alizarin-derived dyes. Alizarin has been used as a prominent red dye, principally for dyeing textile fabrics. Anthraquinone glycosides upon hydrolysis yield the aglycone, which is usually a di-, tri- or tetrahydroxyanthraquinone or a derivative of these compounds. While free anthraquinone aglycones exhibit therapeutic activity, glycosides that enhance solubility are accepted as key active components with various pharmacological actions such as antileukemic, antiseptic, anti-cancer, and antitumor activity [16,17].

Recently, the synthesis of anthraquinone derivatives has attracted significant interest. Various synthesis methods have been reported, the most common of which is the intramolecular condensation of aryl and *O*-arylbenzoic acids, using fuming sulfuric acid, benzoyl chloride, concentrated sulfuric acid, benzoyl chloride, zinc chloride, and $POCl_3/P_2O_3C_{14}$ as catalyst, which produces anthraquinone derivatives [18]. Anthraquinone and its associated derivatives were previously synthesized by a chemical pathway, although this method was expensive and involved several hurdles [19]. This report is based on the utilization of indigenous *E. coli* sugar (uridine diphosphate (UDP)-glucose) as a sugar donor which will be utilized by the glycosyltransferase to conjugate to different anthraquione derivatives. This process is inexpensive and environmentally friendly. We designed a scheme to consider wild type *E. coli* BL21 (DE3) strain. We then expressed glycosyltransferases from *Bacillus licheniformis* DSM13 (YjiC) and biotransformed three anthraquionones into their respective glucosides (Figure 1). The anticancer activities of all derivatives were assessed and the results were significant compared with those of the corresponding aglycones.

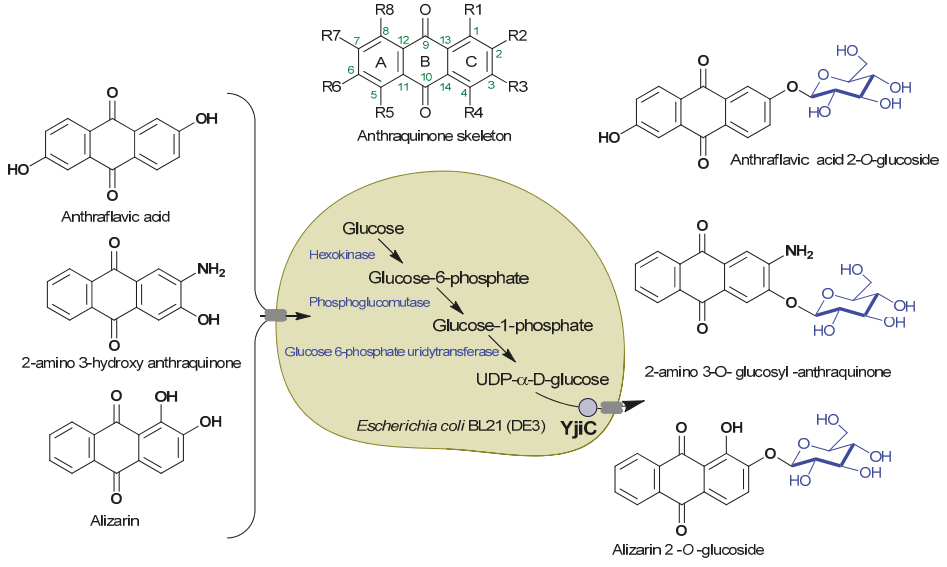

Figure 1. Scheme showing pathway and utilizing *Escherichia coli* indigenous UDP-glucose by *Bacillus* glycosyltransferase for modification of selected anthraquinones into respective glucosides.

2. Results

2.1. Biotransformation of Anthraquinones

The approach was to biosynthesize anthraquinone glucoside utilizing *E. coli* indigenous UDP-glucose as a sugar donor to the expressing glycosyltransefrase (Figure 1). Cultures were prepared for biotransformation reactions with recombinant strain expressing pET28a-YjiC, as explained in the

Materials and Methods section. Three anthraquinones: 2-amino-3-hydroxyanthraquinone, anthraflavic acid, and alizarin were chosen for biotransformation.

Anthraquinones were supplied exogenously to each flask of *E. coli* BL21 (DE3) harboring pET28a-YjiC culture after 20 h of IPTG induction at a final concentration of 0.2 mM. Cultures were allowed to undergo biotransformation for up to 60 h and were then harvested using a double volume of ethyl acetate and analyzed by analytical HPLC-PDA, as described in the Materials and Methods section.

While analyzing the HPLC-PDA of each sample, product peaks appeared at shorter retention times (t_R) than the substrate peak in each reaction mixture, as expected. New peaks at t_R ~ 18.9 min for 2-amino-3-hydroxyanthraquinone-*O*-glucoside, of which the substrate peak was at t_R 21.7 min, t_R ~ 17.3 min for anthraflavic acid-*O*-glucoside, of which the substrate peak was at t_R 20.8 min, and t_R ~ 19.4 min for alizarin-*O*-glucoside, of which the substrate peak was detected at t_R 23.4 min at the UV absorbance of 420 nm (Figure 2).

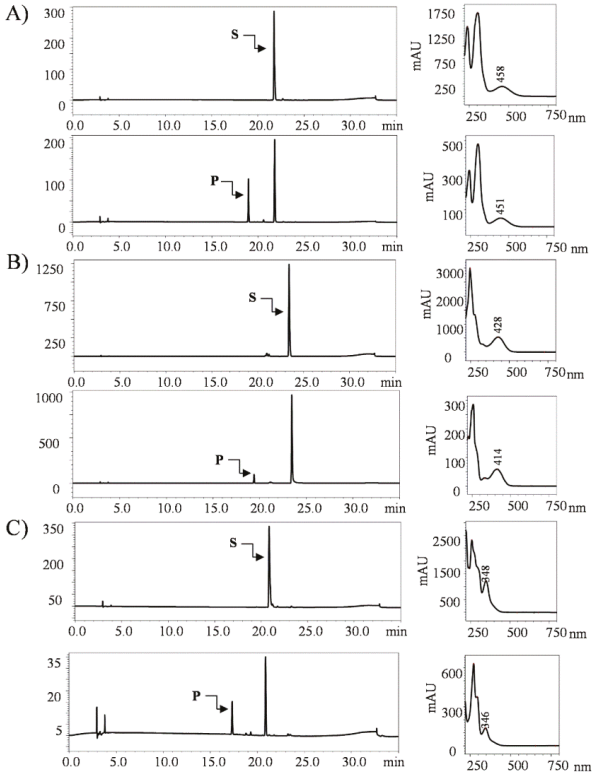

Figure 2. HPLC-PDA chromatogram of biotransformation reaction mixtures compared with respective standards. S refers to the substrate peak and P refers to the product. (**A**) 2-amino-3-hydroxyanthraquinone, (**B**) alizarin, and (**C**) anthraflavic acid.

These product peaks detected from the glycosylation systems were further analyzed by LC-QTOF-ESI/MS in positive ion mode. The mass spectra displayed an exact mass of 2-amino-3-hydroxyanthraquinone $[M + H]^+$ m/z^+ ~ 240.0660, while the mass spectrum of $[M + H]^+$ m/z^+ ~ 402.1175 resembled the glucose conjugated derivative of 2-amino-3-hydroxyanthraquinone. Similarly, anthraflavic acid conjugated to glucose $[M + H]^+$ m/z^+ ~ 403.1025 and the alizarin conjugated to glucose (which was $[M + H]^+$ m/z^+ ~ 403.1015) were assumed from the mass analysis as respective

mass spectra. The mass spectra were obtained along with their sister fragment of anthraflavic acid $[M + H]^+$ m/z^+ ~241.0500 and alizarin $[M + H]^+$ m/z^+ ~ 241.0490 (Figure 3). In this experiment, while we can detect these substrates and their products, the product level was not easily detected. Therefore, we used another experiment to improve the conversion.

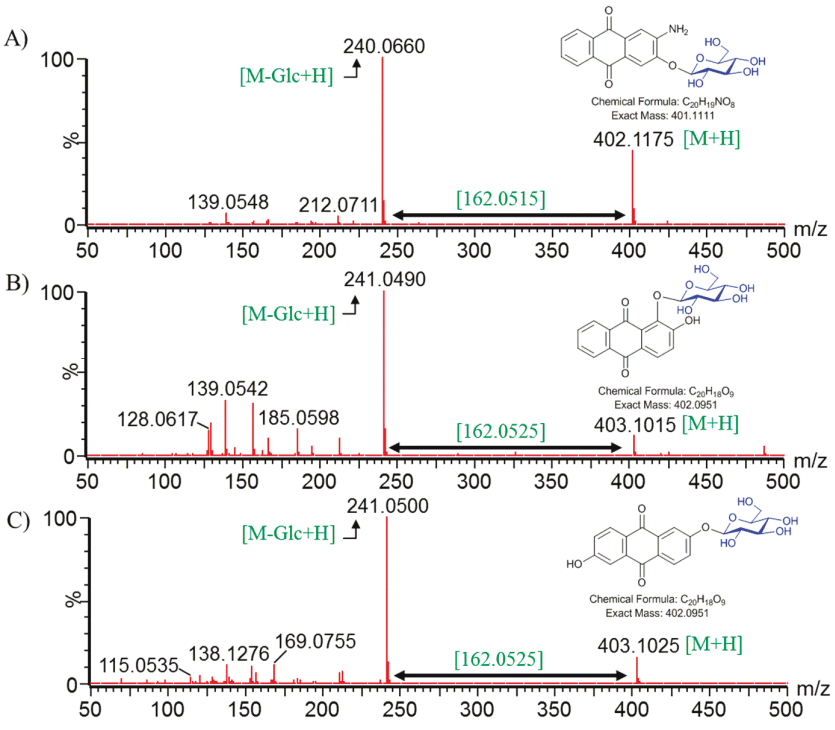

Figure 3. HQ-QTOF ESI/MS analyses of glycosylated (**A**) 2-amino-3-hydroxyanthraquinone; (**B**) Alizarin; and (**C**) anthraflavic acid confirmed by comparing the mass fragments.

2.2. Glucose Supplementation for Production Optimization in Shake Flask

After validating that *E. coli* BL21 (DE3) expressing pET28a-YjiC can biotransform the supplied anthraquinones to their respective glucosides, we considered the optimization of the biotransformation of anthraquinones in shake flasks. Substrates were fed the same amount of 0.2 mM concentration in each flask, while the flasks without the feeding substrates were kept as the control. Samples of 1 mL culture broth from each flask were drawn in each 12 h interval until 60 h. Half of a 0.5 mL sample of culture broth was analyzed for cell density while 0.5 mL of the culture broth was extracted using double volume of ethyl acetate for HPLC sample preparation. While analyzing the production through HPLC, the maximum production of anthraquinone glucoside was achieved from 36 h culture broth (Figure 4).

To enhance the production level of anthraquinone glucosides, we decided to supply extra glucose as carbon source, as reported previously [20] Different concentrations (0%, 4%, and 8%) of glucose were supplemented in separate strain cultures. The production profile of each glucoside changed at different time intervals (from 0 h to 60 h). Previously, while the yields were found to be highest at ~36 h, when these strains were supplemented with glucose, the result showed that production was highest at 48 h (Figure 4). The HPLC-PDA analysis at 48 h resulted in the conversion of approximately 53.89% of alizarin to alizarin-*O*-glucoside in the 4% glucose supplement, while it resulted in the

conversion of 5.2% and 42.8% in the 0% and 8% glucose supplements, respectively. Similarly, ~28% and 84.6% anthraflavic acid *O*-glucoside were found in the 0% and 8% glucose supplements in the anthraflavic acid reaction mixture, while 87.5% of the product formation was measured after feeding 4% glucose. The conversion of 2-amino-3-hydroxyanthraquinone to glucoside was limited to 50%, 53.8%, and 52.2% in 0%, 4%, and 8% glucose supplement, respectively (Figure 4 and Figure S1). In each biotransformation reaction, the product formation decreased after 48 h, while the cell growth did not seem to be hampered (data not shown). The decrease in glucoside concentration could be due to the low stability or the deglycosylation properties of YjiC [21].

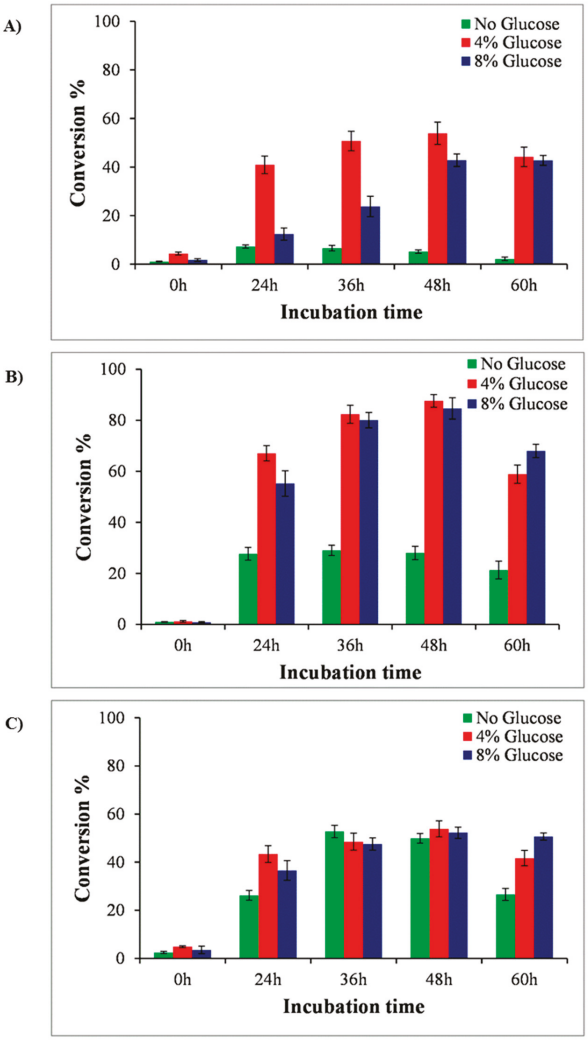

Figure 4. Production profile of anthraquinone-*O*-glucoside at different incubation time intervals and glucose supplementations. (**A**) Alizarin, (**B**) anthraflavic acid, and (**C**) 2-amino-3-hydroxyanthraquinone.

2.3. Comparative Anticancer Activity of Anthraquinone and Their Glucoside Derivatives

Previous studies have revealed that the anticancer effects of anthraquinones are associated with their suppressive activities of cancer cell proliferation. We thus evaluated the effects of 2-amino-3-hydroxyanthraquinone, anthraflavic acid, alizarin, and their glycosylated derivatives on the proliferation of the AGS, Hela, and HepG2 cell lines. The inhibitory effect of anthraflavic acid-*O*-glucoside on cancer cell growth was comparable to that of anthraflavic acid. Besides, 2-amino-3-hydroxyanthraquinone-*O*-glucoside exhibited greater growth inhibitory effect than 2-amino-3-hydroxyanthraquinone. Furthermore, the inhibitory effects of alizarin-*O*-glucoside were higher than any other anthraquinone glucosides (Figure 5). This result demonstrated the positive inhibitory effect of alizarin-*O*-glucoside on test cancer cell lines compared to other compounds.

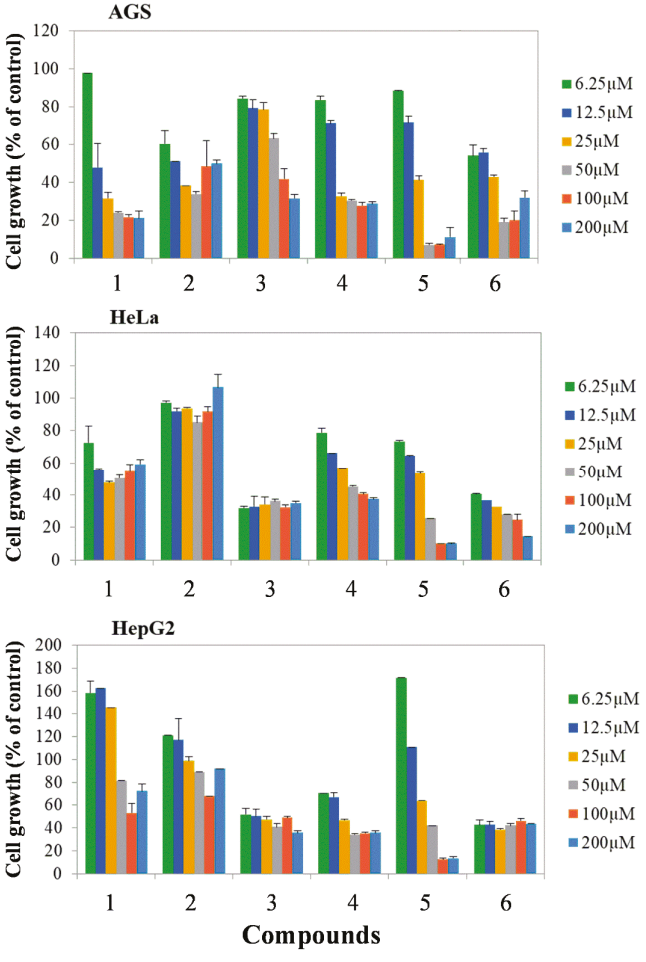

Figure 5. Inhibitory effects of anthraquinones and their derivatives on cancer cell AGS (gastric cancer cell), HeLa (cervical cancer cell), and HepG2 (Liver cancer cell) growth. (1) Anthraflavic acid; (2) Alizarin; (3) 2-amino-3-hydroxyanthraquinone; (4) Anthraflavic acid-*O*-glucoside; (5) Alizarin-*O*-glucoside; (6) 2-amino-3-*O*-glucoxyanthraquinone.

2.4. Scale up Production of Alizarin-O-Glucoside in Bioreactor

Based on the anticancer activity of alizarin-*O*-glucoside, we carried out a scale-up experiment for the same molecule to study the feasibility of microbial biosynthesis in a lab scale fermentor. The reaction culture broth was harvested at a regular time interval of 12 h and analyzed by HPLC–PDA to monitor the percentage conversion of alizarin into its glycosides. The HPLC-PDA analysis at 48 h resulted in the conversion of approximately 67% of alizarin to alizarin-*O*-glucoside higher than in the flask (~53.89%). From the 3-L bioreactor, the production of ~265.32 mg of alizarin-*O*-glucoside was achieved (Figure 6).

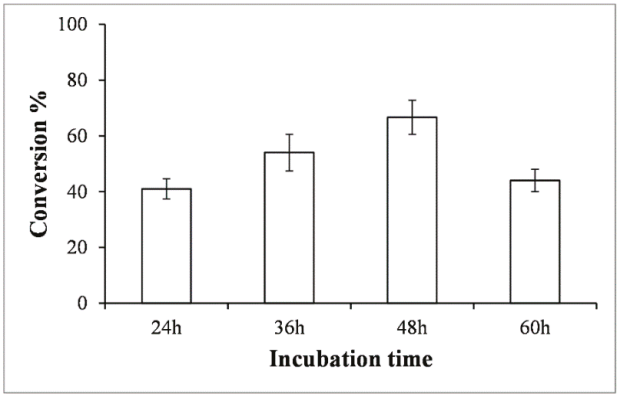

Figure 6. Percentage conversion of alizarin-2-*O*-*β*-D-glucoside in bioreactor at different incubation time intervals.

2.5. Structural Elucidation of Potential Anthraquinone Glucoside Derivative

The product alizarin-*O*-glucoside was purified using prep-HPLC. The purified fraction was concentrated using a rotary evaporator, then lyophilized to remove water content, and then subjected to various NMR analyses. An anomeric proton was detected at 5.18 ppm with *J* value 7.4 Hz referring the conjugation of glucose at beta (*β*) configuration while anomeric carbon was at 100 ppm (Figure 7, Figures S4 and S5, and Table 1). Evidence was further gathered from the proton NMR analysis of the glucoside product of alizarin, by a missing singlet peak for the hydroxyl group in 2-OH, while the similar peak for 1-OH is intact at 12.62 ppm (Figures S2 and S4). This indicates that the possible sugar conjugation is at 2-OH of alizarin. This result was further supported the correlation between the observed anomeric carbon and anomeric proton revealed by HSQC (Figure S6). The carbon number 2 (C-2) of the alizarin signal appearing at *δ* 151.57 ppm has a direct relation with the observed anomeric proton at *δ* 5.18 ppm in HMBC (Figure S7). This confirms that the glycosylation position was at 2-OH of alizarin, and thus the product is alizarin 2-*O*-*β*-D-glucoside. Furthermore, the spectra for glucose moieties were present at respective places in both ^{1}H- (3.0–5.5 ppm) and ^{13}C-NMR (60–100 ppm) analyses. The NMR analyses were compared with the previously published report [22] and spectral database for organic compounds SDBS (http://sdbs.db.aist.go.jp).

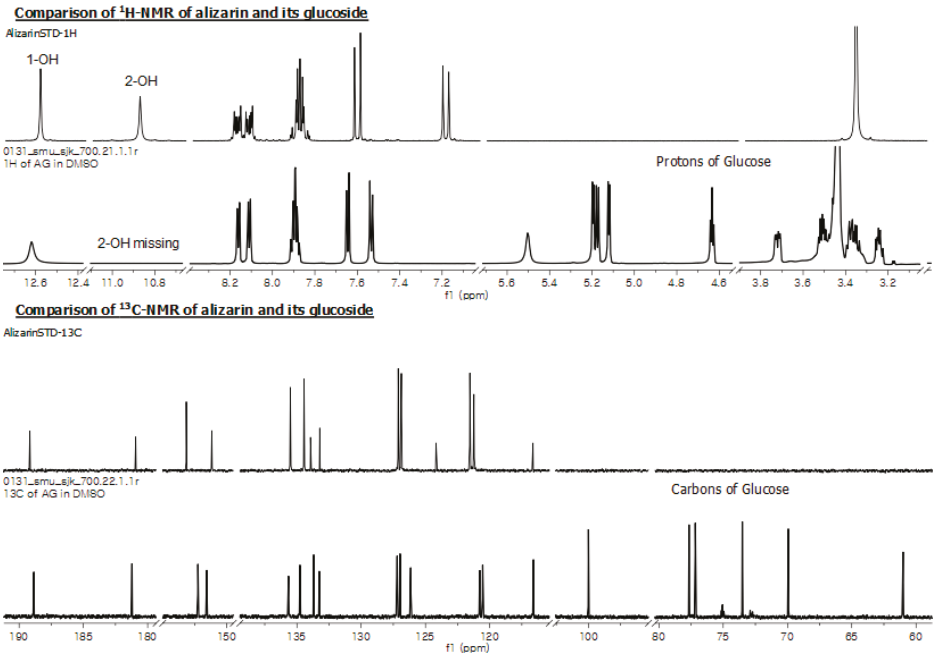

Figure 7. ^{1}H- and ^{13}C-NMR of alizarin and alizarin-2-*O*-*β*-D-glucoside.

Table 1. Comparison of ^{1}H- and ^{13}C-NMR spectra of alizarin and alizarin 2-*O*-glucoside measured in DMSO-d_6. Multiplicities are indicated by s (singlet), d (doublet), t (triplet), q (quartet), and m (multiplet), including coupling constant *J*.

Position	^{1}H-NMR		^{13}C-NMR	
	Alizarin	Alizarin 2-*O*-*β*-D-Glucoside	Alizarin	Alizarin 2-*O*-*β*-D-Glucoside
1-OH	12.59 (*s*, 1H)	12.62 (*s*, 1H)	153.15	155.25
2-OH	10.88 (*s*, 1H)	-	151.17	151.56
3	7.20 (*d*, *J* = 8.3Hz, 1H)	7.53 (*d*, *J* = 8.55Hz, 1H)	121.55	120.78
4	7.62 (*d*, *J* = 8.3Hz, 1H)	7.64 (*d*, *J* = 8.45Hz, 1H)	121.23	120.55
5	8.15 (*m*, 1H)	8.14 (*ddd*, *J* = 35.05, 7.19, 1.82 Hz, 1H)	126.88	126.97
6	7.89 (*m*, 1H)	7.89 (*td*, *J* = 6.81, 6.78, 1.72 Hz, 1H)	133.44	134.76
7	7.89 (*m*, 1H)	7.89 (*td*, *J* = 6.81, 6.78, 1.72 Hz, 1H)	135.51	135.65
8	8.15 (*m*, 1H)	8.14 (*ddd*, *J* = 35.05, 7.19, 1.82 Hz, 1H)	127.12	127.20
9	-	-	180.93	181.21
10	-	-	189.16	188.85
11	-	-	133.22	133.26
12	-	-	133.94	133.69
13	-	-	116.64	116.60
14	-	-	124.17	126.14
1′	-	5.17 (*d*, *J* = 7.4 Hz, 1H)	-	100.00
2′	-	3.36 (*ddd*, *J* = 17.8, 15.0, 8.8 Hz, 1H)	-	73.51
3′	-	3.36 (*ddd*, *J* = 17.8, 15.0, 8.8 Hz, 1H)	-	77.17
4′	-	3.49 (*m*, 1H)	-	77.66
5′	-	3.25 (*dd*, *J* = 9.21, 5.23 Hz, 1H)	-	69.94
6′a	-	3.72 (*ddd*, *J* = 11.92, 5.33, 2.13 Hz, 1H)	-	61.01
6′b		3.49 (m, 1H)		

3. Discussion

Anthraquinones are the largest group of natural pigments, with potential applications in various fields, such as an anticancer, antibacterial agents, and anti-inflammatory agents in pharmaceutical medicine [2,23,24]. The industrial significance of anthraquinones is as synthetic dyes providing brilliant colors, providing the natural red chromogen [25], and in the application of the production of hydrogen peroxide [26], etc. These phenolic compounds can be naturally obtained from various sources such as plant, bacteria, fungi, and lichens [27,28]. These compounds are attracting more attention due to the various key factors as aforementioned. While type II polyketide synthase is responsible for anthraquinone biosynthesis in fungus, reports regarding its biosynthesis and modification in microbial hosts are quite limited [29]. The microbial production of such valuable compounds is performed using simple biotransformation techniques, or is used to enhance production using genetic engineering, the synthetic biological tool is an affirmative practice and certainly increases yields [30]. We considered a versatile post-modifying enzyme, the glycosyltransferase (YjiC), that has revealed potential in glycosylating various classes of natural products including anthraquinone itself [31–33]. A zero engineered wild type *E. coli* strain was considered to express YjiC for whole-cell biotransformation. The YjiC could catalyze glycosylation reaction over different anthraquinones that were fed exogenously and were confirmed by HPLC-PDA and HQ-QTOF ESI/MS (Figures 2 and 3). Among the products, alizarin-*O*-glucoside, 2-amino-3-*O*-glucoxy anthraquinone, and anthraflavic acid-*O*-glucoside were confirmed by mass analysis (Figure 3) while alizarin-*O*-glucoside was elucidated using various NMR analyses.

For production enhancement, glucose was used as a supplemental carbon source. Different concentrations of glucose affected the yield and cell density. As can be seen in Figure 4, while a high concentration of glucose (8%) improved the production level, maximum cell growth was achieved within 24 h (growth curve not shown). However, 4% glucose supplement was optimized and favored enhancement in production by maintaining the cell growth and production yield within 48 h compared to the previous experiment (Figure 2).

Microbial production of emodin *O*-glucoside, aloe-emodin *O*-glucoside using YjiC [33], chrysophanol 8-*O*-*β*-D-glucoside, physcion 8-*O*-*β*-D-glucoside, emodin 6-*O*-*β*-D-glucoside, and aloe-emodin 1-*O*-*β*-D-glucoside were produced by screening 21 different fungal strains for respective anthraquinones biotransformation reported previously [34]. However, all of their biological activities remain unclear, although emodin and aloe-emodin glucoside have shown anti-proliferative activity against some cancer cell lines [33]. Since anthraquinones are potential anticancer agents [35], we synthesized three different *O*-glucosides of 2-amino-3-hydroxyanthraquinone, anthraflavic acid, and alizarin in recombinant *E. coli* strains. These compounds were investigated for anticancer activity against gastric cancer-AGS, uterine cervical cancer-HeLa and liver cancer-HepG2 cells (Figure 5). During the anti-proliferative assay using AGS, HeLa, and HepG2 cancer cell lines, the anthraflavic acid *O*-glucoside and 2-amino-3-*O*-glucosyl anthraquinone revealed more enhanced inhibitory activity than its aglycones, while alizarin *O*-glucoside was more effective than alizarin and other compounds (Figure 5). Although this is a preliminary study for anti-cancer assay, this result suggests that this compound could be developed as an anticancer lead agent in the future. At this point, we needed to determine the exact chemical structure of alizarin *O*-glucoside. Thus, the prep-HPLC purified compound was analyzed with various NMR spectroscopies to elucidate the chemical structure to be alizarin-2-*O*-*β*-D-glucoside (Figure 7). Since other molecules exhibited less activity than alizarin-2-*O*-*β*-D-glucoside, we did not require further structural elucidation of these compounds.

This study provides a comprehensive view of the modification of anthraquinones via biotransformation approach, expressing glycosyltransferase in *E. coli* strain. Anticancer activities of these compounds were assayed against three different cancer cell lines. Among the synthesized derivatives of anthraquinones, alizarin-2-*O*-*β*-D-glucoside was the most effective comparatively in low concentration. This compound could be further investigated in vivo to validate its further potency.

4. Materials and Methods

4.1. General Procedures

Anthraquinones (2-amino-3-hydroxyanthraquinone, anthraflavic acid, and alizarin) were purchased from Tokyo Chemical Industry (Tokyo, Japan). All other chemicals and reagents were of highest chemical grade. *E. coli* BL21 (DE3, Stratagene, La Jolla, CA, USA) was used as expression and biotransformation hosts. Restriction enzymes were used either from Takara Bio. Inc. (Kusatsu, Japan) or Promega (Madison, WI, USA). Luria-Bertani (LB) plates and broth media supplemented with an appropriate antibiotic (kanamycin 50 μg/mL) was used for the *E. coli* growth, colony selection, culture preparation, and biotransformation. Fermentation was conducted in LB medium to enhance production and collection for biological activity.

4.2. Vectors and Recombinant Strains

The previously constructed recombinant vector pET28a-YjiC [36] was used for recombinant strain construction. The vector was confirmed by restriction endonuclease activity digestion with *Bam*HI/*Xho*I, followed by transformation into wild type *E. coli* BL21 (DE3) for biotransformation study.

4.3. Culture Preparation and Whole Cell Biotransformation

Seed culture of *E. coli* strains harboring pET28a-YjiC was prepared in 5 mL LB medium supplemented with 50 μg/mL kanamycin for the maintenance of recombinants in each case, and was then incubated overnight at 37 °C. Approximately 500 μL of seeds were transferred to the same medium (50 mL) and incubated at 37 °C until the cells' optical density reached 600 nm (OD_{600nm}) reached 0.5–0.7, 0.5 mM isopropyl *β*-D-1-thiogalactopyranoside (IPTG) was added to induce protein expression, followed by incubation for 18 h at 20 °C. Since substrates such as 2-amino-3-hydroxyanthraquinone, anthraflavic acid, and alizarin are dissolved in DMSO, we prepared 50 mM stock of each substrate for exogenous supply to the 20 h incubated induced culture prepared. Each substrate at a concentration of 0.2 mM was fed and was allowed to biotransform into the respective products. At the same time, in each case, recombinant strains expressing only vector pET28a(+) without the gene were also fed by the same concentration of anthraquinones as that for the control experiment. After 60 h of incubation, all biotransformation cultures (including controls) were harvested by transforming into a separating funnel followed by the addition of double volume of ethyl acetate and vertical shaking for 30 min then the aqueous and organic layers of the cultures were allowed to settle for another 30 min. The organic ethyl acetate layer in each case was transferred and evaporated using a rotatory evaporator. The final remaining sample was dissolved in 1 mL methanol. This sample was directly analyzed using a high performance liquid chromatogram connected to a photo diode array (HPLC-PDA) and high-resolution quadruple time-of-flight electrospray ionization-mass spectrometry (HQ-QTOF ESI/MS) analysis.

4.4. Whole Cell Biocatalysis in Bioreactor

The recombinant strain of *E. coli* BL21 (DE3) harboring pET28a-YjiC was cultured and the seed was prepared for fermentation. Fermentation was conducted under aerobic condition in LB medium, supplementing glucose as the carbon source. Most protocols followed were similar to those described in our previous reports [20,37]. For the production of anthraquinones glucoside on a large scale, we used a 5-L fermentor system (Biotron, Incheon, Korea). We prepared 3-L of LB medium for fermentation. The seed culture of the recombinant strain expressing glycosyltransferase was cultured in a shake flask (100 mL medium) as an inoculum for the fermentor. Culture was grown overnight at 37 °C in a shaking incubator. For fermentation, the pH meter and the dissolved oxygen (DO) probe were calibrated according to the manufacturer's protocol. The pH was maintained at 7.0 through the process, using commercially available ammonium hydroxide, while the DO level was maintained at >95% during the entire fermentation period. When the optical density of the culture at 600 nm reached 10, the culture was induced by lactose and the temperature was lowered to 20 °C. After 6 h of

culture induction, 240 mg of anthraquinone including 2-amino-3-hydroxyanthraquinone, anthraflavic acid, and alizarin (approximately 0.3 mM final concentration) was added to the culture medium for biotransformation. The fermentor was continuously run for 60 h, maintaining the DO and pH, as mentioned. In each 12-h interval, 100 mL of 50% glucose (autoclaved) was supplied as the carbon source for proper growth. At the end of fermentation, the culture medium was harvested, adding a double volume of ethyl acetate in a separating funnel while vigorously shaking. The aqueous and organic layers were then left to settle. The organic layer was then evaporated using a rotary evaporator to concentrate the samples. The final samples were dissolved in methanol and subjected to purify the products using preparative-HPLC.

4.5. Analytical Procedures

From the samples prepared, 20 μL volume was injected and directly analyzed by HPLC-PDA (Shimadzu, Kyoto, Japan; SPD-M20A Detector) using a reverse phase C_{18} column (Mightysil-RP-18GP, 250 × 4.6mm, Kanto Chemical, Tokyo, Japan). The binary mobile phase was composed of solvent A (HPLC grade water + 0.05% trifluoro acetic acid) and solvent B (100% acetonitrile). The total flow rate was maintained as 1 mL/min for a 35-min program. ACN concentrations were 10% (0–10 min), 20% (10–25 min), 100% (25–28 min), 70% (28–30 min), and 10% (30–35 min).

Products were purified by prep-HPLC with a C_{18} column (YMC-Pack ADS-AQ (250 × 20 mm I.D., 10 μm) connected to a UV detector set at 420 nm using a 35 min binary program with ACN concentrations. The ACN concentrations were as follows: 10% (0–10 min), 20% (10–15 min), 50% (15–20 min), 70% (20–25 min), 90% (25–30 min), 50% (30–34 min), and 20% (34–35 min). Purified products were then completely dried in a lyophilizer and used for structural elucidation and bioactivity.

High resolution quadruple time-of-flight electrospray ionization-mass spectrometry (HQ-QTOF ESI/MS) spectra were obtained on ACQUITY (UPLC; Waters, Milford, MA, USA) coupled with SYNAPT G2-S (Waters, Milford, MA, USA). For structural elucidation of biotransformed metabolites, samples including the standards were dissolved in dimethyl-sulfoxide-d_6 (Sigma-Aldrich, St. Louis, MO, USA). Nuclear magnetic resonance (NMR) was conducted by analyzing ^{1}H-, ^{13}C-NMR with two 2D NMR spectroscopies (heteronuclear single-quantum correlation [HSQC] and heteronuclear multiple-bond correlation [HMBC]). Standard molecules were analyzed using a 300 MHz Bruker BioSpin NMR instrument (Karlsruhe, Germany). Structures of metabolites were elucidated using MestReNova 11.0 program (Mestrelab Research S.L., Santiago de Compostela, Spain).

4.6. Inhibitory Effects of Derivatives on Cancer Cell Growth

Gastric carcinoma cells (AGS) were maintained at the Roswell Park Memorial Institute (RPMI) 1640 medium containing 10% fetal bovine serum (FBS). Cervical carcinoma (HeLa) and hepatocarcinoma cells (HepG2) were grown in Dulbecco's modified Eagle's medium (DMEM) supplemented with 10% FBS. All cells were maintained at 37 °C in a humidified 5% CO_2 incubator. For cell growth assay, various cancer cells were plated at 2×10^3 cells/well in 96-well culture plates. Compounds were added to each well with various concentrations, and the cells were incubated for 72 h. Cell growth was measured using a 3-(4,5-dimethylthiazol-2-yl)-2,5-diphenyltetrazolium bromide (MTT) colorimetric assay. 50 μL of MTT (2 mg/mL stock solution) was added and the plates were incubated for an additional 4 h. After removal of the medium, 100 μL of DMSO was added. Absorbance was measured at 540 nm using a Multiskan® Spectrum microplate spectrophotometer (Thermo Scientific, Waltham, MA, USA,).

Supplementary Materials: The following are available online at, Figure S1: Comparison of glucose concentration based on the recombinant strain in 48 h incubation. Maximum conversion of anthraquinone to respective anthraquinone glycosides were achieved while supplementing 4% additional glucose in the medium. (A) Alizarin; (B) Anthraflavic acid; (C) 2-amino 3-hydroxyanthraquinone. S stands for substrate peak while P stands for product, Figure S2: ^{1}H-NMR of alizarin, Figure S3: ^{13}C-NMR of alizarin, Figure S4: ^{1}H-NMR of alizarin-2-*O*-*β*-D-glucoside, Figure S5: ^{13}C-NMR of alizarin-2-*O*-*β*-D-glucoside, Figure S6: HSQC correlation of alizarin 2-*O*-*β*-D-glucoside, Figure S7: HMBC correlation of alizarin 2-*O*-*β*-D-glucoside.

Author Contributions: T.T.H.N. conceived and designed the experiments. J.M.H. performed the anticancer activity experiments. T.T.H.N. and P.P. performed other experiments, analyzed the data and wrote the manuscript. H.J.J., R.P.P. and Y.I.P. revised the manuscript. J.K.S. revised the manuscript and is supervision. All authors read and approved the final manuscript.

Funding: This work was supported by a grant from the Next-Generation BioGreen 21 Program (SSAC, grant#: PJ013137 (JKS), PJ013206 (YIP)), Rural Development Administration, Korea.

Conflicts of Interest: The authors declare no conflict of interest.

References

1. Dave, H.; Ledwani, L. A review on anthraquinones isolated from Cassia species and their applications. *Indian J. Nat. Prod. Resour.* **2012**, *3*, 291–319.
2. Kanokmedhakul, K.; Kanokmedhakul, S.; Phatchana, R. Biological activity of Anthraquinones and Triterpenoids from *Prismatomeris fragrans*. *J. Ethnopharmacol.* **2005**, *100*, 284–288. [CrossRef] [PubMed]
3. Kosalec, I.; Kremer, D.; Locatelli, M.; Epifano, F.; Genovese, S.; Carlucci, G.; Randic, M.; Zovko Koncic, M. Anthraquinone profile, antioxidant and antimicrobial activity of bark extracts of *Rhamnus alaternus*, *R. fallax*, *R. intermedia* and *R. pumila*. *Food Chem.* **2013**, *136*, 335–341. [CrossRef] [PubMed]
4. Sittie, A.A.; Lemmich, E.; Olsen, C.E.; Hviid, L.; Kharazmi, A.; Nkrumah, F.K.; Christensen, S.B. Structure-activity studies: In vitro antileishmanial and antimalarial activities of anthraquinones from *Morinda lucida*. *Planta Med.* **1999**, *65*, 259–261. [CrossRef] [PubMed]
5. Rath, G.; Ndonzao, M.; Hostettmann, K. Antifungal anthraquinones from *Morinda lucia*. *Int. J. Pharmacogn.* **1995**, *33*, 107–114. [CrossRef]
6. Younos, C.; Rolland, A.; Fleurentin, J.; Lanhers, M.; Misslin, R.; Mortier, F. Analgesic and Behavioural Effects of *Morinda citrifolia*. *Planta Med.* **1990**, *56*, 430–434. [CrossRef] [PubMed]
7. Koumaglo, K.; Gbeassor, M.; Nikabu, O.; de Souza, C.; Werner, W. Effects of three compound extracted from *Morinda lucida* on *Plasmodium falciparum*. *Planta Med.* **1991**, *58*, 533–534. [CrossRef] [PubMed]
8. Akhtar, M.N.; Zareen, S.; Yeap, S.K.; Ho, W.Y.; Lo, K.M.; Hasan, A.; Alitheen, N.B. Total synthesis, cytotoxic effects of damnacanthal, nordamnacanthal and related anthraquinone analogues. *Molecules* **2013**, *18*, 10042–10055. [CrossRef] [PubMed]
9. Ismail, N.H.; Mohamad, H.; Mohidin, A.; Lajis, N.H. Antioxidant activity of anthraquinones from *Morinda elliptica*. *Nat. Prod. Sci.* **2002**, *8*, 48–51.
10. Al-Otaibi, J.S.; EL Gogary, T.M. Synthesis of novel anthraquinones: Molecular structure, molecular chemical reactivity descriptors and interactions with DNA as antibiotic and anti-cancer drugs. *J. Mol. Struct.* **2017**, *1130*, 799–809. [CrossRef]
11. Feng, Y.; Huang, S.; Dou, W.; Zhang, S.; Chen, J.H.; Shen, Y.; Shen, J.H.; Leng, Y. Emodin, a natural product, selectively inhibits 11β-hydroxysteroid dehydrogenase type 1 and ameliorates metabolic disorder in diet-induced obese mice. *Br. J. Pharmacol.* **2010**, *161*, 113–126. [CrossRef] [PubMed]
12. Alam, Z.; Al-Mahdi, Z.; Zhu, Y.; McKee, Z.; Parris, D.S.; Parikh, H.I.; Kellogg, G.E.; Kuchta, A.; McVoy, M.A. Anti-cytomegalovirus activity of the anthraquinone atanyl blue PRL. *Antivir. Res.* **2015**, *114*, 86–95. [CrossRef] [PubMed]
13. Srinivas, G.; Babykutty, S.; Sathiadevan, P.P.; Srinivas, P. Molecular mechanism of emodin action: Transition from laxative ingredient to an antitumor agent. *Med. Res. Rev.* **2007**, *27*, 591–608. [CrossRef] [PubMed]
14. Twycross, R.; Sykes, N.; Mihalyo, M.; Wilcock, A. Stimulant Laxatives and Opioid-Induced Constipation. *J. Pain Symptom Manag.* **2012**, *43*, 306–313. [CrossRef] [PubMed]
15. Hunger, K. *Industrial Dyes: Chemistry, Properties, Applications*; Wiley-VCH: Weinheim, Germany, 2003.
16. Huang, Q.; Lu, G.; Shen, H.M.; Chung, M.C.M.; Choon, N.O. Anti-cancer properties of anthraquinones from rhubarb. *Med. Res. Rev.* **2007**, *27*, 609–630. [CrossRef] [PubMed]
17. Malik, E.M.; Müller, C.E. Anthraquiononones as pharmacological tools and drugs. *Med. Res. Rev.* **2016**, *36*, 705–748. [CrossRef] [PubMed]
18. Madje, B.R.; Shelke, K.F.; Sapkal, S.B.; Kakade, G.K.; Shingare, M.S. An efficient one-pot synthesis of anthraquinone derivatives catalyzed by alum in aqueous media. *Green Chem. Lett. Rev.* **2010**, *3*, 269–273. [CrossRef]

19. Seidel, N.; Hahn, T.; Lirbing, S.; Seichter, W.; Kortus, J.; Weber, E. Synthesis and properties of new 9,10-anthraquinone derived compounds for molecular electronics. *New J. Chem.* **2013**, *37*, 601–610. [CrossRef]
20. Pandey, R.P.; Li, T.F.; Kim, E.H.; Yamaguchi, T.; Park, Y.I.; Kim, J.S.; Sohng, J.K. Enzymatic synthesis of novel phloretin glucosides. *Appl. Environ. Microbiol.* **2013**, *79*, 3516–3521. [CrossRef] [PubMed]
21. Pandey, R.P.; Malla, S.; Simkhada, D.; Kim, B.G.; Sohng, J.K. Production of 3-*O*-xylosyl quercetin in *Escherichia coli*. *Appl. Microbiol. Biotechnol.* **2013**, *97*, 1889–1901. [CrossRef] [PubMed]
22. Parajuli, P.; Pandey, R.P.; Trang, N.T.H.; Chaudhary, A.K.; Sohng, J.K. Synthetic sugar cassettes for the efficient production of flavonol glycosides in *Escherichia coli*. *Microb. Cell Fact.* **2015**, *14*, 76. [CrossRef] [PubMed]
23. Pandey, P.; Parajuli, P.; Shin, J.Y.; Lee, J.; Lee, S.; Hong, Y.S.; Park, Y.I.; Kim, J.S.; Sohng, J.K. Enzymatic biosynthesis of novel resveratrol glucoside and glycoside derivatives. *Appl. Environ. Microbiol.* **2014**, *80*, 7235–7243. [CrossRef] [PubMed]
24. Kalidhar, S.B. Structural elucidation in anthraquinones using ^{1}H NMR glycosylation and alkylation shifts. *Phytochemistry* **1989**, *28*, 3459–3463. [CrossRef]
25. Manojlovic, N.T.; Solujic, S.; Sukdolak, S.; Krstic, L.J. Isolation and antimicrobial activity of anthraquinone from some species of the lichen genus Xanthoria. *J. Serb. Chem. Soc.* **2000**, *65*, 555–560. [CrossRef]
26. Chien, S.C.; Wu, Y.C.; Chen, Z.W.; Yang, W.C. Naturally occurring anthraquinones: Chemistry and therapeutic potential in autoimmune diabetes. *Evid. Based Complement. Altern. Med.* **2015**, *2015*, 357357. [CrossRef] [PubMed]
27. Gürses, A.; Açıkyıldız, M.; Güneş, K.; Sadi Gürses, M. *Dyes Pigments*; Springer: Basel, Switzerland, 2016; p. 88.
28. Chen, Q. Development of an anthraquinone process for the production of hydrogen peroxide in a trickle bed reactor-From bench scale to industrial scale. *Chem. Eng. Process. Process Intensif.* **2008**, *47*, 787–792. [CrossRef]
29. Wink, M. Biochemistry of Plant Secondary Metabolism. In *Annual Plant Reviews*, 2nd ed.; Wiley-Blackwell: Oxford, UK, 2010; Volume 40, pp. 483–485.
30. Duval, J.; Pecher, V.; Poujol, M.; Lesellier, E. Research advances for the extraction, analysis and uses of anthraquinones: A review. *Ind. Crops Prod.* **2016**, *94*, 812–833. [CrossRef]
31. Brachmann, A.O.; Joyce, S.A.; Kodama, H.J.; Schwar, G.; Clarke, D.J.; Bode, H.B. A type II polyketide synthase is responsible for anthraquinone biosynthesis in *Photorhabdus luminescens*. *ChemBioChem* **2007**, *8*, 1721–1728. [CrossRef] [PubMed]
32. Pandey, R.P.; Parajuli, P.; Koffas, M.A.G.; Sohng, J.K. Microbial production of natural and non-natural flavonoids: Pathway engineering, directed evolution and systems/synthetic biology. *Biotechnol. Adv.* **2016**, *34*, 634–662. [CrossRef] [PubMed]
33. Pandey, R.P.; Gurung, R.B.; Parajuli, P.; Koirala, N.; Tuoi, L.T.; Sohng, J.K. Assessing acceptor substrate promiscuity of YjiC-mediated glycosylation toward flavonoids. *Carbohydr. Res.* **2014**, *393*, 26–31. [CrossRef] [PubMed]
34. Parajuli, P.; Pandey, R.P.; Pokhrel, A.R.; Ghimire, G.P.; Sohng, J.K. Enzymatic glycosylation of the topical antibiotic mupirocin. *Glycoconj. J.* **2014**, *31*, 563–572. [CrossRef] [PubMed]
35. Ghimire, G.P.; Koirala, N.; Pandey, R.P.; Jung, H.J.; Sohng, J.K. Modification of emodin and aloe-emodin by glycosylation in engineered *Escherihia coli*. *World J. Microbiol. Biotechnol.* **2015**, *31*, 611–619. [CrossRef] [PubMed]
36. Zhang, W.; Ye, M.; Zhan, J.; Chen, Y.; Guo, D. Microbial glycosylation of four free anthraquinones by *Absidia coerulea*. *Biotechnol. Lett.* **2004**, *26*, 127–131. [CrossRef] [PubMed]
37. Nam, W.; Kim, S.; Nam, S.; Friedman, M. Structure-Antioxidative and Anti-Inflammatory Activity Relationships of Purpurin and Related Anthraquinones in Chemical and Cell Assays. *Molecules* **2017**, *22*, 265. [CrossRef] [PubMed]

Sample Availability: Samples of the compounds are available from the authors.

molecules

MDPI

Article

Zeylenone Induces Mitochondrial Apoptosis and Inhibits Migration and Invasion in Gastric Cancer

Shuxian Yang, Yonghong Liao, Liyong Li, Xudong Xu and Li Cao *

Institute of Medicinal Plant Development, Chinese Academy of Medical Sciences & Peking Union Medical College, Beijing 100193, China; Yangshuxianlove@163.com (S.Y.); yhliao@implad.ac.cn (Y.L.); lly0916@sina.com (L.L.); xdxu@implad.ac.cn (X.X.)

* Correspondence: lcao@implad.ac.cn; Tel.: +86-10-57833222

Received: 8 August 2018; Accepted: 23 August 2018; Published: 27 August 2018

Abstract: The mortality of gastric cancer (GC) is increasing due to its high rates of recurrence and metastasis. Zeylenone (Zey), a type of naturally occurring cyclohexene oxide, was demonstrated to be effective in cancer patients. The aim of this study is to explore the anti-cancer effect of Zey against gastric cancer both in vitro and in vivo, as well as the underlying mechanisms. We found that Zey inhibited gastric tumor growth, as demonstrated by in vitro gastric cancer cell lines and in a human gastric cancer xenograft mouse model. Furthermore, Zey induced substantial apoptosis through a mitochondrial apoptotic pathway, involving mitochondrial transmembrane potential loss, caspase-3 activation, anti-apoptotic protein downregulation, and pro-apoptotic protein upregulation. Notably, we revealed for the first time that Zey suppressed invasion and migration by wound healing and transwell chamber assays. Through Western blotting, we further explored the potential mechanism of Zey's anti-cancer activity. We found that Zey downregulated the expression of matrix metalloproteinase 2/9 (MMP 2/9) and inhibited the phosphorylation of AKT and ERK. In short, Zey, which induced mitochondrial apoptosis and inhibited proliferation, migration, and invasion, may be developed as a novel drug for the treatment of gastric cancer.

Keywords: Zeylenone; gastric cancer; invasion; migration; apoptosis

1. Introduction

Gastric cancer (GC) represents a health threat as the fourth most common cancer and the second leading cause of cancer death worldwide [1,2]. Studies showed that more than 950,000 new diagnoses are made every year, and an estimated 720,000 patients died from gastric cancer in 2012 [3]. Even with the rapid improvement of healthcare and detection [4], gastric cancer is still a nightmare, and the relative five-year survival rates for GC are only about 20% in most areas of the world [5]. Thus, the burden of gastric cancer remains high, especially in Asia, Latin America, and central and eastern Europe [6]. Furthermore, gastric cancer is characterized by uncontrolled cell proliferation and metastasis [2]. Therefore, most patients do not die due to the primary cancer, but from metastatic cancer [7]. However, research into the field of metastasis, compared with other key events such as proliferation, is lacking. Hence, identifying new drugs with anti-metastasis and anti-proliferation characteristics is now the focus in GC treatment.

Naturally occurring bioactive phytochemicals with low toxicity emerged as promising options for the development of effective alternatives for conventional treatments. Zeylenone (Zey) [8], isolated from ethanol extracts of the leaves of *Uvaria grandiflora* Roxb., is a cyclohexene oxide [9], which exhibits anti-cancer activity and is regarded as a soft drug. In 2010–2012, we successfully attained mPEG-PLGA-loaded Zeylenone nanomicelles, which improved the solubility and stability of Zey and achieved sustained release. The drug-loaded micelles were also characterized in terms of drug encapsulation, dynamic size, zeta potential, drug stability, and release, involving not just in vitro

release assays, but also in vivo pharmacokinetic studies [8]. In addition, previous studies by our group indicated that Zey displayed strong cytotoxic activity against acute lymphoblastic leukemia cells [10] and cervical cancer cells [11] in a dose-dependent manner, indicating its strong antitumor activity. However, to the best of our knowledge, the effect of Zey on gastric cancer is yet to be studied in detail, especially the effect of Zey on gastric cancer invasion and migration.

In view of the above, there is an interest in studying the potential effects and mechanisms of Zey against GC. In this study, we found that Zey inhibited gastric tumor growth, as demonstrated by in vitro gastric cancer cell lines and in a human gastric cancer xenograft mouse model. Our further studies revealed that Zey induced substantial apoptosis of GC cells, which was associated with the mitochondrial apoptotic pathway. In addition, Zey also suppressed the invasion and migration of gastric cancer cells by wound healing and transwell chamber assays.

The activation of the AKT and ERK pathway is necessary for tumor initiation and progression, including cell growth, metastasis, and resistance to chemotherapy [12]; thus, these pathways are worth studying [13]. ERK is an important member of the MAPK family, which plays a central role in regulating the expressions of matrix metalloproteinases (MMPs) [14]. MMPs, a family of zinc-dependent neutral endopeptidases, are involved in the metastasis of cancer because of their ability to hydrolyze various extracellular matrix (ECM) components [15]. Of note, MMP-2 and MMP-9 can degrade most ECM components, accelerating metastasis [16]. Through Western blotting, we further explored the potential mechanism of Zey's anti-cancer activity. We found that Zey suppressed the metastasis of gastric cancer cells by decreasing protein levels of MMP-2 and MMP-9 and inhibiting the phosphorylation of AKT, ERK, and mTOR. According to the above experimental results, we conclude that Zey may be developed into a novel therapeutic agent for gastric cancer treatment due to its strong ability to inhibit migration and invasion and to induce apoptosis.

2. Results

2.1. Zey Inhibits Gastric Cancer Cell Proliferation

The chemical structure of Zey is shown in Figure 1A. An MTT assay and colony formation assay were performed to determine the anti-proliferative effect of Zey on SGC7901 and MGC803 cells. As shown in Figure 1B,C, Zey treatments reduced the cell viability of the SGC7901 and MGC803 cells in a dose-dependent manner without severe toxicity to normal gastric epithelial cells (GES-1). Similar results from a colony formation assay confirmed that Zey-treated groups exhibited smaller and fewer colonies compared to untreated cells (Figure 1D,E). However, low concentrations of Zey (<3 μM) did not significantly inhibit cell viability. IC_{50} values of Zey were detected as 13.21 μM for SGC7901 cells and 13.42 μM for MGC803 cells. These data together indicated that Zey has anti-proliferation activity in gastric cancer cells.

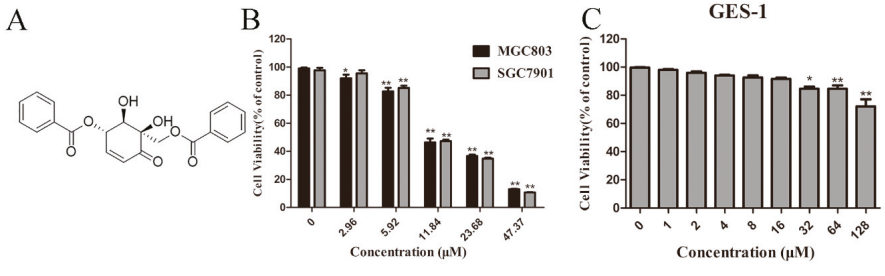

Figure 1. *Cont.*

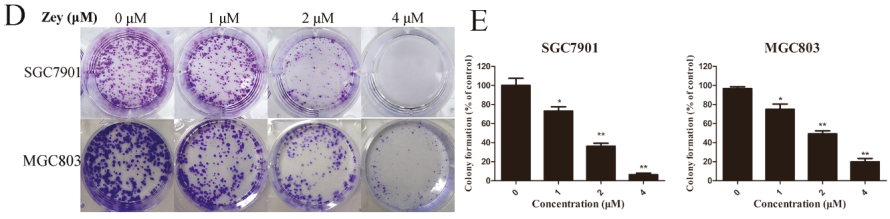

Figure 1. Zeylenone (Zey) effectively suppresses cell viability and colony formation in SGC7901 and MGC803 cells. (**A**) Chemical structure of Zey. (**B**) Zey suppresses the viability of SGC7901 and MGC803 cells determined in an MTT assay. Cells were treated with Zey (0, 2.96, 5.92, 11.84, 23.68, or 47.37 μM) for 24 h. Data are expressed as means ± SD of three distinct experiments. The cell viability of the control (DMSO only) is indicated as 100%. * $p < 0.05$ and ** $p < 0.01$ vs. control cells. (**C**) Zey suppresses the viability of normal gastric epithelial (GES-1) cells determined in an MTT assay. GES-1 cells were treated with Zey (0, 1, 2, 4, 8, 16, 32, 64, or 128 μM) for 24 h. Data are expressed as means ± SD of three distinct experiments. * $p < 0.05$ and ** $p < 0.01$ vs. control cells. (**D**) Representative images of colonies after SGC7901 and MGC803 cells were treated with Zey for 12 days. (**E**) Statistical analysis of colony numbers from three independent experiments. * $p < 0.05$ and ** $p < 0.01$ vs. control cells.

2.2. Zey Induces Gastric Cancer Cell Apoptosis

We further evaluated whether Zey inhibited cell proliferation by inducing cancer cell apoptosis. Firstly, Hoechst 33258 staining was used to study the morphological changes of GC cells. Based on IC_{50} values, we chose 3.3, 6.6, and 13.2 μM as treatments for GC cells. After Hoechst 33258 staining, an increased number of cells with bright nuclear condensation or fragmented nuclei, which was regarded as characteristic of cell apoptosis, was observed after Zey treatment, while control cells exhibited round nuclei and the chromatin were well distributed (Figure 2A).

Next, we further assessed apoptosis using annexin V-FITC/PI apoptosis staining. After treatment with Zey for 12 h, the apoptosis rate significantly increased in a dose-dependent manner in SGC7901 and MGC803 cells (Figure 2B–E). With the treatment time of Zey extended to 24 h, at 13.2 μM, the apoptosis rates of SGC7901 and MGC803 cells reached up to 48.21% and 64.58% ($p < 0.01$), respectively. Thus, Zey induced gastric carcinoma cell apoptosis in a dose- and time-dependent manner.

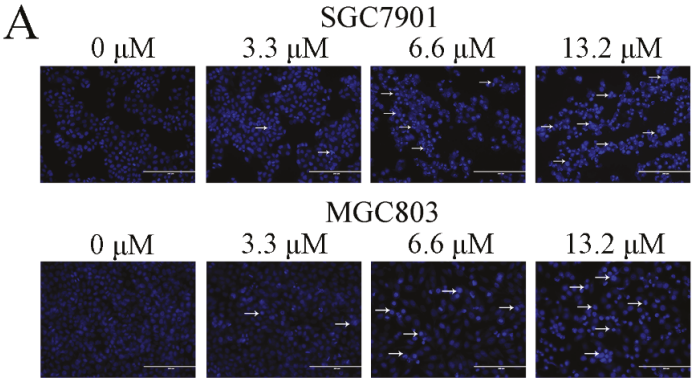

Figure 2. *Cont.*

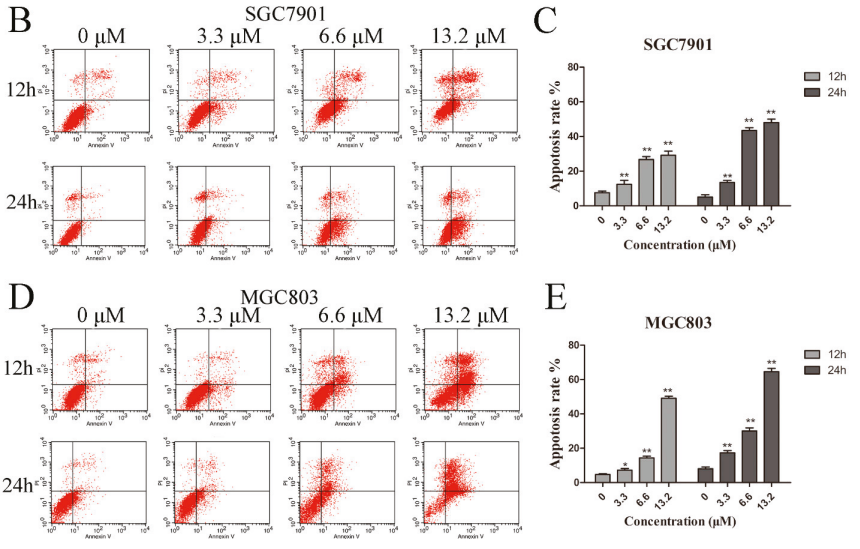

Figure 2. Zey induces apoptosis in SGC7901 and MGC803 cells. (**A**) Morphological changes of apoptosis were detected by Hoechst 33258 staining. Images are shown under a fluorescence microscope with a magnification of 200×. (**B**,**C**) Apoptosis of SGC7901 cells detected by the Annexin V-FITC/PI staining test and the ratio of apoptotic cells. The data represented the means ± SD for triplicate determinations. * $p < 0.05$ and ** $p < 0.01$ vs. control cells. (**D**,**E**) Apoptosis of MGC803 cells detected by the Annexin V-FITC/PI staining test and the ratio of apoptotic cells, including early apoptotic cells (lower right quadrant) and late apoptotic cells (upper right quadrant). The data represented the means ± SD for triplicate determinations. * $p < 0.05$ and ** $p < 0.01$ vs. control cells.

2.3. Zey Induces Apoptosis in Gastric Cancer Cells via the Mitochondrial Apoptosis Pathway

To understand the underlying mechanism via which Zey induces apoptosis in GC cells, we investigated changes in the mitochondrial membrane potential and the level of corresponding proteins involved in apoptosis.

Initially, cells treated with or without Zey were stained with JC-1, and the changes in mitochondrial membrane potential were analyzed by flow cytometry. As shown in Figure 3A,B, when the concentration of Zey was 3.3 μM, the effect was obvious neither in SGC7901 cells nor in MGC803 cells. However, Zey treatment at 13.2 μM induced a loss of mitochondrial membrane potential ($p < 0.01$).

Next, we further measured the effect of Zey on proteins related to apoptosis with Western blotting (Figure 3C). Zey treatment induced a significant decline in anti-apoptotic proteins Bcl-xl and Bcl-2 while significantly increasing the pro-apoptotic protein Bax. Consistently, Zey treatment markedly decreased the levels of pro-caspase-3, indicating that Zey treatment induced gastric cancer cell apoptosis via caspase-3 activation and the involvement of anti-apoptotic proteins Bcl-xl and Bcl-2 and pro-apoptotic protein Bax.

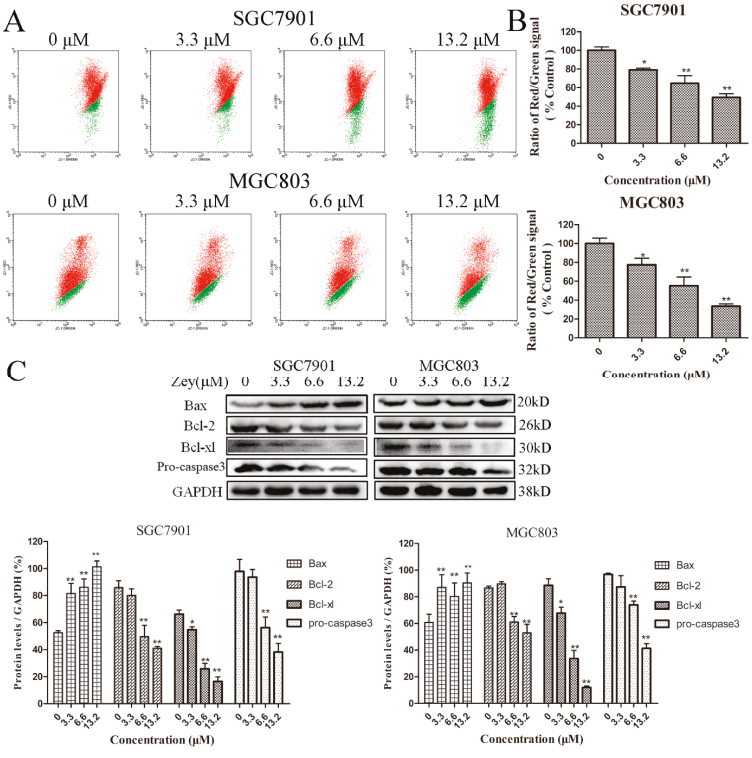

Figure 3. Zey induces apoptosis of SGC7901 and MGC803 cells through the initiation of the mitochondrial pathway. (**A**) Zey induced a loss of mitochondrial membrane potential in SGC7901 and MGC803 cells. Cells were treated with increasing concentrations of Zey for 24 h, and mitochondrial membrane potential was analyzed by flow cytometry after cells were stained with JC-1. (**B**) Quantitative analysis of the ratio of red to green fluorescence. The data represented the means ± SD for triplicate determinations. * $p < 0.05$ and ** $p < 0.01$ vs. control cells. (**C**) Apoptosis-related protein expression was detected by Western blot analysis in SGC7901 and MGC803 cells. Cells were incubated with Zey (0, 3.3, 6.6, or 13.2 μM) for 24 h, and whole-cell lysates were analyzed. The data represented the means ± SD for triplicate determinations. * $p < 0.05$ and ** $p < 0.01$ vs. control cells.

2.4. Zey Inhibits the Migration and Invasion of Gastric Cancer Cells

Previous studies demonstrated that cancer metastasis is highly related to cellular motility and degradation of the ECM [17]. We first examined the effect of Zey on motility in gastric cancer cells using a wound-healing assay. According to the cell viability data (Figure 1B), we chose Zey concentrations at 1, 2, and 4 μM (with a cell viability rate >93%). As shown in Figure 4A,B, the wound-healing ability in SGC7901 cells decreased gradually in a dose-dependent manner with raised concentrations of Zey, consistent with the results in MGC803 cells. Of note, when the concentration of Zey increased to 2 μM and 4 μM, the wound-healing rates of SGC7901 and MGC803 cells were reduced to 20.50% and 25.82% at 2 μM and to 17.94% and 13.62% at 4 μM, respectively. At a low concentration (1 μM), the effect was not as significant ($p > 0.05$).

Next, the effect of Zey on migration and invasion was also further determined with a transwell chamber assay. After treatment with Zey (0, 1, 2, or 4 μM) for 24 h, the number of Zey-treated SGC7901 cells that invaded the lower chamber was significantly less than the control group ($p < 0.01$,

Figure 4C,D). At 4 μM, the invasion and migration rates of SGC7901 were 17.6% and 10.5%, respectively. Then, the same effects were also discovered in MGC803 cells, with percentages of 25.7% and 21.1%, respectively. It can be seen that the effect of Zey on inhibiting invasion and migration in MGC803 cells was not as obvious as in SGC7901 cells. Collectively, these findings showed that Zey could inhibit migration and invasion of GC cells in a dose-dependent manner.

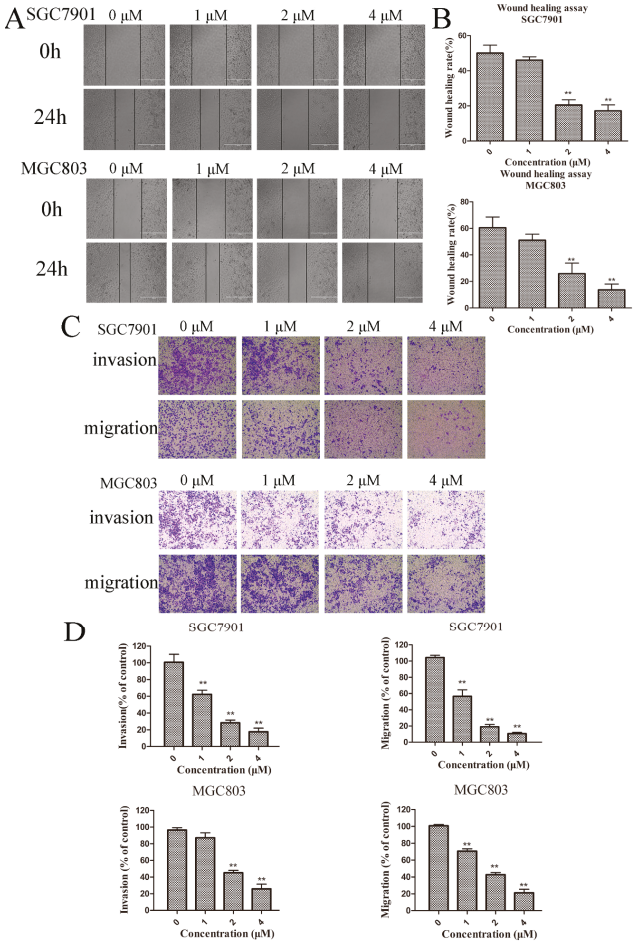

Figure 4. Zey inhibits the migration and invasion in SGC7901 and MGC803 cells. (**A**) Wound-healing assay in SGC7901 and MGC803 cells. After making a linear wound, cells were incubated with different concentrations of Zey (0, 1, 2, or 4 μM) in serum-free RPMI-1640 for an additional 24 h. Wound healing was photographed at 0 and 24 h using a microscope with a magnification of 100×. (**B**) Quantitative analysis of the ratio of wound healing. The data represented the means ± SD for triplicate determinations. * $p < 0.05$ and ** $p < 0.01$ vs. control cells. (**C**) Invasion and migration assay in SGC7901 and MGC803 cells. Images are shown under a light microscope with a magnification of 100×. (**D**) Quantitative analysis of the ratio of invasion/migration in SGC7901 and MGC803 cells. The data represented the means ± SD of three distinct experiments. The control cells were regarded as 100% in the invasion/migration index calculation. * $p < 0.05$ and ** $p < 0.01$ vs. control cells.

2.5. Zey Attenuates AKT/MMP2/MMP9 and ERK Signaling Pathways in Gastric Cancer Cells

To further understand the experimental results mentioned above, we continued exploring the possible mechanisms with Western blotting, particularly with MMP-2 and MMP-9 [18]. As shown in Figure 5A,B, Zey (6.6 and 13.2 μM) treatment significantly reduced the expressions of MMP-2 and MMP-9 compared with the control group ($p < 0.01$). With the concentration of Zey increased to 6.6 μM and 13.2 μM, the inhibitory effect on the activity of MMP-2 and MMP-9 appeared to be more obvious. Activation of AKT accelerated cancer progression and distant metastasis. Our result showed that Zey blocked the phosphorylation of AKT and ERK in SGC7901 and MGC803 cells, and the result was consistent between SGC7901 and MGC803 cells. Collectively, these data indicated that the antitumor effect of Zey on SGC7901 and MGC803 cells is tightly correlated with the AKT/MMP2/MMP9 and ERK signaling pathways.

2.6. Zey Suppresses Tumor Growth in a Mouse Xenograft Model

To further validate the antitumor activity of Zey in vivo, we developed a xenograft model of GC, and tested the effects of Zey on tumor growth. After treatment with Zey for 10 days, the tumor growth in the Zey treatment groups was significantly slower compared with the control groups (Figure 6A). In detail, no significant difference in the tumor volume of the different groups was observed at the beginning of treatment. At the end of treatment, as expected, the tumor volume was smaller in the Zey (30 mg/kg) groups compared with the control groups ($p < 0.01$), as was paclitaxel. Alternatively, the isolated tumor weight was also remarkably reduced in the Zey-treated group (30 mg/kg) than in the control group (Figure 6B,C). Simultaneously, the tumor inhibition rates of Zey were 47.95% (30 mg/kg) and 48.11% (15 mg/kg) in the paclitaxel group compared to the control group (Figure 6B). Moreover, the mouse body weights in the Zey-treated groups slightly decreased, but not obviously ($p > 0.05$), indicating that Zey was not significantly toxic (Figure 6D). Together, these data indicated that Zey could effectively inhibit gastric tumor growth in vivo. In the in vivo experiments reported here, the Zey was mPEG-PLGA-loaded Zeylenone nanomicelles.

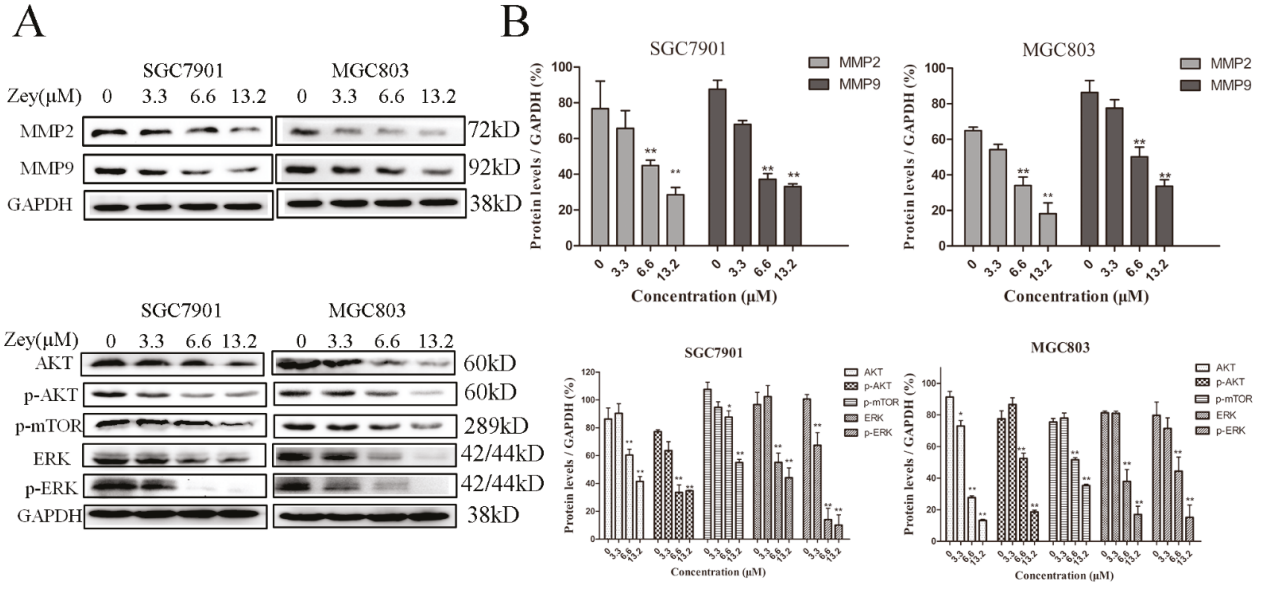

Figure 5. Zey attenuates AKT/matrix metalloproteinase 2 (MMP2)/MMP9, and ERK pathways in SGC7901 and MGC803 cells. (**A**) Immunoblot analyses of AKT, phosphorylated (p)-AKT, MMP-2, MMP-9, p-mTOR, ERK, and p-ERK in Zey-treated SGC7901 and MGC803 cells. (**B**) Quantitative analysis of protein levels. GAPDH was used to confirm equal protein loading. The data represented the means ± SD for triplicate determinations. * $p < 0.05$ and ** $p < 0.01$ vs. control cells.

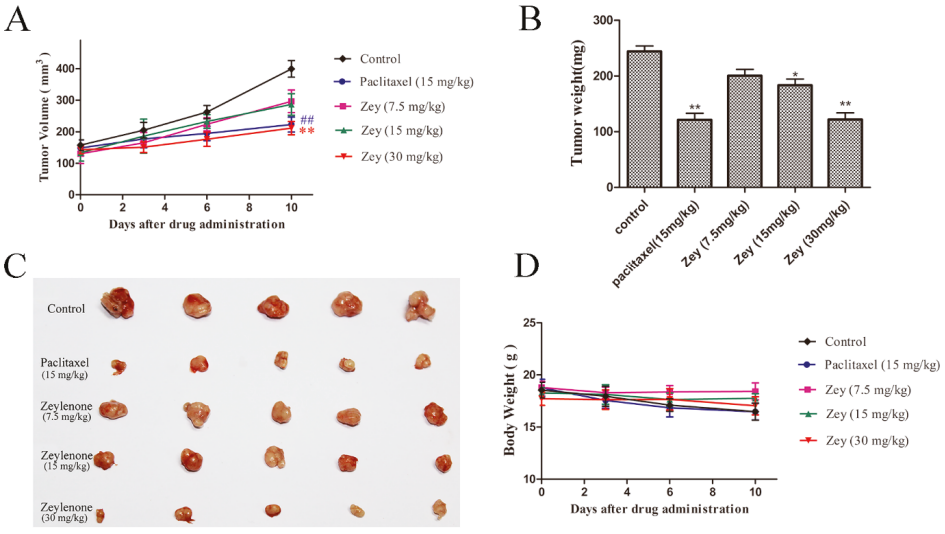

Figure 6. Zey inhibits tumor growth in nude BALB/c mice bearing BGC823 xenografts. BGC823 cells were transplanted subcutaneously to BALB/c nude mice and administered Zey (7.5, 15, and 30 mg/kg), paclitaxel (15 mg/kg), and saline (as the negative control) for 10 days. (**A**) Tumor volume was recorded every two days. Mean ± SD (n = 5). $^{\#\#}$ $p < 0.01$ and ** $p < 0.01$ vs. control group. (**B**) Tumor weight of each group. On day 10 after inoculation, the mice were sacrificed, and the tumor tissues were isolated, weighed, and summarized. Mean ± SD (n = 5). * $p < 0.05$ and ** $p < 0.01$ vs. control group. (**C**) Photographs of tumors in each group. (**D**) Body weight was measured every two days. Mean ± SD (n = 5).

3. Discussion

In the present study, we attempted to identify novel functions of Zey and proposed that Zey may be a potent suppressor of gastric cancer cells. On the other hand, the therapeutic efficacy of Zey against gastric cancer and the potential mechanism remained unclear. Therefore, we evaluated the anti-cancer effects of Zey both in vitro and in a mouse xenograft model and further investigated the underlying mechanisms.

Gastric cancer is one of the most common malignant diseases and ranks second in mortality among all cancers worldwide [19,20]. Although the detection of early gastric cancer improved, long-term survival remains poor. Firstly, Zey showed strong antitumor activity against SGC7901 and MGC803 cells, and therefore, we performed a further and deeper study of Zey in gastric cancer.

Previous studies showed that apoptosis induction played an important role in the inhibition of cancer cells [21]. Relevant studies confirmed that the imbalance between pro-apoptotic proteins, such as Bax, versus anti-apoptotic factors, such as Bcl-2 and Bcl-xl, can result in decreased mitochondrial membrane integrity, leading to the release of cytochrome C and AIF from mitochondria to the cytoplasm. The released cytochrome C then activates caspase, which finally leads to apoptosis [22]. Consistently, in this study, we found that Zey treatment induced apoptosis by dose-dependently decreasing the levels of anti-apoptotic proteins, including Bcl-2 and Bcl-xl, and increasing the expression of the pro-apoptotic protein Bax. Moreover, Zey led to cell apoptosis with the loss of mitochondrial membrane potential, and apoptotic morphological alterations were also observed in GC cells. Taken together, increased apoptosis might be responsible for cancer growth inhibition by Zey [11].

Notably, metastasis, as one of the most important factors of cancer, limits tumor prognosis and increases cancer-related mortality. Therefore, we first found that Zey suppressed both migration and invasion in SGCC7901 and MGC803 cells. To explore the mechanism, we examined the expression of MMPs. Previous studies showed that MMP-2 [23] and MMP-9 [24] were overexpressed in gastric cancer, which accelerated the invasion of tumor cells in vitro and in vivo. In other words, the activation of MMPs led to the spread of tumor cells from their original locations. In our study, we confirmed that Zey treatment markedly reduced MMP-2/9 expression in SGC7901 and MGC803 cells, which implied that Zey, as an inhibitor of MMP expression [25], may be developed into an early treatment to prevent cancer metastasis [26].

In addition, we also focused on the ERK and AKT pathways because they serve critical roles in regulating both the expression of MMPs and cell apoptosis [27]. High expression levels of AKT and phosphorylated (p)-AKT were observed in 74% and 78% of gastric tumors, respectively [28]. Additionally, aberrant AKT activation plays a substantial role in invasion and metastasis. Likewise, ERK is an important member of the MAPK family, which plays a central role in regulating the expressions of MMPs [29]. Based on the above results, we tested the related proteins using Western blot assays. As expected, Zey decreased the expressions of AKT, p-AKT, p-mTOR, ERK, and p-ERK, which may partly account for the proliferative inhibition and suppressive migration observed in the GC cells. However, to some extent, a limitation of our study is that we did not identify the inhibitory target of Zey in these pathways. Therefore, further studies are needed.

To determine whether Zey inhibits tumor growth in vivo, a human gastric cancer xenograft mouse model was used. We found that Zey administered at 30 mg/kg slowed the growth of BGC823 tumors, resulting in a significantly decreased tumor weight on day 10 in the Zey-treated group compared to control mice ($p < 0.01$). Moreover, the treatments of Zey at 30 mg/kg every two days and paclitaxel at 15 mg/kg every two days caused similar proliferation inhibition profiles (inhibition rate at 47.95% and 48.11%, respectively). This was evidence that Zey may be a cytotoxic drug. These findings in vivo were certainly consistent with the observations in vitro and further indicate that Zey may be a potential candidate as an active agent against gastric cancer.

Since Zeylenone was discovered in 1997, we completed pre-clinical studies, including pharmacochemistry [9], structural-activity relationship (SAR) studies [30], drug dosage forms [8], and quantitative analysis of differential protein expression in cervical cancer cells [11]. In the experiments reported here, we mainly discussed the pharmacodynamics and potential mechanism of Zey in gastric cancer. Firstly, we confirmed that Zey inhibited the proliferation of gastric cancer cells in vitro. Then, we went back to the tumor-bearing mice to verify the inhibition of tumor growth in vivo. Finally, we returned to the experiments in vitro again to explore Zey's anti-cancer activity and underlying mechanism. Based on our current preclinical findings, Zey shows promise for development as a novel therapeutic agent in gastric cancer treatment [31]. In the future, when we complete the safety evaluation and pharmacodynamics study, we can go from non-clinical research to clinical research, and we hope that Zey can be used in humans someday.

In summary, our study demonstrated potential effects of Zey on gastric carcinoma using diverse gastric cell lines and a human gastric cancer xenograft mouse model. It may be possible in the future to develop a therapeutic strategy or novel drug for patients with gastric cancer.

4. Materials and Methods

4.1. Materials

Preparations of Zeylenone (Zey) and mPEG-PLGA-loaded Zeylenone nanomicelles were described previously [8]. Zey used for the in vitro studies was stored as 150 mM solutions in DMSO at −20 °C and further diluted to desired working concentrations before use (DMSO concentration <1%). The mPEG-PLGA-loaded Zeylenone nanomicelles used for the in vivo studies were stored in a dry container at room temperature.

RPMI-1640, DMEM, and fetal bovine serum (FBS) were purchased from Corning Inc. (Corning, NY, USA). MTT, Hoechst 33258, and fluorescent dye JC-1 were purchased from Sigma Aldrich (St. Louis, MO, USA). Antibodies against Bcl-2, Bcl-xl, MMP-9, and MMP-2 were purchased from Santa Cruz Biotechnology (Santa Cruz, CA, USA). Antibodies against Bax, p-AKT, AKT, p-mTOR, pro-caspase3, p-ERK, ERK, and GAPDH, as well as all secondary antibodies, were purchased from Cell Signaling Technology (Danvers, MA, USA). An Annexin V-FITC/PI kit and Matrigel matrix were obtained from BD Biosciences (San Jose, CA, USA).

4.2. Cell Lines and Cell Culture

Human gastric carcinoma cell lines, SGC7901, MGC803, and BGC823, and the human normal gastric epithelial cell line, GES-1, were all obtained from the Chinese Academy of Medical Sciences Basic Medicine Cell Center (Beijing, China). SGC7901, MGC803, and BGC823 cells were maintained in RPMI-1640 media containing 10% FBS and 1% penicillin/streptomycin in a 37 °C humidified incubator with 5% CO_2. GES-1 cells were cultured in DMEM media under the same conditions.

4.3. Ethics Statement and Animals

All animal experiments and care were performed in accordance with the National Institutes of Health regulations for the care and use of animals in research. All mouse protocols were approved by the Animal Ethics Committee at the Institute of Medicinal Plant Development, Chinese Academy of Medical Sciences (No. SLXD-2017051634) and were in compliance with the Chinese Association for Laboratory Animal Sciences guidelines.

Female BALB/c nude mice (14–16 g) were purchased from SPF Biotechnology Co., Ltd. (Certificate no. SCXK-2016-0002, Beijing, China) and were maintained on a 12-h light/dark cycle with controlled humidity (50–70%) and temperature (20–24 °C).

4.4. Cell Viability Assay by MTT

Cells cultured in 96-well plates at a density of 5×10^3 cells/well were treated with various concentrations of Zey for 24 h, and cell viability was measured with an MTT assay, as previously described [32].

4.5. Colony Formation Assay

Cells (400 cells/well, six-well plates) were treated with Zey (0, 1, 2, or 4 μM) and were incubated in a 37 °C humidified atmosphere with 5% CO_2 for 12 days. Cell aggregates containing 50 or more cells were considered colonies. The colonies were fixed with methanol, stained with 0.1% Coomassie blue, and then counted under a microscope.

4.6. Hoechst 33258 Staining

SGC7901 and MGC803 cells were treated with different concentrations of Zey for 24 h. After washing with phosphate-buffered saline (PBS), the cells were stained with Hoechst 33258 (10 μg/mL) for 20 min. Nuclear morphology changes were observed and then captured using a fluorescence microscope (Olympus, Tokyo, Japan).

4.7. Flow Cytometric Analysis of Apoptosis

Cells cultured in six-well plates were treated with Zey (SGC7901 and MGC803: 0, 3.3, 6.6, and 13.2 μM) for 12 h and 24 h, respectively. After harvesting and washing twice with PBS, the cells were stained with annexin-V-FITC and PI according to the manufacturer's directions. The stained cells (10^4 cells) were then analyzed immediately using an FACS Calibur flow cytometer (Becton Dickinson, CA, USA), and the results were expressed as a percentage of living (AnnV−, PI−), early apoptotic (AnnV+, PI−), and late apoptotic/dead cells (AnnV+, PI+). Apoptotic rates were

reported as the percentage of apoptotic cells (including early apoptotic cells and late apoptotic cells) among total cells.

4.8. JC-1 for Mitochondrial Transmembrane Potential Study

To investigate whether apoptosis was related to the mitochondrial apoptosis pathway, we measured the change of mitochondrial transmembrane potential using JC-1 [33]. Cells were treated with different concentrations of Zey (SGC7901 and MGC803: 0, 3.3, 6.6, or 13.2 μM) for 24 h. The cells were then collected and stained with 10 μg/mL JC-1 for 30 min in the dark at 37 °C. After washing twice with PBS, the cells were analyzed by flow cytometry. The highly negative membrane potential in mitochondria produces JC-1 red fluorescence. Loss of mitochondrial transmembrane potential results in green fluorescence and loss of the red fluorescence.

4.9. Wound-Healing Assays

Wound-healing assays were performed to investigate migration under Zey treatment. When cell density in 24-well plates was approximately 90%, a sterile 10-μL pipette tip was used to make a linear wound. Cells were washed to remove superfluous floating cells and debris, then co-incubated with different concentrations of Zey (0, 1, 2, or 4 μM, with a cell viability rate >93%) in serum-free RPMI-1640 for an additional 24 h. Wound healing was photographed at 0 and 24 h using a microscope. The width of the wound was measured by ImageJ software (National Institutes of Health, Bethesda, MD, USA). The wound-healing ratio (%) = (wound area at 0 h − wound area at 24 h)/wound area at 0 h × 100%.

4.10. Invasion and Migration Assay

For invasion and migration assays, 8.0-μm-pore-size transwell chambers (Costar, Corning Inc., Corning, NY, USA) were used [34]. Transwell chambers were coated with Matrigel (dilution 1:5) for the invasion assays. After solidification, the cells (4×10^4) treated with Zey were seeded on the upper transwell chamber insert in 24-well plates and cultured in serum-free RPMI-1640 medium. Meanwhile, 500 μL of RPMI-1640 medium containing 10% FBS was added to the 24-well plates. After 24 h, non-invading cells on the upper surface of the membranes were wiped out by cotton swab and those on the underside were stained with 0.1% crystal violet and counted under a light microscope with a magnification of 100×. For each replicate, the cells in 10 randomly selected fields were determined, and the counts were averaged. The invasion rate (%) = the number of migrated cells at 1, 2, or 4 μM/the number of migrated cells at 0 μM × 100%. Similar methods were performed for migration assays, except Matrigel was not used.

4.11. Western Blot Analyses

Cells were exposed to Zey (SGC7901 and MGC803: 0, 3.3, 6.6, or 13.2 μM) for 24 h. The detailed steps for electrophoresis, transfer, and immunoblotting were described previously [35]. Antibodies used in this study were mentioned in the Materials and Methods section. All experiments were performed in triplicate, and levels of protein expression were quantified using the Image J software.

4.12. Tumor Xenograft Study

A total of 2×10^7 BGC823 human gastric cancer cells were inoculated subcutaneously on the right flanks of mice. The mouse body weight and tumor size were measured every two days. The tumor volume (V) was calculated using the formula $V = (L \times W^2)/2$, where L is the largest diameter and W is the diameter perpendicular to width. When tumors reached 100–150 mm^3, the mice were randomized to five groups (n = 5) and treated with vehicle (saline), mPEG-PLGA-loaded Zeylenone micelles (containing Zeylenone 7.5, 15, or 30 mg/kg, once every two days, tail vein injection), and paclitaxel

(15 mg/kg, once every two days, tail vein injection) for a total of 10 days. Subsequently, the mice were then euthanized, and the tumors were excised, weighed, fixed, and stored.

4.13. Statistical Analysis

All experiments were performed in triplicate, and data were presented as the means ± SD. The GraphPad Prism 6.0 software (GraphPad Software, La Jolla, CA, USA) was used for statistical analysis. The statistical significance of group differences was analyzed using one-way (ANOVA) and a Tukey's post hoc test (*t*-test), and $p < 0.05$ was considered to be statistically significant.

Author Contributions: S.Y. and L.C. conceived and designed the experiments; S.Y. performed the experiments; L.L., Y.L., and X.X. analyzed the data; S.Y. wrote the manuscript. All authors reviewed the manuscript.

Funding: This work was financially supported by the Fundamental Research Funds for the Central Universities and by the CAMS Innovation Fund for Medical Sciences (CIFMS) (No. 2016-I2M-1-012). This work was also supported by the Key Laboratory of Bioactive Substances and Resources Utilization of Chinese Herbal Medicine, Ministry of Education, and by the Beijing Key Laboratory of Innovative Drug Discovery of Traditional Chinese Medicine (Natural Medicine), and the Translational Medicine, Institute of Medical Plant Development, Peking Union Medical College and Chinese Academy of Medical Sciences.

Conflicts of Interest: The authors declare no conflict of interest.

References

1. Van Cutsem, E.; Sagaert, X.; Topal, B.; Haustermans, K.; Prenen, H. Gastric Cancer. *Lancet* **2016**, *388*, 2654–2664. [CrossRef]
2. Karimi, P.; Islami, F.; Anandasabapathy, S.; Freedman, N.D.; Kamangar, F. Gastric cancer: Descriptive epidemiology, risk factors, screening, and prevention. *Cancer Epidemiol. Biomark. Prev.* **2014**, *23*, 700–713. [CrossRef] [PubMed]
3. Ferlay, J.; Steliarovafoucher, E.; Lortettieulent, J.; Rosso, S.; Coebergh, J.W.; Comber, H.; Forman, D.; Bray, F. Cancer incidence and mortality patterns in europe: Estimates for 40 countries in 2012. *Eur. J. Cancer* **2013**, *49*, 1374–1403. [CrossRef] [PubMed]
4. Jemal, A.; Center, M.M.; Desantis, C.; Ward, E.M. Global patterns of cancer incidence and mortality rates and trends. *Cancer Epidemiol. Biomark. Prev.* **2010**, *19*, 1893–1907. [CrossRef] [PubMed]
5. Cunningham, S.C.; Kamangar, F.; Kim, M.P.; Hammoud, S.; Haque, R.; Maitra, A.; Montgomery, E.; Heitmiller, R.E.; Choti, M.A.; Lillemoe, K.D. Survival after gastric adenocarcinoma resection: Eighteen-year experience at a single institution. *J. Gastrointest. Surg.* **2005**, *9*, 718–725. [CrossRef] [PubMed]
6. Ferro, A.; Peleteiro, B.; Malvezzi, M.; Bosetti, C.; Bertuccio, P.; Levi, F.; Negri, E.; La, V.C.; Lunet, N. Worldwide trends in gastric cancer mortality (1980–2011), with predictions to 2015, and incidence by subtype. *Eur. J. Cancer* **2014**, *50*, 1330–1344. [CrossRef] [PubMed]
7. Mehlen, P.; Puisieux, A. Metastasis: A question of life or death. *Nat. Rev. Cancer* **2006**, *6*, 449–458. [CrossRef] [PubMed]
8. Hu, X.; Han, R.; Quan, L.H.; Liu, C.Y.; Liao, Y.H. Stabilization and sustained release of zeylenone, a soft cytotoxic drug, within polymeric micelles for local antitumor drug delivery. *Int. J. Pharm.* **2013**, *450*, 331–337. [CrossRef] [PubMed]
9. Liao, Y.H.; Xu, L.Z.; Yang, S.L.; Dai, J.; Zhen, Y.S.; Zhu, M.; Sun, N.J. Three cyclohexene oxides from uvaria grandiflora. *Phytochemistry* **1997**, *45*, 729–732.
10. Sun, L.H.; Dang, H.X.; Lan-Lan, B.U.; Liao, Y.H.; You-Hua, Y.U.; Liu, X.M. Effects of zeylenone on the proliferation and apoptosis of acute lymphoblastic leukemia cells. *J. Tradit. Chin. Med. Univ. Hunan* **2012**. Available online: http://en.cnki.com.cn/Article_en/CJFDTOTAL-HNZX201209005.htm (accessed on 8 August 2018).
11. Zhang, L.; Jin, J.; Zhang, L.; Hu, R.; Gao, L.; Huo, X.; Liu, D.; Ma, X.; Wang, C.; Han, J. Quantitative analysis of differential protein expression in cervical carcinoma cells after zeylenone treatment by stable isotope labeling with amino acids in cell culture. *J. Proteom.* **2015**, *126*, 279–287. [CrossRef] [PubMed]
12. Tsai, J.P.; Lee, C.H.; Ying, T.H.; Lin, C.L.; Lin, C.L.; Hsueh, J.T.; Hsieh, Y.H. Licochalcone a induces autophagy through pi3k/akt/mtor inactivation and autophagy suppression enhances licochalcone a-induced apoptosis of human cervical cancer cells. *Oncotarget* **2015**, *6*, 28851–28866. [CrossRef] [PubMed]

13. Matsuoka, T.; Yashiro, M. The role of pi3k/akt/mtor signaling in gastric carcinoma. *Cancers* **2014**, *6*, 1441–1463. [CrossRef] [PubMed]
14. Chen, P.N.; Hsieh, Y.S.; Chiou, H.L.; Chu, S.C. Silibinin inhibits cell invasion through inactivation of both pi3k-akt and mapk signaling pathways. *Chem. Biol. Int.* **2005**, *156*, 141–150. [CrossRef] [PubMed]
15. Kilian, M.; Gregor, J.I.; Heukamp, I.; Hanel, M.; Ahlgrimm, M.; Schimke, I.; Kristiansen, G.; Ommer, A.; Walz, M.K.; Jacobi, C.A. Matrix metalloproteinase inhibitor ro 28-2653 decreases liver metastasis by reduction of mmp-2 and mmp-9 concentration in bop-induced ductal pancreatic cancer in syrian hamsters: Inhibition of matrix metalloproteinases in pancreatic cancer. *Prostaglandins Leukot. Essent. Fat. Acids* **2006**, *75*, 429–434. [CrossRef] [PubMed]
16. Chen, Z.R.; He, T.F.; Zhao, K.; Xing, C.G. Anti-metastatic activity of fangchinoline in human gastric cancer ags cells. *Oncol. Let.* **2017**, *13*, 655–660. [CrossRef] [PubMed]
17. Wan, B.; Zhu, J.; Chang, Q.; Zhou, H.; Shi, Z.; Min, L.; Cai, Y.; Guan, H. Alpha, 2′-dihydroxy-4,4′-dimethoxydihydrochalcone inhibits cell proliferation, invasion, and migration in gastric cancer in part via autophagy. *Biomed. Pharmacother.* **2018**, *98*, 709–718. [CrossRef] [PubMed]
18. Gao, J.; Liu, X.; Yang, F.; Liu, T.; Yan, Q.; Yang, X. By inhibiting ras/raf/erk and mmp-9, knockdown of epcam inhibits breast cancer cell growth and metastasis. *Oncotarget* **2015**, *6*, 27187–27198. [CrossRef] [PubMed]
19. Piazuelo, M.B.; Correa, P. Gastric cancer: Overview. *Colomb. Med.* **2013**, *44*, 192–201. [PubMed]
20. Katona, B.W.; Rustgi, A.K. Gastric cancer genomics: Advances and future directions. *Cell. Mol. Gastroenterol. Hepatol.* **2017**, *3*, 211–217. [CrossRef] [PubMed]
21. Giuseppa, P.; Daniela, T.; Claudia, C.; Alessia, G.; Gabriella, D.O. Apoptosis as anticancer mechanism: Function and dysfunction of its modulators and targeted therapeutic strategies. *Aging* **2016**, *8*, 603–619.
22. Taylor, R.C.; Cullen, S.P.; Martin, S.J. Apoptosis: Controlled demolition at the cellular level. *Nat. Rev. Mol. Cell Biol.* **2008**, *9*, 231–241. [CrossRef] [PubMed]
23. Mönig, S.P.; Baldus, S.E.; Hennecken, J.K.; Spiecker, D.B.; Grass, G.; Schneider, P.M.; Thiele, J.; Dienes, H.P.; Hölscher, A.H. Expression of mmp-2 is associated with progression and lymph node metastasis of gastric carcinoma. *Histopathology* **2001**, *39*, 597–602. [CrossRef] [PubMed]
24. Kabashima, A.; Maehara, Y.; Kakeji, Y.; Baba, H.; Koga, T.; Sugimachi, K. Clinicopathological features and overexpression of matrix metalloproteinases in intramucosal gastric carcinoma with lymph node metastasis. *Clin. Cancer Res. Off. J. Am. Assoc. Cancer Res.* **2000**, *6*, 3581–3584.
25. Trusolino, L.; Comoglio, P.M. Scatter-factor and semaphorin receptors: Cell signalling for invasive growth. *Nat. Rev. Cancer* **2002**, *2*, 289–300. [CrossRef] [PubMed]
26. Murray, G.I.; Duncan, M.E.; Arbuckle, E.; Melvin, W.T.; Fothergill, J.E. Matrix metalloproteinases and their inhibitors in gastric cancer. *Gut* **1998**, *43*, 791–797. [CrossRef] [PubMed]
27. Zhu, X.; Jiang, X.; Li, A.; Sun, Y.; Liu, Y.; Sun, X.; Feng, X.; Li, S.; Zhao, Z. S-allylmercaptocysteine suppresses the growth of human gastric cancer xenografts through induction of apoptosis and regulation of mapk and pi3k/akt signaling pathways. *Biochem. Biophys. Res. Commun.* **2017**, *491*, 821–826. [CrossRef] [PubMed]
28. Nam, S.Y.; Lee, H.S.; Jung, G.A.; Choi, J.; Cho, S.J.; Min, K.K.; Kim, W.H.; Lee, B.L. Akt/pkb activation in gastric carcinomas correlates with clinicopathologic variables and prognosis. *J. Pathol. Microbiol. Immunol.* **2003**, *111*, 1105–1113. [CrossRef]
29. You, J.; Mi, D.; Zhou, X.; Qiao, L.; Zhang, H.; Zhang, X.; Ye, L. A positive feedback between activated extracellularly regulated kinase and cyclooxygenase/lipoxygenase maintains proliferation and migration of breast cancer cells. *Endocrinology* **2009**, *150*, 1607–1617. [CrossRef] [PubMed]
30. Liu, A.; Xu, L.; Zou, Z. Studies on chemical constituents of uvaria tonkinensis Var. Subglabra. *China J. Chin. Mater. Med.* **2009**, *34*, 567–570.
31. Al-Batran, S.E.; Jager, E.; Scholz, M. Chemotherapy for advanced gastric cancer. *J. Clin. Oncol.* **2007**, *25*, 729–730. [CrossRef] [PubMed]
32. Chang, C.T.; Hseu, Y.C.; Thiyagarajan, V.; Lin, K.Y.; Way, T.D.; Korivi, M.; Liao, J.W.; Yang, H.L. Chalcone flavokawain b induces autophagic-cell death via reactive oxygen species-mediated signaling pathways in human gastric carcinoma and suppresses tumor growth in nude mice. *Arch. Toxicol.* **2017**, *91*, 3341–3364. [CrossRef] [PubMed]
33. Chu, J.H.; Zhao, C.R.; Song, Z.Y.; Wang, R.Q.; Qin, Y.Z.; Li, W.B.; Qu, X.J. 1082-39, an analogue of sorafenib, inhibited human cancer cell growth more potently than sorafenib. *Biomed. Pharmacother.* **2014**, *68*, 335–341. [CrossRef] [PubMed]

34. Xu, Y.H.; Li, Z.L.; Qiu, S.F. IFN-γ induces gastric cancer cell proliferation and metastasis through upregulation of integrin β3-mediated NF-κB signaling. *Transl. Oncol.* **2018**, *11*, 182–192. [CrossRef] [PubMed]
35. Zhang, L.; Si, J.; Li, G.; Li, X.; Zhang, L.; Gao, L.; Huo, X.; Liu, D.; Sun, X.; Cao, L. Umbelliprenin and lariciresinol isolated from a long-term-used herb medicine ferula sinkiangensis induce apoptosis and g0/g1 arresting in gastric cancer cells. *R. Soc. Chem.* **2015**, *5*, 91006–91017. [CrossRef]

Sample Availability: Samples of the compound Zeylenone (Zey) are available from the authors.

molecules

MDPI

Article

JNK Inactivation Induces Polyploidy and Drug-Resistance in Coronarin D-Treated Osteosarcoma Cells

Chang-Te Hsu [1,†], Yi-Fu Huang [2,†], Chen-Pu Hsieh [1,2], Chia-Chieh Wu [1,2,3,4,*] and Tai-Shan Shen [1,*]

1 Department of Orthopedic Surgery, Changhua Christian Hospital, Changhua 50006, Taiwan; 169485@cch.org.tw (C.-T.H.); 51114@cch.org.tw (C.-P.H.)
2 Orthopedics & Sports Medicine Laboratory, Changhua Christian Hospital, Changhua 50006, Taiwan; 181064@cch.org.tw
3 Institute of Biomedical Sciences, National Chung Hsing University, 145 Xingda Rd., South Dist, Taichung 40227, Taiwan
4 School of Medicine, Kaohsiung Medical University, Kaohsiung 80708, Taiwan
* Correspondence: 50560@cch.org.tw (C.-C.W.); 162509@cch.org.tw (T.-S.S.); Tel.: +886-4-7238595 (C.-C.W. & T.-S.S.); Fax: +886-4-7228289 (C.-C.W. & T.-S.S.)
† These authors have contributed equally to this work.

Received: 27 July 2018; Accepted: 21 August 2018; Published: 23 August 2018

Abstract: Inhibition of proliferating cells is a critical strategy for cancer therapy. In this study, we demonstrated that coronarin D, a natural component extracted from the rhizomes of *Hedychium coronarium*, significantly suppressed the proliferation of osteosarcoma cells. The treatment with coronarin D resulted in the activation of caspase-3 and apoptosis. This treatment induced the accumulation of cyclin B1 and DNA condensation indicating the treated osteosarcoma cells were arrested in mitotic phase. Furthermore, the treatment with coronarin D increased the levels of phosphorylated c-Jun NH2-terminal kinase (JNK) in human osteosarcoma cells. Pretreatment with JNK inhibitor blocked the accumulation of cyclin B1 and DNA condensation, resulting the accumulation of tetraploid cells in coronarin D-treated osteosarcoma HOS cells, indicating JNK inactivation blocked the mitotic entry and arrested cells in the 4 N state. After adaptation, the arrested tetraploid cells continued to duplicate their DNA resulting in polyploidy. Interestingly, when the arrested mitotic cells induced by coronarin D were treated with JNK inhibitor, the accumulated cyclin B1 and DNA condensation were immediately eliminated. These arrested 4 N cells loss the ability to undergo cytokinesis, and ultimately continued to duplicate DNA upon prolonged arrest resulting in the production of polyploid populations. JNK inactivation, either by the pretreatment with JNK inhibitor or the treatment with JNK inhibitor in coronarin D-induced mitotic cells, both caused resistance to coronarin D-induced cell death. Taken together, our findings indicate that coronarin D induces the apoptosis and mitosis arrest in human osteosarcoma cells. JNK has a crucial role in coronarin D-induced mitosis arrest and apoptosis. We hypothesize that functional evaluation of JNK may produce more specific and effective therapies in coronarin D-related trail for treatment of human osteosarcoma.

Keywords: coronarin D; JNK; osteosarcoma

1. Introduction

Osteosarcoma is the most common type of primary malignant bone tumor. It arises from osteoid tissue in the bone during periods of rapid growth and predominately affects adolescents and young adults. Current osteosarcoma treatments include surgical resection, chemotherapy, and radiotherapy. The 5-year survival rate for patients remains at 60–70%. Osteosarcoma is characterized by a high

propensity for metastasis. Once this tumor exhibits the ability to invade, the 5-year survival rate for patients with metastatic osteosarcoma decreases dramatically to approximately 20%. It has remained virtually unchanged over the past 30 years [1,2]. Therefore, there is an urgent need for newer effective cures for patients with osteosarcoma, especially for patients suffering from advanced osteosarcoma.

Recent progress has focused on the chemoprevention by natural products for their antigrowth activity against cancer cells [3]. These compounds may exhibit less side effects compared to synthetic chemicals. For example, taxol is isolated from the bark of Taxus brevifolia. It is a microtubule-stabilizing agent used to treat a number of types of cancers including ovarian, breast, and lung cancer [4,5]. Coronarin D, a natural product extracted from the rhizomes of *Hedychium coronarium*, has been shown to possess antimicrobial and antifungal activity [6,7]. Moreover, it has proven to have anti-inflammatory effects and apoptosis potential in cells [8]. The activity of coronarin D in antitumor is unclear. In this study, we evaluated the potential antitumor effect of coronarin D against osteosarcoma.

2. Results

2.1. Coronarin D Reduced Osteosarcoma Cell Viability and Proliferation

Coronarin D is a labdane-type diterpene (Figure 1A). Cell Viability of osteosarcoma cells after exposure to various concentrations of coronarin D (0–200 nM) was tested by MTT assay. The results showed that coronarin D significantly inhibited the growth of osteosarcoma HOS cells and MG-63 cells in a dose- and time-dependent manner, and had a minor cytotoxic effect in human fibroblast cell line MRC-5. (Figure 1B). The half maximal inhibitory concentration (IC_{50}) calculated based on data of the MTT assays for HOS cells were 58.8 nM at 24 h and 51.18 nM at 48 h, those for MG-63 cells were 65.87 nM at 24 h and 61.9 nM at 48 h, and those for MRC-5 cells were 697.39 nM at 24 h and 492.42 nM at 48h. We also examined the effect of coronarin D on cell proliferative capacity by colony formation assays. The results showed that the treatment of coronarin D reduced colony number in a dose-dependent manner in osteosarcoma HOS cells. These data indicate that coronarin D has the potential to reduce the viability of osteosarcoma cells.

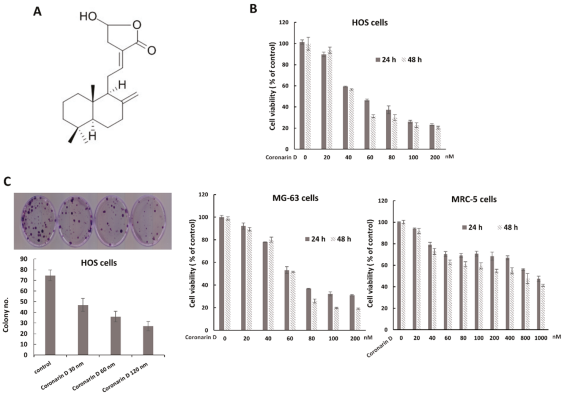

Figure 1. Coronarin D inhibits cell viability of osteosarcoma. (**A**) The chemical structure of coronarin D. (**B**) Coronarin D inhibits osteosarcoma cell growth in a dose- and time-dependent manner. MTT assays were performed with osteosarcoma HOS and MG-63 cells, or human fibroblast cell line MRC-5 exposed to coronarin D in the indicated concentations. Data are expressed as mean ± SD of three independent experiments. (**C**) Coronarin D reduces colony formation of osteosarcoma. HOS cells were plated in colony formation assays after treatment with coronarin D for 6 h. Five-hundred cells were plated per dish. All experiments were performed in triplicate, and the figure above shows a representative example.

2.2. Coronarin D Induces Apoptosis and Cell Arrest

To determine whether programmed cell death was involved in the antiproliferative effect of coronarin D, we analyzed cell for apoptosis by Annexin V staining and the expression of apoptosis-related proteins by Western blotting. Coronarin D treatment induced a significant increase of Annexin V positive cells (Figure 2A), and upregulated the expressions of apoptosis-related proteins, cleaved caspase 3, and cleaved PARP in human osteosarcoma cells (Figure 2B). The data indicate that coronarin D treatment induces apoptosis in human osteosarcoma cells. Furthermore, the caspase inhibitor, ZVAD-FMK, rescued the decreased cell survival caused by coronarin D treatment (Figure 2C). These data indicate that coronarin D suppresses cell survival by caspase-dependent apoptosis.

The analysis of cell cycle distribution in treated cells were performed by PI staining and flow cytometry. The data showed the number of 4 N cells were significantly increased in coronarin D-treated HOS cells indicating coronarin D may arrest cells in mitosis (Figure 3A). To confirm the state of 4 N cells accumulated by the treatment of coronarin D, the mitosis markers, cyclin B1 and phospho-histone H3 at Ser10, were analyzed in coronarin D-treated osteosarcoma cells. The data showed that cyclin B1 was significantly increased in HOS and MG-63 cells, and phospho-histone H3 at Ser10 was increased in MG-63 cells after the exposure of coronarin D (Figure 3B). The number of cells with DNA condensation were increased in coronarin D-treated HOS cells (Figure 3C). Therefore, the 4 N cells accumulated by the treatment of coronarin D should be arrested in mitotic phase. Taken together, these data indicate that coronarin D suppresses cell proliferation by apoptosis and mitosis arrest in human osteosarcoma cells.

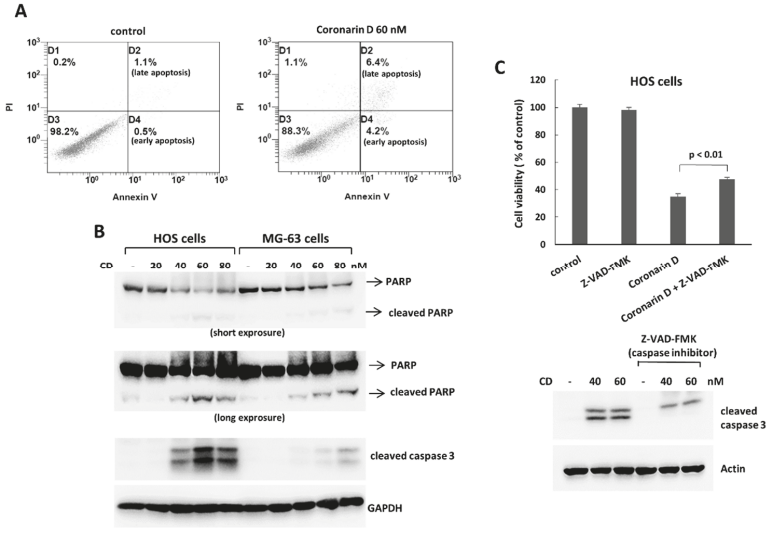

Figure 2. Coronarin D induces apoptosis in osteosarcoma cells. Osteosarcoma cells were treated with coronarin D for 24 h. To detect apoptosis, the HOS cells were stained with Annexin V and propidium iodide, and analyzed using flow cytometry (**A**). Expression of apoptosis-related proteins was measured by Western blotting in HOS cells and MG-63 cells (**B**). (**C**) Caspase inhibitor blocks the antiproliferative effect caused by coronarin D treatment. HOS cells were treated with coronarin D (60 nM) for 24 h in the absence or presence of caspase inhibitor, ZVAD-FMK (10 μM). The treated cells were processed with Western blotting to analyze the caspase 3 activation and MTT assay to determine cell viability.

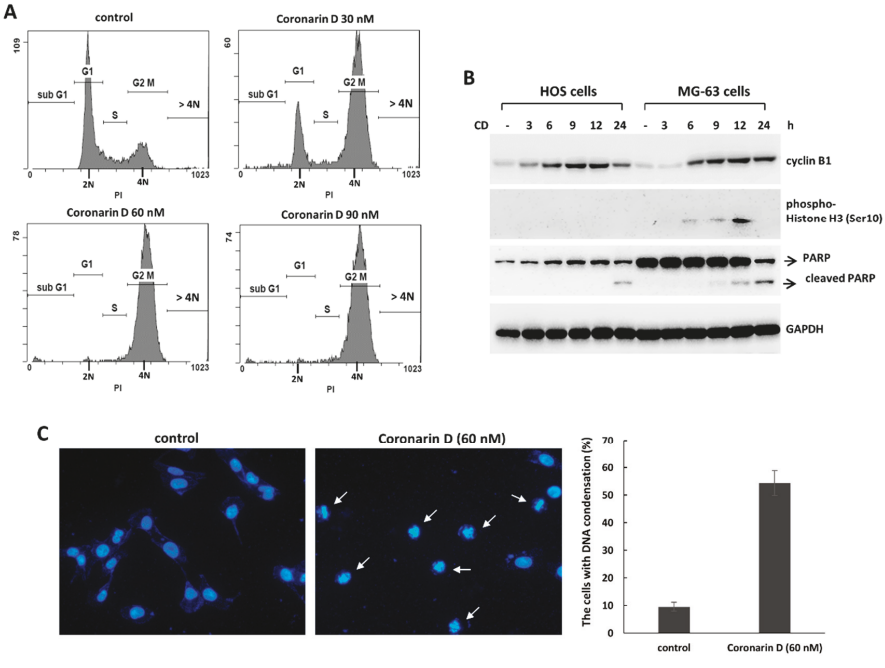

Figure 3. Coronarin D induces M phase arrest in osteosarcoma cells. HOS cells were treated with indicated concentrations of coronarin D for 12 h. The cells were stained with propidium iodide and analyzed by flow cytometer (**A**). (**B**) Coronarin D induces the accumulation of mitosis phase marker in osteosarcoma cells. HOS cells and MG-63 cells were treated with coronarin D (60 nM). The treated cells were harvested in the indicated time points, and analyzed by Western blotting. (**C**) Coronarin D induced DNA condensation in HOS cells. HOS cells were treated with coronarin D (60 nM) for 6 h. The cells were stained with 4,6-diamidino-2-phenylindole (DAPI) for labeling nucleus (blue color), and mitosis cells (white arrows) were observed under microscopic analysis.

2.3. The Pretreatment with JNK Inhibitor Blocks the Mitotic Entry and Induces Polyploidy and Drug-Resistance in Coronarin D-Treated HOS Cells

MAPK signaling plays an important role in many cellular processes including cell division, differentiation, proliferation, and apoptosis [9]. In this study, we found that treatment of coronarin D resulted in increased expression of phospho-JNK following the accumulation of cyclin B1 (Figure 4A). To demonstrate that the role of JNK activation in coronarin D-triggered mitosis arrest and apoptosis, we pretreated HOS cells with the JNK inhibitor (SP600125) (20 μM) for 1 h, and then cotreated cells with coronarin D. This inhibitor induced the accumulation of 4 N cells (Figure 4B) without increased cyclin B1 (Figure 4A) and rounded mitotic cells (Figure 4C) suggesting that JNK inactivation blocked the mitotic entry of coronarin D-treated HOS cells and arrested the cells in 4 N state. After adaption, the arrested 4 N cells continued to duplicate their DNA resulting in the production of polyploid population (Figure 4B). Importantly, JNK inactivation inhibited the formation of cleaved caspase3, PARP, and JNK downstream targets, Bax (Figure 5A) in the coronarin D-treated HOS cells, and blocked the antiproliferative effect induced by coronarin D (Figure 5B). We therefore conclude JNK inactivation cause the resistance to coronarin D-induced cell death.

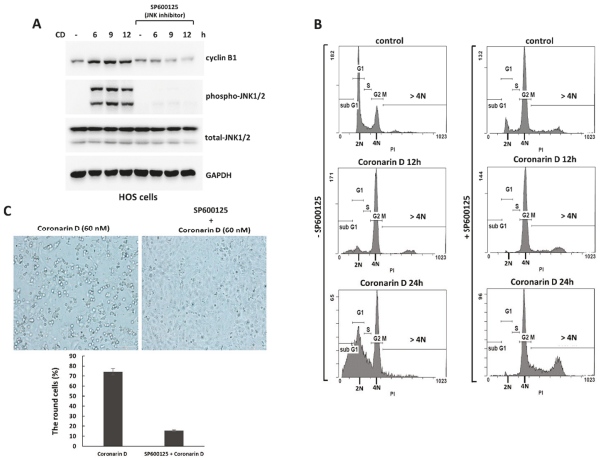

Figure 4. JNK inactivation blocks mitotic entry and induces polyploidy in coronarin D-treated HOS cells. (**A**) JNK inhibitor inhibited the accumulation of cyclin B1 in HOS cells. HOS cells were pretreated with JNK inhibitor, SP600125 (20 μM) for 1 h, and cotreated with coronarin D (60 nM) and harvested in the indicated time points. The treated cells were analyzed by Western blotting using the indicated antibodies. (**B**) JNK inhibitor induces polyploidy in coronarin D-treated HOS cells. HOS cells were treated as described in (**A**). The treated cells were harvested in the indicated time points. The cells were stained with propidium iodide and analyzed by a flow cytometer. (**C**) Round mitotic cells were greatly reduced by cotreatment with SP600125. Phase-contrast photomicrographs of HOS cells treated with coronarin D (60 nM) in the absence or presence of JNK inhibitor (SP600125) (20 μM) for 12 h.

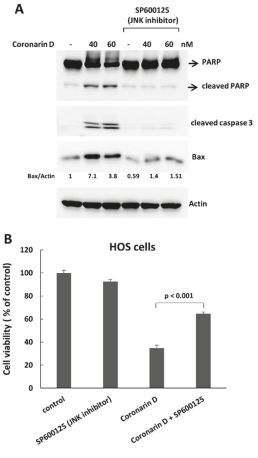

Figure 5. JNK inactivation inhibits coronarin D-induced cell death. (**A**) JNK inactivation suppresses coronarin D-induced cell death. HOS cells were pretreated with JNK inhibitor (SP600125) (20 μM) for 1 h, and cotreated with coronarin D for 24 h. The treated cells were processed with Western blotting to analyze the caspase 3 activation and Bax level. Numbers indicate relative levels of Bax after normalization to Actin. (**B**) JNK inhibitor blocks the antiproliferative effect caused by coronarin D treatment. HOS cells were pretreated with JNK inhibitor (SP600125) (20 μM) for 1 h, and cotreated with coronarin D (80 nM) for 24 h. The treated cells were processed with MTT assay to determine cell viability.

2.4. JNK Inactivation Eliminates the Accumulated Cyclin B1 and Induces Polyploidy in Coronarin D-Induced M Phase Arrest Cells

To precisely analysis the role of JNK activation in coronarin D-induced mitosis, We first treated cells with coronarin D for 12 h to induce the accumulation of mitotic cells, and then cotreated with JNK-specific inhibitor (SP600125) (20 μM) in these arrested mitotic cells (Figure 6A). Once JNK activity was blocked in the arrested mitotic cells, the accumulated cyclin B1 (Figure 6B) and DNA condensation (the data not shown) were immediately eliminated. These arrested 4 N cells lost the ability to undergo cytokinesis, and ultimately continued to duplicate DNA upon prolonged arrest resulting in the production of polyploid populations and drug resistance toward lower level of activated caspase 3 (Figure 6B,C). These data support the hypothesis the JNK activation play an essential role in the coronarin D-induced mitotic arrest and apoptosis.

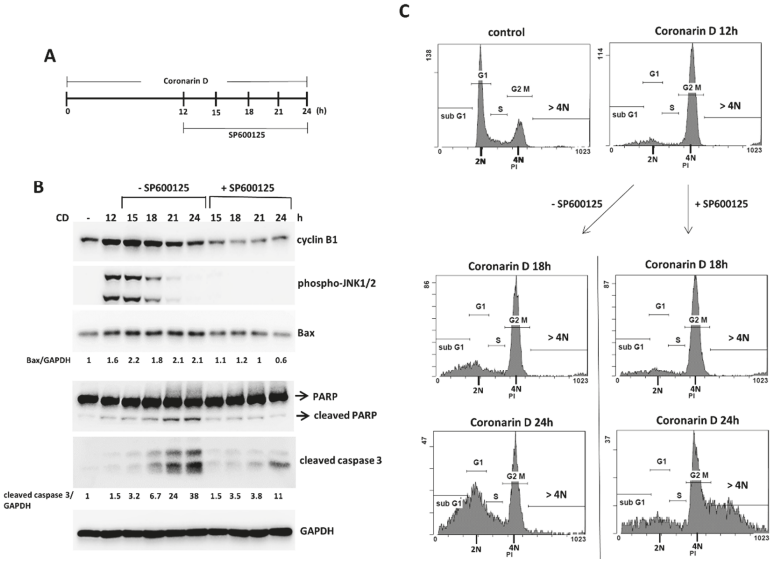

Figure 6. JNK inactivation eliminates the accumulation of cyclin B1 and induces polyploid in coronarin D-induced M phase arrest cells. (**A**) Schedule of drug treatment. HOS cells were treated with coronarin D for 12 h, and coronarin D treatment was continued with or without JNK inhibitor (SP600125) (20 μM). The treated cells were harvested at the indicated time points and analyzed by Western blotting using the indicated antibodies (**B**) and by flow cytometry (**C**). Numbers indicate relative levels of Bax or cleaved caspase 3 after normalization to GAPDH (**B**).

3. Discussion

Coronarin D, a natural product extracted from the rhizomes of *Hedychium coronarium*, has been shown to possess antimicrobial and antifungal activity [6,7]. It has been proven to have anti-inflammatory effects and apoptosis potential in cells [8]. The antitumor activity of coronarin D is uncertain. Limited work has been published showing that coronarin D induces reactive oxygen species-mediated cell death in human nasopharyngeal cancer cells [10]. In this report, we demonstrated that coronarin D suppressed the proliferation of osteosarcoma cells significantly by mitotic arrest and apoptosis. In addition, we showed that the function of JNK in coronarin D-induced effects.

The JNK pathway is predominantly activated by stress stimuli such as cytokines, growth factors, and ultraviolet irradiation. Although activation of JNK is classically thought to induce cell death, several reports have presented that the activity of JNK is also involved in control of the cell cycle [11–14].

In breast cancer cells, inhibition of JNK reduces G2/M transit and causes endoreduplication (cellular DNA content >4 N) [15]. In retinal progenitor cells, JNK is phosphorylated preferentially during the early stages of mitosis, and inhibition of JNK induces mitotic arrest [16]. In this report, we showed that the treatment with coronarin D resulted in the accumulation of cyclin B1, DNA condensation, and arrested cells in mitotic phase following JNK activation in osteosarcoma cells. Blocking JNK activation with JNK inhibitor prevented the accumulation of cyclin B1 and rounded morphology, inhibited mitotic progression, and arrested cells in the 4 N state in coronarin D-treated osteosarcoma cells. Upon prolonged arrest, these arrested cells ultimately continued to duplicate DNA resulting in the production of polyploid populations and drug resistance.

It is unclear how JNK regulates mitosis progression. In NIH-3T3 cells, the inactivation of JNK by SP600125 inhibits expression of Aurora B, blocks phosphorylation of Histone H3 at serine 10, and prevents mitosis entry with sustained expression of cyclin B1 [17]. In this report, we observed that the pretreatment with JNK inhibitor prevented the accumulation of cyclin B1 in coronarin D-exposed osteosarcoma cells. Furthermore, in arrested mitotic cells induced by coronarin D, treatment with JNK inhibitor immediately eliminated the accumulated cyclin B1. These results indicated that the roles of JNK activation in mitotic progression may be associated with cyclin B1 in coronarin D-treated osteosarcoma cells.

Our data showed that the treatment with JNK inhibitor suppressed the activation of caspase 3 and rescued the cell viability in coronarin D-treated osteosarcoma cells indicating JNK has crucial role in coronarin D-induced cell death. How did the inactivation of JNK suppress coronarin D-induced cell death? One possibility is that the inhibition of JNK suppresses mitotic entry, thereby preventing coronarin D-induced cell death in mitosis. The formation of polyploidy has been shown to drive resistance to chemotherapy in tumors [18–20]. We believe that the polyploidy induced by JNK inactivation may cause resistance to coronarin D-induced cell death in osteosarcoma cells. Taken together with the above data, our findings show that coronarin D induces apoptosis and mitosis arrest in human osteosarcoma cells. JNK has a crucial role in coronarin D-induced mitosis arrest and apoptosis. Functional evaluation of JNK may produce more precise and effective therapies in coronarin D-related trail for treatment of human osteosarcoma.

4. Materials and Methods

4.1. Cell Culture and Reagents

Human HOS and MG-63 osteosarcoma cells, and human fibroblast cell line MRC-5 were purchased from the Bioresource Collection and Research Center (Hsinchu, Taiwan). MRC-5, HOS, and MG-63 cells were maintained in Minimum Essential Medium (#11095-080; Gibco, Carlsbad, CA, USA) supplemented with 10% fetal bovine serum (Gibco), 1% penicillin/streptomycin (Gibco). JNK inhibitor (SP600125) and z-VAD-FMK were purchased from Santa Cruz Biotechnology. Coronarin D (purity > 95%) was purchased from ChemFaces (Wuhan, Hubei, China).

4.2. MTT Assay

The human osteosarcoma HOS and MG-63 cells were seeded in 24-well plates for 24 h. The cells were exposed to different concentrations of carnosol for 24 h. At the end of the assay time, 20 μL of MTT solution (5 mg/mL) (Invitrogen, Carlsbad, CA, USA) was added to each well, and then incubated for 2 h at 37 °C. After removing the cultured medium, 200 μL of dimethyl sulfoxide (DMSO) was added to each well. Absorbance at 590 nm of the dissolved formazan product was read using a spectrophotometric plate reader (Thermo Multiskan SPECTRUM, Thermo Fisher Scientific, Waltham, MA, USA). The half maximal inhibitory concentration (IC_{50}) for HOS and MG-63 cells were calculated by the "Forecast" function in Microsoft Excel.

4.3. Flow Cytometry Analysis

Cells were fixed with ice-cold 100% ethanol and kept on −20 °C for 24 h. Cells were rehydrated with cold PBS, and then resuspended in PBS with propium iodine (40 μg/mL) (#P4170; Sigma-Aldrich, St. Louis, MO, USA) and Ribonuclease A (0.2 μg/mL) at room temperature for 30 min in the dark. Samples were analyzed by a Cytomics™ FC500 flow cytometer (Beckman Coulter; Brea, CA, USA).

4.4. Apoptosis Assay

Cell apoptosis was determined by flow cytometry using the Annexin-V-FITC staining kit (Becton Dickinson, San Jose, CA, USA) according to the manufacturer's instructions. Briefly, the treated cells were trypsinized, and washed twice by cold PBS. The cells were incubated with 100 μL of 1× binding buffer with 5 μL of FITC Annexin V and 5 μL of propidium iodide for 15 min at room temperature (RT) in the dark. After incubation, 400 μL of 1× binding buffer was added to each tube, and the fluorescence was detected by a Cytomics™ FC500 flow cytometer (Beckman Coulter, Miami, FL, USA).

4.5. Cell Lysis and Immunoblotting

Cells were lysed in TEGN buffer (10 mM Tris, pH 7.5, 1 mM EDTA, 420 mM NaCl, 10% glycerol, and 0.5% Nonidet P-40) containing a protease inhibitor cocktail (Roche, Mannheim, Germany), phosphatase inhibitors (Roche), and 1 mM dithiothreitol (DTT). For Western blotting, the cell lysates were boiled in protein sample buffer (2 M β-mercaptoethanol, 12% sodium dodecyl sulfate (SDS), 0.5 M Tris, pH 6.8, 0.5 mg/mL bromophenol blue, and 30% glycerol). The samples were analyzed by SDS-polyacrylamide gel electrophoresis (PAGE). Antibodies used were the following: cleaved caspase-3 (#9661; Cell Signaling, Danvers, MA, USA), actin (A2066; Sigma-Aldrich, St. Louis, MO, USA), PARP (#9542; Cell Signaling), GAPDH (#2118; Cell Signaling), Cyclin B1 (#05-373SP; EMD Millipore, Temecula, CA, USA), SAPK/JNK (#9258; Cell Signaling), phospho-JNK (Thr183/Tyr185, Thr221/Tyr223) (#07-175; EMD Millipore, Temecula, CA, USA), and phospho-histone H3 (Ser10) (#9701; Cell Signaling).

4.6. Statistical Analysis

All data were obtained from at least three separate experiments and are expressed as mean ± SD. Statistical comparisons of differences between groups were conducted using the Student's *t*-test. A p value less than 0.05 was considered to represent statistical significance. All statistical analyses were performed using the software package GraphPad Prism (Version 4.0, GraphPad Software; San Diego, CA, USA).

Author Contributions: Conceived and designed the experiments: T.-S.S., C.-C.W., C.-P.H., C.-T.H., and Y.-F.H.; Performed the experiments: C.-T.H. and Y.-F.H.; Analyzed the data: T.-S.S., C.-C.W., C.-P.H., C.-T.H., and Y.-F.H.; Contributed reagents/materials/analysis tools: C.-P.H. and Y.-F.H.; Wrote the paper: Y.-F.H., T.-S.S., and C.-C.W.

Funding: This research received no external funding.

Acknowledgments: This study was supported by grants 106-CCH-IRP-018 from the Changhua Christian Hospital Research Foundation, Changhua City, Taiwan.

Conflicts of Interest: The authors declare no conflict of interest.

References

1. Broadhead, M.L.; Clark, J.C.; Myers, D.E.; Dass, C.R.; Choong, P.F. The Molecular Pathogenesis of Osteosarcoma: A Review. *Sarcoma* **2011**, *2011*, e959248. [CrossRef] [PubMed]
2. Lindsey, B.A.; Markel, J.E.; Kleinerman, E.S. Osteosarcoma Overview. *Rheumatol. Ther.* **2017**, *4*, 25–43. [CrossRef] [PubMed]
3. Dai, X.; Wang, L.; Deivasigamni, A.; Looi, C.Y.; Karthikeyan, C.; Trivedi, P.; Chinnathambi, A.; Alharbi, S.A.; Arfuso, F.; Dharmarajan, A.; et al. A Novel Benzimidazole Derivative, Mbic Inhibits Tumor Growth and Promotes Apoptosis Via Activation of Ros-Dependent Jnk Signaling Pathway in Hepatocellular Carcinoma. *Oncotarget* **2017**, *8*, 12831–12842. [CrossRef] [PubMed]

4. Mukherjee, A.K.; Basu, S.; Sarkar, N.; Ghosh, A.C. Advances in Cancer Therapy with Plant Based Natural Products. *Curr. Med. Chem.* **2001**, *8*, 1467–1486. [CrossRef] [PubMed]
5. Weaver, B.A. How Taxol/Paclitaxel Kills Cancer Cells. *Mol. Biol. Cell* **2014**, *25*, 2677–2681. [CrossRef] [PubMed]
6. Kaomongkolgit, R.; Jamdee, K.; Wongnoi, S.; Chimnoi, N.; Techasakul, S. Antifungal Activity of Coronarin D against Candida Albicans. *Oral Surg. Oral Med. Oral Pathol. Oral Radiol.* **2012**, *114*, 61–66. [CrossRef] [PubMed]
7. Reuk-ngam, N.; Chimnoi, N.; Khunnawutmanotham, N.; Techasakul, S. Antimicrobial Activity of Coronarin D and Its Synergistic Potential with Antibiotics. *Biomed. Res. Int.* **2014**, *2014*, 581985. [CrossRef] [PubMed]
8. Kunnumakkara, A.B.; Ichikawa, H.; Anand, P.; Mohankumar, C.J.; Hema, P.S.; Nair, M.S.; Aggarwal, B.B. Coronarin D, a Labdane Diterpene, Inhibits Both Constitutive and Inducible Nuclear Factor-Kappa B Pathway Activation, Leading to Potentiation of Apoptosis, Inhibition of Invasion, and Suppression of Osteoclastogenesis. *Mol. Cancer Ther.* **2008**, *7*, 3306–3317. [CrossRef] [PubMed]
9. Dhanasekaran, D.N.; Reddy, E.P. Jnk-Signaling: A Multiplexing Hub in Programmed Cell Death. *Genes Cancer* **2017**, *8*, 682–694. [PubMed]
10. Chen, J.C.; Hsieh, M.C.; Lin, S.H.; Lin, C.C.; Hsi, Y.T.; Lo, Y.S.; Chuang, Y.C.; Hsieh, M.J.; Chen, M.K. Coronarin D Induces Reactive Oxygen Species-Mediated Cell Death in Human Nasopharyngeal Cancer Cells through Inhibition of P38 Mapk and Activation of Jnk. *Oncotarget* **2017**, *8*, 108006–108019. [CrossRef] [PubMed]
11. Du, L.; Lyle, C.S.; Obey, T.B.; Gaarde, W.A.; Muir, J.A.; Bennett, B.L.; Chambers, T.C. Inhibition of Cell Proliferation and Cell Cycle Progression by Specific Inhibition of Basal Jnk Activity: Evidence That Mitotic Bcl-2 Phosphorylation Is Jnk-Independent. *J. Biol. Chem.* **2004**, *279*, 11957–11966. [CrossRef] [PubMed]
12. Gutierrez, G.J.; Tsuji, T.; Cross, J.V.; Davis, R.J.; Templeton, D.J.; Jiang, W.; Ronai, Z.A. Jnk-Mediated Phosphorylation of Cdc25c Regulates Cell Cycle Entry and G(2)/M DNA Damage Checkpoint. *J. Biol. Chem.* **2010**, *285*, 14217–14228. [CrossRef] [PubMed]
13. Guo, X.X.; An, S.; Yang, Y.; Liu, Y.; Hao, Q.; Tang, T.; Xu, T.R. Emerging Role of the Jun N-Terminal Kinase Interactome in Human Health. *Cell Biol. Int.* **2018**, *42*, 756–768. [CrossRef] [PubMed]
14. Li, Y.S.; Deng, Z.H.; Zeng, C.; Lei, G.H. Jnk Pathway in Osteosarcoma: Pathogenesis and Therapeutics. *J. Recept. Signal Transduct.* **2016**, *36*, 465–470. [CrossRef] [PubMed]
15. Mingo-Sion, A.M.; Marietta, P.M.; Koller, E.; Wolf, D.M.; Van Den Berg, C.L. Inhibition of jnk reduces g^2/m transit independent of p53, leading to endoreduplication, decreased proliferation, and apoptosis in breast cancer cells. *Oncogene* **2004**, *23*, 596–604. [CrossRef] [PubMed]
16. Ribas, V.T.; Gonçalves, B.S.; Linden, R.; Chiarini, L.B. Activation of c-jun n-terminal kinase (jnk) during mitosis in retinal progenitor cells. *PLoS ONE* **2012**, *7*, e34483. [CrossRef] [PubMed]
17. Oktay, K.; Buyuk, E.; Oktem, O.; Oktay, M.; Giancotti, F.G. The c-jun n-terminal kinase jnk functions upstream of aurora b to promote entry into mitosis. *Cell Cycle* **2008**, *7*, 533–541. [CrossRef] [PubMed]
18. Castedo, M.; Coquelle, A.; Vitale, I.; Vivet, S.; Mouhamad, S.; Viaud, S.; Zitvogel, L.; Kroemer, G. Selective resistance of tetraploid cancer cells against dna damage-induced apoptosis. *Ann. N. Y. Acad. Sci.* **2006**, *1090*, 35–49. [CrossRef] [PubMed]
19. Mittal, K.; Donthamsetty, S.; Kaur, R.; Yang, C.; Gupta, M.V.; Reid, M.D.; Choi, D.H.; Rida, P.C.G.; Aneja, R. Multinucleated Polyploidy Drives Resistance to Docetaxel Chemotherapy in Prostate Cancer. *Br. J. Cancer* **2017**, *116*, 1186–1194. [CrossRef] [PubMed]
20. Sharma, S.; Zeng, J.-Y.; Zhunag, C.; Zhang, R.; Wang, M. Abstract 921: Small-molecule inhibitor bms-777607 induces breast cancer cell polyploidy with increased resistance to cytotoxic chemotherapy agents. *Cancer Res.* **2013**, *73*, 921. [CrossRef]

Sample Availability: Not Available.

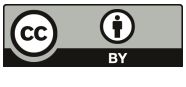

molecules

MDPI

Article

Novel Polyketides Produced by the Endophytic Fungus *Aspergillus Fumigatus* from *Cordyceps Sinensis*

Da-Le Guo [1], Xiao-Hua Li [1], Dan Feng [1], Meng-Ying Jin [1], Yu-Mei Cao [1], Zhi-Xing Cao [1], Yu-Cheng Gu [2], Zhao Geng [3], Fang Deng [1,*] and Yun Deng [1,*]

1 The Ministry of Education Key Laboratory of Standardization of Chinese Herbal Medicine, State Key Laboratory, Breeding Base of Systematic Research Development and Utilization of Chinese Medicine Resources, School of Pharmacy, Chengdu University of Traditional Chinese Medicine, Chengdu 611137, China; guodale@cdutcm.edu.cn (D.-L.G.); 18844144528@163.com (X.-H.L.); 18408210828@163.com (D.F.); ivyweilan@163.com (M.-Y.J.); maycao12@163.com (Y.-M.C.); caozhixing007@163.com (Z.-X.C.)

2 Syngenta Jealott's Hill International Research Centre, Berkshire RG42 6EY, UK; yucheng.gu@syngenta.com

3 Sichuan Institute of Food and Drug Control, Chengdu 611731, China; gengzhao713@hotmail.com

* Correspondence: dengfang@cdutcm.edu.cn (F.D.); dengyun@cdutcm.edu.cn (Y.D.); Tel.: +86-28-6180-0232 (Y.D.)

Received: 21 June 2018; Accepted: 7 July 2018; Published: 13 July 2018

Abstract: Five new polyketides, including two pairs of enantiomers and a racemate, were isolated from the fermentation broth of *Aspergillus fumigatus*, an endophytic fungus isolated from *Cordyceps sinensis*. Their structures were identified using one-dimensional (1D) and two-dimensional (2D) NMR experiments, and the absolute configurations of the enantiomers were confirmed using electronic circular dichroism (ECD) calculations. Compounds **1a** and **2a** exhibited inhibitory activity against the MV4-11 cell line in vitro, with IC_{50} values of 23.95 μM and 32.70 μM, respectively.

Keywords: *Aspergillus fumigatus*; *Cordyceps sinensis*; isochromanes; chiral resolution; ECD calculation; cytotoxicity

1. Introduction

Aspergillus fumigatus (*A. fumigatus*) is an omnipresent saprophytic fungus normally residing in the soil or decaying organic matter [1], and it has the ability to produce secondary metabolites that meet its survival requirements under various environmental conditions [2]. Previous chemical investigations revealed the constituents to be terpenes [3,4], phenolics [5], diketopiperazine [6], and other nitrogen compounds [7,8], which exhibit a variety of biological activities. For instance, fumagillin, which is a typical secondary metabolite from *A. fumigatus*, has the capacity to inhibit angiogenesis in tumor cells [9].

With the purpose of searching compounds with novel structures and bio-activities from endophytes of traditional Chinese medicine (TCM), *A. fumigatus*, as an endophytic fungus of *Cordyceps sinensis*, was chosen, and three new isochromanes were isolated from its fermentation broth (Figure 1). These polyketides were presumed to be the mixtures of enantiomers due to their approximate-to-zero optical rotation. Chiral resolution was further applied to two of these racemates, and it yielded two pairs of enantiomers. The absolute configurations of these enantiomers were further verified using quantum-chemical electronic circular dichroism (ECD) calculations. Details of the isolation, structure identification, and cytotoxicity evaluation of these new compounds are reported herein.

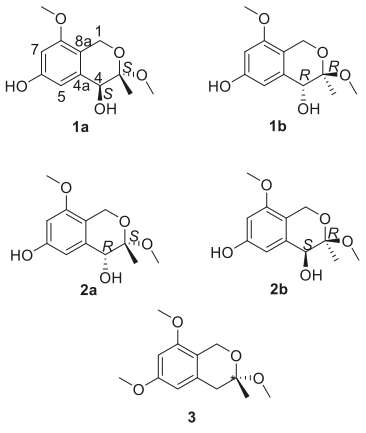

Figure 1. The structures of compounds obtained from *Aspergillus fumigatus*.

2. Results and Discussion

Compound **1** (Figure 1) was obtained as a yellow gum. The molecular formula of **1** was established using HRESIMS as $C_{12}H_{16}O_5$ (found 263.0897, calculated for $[M + Na]^+$ 263.0890). The infrared (IR) spectrum showed intense absorption bands of hydroxy at ν_{max} 3397.5 cm^{-1} (OH), and 1613.2 cm^{-1} and 1371.6 cm^{-1} (phenyl), as well as a methylene band at 2932.1 cm^{-1}. The ^1H NMR spectrum displayed two aromatic proton signals at δ 6.38 (1H, d, J = 2.2 Hz, H-5) and 6.33 (1H, d, J = 2.2 Hz, H-7), two methoxyl signals at δ 3.76 (3H, s, 8-OMe) and 3.30 (3H, s, 3-OMe), one oxymethylene signal at δ 4.46 (1H, d, J = 15.3 Hz, H-1) and 4.41 (1H, d, J = 15.3 Hz, H-1), and one methine signal at δ 4.00 (1H, s, H-4) and 1.46 (3H, s, 3-Me). The ^{13}C NMR and DEPT spectra of Compound **1** exhibited 12 carbon signals, including six aromatic carbons at δ 158.4 (C-8), 157.2 (C-6), 137.3 (C-4a), 114.2 (C-8a), 109.0 (C-5), and 99.0 (C-7), a quaternary carbon at δ 101.5 (C-3), one methine carbon at δ 70.4 (C-4), one methylene carbon at δ 60.7 (C-1), two methoxyl carbons at δ 55.8 (8-OMe) and 49.8 (3-OMe), and a methyl signal at δ 19.1 (C-3). The HMBC correlations of H-1/C-8 and C-3, H-5/C-4, 3-Me/C-3 and C-4, 3-OMe/C-3, and 8-OMe/C-8, as well as the NOESY correlations of H-7/8-OMe confirmed the presence of an isochromane scaffold, and the primary structure of **1** was established as 3,8-dimethoxy-3-methylisochromane-4,6-diol (Figure 2). The NOESY correlations of H-4/3-OMe indicated that the relative configuration of **1** should be 3R*,4R* (Figure 3). Compound **1** was presumed to be a mixture of enantiomers, as its optical rotation was approximate to zero. Further chiral HPLC analysis confirmed the presence of a pair of anticipated enantiomers. Subsequent chiral resolution was applied, and two enantiomers, **1a** and **1b**, were obtained successfully. The ECD experiment and ECD calculation of **1** were conducted to determine its absolute configuration. The calculated ECD spectra of 3S, 4S-**1** fitted the experimental spectrum of **1a** nicely, while the calculated ECD spectra of 3R, 4R-**1** matched the experimental spectra of **1b** quite well, allowing the absolute configurations of **1a** and **1b** to be determined as 3S, 4S and 3R, 4R, respectively.

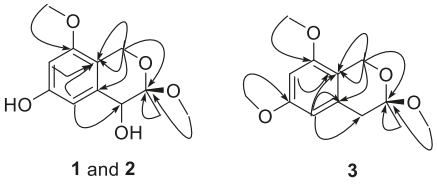

Figure 2. Key HMBC correlations of Compounds **1**–**3**.

Compound **2** (Figure 1) was obtained as a yellow gum. It was assigned the same molecular formula, $C_{12}H_{16}O_5$, as **1** on the basis of HRESIMS. The NMR spectra of **2** were similar to those of **1**, which indicated that it was an epimer of **1**. Both the changes in chemical shift of H-4 (δ 4.36), C-4 (δ 72.6), and C-3 (δ 99.5), and the absence of NOESY correlation of H-4/3-OMe indicated its relative configuration should be 3R*,4S*. Based on its optical rotation, chiral separation was applied, and it successfully produced a pair of enantiomers. The ECD experiment and ECD calculation of **2b** were conducted to determine its absolute configuration. The results (Figure 4) indicated that the calculated ECD curve of 3R, 4S-**2** was similar to the experimental ECD spectrum of (+)-**2** (**2b**), which designated the configuration of (+)-**2** as 3R, 4S-3,8-dimethoxy-3-methylisochromane-4,6-diol. On the other hand, (−)-**2** was assigned to be 3S, 4R-3,8-dimethoxy-3-methylisochromane-4,6-diol (**2a**) accordingly.

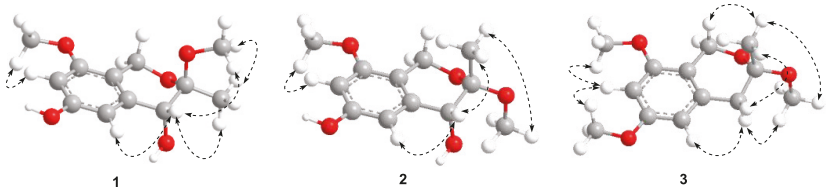

Figure 3. The key NOESY correlations of Compounds **1**–**3**.

Compound **3** (Figure 1) was isolated as a yellow gum. Its molecular formula was established as $C_{13}H_{18}O_4$ on the basis of the HRESIMS through the pseudo-molecular ion peak at m/z 261.1107 $[M + Na]^+$ (calculated for 261.1097). The ^1H and ^{13}C NMR spectra indicated that **3** possessed a similar structure to **1** and **2** except for a methylene (δ_H: 2.85, d, J = 16.4 Hz, 2.73, d, J = 16.4 Hz; δ_C: 39.8) instead of a methine group at C-4, and the presence of another methoxyl (δ_H: 3.78; δ_C: 55.7). The HMBC correlation of 6-Me/C-6 readily located this methoxyl at C-6. Thus, **3** was elucidated to be 3,6,8-trimethoxy-3-methylisochromane.

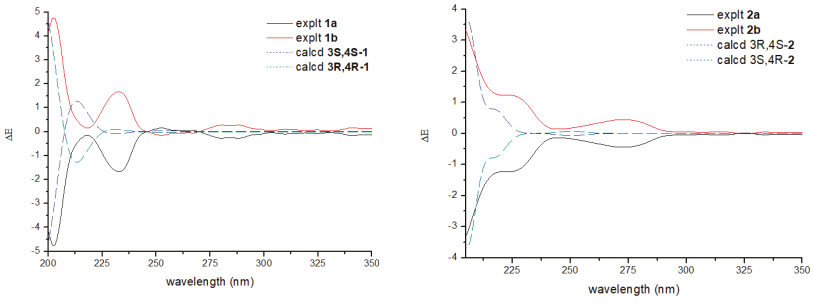

Figure 4. Experimental electronic circular dichroism (ECD) spectra of Compounds **1** and **2** and their calculated curves.

The MTT method was applied to evaluate the cytotoxicity of these compounds against MDA-ME-231 and MV4-11 cancer cell lines. Compounds **1a** and **2a** showed moderate growth inhibition against the MV4-11 cell line with IC_{50} values of 23.95 μM and 32.70 μM, respectively.

3. Materials and Methods

3.1. General Experimental Procedures

The UV spectra were measured on a PerkinElmer Lambda 35 UV-VIS spectrophotometer (PerkinElmer, Waltham, MA, USA). The IR spectra were recorded on a PerkinElmer Spectrum One

Fourier-transform IR (FT-IR) spectrometer, (PerkinElmer, Waltham, MA, USA). The ECD spectra were obtained on a JASCO (Oklahoma City, OK, USA) J-810 spectrometer. The optical rotations were measured on a JASCO (Oklahoma City, OK, USA) P-1020 polarimeter. The NMR spectra were recorded on a Bruker (Billerica, MA, USA) 400 spectrometer, for one-dimensional (1D) and two-dimensional (2D) NMR. The HRESIMS data were recorded on a Bruker (Billerica, MA, USA) Micro TOF-Q II mass spectrometer. Preparative HPLC was performed on a Hanbon Sci. & Tech. (Huaian, Jiangsu, China) NP7000 serials instrument equipped with a Hanbon Sci. & Tech. (Huaian, Jiangsu, China) NU3000 serials UV detector, using a Kromasil 100-5-C_{18} column (10 × 250 mm, 5μm; Akzo Nobel Pulp and Performance Chemicals AB, Bohus, Sweden) for normal separation, and a column Chiralpak IC column (4.6 × 250 mm, 5 μm; Chiral Technologies, West Chester, PA, USA) for chiral resolution. Column chromatography (CC) was performed on a silica gel (200–300 mesh; Qingdao Marine Chemical Inc., Qingdao, China) and a Sephadex LH-20 (GE-Healthcare Bio-Sciences AB, Uppsala, Sweden). All solvents used were of analytical grade.

3.2. Fungal Material

The *A. fumigatus* strain was separated from *Cordyceps sinensis* collected in Xiahe county, China in May 2017. The fungus was identified using morphological observation and sequence (GenBank acccession No. MG519287) analyses of the ITS region of recombinant DNA (rDNA). The identified strain was inoculated into 24,500 mL Erlenmeyer flasks, each containing 200 mL of potato dextrose agar (PDA) at room temperature, agitated on an orbital shaker at 200 rpm for seven days to produce the seed culture. The fermentation was carried out in one hundred and twenty 1000 mL Fernbach flasks, each containing 10 mL of seed culture and 400 mL of medium (soluble starch 0.8%, peptone 0.5%, NaCl 0.2%, $CaCO_3$ 0.2%, $MgSO_4 \cdot 7H_2O$ 0.05%, and K_2HPO_4 0.05%), and was incubated at 25 °C on a rotary shaker at 200 rpm for 15 days.

3.3. Fractionation and Isolation

The culture was filtered to separate the mycelia and the broth. The broth was firstly extracted with petroleum ether, followed by ethyl acetate. The ethyl acetate solution was concentrated to a brown residue (9.3 g). The crude extract was fractionated using liquid chromatography on a silica gel (6 × 30 cm) with a gradient elution of $CHCl_3$/MeOH. The fractions eluted with a ratio of 75:25 were combined, (1.08 g) and were further subjected to Sephadex LH-20 column chromatography (4 × 180 cm; mobile phase $CHCl_3$/MeOH, 1:1), which afforded three sub-fractions (Fr.1–Fr.3). Fr.3 (91 mg) was purified using a preparative HPLC with a reversed-phase column (5u 100 A; 10 × 250 mm; mobile phase MeOH/H_2O, 65:35) to furnish Compounds **1** (3.0 mg), **2** (1.9 mg), and **3** (2.9 mg). Compound **1** was further separated using HPLC with a Chiralpak IC column (mobile phase n-hexane/isopropanol, 85:15) to yield Compounds **1a** (0.33 mg, R_t 10.4 min) and **1b** (0.42 mg, R_t 20.6 min), while Compound **2** was further separated under the same conditions to give Compounds **2a** (0.16 mg, R_t 8.1 min) and **2b** (0.26 mg, R_t 28.5 min).

3.3.1. 3R,4S-3,8-Dimethoxy-3-methylisochromane-4,6-diol (**1a**)

Yellow gum, $[\alpha]_D^{20}$ = +167.9 (c = 0.02, MeOH), IR (KBr): 3397.5, 2932.1, 1613.2, 1371.6, 1055.3 cm^{-1}; λ_{max} 207.3 (3.74), 281.5 (2.72); ^1H (CD_3OD, 400 MHz) and ^{13}C NMR (CD_3OD, 100 MHz) spectroscopic data (see Table 1 and Supplementary Material); HRESIMS *m*/*z* 263.0897 $[M + Na]^+$ (calculated for $C_{12}H_{16}O_5Na^+$, 263.0890).

Table 1. The ^{1}H (400 MHz) and ^{13}C (100 MHz) NMR data (δ in ppm, multiple J in Hz) of Compounds **1**–**3**.

Position	**1** [a]		**2**		**3**	
	δ_H	δ_C	δ_H	δ_C	δ_H	δ_C
1	4.41, d, 15.3 Hz 4.46, d, 15.3 Hz	60.7	4.56, d, 15.2 Hz 4.43, d, 15.2 Hz	60.6	4.65, d, 15.1 Hz 4.44, d, 15.1 Hz	60.2
2	-	-	-	-	-	-
3	-	101.5	-	99.5	-	98.8
4	4.00, s	70.4	4.36, s	72.6	2.85, d, 16.4 Hz 2.73, d, 16.4 Hz	39.8
4a	-	137.3	-	138.6	-	134.4
5	6.38, d, 2.2 Hz	109.0	6.63, d, 2.1 Hz	105.5	6.33, d, 2.1 Hz	105.5
6	-	157.2	-	158.5	-	161.0
7	6.33, d, 2.2 Hz	99.0	6.28, d, 2.1 Hz	97.9	6.33 d, 2.1 Hz	96.9
8	-	158.4	-	156.8	-	157.4
8a	-	114.2	-	114.6	-	115.2
3-Me	1.46, s	19.1	1.49, s	20.5	1.44, s	23.4
3-OMe	3.30, s	49.8	3.31, s	49.1	3.28, s	48.8
6-OMe	-	-	-	-	3.78	55.7
8-OMe	3.76, s	55.8	3.75, s	55.8	3.72	55.8

[a] Compounds **1**–**3** were measured in CD_3OD.

3.3.2. 3R,4R-3,8-Dimethoxy-3-methylisochromane-4,6-diol (**1b**)

Yellow gum, $[\alpha]_D^{20} = -167.9$ (c = 0.01, MeOH), spectrometric (UV, IR, NMR, MS, and HRESIMS) data are the same as those of **1a**.

3.3.3. 3S,4R-3,8-Dimethoxy-3-methylisochromane-4,6-diol (**2a**)

Yellow gum, $[\alpha]_D^{20} = -260.1$ (c = 0.01, MeOH), IR (KBr): 3421.1, 2940.8, 1623.6, 1384.6, 1061.2 cm^{-1}; λ_{max} 211.1 (3.76), 282.2 (2.73); ^{1}H (CD_3OD, 400 MHz) and ^{13}C NMR (CD_3OD, 100 MHz) spectroscopic data (see Table 1); HRESIMS m/z 263.0893 $[M + Na]^+$ (calculated for $C_{12}H_{15}O_5Na^+$, 263.0890).

3.3.4. 3R,4S-3,8-Dimethoxy-3-methylisochromane-4,6-diol (**2b**)

Yellow gum, $[\alpha]_D^{20} = +260.1$ (c = 0.01, MeOH), spectrometric (UV, IR, NMR, MS, and HRESIMS) data are the same as those of **2a**.

3.3.5. 3,6,8-Trimethoxy-3-methylisochromane (**3**)

Yellow gum, $[\alpha]_D^{20} = +0.9$ (c = 0.11, MeOH), IR (KBr): 3435.5, 2923.0, 1638.5, 1384.2, 1074.7 cm^{-1}; λ_{max} 210.6 (3.85), 281.0 (2.97); ^{1}H (CD_3OD, 400 MHz) and ^{13}C NMR (CD_3OD, 100 MHz) spectroscopic data (see Table 1); HRESIMS m/z 261.1107 $[M + Na]^+$ (calculated for $C_{12}H_{16}O_4Na^+$, 261.1097).

3.4. MTT Assay

The MV4-11 and MDA-ME-231 cells (American Type Culture Collection, Manassas, VA, USA) were grown in DMEM or IMDM medium containing 10% FBS in 5% CO_2 at 37 °C. When the cells entered the exponential growth phase, they were seeded in a 96-well plate and incubated overnight. Afterward, media containing various concentrations of tested compounds from 3.125 μM to 100 μM were added to each well. Additionally, 0.1% DMSO was used as a blank control, while taxol was used as a positive control. After the incubation period (72 h at 37 °C), 20 μL/well of MTT reagent (5 mg/mL) was added, and the wells were incubated for 2–4 h, before 50 μL/well of 20 acidified SDS was added to lyse the cells. Finally, the absorbance was measured at 570 nm to evaluate the inhibition effects of the tested compounds on cell growth. All experiments were performed in triplicate.

4. Conclusions

Among the five new compounds obtained from a TCM-related strain *A. fumigatus*, two pairs of novel enantiomers were discovered. The MTT method was used to detect the cytotoxicity of these compounds against MDA-ME-231 and MV4-11 cells. Compounds **1a** and **2a** exhibited moderate cytotoxic activity against the MV4-11 cell line with IC_{50} values of 23.95 μM and 32.70 μM, respectively.

Supplementary Materials: The following are available online, Pages 1–3: The computational details; Figures S1–S2: HPLC chromatograms of **1** and **2** using a Chiralpak IC column; Figures S3–S23: MS and NMR spectra of Compounds **1**–**3**.

Author Contributions: D.-L.G. and Y.D. conceived and designed the experiments; X.-H.L., M.-Y.J. and Y.-M.C., performed the experiments; D.-L.G., Z.-X.C., and Z.G. analyzed the data; D.F. contributed materials; Y.-C.G. and F.D. wrote the paper.

Funding: This work was financially supported by grants from the National Natural Sciences Foundation of China (81373961); Sichuan Provincial Youth Science and Technology Innovation Team (2016TD0006, 2015TD0028); Project Funded by China Postdoctoral Science Foundation (2017M622985); and Project Funded by Department of Education in Sichuan Province (18ZA0191).

Acknowledgments: The authors wish to thank Jing Yang (KIB CAS, China) for the help in ECD calculation.

Conflicts of Interest: No potential conflict of interest was reported by the authors.

References

1. Haas, H. Fungal siderophore metabolism with a focus on *Aspergillus fumigatus*. *Nat. Prod. Rep.* **2014**, *31*, 1266–1276. [CrossRef] [PubMed]
2. Kwon-Chung, K.J.; Sugui, J.A. *Aspergillus fumigatus*—What makes the species a ubiquitous human fungal pathogen? *PLoS Pathog.* **2013**, *9*, e1003743. [CrossRef] [PubMed]
3. Chu, M.; Mierzwa, R.; He, L.; Xu, L.; Patel, M.; Patel, D.; Chan, T.M. Structure of Sch 528647: A new antitumor antibiotic related to Fumagillin. *J. Antibiot.* **2001**, *54*, 1096–1099. [CrossRef] [PubMed]
4. Wang, Y.; Li, D.H.; Li, Z.L.; Sun, Y.J.; Hua, H.M.; Liu, T.; Bai, J. Terpenoids from the Marine-Derived Fungus *Aspergillus fumigatus* YK-7. *Molecules* **2016**, *21*, 31. [CrossRef] [PubMed]
5. Cutler, H.G.; Lauren, D.R.; Wilkins, A.L.; Holland, P.T.; Hill, R.A.; Dugan, F.M. Ruakuric acid: A natural product from *Aspergillus fumigatus*. *Phytochemistry* **1996**, *43*, 209–214. [CrossRef]
6. Wang, F.Z.; Fang, Y.C.; Zhu, T.J.; Zhang, M.; Lin, A.Q.; Gu, Q.Q.; Zhu, W.M. Seven new prenylated indole diketopiperazine alkaloids from holothurian-derived fungus *Aspergillus fumigatus*. *Tetrahedron* **2008**, *64*, 7986–7991. [CrossRef]
7. Magotra, A.; Kumar, M.; Kushwaha, M.; Awaschi, P.; Raina, C.; Gupta, A.P.; Shah, B.A.; Gandhi, S.G.; Chaubey, A. Epigenetic modifier induced enhancement of fumiquinazoline C production in *Aspergillus fumigatus* (GA-L7): An endophytic fungus from *Grewia asiatica* L. *ABM Express* **2017**, *7*, 43. [CrossRef] [PubMed]
8. Shi, Y.S.; Zhang, Y.; Chen, X.Z.; Zhang, N.; Liu, Y.B. Metabolites produced by the endophytic fungus *Aspergillus fumigatus* from the stem of *Erythrophloeum fordii oliv*. *Molecules* **2015**, *20*, 10793–10799. [CrossRef] [PubMed]
9. Sin, N.; Meng, L.H.; Wang, M.Q.W.; Wen, J.J.; Bornmann, W.G.; Crews, C.M. The anti-angiogenic agent fumagillin covalently binds and inhibits the methionine aminopeptidase, MetAP-2. *Proc. Natl. Acad. Sci. USA* **1997**, *94*, 6099–6103. [CrossRef] [PubMed]

Sample Availability: Samples of the compounds **1a**, **1b**, and **3** are available from the authors.

molecules

MDPI

Article

Cytotoxic Triterpenes from *Salacia crassifolia* and Metabolite Profiling of Celastraceae Species

Laila S. Espindola [1,2,*], Renata G. Dusi [1,2], Daniel P. Demarque [1], Raimundo Braz-Filho [3], Pengcheng Yan [2,4], Heidi R. Bokesch [2,5], Kirk R. Gustafson [2] and John A. Beutler [2]

1 Laboratório de Farmacognosia, Universidade de Brasília, Campus Universitário Darcy Ribeiro, Brasília 70910-900, Brazil; renatadusi@hotmail.com (R.G.D.); dpdemarque@gmail.com (D.P.D.)
2 Molecular Targets Program, National Cancer Institute, Frederick, MD 21702, USA; yanpc@wzmc.edu.cn (P.Y.); bokeschh@mail.nih.gov (H.R.B.); gustafki@mail.nih.gov (K.R.G.); beutlerj@mail.nih.gov (J.A.B.)
3 FAPERJ/Departamento de Química, Universidade Federal Rural do Rio de Janeiro, Seropédica, RJ and Laboratório de Ciências Químicas, Universidade Estadual do Norte Fluminense, Campos dos Goytacazes, Rio de Janeiro 28013-602, Brazil; braz@uenf.br
4 School of Pharmaceutical Sciences, Wenzhou Medical University, Wenzhou 325035, China
5 Basic Science Program, Leidos Biomedical Research, Inc., Frederick National Laboratory for Cancer Research Sponsored by the National Cancer Institute, Frederick, MD 21702, USA
* Correspondence: darvenne@unb.br; Tel.: +55-61-3107-2016

Academic Editor: Roberto Fabiani
Received: 2 June 2018; Accepted: 18 June 2018; Published: 20 June 2018

Abstract: The new pentacyclic triterpene 11β-hydroxypristimerin (**1**), along with the known metabolites pristimerin (**2**), 6-oxopristimerol (**3**) and vitideasin (**4**), were isolated from a *Salacia crassifolia* root wood extract, following a bioassay-guided fractionation approach. Both the extract and the purified triterpenes displayed pronounced cytotoxic activity against human cancer cell lines. The NCI-60 cell line screen revealed that compound **2** was the most active, with a mean GI_{50} of 0.17 μM, while compound **1** had a mean GI_{50} of 8.7 μM. A COMPARE analysis of the screening results showed that pristimerin is likely to be the main compound responsible for the cytotoxic activity of the extract (mean GI_{50} of 0.3 $\mu g \cdot mL^{-1}$). A targeted search for pristimerin and related derivatives using LC-MS/MS revealed the presence of pristimerin (**2**) and 6-oxopristimerol (**3**) in all Celastraceae species examined and in all plant parts tested, while vitideasin (**4**) was only detected in the genus *Salacia*.

Keywords: cytotoxic activity; NCI-60 cancer cell line; pristimerin; *Salacia crassifolia*; Celastraceae; Brazilian Cerrado biome; *Salacia elliptica*; *Cheiloclinium cognatum*; *Plenckia populnea*

1. Introduction

Anticancer drugs derived from plants such as vinblastine, vincristine, etoposide, teniposide, paclitaxel (Taxol®), docetaxel, topotecan and irinotecan continue to have significant therapeutic value [1]; however, cancer remains a leading cause of death worldwide. In the research described below, we utilized bioassay-guided isolation of the cytotoxic constituents in selected plant extracts, the same approach that led to the discovery of some of these antitumor agents.

The Cerrado biome of Brazil has proven to be a rich source of cytotoxic plant extracts [2]. *Salacia crassifolia* (Mart. ex Schult.) G. Don, Celastraceae, popularly known as Bacupari-do-Cerrado, has been used by traditional communities to treat cancer [3]. It is a tree from the Cerrado biome adapted to the region's dry climate with a well-developed root system. This species is cultivated for its edible fruit, used as an ornamental plant, and used for reforestation and restoration of degraded

environments. Beyond its use against cancer, *S. crassifolia* is utilized in traditional medicine as an antimicrobial and anti-inflammatory agent [3]. Previous phytochemical investigations of the hexane extract of the leaves of *S. crassifolia* led to the isolation of friedelanes [4], commonly found in the leaves of Celastraceae species, and known as precursors of quinone methide triterpenoids found in the roots of these species [5,6]. Twenty-one extracts from *S. crassifolia*, *Salacia elliptica* (Mart.) G. Don, *Cheiloclinium cognatum* (Miers) A.C. Sm., and *Plenckia populnea* Reissek were analyzed by mass spectrometry to verify the distribution of pentacyclic triterpenoids in different plant parts of various Celastraceae species. In order to probe the cytotoxic potential and chemical profile of *S. crassifolia*, the hexane extract of its root wood was evaluated by high-throughput screening (HTS) against diverse tumor cells, together with the NCI-60 cell line screen [7]. Herein, we report the bioassay-guided isolation and structure elucidation of compounds **1**–**4** and their cytotoxic activity.

2. Results and Discussion

In our search for new cytotoxic agents, the hexane extract of *S. crassifolia* root wood was selected by preliminary high-throughput screening of Cerrado plant extracts, tested at 10 $\mu g \cdot mL^{-1}$ in eight cancer cell lines: Colo205 and KM12 (colon cancer), A498 and U031 (renal cancer), HEP3B and SKHEP (liver cancer), and MG63 and MG63.3 (osteosarcoma). While cytotoxic activity was observed in most cell lines, the extract did not inhibit the growth of either of the hepatic cancer cell lines. Dose-response experiments were then conducted with the root wood extract (N192803) in the colon, renal, and osteosarcoma cell lines. Based on its ^{1}H NMR profile and selective cytotoxic activity, this extract was subsequently submitted for testing in the NCI-60 tumor cell assay [7].

2.1. Dose-Response Results

The extract of *S. crassifolia* root wood was cytotoxic against the KM12 colon cancer cell line (IC_{50} 1.7 $\mu g \cdot mL^{-1}$), but had no activity against Colo205 colon cancer cells at 20 $\mu g \cdot mL^{-1}$. Likewise, it was active against the A498 renal cancer cell line (IC_{50} 1.6 $\mu g \cdot mL^{-1}$), but showed no inhibitory activity at 20 $\mu g \cdot mL^{-1}$ for U031 renal cancer cells. Divergent activity in two renal cancer cell lines and two colon cancer cell lines provided evidence of potential selectivity among other cancer cell types, which can be further assessed in the NCI-60 cell screen. We considered this a favorable sign to justify a detailed study of this extract. When tested against osteosarcoma MG63 (non-metastatic) and MG63.3 (metastatic) cells, the extract inhibited cell growth with an IC_{50} of 3.7 $\mu g \cdot mL^{-1}$ and 5.7 $\mu g \cdot mL^{-1}$, respectively. Since these two related cell lines differ in their metastatic potential, the similar potency indicated that the sample does not differentially target metastatic osteosarcoma cells.

2.2. Extract NCI-60 Results

The hexane extract of *S. crassifolia* root wood (N192803) was submitted to both the NCI-60 cell line one-dose and five-dose screens. The mean GI_{50} (50% growth inhibition) was 0.3 $\mu g \cdot mL^{-1}$, a 3-fold lower concentration than its mean total growth inhibition (TGI) and 15-fold lower than the mean LC_{50} (Figure 1). The GI_{50} ranged from a low of 0.17 $\mu g \cdot mL^{-1}$ for the HCT-15 colon cancer cell line, to a high of 2.3 $\mu g \cdot mL^{-1}$, and growth inhibitory activity was observed in leukemia, melanoma, lung, colon, brain, ovarian, breast, prostate, and kidney cancer cell lines (Supplementary Materials).

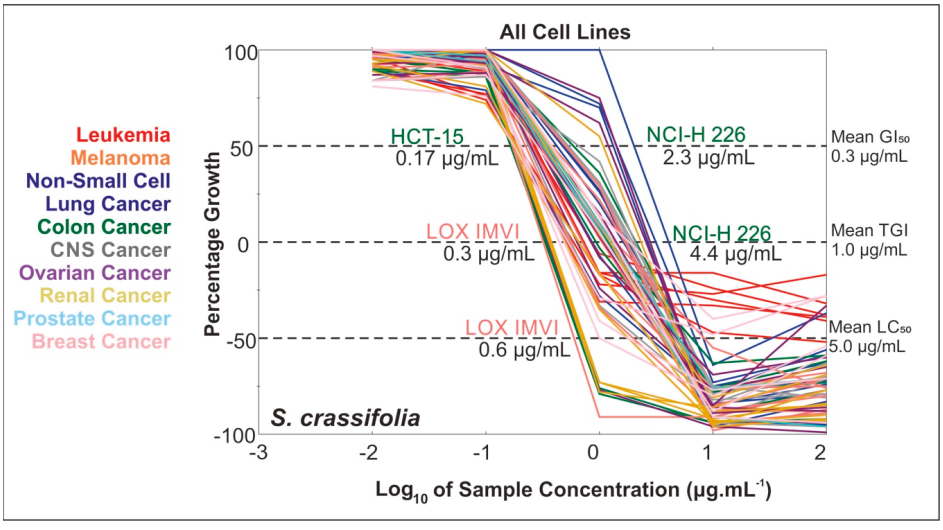

Figure 1. NCI-60 dose-response curves for the *Salacia crassifolia* root wood extract. Percentage growth of 100: cell growth is comparable to the control; percentage growth of 0: cells are still viable but no net cell growth relative to time zero; percentage growth of −100: complete cell killing, no cells are viable.

2.3. Bioassay-Guided Fractionation of S. crassifolia

In order to identify the active compounds, the root wood hexane extract was initially fractionated on diol Solid Phase Extraction cartridges to give fractions of increasing polarity (A–E). Fraction B was eluted with CH_2Cl_2-EtOAc (20:1) and it showed an IC_{50} of 3.8 µg·mL^{-1} and 1.9 µg·mL^{-1} in renal (A498 and UO31), and 14.9 µg·mL^{-1} and 16.5 µg·mL^{-1} in osteosarcoma (MG63 and MG63.3) cancer cell lines. It was further fractionated on a Sephadex LH-20 column, giving 11β-hydroxypristimerin (**1**) in fraction B3 after final purification on HPLC; pristimerin (**2**) in fraction B5 and 6-oxopristimerol (**3**) in fraction B9. Another portion of fraction B3 after separation on a silica gel column gave vitideasin (**4**) in fraction B3-1, and compound **2** in B3-2. Fractions A and C from the initial diol fractionation also showed cytotoxicity in renal and osteosarcoma cell lines (Supplementary Materials). Investigation of these fractions showed that **2** is also a major component, thus explaining their growth inhibitory activity.

Compound **2** is the major secondary metabolite of the *S. crassifolia* extract, accounting for 69% of fraction B3, and it was present in fractions B2 to B7. Gonçalves et al. [8] reported the presence of **2** in a mixture containing another colorless compound that was obtained from the roots of *S. crassifolia*, and this mixture showed notably weaker antimicrobial activity than commercially available pristimerin. In this current study, the availability of high resolution chromatographic and spectroscopic techniques allowed the isolation and characterization of structurally similar compounds (**1**–**4**) (Figure 2) with differential cytotoxic potencies, as seen between **1** and **2**. Carvalho et al. [9] reported that Gonçalves et al. [10] isolated maytenin from *S. crassifolia*, but, in fact, Gonçalves described the isolation of maytenin from *Maytenus ilicifolia*.

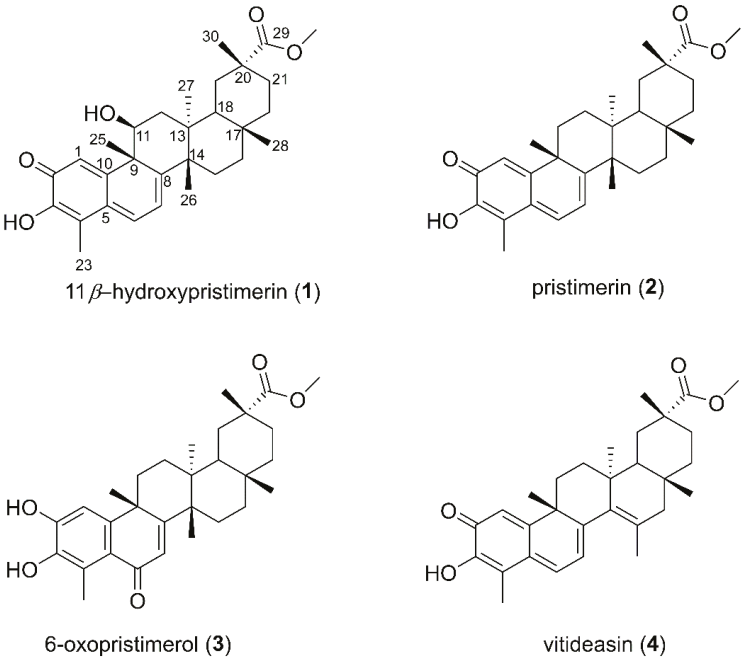

Figure 2. The structure of compounds isolated from *Salacia crassifolia*. 11β-hydroxypristimerin (**1**), pristimerin (**2**), 6-oxopristimerol (**3**) and vitideasin (**4**).

2.4. Identification of Isolated Compounds from Salacia crassifolia

From a portion of the diol fraction B, 11β-hydroxypristimerin (**1**), a previously unreported compound, was isolated (see experimental for more details). The mass spectrum of **1** helped establish the molecular formula as $C_{30}H_{38}O_4$ (m/z 463.2849; $[M\text{-}H_2O + H]^+$; error = 0.2 ppm). In the ^1H NMR data (Supplementary Materials), we observed signals for three olefinic protons (H-1, H-6 and H-7) and, in the ^{13}C spectrum, we observed eight olefinic carbons (C-1, C-3, C-4, C-5, C-6, C-7, C-8 and C-10) and a carbonyl carbon (C-2, δ 178.8). H-1, an α-carbonyl olefinic proton, was observed as a singlet (δ 7.32). H-6 and H-7 signals were observed as doublets at δ 6.88 and δ 6.28 (J = 7.2 Hz), respectively. Hence, compound **1** was characterized as a quinonemethide triterpene with a methyl ester group substituted in ring-E (carbonyl C-29 δ 178.7; methoxyl C-31 δ 51.8, H-31 δ 3.60). The NMR data for **1** closely matched those reported for pristimerin **2** [11,12]. The only significant difference was an oxymethine assigned at C-11 (H-11, δ 4.57; dd, J = 12.2, 6.4 Hz) based on its coupling with H_2-12. Molecular formula requirements established a hydroxy substituent at this position and the large vicinal coupling constants required an axial (β) orientation of H-11. Our spectroscopic analyses along with biogenetic considerations allowed assignment of the structure **1** as 11β-hydroxypristimerin.

Pristimerin (**2**) was identified in fraction B5, and 6-oxopristimerol (**3**) was detected in fraction B9. The ^1H and ^{13}C NMR data of these compounds were compared with literature values [11] to assure proper identification of the structures (NMR spectra and data are available in Supplementary Materials). LC-MS/MS analysis of pristimerin (**2**) indicated a molecular formula of $C_{30}H_{40}O_4$ with the presence of a protonated ion ($[M + H]^+$ m/z 465.3004; error: 0.1 ppm) and a sodiated adduct ($[M + Na]^+$ m/z 487.2823; error: 0.4 ppm). When submitted to collisional activation, the protonated molecular ion generated a highly intense fragment at m/z 201.0915. The proposal for this fragmentation involves carbocation formation at C-8, followed by a methyl shift and a pericyclic fragmentation giving rise to

m/*z* 201.0915 (Figure 3). This type of fragmentation pathway for pristimerin (**2**) was used to identify and confirm the presence of related triterpenoids in the extracts and fractions being studied.

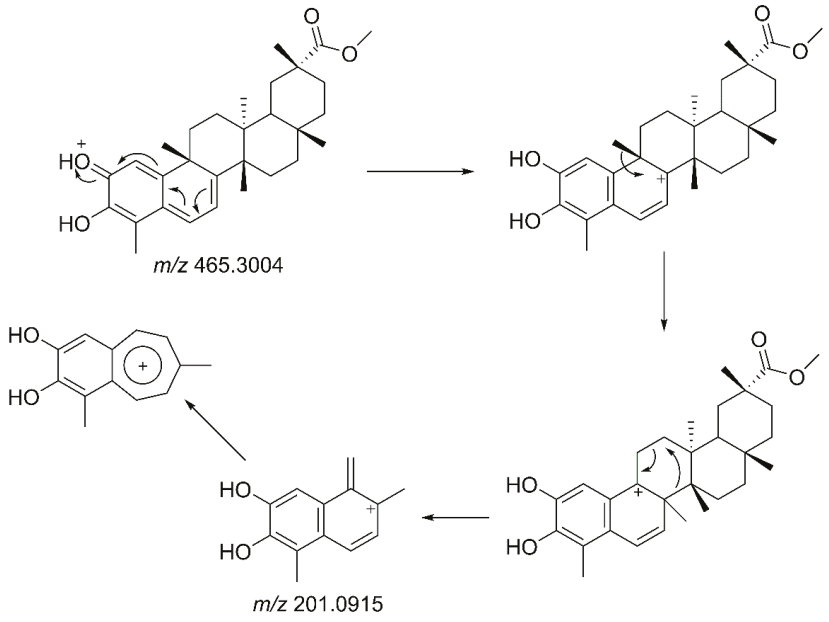

Figure 3. Proposed fragmentation for pristimerin (**2**).

LC-MS/MS analysis of 6-oxopristimerol (**3**) generated both the protonated molecular ion ([M + H]$^+$ $C_{30}H_{41}O_5$ *m*/*z* 481.2949; error: 1 ppm) and the sodiated adduct ([M + Na]$^+$ $C_{30}H_{40}NaO_5$ *m*/*z* 503.2771; error 0.5 ppm). The fragmentation of **3** follows the same pattern as pristimerin (**2**), although, due to the additional oxygen at C-6, the intense fragment ion is at *m*/*z* 217.0860 [12].

The mass spectrum of vitideasin (**4**) showed a protonated molecular ion ([M + H]$^+$ $C_{30}H_{39}O_4$ *m*/*z* 463.2878; error: 6.4 ppm) and its NMR spectroscopic data was compared with literature values [13] (NMR data and spectra are available in Supplementary Materials). Fragmentation of the protonated ion gave rise to a *m*/*z* 201.0899 ion, the same fragment observed with pristimerin (**2**).

In the LC-MS/MS analysis of the *S. crassifolia* root extract, it was possible to identify other triterpene quinonemethide derivatives, such as 6-oxopristimerol derivatives with an extra double bond ([M + H]$^+$ $C_{30}H_{39}O_5$ *m*/*z* 463.2847; error: 0.3 ppm) compared to 6-oxopristimerol (**3**). Fragmentation of the protonated molecule gave rise to an ion at *m*/*z* 217.0853, as seen with **3**. Due to the low yield of this metabolite, NMR analysis for structural assignment was not possible. Another compound identified by MS was a 11β-hydroxypristimerin derivative ([M + H]$^+$ $C_{30}H_{39}O_5$ *m*/*z* 479.2713; error: 17.6 ppm), which also had an extra unsaturation compared with 11β-hydroxypristimerin (**1**). Fragmentation of the protonated molecule gave rise to a *m*/*z* 201.0917 fragment. These results indicate that *S. crassifolia* is a rich source of additional quinonemethide triterpenoids and their derivatives.

2.5. Biological Activity of Isolated Compounds

Compounds **1**, **2**, and **3** were submitted to the NCI-60 cell screen. In this National Cancer Institute screen, which utilizes 60 different human tumor cell lines, **2** exhibited a mean GI_{50} value of 0.23 μM, with individual values ranging from 0.12 μM (UO-31 renal and T-47D breast) to 1.2 μM (A549 non-small cell lung). Compound **1** was less potent, with a mean GI_{50} value of 8.7 μM, with the renal cancer

cell line 786-O being the most sensitive. A COMPARE bioinformatic analysis resulted in a Pearson correlation factor of 0.9 between the crude *S. crassifolia* extract and compound **2**, indicating that it is likely the major compound responsible for the extract activity. A weaker correlation factor of 0.7 was found between the extract and **1** (Figure 4). Although compounds **1** and **2** are structurally similar, their mutual correlation factor was only 0.5, suggesting that a β-hydroxyl group at C-11 altered the mode of action and reduced the potency. In addition, oxidation of C-6 and loss of the quinone moiety in compound **3** drastically reduced its cytotoxic activity, making it ineligible to be tested in a full dose response in the NCI-60 screen. In accordance with the literature, triterpenes with a quinonemethide moiety in the A-ring display more potent cytotoxic activity in cancer cells [14].

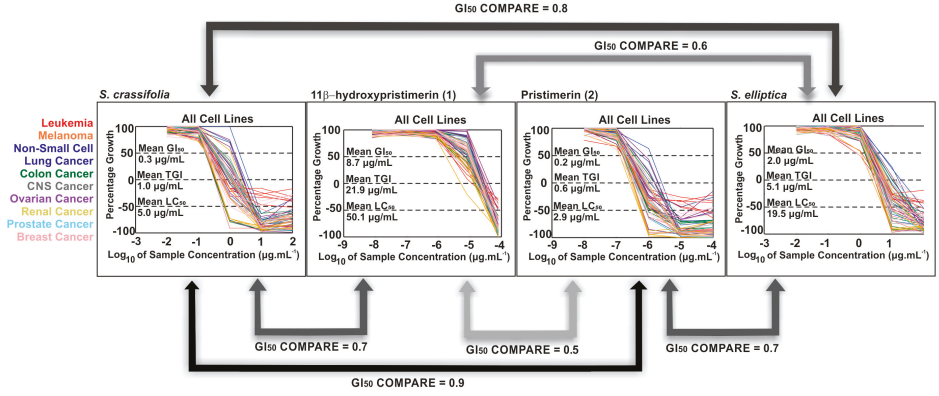

Figure 4. COMPARE correlations between **1**, **2** and *Salacia* extracts.

2.6. LC-MS/MS Analysis of Extracts of Species from the Celastraceae Family

S. crassifolia root is a rich source of compound **2** and other pristimerin-like triterpenes. In order to identify the presence of quinonemethide triterpenes in other Celastraceae species, we performed targeted metabolite analysis of twenty-one different extracts from the leaves, stems, and roots of *S. crassifolia*, *S. elliptica*, *C. cognatum* and *P. populnea*, obtained using hexane, ethyl acetate or ethanol as extraction solvents. The compounds 11β-hydroxypristimerin (**1**), pristimerin (**2**), 6-oxopristimerol (**3**) and vitideasin (**4**) were monitored by LC-MS/MS, as well as the quinonemethide triterpenes isoiguesterin ($[M + H]^+$ 403.3 > 201.3), a salaquinone A derivative ($[M + H]^+$ 451.3 > 201.3), a tingenin B derivative ($[M + H]^+$ 437.3 > 201.3), and tingenone ($[M + H]^+$ 407.3 > 201.3). Of these latter compounds, only salaquinone A was detected in any of the extracts. In Figure 5, we summarize the findings of these analyses in a heatmap generated using the MetaboAnalyst platform [15].

Pristimerin (**2**) is a naturally occurring quinonemethide triterpenoid, restricted to plants of the Celastraceae [16]. Previously, it has shown cytotoxic [17], antimicrobial [4], anti-inflammatory [18], and antioxidant [9] activities. Earlier studies showed that pristimerin is found mainly in the roots of Celastraceae species, while its precursor friedelin, and other similarly cyclized intermediates, are found in the leaves [5,6]. A study of *S. campestris* and *Maytenus aquifolium* suggested a compartmentalized biosynthesis of quinonemethide triterpenoids in the root bark of Celastraceae species [6]. However, we detected pristimerin (**2**) and 6-oxopristimerol (**3**) in all plant parts of all species studied (Figure 5), including leaves, albeit at a lower concentration than in the roots. Detection of pristimerin (**2**) in the hydroalcoholic leaf extract of *Maytenus aquifolium* has previously been reported [19]. Salaquinone A and 11β-hydroxypristimerin were detected in *C. cognatum*, *S. crassifolia* and *S. elliptica* extracts, while vitideasin (**4**) was only detected in *Salacia* extracts (Figure 5).

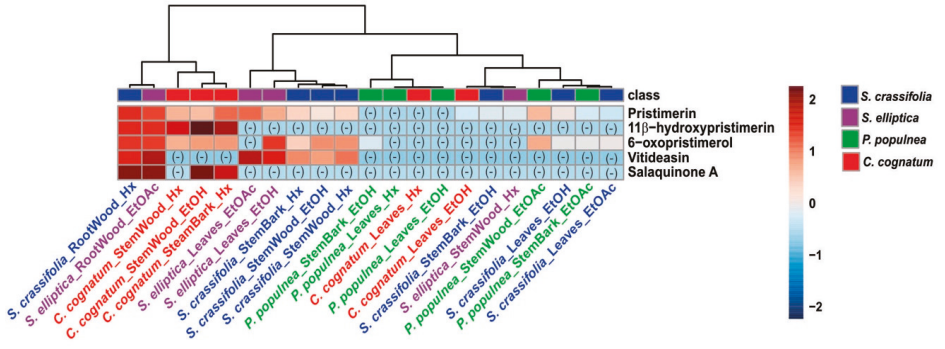

Figure 5. Heatmap and similarity analysis obtained using the MetaboAnalyst platform to analyze the metabolite profile of twenty-one different extracts from leaves, stem and root of *S. crassifolia*, *S. elliptica*, *C. cognatum* and *P. populnea*, obtained using hexane, ethyl acetate and ethanol as extraction solvents.

The ethyl acetate extract of *S. elliptica* root wood showed a mean GI_{50} in the NCI-60 of 2.04 μg·mL^{-1}, 6-fold greater than the GI_{50} of the *S. crassifolia* root wood hexane extract. The leukemia cell line MOLT-4 and breast cancer line T-47D were the most sensitive to this *S. elliptica* extract with a GI_{50} of 0.7 μg·mL^{-1}. The *S. elliptica* extract had only 40% (LC-MS/MS peak area) of **2** relative to *S. crassifolia* and, indeed, it showed a weaker COMPARE correlation coefficient of 0.7 with **2** (Figure 4). The correlation coefficient between the two *Salacia* extracts was 0.8. The only two extracts that met the criteria for NCI-60 dose response testing were from the roots of *S. elliptica* and *S. crassifolia*, where **2** is more abundant, reinforcing that **2** is the predominant active compound in the extracts. Carneiro et al. [20] showed that the methanolic extract of *S. crassifolia* stem bark had no in vivo cytotoxic activity. In a similar finding from our study, the ethanolic extract of *S. crassifolia* stem bark was not active in any of the eight cancer cell lines in preliminary HTS. The lack of cytotoxic activity of these polar extracts is consistent with the low abundance of **2**, as seen in Figure 5. The *C. cognatum* stem bark hexane extract selectively inhibited 87% of MG63 cells at 10 μg·mL^{-1}, and it had only 12.5% (LC-MS/MS peak area) of the pristimerin content, relative to the *S. crassifolia* extract (Figure 5).

In summary, the Brazilian Cerrado environment provides a rich source of bioactive plant metabolites. In particular, species of the Celastraceae offer numerous bioactive quinonemethide triterpenes, some of which have selective effects on cancer cell growth. In the case of *Salacia* species, the roots were rich in pristimerin (**2**). Compound **2** showed selective inhibitory activity towards a variety of human tumor cell lines and it was primarily responsible for the cytotoxic activity of the crude extracts. A co-occurring metabolite was identified as 11*β*-hydroxypristimerin (**1**), which is a new member of this triterpenoid class. These results demonstrate that the combined use of a targeted search for pristimerin and derivatives, cytotoxicity screening, and COMPARE analysis can efficiently identify the plant species and plant parts containing these and other growth inhibitory compounds.

3. Materials and Methods

3.1. General Experimental Procedures

UV absorption spectra were obtained using a Varian Cary 50 Bio UV−visible spectrophotometer (Agilent, Santa Clara, CA, USA). IR spectra were measured using a Perkin-Elmer FT-IR Spectrometer, SPECTRUM 2000 (Waltham, MA, USA). NMR spectra were acquired on a Bruker Avance III spectrometer (Billerica, MA, USA) operating at 600 MHz for ^{1}H and 150 MHz for ^{13}C and equipped with a 3 mm cryogenically cooled probe. ^{1}H and ^{13}C spectra were referenced to the residual deuterated solvent peaks. HRESIMS data were acquired on an Agilent 6530 Accurate Mass Q-TOF instrument

(Santa Clara, CA, USA) and on a TripleTOF 5600 mass spectrometer (AB SCIEX, Framingham, MA, USA). Diol SPE fractionation of the extract was performed on DIO Spe-ed SPE cartridges (Applied Separations, Allentown, PA, USA), and subsequent fractions were separated on Sephadex LH-20 (GE Healthcare, Chicago, IL, USA). These fractions were then separated on silica gel. Sephadex LH-20 and silica gel columns were attached to a UA-6 UV detector and Foxy 200 fraction collector (Teledyne Isco, Lincoln, NE, USA). Final purifications were performed using a Varian ProStar HPLC with the indicated gradient and column. All solvents and chemicals used were of analytical grade.

3.2. Plant Extracts

Salacia crassifolia (Mart. ex Schult.) G. Don, Celastraceae, identified by esteemed Cerrado specialist botanist Prof. José Elias de Paula, was collected in August 2007, from the Cerrado *sensu stricto-campo aberto* of the Cerrado biome, Santo Antônio do Descoberto, Goiás State, at an altitude of 1169 m; 15°47′51.8″ S 48°17′44.3″ W. A voucher specimen was deposited in the Herbarium of the Universidade de Brasília under the accession number (UB) 3776. *Salacia elliptica* (Mart.) G. Don was collected in August 2007 at 1112 m; 15°49′00.5″ S 48°19′14.2″ W, Cerrado *campo sujo* ecosystem, voucher (UB) 3819. *Plenckia populnea* Reissek was collected in June 2007 at 1.243 m; 15°39′939″ S 47°53′195″ W, voucher (UB) 3747. *Cheiloclinium cognatum* (Miers) A.C. Sm. was collected in February 2009 at 961 m; 15°46′32.7″ S 47°38′59.5″ W, voucher (UB) 3805.

3.3. Antiproliferative Bioassay

The formazan endpoint assay developed by the Assay Development and Screening Section of the Molecular Targets Laboratory was used for the antiproliferative bioassays. The tests were carried out as described previously [21]. HTS was used to screen the hexane extract of *S. crassifolia* root wood at 10 $\mu g \cdot mL^{-1}$ in eight cancer cell lines: Colo205 and KM12 (colon cancer), A498 and U031 (renal cancer), HEP3B and SKHEP (liver cancer) and MG63 and MG63.3 (osteosarcoma). The extract was then further tested in dose response, from 20 $\mu g \cdot mL^{-1}$ to 1.3 $\mu g \cdot mL^{-1}$, in colon, renal and osteosarcoma cell lines, as well as in the NCI-60 cell assay. This screen utilizes 60 different human tumor cell lines, representing leukemia, melanoma and cancers of the lung, colon, brain, ovary, breast, prostate, and kidney. Three endpoints are calculated: (1) GI_{50}, the concentration yielding a growth percent of 50 (i.e., 50% growth inhibition), (2) TGI, the concentration yielding a growth percent of 0, or Total Growth Inhibition, and (3) LC_{50}, the concentration yielding a growth percent of −50, or lethality in 50% of the starting cells [7].

3.4. Bioassay-Guided Isolation of Compounds

The dried and powdered root wood (315.4 g) of *S. crassifolia* was subjected to repeated maceration with hexane, and the solvent was concentrated to dryness under reduced pressure at 30 °C yielding crude extract (3.2977 g). The extract was fractionated by solid phase extraction chromatography using a stepwise fractionation (2 g, 6 mL Diol cartridge, Applied Separations, Allentown, PA, USA). For the procedure, 864.3 mg of extract was dissolved in 12.8 mL of 1:1 CH_2Cl_2/MeOH and the soluble portion applied to 8 diol cartridges. After drying overnight, each cartridge was sequentially eluted with 6 mL of the following: 9:1 Hexane/CH_2Cl_2 (fraction A = 217.1 mg), 20:1 CH_2Cl_2/EtOAc (fraction B = 527.7 mg), EtOAc (fraction C = 82.7 mg), 5:1 EtOAc/MeOH (fraction D = 25.5 mg) then MeOH (fraction E = 9.9 mg). The fractions collected were dried under nitrogen gas, submitted for bioassay and analyzed by ^{1}H NMR. Renal (UO-31 and A498) and osteosarcoma (MG63 and MG63.3) cancer cell lines were used for bioassay-guided isolation. Based on the biological results, a portion (373.65 mg) of fraction B was solubilized in 7.5 mL of hexane/CH_2Cl_2/MeOH (2:5:1) and fractionated on 3 Sephadex LH-20 columns using the same solvent mixture. For each column, 72 fractions were collected and combined in 10 fractions (B1 to B10) based on the UV chromatogram. The fractions collected were dried under nitrogen gas and analyzed by ^{1}H NMR. A portion of the combined B3 fraction (71.4 mg) was subjected to silica gel column chromatography eluted with mixtures of CH_2Cl_2/EtOAc (92:8, 90:10, 85:15, 80:20, 70:30, 50:50, 40:60, 0:100) to yield 5 fractions: B3-1 (4.6 mg), B3-2 (49.29 mg), B3-3 (1.8 mg),

B3-4 (8.05 mg) and B3-5 (7.1 mg). Another portion of the B3 fraction was purified using a Phenomenex Luna C8 (5 μ, 300 Å, 250 × 4.6 mm) column with 80% to 92% acetonitrile in water gradient (0–30 min), monitoring at 254 nm.

11β-Hydroxypristimerin (1): UV (MeOH) λ (log ε) 205 (4.34), 280 (3.54), 400 (3.30) nm; ^{1}H NMR ($CDCl_3$, 600 MHz) δ 7.32 (1H, s, H-1), 6.88 (1H, d, *J* = 7.2 Hz, H-6), 6.28 (1H, d, *J* = 7.2 Hz, H-7), 4.57 (1H, dd, *J* = 12.2, 6.4 Hz, H-11), 3.60 (3H, s, OCH_3), 2.40, 1.74 (each 1H, m, H_2-19), 2.38, 2.01 (each 1H, m, H_2-12), 2.24, 1.40 (each 1H, m, H_2-21), 2.19 (3H, s, H_3-23), 2.00, 0.98 (each 1H, m, H_2-22), 1.87, 1.51 (each 1H, m, H_2-16), 1.64 (3H, s, H_3-25), 1.62, 1.58 (each 1H, m, H_2-15), 1.59 (1H, m, H-18), 1.30 (3H, s, H_3-26), 1.20 (3H, s, H_3-30), 1.10 (3H, s, H_3-28), 0.61 (3H, s, H_3-27), ^{13}C NMR ($CDCl_3$, 125 MHz) δ 178.8 (C, C-2), 178.7 (C, C-29), 167.2 (C, C-8), 161.6 (C, C-10), 145.9 (C, C-3), 132.2 (CH, C-6), 128.6 (C, C-5), 121.6 (CH, C-1), 118.8 (C, C-7), 118.0 (C, C-4), 65.3 (CH, C11), 51.8 (CH_3, $COOCH_3$), 48.1 (C, C-9), 44.9 (C, C-14), 43.9 (CH, C-18), 43.4 (CH_2, C-12), 40.6 (C, C-13), 40.4 (C, C-20), 36.2 (CH_2, C-16), 34.4 (CH_3, C-25), 34.3 (CH_2, C-22), 32.7 (CH_3, C-30), 31.4 (CH_3, C-28), 30.87 (C, C-17), 30.81 (CH_2, C-19), 29.7 (CH_2, C-21), 28.7 (CH_2, C-15), 21.4 (CH_3, C-26), 18.5 (CH_3, C-27), 10.4 (CH_3, C-23). HRESIMS *m*/*z* 463.2849 (calcd. for $C_{30}H_{38}O_4 + H^+$; [M − H_2O + H]; error = 0.2 ppm).

3.5. LC-MS/MS Analysis of Isolated Compounds

For analysis of isolated compounds, an HPLC ekspert ultraLC 100 coupled with a TripleTOF 5600 mass spectrometer (AB SCIEX, Framingham, MA, USA) was used. For chromatographic separation, a Shim-pack XR-ODS C_{18} column (5 cm × 2.0 mm, 2.2 μm particle size) (Shimadzu, Kyoto, Japan) was used, coupled with a pre-column with the same material. The mobile phases were water and methanol (both with 0.1% of formic acid). The elution method initiated with 5% of methanol was kept isocratic for 1.0 min, which was then increased to 95% over 10 min. Four minutes were added to the method to wash and stabilize the column. The injection volume was 2 μL, and the column temperature was 40 °C. The positive ionization mode was employed and the ionization source parameters were CUR 22 (Curtain Gas), source temperature 450 °C, ionization voltage (IS) 5500 V, Gas1 (nebulization gas) 45, Gas2 (turbo heaters gas) 45 and DP 100 (declustering potential).

3.6. LC-MS/MS Analysis of Extracts of Species from the Celastraceae Family: Targeted Search for Pristimerin and Derivatives

Twenty-one different extracts from *P. populnea*, *C. cognatum*, *S. crassifolia* and *S. elliptica* were analyzed using an HPLC (Shimadzu LC-20AD, Kyoto, Japan) coupled with an ESI triple quadrupole mass spectrometer (ABSciex API 3200). For chromatographic separation, a Supelco Ascentis Express C_{18} column (15 cm × 4.6 mm, 2.7 μm particle size) (Bellefonte, PA, USA) was used. The mobile phases were water and methanol (both with 0.1% of formic acid). The elution method initiated with 70% of methanol, which was then increased to 100% for 5 min and kept isocratic until 11 min. Four minutes were added to stabilize the column. The injection volume was 10 μL, the column temperature was 45 °C and the autosampler temperature was 15 °C. The positive ionization mode was employed and the ionization source parameters were CUR 12 (Curtain Gas), source temperature 500 °C, ionization voltage (IS) 4500 V, CAD gas (collisionally-activated dissociation gas) 5, Gas1 (nebulization gas) 40 and Gas2 (turbo heaters gas) 40. The parameters DP (declustering potential) was 45, EP (entrance potential) 10, CE (collision energy) 25, CXP (collision cell exit potential) 3 and DT (Dwell time) 100. The transitions monitored were 465.3 > 201.2 (pristimerin), 481.3 > 201.2 (11β-hydroxypristimerin), 481.3 > 217.3 (6-oxopristimerol), 463.3 > 201.3 (vitideasin). Other quinonemethides triterpenes were also monitored, as 403.3 > 201.3 (isoiguesterin), 451.3 > 201.3 (salaquinone A derivative), 437.3 > 201.3 (tingenin B derivative) and 407.3 > 201.3 (tingenone). The area values were analysed in MetaboAnalyst 4.0 [15] (McGill University, Montreal, Canada) using log transformation and autoscaling for data scaling (mean-centered and divided by the standard deviation of each variable). The heatmap was built using Euclidean distance measure and Ward clustering algorithm. The data was grouped according to the species.

Supplementary Materials: The following are available online: Detailed biological results, COMPARE correlations between the NCI-60 tested compounds and extracts; and the spectroscopic data of Compounds **1**, **2**, **3** and **4**.

Author Contributions: Conceptualization, L.S.E.; Methodology, L.S.E. and R.G.D.; Validation, L.S.E., K.R.G., H.R.B. and J.A.B.; Formal Analysis, J.A.B. and L.S.E.; Investigation, L.S.E., R.G.D., D.P.D., H.R.B. and P.I.; Resources, L.S.E., K.R.G., J.A.B. and H.R.B.; Data Curation, L.S.E. and D.P.D.; Writing—Original Draft Preparation, L.S.E., D.P.D. and R.G.D.; Writing—Review and Editing, L.S.E., R.G.D., D.P.D., K.R.G., H.R.B. and J.A.B.; Visualization, L.S.E., R.G.D. and D.P.D.; Supervision, L.S.E.; Project Administration, L.S.E.; Funding Acquisition, L.S.E., K.R.G., and J.A.B.; Targeted search for pristimerin and derivatives, D.P.D.; LC-MS/MS analysis, D.P.D.; Structural elucidation, R.B.-F., L.S.E., R.G.D., D.P.D., P.I. and K.R.G.

Funding: The authors wish to thank the Brazilian scientific research agency *CNPq*—Process 249213/2013-3. The Special Fund for ArboControl Brasil Project, Process TED74/2016 (FNS/UnB) for providing a postdoctoral fellowship to D.P. Demarque and supporting R.G. Dusi. This research was also supported in part by the Intramural Research Program of the NIH, National Cancer Institute, Center for Cancer Research and with federal funds from the National Cancer Institute, National Institutes of Health, under contract HHSN261200800001E. The content of this publication does not necessarily reflect the views or policies of the Department of Health and Human Services, nor does it mention trade names, commercial products, or organizations implying endorsement by the U.S. Government. Article processing charges were sponsored by MDPI.

Acknowledgments: This paper is dedicated to the memory of the botanist Professor José Elias de Paula for the legacy left to the Laboratório de Farmacognosia of Universidade de Brasília. We have obtained authorization to access the plant samples used for research from the Council for the Genetic Heritage Management (CGen)/ Brazilian Institute of the Environment and Renewable Natural Resources (IBAMA) n. 06/2012—Process 02000.002272/2006-73; and official permission to export the Brazilian Cerrado plant extracts from the CGen/IBAMA—Exportation License n. 14BR014583/DF. The authors thank Norberto Peporine Lopes and Guilherme D. Brand for allowing us to perform the LC-MS/MS analysis in their laboratories.

Conflicts of Interest: The authors declare no conflict of interest.

References

1. Cragg, G.M.; Grothaus, P.G.; Newman, D.J. New horizons for old drugs and drug leads. *J. Nat. Prod.* **2014**, *77*, 703–723. [CrossRef] [PubMed]
2. de Mesquita, M.L.; de Paula, J.E.; Pessoa, C.; de Moraes, M.O.; Costa-Lotufo, L.V.; Grougnet, R.; Michel, S.; Tillequin, F.; Espindola, L.S. Cytotoxic activity of Brazilian Cerrado plants used in traditional medicine against cancer cell lines. *J. Ethnopharmacol* **2009**, *123*, 439–445. [CrossRef] [PubMed]
3. Attuch, I.M. Conhecimentos tradicionais do Cerrado: Sobre a memória de Dona Flor, raizeira e parteira. Master's Thesis, Universidade de Brasília, Brasília, Brazil, 2006.
4. Rodrigues, V.G.; Duarte, L.P.; Silva, R.R.; Silva, G.D.F.; Mercadante-Simoes, M.O.; Takahashi, J.A.; Matildes, B.L.G.; Fonseca, T.H.S.; Gomes, M.A.; Vieira, S.A. Salacia crassifolia (Celastraceae): Chemical constituents and antimicrobial activity. *Quim. Nova* **2015**, *38*, 237–242. [CrossRef]
5. Shan, W.G.; Zhang, L.W.; Xiang, J.G.; Zhan, Z.J. Natural friedelanes. *Chem. Biodivers.* **2013**, *10*, 1392–1434. [CrossRef] [PubMed]
6. Corsino, J.; de Carvalho, P.R.; Kato, M.J.; Latorre, L.R.; Oliveira, O.M.; Araujo, A.R.; Bolzani, V.D.; Franca, S.C.; Pereira, A.M.; Furlan, M. Biosynthesis of friedelane and quinonemethide triterpenoids is compartmentalized in Maytenus aquifolium and Salacia campestris. *Phytochemistry* **2000**, *55*, 741–748. [CrossRef]
7. Shoemaker, R.H. The NCI60 human tumour cell line anticancer drug screen. *Nature Reviews. Cancer* **2006**, *6*, 813–823. [CrossRef] [PubMed]
8. Gonçalves de Lima, O.; Coelho, J.S.B.; Maciel, G.M.; Heringer, E.P.; Gonçalves de Lima, C. Substancias antimicrobianas de plantas superiores-Comunicação XXXIX-Identificação de pristimerina como um componente ativo do "Bacupari" do Araguaia, Salacia crassifolia (Mart.) G. Don. (Hippocrateaceae). *Rev. Inst. Antibiót. (Recife)* **1972**, *12*, 19–24.
9. Carvalho, P.R.; Silva, D.H.; Bolzani, V.S.; Furlan, M. Antioxidant quinonemethide triterpenes from Salacia campestris. *Chem. Biodivers.* **2005**, *2*, 367–372. [CrossRef] [PubMed]
10. Gonçalves de Lima, O.; Coelho, J.S.B.; Weigert, E.; D'Albuquerque, I.L.; Lima, D.A.; Souza, M.A.M. Substancias antimicrobianas de plantas superiores-Comunicação XXXVI-Sobre a presença de maitenina e pristimerina na parte cortical das raízes de Maytenus ilicifolia, procedente do Brasil Meridional. *Rev. Inst. Antibiót. (Recife)* **1971**, *11*, 35–38.

11. Gunatilaka, A.A.L.; Chandrasiri, H.; Kikuchi, T.; Tezuka, Y. ^{1}H and ^{13}C NMR analysis of three Quinone-Methide Triterpenoids. *Magn. Reson. Chem.* **1989**, *27*, 803–811. [CrossRef]
12. Shirota, O.; Morita, H.; Takeya, K.; Itokawa, H. Cytotoxic aromatic triterpenes from Maytenus ilicifolia and Maytenus chuchuhuasca. *J. Nat. Prod.* **1994**, *57*, 1675–1681. [CrossRef] [PubMed]
13. De Almeida, M.T.; Rios-Luci, C.; Padron, J.M.; Palermo, J.A. Antiproliferative terpenoids and alkaloids from the roots of Maytenus vitis-idaea and Maytenus spinosa. *Phytochemistry* **2010**, *71*, 1741–1748. [CrossRef] [PubMed]
14. Salvador, J.A.R.; Leal, A.S.; Valdeira, A.S.; Goncalves, B.M.F.; Alho, D.P.S.; Figueiredo, S.A.C.; Silvestre, S.M.; Mendes, V.I.S. Oleanane-, ursane-, and quinone methide friedelane-type triterpenoid derivatives: Recent advances in cancer treatment. *Eur. J. Med. Chem.* **2017**, *142*, 95–130. [CrossRef] [PubMed]
15. Xia, J.; Wishart, D.S. Using MetaboAnalyst 3.0 for comprehensive metabolomics data analysis. *Curr. Protoc. Bioinforma.* **2016**, *55*, 14–10. [CrossRef] [PubMed]
16. Dirsch, V.M.; Kiemer, A.K.; Wagner, H.; Vollmar, A.M. The triterpenoid quinonemethide pristimerin inhibits induction of inducible nitric oxide synthase in murine macrophages. *Eur. J. Pharmacol.* **1997**, *336*, 211–217. [CrossRef]
17. Yousef, B.A.; Hassan, H.M.; Zhang, L.Y.; Jiang, Z.Z. Anticancer potential and molecular targets of pristimerin: A mini-review. *Curr. Cancer Drug Targets* **2017**, *17*, 100–108. [CrossRef] [PubMed]
18. Tong, L.; Nanjundaiah, S.M.; Venkatesha, S.H.; Astry, B.; Yu, H.; Moudgil, K.D. Pristimerin, a naturally occurring triterpenoid, protects against autoimmune arthritis by modulating the cellular and soluble immune mediators of inflammation and tissue damage. *Clin. Immunol.* **2014**, *155*, 220–230. [CrossRef] [PubMed]
19. Nossack, A.C.; Celeghini, R.M.D.; Lancas, F.M.; Yariwake, J.H. HPLC-UV and LC-MS analysis of quinonemethides triterpenes in hydroalcoholic extracts of "espinheira santa" (Maytenus aquifolium Martius, Celastraceae) leaves. *J. Braz. Chem. Soc.* **2004**, *15*, 582–586. [CrossRef]
20. Carneiro, C.C.; Silva, C.R.; Menezes, A.C.; Pérez, C.N.; Chen-Chen, L. Assessment of genotoxic, cytotoxic, and protective effects of *Salacia crassifolia* (Mart. Ex. Schult.) G. Don. stem bark fractions in mice. *Genet. Mol. Res.* **2013**, *12*, 2167–2177. [CrossRef] [PubMed]
21. Cho, N.; Ransom, T.T.; Sigmund, J.; Tran, T.; Cichewicz, R.H.; Goetz, M.; Beutler, J.A. Growth inhibition of colon cancer and melanoma cells by versiol derivatives from a Paraconiothyrium species. *J. Nat. Prod.* **2017**, *80*, 2037–2044. [CrossRef] [PubMed]

Sample Availability: Samples of the compounds are not available from the authors.

molecules

MDPI

Review

Anti-Cancer Activity of Porphyran and Carrageenan from Red Seaweeds

Zhiwei Liu [1,2], Tianheng Gao [3], Ying Yang [4], Fanxin Meng [1], Fengping Zhan [1], Qichen Jiang [4,*] and Xian Sun [1,5,*]

1 School of Pharmacy and Food Sciences, Zhuhai College of Jilin University, Zhuhai 519041, China; zwliumost@126.com (Z.L.); mfx@jluzh.edu.cn (F.M.); ZhanFengping@163.com (F.Z.)
2 School of Environment and Energy, South China University of Technology, Guangzhou 510006, China
3 Institute of Marine Biology, College of Oceanography, Hohai University, Nanjing 210017, China; gaotianheng928@hhu.edu.cn
4 Freshwater Fisheries Research Institute of Jiangsu Province, 79 Chating East Street, Nanjing 210017, China; sanbao1120@gmail.com
5 School of Marine Sciences, Sun Yat-Sen University, Guangzhou 510275, China
* Correspondence: qichenjiang@live.cn (Q.J.); imytian@163.com (X.S.); Tel.: +86-25-86618250 (Q.J.); +86-756-7626350 (X.S.)

Academic Editor: Roberto Fabiani
Received: 27 October 2019; Accepted: 24 November 2019; Published: 25 November 2019

Abstract: Seaweeds are some of the largest producers of biomass in the marine environment and are rich in bioactive compounds that are often used for human and animal health. Porphyran and carrageenan are natural compounds derived from red seaweeds. The former is a characteristic polysaccharide of *Porphyra*, while the latter is well known from *Chondrus*, *Gigartina*, and various *Eucheuma* species, all in Rhodophyceae. The two polysaccharides have been found to have anti-cancer activity by improving immunity and targeting key apoptotic molecules and therefore deemed as potential chemotherapeutic or chemopreventive agents. This review attempts to review the current study of anti-cancer activity and the possible mechanisms of porphyran and carrageenan derived from red seaweeds to various cancers, and their cooperative actions with other anti-cancer chemotherapeutic agents is also discussed.

Keywords: seaweed; porphyran; carrageenan; anti-cancer

1. Introduction

Cancers are serious diseases of various etiologies, especially that of unhealthy eating habits and lifestyle. In 2018, about 9.6 million cancer-related deaths and 18 million new cases were estimated by the World Health Organization (WHO) [1]. Uncontrolled growth, invasiveness, and metastasis are characteristics of tumor cells evoked by acquired genetic changes [2]. With tumor development, unbalanced programmed cell death, disordered signaling pathways, angiogenesis, and poor immune response disrupt various homeostatic pathways. Such deregulated pathways are the main targets of cancer treatment by chemotherapy [3]. According to the characteristics and stage of the tumor, combined therapy is applied in cancer treatment including surgery, chemotherapy, radiation therapy, and immunotherapy. The ultimate aim of all treatments is to destroy the tumor cells in the achievement of cancer treatment, while avoid damaging normal cells as far as possible. Unfortunately, severe side effects are often unavoidable, limiting the efficacy of treatment. Chemotherapy is commonly and effectively used in cancer therapeutics, exerting cytotoxicity on rapidly dividing and proliferating cells, not only including malignant cells, but also normal cells with high-proliferating potential. Thus, chemotherapy usually brings serious side effects including anemia, appetite loss, delirium, alopecia,

peripheral neuropathy, and irreversible damage to vital organs [4]. In addition, drug tolerance is also an issue in cancer treatment, which would weaken the treatment effects. Targeted therapy could avoid the side effects in part, but not always completely. Monoclonal antibodies are generally safer than chemotherapy only with mild allergic reactions such as urticaria for the design of a specifically targeted treatment to the cancer antigens located on tumor cells. However, severe reactions are still hard to avoid. For instance, patients who have a high burden of tumor cells in their circulation would face a high risk of tumor lysis syndrome and other severe complications such as anaphylactic reactions and myocardial infarction in occasional cases [5]. Therefore, developing low side-effect and better-tolerated anti-cancer agents is compelling.

Natural products are attractive sources for the development of new medicinal and therapeutic agents for their cell selective and fewer adverse effects. In this context, it is significant to develop natural products in cancer treatment. According to reports, natural origins are the main origins for approved drugs in the treatment of cancer, occupying almost 60% [6]. Though the development of marine natural products is still in its embryonic stage, it is anticipated that marine natural products will become an invaluable source for the development of new medicinal and therapeutic agents in cancer treatment because of their large habitat (covering ~70% of the Earth's surface), high biodiversity (95% of world biodiversity), and the specific conditions under which some species live [7,8]. It has great scope in which discover new anti-cancer medicine for large production, biological activity, and have unique chemicals. Over the last few decades, pharmaceutical companies and academic institutions have made significant efforts in deriving and identifying new marine products from marine organisms, with more than 3000 new anti-cancer compounds [9]. Of particular interest are the products derived from seaweeds with anti-cancer potential in natural marine products.

Seaweeds are widely distributed in cold, temperate, and tropical zones and play vital roles in sustaining the biodiversity and ecology of marine ecosystems. Several species of economic value such as *Laminaria*, *Porphyra*, and *Gracilaria* are cultured in the coastal waters of many countries [10]. Seaweeds are low in lipids, rich in proteins, minerals, vitamins, antioxidants, phytochemicals, polyunsaturated fatty acids, and are also a source of a vast number of novel compounds with unique health benefits such as essential amino acids and their proteins as well as essential minerals [11,12]. Epidemiological studies have shown that a seaweed-rich diet reduces the incidence of obesity, cancer, and heart and cerebrovascular diseases [13]. A large number of studies have uncovered the anti-cancer activities of seaweeds and numerous seaweed-derived compounds that have been shown to be effective through multiple mechanisms such as the inhibition of cancer cell growth, invasiveness and metastasis as well as by the induction of apoptosis in cancer cells. Some of the substances have been developed into drugs for cancer treatment [3,14–17]. In recent years, natural compounds extracted from marine algae have been proposed as effective in inhibiting tumor growth, adhesion, invasion, and migration [15].

Polyphenols and sulfated polysaccharides are the predominant belongings of seaweed, possessing an array of pharmacological properties [6]. Polysaccharides are found in the intracellular space and in the fibrillar cell walls of seaweeds [2]. Recently, considerable attention has been focused on polysaccharides isolated from natural sources. Such polysaccharides, which are the main storage compounds in seaweed, are polymers of hexoses or other monosaccharides with antioxidant, anti-cancer, anti-coagulant, and anti-inflammatory properties and are widely included in commercial products [18–20]. Small differences in structures in these polysaccharides determine their distinctive properties. These large molecules are divided into either homopolysaccharides or homoglycans and heteropolysaccharides or heteroglycans. Both are distinguished by a monomeric unit, which is of only one kind in the former such as cellulose and starch, or two or more kinds in the latter. Additionally, the polymers are divided into brown, red, green, and blue polysaccharides, according to the type of seaweed from which they are derived. The former two polysaccharides have attracted more attention and are widely applied. Alginic acid, fucoidan (sulfated fucose), and laminaran (β-1,3 glucan) are derived from brown seaweed. Agars, carrageenans, xylans, floridean starch (amylopectin-like glucan), water-soluble sulfated galactans, and porphyrans are from red algae. Green seaweeds contain sulfuric acid polysaccharides, sulfated

galactans, and xylans. Seaweed polysaccharides are diverse and characteristic of specific species and vary with season. Up to 76% of the dry weight is polysaccharide in some genera such as *Ascophyllum*, *Porphyra*, and *Palmaria* [21]. This review attempts to review the current study of anti-cancer activity and the possible mechanism of porphyran and carrageenan derived from red seaweeds to various cancers, and their cooperative action with other anti-cancer chemotherapeutic agents is also discussed. The keywords, "red seaweed", "cancer", "polysaccharide", "porphyran", and "carrageenan" were searched in "Google Scholar" and "Web of Science" in the period between 1980 and 2019.

2. Anti-Cancer Activity from Red Seaweeds

Edible red seaweeds have been considered as a healthy and beneficial food in Asia such as Japan, China, Thailand, and South Korea for a long time. Red seaweed cultivation has significantly grown rapidly since the early 20th century due to the continuous increase in demand for food and industry [10]. *Kappaphycus*, *Eucheuma*, *Gracialria,* and *Porphyra* are the main species largely cultivated in Indonesia and China. Bioactive compounds of seaweeds are synthesized in accordance with seaweed growth stage and the ability to interact with environmental changes such as radiation, water pressure, and salinity [7]. Phycobiliproteins, carotenoids, pigments, terpenes, polyphenols, phlorotannins, and polysaccharides are the major contributors to seaweeds, with various types and amounts in different species [3,11,22]. Terpenes, polysaccharides, and polyphenols are of major interest for their anti-cancer activity [2,3,23].

The anti-cancer effects of seaweed could be as nutrients and cytotoxic properties [19]. As a nutrient source, seaweed limits the development of cancers, probably by enhancing antioxidant properties. Through the mechanisms of carcinogenesis promoted by oxidative processes, it is obvious that antioxidants play vital roles in the later stages of cancer development. Thus, antioxidants are deemed as a feasible manner to regress premalignant lesions and inhibit cancer development [6]. Meanwhile, natural seaweed products have cytotoxic properties when concentrated. Researchers have reported that a sulfated polysaccharide from *Champia feldmannii* did not show obvious in vitro cytotoxicity, but was antitumor against sarcoma 180 in mice, probably associated with its immune stimulating properties [24]. A sulfated polysaccharide isolated from *Gracilaria lemaneiformis* exhibited remarkable anti-cancer and immunomodulatory activities against transplanted H22 hepatoma cells in ICR (Institute of Cancer Research) mice. Marked inhibition of tumor growth, promotion of splenocyte proliferation, macrophage phagocytosis, and the level of increments of IL-2 and $CD8^+$ T cells in blood [25] were all affected. The in vitro and in vivo anti-cancer studies of the sulfated polysaccharide isolated from *C. feldmannii* was carried out in Swiss mice. Though the in vitro cytotoxicity of the polysaccharide was not significant, the in vivo anti-cancer effect was measurable. The increased immune stimulation including increasing both the production of specific antibodies and the production of OVA-specific antibodies as well as inducing a discreet hyperplasia of lymphoid follicles of the white pulp in the spleen, were associated with anti-cancer activity [24]. Anti-cancer effects were also demonstrated in the polysaccharides derived from other seaweeds, especially fucoidan from brown seaweeds. The anti-cancer activity of fucoidans has been reported in many types of cancers such as lung cancer [26,27], gastric cancer [26], breast cancer [28], and liver cancer HepG2 cell [29]. In the following section, porphyran and carrageenan, the polysaccharides derived from red seaweeds, are described in detail.

Anti-cancer activity has also been proven in other compounds. Terpenes and their derivations, halogenated monoterpenes, are compounds of seaweeds, usually as secretin outside the cell to defend against environmental stress with high anti-cancer activity. The halogenated monoterpene halomon [6(*R*)-bromo-3(*S*)-bromomethyl)-7-methyl-2,3,7-trichloro-1-octene] was the first monoterpene isolated from *Portieria hornemannii* [30] with sub-micromolar activity ($IC_{50} \leq 0.9$ μM) against at least one cancer cell line including renal-, brain-, and colon-derived solid tumor cell lines [31]. Other halogenated monoterpenes isolated from the red seaweeds *Plocamium suhrii* and *Plocamium cornutum,* showed greater antiproliferative activity on an esophageal cancer cell line (WHCO1) when compared with cisplatin, well-known as an anti-cancer drug [32]. Phenolic compounds are composed of a single

aromatic ring and possess large, broad biological activities due to the ring bearing one or more hydroxyl groups [4,33]. Bromophenols, polyphenolics compounds with one or more bromine substituents, are most commonly found in red seaweeds [34]. A polyphenol-rich extract from *Eucheuma cottonii* was proven to have selective cytotoxicity in estrogen-dependent MCF-7 and estrogen-independent MB-MDA-231 human breast-cancer cells (IC_{50} values of 20 and 42 μg/mL, respectively) depending on dose. Polyphenol showed anti-cancer activity by inducing apoptosis, downregulating the endogenous estrogen biosynthesis, and improving antioxidative status [35]. Additionally, polyphenols from red seaweed *Corallina officinalis* have been applied in nano-biotechnology and biosynthesized to gold nanoparticles as a reducing and stabilizing agent. The gold nanoparticles showed cytotoxic activity against MCF-7 cells depending on the dose of gold nanoparticles and the polyphenol content [36]. Pheophorbide a (Pa) is a product of chlorophyll breakdown, having been applied in the photodynamic therapy of cancer as a chlorine-based photosensitizer [37]. Pa-mediated photodynamic therapy (PDT) was used in treating 7,12-dimethylbenz[*a*]anthracene (DMBA)/12-*O*-tetradecanoylphorobol-13-acetate (TPA)-induced mouse papillomas with marked downregulation of proliferating cell nuclear antigen expression [37]. The Pa isolated from *Grateloupia elliptica* was proven to have specific anti-cancer activity toward various cancer cells lines including B16-BL6, HeLa, SiHa, SK-OV-3, and U87MG cells, especially in U87 MG glioblastoma cells [6]. The Pa induced G0/G1 arrest of U87 MG cells in the absence of direct photo-irradiation, causing late apoptosis and DNA degradation under dark conditions. These results suggest that Pa isolated from *G. elliptica* is a potential glioblastoma-specific anti-cancer agent without side effects on normal cells.

3. Porphyran

Porphyran is a characteristic polysaccharide of *Porphyra*, also a red seaweed. Various species are "Nori", which is marketed in sheets of dried seaweed and is popular in East and Southeast Asia as well as globally, especially as a wrap for sushi. Porphyran is a galactose, highly substituted by the 6-*O*-sulfation of L-galactose units and 6-*O*-methylation of D-galactose units (Figure 1) [38,39]. Various methods including hot water extraction, radical degradation, and ultrasonic treatment have been used to extract porphyrans from red seaweeds. Porphyrans have been reported to be hypolipidemic, anti-cancer, and anti-inflammatory in human beings. Porphyran inhibits NO production in macrophages by blocking NF-B activation in the mouse macrophages of RAW264.7 cells that were stimulated with lipopolysaccharides. This may explain some of the anti-inflammatory effects of porphyran [40]. It has been reported that porphyrans have the potential to prevent hyperlipidemia due to its excellent antioxidant activities in mice [14]. Previous studies have shown that porphyrans inhibited lipid synthesis in HepG2 cells and also decreased apolipoprotein B100 secretion, realizing its hypolipidemic effect [41]. Oral porphyran alleviates liver damage induced by the high-fat diet of ICR mice, implicating the use of porphyran as a dietary hypolipidemic component [42]. Furthermore, porphyran was proven to be effective and potential in anti-cancer by various studies (Table 1, Figure 2).

Generally, porphyran is non-toxic on normal cells, although toxic for cancer cells, and induces cell death in a dose-dependent manner [43]. In vitro anti-proliferative activity of crude and purified porphyran, also in a dose-dependent manner, was reported in HT-29 colon cancer cells and AGS gastric cancer cells. The polysaccharide portion of the crude porphyran was thought to account for anti-proliferative activity via apoptosis, as indicated by increased caspase-3 activity [44]. The anti-cancer activity of porphyran against Ehrlich carcinoma and Meth-A fibrosarcoma has been demonstrated in mice tumor models [45,46]. Similar results have been reported in cancer cells of AGS and HT-29, the proliferation of which was arrested by *Porphyran-chungkookjang*, prepared by adding 5% *(w/w)* porphyran into fermented *Bacillus subtilis* [47]. The methanol extract of *porphryan-chungkookjang* showed higher anti-cancer effects than the *chungkookjang*.

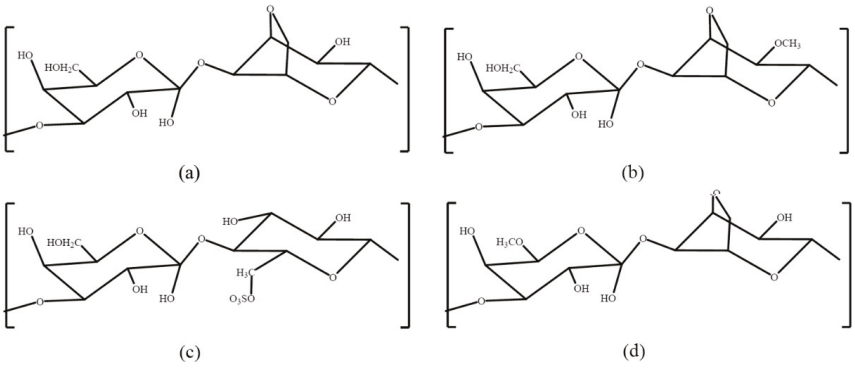

Figure 1. Typical repetitive structures in porphyran [38]: (**a**) G-A; (**b**) G-A2M; (**c**) G-L6S; (**d**) G6M-A. G: 1,3-linked β-D-galactose; A: 1,4-linked 3,6-anhydro-α-L-galactose; A2M: 1,4-linked 2-*O*-methyl-3,6-anhydro-α-L-galactose; L6S: 1,4-linked α-L-galactose 6-sulfate; G6M: 1,3-linked 6-*O*-methyl-β-D-galactose.

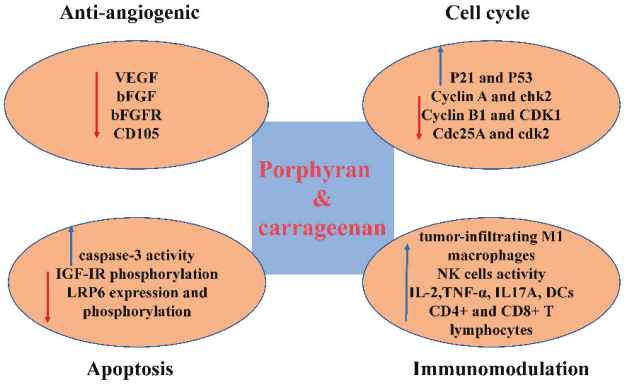

Figure 2. Possible mechanism in the anti-cancer activity of porphyran and carrageenan.

One study revealed that AGS gastric cancer cells were effectively controlled by porphyrin, which decreased cell proliferation and induced apoptosis. Negative regulation of IGF-IR phosphorylation and activation of caspase-3 is a porphyran effect [47]. Other investigations showed that a polysaccharide from *Porphyra yezoensis* arrested the cancer cell cycle at either the G0/G1 or G2/M check points [48]. Cell proliferation was also inhibited in the HeLa line, which were induced by porphyran. The cell cycle was blocked in the G2/M phase by regulating and controlling the expression of p21, p53, cyclin B1, and CDK1 [49].

There is growing evidence that the biological activities of polysaccharides are dependent on their molecular weight, conformational state, chemical components, and glycosidic bonds [50,51]. Molecular weight is especially important because it is related to viscosity, water-solubility, conformation, and other basic properties of polysaccharides [38,52]. Lower molecular weight porphyrans have a higher antioxidant activity [39,53]. Although discolored due to a lack of nutrients that reduces their commercial value considerably, in cultured *P. yezoensis*, a higher level of porphyran was found in the discolored organisms. It has greater ROS-scavenging activity, likely due to the lower mean molecular mass of the porphyran [54]. Additionally, oligo-porphyran, the acid hydrolysis product of porphyran, has the potential to prevent and treat various pathologies such as Parkinson's disease and acute renal failure. Previous studies have suggested that oligo-porphyran protects renal morphology

and function in rats with renal impairment [39]. They also ameliorate neurobehavioral defects by regulating the PI3K/Akt/Bcl-2 pathway in Parkinsonian mice [55]. The anti-cancer response to porphyran shows varying results. For example, porphyran derived from *P. yezoensis* was degraded by gamma irradiation so that the exposure dose of irradiation was higher and the molecular weight of porphyrans lower [49]. No significant changes in the contents of sulfate, monosaccharide composition, and 3,6-anhydroanhydro-α-L-galactose were detected in the three polysaccharides. These inhibited the cancer cell lines of HeLa and Hep3B more effectively than the degraded products. This discovery contradicts other studies that concluded that lower molecular weight porphyrans exert more anti-cancer activity [38]. The relationship between the molecular weight of porphyrans and their anti-cancer activity along with their conformation should be studied further.

Table 1. Anti-cancer activity and possible mechanisms of porphyran.

Source	Target	Type of Activity	Possible Mechanisms	References
P. yezoensis	Mice implanted with Ehrlich carcinoma and Meth A fibrosarcoma	Appreciable inhibition of tumor growth	Not referred	[45,46]
	AGS and HT-29 cancer cells	Antiproliferation		[47]
	SGC-7901 and 95D cancer cell lines			[38]
	Hep3B cells	Antiproliferation and cell cycle blocked in the G2/M phase	Upregulation of p21 and p53, while negatively regulating cyclin B1and CDK1	[49]
	HO-8910, MCF-7, K562, and SMMC-7721 cells	Antiproliferation and cell cycle arrested at the G0/G1or the G2/M check points	Not referred	[48]
	HT-29 colon cancer cells and AGS gastric cancer cells	Antiproliferation and apoptosis induced	Increasing caspase-3 activity	[44]
Commodity provided by Korea Bio Polymer (KBP) company	AGS human gastric cancer cells.		Negatively regulating IGF-IR phosphorylation and inducing caspase-3 activation	[43]

4. Carrageenan

Carrageenan is a highly sulfated polysaccharide found in *Chondrus*, *Gigartina*, and various *Eucheuma* species in the red algal family Rhodophyceae [38]. It is widely used in food and pharmaceutical industries as a stabilizer, a gelling agent, thickener, binder, and additive [56]. D-galactopyranosyl with one or two sulfate groups is the base unit of carrageenans, linked via alternated (1→3)-β-D-and (1→4)-α-D-glucoside (Figure 3) [56–58]. The number and position of the sulfate groups divide carrageenans into α-carrageenan, β-carrageenan, γ-carrageenan, δ-carrageenan, θ-carrageenan, ι-carrageenan, κ-carrageenan, λ-carrageenan, μ-carrageenan, and ν-carrageenan (Figure 3), and of these, κ-, ι-, and λ-carrageenans, are of commercial significance [59]. Acidic hydrolysis is effective in analyzing their structures through reductive hydrolysis [60,61], and enzymatic hydrolysis is preferred in industrial production [62]. Although carrageenan is generally regarded as safe [38], its consumption is reported to cause colitis [63–65]. It is also reported to induce paw edema and pleurisy in experimental rats, which is widely used to study anti-inflammatory activity and the mechanisms involved in inflammation [66–70]. Carrageenan induces thrombosis in a tail thrombosis model and is frequently used to study the mechanisms of antithrombosis and thrombolysis in small laboratory animals [71–73]. Growing evidence suggests the anti-cancer ability of carrageenan (Table 2, Figure 2).

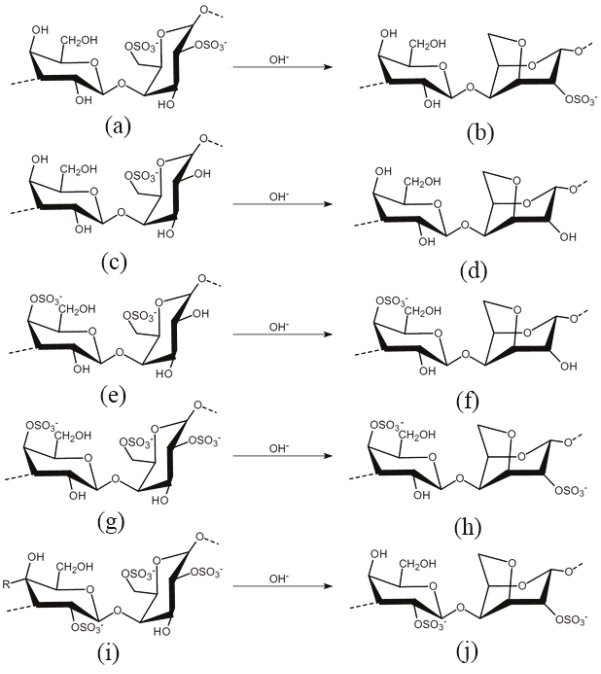

Figure 3. Chemical structure of carrageenans [64]: (**a**) δ-carrageenan; (**b**) α-carrageenan; (**c**) γ-carrageenan; (**d**) β-carrageenan; (**e**) μ-carrageenan; (**f**) κ-carrageenan; (**g**) ν-carrageenan; (**h**) ι-carrageenan; (**i**) λ-carrageenan; and (**j**) θ-carrageenan.

Natural anti-cancer defense mechanisms in the host play an important role in cancer treatment combined with a variety of therapeutic approaches including new anti-cancer drugs that enhance immunity [74]. Seaweed polysaccharides are reported to regulate immune responses by activating immune cells and other generalized immune responses. Immunomodulating activity induced by carrageenan has been studied in the treatment of tumors by several researchers. λ-carrageenan was reported to inhibit tumor growth in B16-F10- and 4T1-bearing mice through intratumoral injection [75]. Meanwhile, immune response to the tumor was enhanced by promoting tumor-infiltrating M1 macrophages in the spleen, which secreted higher levels of IL17A in the spleen and TNF-α in the tumor. Humoral and cell-mediated immunity in S180-bearing mice was also reported to be enhanced by carrageenan oligosaccharides extracted from *Kappaphycus striatum* and led to potent tumor therapeutic activity [76].

The selective cytotoxic effects of carrageenans on cancer cells have been demonstrated in several investigations. Such studies have shown that concentrations of 250–2500 μg/mL of both κ-carrageenan and λ-carrageenan inhibited human cervical carcinoma cells by not only arresting the cell cycle at specific phases, but also by delaying the time of it [56]. κ-carrageenan delayed the cell cycle in the G2/M phase while λ-carrageenan delayed both G1 and G2/M phases. However, κ-selenocarrageenan (i.e., κ-carrageenan with selenium) is anti-proliferative on the human hepatoma cell line. It blocks the cell cycle in the S phase [77]. However, native ι-carrageenan showed no significant anti-proliferation in the human osteosarcoma cell line in either in vitro or in vivo assays. Degraded ι-carrageenan [78] suppressed tumor growth, induced apoptosis, and arrested the G1 phase, which improved the survival rate of tumor-bearing mice. Downregulation of the Wnt/β-catenin signaling pathway was responsible for that.

Table 2. Anti-cancer activity and possible mechanisms of carrageenans.

Source	Target	Type of Activity	Possible Mechanisms	References
λ-carrageenan purchased from Sigma-Aldrich	B16-F10 and 4T1 bearing mice	Inhibition of tumor growth and improving immune system	Increasing the number of tumor-infiltrating M1 macrophages, DCs, and more activated $CD4^+$ $CD8^+$ T lymphocytes and enhancing the secretion of IL17A in spleen and significantly increase the level of TNF-α in tumor	[75]
Carrageenan oligosaccharides derived from *Kappaphycus striatum*	S180-bearing mice		Increase macrophage phagocytosis, the form of antibody secreted by spleen cells, spleen lymphocyte proliferation, NK cells activity, serumal IL-2 and TNF-a level	[76]
κ-carrageenan and λ-carrageenan purchased from Sigma-Aldrich	HeLa cells	Cell cycle delayed in G2/M phase or in both G1 and G2/M phase	Not referred	[56]
κ-selenocarrageenan consisted of selenium and κ-carrageenan	HepG2 cells	Cell cycle delayed in S phase	Upregulating Cyclin A and chk2 protein and down-regulating Cdc25A and cdk2 expression.	[77]
ι-Carrageenan	Human osteosarcoma cell line	Apoptosis induced and Cell cycle delayed in G1 phase	Downregulation of the Wnt/β-catenin signaling pathway through suppressing LRP6 expression and phosphorylation	[78]
κ-carrageenan oligosaccharides prepared from κ-carrageenan with enzyme	MCF-7 xenograft tumor	Antiproliferation and anti-angiogenic	Negative regulation of human VEGF, bFGF, bFGFR, and CD105	[79]

Angiogenesis plays a vital role in cancer development. Therefore, anti-angiogenic activity is widely explored in cancer treatment. As they have better anti-angiogenic activity than the standard compound, suramin, carrageenans have been defined as angiogenesis inhibitors [70,80,81]. The anti-angiogenic activity of κ-carrageenan oligosaccharides was shown in ECV304 cells and the CAM (Chicken chorioallantoic membrane) model to inhibit the proliferation, migration, and tube formation of cells [79]. Moreover, the oligosaccharides inhibited new blood vessel formation with the negative regulation of human VEGF, bFGF, bFGFR, and CD105 in MCF-7 xenograft tumors. The negative effect on tumor blood vessel endothelial cell differentiation was also demonstrated in human umbilical vein endothelial cells and were affected by λ-carrageenan oligosaccharides at relatively low concentrations (150–300 μg/mL) [82] by the downregulation of intracellular matrix metalloproteinase (MMP-2) expression.

The biological activities of sulfated polysaccharides are a function of structural features such as the amount and position of sulfation and molecular weight. That is, the chemical modification of carbohydrates leads to variations in their biological activities [83]. For example, λ-carrageenan can be degraded into five products, all with different molecular weights and all showing anti-cancer effects, probably through immunomodulation. Lower molecular weight products, 15 and 9.3 kDa, showed higher anti-cancer and immunomodulation effects [83]. Selective chemical sulfation in the carrageenan backbone plays a measurable effect on its anticoagulant activity, which would be promoted by the substitution by sulfate at C6 of β-D-Galp and C2 of 3,6-anhydro-α-D-Galp units [84]. Another example, sulfate at C2 of the β-D-GalAp units, showed a more positive effect on the anticoagulation than at C4. Additionally, the partially oxidized molecule promoted the anticoagulant effect of the κ-carrageenan derivative more than the fully oxidized molecule [85]. Anti-cancer and immunomodulation activities

of κ-carrageenan oligosaccharides from *Kappaphycus striatum* were enhanced by sulfation, acetylation, and phosphorylation where the sulfated derivative was the most effective. Chemical modifications also promoted oxidant activity by κ-carrageenan oligosaccharides [86].

5. Combination with Conventional Anti-Cancer Drugs

Toxicity analyses have proven that polysaccharides are potent anti-cancer agents and effective adjuvants in cancer immunotherapy. 5-Fluorouracil (5-Fu), a thymidylate synthase inhibitor, has been widely used to treat cancer for several decades. However, it is limited by undesirable side effects [87–89]. When the drug was fixed at the 6-position with low molecular weight porphyran in order to obtain a water-soluble macromolecule prodrug, it led to a slow release of 5-Fu and prolonged the duration of anti-cancer activity and reduced the side effects [88]. The mixture and conjugate enhanced the anti-cancer activity of 5-Fu and immunocompetence recovered the damage in transplanted S180 tumor mice. The medical effect of the λ-carrageenan on anti-cancer activity and immunosuppression by 5-Fu were explored on transplanted S180 tumor mice [90]. Though the individual use of the λ-carrageenan sample or 5-Fu at low dose only exerted low anti-cancer activity, a mixture of the two samples at the same dose increased the activity. Meanwhile, λ-carrageenan enhanced immunocompetence that had been damaged by 5-Fu by increasing the weight of the spleen, activating lymphocyte proliferation, recovering the level of TNF-α, and reactivating the decreased spleens and white pulps. Similar research supports this result in H-22 tumor mice [91].

Gold nanoparticles (AuNPs) have been widely used in catalysis, photothermal therapy, and targeted drug delivery [92]. The κ-carrageenan oligosaccharide was reported as a reducing and capping agent to prepare AuNPs, which showed significant cytotoxic activities to HCT-116 and MDA-MB-231 cells [93]. Furthermore, maghemite nanoparticles have been reported to be electrostatically entrapped by ι-carrageenans in the sulfate groups [94]. In vitro anti-cancer efficacy of the biocompatible ι-carrageenan-γ-maghemite nanocomposite was demonstrated in the human colon cancer cell line by inducing cell apoptosis by following the ROS-mediated mitochondrial pathway, combined with downregulation of the expression levels of mRNA of XIAP and PARP-1, and the upregulation of caspase3, Bcl-2, and Bcl-xL.

6. Conclusions

The ideal cancer treatment eradicates tumor cells without damage to healthy tissues. Due to the side effects of current treatments, more attention is being paid to the selective toxicity of seaweed polysaccharides that are nontoxic to normal cells, but toxic to tumor cells. Several in vitro and in vivo studies have demonstrated that porphyrans and carrageenans have strong anti-cancer properties. Moreover, when combined with conventional drugs, these polysaccharides not only showed more effective anti-cancer activity, but also enhanced immunocompetence that had been damaged by drugs such as by increasing the weight of the spleen, activating lymphocyte proliferation, recovering the level of TNF-α, and reactivating the decreased spleens and white pulps.

Author Contributions: Literature search and writing of the manuscript, Z.L. and T.G.; Provided skilled assistance and supervised the overall preparation of the manuscript, Y.Y. and X.S.; Proposed and prepared the figures, F.M.; Literature search and manuscript editing, F.Z. and Q.J.; Contributed to the conception of the idea and revised the manuscript with critical reviews and comments, X.S.

Funding: This research received no external funding.

Acknowledgments: We are grateful to Larry B. Liddle from Long Island University for his language assistance.

Conflicts of Interest: The authors declare no conflicts of interest.

References

1. Global Cancer Observatory. Available online: http://gco.iarc.fr/ (accessed on 18 November 2019).
2. Senthilkumar, K.; Manivasagan, P.; Venkatesan, J.; Kim, S.-K. Brown seaweed fucoidan: Biological activity and apoptosis, growth signaling mechanism in cancer. *Int. J. Biol. Macromol.* **2013**, *60*, 366–374. [CrossRef] [PubMed]
3. Atashrazm, F.; Lowenthal, R.; Woods, G.; Holloway, A.; Dickinson, J. Fucoidan and Cancer: A Multifunctional Molecule with Anti-Tumor Potential. *Mar. Drugs* **2015**, *13*, 2327–2346. [CrossRef] [PubMed]
4. Gutiérrez-Rodríguez, A.G.; Juárez-Portilla, C.; Olivares-Bañuelos, T.; Zepeda, R.C. Anticancer activity of seaweeds. *Drug Discov. Today* **2018**, *23*, 434–447. [CrossRef] [PubMed]
5. Dotan, E.; Aggarwal, C.; Smith, M.R. Impact of Rituximab (Rituxan) on the Treatment of B-Cell Non-Hodgkin's Lymphoma. *Pharm. Ther.* **2010**, *35*, 148–157.
6. Sithranga Boopathy, N.; Kathiresan, K. Anticancer Drugs from Marine Flora: An Overview. *J. Oncol.* **2010**, *2010*, 214186. [CrossRef] [PubMed]
7. Appeltans, W.; Ahyong, S.T.; Anderson, G.; Angel, M.V.; Artois, T.; Bailly, N.; Bamber, R.; Barber, A.; Bartsch, I.; Berta, A.; et al. The Magnitude of Global Marine Species Diversity. *Curr. Biol.* **2012**, *22*, 2189–2202. [CrossRef] [PubMed]
8. Jimeno, J.; Faircloth, G.; Sousa-Faro, J.F.; Scheuer, P.; Rinehart, K. New Marine Derived Anticancer Therapeutics – A Journey from the Sea to Clinical Trials. *Mar. Drugs* **2004**, *2*, 14–29. [CrossRef]
9. Cho, M.; Park, G.-M.; Kim, S.-N.; Amna, T.; Lee, S.; Shin, W.-S. Glioblastoma-Specific Anticancer Activity of Pheophorbide a from the Edible Red Seaweed *Grateloupia elliptica*. *J. Microbiol. Biotechnol* **2014**, *24*, 346. [CrossRef]
10. Yang, Y.; Chai, Z.; Wang, Q.; Chen, W.; He, Z.; Jiang, S. Cultivation of seaweed *Gracilaria* in Chinese coastal waters and its contribution to environmental improvements. *Algal Res.* **2015**, *9*, 236–244. [CrossRef]
11. Lange, K.W.; Hauser, J.; Nakamura, Y.; Kanaya, S. Dietary seaweeds and obesity. *Food Sci. Hum. Wellness* **2015**, *4*, 87–96. [CrossRef]
12. Miyashita, K.; Mikami, N.; Hosokawa, M. Chemical and nutritional characteristics of brown seaweed lipids: A review. *J. Funct. Foods* **2013**, *5*, 1507–1517. [CrossRef]
13. Olivares-Bañuelos, T.; Gutiérrez-Rodríguez, A.G.; Méndez-Bellido, R.; Tovar-Miranda, R.; Arroyo-Helguera, O.; Juárez-Portilla, C.; Meza-Menchaca, T.; Aguilar-Rosas, L.E.; Hernández-Kelly, L.C.R.; Ortega, A.; et al. Brown Seaweed *Egregia menziesii*'s Cytotoxic Activity against Brain Cancer Cell Lines. *Molecules* **2019**, *24*, 260. [CrossRef]
14. Wang, X.; Li, W.; Xiao, L.; Liu, C.; Qi, H.; Zhang, Z. In vivo antihyperlipidemic and antioxidant activity of porphyran in hyperlipidemic mice. *Carbohydr. Polym.* **2017**, *174*, 417–420. [CrossRef] [PubMed]
15. Pádua, D.; Rocha, E.; Gargiulo, D.; Ramos, A.A. Bioactive compounds from brown seaweeds: Phloroglucinol, fucoxanthin and fucoidan as promising therapeutic agents against breast cancer. *Phytochem. Lett.* **2015**, *14*, 91–98. [CrossRef]
16. Sun, X.; Zhong, Y.; Luo, H.; Yang, Y. Selenium-Containing Polysaccharide-Protein Complex in Se-Enriched *Ulva fasciata* Induces Mitochondria-Mediated Apoptosis in A549 Human Lung Cancer Cells. *Mar. Drugs* **2017**, *15*, 215. [CrossRef] [PubMed]
17. Geng, L.; Wang, J.; Zhang, Z.; Yue, Y.; Zhang, Q. Structure and Bioactivities of Porphyrans and Oligoporphyrans. *Curr. Pharm. Des.* **2019**. [CrossRef]
18. Sanjeewa, K.K.A.; Jayawardena, T.U.; Kim, S.-Y.; Kim, H.-S.; Ahn, G.; Kim, J.; Jeon, Y.-J. Fucoidan isolated from invasive *Sargassum horneri* inhibit LPS-induced inflammation via blocking NF-κB and MAPK pathways. *Algal Res.* **2019**, *41*, 101561. [CrossRef]
19. Murphy, C.; Hotchkiss, S.; Worthington, J.; McKeown, S.R. The potential of seaweed as a source of drugs for use in cancer chemotherapy. *J. Appl. Phycol.* **2014**, *26*, 2211–2264. [CrossRef]
20. Yu, Y.; Shen, M.; Song, Q.; Xie, J. Biological activities and pharmaceutical applications of polysaccharide from natural resources: A review. *Carbohydr. Polym.* **2018**, *183*, 91–101. [CrossRef]
21. Holdt, S.L.; Kraan, S. Bioactive compounds in seaweed: Functional food applications and legislation. *J. Appl. Phycol.* **2011**, *23*, 543–597. [CrossRef]

22. de Souza, L.A.R.; Dore, C.M.P.; Castro, A.J.; de Azevedo, T.C.; de Oliveira, M.T.B.; Maria de Fátima, V.M.; Benevides, N.M.; Leite, E.L. Galactans from the red seaweed *Amansia multifida* and their effects on inflammation, angiogenesis, coagulation and cell viability. *Biomed. Prev. Nutr.* **2012**, *2*, 154–162. [CrossRef]
23. Peng, J.; Yuan, J.-P.; Wu, C.-F.; Wang, J.-H. Fucoxanthin, a marine carotenoid present in brown seaweeds and diatoms: Metabolism and bioactivities relevant to human health. *Mar. Drugs* **2011**, *9*, 1806–1828. [CrossRef] [PubMed]
24. Lins, K.O.A.L.; Bezerra, D.P.; Alves, A.P.N.N.; Alencar, N.M.N.; Lima, M.W.; Torres, V.M.; Farias, W.R.L.; Pessoa, C.; de Moraes, M.O.; Costa-Lotufo, L.V. Antitumor properties of a sulfated polysaccharide from the red seaweed *Champia feldmannii* (Diaz-Pifferer). *J. Appl. Toxicol.* **2009**, *29*, 20–26. [CrossRef] [PubMed]
25. Fan, Y.; Wang, W.; Song, W.; Chen, H.; Teng, A.; Liu, A. Partial characterization and anti-tumor activity of an acidic polysaccharide from *Gracilaria lemaneiformis*. *Carbohydr. Polym.* **2012**, *88*, 1313–1318. [CrossRef]
26. Han, J.G.; Syed, A.Q.; Kwon, M.; Ha, J.H.; Lee, H.Y. Antioxident, immunomodulatory and anticancer activity of fucoidan isolated from *Fucus vesiculosus*. *J. Biotechnol.* **2008**, *136*, S571. [CrossRef]
27. Hsu, H.Y.; Lin, T.-Y.; Lu, M.-K.; Leng, P.-J.; Tsao, S.-M.; Wu, Y.-C. Fucoidan induces Toll-like receptor 4-regulated reactive oxygen species and promotes endoplasmic reticulum stress-mediated apoptosis in lung cancer. *Sci. Rep.* **2017**, *7*, 44990. [CrossRef]
28. Yamasaki-Miyamoto, Y.; Yamasaki, M.; Tachibana, H.; Yamada, K. Fucoidan Induces Apoptosis through Activation of Caspase-8 on Human Breast Cancer MCF-7 Cells. *J. Agric. Food Chem.* **2009**, *57*, 8677–8682. [CrossRef]
29. Yan, M.-D.; Lin, H.-Y.; Hwang, P.-A. The anti-tumor activity of brown seaweed oligo-fucoidan via lncRNA expression modulation in HepG2 cells. *Cytotechnology* **2019**, *71*, 363–374. [CrossRef]
30. Fuller, R.W.; Cardellina, J.H.; Kato, Y.; Brinen, L.S.; Clardy, J.; Snader, K.M.; Boyd, M.R. A pentahalogenated monoterpene from the red alga *Portieria hornemannii* produces a novel cytotoxicity profile against a diverse panel of human tumor cell lines. *J. Med. Chem.* **1992**, *35*, 3007–3011. [CrossRef]
31. Rocha, D.; Seca, A.; Pinto, D. Seaweed Secondary Metabaolites In Vitro and In Vivo Anticancer Activity. *Mar. Drugs* **2018**, *16*, 410. [CrossRef]
32. Antunes, E.M.; Afolayan, A.F.; Chiwakata, M.T.; Fakee, J.; Knott, M.G.; Whibley, C.E.; Hendricks, D.T.; Bolton, J.J.; Beukes, D.R. Identification and in vitro anti-esophageal cancer activity of a series of halogenated monoterpenes isolated from the South African seaweeds *Plocamium suhrii* and *Plocamium cornutum*. *Phytochemistry* **2011**, *72*, 769–772. [CrossRef] [PubMed]
33. Li, Y.-X.; Wijesekara, I.; Li, Y.; Kim, S.-K. Phlorotannins as bioactive agents from brown algae. *Process Biochem.* **2011**, *46*, 2219–2224. [CrossRef]
34. Catarino, M.D.; Silva, A.M.S.; Cardoso, S.M. Fucaceae: A Source of Bioactive Phlorotannins. *Int. J. Mol. Sci.* **2017**, *18*, 1327. [CrossRef] [PubMed]
35. Namvar, F.; Mohamed, S.; Fard, S.G.; Behravan, J.; Mustapha, N.M.; Alitheen, N.B.M.; Othman, F. Polyphenol-rich seaweed (*Eucheuma cottonii*) extract suppresses breast tumour via hormone modulation and apoptosis induction. *Food Chem.* **2012**, *130*, 376–382. [CrossRef]
36. ElKassas, H.Y.; ElSheekh, M.M. Cytotoxic activity of biosynthesized gold nanoparticles with an extract of the red seaweed *Corallina officinalis* on the MCF-7 human breast cancer cell line. *Asian Pac. J. Cancer Prev. APJCP* **2014**, *15*, 4311. [CrossRef]
37. Zhang, X.; Choi, E.J.; Zheng, Z.; Zhu, L.; Cho, S.B.; Kim, K.-Y.; Kim, J.; Cha, I.-H. Apoptotic effect of pheophorbide a-mediated photodynamic therapy on DMBA/TPA-induced mouse papillomas. *Lasers Med. Sci.* **2015**, *30*, 51–57. [CrossRef]
38. Yu, X.; Zhou, C.; Yang, H.; Huang, X.; Ma, H.; Qin, X.; Hu, J. Effect of ultrasonic treatment on the degradation and inhibition cancer cell lines of polysaccharides from *Porphyra yezoensis*. *Carbohydr. Polym.* **2015**, *117*, 650–656. [CrossRef]
39. Wang, J.; Hou, Y.; Duan, D.; Zhang, Q. The Structure and Nephroprotective Activity of Oligo-Porphyran on Glycerol-Induced Acute Renal Failure in Rats. *Mar. Drugs* **2017**, *15*, 135. [CrossRef]
40. Jiang, Z.; Hama, Y.; Yamaguchi, K.; Oda, T. Inhibitory effect of sulphated polysaccharide porphyran on nitric oxide production in lipopolysaccharide-stimulated RAW264.7 macrophages. *J. Biochem. (Tokyo)* **2012**, *151*, 65–74. [CrossRef]

41. Inoue, N.; Yamano, N.; Sakata, K.; Nagao, K.; Hama, Y.; Yanagita, T. The Sulfated Polysaccharide Porphyran Reduces Apolipoprotein B100 Secretion and Lipid Synthesis in HepG2 Cells. *Biosci. Biotechnol. Biochem.* **2009**, *73*, 447–449. [CrossRef]
42. Cao, J.; Wang, S.C.; Xu, L.W.; He, J.B.; Xu, X.M. Extraction of Porphyran from *Porphyra yezoensis* for Gel Formulation Preparation. *Key Eng. Mater.* **2014**, *636*, 133–137. [CrossRef]
43. Kwon, M.-J.; Nam, T.-J. Porphyran induces apoptosis related signal pathway in AGS gastric cancer cell lines. *Life Sci.* **2006**, *79*, 1956–1962. [CrossRef]
44. Kwon, M.-J.; Nam, T.-J. Chromatographically Purified Porphyran from *Porphyra yezoensis* Effectively Inhibits Proliferation of Human Cancer Cells. *Food Sci. Biotechnol.* **2007**, *16*, 873–878.
45. Noda, H.; Amano, H.; Arashima, K.; Hashimoto, S.; Nisizawa, K. Antitumour Activity of Polysaccharides and Lipids from Marine Algae. *Nippon Suisan Gakkaishi* **1989**, *55*, 1265–1271. [CrossRef]
46. Noda, H.; Amano, H.; Arashima, K.; Nisizawa, K. Antitumor activity of marine algae. *Hydrobiologia* **1990**, *204–205*, 577–584. [CrossRef]
47. Min, H.-K.; Kim, H.-J.; Chang, H.-C. Growth-inhibitory Effect of the Extract of *Porphyran-Chungkookjang* on Cancer Cell. *J. Korean Soc. Food Sci. Nutr.* **2008**, *37*, 826–833. [CrossRef]
48. Zhang, L.-X.; Cai, C.-E.; Guo, T.-T.; Gu, J.-W.; Xu, H.-L.; Zhou, Y.; Wang, Y.; Liu, C.-C.; He, P.-M. Anti-cancer effects of polysaccharide and phycocyanin from *Porphyra yezoensis*. *J. Mar. Sci. Technol.* **2011**, *19*, 6.
49. He, D.; Wu, S.; Yan, L.; Zuo, J.; Cheng, Y.; Wang, H.; Liu, J.; Zhang, X.; Wu, M.; Choi, J.; et al. Antitumor bioactivity of porphyran extracted from *Pyropia yezoensis* Chonsoo2 on human cancer cell lines. *J. Sci. Food Agric.* **2019**, *99*, 6722–6730. [CrossRef]
50. Ma, C.; Feng, M.; Zhai, X.; Hu, M.; You, L.; Luo, W.; Zhao, M. Optimization for the extraction of polysaccharides from *Ganoderma lucidum* and their antioxidant and antiproliferative activities. *J. Taiwan Inst. Chem. Eng.* **2013**, *44*, 886–894. [CrossRef]
51. Chen, T.; Zhao, X.; Wu, J.; Yu, D.; Wu, Y. Supercritical fluid CO_2 extraction, simultaneous determination of components in ultra-fine powder of Ganoderma sinense by HPLC–ESI-MS method. *J. Taiwan Inst. Chem. Eng.* **2011**, *42*, 428–434. [CrossRef]
52. Liu, W.; Wang, H.; Pang, X.; Yao, W.; Gao, X. Characterization and antioxidant activity of two low-molecular-weight polysaccharides purified from the fruiting bodies of *Ganoderma lucidum*. *Int. J. Biol. Macromol.* **2010**, *46*, 451–457. [CrossRef] [PubMed]
53. Zhao, T.; Zhang, Q.; Qi, H.; Zhang, H.; Niu, X.; Xu, Z.; Li, Z. Degradation of porphyran from *Porphyra haitanensis* and the antioxidant activities of the degraded porphyrans with different molecular weight. *Int. J. Biol. Macromol.* **2006**, *38*, 45–50. [CrossRef] [PubMed]
54. Isaka, S.; Cho, K.; Nakazono, S.; Abu, R.; Ueno, M.; Kim, D.; Oda, T. Antioxidant and anti-inflammatory activities of porphyran isolated from discolored nori (*Porphyra yezoensis*). *Int. J. Biol. Macromol.* **2015**, *74*, 68–75. [CrossRef] [PubMed]
55. Liu, Y.; Geng, L.; Zhang, J.; Wang, J.; Zhang, Q.; Duan, D.; Zhang, Q. Oligo-Porphyran Ameliorates Neurobehavioral Deficits in Parkinsonian Mice by Regulating the PI3K/Akt/Bcl-2 Pathway. *Mar. Drugs* **2018**, *16*, 82. [CrossRef] [PubMed]
56. Prasedya, E.S.; Miyake, M.; Kobayashi, D.; Hazama, A. Carrageenan delays cell cycle progression in human cancer cells in vitro demonstrated by FUCCI imaging. *BMC Complement. Altern. Med.* **2016**, *16*, 270. [CrossRef] [PubMed]
57. Weiner, M.L. Food additive carrageenan: Part II: A critical review of carrageenan in vivo safety studies. *Crit. Rev. Toxicol.* **2014**, *44*, 244–269. [CrossRef]
58. Chandrasekaran, R.; Bian, W.; Okuyama, K. Three-dimensional structure of guaran. *Carbohydr. Res.* **1998**, *312*, 219–224. [CrossRef]
59. Fedorov, S.; Ermakova, S.; Zvyagintseva, T.; Stonik, V. Anticancer and Cancer Preventive Properties of Marine Polysaccharides: Some Results and Prospects. *Mar. Drugs* **2013**, *11*, 4876–4901. [CrossRef]
60. Mendoza, W.G.; Ganzon-Fortes, E.T.; Villanueva, R.D.; Romero, J.B.; Montano, M.N.E. Tissue age as a factor affecting carrageenan quantity and quality in farmed *Kappaphycus striatum* (Schmitz) Doty ex Silva. *Bot. Mar.* **2006**, *49*, 57–64. [CrossRef]
61. Knutsen, S.H.; Moe, S.T.; Larsen, B.; Grasdalen, H. Molecular cut-off values of dialysis membranes for alginate and kappa-carrageenan oligosaccharides. *Hydrobiologia* **1993**, *260–261*, 667–672. [CrossRef]

62. Cheong, K.-L.; Qiu, H.-M.; Du, H.; Liu, Y.; Khan, B.M. Oligosaccharides Derived from Red Seaweed: Production, Properties, and Potential Health and Cosmetic Applications. *Molecules* **2018**, *23*, 2451. [CrossRef] [PubMed]
63. Shang, Q.; Sun, W.; Shan, X.; Jiang, H.; Yu, G. Carrageenan-induced colitis is associated with decreased population of anti-inflammatory bacterium, *Akkermansia muciniphila*, in the gut microbiota of C57BL/6J mice. *Toxicol. Lett.* **2017**, *279*, 87–95. [CrossRef] [PubMed]
64. Necas, J.; Bartosikova, L. Carrageenan: A review. *Veterinární Medicína* **2013**, *58*, 187–205. [CrossRef]
65. Li, Y.-Y.; Huang, S.-S.; Lee, M.-M.; Deng, J.-S.; Huang, G.-J. Anti-inflammatory activities of cardamonin from *Alpinia katsumadai* through heme oxygenase-1 induction and inhibition of NF-κB and MAPK signaling pathway in the carrageenan-induced paw edema. *Int. Immunopharmacol.* **2015**, *25*, 332–339. [CrossRef] [PubMed]
66. Ceccarelli, M.; Bani, D.; Cinci, L.; Nistri, S.; Uliva, C.; Ragazzo, E.; Vannacci, A.; Manoni, M.; Gori, A.M.; Abbate, R.; et al. Anti-inflammatory effects of low molecular weight heparin derivative in a rat model of carrageenan-induced pleurisy. *J. Cell. Mol. Med.* **2009**, *13*, 2704–2712. [CrossRef] [PubMed]
67. Ghorbanzadeh, B.; Mansouri, M.; Hemmati, A.; Naghizadeh, B.; Mard, S.; Rezaie, A. A study of the mechanisms underlying the anti-inflammatory effect of ellagic acid in carrageenan-induced paw edema in rats. *Indian J. Pharmacol.* **2015**, *47*, 292. [CrossRef]
68. Shree, N.; Venkategowda, S.; Venkatranganna, M.V.; Bhonde, R.R. Treatment with adipose derived mesenchymal stem cells and their conditioned media reverse carrageenan induced paw oedema in db/db mice. *Biomed. Pharmacother.* **2017**, *90*, 350–353. [CrossRef]
69. Karama, Z.B.; Samar, M.; Amina, T.; Lobna, J.; Mohamed, T.; Slim, T. Effects of *Juniperus phoenicea* Hydroalcoholic Extract on Inflammatory Mediators and Oxidative Stress Markers in Carrageenan-Induced Paw Oedema in Mice. *BioMed Res. Int.* **2018**, 1–11. [CrossRef]
70. Ashraf, S.; Mapp, P.I.; Walsh, D.A. Angiogenesis and the persistence of inflammation in a rat model of proliferative synovitis. *Arthritis Rheum.* **2010**, *62*, 1890–1898. [CrossRef]
71. Arslan, R.; Bektas, N.; Bor, Z.; Sener, E. Evaluation of the antithrombotic effects of *Crataegus monogyna* and *Crataegus davisii* in the carrageenan-induced tail thrombosis model. *Pharm. Biol.* **2015**, *53*, 275–279. [CrossRef]
72. Ma, N.; Liu, X.W.; Yang, Y.J.; Li, J.Y.; Mohamed, I.; Liu, G.R.; Zhang, J.Y. Preventive Effect of Aspirin Eugenol Ester on Thrombosis in κ-Carrageenan-Induced Rat Tail Thrombosis Model. *PLoS ONE* **2015**, *10*, e0133125. [CrossRef] [PubMed]
73. Zhang, Y.-L.; Xi, M.-Z.; Choi, Y.-B.; Lee, B.-H. Antithrombotic Effect of Fermented *Ophiopogon japonicus* in Thrombosis-Induced Rat Models. *J. Med. Food* **2017**, *20*, 637–645. [CrossRef]
74. Ehrke, M.J. Immunomodulation in cancer therapeutics. *Int. Immunopharmacol.* **2003**, *3*, 1105–1119. [CrossRef]
75. Luo, M.; Shao, B.; Nie, W.; Wei, X.-W.; Li, Y.-L.; Wang, B.-L.; He, Z.-Y.; Liang, X.; Ye, T.-H.; Wei, Y.-Q. Antitumor and Adjuvant Activity of λ-carrageenan by Stimulating Immune Response in Cancer Immunotherapy. *Sci. Rep.* **2015**, *5*, 1–12. [CrossRef] [PubMed]
76. Yuan, H.; Song, J.; Li, X.; Li, N.; Dai, J. Immunomodulation and antitumor activity of κ-carrageenan oligosaccharides. *Cancer Lett.* **2006**, *243*, 228–234. [CrossRef]
77. Ling, N. Growth Inhibition and Cell Cycle Arrest of Kappa-Selenocarrageenan and Paclitaxel on HepG2 Cells. *Adv. Mater. Res.* **2011**, *343–344*, 530–534. [CrossRef]
78. Jin, Z.; Han, Y.-X.; Han, X.-R. Degraded Iota-Carrageenan Can Induce Apoptosis in Human Osteosarcoma Cells Via the Wnt/β-Catenin Signaling Pathway. *Nutr. Cancer* **2013**, *65*, 126–131. [CrossRef]
79. Yao, Z.; Wu, H.; Zhang, S.; Du, Y. Enzymatic preparation of κ-carrageenan oligosaccharides and their anti-angiogenic activity. *Carbohydr. Polym.* **2014**, *101*, 359–367. [CrossRef]
80. Paper, D.H.; Vogl, H.; Franz, G.; Hoffman, R. Defined carrageenan derivatives as angiogenesis inhibitors. *Macromol. Symp.* **1995**, *99*, 219–225. [CrossRef]
81. Poupard, N.; Badarou, P.; Fasani, F.; Groult, H.; Bridiau, N.; Sannier, F.; Bordenave-Juchereau, S.; Kieda, C.; Piot, J.-M.; Grillon, C.; et al. Assessment of Heparanase-Mediated Angiogenesis Using Microvascular Endothelial Cells: Identification of λ-Carrageenan Derivative as a Potent Anti Angiogenic Agent. *Mar. Drugs* **2017**, *15*, 134. [CrossRef]
82. Chen, H.; Yan, X.; Lin, J.; Wang, F.; Xu, W. Depolymerized Products of λ-Carrageenan as a Potent Angiogenesis Inhibitor. *J. Agric. Food Chem.* **2007**, *55*, 6910–6917. [CrossRef] [PubMed]

83. Yuan, H.; Song, J.; Li, X.; Li, N.; Liu, S. Enhanced immunostimulatory and antitumor activity of different derivatives of κ-carrageenan oligosaccharides from *Kappaphycus striatum*. *J. Appl. Phycol.* **2011**, *23*, 59–65. [CrossRef]
84. de Araújo, C.A.; Noseda, M.D.; Cipriani, T.R.; Gonçalves, A.G.; Duarte, M.E.R.; Ducatti, D.R.B. Selective sulfation of carrageenans and the influence of sulfate regiochemistry on anticoagulant properties. *Carbohydr. Polym.* **2013**, *91*, 483–491. [CrossRef] [PubMed]
85. dos Santos-Fidencio, G.C.; Gonçalves, A.G.; Noseda, M.D.; Duarte, M.E.R.; Ducatti, D.R.B. Effects of carboxyl group on the anticoagulant activity of oxidized carrageenans. *Carbohydr. Polym.* **2019**, *214*, 286–293. [CrossRef] [PubMed]
86. Yuan, H.; Zhang, W.; Li, X.; Lü, X.; Li, N.; Gao, X.; Song, J. Preparation and in vitro antioxidant activity of κ-carrageenan oligosaccharides and their oversulfated, acetylated, and phosphorylated derivatives. *Carbohydr. Res.* **2005**, *340*, 685–692. [CrossRef] [PubMed]
87. Ouchi, T.; Yuyama, H.; Vogl, O. Synthesis of poly (ethylene glycol)-bound 3-(5-fluorouracil-1-yl) propanoic acid, its hydrolysis reactivity and antitumor activity. *Makromol. Chem. Rapid Commun.* **1985**, *6*, 815–819. [CrossRef]
88. Wang, X.; Zhang, Z. The antitumor activity of a red alga polysaccharide complexes carrying 5-fluorouracil. *Int. J. Biol. Macromol.* **2014**, *69*, 542–545. [CrossRef]
89. Raymond, E.; Buquet-Fagot, C.; Djelloul, S.; Mester, J.; Cvitkovic, E.; Allain, P.; Louvet, C.; Gespach, C. Antitumor activity of oxaliplatin in combination with 5-fluorouracil and the thymidylate synthase inhibitor AG337 in human colon, breast and ovarian cancers. *Anticancer. Drugs* **1997**, *8*, 876–885. [CrossRef]
90. Zhou, G.; Xin, H.; Sheng, W.; Sun, Y.; Li, Z.; Xu, Z. In vivo growth-inhibition of S180 tumor by mixture of 5-Fu and low molecular λ-carrageenan from *Chondrus ocellatus*. *Pharmacol. Res.* **2005**, *51*, 153–157. [CrossRef]
91. Zhou, G.; Sheng, W.; Yao, W.; Wang, C. Effect of low molecular λ-carrageenan from *Chondrus ocellatus* on antitumor H-22 activity of 5-Fu. *Pharmacol. Res.* **2006**, *53*, 129–134. [CrossRef]
92. Mohammad Ali Faramarzi. Armin Sadighi Insights into biogenic and chemical production of inorganic nanomaterials and nanostructures. *Adv. Colloid Interface Sci.* **2012**, *189–190*, 1–20.
93. Chen, X.; Zhao, X.; Gao, Y.; Yin, J.; Bai, M.; Wang, F. Green Synthesis of Gold Nanoparticles Using Carrageenan Oligosaccharide and Their In Vitro Antitumor Activity. *Mar. Drugs* **2018**, *16*, 277. [CrossRef] [PubMed]
94. Raman, M.; Devi, V.; Doble, M. Biocompatible ι-carrageenan-γ-maghemite nanocomposite for biomedical applications – synthesis, characterization and in vitro anticancer efficacy. *J. Nanobiotechnol.* **2015**, *13*, 18. [CrossRef] [PubMed]

molecules

MDPI

Review

Structural Modifications of Nature-Inspired Indoloquinolines: A Mini Review of Their Potential Antiproliferative Activity

Ning Wang [1,2], Marta Świtalska [3], Li Wang [1,4], Elkhabiry Shaban [1,5], Md Imran Hossain [1,6], Ibrahim El Tantawy El Sayed [1,7,*], Joanna Wietrzyk [3,*] and Tsutomu Inokuchi [1,*]

1 Division of Chemistry and Biotechnology, Graduate School of Natural Science and Technology, Okayama University, 3-1-1 Tsushima-naka, Kita-ku, Okayama 700-8530, Japan; wn12171982@sina.com (N.W.); liwang_512@163.com (L.W.); shaban_nrc@yahoo.com (E.S.); imranju7@yahoo.com (M.I.H.)
2 Department of Materials Science and Engineering, Yingkou Institute of Technology, Yingkou 115014, China
3 Hirszfeld Institute of Immunology and Experimental Therapy, Polish Academy of Sciences, 12R. Weigla Street, 53-114 Wroclaw, Poland; switalska@iitd.pan.wroc.pl
4 Department of Medicinal Chemistry, School of Pharmacy, Southwest Medical University, Luzhou 646000, China
5 Dyeing, Printing and Textile Auxiliaries Department, Textile Research Division, National Research Centre, 33 El-Bohouth Street, Dokki, Giza 12622, Egypt
6 Department of BioMolecular Sciences, School of Pharmacy, University of Mississippi, 419 Faser Hall, MS 38677, USA
7 Chemistry Department, Faculty of Science, El Menoufia University, Shebin El Koom 32511, Egypt
* Correspondence: ibrahimtantawy@yahoo.co.uk (I.E.T.E.S.); wietrzyk@iitd.pan.wroc.pl (J.W.); inokuchi@cc.okayama-u.ac.jp (T.I.)

Academic Editor: Roberto Fabiani
Received: 24 April 2019; Accepted: 1 June 2019; Published: 5 June 2019

Abstract: Cryptolepine, neocryptolepine and isocryptolepine are naturally occurring indoloquinoline alkaloids with various spectrum of biological properties. Structural modification is an extremely effective means to improve their bioactivities. This review enumerates several neocryptolepine and isocryptolepine analogues with potent antiproliferative activity against MV4-11 (leukemia), A549 (lung cancer), HCT116 (colon cancer) cell lines in vitro. Its activity towards normal mouse fibroblasts BALB/3T3 was also evaluated. Furthermore, structure activity relationships (SAR) are briefly discussed. The anticancer screening of neocryptolepine derivatives was performed in order to determine their cytotoxic and growth inhibitory activities across the JFCR39 cancer cell line panel.

Keywords: cryptolepine; neocryptolepine; isocryptolepine; antiproliferative activity; structure activity relationships

1. Introduction

1.1. Antitumoral Activity of Cryptolepine

Cryptolepine (**1**), neocryptolepine (**2**), and isocryptolepine (**3**) are typical indoloquinoline alkaloids isolated from the roots of *Cryptolepis sanguinolenta* [1,2].

These alkaloids are composed of the tetracyclic indoloquinoline ring system, which only differ with respect to the orientation and site of their indole and quinoline ring junctures (Figure 1). By introducing the appropriate motif at the certain positions, their derivatives can increase better biological activity than the mother core [3].

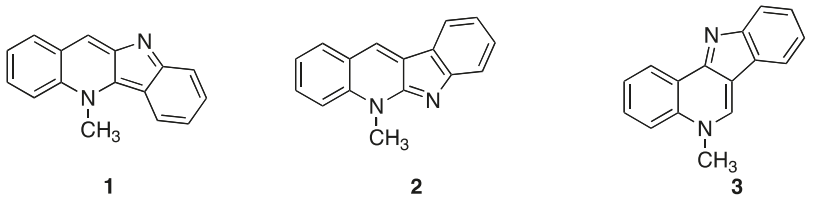

Figure 1. Structures of typical indoloquinolines from *Cryptolepis sanguinolenta*.

Many researchers have achieved the structural modification of cryptolepine scaffold for the purpose of improving antitumor activity, while the pharmacological properties of the analogues are being studied deeply.

The bioactivities of many antitumoral agents are related to their interactions with the DNA molecule, which is regarded as a classical target for these drugs in clinical use. The basic mechanism of antitumoral activity of these drugs is to affect the replication, expression, transcription and other physiological functions of the DNA, which causes the tumor cell death [4].

In 1990, Yamato et al. synthesized the indoloquinoline derivatives **4** (Figure 2), and screened its biological properties in vitro and in vivo. The compounds **4** showed potential antitumor activity (P388 leukemia in mice), DNA intercalative property, and ability to induce topoisomerase II dependent DNA cleavage [5].

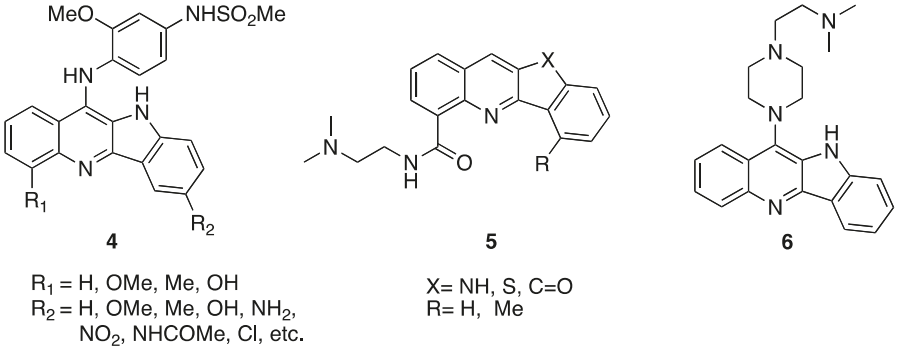

Figure 2. Structures of cryptolepine derivatives.

In 1997, Deady et al. studied a series of cryptolepine derivatives **5** and evaluated their antitumoral activity in a series of murine and human tumor cell lines such as the mice lung cancer cells (LLC), mice leukemia cells (P388), human leukocyte cells (JL). These compounds appear to be mixed topoisomerase I/II inhibitors in the human leukemia cell lines studied [6].

In 1998, Bonjean et al. verified the cryptolepine alkaloids bound tightly to DNA as a typical intercalating agent by various means of absorption, such as fluorescence, circular, and linear dichroism, as well as by a relaxation assay using DNA topoisomerases. At the same time, they provided direct evidence that DNA is the primary target of cryptolepine. The mechanism of the compounds inhibiting tumor cell proliferation is mainly based on the synthesis of DNA inhibition, not the inhibition of proteins and RNA [7].

In 2002, Lisgarten, John N., reported that cryptolepine interacts with the DNA fragment $d(CCTAGG)_2$ in a base-stacking intercalation mode by using X-ray crystallography. It was found that cryptolepine intercalated between pyrimidine bases of the fragment in the form of π-π accumulation. This is the first single crystal structure of DNA intercalator complex, which is the small molecule to bind a non-alternating (pyrimidine-pyrimidine) DNA sequence [8].

In 2012, Boddupally et al. have synthesized a series of 11-substituted cryptolepine derivatives **6** (Figure 2). The compound **6** showed the most potent anticancer activity with IC_{50} = 0.97 μM against HCT-116 colon cancer cell line and IC_{50} = 2.33 μM against Raji lymphoma cells in further cytotoxic test in vitro. At the same time, this compound showed a strong inhibition of c-MYC expression [9].

Gu and Lu demonstrated the binding of aniline-substituted cryptolepine derivatives with calf-thymus DNA presumably via an intercalation mechanism and studied the binding mode of these derivatives with duplex DNA by Surflex-dock software. They reported that these derivatives intercalated into the base-pairs, and reacted with DNA via mainly π-π interaction with medium, moreover the functional groups substituted on aniline ring affected the binding abilities [10,11].

The aim of this review is to present an overview of the potential of neocryptolepine and isocryptolepine as scaffolds for the design and development of new anticancer drugs. Both compounds have also the linearly arranged tetracyclic plane as same as cryptolepine, so they can be expected as candidates of antitumoral agent, although they have a slightly weaker capability to intercalate into DNA and inhibit human topoisomerase II [12].

1.2. Antitumoral Activity of Neocryptolepines and Isocryptolepines

In our group, we have synthesized an array of novel neocryptolepine derivatives **7**, and their congeners **8**, 11-aminoalkylamino-substituted chromeno[2,3-*b*]indoles **9**, and isocryptolepine derivatives **10** (Figure 3). Then the antiproliferative activities of these compounds were tested in vitro against MV4-11 (human leukemia), HCT116 (human colon cancer), and A549 (human non-small cell lung cancer) and BALB/3T3 (normal murine fibroblasts) cell lines.

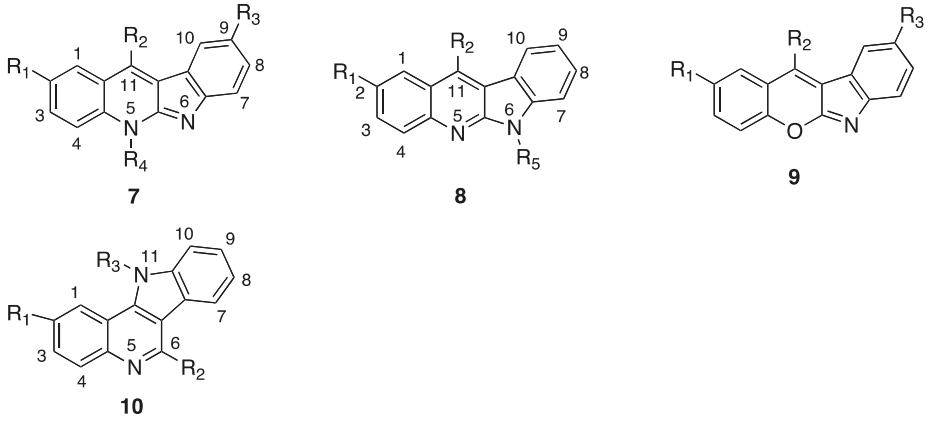

Figure 3. Structure of neocryptolepine derivatives **7**, **8**, chromeno[2,3-*b*]indoles **9**, and isocryptolepine derivatives **10**.

We focused our attention on modifying the neocryptolepine structure at four positions: (1) the side chain at C11, introducing the various amino groups, e.g., -$NH(CH_2)_nNH_2$ (n = 2,3,4), -$NH(CH_2)_3N(C_2H_5)_2$, -$NH(CH_2)_3OH$, -$NHCH_2CH(OH)CH_2NH_2$, -$NHCH_2CH(CH_3)CH_2NH_2$, -$NHCH_2CH(CH_3)NH_2$, -$NHCH_2C(CH_3)_2NH_2$, and so on; (2) replacing the H atom at C2 with MeO, Br, Cl, Me, and replacing H at C9 with COOMe; (3) altering the Me from N5 to N6, (4) changing the N5 to O atom and (5) incorporating metal ion coordinated with diamine side chain [13–18].

In addition, we have also engaged in modifying isocryptolepine derivatives in three ways: the amino substituent effect at C6, and N11 methyl localization effect, and the substituent group effect at C2 of quinoline moiety [19].

Some compounds with higher antiproliferative activity are listed in Tables 1 and 2. The SAR (structure activity relationships) studies reveal that the most necessary strategy is introducing

ω-aminoalkylamino group in the side chain. Among the tested 84-neocryptolepine derivatives and 44-isocryptolepine derivatives, the most potent compounds with higher activity contain the -$NH(CH_2)_3NH_2$ side chain.

Table 1. Cytotoxic effect of neocryptolepine derivatives [13–16].

No.	Substituent					IC_{50} μM			
	R_1	R_2	R_3	R_4	R_5	BALB/3T3	MV4-11	A549	HCT116
7a	H	$NH(CH_2)_3NH_2$	H	Me	-	0.884 ± 0.115	0.066 ± 0.023	0.205 ± 0.079	0.302 ± 0.056
7b	Cl	$NH(CH_2)_3NH_2$	H	Me	-	0.401 ± 0.015	0.068 ± 0.018	0.761 ± 0.169	0.195 ± 0.044
7c	Br	$NH(CH_2)_3NH_2$	H	Me	-	0.869 ± 0.018	0.012 ± 0.002	0.543 ± 0.256	0.274 ± 0.050
7d	OMe	$NH(CH_2)_3NH_2$	H	Me	-	0.978 ± 0.021	0.102 ± 0.021	0.407 ± 0.117	0.155 ± 0.042
7e	Cl	$NHCH_2CH(OH)CH_2NH_2$	H	Me	-	0.896 ± 0.042	0.042 ± 0.014	0.197 ± 0.028	0.138 ± 0.050
7f	Br	$NHCH_2CH(OH)CH_2NH_2$	H	Me	-	0.864 ± 0.015	0.057 ± 0.015	0.190 ± 0.027	0.117 ± 0.055
7g	H	$NH(CH_2)_3NH_2$	COOMe	Me	-	0.933 ± 0.047	0.044 ± 0.011	0.820 ± 0.456	0.176 ± 0.055
7h	Br	$NH(CH_2)_3NH_2$	COOMe	Me	-	0.773 ± 0.023	0.050 ± 0.016	0.302 ± 0.138	0.164 ± 0.070
7i	Cl	$NH(CH_2)_3NH_2$	COOMe	Me	-	0.833 ± 0.030	0.056 ± 0.035	0.194 ± 0.063	0.116 ± 0.078
7j	Cl	$NH(CH_2)_3NH_2$	Br	Me	-	0.834 ± 0.067	0.076 ± 0.034	0.464 ± 0.011	0.284 ± 0.142
8	Cl	$NH(CH_2)_2NH_2$	H	-	Me	0.437 ± 0.400	0.456 ± 0.123	8.282 ± 0.585	6.989 ± 1.416
9	OMe	$NH(CH_2)_2NH_2$	H	-	-	6.87 ± 1.74	0.12 ± 0.07	9.29 ± 1.10	1.93 ± 0.24
		Cisplatin				8.53 ± 3.53	2.36 ± 0.68	7.83 ± 2.60	3.47 ± 0.77
		Doxorubicin HCl				1.08 ± 0.03	0.006 ± 0.002	0.33 ± 0.10	0.39 ± 0.10

Table 2. Cytotoxic effect of isocryptolepine derivatives [17].

No.	Substituent			IC_{50} μM			
	R_1	R_2	R_3	BALB/3T3	MV4-11	A549	HCT116
10a	H	$NH(CH_2)_3NH_2$	H	1.05 ± 0.13	0.12 ± 0.01	0.17 ± 0.05	0.26 ± 0.11
10b	OMe	$NH(CH_2)_3NH_2$	H	0.31 ± 0.03	0.12 ± 0.05	0.16 ± 0.03	0.07 ± 0.03
10c	NO_2	$NH(CH_2)_3NH_2$	H	0.36 ± 0.15	0.15 ± 0.06	0.35 ± 0.22	0.10 ± 0.02
10d	H	$NH(CH_2)_3NH_2$	Me	0.95 ± 0.24	0.11 ± 0.04	0.18 ± 0.03	0.06 ± 0.02
10e	NO_2	$NH(CH_2)_3NH_2$	Me	0.08 ± 0.02	0.05 ± 0.01	0.11 ± 0.07	0.01 ± 0.00
10f	H	$NH(CH_2)_3NH(CH_3)_2$	H	1.18 ± 0.20	0.41 ± 0.31	0.87 ± 0.27	0.55 ± 0.17
10g	Cl	$NH(CH_2)_3NH(CH_3)_2$	Me	0.82 ± 0.08	0.08 ± 0.03	0.57 ± 0.31	0.10 ± 0.02

Among them, 11-(3-amino-2-hydroxy)propylamino derivatives **7e** and **7f** were the most cytotoxic with a mean IC_{50} value of 0.042 μM and 0.057 μM against the MV4-11 cell line, 0.197 μM and 0.190 μM against the A549 cell line, and 0.138 μM and 0.117 μM against the HCT116 cell line.

We propose the reason that the amino terminus domain in the side chain would react with negative charged phosphate groups in DNA, which increases the insertion ability of the complex to DNA.

The methyl localization effect is an important additional contributor to increase the activity. The activity is greatly reduced (10~30 fold lower) by changing the Me group from N5 to N6 (i.e., **8**) of neocryptolepine derivatives. The Me group can increase the activity of isocryptolepine derivatives, as found by a comparison of the compounds **10e** and **10c**.

Replacing H atom at the C2 with MeO, Br, Cl, Me, or replacing H at C9 by COOMe can improve the antiproliferactive activity of neocryptolepine derivatives. Each group contributes differently to the antiproliferactive activity of different tumor cells. For example, **7c** with Br at C2 shows the best antiproliferactive activity against MV4-11 leukemia cells, and this modification did not increase antiproliferactive activity against normal BALB/3T3 cells, but unexpectedly it decreases 2-fold the antiproliferactive activity against A549 lung cancer cells. It can be suggested that this modification increases the selectivity of the tested compound, improving their effect on leukemic cells, without increasing possible adverse effects on normal cells. The substituent effect at C2 of isocryptolepine core also can change the activity; NO_2 is the effective group to increase the activity against cancer but unfortunately also normal cells (**10c** and **10e**). Therefore, we must examine our best to find an effective substituent for further improving the activity.

We boldly tried to replace the 5-nirtogen atom with oxygen atom, forming **9**, which significantly drop the antiproliferactive activity [16].

From all the assay data, isocryptolepine analogues are more potential as the anticancer drug candidates in comparison with the neocrytolepine analogues, compound **10e** (or **10a**) shows the higher antiproliferactive activity against A549 and HCT116 cancer cell, and lower antiproliferactive activity against normal cells comparing **7a**, when amino-substituent is $NH(CH_2)_3NH_2$ and substituent group is H at C2.

The mode of neocryptolepine and isocryptolepine binding to DNA was studied using UV-VIS absorption spectroscopy with salmon fish sperm DNA. From the DNA binding studies, it can be proven that the methyl localization effect and the substituent group effect at C2 of quinoline moiety influence the capability to intercalate into DNA. Two effects improve the activity of isocryptolepine to interact with DNA, the binding constant of **10f**-DNA was 1.05×10^6 L/mol and **10g**-DNA was 4.84×10^6 L/mol [19]. The activity of neocryptolepine to interact with DNA varied; the binding constant of **7c**-DNA was 2.93×10^5 and **8**-DNA was 3.28×10^5 L/mol [13].

In a series of neocrytolepine analogues, **7c** shows the best antiproliferactive activity against MV4-11 leukemia with IC_{50} 0.012 ± 0.002 μM. Compounds **7f** and **7i** show almost the same highest antiproliferactive activity against A549 lung cancer cells with IC_{50} 0.190 ± 0.027 μM and 0.194 ± 0.063 μM, and the antiproliferative activity against HCT116 colon cancer cells with IC_{50} 0.117 ± 0.055 μM and 0.116 ± 0.078 μM. Analogue **7b** unfortunately shows 2-fold higher cytotoxic activity against normal BALB/3T3 cells with the IC_{50} 0.401 ± 0.015 μM than other studied neocrytolepine analogues and 20-fold higher than cisplatin [13].

In series of isocryptolepine analogues, **10e** shows the best antiproliferactive activity against cancer cell lines with IC_{50} 0.05 ± 0.01 μM (MV4-11), IC_{50} 0.11 ± 0.07 μM (A549), and IC_{50} 0.01 ± 0.00 μM (HCT116). Unfortunately, this compound had also 4~15 fold higher cytotoxic activity against normal BALB/3T3 cells with the IC_{50} 0.08 ± 0.02 μM. These two simultaneous modifications at C2-NO_2 and at N11-Me showed 15- and 100-fold increased cytotoxicity of **10e** in comparison to doxorubicin and cisplatin, cytostatic used as a control.

In 2016, in vitro antiproliferative activities of neocryptolepine derivatives were evaluated by Okada (Table 3). The compounds **7a** and **7d** showed the highest anticancer activity, having IC_{50} values of 0.50 μM and 0.20 μM against the breast cancer MDA-MB-453 cell line, at the same time **7a** having 0.64 μM and 2.7 μM against WiDr (colon adenocarcinoma) and SKOv3 (ovarian cancer) cell lines, **7d** having 0.37 μM and 1.3 μM against WiDr (colon adenocarcinoma) and SKOv3 (ovarian cancer) cell lines.

Table 3. Antiproliferative activity of neocryptolepine derivatives against cell lines of the breast cancer MDA-MB-453, WiDr (colon adenocarcinoma) and SKOv3 (ovarian cancer).

Compound	MDA-MB-453 IC_{50}(μM)	WiDr IC_{50}(μM)	SKOv3 IC_{50}(μM)
Neocryptolepine	7.48 ± 4.42	N.T.	N.T.
7a	0.50 ± 0.24	0.64 ± 0.13	2.7 ± 0.42
7d	0.20 ± 0.09	0.37 ± 0.07	1.3 ± 0.18
Cisplatin	7.6 ± 0.7 [a]	8.84 ± 0.52 [c]	18.2 ± 0.1 [d]
Doxorubicin	0.086 ± 0.006 [b]	0.089 [e]	0.52

N.T.: not tested, [a] Rakic et al. (2012), [b] Sandhu et al. (2012), [c] Kuo et al. (2010), [d] Ganta et al. (2014), [e] Molphy et al. (2014).

Recently, we reported the in vitro antiproliferative activity of 11-substituted neocryptolepines with branched ω-aminoalkylamino chain. These 2-substituted 5-methyl-indolo[2,3-*b*]quinoline derivatives were prepared by nucleophilic aromatic substitution (S_NAr) of 11-chloroneocryptolepines **2** with appropriate 1,2- and 1,3-diamines (Scheme 1). Many of the prepared neocryptolepine derivatives showed submicromolar antiproliferative activity of less than μM against the human leukemia MV4-11 cell line (Table 4).

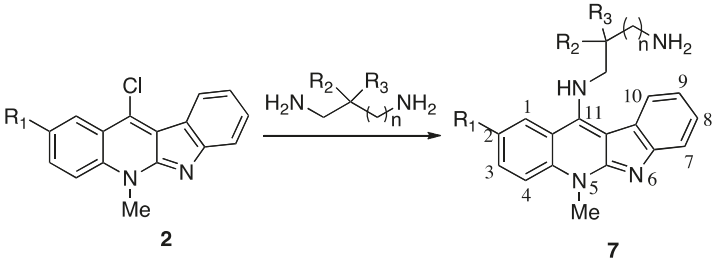

Scheme 1. Synthesis of 11-aminoalkylamino-5-methylindolo[2,3-*b*]quinolines.

Table 4. Antiproliferative activity of 11-aminoalkylamino-5-methyl-indolo[2,3-*b*]quinolines against cell lines of MV4-11, A549 and HCT116, and cytotoxicity against normal mice fibroblast BALB/3T3 [15].

No.	Substituent		IC_{50} μM			
Compounds	**R_1**	**C11-Substituent**	**MV4-11**	**BALB/3T3**	**A549**	**HCT116**
Cisplatin		-	2.820 ± 0.450	8.700 ± 0.097	9.870 ± 2.400	8.500 ± 0.540
Doxorubicin HCl		-	0.006 ± 0.002	1.078 ± 0.033	0.329 ± 0.097	0.390 ± 0.098
2a	H	Cl	1.312 ± 0.262	-	-	-
2b	Br	Cl	0.810 ± 0.145	-	-	-
7l	H	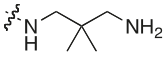	0.150 ± 0.060	4.789 ± 2.018	1.512 ± 0.198	1.262 ± 0.361
7m	Cl	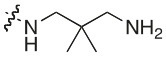	0.119 ± 0.043	9.131 ± 0.844	1.455 ± 0.168	1.373 ± 0.351
7n	Me		0.105 ± 0.027	10.558 ± 0.330	1.795 ± 0.270	2.370 ± 0.481
7o	Cl	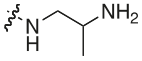	0.103 ± 0.014	1.018 ± 0.017	1.269 ± 0.118	1.204 ± 0.283
7p	Br	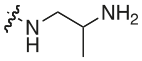	0.078 ± 0.020	0.939 ± 0.018	0.988 ± 0.164	0.842 ± 0.367

For further studying cytotoxic and growth inhibitory activities of neocryptolepine derivatives, the anticancer screening was performed across the JFCR39 cancer cell line panel, evaluated at five concentration levels (100, 10, 1.0, 0.1, and 0.01 μM) (Table 5). The results (the means of GI_{50}, TGI, and LC_{50} values) showed that **7d** have potent anticancer activity against the melanoma (LOX-IMVI) and lung (NCIH522, A549, and DMS273) cancer cell lines in the JFCR39 panels. Compound **7d** shows a notable cytotoxicity against the breast (BSY-1, LC_{50} = 0.82 μM), CNS (SF-539, LC_{50} = 0.60 μM, SNB-75, LC_{50} = 0.91 μM), colon (HCC2998, LC_{50} = 0.74 μM), lung (NCI-H522, LC_{50} = 0.71 μM, A549, LC_{50} = 0.85, DMS273, LC_{50} = 0.70, DMS114, LC_{50} = 0.72 μM), and ovarian (VCAR-4, LC_{50} = 0.48 μM) cancer cell lines [20].

Table 5. Growth inhibitory (GI_{50}) and cytotoxic (LC_{50}) activities of compounds **7d**, **7k** and **7q** across the JFCR 39 panel.

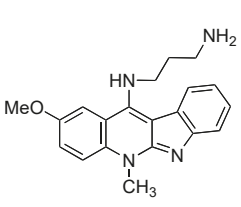

7d

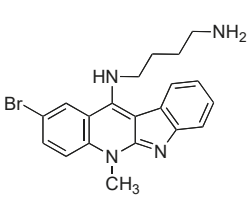

7k

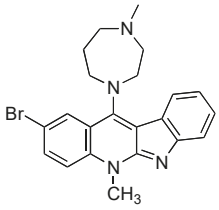

7q

Tissue of Origin	Cell Line	7d			7k			7q		
		GI 50 (μM)	**TGI (μM)**	**IC50 (μM)**	**GI 50 (μM)**	**TGI (μM)**	**IC50 (μM)**	**GI 50 (μM)**	**TGI (μM)**	**IC50 (μM)**
Breast	HBC-4	0.06	0.80	9.5	0.08	0.61	6.1	1.3	4.3	19
	BSY-1	0.11	0.30	0.82	0.12	0.35	3.5	2.0	5.2	20
	HBC-5	0.06	0.33	3.4	0.09	0.41	4.1	0.86	10	53
	MCF-7	0.04	0.24	17	0.03	0.31	3.1	0.87	7.9	44
	MDA-MB-231	0.08	0.33	6.9	0.07	0.34	3.4	0.50	4.1	44
CNS	U251	0.04	0.47	17	0.05	0.55	7.9	0.7	13	58
	SF-268	0.05	0.59	26	0.06	0.75	4.7	0.94	14	76
	SF-295	0.10	0.81	14	0.11	0.55	2.9	1.3	14	49
	SF-539	0.05	0.20	0.60	0.07	0.23	0.63	0.7	3.9	22
	SNB-75	0.13	0.34	0.91	0.15	0.38	0.93	3.3	15	42
	SNB-78	0.12	0.78	25	0.20	0.98	5.2	2.9	20	62
Colon	HCC2998	0.05	0.22	0.74	0.07	0.23	0.69	1.0	2.9	8.0
	KM-12	0.06	0.64	23	0.09	0.59	4.6	0.72	7.0	64
	HT-29	0.04	0.54	24	0.06	0.64	28	0.56	5.6	46
	HCT-15	0.72	6.9	50	1.0	3.7	100	0.58	5.8	49
	HCT-116	0.04	0.57	22	0.04	0.80	5.1	0.43	2.3	15
Lung	NCI-H23	0.06	0.28	1.8	0.07	0.36	2.5	1.2	4.8	98
	NCI-H226	0.08	0.49	25	0.09	0.63	6.2	0.74	4.8	44
	NCI-H522	0.04	0.20	0.71	0.04	0.18	0.57	0.42	1.8	5.5
	NCI-H460	0.05	0.27	3.4	0.05	0.23	1.7	0.45	2.6	20
	A549	0.06	0.23	0.85	0.05	0.26	1.9	0.68	2.5	8.3
	DMS273	0.04	0.18	0.70	0.05	0.18	0.61	0.42	1.6	4.7
	DMS114	0.08	0.26	0.72	0.10	0.33	1.10	1.1	3.7	18
Melanoma	LOX-IMVI	0.03	0.11	1.1	0.03	0.11	0.75	0.31	1.5	7.6
Ovarian	OVCAR-3	0.06	0.28	8.0	0.05	0.30	42	0.64	4.6	82
	OVCAR-4	0.04	0.15	0.48	0.04	0.16	59	0.52	2.7	19
	OVCAR-5	0.05	0.35	9.5	0.05	0.26	42	0.56	3.1	32
	OVCAR-8	0.05	0.33	23	0.05	0.43	100	0.48	3.4	100
	SK-OV-3	0.13	1.0	20	0.13	1.2	54	1.2	7.4	51
Renal	RXF-631L	0.27	1.4	7.4	0.19	0.67	3.0	1.1	3.0	18
	ACHN	0.27	2.1	20	0.25	2.2	10	0.7	7.1	51
Stomach	St-4	0.06	0.43	3.8	0.12	0.60	3.7	0.72	4.9	44
	MKN1	0.09	0.38	12	0.11	0.47	3.1	1.1	3.6	14
	MKN7	0.04	0.34	23	0.06	0.48	36	0.9	8.0	69
	MKN28	0.05	0.9	37	0.05	1.1	58	0.55	12	100
	MKN45	0.05	1.0	28	0.05	1.1	8.0	0.44	6.2	100
	MKN74	0.05	1.0	52	0.06	0.94	8.0	0.56	6.8	100
Prostate	DU145	0.1	0.34	17	0.09	0.43	3.3	1.2	4.0	22
	PC-3	0.16	1.3	70	0.16	1.3	22	2.0	12	56

CNS: Central nervous system; GI50: 50% growth inhibition concentration (μM); TGI: Total Growth inhibition concentration (μM); LC_{50}: Lethal concentration (μM).

Table 5 shows that all of the compounds are highly potent against the melanoma (LOX-IMVI) and lung (NCI-H522, A549, and DMS273) cancer cell lines in the JFCR39 panels. Compounds

7d and **7k** are more potent than compound **7q** towards the cancer cell lines in the JFCR39 panel. Compounds **7d** and **7k** show a similar growth inhibitory activity (GI_{50} > 0.01 μM) against the 31 and 28 cell lines, respectively, of the JFCR39 panel. Compound **7k** shows a notable cytotoxicity against the breast (BSY-1, LC_{50} = 0.82 μM), CNS (SF-539, LC_{50} = 0.60 μM, SNB-75, LC_{50} = 0.91 μM), colon (HCC2998, LC_{50} = 0.74 μM), lung (NCI-H522, LC_{50} = 0.71 μM, A549, LC_{50} = 0.85, DMS273, LC_{50} = 0.70, DMS114, LC_{50} = 0.72) and ovarian (VCAR-4, LC_{50} = 0.48 μM) cancer cell lines. Compound **7q** shows a mentionable cytotoxicity for the CNS (SF-539, LC_{50} = 0.63 μM, SNB-75, LC_{50} = 0.93 μM), colon (HCC2998, LC_{50} = 0.69 μM), lung (NCI-H522, IC_{50} = 0.57 μM, DMS273, LC_{50} = 0.61 μM), and melanoma (LOX-IMVI, LC_{50} = 0.75 μM) cancer cell lines. Compound **7q** displayed a strong growth inhibitory activity (GI_{50} < 1 μM) for 28 panels in the JFCR39 panel of the various cell lines. DMS273 (lung cancer) and NCI-H522 (lung cancer) are the most sensitive cell lines of the 39 cell lines (GI_{50} = 0.42 μM for both and LC_{50} = 4.7 μM and 5.5 μM respectively). Compound **7q** also showed a strong antitumor effect on LOX-IMVI (melanoma, GI_{50} = 0.3 μM, LC_{50} = 7.6 μM).

In our group, we achieved the synthesis of the artemisinin-indoloquinoline hybrids and studied their antiproliferative activity (Figure 4). The artemisinin-neocryptolepine hybrids **11a**, **11b** and the artemisinin-isocryptolepine hybrids **12** showed the potent antiproliferative activity, based on the data in Table 6.

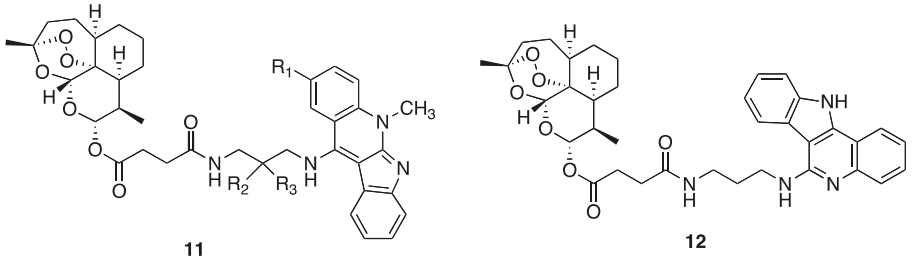

Figure 4. Structures of artemisinin-neocryptolepine hybrids.

Table 6. Antiproliferative activity of the artemisinin-indoloquinoline hybrids against cell line of MV4-11, A549 and HCT116, and cytotoxicity against normal mice fibroblast BALB/3T3 [21].

Compound	R_1	R_2	R_3	MV4-11	A549	HCT116	BALB/3T3
11a	Cl	CH_3	CH_3	0.072 ± 0.022	4.555 ± 2.086	0.893 ± 0.397	6.423 ± 0.996
11b	CO_2Me	CH_3	CH_3	0.075 ± 0.001	5.060 ± 0.911	2.206 ± 0.687	5.945 ± 1.163
12	CO_2Me	H	H	0.086 ± 0.020	0.649 ± 0.080	0.130 ± 0.014	0.768 ± 0.155

In 2017, Li Wang synthesized the novel tacrine-neocryptolepine hybrids, and evaluated as inhibitors of human AChE (hAChE) and human BuChE (hBuChE) (Figure 5). Compound **13** was a highly potent hAChEI having IC_{50} = 0.95 ± 0.04 nM, and a highly potent hBuChE having IC_{50} = 2.29 ± 0.14 nM [22].

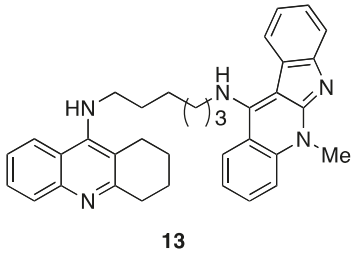

Figure 5. Structure of tacrine-neocryptolepine hybrids.

2. Compare Study

The COMPARE analysis assesses the correlation coefficient between the fingerprints of the test compounds and those of the various reference compounds [23]. This system provides an information intensive approach to identify the molecular targets of new compounds. The JFCR39 COMPARE analysis-guided assay is a successful means to find new anticancer drug candidates. The COMPARE analysis is carried out by calculation of the Pearson correlation coefficient (r value) between the fingerprints of compounds X and Y. The r value is then used to determine the degree of similarity, that is, the higher the r value, the greater the similarity of X to Y. Generally, an r value of $0.5 < r < 0.75$ between two agents suggests they might have a similar mechanism of action (Figure 6).

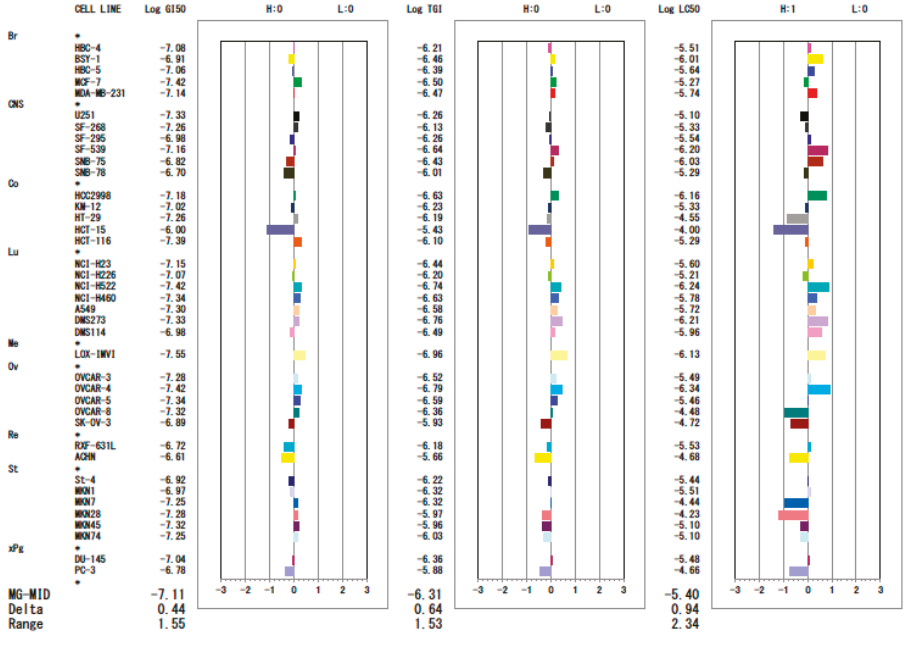

(**A**)

Figure 6. *Cont.*

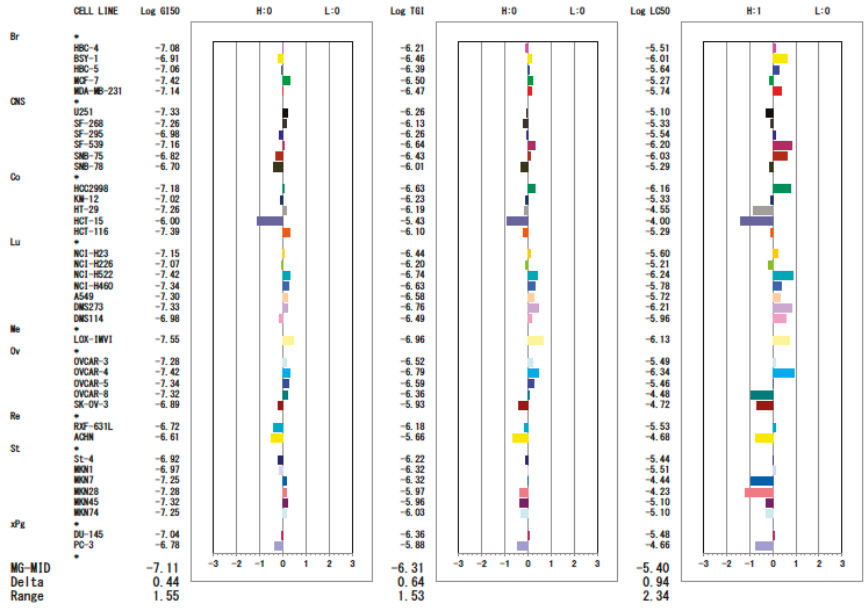

(**B**)

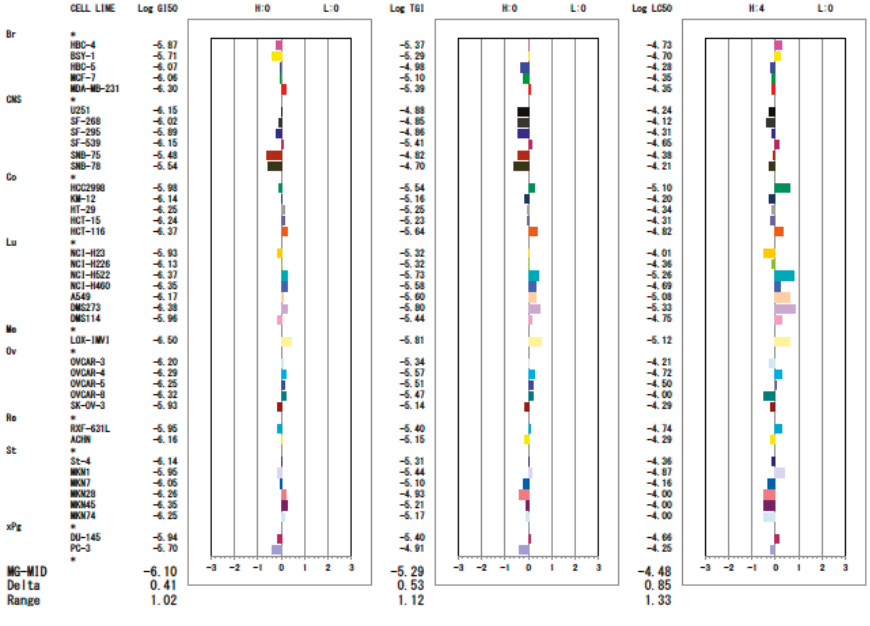

(**C**)

Figure 6. Growth inhibitory- and cytotoxic activities of compounds (**A**) **7d**, (**B**) **7k**, and (**C**) **7q** across a panel of the JFCR39 cell lines. The mean graph was produced by computer processing of the 50% growth inhibition (GI_{50}) and the 50% lethal concentration (LC_{50}) values. The logarithm of the GI_{50} and the LC_{50} values for each cell line is indicated. The X-axis shows the difference on a logarithmic scale between the mean of Log GI_{50}/Log LC_{50} values for all 39-cell lines (MG-MID, expressed as 0 in the

fingerprint) and the Log GI50/Log LC_{50} for each cell line in the JFCR39 panel. Columns to the right of 0 indicate the sensitivity of the cell lines to a given compound, and columns to the left indicate their resistance. The MG-MID mean of the Log GI_{50}/Log LC_{50} values for all 39 cell lines; delta difference between the MG-MID and the Log GI_{50}/Log LC_{50} value for the most sensitive cell line; range difference between the Log GI_{50}/Log LC_{50} values for the most resistant cell line and the most sensitive cell line.

The COMPARE analysis revealed that compounds **7d** and **7k** have a very good match to actinomycin D (r = 0.7 for both). Similarly, compound **7k** has a slight similarity to paclitaxel (r = 0.64). Compound **7q** shows some resemblance to vindesine sulfate (r = 0.58) and aclarubicinHCl (r = 0.57).

3. Conclusions

Indoloquinoline alkaloids are important scaffolds for antitumoral drug development. This review discussed the SAR of neocryptolepine and isocryptolepine, and presents the useful methods for improving the antitumoral activity of neocryptolepine and isocryptolepine analogues. The amino substituent effect and methyl localization effect are now available strategies, but the substituent group effect at the benzene ring of the quinoline moiety has no effect on regular SAR. Thus, the antitumoral activity is highly related to the activity of interacting with DNA. The computer-assisted database analysis, COMPARE, suggested that **7d** and **7k** have a mode of action similar to actinomycin D. It also suggested that **7l** has a mode of action similar to vindesine sulfate or aclarubicin HCl. However, the new compounds may have other unique modes of action since the correlation coefficients (r) were at relatively low levels, which present an interesting possibility to examine in further studies.

Funding: This study was partially supported by the Adaptable and Seamless Technology Transfer Program from Japan Science and Technology Agency (JST), No. AS242Z02199Q, and Menoufia University, No. Ib-C2013.

Conflicts of Interest: The authors declare no conflict of interest.

References

1. Oliver-Bever, B. *Medicinal Plants in Tropical West Africa*; Cambridge University Press: Cambridge, UK, 1986; p. 41.
2. Cimanga, K.; Bruyne, T.; Pieters, L.; Claeys, M.; Vlietinck, A. New alkaloids from Cryptolepis sanguinolenta. *Tetrahedron Lett.* **1996**, *37*, 1703–1706. [CrossRef]
3. Bailly, C.; Laine, W.; Baldeyrou, B.; De Pauw-Gillet, M.C.; Colson, P.; Houssier, C.; Cimanga, K.; Van Miert, S.; Vlietinck, A.J.; Pieters, L. DNA intercalation topoisomerase II inhibition and cytotoxic activity of the plant alkaloid neocryptolepine. *Anti-Cancer Drug Des.* **2000**, *15*, 191–201.
4. Hurley, L. DNA and its associated processes as targets for cancer therapy. *Nat. Rev. Cancer* **2002**, *2*, 188–200. [CrossRef]
5. Yamato, M.; Hashigaki, K.; Takeuchi, Y.; Ikeda, Y. Synthesis and antitumor activity of fused tetracyclic quinoline derivatives. 1. *J. Med. Chem.* **1989**, *32*, 1295–1300. [CrossRef] [PubMed]
6. Deady, L.W.; Kaye, A.J.; Finlay, G.J.; Baguley, B.C.; Denny, W.A. Synthesis and antitumor properties of N-[2-(Dimethylamino)ethyl] carboxamide derivatives of fused tetracyclic quinolines and quinoxalines: A new class of putative Topoisomerase inhibitors. *J. Med. Chem.* **1997**, *40*, 2040–2046. [CrossRef] [PubMed]
7. Bonjean, K.; De Pauw-Gillet, M.C.; Defresne, M.P.; Colson, P.; Houssier, C.; Dassonneville, L.; Bailly, C.; Greimers, R.; Wright, C.; Quetin-Leclercq, J.; et al. The DNA intercalating alkaloid cryptolepine interferes with Topoisomerase II and inhibits primarily DNA synthesis in B 16 melanoma cells. *Biochemistry* **1998**, *37*, 5136–5146. [CrossRef] [PubMed]
8. Lisgartent, J.N.; Coll, M.; Portugal, J.; Wright, C.W.; Aymami, J. The antimalarial and cytotoxic drug cryptolepine intercalates into DNA at cytosine-cytosine sites. *Nat. Struct. Biol.* **2002**, *9*, 57–60. [CrossRef] [PubMed]

9. Boddupally, P.V.L.; Hahn, S.; Beman, C.; De, B.; Brooks, T.A.; Gokhale, V.; Hurley, L.H. Anticancer Activity and Cellular Repression of c-MYC by the GQuadruplex-Stabilizing 11-Piperazinylquindoline is Not Dependent on Direct Targeting of the G-Quadruplex in the c-MYC Promoter. *J. Med. Chem.* **2012**, *55*, 6076–6086. [CrossRef]
10. Zhou, J.L.; Lu, Y.J.; Ou, T.-M.; Zhou, J.-M.; Huang, Z.-S.; Zhu, X.-F.; Du, C.-J.; Bu, X.-Z.; Ma, L.; Gu, L.-Q.; et al. Synthesis and evaluation of quindoline derivatives as G-quadruplex inducing and stabilizing ligands and potential inhibitors of telomerase. *J. Med. Chem.* **2005**, *48*, 7315–7321. [CrossRef]
11. Lu, Y.J.; Ou, T.M.; Tan, J.H.; Hou, J.Q.; Shao, W.Y.; Peng, D.; Sun, N.; Wang, X.D.; Wu, W.B.; Bu, X.Z.; et al. 5-*N*-methylated quindoline derivatives as telomeric G-quadruplex stabilizing ligands: Effects of 5-N positive charge on quadruplex binding affinity and cell proliferation. *J. Med. Chem.* **2008**, *51*, 6381–6392. [CrossRef]
12. Guittat, L.; Alberti, P.; Rosu, F.; Van Miert, S.; Thetiot, E.; Pieters, L.; Gabelica, V.; De Pauw, E.; Ottaviani, A.; Riou, J.-F.; et al. Interaction of cryptolepine and neocryptolepine with unusual DNA structures. *Biochimie* **2003**, *85*, 535–547. [CrossRef]
13. Wang, L.; Switalska, M.; Mei, Z.-W.; Lu, W.-J.; Takahara, Y.; Feng, X.-W.; El-Sayed, I.E.-T.; Wietrzyk, J.; Inokuchi, T. Synthesis and in vitro antiproliferative activity of new 11-aminoalkylamino-substituted 5H- and 6H-indolo[2,3-*b*]quinolines; structure–activity relationships of neocryptolepines and 6-methyl congeners. *Bioorg. Med. Chem.* **2012**, *20*, 4820–4829. [CrossRef] [PubMed]
14. Lu, W.; Switalska, M.; Wang, L.; Yonezawa, M.; El-Sayed, I.E.-T.; Wietrzyk, J.; Inokuchi, T. In vitro antiproliferative activity of 11-aminoalkylaminosubstituted 5H-indolo[2,3-*b*]quinolines; improving activity of neocryptolepines by installation of ester substituent. *Med. Chem. Res.* **2013**, *22*, 4492–4504. [CrossRef]
15. Shaban, E.; Switalska, M.; Wang, L.; Wang, N.; Xiu, F.; Hayashi, I.; Ngoc, T.A.; Nagae, S.; El-Ghlban, S.; Shimoda, S.; et al. Synthesis and In Vitro Antiproliferative Activity of 11-Substituted Neocryptolepines with a Branched ω-Aminoalkylamino Chain. *Molecules* **2017**, *22*, 1954. [CrossRef] [PubMed]
16. Peng, W.; Świtalska, M.; Wang, L.; Mei, Z.-W.; Edazawa, Y.; Pang, C.-Q.; El-Sayed, I.E.-T.; Wietrzyk, J.; Inokuchi, T. Synthesis and in vitro antiproliferative activity of new 11-aminoalkylaminosubstituted chromeno[2,3-*b*]indoles. *Eur. J. Med. Chem.* **2012**, *58*, 441–451. [CrossRef] [PubMed]
17. Emam, S.; El Sayed, I.; Ayad, M.; Hathout, H. Synthesis, characterization and anticancer activity of new Schiff bases bearing neocryptolepine. *J. Mol. Struct.* **2017**, *1146*, 600–619. [CrossRef]
18. Emam, S.; El Sayed, I.; Nassar, N. Transition metal complexes of neocryptolepine analogues Part I: Synthesis, spectroscopic characterization, and in vitro anticancer activity of Copper(II) Complexes, Spectrochim. *Mol. Biomol. Spectrosc.* **2015**, *138*, 942–953. [CrossRef]
19. Wang, N.; Świtalska, M.; Wu, M.-Y.; Imai, K.; Ngoc, T.A.; Pang, C.-Q.; Wang, L.; Wietrzyk, J.; Inokuchi, T. Synthesis and in vitro cytotoxic effect of 6-amino-substituted 11H- and 11Me-indolo[3,2-*c*]quinolines. *Eur. J. Med. Chem.* **2014**, *78*, 314–323. [CrossRef]
20. Okada, M.; Mie, Z.-W.; Hossain, M.I.; Wang, L.; Tominaga, T.; Takebayashi, T.; Murakami, M.; Yasuda, M.; Shigehiro, T.; Kasai, T.; et al. Synthesis and in vitro cancer cell growth inhibition evaluation of 11-amino-modified 5-Me-indolo[2,3-*b*]quinolines and their COMPARE analyses. *Med. Chem. Res.* **2016**, *25*, 879–892. [CrossRef]
21. Wang, L.; Świtalska, M.; Wang, N.; Du, Z.-J.; Fukumoto, Y.; Diep, N.K.; Kiguchi, R.; Nokami, J.; Wietrzyk, J.; Inokuchi, T.; et al. Design, Synthesis, and Biological Evaluation of Artemisinin-Indoloquinoline Hybrids as Potent Antiproliferative Agents. *Molecules* **2014**, *19*, 19021–19033. [CrossRef]
22. Wang, L.; Moraleda, I.; Iriepa, I.; Romero, A.; López-Muñoz, F.; Chioua, M.; Inokuchi, T.; Bartolini, M.; Marco-Contelles, J. 5-Methyl-N-(8-(5,6,7,8-tetrahydroacridin-9-ylamino)octyl)-5H-indoloij2,3-b]quinolin-11 -amine: A highly potent human cholinesterase inhibitor. *Med. Chem. Commun.* **2017**, *8*, 1307–1317. [CrossRef] [PubMed]
23. Kong, D.; Yamori, T. JFCR39, a panel of 39 human cancer cell lines, and its application in the discovery and development of anticancer drugs. *Bioorg. Med. Chem.* **2012**, *20*, 1947–1951. [CrossRef] [PubMed]

molecules

MDPI

Review

Pleiotropic Pharmacological Actions of Capsazepine, a Synthetic Analogue of Capsaicin, against Various Cancers and Inflammatory Diseases

Min Hee Yang [1], Sang Hoon Jung [1], Gautam Sethi [2,*] and Kwang Seok Ahn [1,3,4,*]

1 KHU-KIST Department of Converging Science and Technology, Kyung Hee University, Seoul 02447, Korea; didmini@naver.com (M.H.Y.); shjung507@gmail.com (S.H.J.)
2 Department of Pharmacology, Yong Loo Lin School of Medicine, National University of Singapore, Singapore 117600, Singapore
3 Department of Science in Korean Medicine, Kyung Hee University, 24 Kyungheedae-ro, Dongdaemun-gu, Seoul 02447, Korea
4 Comorbidity Research Institute, College of Korean Medicine, Kyung Hee University, 24 Kyungheedae-ro, Dongdaemun-gu, Seoul 02447, Korea
* Correspondence: phcgs@nus.edu.sg (G.S.); ksahn@khu.ac.kr (K.S.A.); Tel.: +65-6516-3267 (G.S.); +82-2-961-2316 (K.S.A.)

Academic Editor: Roberto Fabiani
Received: 18 February 2019; Accepted: 8 March 2019; Published: 12 March 2019

Abstract: Capsazepine is a synthetic analogue of capsaicin that can function as an antagonist of TRPV1. Capsazepine can exhibit diverse effects on cancer (prostate cancer, breast cancer, colorectal cancer, oral cancer, and osteosarcoma) growth and survival, and can be therapeutically used against other major disorders such as colitis, pancreatitis, malaria, and epilepsy. Capsazepine has been reported to exhibit pleiotropic anti-cancer effects against numerous tumor cell lines. Capsazepine can modulate Janus activated kinase (JAK)/signal transducer and activator of the transcription (STAT) pathway, intracellular Ca^{2+} concentration, and reactive oxygen species (ROS)-JNK-CCAAT/enhancer-binding protein homologous protein (CHOP) pathways. It can inhibit cell proliferation, metastasis, and induce apoptosis. Moreover, capsazepine can exert anti-inflammatory effects through the downregulation of lipopolysaccharide (LPS)-induced nuclear transcription factor-kappa B (NF-κB), as well as the blockage of activation of both transient receptor potential cation channel subfamily V member 1 (TRPV1) and transient receptor potential cation channel, subfamily A, and member 1 (TRPA1). This review briefly summarizes the diverse pharmacological actions of capsazepine against various cancers and inflammatory conditions.

Keywords: capsazepine; cancer; inflammatory diseases; ROS; TRPV1

1. Introduction

Capsaicin (8-Methyl-*N*-vanillyl-trans-6-nonenamide) is the commonly found pungent ingredient in hot chili peppers [1,2]. Capsaicin can act as a pharmacological agent that can regulate inflammation and pain using specific receptors of afferent sensory neurons [3]. The transient receptor potential vanilloid type 1 (TRPV1) channel can be activated by capsaicin [1]. TRPV1 is a ligand-gated non-selective, cation channel, and it was first reported in sensory neurons such as dorsal root ganglion (DRG) [4]. As soon as the TRPV1 channel is activated, uptake of calcium (Ca^{2+}) ion is rapidly increased [5]. Ca^{2+} plays an important role in diverse signal transduction pathways [5], including cell proliferation, cell death, neural excitation, neurotransmitter release, etc.

Capsazepine(*N*-[2-(4-Chlorophenyl)ethyl]-1,3,4,5-tetrahydro-7,8-dihydroxy-2*H*-2-benzazepine-2 carbothioamide) is a synthetic analogue of capsaicin [1]. It was first discovered and characterized

by the Sandoz (now Novartis) [1], and it was modified on the chemical backbone of capsaicin [6], (Figure 1). Interestingly, capsazepine (10 μM) can also reversibly reduce the response to capsaicin (500 nM) of voltage-clamped DRG neurons in rats [1]. Moreover, capsazepine can act as a potent blocker of TRPV1 channels. It can bind to the pores of transmembrane domain on TRPV1 channel and can interact with all monomers residues of this channel [3]. Capsazepine can also exhibit several pharmacological effects via blocking TRPV1 channel and thereby suppressing the influx of Ca^{2+} [5]. It can thus be effectively used for the prevention and treatment of various cancers and inflammatory conditions, although its clinical use has been hampered, owing to its poor pharmacokinetic properties (Figure 2).

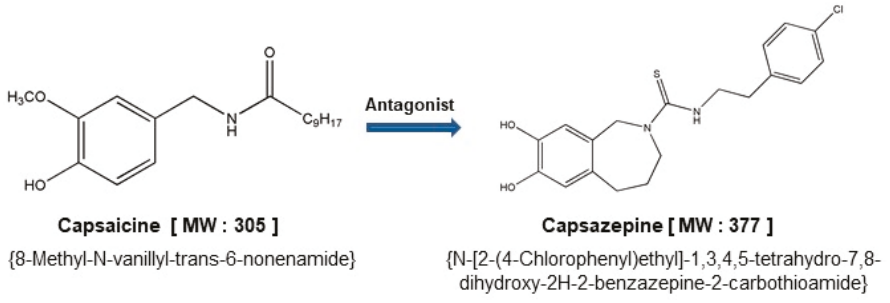

Figure 1. The chemical structures of capsaicin and capsazepine.

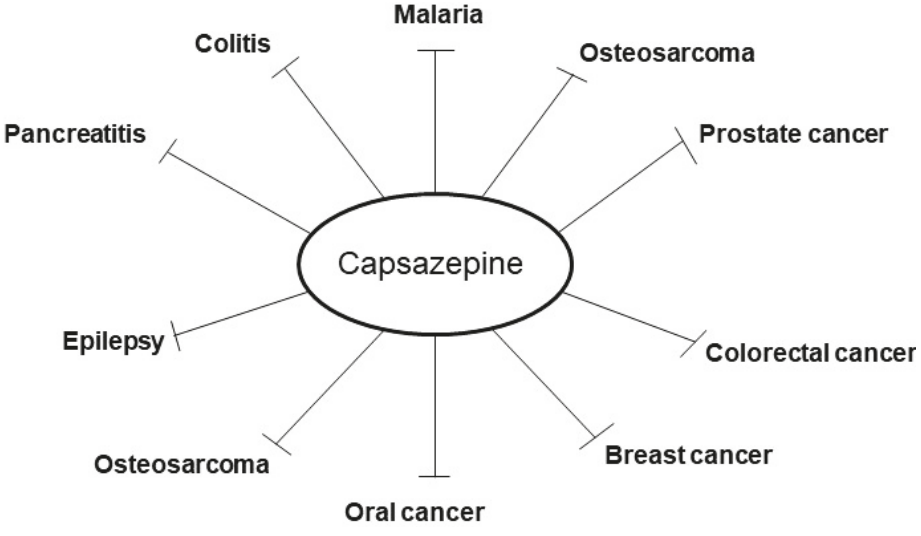

Figure 2. Pharmacological properties of capsazepine.

Additionally, capsazepine has been also reported to target various other receptors including other TRP channels such as TRPV4 and TRPM8 [7–9]. It can also block nicotinic acetylcholine receptors and voltage-activated calcium channels in rats [7,8]. Interestingly, Docherty et al. reported that capsazepine can mediate human hyperpolarization-activated cyclic nucleotide-gated two and four channels and inhibit currents in the HEK293 cells concentration dependently [9]. This finding can also partly explain the reported anti-nociceptive effects of capsazepine [9].

2. Pharmacological Actions of Capsazepine in Tumor Cell Lines

2.1. Anti-Cancer Effects of Capsazepine In Vitro

Several compounds derived from Mother Nature can function as potent anti-cancer agents that can abrogate the process of tumorigenesis [10–26]. Capsazepine has been reported to exert significant anti-proliferative effects against multiple tumor types *in vitro*, as summarized in Table 1. The mechanisms underlying the anti-cancer/growth inhibitory effects include the inhibition of activation of Janus activated kinase (JAK)/signal transducer and activator of transcription (STAT) pathway, calcium ion influx, ROS-JNK-CHOP pathway, and modulation of other important signal transduction pathways (Figure 3).

Table 1. Anti-cancer effects of capsazepine *in vitro*.

Origin	Cell Lines	Concentrations	Molecular Targets	Mechanism of Actions	Ref.
Prostate	DU145	1, 2.5, 5 μM for 6, 24 h	STAT3, JAK↓	Apoptosis↑	[27]
	LNCaP				[27]
	PC-3	200 μM from for 5 h	Intracellular Ca^{2+} concentration↑	Apoptosis↑	[4]
Breast	MDA-MB-231	25 μM for 48 h	System x_c^- (xCT), cystine	ROS↑ Apoptosis↑	[28]
Colon	HCT166	10, 30 μM for 6, 24 h	ROS, JNK, CHOP	Apoptosis↑	[5]
Oral	SCC4	30, 60, 90 μM for 24 h	ROS	cell proliferation↓ Apoptosis↑	[29]
	SCC25				
	HSC3				
Bone	MG63	50, 100, 150, 200 μM for 4 h	Intracellular Ca^{2+} concentration↑	Tumor cell multiplication↓	[30]

2.1.1. Prostate Cancer

Signal transducer and activator of transcription (STAT) proteins activation associated with cell proliferation, survival, and angiogenesis [27,31–40]. STAT3 is frequently hyper-activated in tumor cells and regulates the expression of oncogenic genes [31]. Capsazepine was found to induce substantial apoptosis in DU145 and PC-3 prostate cells by inhibiting STAT3 activation [27]. The suppression of STAT3 was caused through the inhibition of upstream Janus activated kinase-1, 2 (JAK1, JAK2), and c-Src kinases. Moreover, capsazepine induced the expression of PTPε both protein and mRNA levels that may mediate the STAT3 inhibitory effects of the drug [27]. Capsazepine also decreases the expression of various oncogenic proteins, invasion, and promoted apoptosis in prostate cancer [27].

While capsazepine has been known to be a potent blocker of the TRPV1 channel. Huang et al. reported that capsazepine can exhibit anticancer effects in prostate cancer by inducing intracellular Ca^{2+} concentration. There are two different ways to store Ca^{2+}. For example, IP_3-sensitive Ca^{2+} stores release Ca^{2+} into the cytosol when cells are stimulated by an endogenous agent, whereas IP_3-insensitive Ca^{2+} stores can release Ca^{2+} into the cytosol when cells are stimulated by the exogenous agent [4]. Human PC-3 cells can store Ca^{2+} in the endoplasmic reticulum [4]. Capsazepine induced intracellular Ca^{2+} concentration by Ca^{2+} influx, and thereby releasing Ca^{2+} from the endoplasmic reticulum [4]. Interestingly, capsazepine causes the release of Ca^{2+} from the endoplasmic reticulum in a phospholipase C independent manner as the U73122, an inhibitor of phospholipase C, treatment did not significantly effect capsazepine-induced Ca^{2+} release [4].

2.1.2. Breast Cancer

System x_c^- (xCT), the functional unit of cys-tine/glutamate antiporter, has been found to be elevated in many tumor types in response to high ROS concentrations [28]. When this antiporter is upregulated, it can promote cell survival by inducing cysteine uptake and promoting glutathione (GSH) production [28]. High glutamate released by System x_c^- (xCT) has been associated with cancer-induced

bone pain (CIBP) during distal breast metastasis [28]. The exchange of cystine for glutamate generally occurs at a stoichiometric ratio of 1:1 induced by the intracellular concentration of glutamate [28]. Therefore, the inhibition of System x_c^- (xCT) can induce the downregulation of glutamate release, and thus reduce mechanical hyperalgesia associated with CIBP [28]. Capsazepine was found to significantly inhibit System x_c^- (xCT) by blocking the uptake of cysteine [28]. Capsazepine was also found to induce ROS production, which led to a substantial programmed cell death in MDA-MB-231 cells [28].

2.1.3. Colorectal Cancer

TNF-related apoptosis-inducing ligand (TRAIL) has the role of anti-cancer effects [5]. TRAIL can bind to the death receptors and activate the extrinsic apoptotic cell death pathway [5,41–44]. TRAIL can induce cancer apoptosis by increasing the activation of death receptors DR4 and DR5. DR induction has been related to the increased activation of CCAAT/enhancer-binding protein homologous protein (CHOP), ROS production, as well as to the augmented JNK phosphorylation [45,46]. Interestingly, capsazepine was found to induce TRAIL receptor expression by upregulating both DR4 and DR5 receptors through JNK activation in colorectal HCT116 cells [5]. It also required ROS and CHOP to exert these effects [5]. Capsazepine also decreased the expression of cell survival proteins and increases the pro-apoptotic proteins [5].

2.1.4. Oral Cancer

Gonzales et al. reported that capsazepine can exhibit both cytotoxic and anti-tumor effects in oral squamous cell carcinoma (OSCC) [29]. These effects were associated with the production of ROS independently of its action on the TRPV1 channel [29]. ROS can regulate the activation of various signaling molecules including NF-κB, STAT3, JNK, hypoxia-inducible factor-1α, kinases, growth factors, cytokines and other proteins, and enzymes [29,35,38,47–52]. It has been closely linked to cell proliferation, survival, invasion, and metastasis of cancer [48,53]. It is well known that cancer cells undergo oxidative stress due to increased metabolic activity resulting in a subtle balance between ROS levels and cellular antioxidant capabilities. When ROS levels are increased above basal level, the subtle balance may be disrupted and thus trigger ROS induced apoptosis. Vanilloids such as capsazepine have been found to increase ROS and thus alter the balance between normal ROS contents and cellular antioxidant capabilities [29,54,55]. Capsazepine was also observed to augment apoptosis in a concentration-dependent manner in SCC4, SCC25, and HSC3 cells [29].

2.1.5. Osteosarcoma

Capsazepine can also exert potent anti-cancer effects on MG63 osteosarcoma cells [30]. Capsazepine can induce intracellular Ca^{2+} increase by causing extracellular Ca^{2+} influx [30]. Moreover, capsazepine can cause intracellular Ca^{2+} release from endoplasmic reticulum via a phospholipase C-independent manner [30]. It was also noted to attenuate cell proliferation in a concentration dependent manner [30]. The multiple oncogenic targets modulated upon capsazepine treatment are briefly summarized in Figure 3.

2.2. Anti-Cancer Effects of Capsazepine In Vivo

2.2.1. Prostate Cancer

Capsazepine has been reported to exhibit anti-cancer effects in prostate cancer in preclinical settings [27]. Capsazepine administered at doses of 1 mg/kg and 5 mg/kg three times a week for up to 20 days abrogated tumor growth in the xenograft prostate cancer mouse model [27]. Additionally, capsazepine treatment caused reduction in phosphorylation of STAT3 and increased PTPε protein levels in tumor tissues [27].

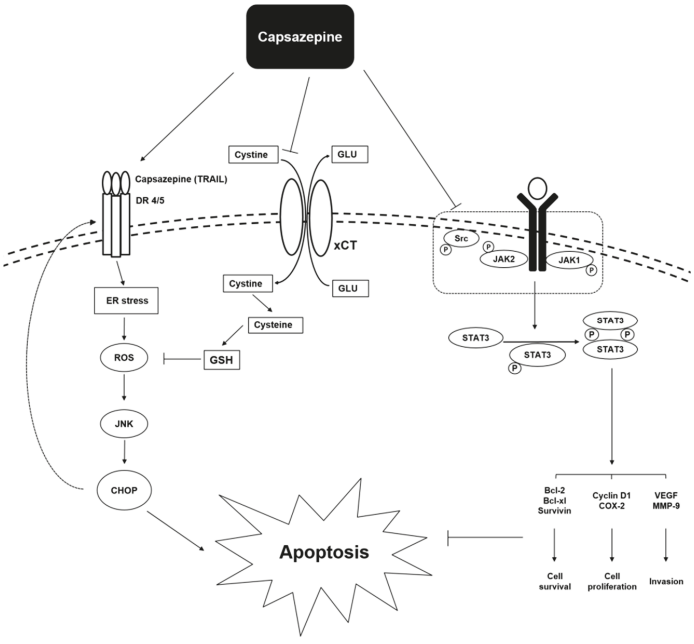

Figure 3. Potential mechanisms underlying reported anti-cancer effects of capsazepine.

2.2.2. Breast Cancer

Capsazepine can regulate System x_c^- activity under *in vivo* conditions as well [28]. MDA-MB-231 grafted BALB/c nude mice was treated with high (10 mg/kg) and low (5 mg/kg) doses of capsazepine for three days/week and it was found to delay the CIBP-induced nociceptive behaviors [28].

2.2.3. Oral Cancer

Capsazepine treatment in oral squamous cell carcinoma (OSCC) xenograft mouse model was observed to attenuate tumor growth [29]. HSC3, SCC4, and SCC25 xenografts were treated with 0.02, 0.04 mg capsazepine for 12, 16, or 18 days, respectively. Anti-tumor effects of capsazepine has no adverse effects on non-malignant tissues *in vivo* [29] (Table 2).

Table 2. Anti-cancer effects of Capsazepine on animal studies.

Disease	Animal Model	Dosage	Outcome	Ref.
Prostate cancer	mice	1, 5 mg/kg/day for 20 days	Tumor growth↓ STAT3↓	[27].
Breast cancer	mice	10, 5 mg/kg/day for 36 days	CIBP-induced nociceptive behaviors	[28]
Oral cancer	mice	0.02, 0.04 mg/day for 12, 16 and 18 days	Tumor growth↓	[29]

3. Effects of Capsazepine on Inflammatory Conditions

Lipopolysaccharide (LPS) can interact with Toll-like receptor 4 (TLR4), leading to the activation of nuclear transcription factor-kappa B (NF-κB), a transcription factor that plays an important role in both inflammation and cancer [56–67]. NF-κB can initiate the transcription of inducible nitric oxide synthase (iNOS), tumor necrosis factor-α(TNF-α), interleukin-6 (IL-6), and other pro-inflammatory mediators [68]. Nitric oxide (NO) is one of the key products generated during an inflammatory

response [69,70]. Capsazepine can downregulate NO production by attenuating iNOS mRNA expression in LPS-stimulated RAW264.7 macrophages [70]. Capsazepine was also found to abrogate LPS-induced NF-κB activation and it was noted that these inhibitory effects were mediated via its antioxidant activity [70].

Capsazepine is an effective blocker at TRPV1 in human, rat, and guinea pig. Capsazepine can block the TRPV1 responses in response to low pH and heat in human and guinea pig with a better efficacy than in rat [71]. Additionally, capsazepine has been reported to reduce both inflammatory and neuropathic mechanical hyperalgesia in guinea pigs, but not in rats [72]

3.1. Colitis

Sensory neurons have two major polymodal ion channel receptors, TRPV1 and transient receptor potential ankyrin 1 (TRPA1) [73]. Sensitization of both TRPA1 and TRPV1 can lead to hyperalgesia and both channels can also exert neurogenic inflammatory effects [73]. TRPA1 was found in DRG and has an important role in peripheral pain [73]. TRPA1 can also exert anti-inflammatory and anti-nociceptive effects similar to TRPV1 [73]. Kistner et al. found that capsazepine can also exhibit inhibitory effects on colitis via the modulation of TRPA1 [73]. They demonstrated this hypothesis by using capsazepine-induced calcium transients in human TRPA1-expressing HEK293t cells and mice [73]. The diverse pro-inflammatory mediators affected by capsazepine treatment are depicted in Figure 4 (Table 3).

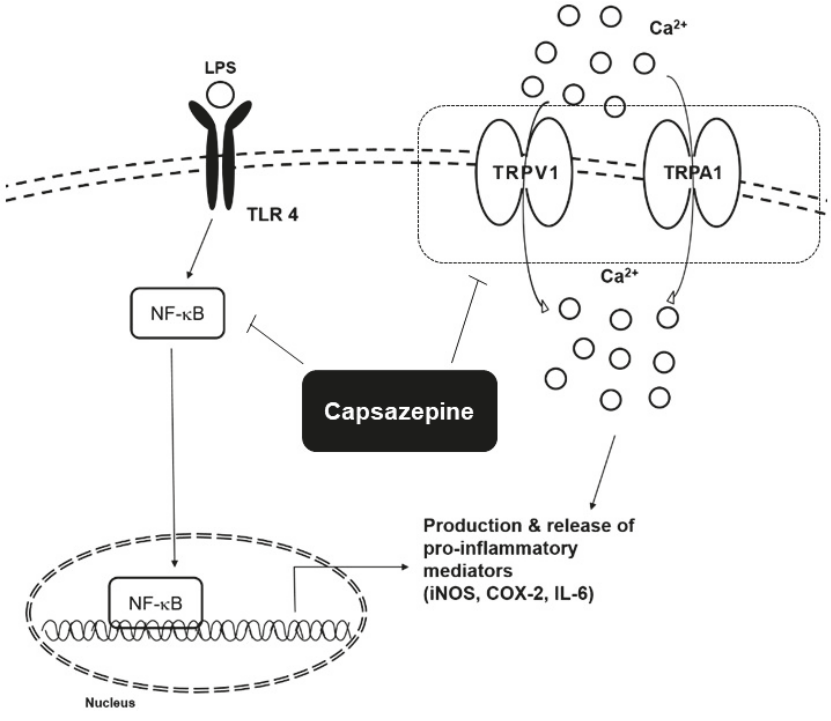

Figure 4. Potential mechanisms regulating anti-inflammatory effects of capsazepine.

Attenuation of experimental colitis by capsazepine has been attributed to its antagonistic effects on TRPV1channel, and were also found to be associated with the inhibition of neurogenic inflammation [74]. For example, repeated capsazepine administration can attenuated trinitrobenzene sulfonic acid (TNBS)-induced colitis in rats [74]. Rats were treated with 37.7×10^{-5} mg/kg/day

of capsazepine enema for six days [74]. Capsazepine was found to downregulate macroscopic damage score (MDS) and MPO scores [74]. Similarly, capsazepine can prevent intestinal inflammation in dextran sulphate sodium (DSS)-induced colitis [75]. Sprague-Dawley rats were treated with 0.1 mg/kg/day for six days [75]. Capsazepine significantly decreased the levels of disease activity index (DAI), myeloperoxidase (MPO) activity in DSS-induced colitis [75].

Table 3. Anti-inflammatory Effects of capsazepine *in vitro*.

Origin	Cell Lines	Concentrations	Molecular Targets	Mechanism of Actions	Ref.
Macrophage	RAW264.7	1, 5, 10 μM for 6 h	NF-κB	Immune response↑	[70]
Kidney	HEK293t	10 μM for 10 s	TRPA1	Inflammation↓	[73]
Hippocampus	Hippocampal ca1 pyramidal cells	10, 100 μM for 20 min	TRPV1	Apoptosis↑, cell proliferation↓	[76]

Table 4. Anti-inflammatory effects of capsazepine in preclinical disease models.

Disease	Animal Model	Dosage	Outcome	Ref.
Colitis	Rat	37.7×10^{-5} mg/kg/day for 6 days	Inflammatory parameter↓	[74]
	Rat	0.1 mg/kg/day for 6 days	DAI, MPO activity↓	[74]
	Rat	1 mg/kg/day for 7 days	Inflammatory parameter↓	[73]
Pancreatitis	Rat	37.7×10^{-3} mg/kg for 30 min before surgery	Inflammatory parameter↓	[76]
Malaria	mice	0.05 mg/kg/day for 6 days	Immune response↑	[77]
Epilepsy	rat	1, 3, 10 mg/kg/day for 7 days	seizure severity↓	[78]
	mice	5 mg/kg/test	antinociceptive effects	[79]
	mice	50 mg/kg	4-AP(4-aminopyridine)-induced epileptic status activity↓	[80]

3.2. Pancreatitis

TRPV1 activation was also found to be involved in acute pancreatitis. Wick et al. reported that the sensory nerves that stimulate pancreas can release TRPV1, substance P (SP), and CGRP in dorsal horn caused during the nociception process [81]. Antagonism of TRPV1, SP, and CGRP receptors can inhibit pancreatitis pain [81]. Additionally, pancreaticobiliary duct obstruction may cause an increase in the pancreatic leukotriene B_4 (LTB_4) concentrations [76]. It can thus mediate TRPV1 activation and causes acute pancreatitis. Rats were pre-treated with capsazepine 37.7×10^{-3} mg/kg sc 30 min before surgery [76]. Capsazepine caused a downregulation of various inflammatory parameters such as myeloperoxidase (MPO) activity, pancreatic edema, and histological damage in leukotriene B_4 (LTB_4)-induced pancreatitis [76].

3.3. Malaria

Malaria is an infectious disease caused by the bite of infectious mosquitoes and the outcome of infection depends on the host's innate immune response [82]. White et al. investigated the role of TRPV1 in malaria for the first time and employed C57BL/6 mice treated with capsazepine 0.05 mg/kg/day for six days [82]. They found that capsazepine was able to regulate the innate immune response to malaria in mice infected with *Plasmodium berghei* ANKA [82].

3.4. Epilepsy

Calcium ion accumulation in hippocampal neurons is a major contributor to epilepsy [80]. Ghazizadeh et al. and Naziroglu et al. investigated that epilepsy effects on oxidative stress [83,84]. They found that Ca^{2+} signaling and the apoptosis in pentylentetrazol (PTZ)-induced hippocampal injury in rats. Shirazi et al. reported that TRPV1 receptors are important for PTZ and amygdala-induced kindling in rats [85]. TRPV1 antagonist, capsazepine can modulate epileptiform activity by anti-convulsant properties [85]. During epilepsy induction, intracellular calcium ion concentration was found to be increased [85]. Capsazepine caused a decrease in intracellular Ca^{2+} concentration [85].

There are many studies anti-epileptic effect of capsazepine [6,27,80,86,87]. Gonzalez-Reyes et al. reported that the capsazepine administration can suppress 4-AP induced ictal activity and propagation of seizure activity *in vitro* (10–100 μM) and *in vivo* (50 mg/kg s.c.) [80]. In addition, capsazepine can act directly on the axons through the blood brain barrier [80]. Nazıroğlu et al. has also shown that capsaicin-induced TRPV1 sensitization can cause Ca^{2+} elevation, thereby increasing apoptosis and epileptic seizures [80]. These processes were reduced by capsazepine (0.1 mM) treatment [87]. Additionally, capsazepine can potentiate the anti-nociceptive effects of morphine in mice [79]. Morphine treatment can induce TRPV1 expression in the DRG, spinal cord upon repeated exposure [79]. Interestingly, TRPV1 antagonists can be used effectively as pharmacological agents against morphine treatment. Santos et al. found that capsazepine treatment can lead to an inhibitory avoidance, thereby leading to a decrease in the rat elevated plus-maze test and thus indicating that TRPV1 may have a key role in regulating anxiety [88]. Similarly, a decreased expression of TRPV1 channels and inhibitory avoidance behavior was observed in rats that received capsazepine in the elevated plus-maze test [69] (Table 4).

3.5. Neurogenic Inflammation

Capsazepine can inhibit neurogenic inflammation mediated by TRPV1 [89,90]. Inflammatory responses caused by the release of inflammatory mediators such as neuropeptide calcitonin gene-related peptide (CGRP) and substance P (SP) from primary afferent nerve terminals are referred to as neurogenic inflammation [89,91]. Inflammatory neuropeptides release by antidromic activation of afferent nociceptors and dorsal root reflexes (DRRs) play a key role in this process [91]. Flores et al. reported that capsazepine (300 μL) abolished the capsaicin-evoked release of immunoreactive CGRP (iCGRP) in Sprague-dawley rats buccal mucosa [92]. Moreover, the neurosecretion of capsaicin-evoked iCGRP via the vanilloid receptor mediated mechanism [92].

Further, capsazepine can inhibit H_2S-induced neurogenic inflammation [89,90,93]. Hydrogen sulfide (H_2S) is a mediator of diverse biological effects [89]. It also contributes to local and systemic inflammation [94]. Sodium hydrogen sulfide (NaHS) used as a donor of H_2S and induces sensory nerve activation in the guinea pig airways [89]. Capsazepine can abrogate NaHS evoked neuropeptide release through desensitization of TRPV1 [89]. Bhatia et al. noted that capsazepine pretreatment (15 mg/kg) in mice can protect H_2S-inducing lung inflammation [90]. Additionally, they found that H_2S is located upstream of TRPV1 activation, and can regulate the release of sensory neuropeptides in sepsis [93].

4. Conclusions and Future Perspectives

In this article, we have briefly reviewed diverse pharmacological actions of capsazepine *in vitro* and *in vivo*. Capsazepine can exert therapeutic effects against various malignancies and inflammatory disorders. It can suppress proliferation and metastasis, induce apoptosis by modulating several oncogenic signaling pathways, and thereby exert its anti-tumoral effects in different cancers. Moreover, capsazepine can reduce the levels of inflammatory mediators such as DAI, and MPO activity, however, the concentrations at which it can exert these pleiotropic anti-tumoral/anti-inflammatory effects may vary depending on the cell types and *in vivo* model systems used for investigation. Additional studies are required to elucidate the unmet potential of capsazepine in suitable animal models and clinical settings.

Author Contributions: M.H.Y. and S.H.J. conceived the project and wrote the manuscript. G.S. and K.S.A. edited the manuscript.

Funding: This work was supported by a National Research Foundation of Korea (NRF) grant funded by the Korean government (MSIP) (NRF-2018R1D1A1B07042969).

Conflicts of Interest: The authors declare no conflict of interests.

Abbreviations

TRPV1	Transient receptor potential vanilloid type 1
DRG	Dorsal root ganglion
STAT	Signal transducer and activator of transcription
JAK1, JAK2	Janus activated kinase-1, 2
GSH	Glutathione
CIBP	Cancer-induced bone pain
ROS	Reactive oxygen species
CHOP	CCAAT/enhancer-binding protein homologous protein
LPS	Lipopolysaccharide
NF-κB	Nuclear transcription factor-kappa B
OSCC	Oral squamous cell carcinoma
TLR4	Toll-like receptor 4
iNOS	Inducible nitric oxide synthase
TNF-α	Tumor necrosis factor-α
IL-6	Interleukin-6
NO	Nitric oxide
TRPA1	Transient receptor potential ankyrin 1
TNBS	Trinitrobenzene sulfonic acid
MDS	Macroscopic damage score
MPO	Myeloperoxidase
DSS	Dextran sulphate sodium
LTB_4	Leukotriene B_4
PTZ	Pentylentetrazol
CGRP	Calcitonin gene-related peptide

References

1. Bevan, S.; Hothi, S.; Hughes, G.; James, I.F.; Rang, H.P.; Shah, K.; Walpole, C.S.; Yeats, J.C. Capsazepine: A competitive antagonist of the sensory neurone excitant capsaicin. *Br. J. Pharm.* **1992**, *107*, 544–552. [CrossRef]
2. Rollyson, W.D.; Stover, C.A.; Brown, K.C.; Perry, H.E.; Stevenson, C.D.; McNees, C.A.; Ball, J.G.; Valentovic, M.A.; Dasgupta, P. Bioavailability of capsaicin and its implications for drug delivery. *J. Control. Release Off. J. Control. Release Soc.* **2014**, *196*, 96–105. [CrossRef] [PubMed]
3. Hellmich, U.A.; Gaudet, R. Structural biology of TRP channels. *Handb. Exp. Pharm.* **2014**, *223*, 963–990.
4. Huang, J.K.; Cheng, H.H.; Huang, C.J.; Kuo, C.C.; Chen, W.C.; Liu, S.I.; Hsu, S.S.; Chang, H.T.; Lu, Y.C.; Tseng, L.L.; et al. Effect of capsazepine on cytosolic $Ca^{(2+)}$ levels and proliferation of human prostate cancer cells. *Toxicol. In Vitro* **2006**, *20*, 567–574. [CrossRef]
5. Sung, B.; Prasad, S.; Ravindran, J.; Yadav, V.R.; Aggarwal, B.B. Capsazepine, a TRPV1 antagonist, sensitizes colorectal cancer cells to apoptosis by TRAIL through ROS-JNK-CHOP-mediated upregulation of death receptors. *Free Radic Biol. Med.* **2012**, *53*, 1977–1987. [CrossRef] [PubMed]
6. Chen, C.Y.; Li, W.; Qu, K.P.; Chen, C.R. Piperine exerts anti-seizure effects via the TRPV1 receptor in mice. *Eur. J. Pharm.* **2013**, *714*, 288–294. [CrossRef]
7. Docherty, R.J.; Yeats, J.C.; Piper, A.S. Capsazepine block of voltage-activated calcium channels in adult rat dorsal root ganglion neurones in culture. *Br. J. Pharmacol.* **1997**, *121*, 1461–1467. [CrossRef] [PubMed]
8. Liu, L.; Simon, S.A. Capsazepine, a vanilloid receptor antagonist, inhibits nicotinic acetylcholine receptors in rat trigeminal ganglia. *Neurosci. Lett.* **1997**, *228*, 29–32. [CrossRef]
9. Zuo, G.F.; Li, M.H.; Zhang, J.X.; Li, B.; Wang, Z.M.; Wang, Q.; Xiao, H.; Chen, S.L. Capsazepine concentration dependently inhibits currents in HEK 293 cells mediated by human hyperpolarization-activated cyclic nucleotide-gated 2 and 4 channels. *Exp. Biol. Med.* **2013**, *238*, 1055–1061. [CrossRef]
10. Deorukhkar, A.; Krishnan, S.; Sethi, G.; Aggarwal, B.B. Back to basics: How natural products can provide the basis for new therapeutics. *Expert Opin. Investig. Drugs* **2007**, *16*, 1753–1773. [CrossRef]
11. Yang, S.F.; Weng, C.J.; Sethi, G.; Hu, D.N. Natural bioactives and phytochemicals serve in cancer treatment and prevention. *Evid Based Complement. Altern. Med.* **2013**, *2013*, 698190. [CrossRef]

12. Tang, C.H.; Sethi, G.; Kuo, P.L. Novel medicines and strategies in cancer treatment and prevention. *Biomed. Res. Int.* **2014**, *2014*, 474078. [CrossRef]
13. Hsieh, Y.S.; Yang, S.F.; Sethi, G.; Hu, D.N. Natural bioactives in cancer treatment and prevention. *Biomed. Res. Int.* **2015**, *2015*, 182835. [CrossRef]
14. Yarla, N.S.; Bishayee, A.; Sethi, G.; Reddanna, P.; Kalle, A.M.; Dhananjaya, B.L.; Dowluru, K.S.; Chintala, R.; Duddukuri, G.R. Targeting arachidonic acid pathway by natural products for cancer prevention and therapy. *Semin. Cancer Biol.* **2016**, *40–41*, 48–81. [CrossRef]
15. Hasanpourghadi, M.; Looi, C.Y.; Pandurangan, A.K.; Sethi, G.; Wong, W.F.; Mustafa, M.R. Phytometabolites Targeting the Warburg Effect in Cancer Cells: A Mechanistic Review. *Curr. Drug Targets* **2017**, *18*, 1086–1094. [CrossRef]
16. Shanmugam, M.K.; Warrier, S.; Kumar, A.P.; Sethi, G.; Arfuso, F. Potential Role of Natural Compounds as Anti-Angiogenic Agents in Cancer. *Curr. Vasc. Pharm.* **2017**, *15*, 503–519. [CrossRef]
17. Shanmugam, M.K.; Kannaiyan, R.; Sethi, G. Targeting cell signaling and apoptotic pathways by dietary agents: Role in the prevention and treatment of cancer. *Nutr. Cancer* **2011**, *63*, 161–173. [CrossRef]
18. Aggarwal, B.B.; Sethi, G.; Baladandayuthapani, V.; Krishnan, S.; Shishodia, S. Targeting cell signaling pathways for drug discovery: An old lock needs a new key. *J. Cell Biochem.* **2007**, *102*, 580–592. [CrossRef]
19. Shanmugam, M.K.; Nguyen, A.H.; Kumar, A.P.; Tan, B.K.; Sethi, G. Targeted inhibition of tumor proliferation, survival, and metastasis by pentacyclic triterpenoids: Potential role in prevention and therapy of cancer. *Cancer Lett.* **2012**, *320*, 158–170. [CrossRef]
20. Shanmugam, M.K.; Lee, J.H.; Chai, E.Z.; Kanchi, M.M.; Kar, S.; Arfuso, F.; Dharmarajan, A.; Kumar, A.P.; Ramar, P.S.; Looi, C.Y.; et al. Cancer prevention and therapy through the modulation of transcription factors by bioactive natural compounds. *Semin. Cancer Biol.* **2016**, *40–41*, 35–47. [CrossRef]
21. Bishayee, A.; Sethi, G. Bioactive natural products in cancer prevention and therapy: Progress and promise. *Semin. Cancer Biol.* **2016**, *40–41*, 1–3. [CrossRef] [PubMed]
22. Tewari, D.; Nabavi, S.F.; Nabavi, S.M.; Sureda, A.; Farooqi, A.A.; Atanasov, A.G.; Vacca, R.A.; Sethi, G.; Bishayee, A. Targeting activator protein 1 signaling pathway by bioactive natural agents: Possible therapeutic strategy for cancer prevention and intervention. *Pharm. Res.* **2018**, *128*, 366–375. [CrossRef] [PubMed]
23. Ko, J.H.; Sethi, G.; Um, J.Y.; Shanmugam, M.K.; Arfuso, F.; Kumar, A.P.; Bishayee, A.; Ahn, K.S. The Role of Resveratrol in Cancer Therapy. *Int. J. Mol. Sci.* **2017**, *18*, 2589. [CrossRef] [PubMed]
24. Jung, Y.Y.; Hwang, S.T.; Sethi, G.; Fan, L.; Arfuso, F.; Ahn, K.S. Potential Anti-Inflammatory and Anti-Cancer Properties of Farnesol. *Molecules* **2018**, *23*, 2827. [CrossRef] [PubMed]
25. Merarchi, M.; Sethi, G.; Fan, L.; Mishra, S.; Arfuso, F.; Ahn, K.S. Molecular Targets Modulated by Fangchinoline in Tumor Cells and Preclinical Models. *Molecules* **2018**, *23*, 2538. [CrossRef]
26. Sethi, G.; Shanmugam, M.K.; Warrier, S.; Merarchi, M.; Arfuso, F.; Kumar, A.P.; Bishayee, A. Pro-Apoptotic and Anti-Cancer Properties of Diosgenin: A Comprehensive and Critical Review. *Nutrients* **2018**, *10*, 645. [CrossRef]
27. Lee, J.H.; Kim, C.; Baek, S.H.; Ko, J.H.; Lee, S.G.; Yang, W.M.; Um, J.Y.; Sethi, G.; Ahn, K.S. Capsazepine inhibits JAK/STAT3 signaling, tumor growth, and cell survival in prostate cancer. *Oncotarget* **2017**, *8*, 17700–17711. [CrossRef]
28. Fazzari, J.; Balenko, M.D.; Zacal, N.; Singh, G. Identification of capsazepine as a novel inhibitor of system xc(−) and cancer-induced bone pain. *J. Pain Res.* **2017**, *10*, 915–925. [CrossRef]
29. Gonzales, C.B.; Kirma, N.B.; De La Chapa, J.J.; Chen, R.; Henry, M.A.; Luo, S.; Hargreaves, K.M. Vanilloids induce oral cancer apoptosis independent of TRPV1. *Oral Oncol.* **2014**, *50*, 437–447. [CrossRef]
30. Teng, H.P.; Huang, C.J.; Yeh, J.H.; Hsu, S.S.; Lo, Y.K.; Cheng, J.S.; Cheng, H.H.; Chen, J.S.; Jiann, B.P.; Chang, H.T.; et al. Capsazepine elevates intracellular Ca2+ in human osteosarcoma cells, questioning its selectivity as a vanilloid receptor antagonist. *Life Sci.* **2004**, *75*, 2515–2526. [CrossRef]
31. Chai, E.Z.; Shanmugam, M.K.; Arfuso, F.; Dharmarajan, A.; Wang, C.; Kumar, A.P.; Samy, R.P.; Lim, L.H.; Wang, L.; Goh, B.C.; et al. Targeting transcription factor STAT3 for cancer prevention and therapy. *Pharm. Ther.* **2016**, *162*, 86–97. [CrossRef]
32. Arora, L.; Kumar, A.P.; Arfuso, F.; Chng, W.J.; Sethi, G. The Role of Signal Transducer and Activator of Transcription 3 (STAT3) and Its Targeted Inhibition in Hematological Malignancies. *Cancers* **2018**, *10*, 327. [CrossRef]

33. Lee, J.H.; Kim, C.; Lee, S.G.; Sethi, G.; Ahn, K.S. Ophiopogonin D, a Steroidal Glycoside Abrogates STAT3 Signaling Cascade and Exhibits Anti-Cancer Activity by Causing GSH/GSSG Imbalance in Lung Carcinoma. *Cancers* **2018**, *10*, 427. [CrossRef]
34. Wong, A.L.A.; Hirpara, J.L.; Pervaiz, S.; Eu, J.Q.; Sethi, G.; Goh, B.C. Do STAT3 inhibitors have potential in the future for cancer therapy? *Expert Opin. Investig. Drugs* **2017**, *26*, 883–887. [CrossRef]
35. Zhang, J.; Ahn, K.S.; Kim, C.; Shanmugam, M.K.; Siveen, K.S.; Arfuso, F.; Samym, R.P.; Deivasigamanim, A.; Lim, L.H.; Wang, L.; et al. Nimbolide-Induced Oxidative Stress Abrogates STAT3 Signaling Cascade and Inhibits Tumor Growth in Transgenic Adenocarcinoma of Mouse Prostate Model. *Antioxid. Redox Signal.* **2016**, *24*, 575–589. [CrossRef]
36. Subramaniam, A.; Shanmugam, M.K.; Ong, T.H.; Li, F.; Perumal, E.; Chen, L.; Vali, S.; Abbasi, T.; Kapoor, S.; Ahn, K.S.; et al. Emodin inhibits growth and induces apoptosis in an orthotopic hepatocellular carcinoma model by blocking activation of STAT3. *Br. J. Pharm.* **2013**, *170*, 807–821. [CrossRef]
37. Subramaniam, A.; Shanmugam, M.K.; Perumal, E.; Li, F.; Nachiyappan, A.; Dai, X.; Swamy, S.N.; Ahn, K.S.; Kumar, A.P.; Tan, B.K.; et al. Potential role of signal transducer and activator of transcription (STAT)3 signaling pathway in inflammation, survival, proliferation and invasion of hepatocellular carcinoma. *Biochim. Biophys. Acta* **2013**, *1835*, 46–60. [CrossRef]
38. Kim, C.; Lee, S.G.; Yang, W.M.; Arfuso, F.; Um, J.Y.; Kumar, A.P.; Bian, J.; Sethi, G.; Ahn, K.S. Formononetin-induced oxidative stress abrogates the activation of STAT3/5 signaling axis and suppresses the tumor growth in multiple myeloma preclinical model. *Cancer Lett.* **2018**, *431*, 123–141. [CrossRef]
39. Jung, Y.Y.; Lee, J.H.; Nam, D.; Narula, A.S.; Namjoshi, O.A.; Blough, B.E.; Um, J.Y.; Sethi, G.; Ahn, K.S. Anti-myeloma Effects of Icariin Are Mediated Through the Attenuation of JAK/STAT3-Dependent Signaling Cascade. *Front. Pharmacol.* **2018**, *9*, 531. [CrossRef]
40. Siveen, K.S.; Sikka, S.; Surana, R.; Dai, X.; Zhang, J.; Kumar, A.P.; Tan, B.K.; Sethi, G.; Bishayee, A. Targeting the STAT3 signaling pathway in cancer: Role of synthetic and natural inhibitors. *Biochim. Biophys. Acta* **2014**, *1845*, 136–154. [CrossRef]
41. Prasad, S.; Kim, J.H.; Gupta, S.C.; Aggarwal, B.B. Targeting death receptors for TRAIL by agents designed by Mother Nature. *Trends Pharmacol. Sci.* **2014**, *35*, 520–536. [CrossRef] [PubMed]
42. Dai, X.; Zhang, J.; Arfuso, F.; Chinnathambi, A.; Zayed, M.E.; Alharbi, S.A.; Kumar, A.P.; Ahn, K.S.; Sethi, G. Targeting TNF-related apoptosis-inducing ligand (TRAIL) receptor by natural products as a potential therapeutic approach for cancer therapy. *Exp. Biol. Med.* **2015**, *240*, 760–773. [CrossRef] [PubMed]
43. Subramaniam, A.; Loo, S.Y.; Rajendran, P.; Manu, K.A.; Perumal, E.; Li, F.; Shanmugam, M.K.; Siveen, K.S.; Park, J.I.; Ahn, K.S.; et al. An anthraquinone derivative, emodin sensitizes hepatocellular carcinoma cells to TRAIL induced apoptosis through the induction of death receptors and downregulation of cell survival proteins. *Apoptosis Int. J. Program. Cell Death* **2013**, *18*, 1175–1187. [CrossRef] [PubMed]
44. Kamat, A.M.; Sethi, G.; Aggarwal, B.B. Curcumin potentiates the apoptotic effects of chemotherapeutic agents and cytokines through down-regulation of nuclear factor-kappaB and nuclear factor-kappaB-regulated gene products in IFN-alpha-sensitive and IFN-alpha-resistant human bladder cancer cells. *Mol. Cancer Ther.* **2007**, *6*, 1022–1030. [CrossRef] [PubMed]
45. Yamaguchi, H.; Wang, H.G. CHOP is involved in endoplasmic reticulum stress-induced apoptosis by enhancing DR5 expression in human carcinoma cells. *J. Biol. Chem.* **2004**, *279*, 45495–45502. [CrossRef] [PubMed]
46. Yoshida, T.; Shiraishi, T.; Nakata, S.; Horinaka, M.; Wakada, M.; Mizutani, Y.; Miki, T.; Sakai, T. Proteasome inhibitor MG132 induces death receptor 5 through CCAAT/enhancer-binding protein homologous protein. *Cancer Res.* **2005**, *65*, 5662–5667. [CrossRef]
47. Dai, X.; Wang, L.; Deivasigamni, A.; Looi, C.Y.; Karthikeyan, C.; Trivedi, P.; Chinnathambi, A.; Alharbi, S.A.; Arfuso, F.; Dharmarajan, A.; et al. A novel benzimidazole derivative, MBIC inhibits tumor growth and promotes apoptosis via activation of ROS-dependent JNK signaling pathway in hepatocellular carcinoma. *Oncotarget* **2017**, *8*, 12831–12842. [CrossRef]
48. Prasad, S.; Gupta, S.C.; Tyagi, A.K. Reactive oxygen species (ROS) and cancer: Role of antioxidative nutraceuticals. *Cancer Lett.* **2017**, *387*, 95–105. [CrossRef]
49. Kim, S.M.; Kim, C.; Bae, H.; Lee, J.H.; Baek, S.H.; Nam, D.; Chung, W.S.; Shim, B.S.; Lee, S.G.; Kim, S.H.; et al. 6-Shogaol exerts anti-proliferative and pro-apoptotic effects through the modulation of STAT3 and MAPKs signaling pathways. *Mol. Carcinog.* **2015**, *54*, 1132–1146. [CrossRef]

50. Woo, C.C.; Hsu, A.; Kumar, A.P.; Sethi, G.; Tan, K.H. Thymoquinone inhibits tumor growth and induces apoptosis in a breast cancer xenograft mouse model: The role of p38 MAPK and ROS. *PLoS ONE* **2013**, *8*, e75356. [CrossRef]
51. Gupta, S.C.; Hevia, D.; Patchva, S.; Park, B.; Koh, W.; Aggarwal, B.B. Upsides and downsides of reactive oxygen species for cancer: The roles of reactive oxygen species in tumorigenesis, prevention, and therapy. *Antioxid. Redox Signal.* **2012**, *16*, 1295–1322. [CrossRef]
52. Park, K.R.; Nam, D.; Yun, H.M.; Lee, S.G.; Jang, H.J.; Sethi, G.; Cho, S.K.; Ahn, K.S. beta-Caryophyllene oxide inhibits growth and induces apoptosis through the suppression of PI3K/AKT/mTOR/S6K1 pathways and ROS-mediated MAPKs activation. *Cancer Lett.* **2011**, *312*, 178–188. [CrossRef] [PubMed]
53. de Sa Junior, P.L.; Camara, D.A.D.; Porcacchia, A.S.; Fonseca, P.M.M.; Jorge, S.D.; Araldi, R.P.; Ferreira, A.K. The Roles of ROS in Cancer Heterogeneity and Therapy. *Oxid. Med. Cell. Longev.* **2017**, *2017*, 2467940. [CrossRef]
54. Sanchez, A.M.; Sanchez, M.G.; Malagarie-Cazenave, S.; Olea, N.; Diaz-Laviada, I. Induction of apoptosis in prostate tumor PC-3 cells and inhibition of xenograft prostate tumor growth by the vanilloid capsaicin. *Apoptosis Int. J. Program. Cell Death* **2006**, *11*, 89–99. [CrossRef] [PubMed]
55. Ziglioli, F.; Frattini, A.; Maestroni, U.; Dinale, F.; Ciufifeda, M.; Cortellini, P. Vanilloid-mediated apoptosis in prostate cancer cells through a TRPV-1 dependent and a TRPV-1-independent mechanism. *Acta Bio-Med. Atenei Parm.* **2009**, *80*, 13–20.
56. Li, F.; Zhang, J.; Arfuso, F.; Chinnathambi, A.; Zayed, M.E.; Alharbi, S.A.; Kumar, A.P.; Ahn, K.S.; Sethi, G. NF-kappaB in cancer therapy. *Arch. Toxicol.* **2015**, *89*, 711–731. [CrossRef] [PubMed]
57. Manu, K.A.; Shanmugam, M.K.; Ramachandran, L.; Li, F.; Fong, C.W.; Kumar, A.P.; Tan, P.; Sethi, G. First evidence that gamma-tocotrienol inhibits the growth of human gastric cancer and chemosensitizes it to capecitabine in a xenograft mouse model through the modulation of NF-kappaB pathway. *Clin. Cancer Res. Off. J. Am. Assoc. Cancer Res.* **2012**, *18*, 2220–2229. [CrossRef] [PubMed]
58. Sethi, G.; Shanmugam, M.K.; Ramachandran, L.; Kumar, A.P.; Tergaonkar, V. Multifaceted link between cancer and inflammation. *Biosci. Rep.* **2012**, *32*, 1–15. [CrossRef] [PubMed]
59. Li, F.; Sethi, G. Targeting transcription factor NF-kappaB to overcome chemoresistance and radioresistance in cancer therapy. *Biochim. Biophys. Acta* **2010**, *1805*, 167–180.
60. Sethi, G.; Tergaonkar, V. Potential pharmacological control of the NF-kappaB pathway. *Trends Pharmacol. Sci.* **2009**, *30*, 313–321. [CrossRef]
61. Ahn, K.S.; Sethi, G.; Aggarwal, B.B. Nuclear factor-kappa B: From clone to clinic. *Curr. Mol. Med.* **2007**, *7*, 619–637. [CrossRef] [PubMed]
62. Liu, L.; Ahn, K.S.; Shanmugam, M.K.; Wang, H.; Shen, H.; Arfuso, F.; Chinnathambi, A.; Alharbi, S.A.; Chang, Y.; Sethi, G.; et al. Oleuropein induces apoptosis via abrogating NF-kappaB activation cascade in estrogen receptor-negative breast cancer cells. *J. Cell. Biochem.* **2018**. [CrossRef]
63. Puar, Y.R.; Shanmugam, M.K.; Fan, L.; Arfuso, F.; Sethi, G.; Tergaonkar, V. Evidence for the Involvement of the Master Transcription Factor NF-kappaB in Cancer Initiation and Progression. *Biomedicines* **2018**, *6*, 82. [CrossRef] [PubMed]
64. Chai, E.Z.; Siveen, K.S.; Shanmugam, M.K.; Arfuso, F.; Sethi, G. Analysis of the intricate relationship between chronic inflammation and cancer. *Biochem. J.* **2015**, *468*, 1–15. [CrossRef] [PubMed]
65. Shanmugam, M.K.; Ahn, K.S.; Lee, J.H.; Kannaiyan, R.; Mustafa, N.; Manu, K.A.; Siveen, K.S.; Sethi, G.; Chng, W.J.; Kumar, A.P. Celastrol Attenuates the Invasion and Migration and Augments the Anticancer Effects of Bortezomib in a Xenograft Mouse Model of Multiple Myeloma. *Front. Pharmacol.* **2018**, *9*, 365. [CrossRef] [PubMed]
66. Manu, K.A.; Shanmugam, M.K.; Ramachandran, L.; Li, F.; Siveen, K.S.; Chinnathambi, A.; Zayed, M.E.; Alharbi, S.A.; Arfuso, F.; Kumar, A.P.; et al. Isorhamnetin augments the anti-tumor effect of capeciatbine through the negative regulation of NF-kappaB signaling cascade in gastric cancer. *Cancer Lett.* **2015**, *363*, 28–36. [CrossRef]
67. Li, F.; Shanmugam, M.K.; Siveen, K.S.; Wang, F.; Ong, T.H.; Loo, S.Y.; Swamy, M.M.; Mandal, S.; Kumar, A.P.; Goh, B.C.; et al. Garcinol sensitizes human head and neck carcinoma to cisplatin in a xenograft mouse model despite downregulation of proliferative biomarkers. *Oncotarget* **2015**, *6*, 5147–5163. [CrossRef]

68. Han, S.; Lee, J.H.; Kim, C.; Nam, D.; Chung, W.S.; Lee, S.G.; Ahn, K.S.; Cho, S.K.; Cho, M.; Ahn, K.S. Capillarisin inhibits iNOS, COX-2 expression, and proinflammatory cytokines in LPS-induced RAW 264.7 macrophages via the suppression of ERK, JNK, and NF-kappaB activation. *Immunopharmacol. Immunotoxicol.* **2013**, *35*, 34–42. [CrossRef]
69. Kasckow, J.W.; Mulchahey, J.J.; Geracioti, T.D., Jr. Effects of the vanilloid agonist olvanil and antagonist capsazepine on rat behaviors. *Prog. Neuropsychopharmacol. Biol. Psychiatry* **2004**, *28*, 291–295. [CrossRef]
70. Oh, G.S.; Pae, H.O.; Seo, W.G.; Kim, N.Y.; Pyun, K.H.; Kim, I.K.; Shin, M.; Chung, H.T. Capsazepine, a vanilloid receptor antagonist, inhibits the expression of inducible nitric oxide synthase gene in lipopolysaccharide-stimulated RAW264.7 macrophages through the inactivation of nuclear transcription factor-kappa B. *Int. Immunopharmacol.* **2001**, *1*, 777–784. [CrossRef]
71. Phillips, E.; Reeve, A.; Bevan, S.; McIntyre, P. Identification of species-specific determinants of the action of the antagonist capsazepine and the agonist PPAHV on TRPV1. *J. Biol. Chem.* **2004**, *279*, 17165–17172. [CrossRef] [PubMed]
72. Walker, K.M.; Urban, L.; Medhurst, S.J.; Patel, S.; Panesar, M.; Fox, A.J.; McIntyre, P. The VR1 antagonist capsazepine reverses mechanical hyperalgesia in models of inflammatory and neuropathic pain. *J. Pharmacol. Exp. Ther.* **2003**, *304*, 56–62. [CrossRef] [PubMed]
73. Kistner, K.; Siklosi, N.; Babes, A.; Khalil, M.; Selescu, T.; Zimmermann, K.; Wirtz, S.; Becker, C.; Neurath, M.F.; Reeh, P.W.; et al. Systemic desensitization through TRPA1 channels by capsazepine and mustard oil—A novel strategy against inflammation and pain. *Sci. Rep.* **2016**, *6*, 28621. [CrossRef]
74. Fujino, K.; Takami, Y.; de la Fuente, S.G.; Ludwig, K.A.; Mantyh, C.R. Inhibition of the vanilloid receptor subtype-1 attenuates TNBS-colitis. *J. Gastrointest. Surg.* **2004**, *8*, 842–847; discussion 847–848. [CrossRef] [PubMed]
75. Kihara, N.; de la Fuente, S.G.; Fujino, K.; Takahashi, T.; Pappas, T.N.; Mantyh, C.R. Vanilloid receptor-1 containing primary sensory neurones mediate dextran sulphate sodium induced colitis in rats. *Gut* **2003**, *52*, 713–719. [CrossRef] [PubMed]
76. Vigna, S.R.; Shahid, R.A.; Nathan, J.D.; McVey, D.C.; Liddle, R.A. Leukotriene B4 mediates inflammation via TRPV1 in duct obstruction-induced pancreatitis in rats. *Pancreas* **2011**, *40*, 708–714. [CrossRef]
77. White, N.J.; Pukrittayakamee, S.; Hien, T.T.; Faiz, M.A.; Mokuolu, O.A.; Dondorp, A.M. Malaria. *Lancet* **2014**, *383*, 723–735. [CrossRef]
78. Cho, S.J.; Vaca, M.A.; Miranda, C.J.; N'Gouemo, P. Inhibition of transient potential receptor vanilloid type 1 suppresses seizure susceptibility in the genetically epilepsy-prone rat. *CNS Neurosci. Ther.* **2018**, *24*, 18–28. [CrossRef]
79. Nguyen, T.L.; Nam, Y.S.; Lee, S.Y.; Kim, H.C.; Jang, C.G. Effects of capsazepine, a transient receptor potential vanilloid type 1 antagonist, on morphine-induced antinociception, tolerance, and dependence in mice. *Br. J. Anaesth.* **2010**, *105*, 668–674. [CrossRef]
80. Gonzalez-Reyes, L.E.; Ladas, T.P.; Chiang, C.C.; Durand, D.M. TRPV1 antagonist capsazepine suppresses 4-AP-induced epileptiform activity in vitro and electrographic seizures in vivo. *Exp. Neurol.* **2013**, *250*, 321–332. [CrossRef]
81. Wick, E.C.; Hoge, S.G.; Grahn, S.W.; Kim, E.; Divino, L.A.; Grady, E.F.; Bunnett, N.W.; Kirkwood, K.S. Transient receptor potential vanilloid 1, calcitonin gene-related peptide, and substance P mediate nociception in acute pancreatitis. *Am. J. Physiol. Gastrointest. Liver Physiol.* **2006**, *290*, G959–G969. [CrossRef]
82. Fernandes, E.S.; Brito, C.X.; Teixeira, S.A.; Barboza, R.; dos Reis, A.S.; Azevedo-Santos, A.P.; Muscara, M.; Costa, S.K.; Marinho, C.R.; Brain, S.D.; et al. TRPV1 antagonism by capsazepine modulates innate immune response in mice infected with Plasmodium berghei ANKA. *Mediat. Inflamm.* **2014**, *2014*, 506450. [CrossRef]
83. Ghazizadeh, V.; Naziroglu, M. Electromagnetic radiation (Wi-Fi) and epilepsy induce calcium entry and apoptosis through activation of TRPV1 channel in hippocampus and dorsal root ganglion of rats. *Metab. Brain Dis.* **2014**, *29*, 787–799. [CrossRef]
84. Naziroglu, M.; Ozkan, F.F.; Hapil, S.R.; Ghazizadeh, V.; Cig, B. Epilepsy but not mobile phone frequency (900 MHz) induces apoptosis and calcium entry in hippocampus of epileptic rat: Involvement of TRPV1 channels. *J. Membr. Biol.* **2015**, *248*, 83–91. [CrossRef]
85. Shirazi, M.; Izadi, M.; Amin, M.; Rezvani, M.E.; Roohbakhsh, A.; Shamsizadeh, A. Involvement of central TRPV1 receptors in pentylenetetrazole and amygdala-induced kindling in male rats. *Neurol. Sci.* **2014**, *35*, 1235–1241. [CrossRef]

86. Manna, S.S.; Umathe, S.N. A possible participation of transient receptor potential vanilloid type 1 channels in the antidepressant effect of fluoxetine. *Eur. J. Pharm.* **2012**, *685*, 81–90. [CrossRef]
87. Naziroglu, M.; Ovey, I.S. Involvement of apoptosis and calcium accumulation through TRPV1 channels in neurobiology of epilepsy. *Neuroscience* **2015**, *293*, 55–66. [CrossRef]
88. Santos, C.J.; Stern, C.A.; Bertoglio, L.J. Attenuation of anxiety-related behaviour after the antagonism of transient receptor potential vanilloid type 1 channels in the rat ventral hippocampus. *Behav. Pharm.* **2008**, *19*, 357–360. [CrossRef]
89. Trevisani, M.; Patacchini, R.; Nicoletti, P.; Gatti, R.; Gazzieri, D.; Lissi, N.; Zagli, G.; Creminon, C.; Geppetti, P.; Harrison, S. Hydrogen sulfide causes vanilloid receptor 1-mediated neurogenic inflammation in the airways. *Br. J. Pharmacol.* **2005**, *145*, 1123–1131. [CrossRef]
90. Bhatia, M.; Zhi, L.; Zhang, H.; Ng, S.W.; Moore, P.K. Role of substance P in hydrogen sulfide-induced pulmonary inflammation in mice. *Am. J. Physiol. Lung Cell. Mol. Physiol.* **2006**, *291*, L896–L904. [CrossRef]
91. Lin, Q.; Li, D.; Xu, X.; Zou, X.; Fang, L. Roles of TRPV1 and neuropeptidergic receptors in dorsal root reflex-mediated neurogenic inflammation induced by intradermal injection of capsaicin. *Mol. Pain* **2007**, *3*, 30. [CrossRef] [PubMed]
92. Flores, C.M.; Leong, A.S.; Dussor, G.O.; Harding-Rose, C.; Hargreaves, K.M.; Kilo, S. Capsaicin-evoked CGRP release from rat buccal mucosa: Development of a model system for studying trigeminal mechanisms of neurogenic inflammation. *Eur. J. Neurosci.* **2001**, *14*, 1113–1120. [CrossRef] [PubMed]
93. Ang, S.F.; Moochhala, S.M.; Bhatia, M. Hydrogen sulfide promotes transient receptor potential vanilloid 1-mediated neurogenic inflammation in polymicrobial sepsis. *Crit. Care Med.* **2010**, *38*, 619–628. [CrossRef]
94. Ang, S.F.; Moochhala, S.M.; MacAry, P.A.; Bhatia, M. Hydrogen sulfide and neurogenic inflammation in polymicrobial sepsis: Involvement of substance P and ERK-NF-kappaB signaling. *PLoS ONE* **2011**, *6*, e24535. [CrossRef] [PubMed]

molecules

MDPI

Review

Dietary Phytochemicals Targeting Cancer Stem Cells

Alena Liskova [1], Peter Kubatka [2,*], Marek Samec [1], Pavol Zubor [1], Milos Mlyncek [3], Tibor Bielik [1], Samson Mathews Samuel [4], Anthony Zulli [5], Taeg Kyu Kwon [6] and Dietrich Büsselberg [4,*]

1 Clinic of Obstetrics and Gynecology, Jessenius Faculty of Medicine, Comenius University in Bratislava, Martin, 03601 Bratislava, Slovakia; alenka.liskova@gmail.com (A.L.); marek.samec@gmail.com (M.S.); Pavol.Zubor@jfmed.uniba.sk (P.Z.); tbielik57@gmail.com (T.B.)

2 Department of Medical Biology, Jessenius Faculty of Medicine, Comenius University in Bratislava, Martin, 03601 Bratislava, Slovakia

3 Department of Obstetrics and Gynecology Faculty Hospital Nitra Constantine the Philosopher University, 949 01 Nitra, Slovakia; mlyncekmilos@hotmail.com

4 Department of Physiology and Biophysics, Weill Cornell Medicine-Qatar, Education City, Qatar Foundation, P.O. Box 24144, Doha 24144, Qatar; sms2016@qatar-med.cornell.edu

5 Institute for Health and Sport, Victoria University, Melbourne, VIC 3011, Australia; Anthony.Zulli@vu.edu.au

6 Department of Immunology and School of Medicine, Keimyung University, Dalseo-Gu, 426 01 Daegu, Korea; kwontk@dsmc.or.kr

* Correspondence: kubatka@jfmed.uniba.sk (P.K.); dib2015@qatar-med.cornell.edu (D.B.)

Received: 8 February 2019; Accepted: 28 February 2019; Published: 4 March 2019

Abstract: There is an increasing awareness of the importance of a diet rich in fruits and vegetables for human health. Cancer stem cells (CSCs) are characterized as a subpopulation of cancer cells with aberrant regulation of self-renewal, proliferation or apoptosis leading to cancer progression, invasiveness, metastasis formation, and therapy resistance. Anticancer effects of phytochemicals are also directed to target CSCs. Here we provide a comprehensive review of dietary phytochemicals targeting CSCs. Moreover, we evaluate and summarize studies dealing with effects of dietary phytochemicals on CSCs of various malignancies in preclinical and clinical research. Dietary phytochemicals have a significant impact on CSCs which may be applied in cancer prevention and treatment. However, anticancer effects of plant derived compounds have not yet been fully investigated in clinical research.

Keywords: cancer stem cells; phytochemicals; plant-derived foods; fruit; vegetable; cell signaling

1. Introduction

Despite progress in anticancer therapy, cancer is a major health problem and one of the leading causes of morbidity worldwide [1,2]. Cancer is characterized by uncontrolled cell growth, invasiveness, and formation of metastasis. Malignant tumours are represented by heterogeneous populations of cancer cells. The heterogeneity may be explained by evolutional accumulation of mutations in one or few cells or by presence of cells with stem-like properties. Cancer stem cells (CSCs) are characterized as a subpopulation of cells with an intrinsic ability of self-renewal and differentiation [3–6]. Dietary phytochemicals are suggested to possess anti-cancer properties with minimal or no side effects [7–9]; moreover, they may also improve the efficacy of chemo- or radiotherapy, and therefore may represent an important strategy to target CSCs [10].

1.1. Aim of the Study

The review focuses on the anticancer effectiveness of dietary phytochemicals, either isolated or as mixtures via targeting CSCs. Firstly, it discusses the basics of CSCs and signaling pathways modulating their stem-like properties. The core of the review is the summary of preclinical and clinical studies evaluating whether dietary phytochemicals target CSCs in various malignancies. Plant-derived dietary compounds which are effective agents against CSCs in preclinical in vitro and in vivo research should be further evaluated in clinical research. We emphasize the need to include dietary phytochemicals in the current clinical research.

1.2. Source of Data

Data were recovered from the biomedical literature published in the English-language literature by use of "cancer stem cells" and "plant-based functional foods" or "phytochemicals" or "fruit" or "vegetables" or "herbs" as either a keyword or medical subject heading (MeSH) term in searches of the PubMed bibliographic database. We emphasize the most recent scientific papers from the years 2013–2019. About 40 studies were selected with the database accessed between December 2018 and February 2019.

2. CSCs (Cancer Stem Cells)

CSCs are multipotent cells exhibiting stem-like properties and possessing the capability of the initiation of tumor growth, invasiveness, and dissemination to distant organs [6,11]. CSCs are like normal stem cells in several ways; however, if the balance of the influence of internal or external factors is not maintained, it may lead to hyperproliferation and metastasis [12]. Moreover, CSCs are resistant to chemical and electromagnetic insults due to their infrequent replication, active drug efflux system, increase in defense against reactive oxygen species and importantly higher ability of DNA repairs which may result in a lower rate of apoptosis [13]. Moreover, autophagy is characterized as a process allowing cells to survive under stress conditions. Accordingly, therapy-resistance and survival of CSCs may be also associated with increase in autophagy activity [14]. CSCs are also characterized by active telomerase expression, increased membrane transport activity [2] and hypoxic niche [12]. The survival of stem cells and CSCs depends on their niche or microenvironment which provides signals regulating their proliferative and self-renewal maintenance [15]. In conclusion, CSCs are related to the development of cancer, metastasis and resistance to conventional anticancer therapies and recurrence or relapse of malignancy. Targeting CSCs is a promising strategy of anti-cancer research [12,16].

2.1. Cancer Stem Cells Markers

CSCs have been recognized in various types of tumors and it is now possible to identify and isolate them using a distinctive profile of surface (e.g. CD24, CD44, CD133, CD49, CXCR4, LGR5) or intracellular markers (e.g. ALDH) [17]. Table 1 lists a brief overview of generally accepted markers associated with CSCs. However, no universal marker for CSCs has been identified [13]. Moreover, their phenotypes exhibit different markers due to the occurrence of epigenetic alterations, possible presence of multiple CSCs pools or technical variations [18]. Importantly, these markers are also present in normal stem cells and other cell types [19]; therefore, a combination of markers is usually required to denote the CSCs population [20]. CSCs markers are also associated with induction of stem-like phenotype of cancer cells via modulation of various molecular pathways (Figure 1). On the contrary, a novel 3D spheroid-based label-retention assay followed by FACS sorting allows the identification and isolation of stem cells at a single cell level which is considered to be a marker-free method of isolation of both normal stem cells and CSCs. Consequently, this method dealing with isolation and characterization of the novel properties of CSCs may be of a great interest in anti-cancer therapeutic strategy [14]. Moreover, the isolation of stem cells can be also helpful in the understanding of the

initiation of carcinogenesis as a result of environmental carcinogens targeting stem cells as was demonstrated by Hu et al. [21] and Prins et al. [22] in in vivo models using prostasphere cells.

Table 1. Markers of CSCs in various tissues.

Cancer type	Marker	References
Brain cancer	$CD34^+/CD38^-/CD133^+/CD44^+$	[6,23]
Breast cancer	$CD44^+/CD24^-/Lineage^-/ALDH1^+/EpCAM^+$	[18,20,23]
Colon cancer	$CD133^+/CD44^+/CD166^+/ALDH1^+/LGR5^+/EpCAM^+$	[6,18,19]
Leukemia	$CD34^+/CD38^-/CD90^-$	[6,18,19]
Liver	$CD133^+/CD90^+/EpCAM^+$	[6]
Lung	$CD133^+/CD44^+/CD90^+$	[2,18]
Ovary	$CD44^+/ALDH1^+/CD133^+$	[6,18]
Pancreas	$CD44^+/CD24^+/CD133^+/EpCAM^+$	[18,23]

Explanatory notes: + presence; $^-$ absence. Abbreviations used: ALDH1-Aldehyde dehydrogenase 1; CD24/34/38/44/90/133/166-Cluster of Differentiation 24/34/38/44/90/133/166; EpCAM-Epithelial Cell Adhesion Molecule.

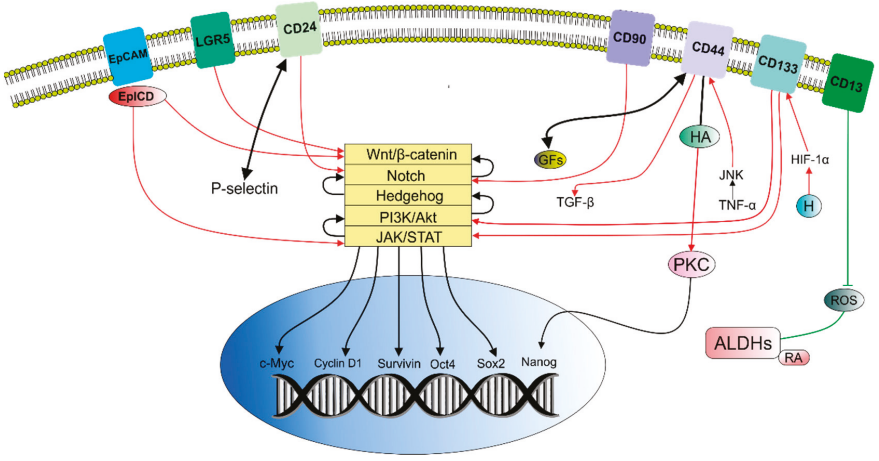

Figure 1. Association between surface markers and promotion of CSCs stem-like properties [3,20,23–41].

Cluster of differentiation 44 (CD44) promotes increase in growth factor beta (TGF-β) leading to Epithelial–mesenchymal transition (EMT). Binding of hyaluronic acid (HA) with CD44 activates Protein kinase C (PKC) which then phosphorylates transcription factor Nanog resulting in upregulation of ATP binding cassette subfamily B member 1 (ABCB1) contributing to multidrug resistance (MDR)). CD44 serves as a coreceptor for growth factors and stimulate CSCs self-renewal. Tumour necrosis factor alfa (TNF-α) upregulates CD44 through Janus kinase (JNK), thus inducing migration, invasion, metastasis or EMT. Cluster of differentiation 24 (CD24) stimulates metastasis formation via interaction with P-selectin and cancer progression and trigger EMT via activation of Notch1signaling. Cluster of differentiation 133 (CD133) is involved in tumour cell proliferation, metastasis, tumorigenesis or therapy resistance—via activation of the phosphatidylinositol-3-kinase (PI3K)/Akt. Hypoxia (H) in stem cells and the tumour microenvironment promote CD133 expansion via upregulation of hypoxia-inducible factor 1-alpha (HIF-1α). Overexpression of CD133 is associated with tumour progression through epidermal growth factor receptor (EGFR)-dependent Akt activation. The role of cluster of differentiation 90 (CD90) in cancer depends on the cancer type and signaling mechanism. For example, cancer stem-like activity is elevated through up-activation of Notch pathway. Increased

expression of cluster of differentiation13 (CD13) reduces reactive oxygen species (ROS) promoting CSCs survival via EMT. Leucine-rich repeat-containing G-protein-coupled 5 (LGR5) promotes proliferation of cancer cells via activation of Wnt/β-catenin pathway. Epithelial cell adhesion molecule (EpCAM) cleavages with its intracellular domain (EpICD) and provide key signals for achieving CSCs properties by modulation of Wnt pathway or LIF/STAT3. Activity of aldehyde dehydrogenase (ALDH) may protect CSCs against cell death caused by ROS. ALDHs metabolizes retinoic acid (RA) thus regulating stem-like properties of CSCs. Aberrantly regulated signaling pathways and cross-talks between them may ultimately influence their target genes such as c-Myc, cyclinD1, Survivin, Nanog, Oct-4, Sox2, etc.

2.2. EMT (Epithelial–Mesenchymal Transition)

EMT is the reversible change occurring usually during embryogenesis in which epithelial cells acquire mesenchymal phenotypes [42]; moreover, EMT is an important process during wound healing and reestablishment of basal and apical polarity [20]. However, EMT is a crucial step in the initiation of tumor metastasis in which cancer cells alter their morphology, loose epithelial cell-cell junctions and obtain migratory properties and metastatic capacity. CSCs are considered to possess enhanced EMT ability, and thus produce metastatic tumors or circulate in the body in a dormant state, until its activation which may occurs years later [2,20]. EMT also supports the resistance of CSCs to therapeutic drugs [6]. The process of EMT is associated with modulation of E-cadherin, N-cadherin, vimentin, C-X-C chemokine receptor type 4 (CXCR4) or cyclooxygenase-2 (COX-2) and also with activation of transcription factors Snail or Twist [20,43]. It is indicated that metastatic cancer cells undergoing EMT may possess a CSCs phenotype [44].

2.3. Molecular or Cellular Signaling of CSCs

Strictly regulated signaling pathways control the activity of stem cells [6]. However, some pathways could be abnormally repressed or activated in human malignancies and these irregularities contribute to the proliferative, differentiation, self-renewal, and survival properties of CSCs via aberrant regulation of target genes, such as c-Myc, cyclin D1, Survivin, Nanog, Oct-4, Sox2 and others. Interestingly, signaling pathways are not linear which means that cross-talk between various pathways occasionally occur and may lead to consequences including promotion of resistance to therapy, CSCs expansion or other fatal consequences [40,41].

2.3.1. Signaling Pathways in CSCs

The evolutionary conserved Notch signaling pathway possesses an important role in the balance of differentiation, cell cycle progression [6], survival, and apoptosis of stem cells. Alterations in this ligand-receptor pathway guide undifferentiated cells toward malignant transformation and acquisition of EMT via increased expression of Notch1, Sox2, Nanog, Oct4 or Lin28; moreover the cross-talks between Notch and other oncogenic signaling pathways also play a crucial role in the development of cancer [41,45]. Notch signaling is considered to be one of the most activated pathways in cancer cells and is an important linkage between angiogenesis and CSCs self-renewal [46].

Wnt signaling pathway is involved in embryonic development and homeostasis of tissues. Evolutionary conserved and highly complex Wnt signaling is considered to encompass two pathways which are not exclusive and cross-talk may occur between them. β-catenin-independent pathway (or noncanonical) with calcium as the major mediator regulates asymmetrical division of cells, cell polarity and migration [40,45]. On the contrary, the transcriptional regulator β-catenin-dependent (canonical) pathway regulates the survival and proliferation of cells [47]. The aberrant activation of Wnt pathway and deregulated expression of Wnt-binding proteins, ligands, inhibitors or other co-regulators is associated with various human malignancies, acquisition of EMT phenotype, self-renewal or cancer cell dedifferentiation into CSCs. Targeting Wnt may be another option of decreasing or eliminating CSCs [41,45].

The Hedgehog (HH) signaling pathway plays a crucial role in the embryonic development, especially the development of skin, hair follicles and sebaceous glands and also in adult brain development [6]. Moreover, HH functions in the regulation of proliferation, maintenance of the stem cells and progenitor cell and self-renewal capacity [48]. There are several Hedgehog homologues which are well studied in mammals including sonic (sHH), desert (dHH), and indian (iHH). Significantly, it is supposed that HH plays an important role in the process of acquiring stem cell-like properties during the EMT [41]. For instance, aberrant activation of sHH/transcription factor GLI1 signaling may lead to changes in expression of GLI1-regulated oncoproteins like N-myc, CyclinD1, Foxm1, and Bcl-2 playing a crucial role in CSCs self-renewal [49].

The phosphatidylinositol-3-kinase (PI3K)/Akt and the mammalian target of rapamycin (mTOR) is a signaling pathway playing crucial role in metabolism, proliferation, angiogenesis, differentiation, and survival of cells [48]. It is abnormally regulated in cancer cells due to mutation, deletion, methylation, amplification or post-translational modifications and is important for regulation of apoptosis, radioresistance, metastasis, and maintenance of CSCs populations. Phosphatase and tensin homolog (PTEN) is suggested to be a negative regulator of PI3K/Akt/mTOR pathway and also to function as a tumour suppressor [50]. Components of PI3K pathway are considered to be the most activated and mutated in human cancers, thus it is important to consider its targeting in cancer treatment [51].

The Janus kinase (JAK) and signal transducer and activator of transcription (STAT) signaling pathway possess and important role in cytokines and growth factor signaling affecting cell growth, proliferation and immune response. Aberrant regulation of the JAK/STAT pathway is associated and implied with maintenance of germ-line stem cell populations in various cancers [48]. Moreover, interleukin-8 (IL-8) is suggested to trigger the activation of STAT3 which may lead to inflammation, ROS production and multidrug resistance (MDR) [52]. More detailed overview of aberrantly regulated CSCs signaling pathways attributed to various malignancies is shown in Table 2. Importantly, this table is adjusted to several concrete cancer types, and thus other abnormally regulated pathways or signaling molecules, which are not mentioned, may be also responsible for the CSCs-phenotype of other malignancies.

Table 2. Cancer stem cells signaling pathways aberrantly regulated in selected malignancies.

Signaling Pathway	Cancer type	Mechanism of action	References
Notch	Brain cancer	↑Notch1 ↑JAG1 ↑DLL1	[6,40,44]
	T cell acute lymphoblastic leukemia	↑ Notch1	
	Breast cancer	↑Notch1 ↑JAG1,	
	Pancreatic cancer	↑Notch1 ↑Notch3 ↑Jag1 ↑Jag2 ↑Hes1	
	Non-Small Lung Cancer	↑ Notch3	
Wnt/β-catenin	Breast cancer	↑LEF-1 ↑TCF-4 ↑cyclin D1 ↑β-catenin ↓SFRP	[6,40,41,47]
	Colorectal carcinoma Brain tumor Prostate cancer	Mutations in APC/β-catenin site	
	Hematologic cancer Skin cancer Lung cancer	↓ WIF-1 ↓SFRP-1 ↓ DKK ↓AXIN2	

Table 2. *Cont.*

Signaling Pathway	Cancer type	Mechanism of action	References
Hedgehog	Colon cancer	↑sHH ↑GLI2	[6,40]
	Medulloblastoma predisposition	Mutations in PTCH1	
	Myeloma	↑SMO ↑GLI1	
	Glioma	↑GLI1 ↑SHH ↑PTCH1	
PI3K/Akt/mTOR	Gastric cancer	↑Akt1	[19]
	Ovarian cancer Pancreatic cancer	↑Akt2	
	T cell acute lymphoblastic leukemia Melanoma Endometrial carcinoma Prostate cancer Glioblastoma	Mutations in PTEN	
JAK/STAT	Breast cancer Gastric cancer Glioblastoma	↑STAT3	[40,53,54]

Explanatory notes: ↓decrease; ↑increase.

Abberant regulation of Notch signaling may be modulated via abnormal expression of Notch ligands including Delta-like (DLL1/3/4) and JAGGED (JAG1/2), Notch receptors (Notch1–4) or Notch target genes (Hes1). Wnt/β-catenin pathway may contribute to cancer-like phenotype of cells via abnormal expression of Secreted frizzled-related proteins (SRFP-1), Wnt inhibitory factor (WIF), Dickkopf-related protein (DKK), Axis inhibition protein 2 (AXIN2) and increased levels of Wnt signaling proteins including Lymphoid enhancer-binding factor 1 (LEF-1) or T-cell factor 4 (TCF-4) binding to which β-catenin influence expression of target genes (eg. Cyclin D or c-Myc). Deregulation of Hedgehog (HH) pathway may be influenced via aberrant expression of HH ligands (sonic, desert, indian), receptors PATCHED (PTCH), transmembrane proteins SMOOTHENED (SMO) or transcription factors Zinc finger proteins (GLI1-3). Abnormal modulation of PI3K/Akt/mTOR may be based on dysregulated Protein kinase B (Akt) or negative regulator of the Phosphatase and tensin homolog (PTEN). JAK/STAT signaling may be deregulated via abnormal expression of Signal transducer and activator of transcription 3 (STAT3).

2.3.2. Apoptotic and Death Resistance Signaling of CSCs

Apoptosis is regulated by an extrinsic or intrinsic pathway. Dysregulated apoptosis is a hallmark of cancer, and failure in signaling either of extrinsic or intrinsic pathways occurs also in CSCs [2,55]. Deficiency in apoptotic pathways of CSCs is induced via various mechanisms. Firstly, upregulation of cFLIPs, FLICE-like inhibitory proteins functioning as negative modulators of death receptor-induced apoptosis, and dysregulated expression of Bcl-2 family members are critical for the survival of CSCs. Additionally, increase in expression of inhibitors of apoptosis proteins (IAPs) is also associated with the tendency of CSCs to evade apoptosis. An increase in survivin, antiapoptotic protein which belongs to IAP family, may also contribute to maintenance of CSCs [55,56]. Furthermore, it is suggested that chemo- or radioresistance of CSCs is dependent on interleukin-4 (IL-4) signaling pathway because upregulation of the already mentioned pathway may result in apoptosis resistance [6]. Increase in autophagy flux is also observed in stem cells; therefore it may be related with therapy resistance of CSCs (Hu et al. [14]). Cancer cells may contain activated nuclear factor-κB (NF-κB) and tumour necrosis factor receptor-1 associated death domain protein (TRADD) which is considered to possess

an important role in NF-κB activation and survival of CSCs [56]. NF-κB enables CSCs to mediate metastasis [40] and cooperates with other pathways which are associated with CSCs, such as Notch, TGF-β or STAT3 [57]. Importantly, activation of nuclear respiratory factor 2 (Nrf-2) may lead to inhibition of NF-κB signaling [58]. In addition, overactivation of ATP-binding (ABC) efflux multidrug resistance transporters, which induce resistance to chemotherapy, was observed to be highly expressed in various CSCs. Moreover, hypoxia-inducible factor 1 (HIF-1) mediating efflux of chemotherapy is implicated in resistance of CSCs to chemotherapy. The use of agents reducing efflux may be a viable strategy targeting CSCs. Activation of enzyme aldehyde dehydrogenase (ALDH) is associated with drug metabolic activities. Restoration of apoptotic processes in CSCs may lead to increased sensitiveness of CSCs to anticancer strategies [56,59].

In conclusion, multiple mechanisms are involved in regulation of the stem-cells related processes of self-renewal, differentiation or apoptosis, many of them are deregulated in CSCs. Figure 2 depicts an overview of signaling pathways involved in the maintenance of CSCs survival, self-renewal, differentiation, and mechanisms of death resistance. Nevertheless, several pharmaceuticals and dietary phytochemicals were suggested to repair these abnormally regulated cellular or molecular signaling pathways in CSCs, and thus function as anticancer agents. In the following chapter we will focus on anticancer effects of dietary phytochemicals (isolated and/or compounds) in CSCs.

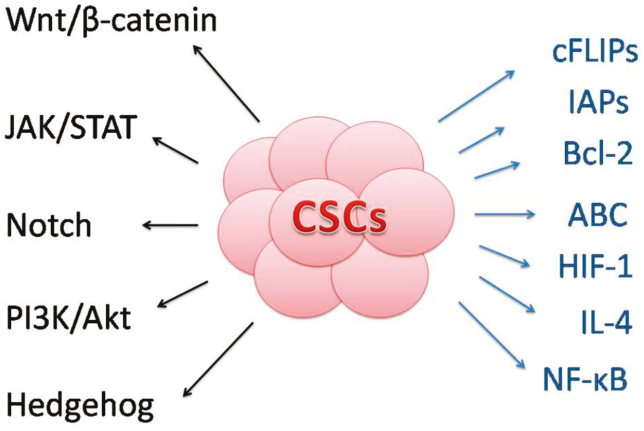

Figure 2. Mechanisms involved in stem-like maintenance and death resistance of CSCs.

Self-renewal, differentiation and maintenance of other stem-like properties may be mediated via modulation of signaling pathways including Notch, Wnt/β-catenin, Hedgehog, PI3K/Akt, JAK/STAT and others. cFLIPS, FLICE-like inhibitory proteins; IAPs, inhibitors of apoptosis proteins; Bcl-2, Bcl-2 family proteins; ABC, ATP-binding efflux multidrug resistance transporters; HIF-1, hypoxia-inducible factor 1; IL-4, interleukin-4; NF-κB, nuclear factor-κB are suggested to modulate CSCs resistance to death and cancer therapies.

3. Natural Compounds Targeting CSCs in Cancer Research

The importance of natural compounds in cancer treatment or prevention is supported by abundant evidence from cancer research [60]. Natural products are a source of bioactive compounds [20] demonstrating antioxidant, proapoptotic, and antiproliferative effects on a variety of cancers, for which existence of CSCs have been reported [61]. Significantly, dietary phytochemicals possess an ability of multilateral targeting of cellular and molecular signaling pathways which are abnormally activated in CSCs [18,59]. Since the first identification of CSCs in the late 1990s, there is great interest of this approach in cancer research [15]. Although, the clear evidence of phytochemicals targeting CSCs was in the early 21st lacking, a possible association between phytochemicals and their potential anti-CSCs

effects was indicated by several studies. Jaiswal et al. [62] and Ryu et al. [63] suggested an active role of curcumin in the Wnt/β-catenin attenuation in colon cancer cells. Moreover, downregulation of Notch1 was observed in pancreatic cancer cells [64]. However, more recent evidence from various preclinical and clinical studies suggests a direct association of natural bioactive compounds either in form of isolated dietary phytochemicals or in a form of plant functional foods in targeting CSCs.

3.1. Preclinical Research

3.1.1. Isolated Phytochemicals

Epigallocatechin-3-gallate (EGCG) is the main constituents of green tea and its protective effects are associated with various human malignancies whereas the combination of EGCG and anticancer therapy is more effective for inhibiting CSCs [65]. Interestingly, EGCG diminished lung CSCs activity in vitro via inhibition of tumorsphere formation, decrease in CSCs markers, suppression of proliferation, and induction of apoptosis. The mechanism of already mentioned effects of EGCG is attributed to the modulation of the Wnt/β-catenin pathway [66]. EGCG also inhibited self-renewal capacity of head and neck CSCs by attenuating the expression of stem cell markers and suppressing sphere forming capacity. Moreover, EGCG augmented cisplatin-mediated chemosensitivity by suppression of ABC transporter genes, inhibited tumor formation and induced apoptosis in xenograft model. The presumed mechanism of the anti-CSCs activity of EGCG is attributed to decrease in transcription level of Notch signaling components [67].

Resveratrol is a protective ingredient widely spread in the traditional Mediterranean diet which is considered to lower the risk of cancer. Resveratrol and its analogue pterostilbene target CSCs via multiple signaling pathways [68]. Resveratrol is characterized as polyphenolic stilbene derivate found in the skin of grapes and berries which possess antioxidant, anti-inflammatory, and anticarcinogenic properties [20]. Resveratrol suppressed the Wnt/β-catenin signaling pathway in breast CSCs in vitro and in vivo, and thus inhibited breast cancer stem cells and induced autophagy [69]. Moreover, resveratrol was found to impair glioma stem cells proliferation and motility by modulating the Wnt signaling and EMT activators in glioblastoma multiforme lines [70]. Furthermore, resveratrol eliminated CSCs of osteosarcoma by reduction of expression of cytokines activating JAK/STAT signaling [71]. Pterostilbene is a bioactive compound of blueberries and grapes gaining an attention due to its chemo-preventive effects in a variety of cancer types. Tumor-associated macrophages (TAM) are suggested to promote metastasis and malignancy; interestingly, it is suggested that pterostilbene influences CSCs/TAM regulation in breast cancer. Pterostilbene suppressed the generation of breast CSCs via modulation of NF-κB/microRNA 448 circuit [72]. Moreover, pterostilbene was found to function as an anticancer stem cell agent via suppressing irradiation-mediated enrichment of CD133+ Mahlavu cells, preventing tumor sphere formation, reducing stemness gene expression and suppressing invasion, migration, and process of EMT in hepatoma CSCs [43].

Genistein is a soy isoflavone functioning as a natural NF-κB inhibitor [73]. Genistein is associated with antitumor effects in various malignancies, especially in breast and prostate cancer. The study evaluating effects of genistein in vitro and in vivo was performed in MCF-7 breast cancer cells and in nude mice. Genistein inhibited breast cancer stem cells through down regulation of Hedgehog-GLI1 signaling pathway [74]. Moreover, genistein was found to inhibit stemness of SKOV3 cells induced by macrophages co-cultured with ovarian cancer stem-like cells thus becoming a potential chemo-preventive agent in human ovarian cancer. Genistein disrupted interaction between OCSLCs and THP-1 macrophages via blocking IL-8/STAT3, reversing M2 polarization of macrophages and inhibiting stemness of SKOV3 cells in co-culture system and co-injection in nude mice [52]. 7-Difluoromethoxyl-5,4′-di-*n*-octyl genistein (DFOG) is a novel synthetic genistein analogue. DFOG inhibited stem-like properties and reverse EMT phenotype in gastric cancer stem-like cells in vitro [75].

Curcumin is a dietary polyphenol derived from *Curcuma longa*. Curcumin targets CSCs through acting on the signaling pathways including Wnt, HH or Notch [76,77]. Importantly, curcumin decreased

CSCs markers in Burkitt lymphoma and acute myeloid leukemia cell line via modulation of self-renewal CSCs mechanisms [78]. Another study evaluated effects of curcumin on the reduction of breast CSCs population for sensitizing cancer cells to mitomycin C. Curcumin sensitized breast cancer cells to chemotherapy via decrease in ABC transporter (ABCG2) expression [79]. Curcumin also suppressed malignant glioma cells growth and induced apoptosis via inhibition of sHH/Gli1 pathway in vitro and in vivo [49]. Curcumin also induced cell cycle arrest via regulation of G0/G1 phase related factors including cyclin D1, cyclin-dependent kinase 2 (CDK-2), nuclear factor erythroid 2–related factor 2 (p21) and cyclin-dependent kinase inhibitor 1 (p27) and apoptosis in prostate cancer cells in vitro via down regulation of Notch signaling [80].

Isothiocyanates (ITCs) suppress cellular proliferation, EMT and self-renewal of CSCs via inhibition of oncogenic signaling pathways such as NF-κB, STAT3 or other pathways which are found to be upregulated in various cancers [81]. Phenethyl isothiocyanate (PEITC) and sulforaphane are most widely investigated isothiocynates of cruciferous plants [82]. Sulforaphane reduced tumor growth of orthotopically implanted primary pancreatic CSCs into NOD/SCID/IL2Rgamma mice, isolated from human pancreatic tumors via modulation of Sonic hedgehog-GLI pathway. Despite reduced expression of sHH components, sulforaphane also inhibited pluripotency maintaining transcription factors and markers of angiogenesis including vascular endothelial growth factor (VEGF) together with platelet-derived growth factor receptor alpha (PDGFRα). Interestingly, all of them are downstream targets for GLI transcription. Sulforaphane also reduced markers of EMT, in which Zinc finger E-box-binding homeobox 1 (Zeb-1) is included [83]. Moreover, sulforaphane inhibited CSCs properties and enhanced therapeutic efficacy of cisplatin in NSCLC through up-regulation of miR-214 which then targeted c-Myc in vitro and in xenografted nude mice [84]. Additionally, sulforaphane suppressed the growth of triple-negative breast cancer stem-like cells in vitro and in vivo via modulation of stem-related embryonic oncogene CRIPTO-1/TDGF1 (CR1) and its homologue CR3. Despite the crypto-modulated pathway, sulforaphane decreased expression of various stem cell markers [85]. PEITC is an effective inhibitor of colorectal CSCs by targeting Wnt/β-catenin pathway in vitro. PEITC reduced the size and number of cell spheroids and expression of CSCs markers and suppressed colony formation and proliferation indicating the repression of self-renewal ability [77]. PEITC also suppressed pluripotency factors, self-renewal capacity, and clonogenicity of CSCs in vitro CSCs model derived from colon cancer cells and in a mouse xenograft model injected with EpCAM-expressing cells [86].

Diallyl trisulfide (DATS) is a garlic derived organosulfur suggested to possess anticancer properties. DATS reduced tumorsphere formation, decreased CSCs markers expression, inhibited proliferation and induced apoptosis via inhibition of Wnt/β-catenin pathway and its target genes in colorectal cancer cell line [87]. Similarly, DATS inhibited the viability of CSCs, decreased expression of CSCs markers, inhibited proliferation and induced apoptosis in human breast cancer cell line also via inhibition of Wnt/ β-catenin pathway [88].

3.1.2. Plant-Derived Functional Foods

Anti-cancer research demonstrated benefits of phytochemicals combinations over isolated phytochemicals [89]. Plant-derived functional foods contain various bioactive compounds, and therefore are effective agents targeting CSCs. Several studies evaluated anti-CSCs effectiveness of plant-functional foods in preclinical research. Green algae *Capsosiphon fluvescens* glycoprotein downregulated the Wnt-1 signaling pathway in human gastric cell line, and therefore inhibited gastric cancer cell migration [90]. Anticarcinogenic effects of plant derived functional foods were evaluated in the chemopreventive models of experimental rat mammary carcinogenesis. Administration of *Origanum vulgare* L. in diet in the lower dose (0.1%) suppressed expression of CD24 by 34% and by 57% in the higher dose (1%). Moreover, the level of expression of EpCAM was decreased by 14% and 10% respectively. Furthermore, dietary administration of *Syzygium aromaticum* L. in high dose (1%) showed decrease in expression of CD24 and CD44 and increase in expression

of ALDH1. These effects on CSCs were associated with significant chemopreventive activity in both studies [91,92]. Pomegranate (*Punica granatum* L.) is a fruit rich in nutrients and bioactive phytochemicals [93]. A pomegranate emulsion was found to possess chemopreventive properties against DMBA-induced mammary tumorigenesis in rats via disruption of Estrogen Receptor and Wnt/β-catenin signaling pathways [94]. Further investigation revealed that preventive effects of pomegranate extract in DMBA-evoked mammary carcinogenesis involve anti-inflammatory regulation of two interrelated pathways NF-κB and Nrf2 [93], and this mechanism may be interrelated with CSCs signaling. *Trianthema portulacastrum* L. is an exotic plant exhibiting various pharmacological properties including antibacterial, antifungal, anti-inflammatory or antioxidant effects. *T. portulacastrum* extract (TPE) was found to prevent DMBA-induced breast carcinogenesis by anti-inflammatory mechanism mediated via modulation of NF-κB and Nrf signaling pathways [94]. Moreover, extract of *Geissospermum vellosii* also known as Pao Pereira, inhibited pancreatic CSCs via modulation of Wnt/β-catenin in vitro and in vivo [95]. Similarly, pancreatic CSCs were inhibited by extract of traditional African plant *Rauwolfia vomitoria* in vivo and in vitro also via modulation of Wnt/β-catenin signaling pathway [96]. Significantly, Chinese bayberry (*Myrica rubra*) leaf proanthocyanidins (BLPs) containing epigallocatechin-3-O-gallate (EGCG) as their terminal and major extension units exhibited inhibitory effects on chemotherapy-resistant OVCAR-3 spheroid cells via modulation of cell viability and sphere and colony formation. Furthermore, BLPs also inhibited self-renewal abilities of CSCs via targeting Wnt/β-catenin signaling pathway [97]. The anticancer benefits of three marine brown seaweed polyphenol extractions including *Hormophysa triquerta* (HT-EA), *Spatoglossum asperum* (SA-EA) or *Padina tetrastromatica* (PT-EA) were explored utilizing pancreatic cancer (PC) stem cells grown ex vivo and mouse model of residual-PC. Results of the study demonstrated the ability of these extracts to target signaling pathways playing critical role in the regulation of EMT, pluripotency and maintenance of CSCs after first-line therapy [98]. Water extract of *Gynura divaricata* (GDE) was found to target liver CSCs in a moderate to weak level and to sensitize Huh7 cell to cisplatin therapy by regulation of Wnt/β-catenin pathway and target genes [99].

Moreover, the efficacy of resveratrol (RSV) in combination with grape seed extract (GSE) was investigating in isolated human colon CSCs in vitro and in an azoxymethane-induced mouse model of colon carcinogenesis in vivo. RSV-GSE suppressed Wnt/β-catenin and induced mitochondrial-mediated apoptosis of CSCs [100]. A summary evaluating the anti-CSCs mechanisms of phytochemicals (isolated or mixtures) is shown in Table 3.

Table 3. Anticancer mechanisms of dietary phytochemicals (isolated or mixtures) targeting CSCs.

Phytochemical (Isolated or Mixture)	Cell Line/Animal Model	Mechanism	References
EGCG	A549, H1299	↓β-catenin ↓CD133 ↓CD44 ↓ALDH1A1 ↓Nanog ↓Oct4	[66]
EGCG/ EGCG and cisplatin	HNSC CSCs BALB/c nude mice	↓Oct4 ↓Sox2 ↓Nanog ↓CD44 ↓ABCC2 ↓ABCG2	[67]
Resveratrol	MCF-7, SUM159 NOD/SCID xenografted mice	→autophagy ↓Wnt/β-catenin	[69]
	GBM2, GBM7, G144, G179, G166, GliNS2, GBM04	↓β-catenin ↓c-Myc ↓Twist1 ↓Snail1	[70]
	MNNG/HOS. MG-63, hFOB1.19	↓JAK2/STAT3 ↓CD133	[71]

Table 3. *Cont.*

Phytochemical (Isolated or Mixture)	Cell Line/Animal Model	Mechanism	References
Pterostilbene	MCF7, MDA-MB-231	↓NF-κB ↓Twist1 ↓vimentin ↑E-cadherin	[72]
	HCC Mahlavu	↓c-Myc ↓COX-2 ↓vimentin ↓CXCR4 ↓Twist1	[43]
Genistein	MCF-7 Nude mice	↓SMO ↓GLI1	[74]
	SKOV3 Nude mice	↓CD 163 ↓p-STAT3 ↓IL-10 ↑IL-12 ↓CD133 ↓CD44	[52]
	GCSLCs	↓ Twist1 ↓N-cadherin ↑E-cadherin ↓CD133 ↓CD44 ↓ALDH1	[75]
Curcumin	BL41-3, Ramos, DG-75, THP-1	↓ALDH+ cells ↓GLI1 ↓Notch1 ↓cyclin D1	[78]
	MCF-7, MDA-MB-231 Athymic mice	↓ABCG2 ↓ABCC1	[79]
	U87, T98G U87-implanted nude mice	↓sHH ↓SMO ↓GLI1 ↓cyclin D1 ↓Bcl-2 ↓FoxM1 ↑Bax/Bcl-2 ratio	[49]
	DU-145	↓cyclin D1 ↓CDK2 ↓Bcl-2 ↑p21 ↑p27 ↑p53	[80]
Sulforaphane	NOD/SCID/IL2Rgamma mice	↓SMO ↓GLI1 ↓GLI2 ↓Nanog ↓Oct-4 ↑Bcl-2 ↓Zeb-1 ↓E-cadherin ↓VEGF ↓PDGFRα	[83]
	BalbC/nude mice	↓CR1 ↓CR3 ↓Nanog ↓ALDHH1A1 ↓Wnt3 ↓Notch4	[85]
	BEAS-2B, H460, H1299, A549	↓c-Myc	[84]
Phenethyl isothiocyanate	DLD-1 SW480	↓size/number of cell spheroids ↓CD133+	[77]
	293T, NCCIT, HCT116 Xenograft model	↓Oct4 ↓Sox-2 ↓Nanog	[86]
Diallyl trisulfide	SW48, DLD-1	↓β-catenin ↓c-Myc ↓cyclin D1	[87]
	MCF-7, SUM159	↓CD44 ↓ALDH1A1 ↓Nanog ↓Oct4	[88]

Table 3. *Cont.*

Phytochemical (Isolated or Mixture)	Cell Line/Animal Model	Mechanism	References
Capsosiphon fulvescens	AGS	↓Wnt-1 ↓β-catenin → G0/G1 arrest	[90]
Origanum vulgare	NMU-induced rat mammary carcinogenesis	↓CD24 ↓EpCAM	[91]
Syzygium aromaticum	NMU-induced rat mammary carcinogenesis	↓CD24 ↓CD44 ↑ALDH1	[92]
Pomegranate extract	DMBA-induced rat mammary carcinogenesis	↓ER-α:ER-β↓β-catenin ↓cyclin D1 ↓COX-2 ↑Nrf2 IκBα degradation and NF-κB translocation blockage	[93]
Trianthema portulacastrum extract	DMBA-induced rat mammary carcinogenesis	↓COX-2 ↑Nrf2 IκBα degradation and NF-κB translocation blockage	[94]
Pao Pereira extract	PANC-1, MIA PaCa-2, AsPC-1, HPAF-II, BxPC-3 in immunocompromised mice	↓Nanog ↓β-catenin	[95]
Rauwolfia vomitoria extract	PANC-1, AsPC-1, HPAF-II, BxPC-3 and MiA PaCa-2 in immunocompromised mice	↓Nanog ↓β-catenin	[96]
Chinese bayberry leaf proanthocyanidins (BLPs)	OVCAR-3	↓β-catenin ↓cyclin D1 ↓c-Myc →G1 arrest	[97]
HT-EA, SA-EA, PT-EA	Panc-1, MiaPaCa-2, Panc-3.27, and BxPC-3 Athymic NCr-nu/nu nude mice	↓Nanog ↓Oct-4 ↓Sox2 ↓N-cadherin	[98]
Water extract of *Gynura divaricata* (GDE)	Huh7, Hep3B	↓β-catenin	[99]
Resveratrol (RSV) and grape seed extracts (GSE)	Human colon CSCs Azoxymethane-induced mice	↓ nuclear translocation of β-catenin ↓c-Myc ↓cyclin D1 ↑p53 ↑Bax/Bcl-2	[100]

Explanatory notes: ↓ decrease; ↑ increase; → induction. Abbreviations used: ABCC1-ATP Binding Cassette Subfamily C Member 1; ABCC2-ATP Binding Cassette Subfamily C Member 2; ABCG2-ATP Binding Cassette Subfamily G Member 2; ALDH1A1-Aldehyde Dehydrogenase 1 Family Member A1; Bcl-2-B-cell Lymphoma Protein Family CD136/133/44/24, Cluster of Differentiation 136/133/44/24; CDK2-Cyclin-dependent Kinase 2; c-Myc, MYC protoonkogene; COX-2-Cyclo- oxygenase 2; CR1-CRIPTO-1/TDGF1, Teratocarcinoma-derived Growth Factor 1, CR3, CRIPTO-3/TDGF1P3, Putative Teratocarcinoma-derived Growth Factor 3; CXCR4-Chemokine Receptor Type 4; EpCAM-Epithelial Cell Adhesion Molecule; ERα-Estrogen Receptor Alfa; ERβ-Estrogen Receptor Beta; FoxM1-Forkhead Box Protein M1; GLI1/2-Zinc Finger Protein 1/2; IL-10/12-Interleukin 10/12; JAK-Janus kinase; NF-κB-Nuclear Factor Kappa-light-chain-enhancer of Activated B cells; Notch1-4-Notch receptors; NRF2-Nuclear Factor Erythroid 2–related Factor 2; p21-Cyclin-dependent Kinase Inhibitor 1; p27-Cyclin-dependent Kinase Inhibitor 1B; p53-Tumour Protein p53; PDGFRα-Platelet-derived Growth Factor Receptor Alpha; pSTAT3-Phospho-Signal Transducer and Activator of Transcription 3; sHH- Sonic Hedgehog; SMO- Transmembrane protein SMOOTHENED; Snail1-Zinc Finger Protein; STAT-Signal Transducer and Activator of Transcription; Twist1-Twist family BHLH Transcription Factor 1/gene; VEGF-Vascular Endothelial Growth Factor; Zeb-1-Zinc finger E-box-binding Homeobox 1.

3.2. Clinical research

Anti-CSCs potential of dietary phytochemicals (isolated or mixtures) was investigated in several previously mentioned preclinical studies [43,49,52,66,67,69–72,74,75,77–80,83–88,90–100]. Significantly, anticancer properties of phytochemicals were evaluated in several clinical trials. Firstly, a phase I pilot study on patients with colon cancer was conducted to evaluate effects of a low dose of resveratrol formulation and resveratrol-containing freeze-dried grape powder (GP) on Wnt signaling in the colon. Results of the trial are based on the expression of Wnt target genes. Resveratrol/GP inhibited Wnt target gene expression in normal colon mucosa; however did not inhibit the Wnt pathway in colon cancer tissue [101]. Moreover, a phase 2 randomized, placebo-controlled trial was conducted on 59 subjects diagnosed with urothelial bladder cancer. The aim of the trial was to investigate whether daily dose of genistein in the form of purified soy extract G-2535 for 14 to 21 days before surgery alter molecular pathways in bladder epithelial tissue. The primary outcome of the study was inhibition of EGFR phosphorylation in a dose of 300mg/d. However, no significant changes were observed in expression of COX-2, Ki67, caspase-3, Akt or p-Akt [102]. Furthermore, a randomized clinical trial on 35 colorectal cancer patients, who were daily administrated 900 mg of ellagitannins-containing pomegranate extract (PE) showed the expression of CRC-genes in normal and cancerous colon tissue was evaluated before (biopsies) and after (surgical specimens) 5–35 days of supplementation. Tissues were also obtained from a control group of patients with no supplementation. The consumption of the PE was significantly associated with a counterbalance effect in the expression of CD44, β-catenin, p21 or others suggesting that the intake of PE modulated the impact on gene expression in a gene- and tissue-specific manner [103]. While searching in the clinical trial database [104], we found few clinical trials which may be partially related to CSCs. A prospective phase II study was initiated in 2015 with the aim to investigate the effect of Fursultiamine, a derivate of vitamin B, combined with concurrent chemo/radiotherapy in esophageal cancer patients (ClinicalTrials.gov Identifier: NCT02423811). Moreover, pancreatic ductal adenocarcinoma (PDA) stem cells were target of a pilot study initiated in 2013 with the aim to find whether the application of freeze-dried broccoli sprouts lead cancer inhibition in patients with advanced PDA (ClinicalTrials.gov Identifier: NCT01879878). However, no results of these clinical trials are available at this time.

Figure 3 shows an overview of dietary phytochemicals (isolated or mixtures) in preclinical or clinical research and their effects on CSCs. Finally, there is number of clinical trials evaluating plant derived foods or dietary supplements in anticancer research; however, we were not successful in finding clinical trials focusing on CSCs specifically.

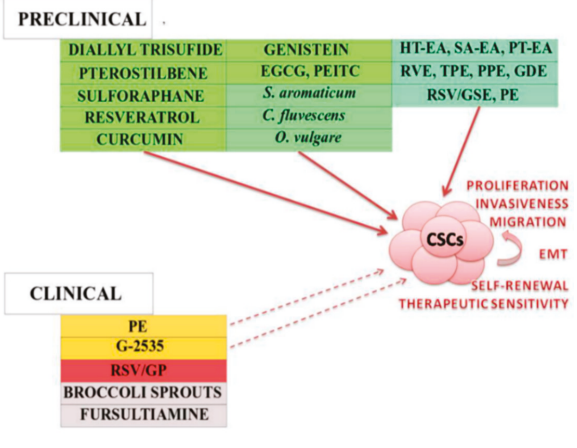

Figure 3. Dietary phytochemicals targeting CSCs in preclinical and clinical cancer research.

Isolated dietary phytochemicals including diallyl trisulfide, pterostilbene, sulforaphane, resveratrol, curcumin, genistein, epigallocatechin-3-gallate (EGCG), phenethyl isothiocyanate (PEITC) and plant functional foods including *S. aromaticum, C. fluvescens, O. vulgare,* Chinese bayberry leaf proanthocyanidins (BLPs) and extracts of pomegranate, *Trianthema portulacastrum, Gynura divaricata, Hormophysa triquerta* (HT-EA), *Spatoglossum asperum* (SA-EA), *Padina tetrastromatica* (PT-EA) and resveratrol in combination with grape seed extracts (GSE) demonstrated anticancer properties via targeting CSCs-mediated pathways and thus modulating CSCs proliferation, invasiveness, migration, self-renewal, EMT and sensitivity to therapeutic approaches in preclinical research. The data evaluating effects of dietary phytochemicals in clinical research were insufficient. Ellagitannins-containing pomegranate extract (PE) and purified soy extract (G-2535) may modulate CSCs signaling at least partially. Resveratrol formulation and resveratrol-containing freeze-dried grape powder RSV/GP did not exhibit any prosperous effects in inhibition of CSCs pathways in cancer tissue. Clinical trials evaluating anticancer effects of broccoli sprouts and fursultiamine were initiated in 2013 and 2015, however no results were reported for these studies.

4. Conclusion and Future Perspectives

There is great evidence suggesting that aberrant regulation of CSCs signaling pathways may lead to deregulation of self-renewal, apoptosis, proliferation, and importantly resistance to anti-cancer therapy. Considering the cancer research, phytochemicals (isolated or mixtures) are suggested to possess antioxidant, antiproliferative, and anticancer properties and also to have the ability to target aberrantly regulated signaling of CSCs. Importantly, the use of plant derived compounds is associated with no or very little adverse events. Phytochemicals are thought to modulate various signaling pathways of CSCs. Cross talk between these pathways influence self-renewal, differentiation, EMT, therapy resistance and other pro-cancer mechanism associated with stem-like cells. Here we summarized the current state of the anticancer effectiveness of different plant-derived dietary phytochemicals in preclinical and clinical research. In vitro and in vivo preclinical studies indicated significant anticancer effects of dietary phytochemicals mediated by CSCs targeting via modulation of signaling pathways, including Wnt, Notch, Hedgehog, or other, as well as via regulation of mechanisms involved in the processes of apoptosis or drug resistance. Based on the comparative preclinical oncology studies, functional foods (characterized by the presence of mixture of phytochemicals) are suggested to exhibit better anti-cancer activities (including the anti-CSCs properties) when compared to isolated phytochemicals. Importantly, each of the preclinical studies included in our review is specific in its aims and uses specifically designed methods. However, individual processes in the cell and therefore processes of carcinogenesis are complex and interconnected. Nevertheless, it would be beneficial to find out if there are associations or discrepancies between studies dealing with the same type of cancer, cell line, model, phytochemical or specific pathway responsible for anti-CSCs effects of particular substance. After all, more specific and comparative studies are needed for such analysis. Despite numerous preclinical studies, clinical research in this area is significantly lagging behind and only a few trials could be identified. On the contrary, we have encountered a large number of clinical studies focused on how are CSCs influenced by synthetic drugs; however, evidence of plant-derived foods or other dietary supplements as anti-CSCs agents is lacking. In conclusion, we emphasize the significant anti-cancer effects of dietary phytochemicals on CSCs in a wide range of cancer types via influencing multiple signaling mechanisms, and thus demonstrating the urgent need for their in-depth investigation in clinical research.

Author Contributions: A.L., P.K., M.S., S.M.S. literature search and writing of the manuscript; P.K., D.B., T.K.K. provided a skilled assistance and supervised the overall preparation of the manuscript; M.S. proposed and prepared the figures; M.M., T.B. contributed to conception of the idea, literature search, manuscript editing; P.Z., A.Z. revised the manuscript with critical reviews and comments.

Acknowledgments: This work was supported by the Scientific Grant Agency of the Ministry of Education of the Slovak Republic under the contracts no. VEGA 1/0136/19, 1/0124/17 and the Slovak Research and Development Agency under the contract no. APVV-16-0021.

Conflicts of Interest: The authors declare no conflict of interest.

References

1. Konrad, C.V.; Murali, R.; Varghese, B.A.; Nair, R. The role of cancer stem cells in tumor heterogeneity and resistance to therapy. *Can. J. Physiol. Pharmacol.* **2017**, *95*, 1–15. [CrossRef] [PubMed]
2. Kim, D.H.; Surh, Y.J. Chemopreventive and Therapeutic Potential of Phytochemicals Targeting Cancer Stem Cells. *Curr. Pharmacol. Rep.* **2015**, *1*, 302–311. [CrossRef]
3. Kozovska, Z.; Gabrisova, V.; Kucerova, L. Colon cancer: Cancer stem cells markers, drug resistance and treatment. *Biomed. Pharmacother.* **2014**, *68*, 911–916. [CrossRef] [PubMed]
4. Oo, A.K.K.; Calle, A.S.; Nair, N.; Mahmud, H.; Vaidyanath, A.; Yamauchi, J.; Khayrani, A.C.; Du, J.; Alam, M.J.; Seno, A.; et al. Up-Regulation of PI 3-Kinases and the Activation of PI3K-Akt Signaling Pathway in Cancer Stem-Like Cells Through DNA Hypomethylation Mediated by the Cancer Microenvironment. *Transl. Oncol.* **2018**, *11*, 653–663. [CrossRef] [PubMed]
5. Alison, M.R.; Islam, S.; Wright, N.A. Stem cells in cancer: Instigators and propagators? *J. Cell Sci.* **2010**, *123*, 2357–2368. [CrossRef] [PubMed]
6. Salem, M.L.; El-Badawy, A.S.; Li, Z. Immunobiology and signaling pathways of cancer stem cells: Implication for cancer therapy. *Cytotechnology* **2015**, *67*, 749–759. [CrossRef] [PubMed]
7. Varghese, E.; Samuel, S.M.; Varghese, S.; Cheema, S.; Mamtani, R.; Büsselberg, D. Triptolide Decreases Cell Proliferation and Induces Cell Death in Triple Negative MDA-MB-231 Breast Cancer Cells. *Biomolecules* **2018**, *8*, 163. [CrossRef] [PubMed]
8. Varghese, E.; Samuel, S.M.; Abotaleb, M.; Cheema, S.; Mamtani, R.; Büsselberg, D. The "Yin and Yang" of Natural Compounds in Anticancer Therapy of Triple-Negative Breast Cancers. *Cancers* **2018**, *10*, 346. [CrossRef] [PubMed]
9. Abotaleb, M.; Samuel, S.M.; Varghese, E.; Varghese, S.; Kubatka, P.; Liskova, A.; Büsselberg, D. Flavonoids in Cancer and Apoptosis. *Cancers* **2019**, *11*, E28. [CrossRef] [PubMed]
10. Lee, CH.; Chen, C.Y. Natural product-based therapeutics for the treatment of cancer stem cells: A patent review (2010–2013). *Expert Opin. Ther. Pat.* **2015**. [CrossRef] [PubMed]
11. Patel, P.; Chen, E.I. Cancer stem cells, tumor dormancy, and metastasis. *Front. Endocrinol.* **2012**, *3*, 125. [CrossRef] [PubMed]
12. Pan, Y.; Ma, S.; Cao, K.; Zhou, S.; Zhao, A.; Li, M.; Qian, F.; Zhu, C. Therapeutic approaches targeting cancer stem cells. *J. Cancer Res. Ther.* **2018**, *14*, 1469–1475. [CrossRef] [PubMed]
13. Wang, T.; Shigdar, S.; Gantier, M.P.; Hou, Y.; Wang, L.; Li, Y.; Shamaileh, H.A.; Yin, W.; Zhou, S.F.; Zhao, X.; et al. Cancer stem cell targeted therapy: Progress amid controversies. *Oncotarget* **2015**, *6*, 44191–44206. [CrossRef] [PubMed]
14. Hu, W.Y.; Hu, D.P.; Xie, L.; Li, Y. Majumdar S1, Nonn L2, Hu H3, Shioda T4, Prins GS5. Isolation and functional interrogation of adult human prostate epithelial stem cells at single cell resolution. *Stem Cell Res.* **2017**, *23*, 1–12. [CrossRef] [PubMed]
15. Moharil, R.B.; Dive, A.; Khandekar, S.; Bodhade, A. Cancer stem cells: An insight. *J. Oral Maxillofac. Pathol.* **2017**, *21*, 463. [CrossRef] [PubMed]
16. Palermo, R.; Ghirga, F.; Piccioni, M.G.; Bernardi, F.; Zhdanovskaya, N.; Infante, P.; Mori, M. Natural products inspired modulators of cancer stem cells-specific signaling pathways Notch and Hedgehog. *Curr. Pharm. Des.* **2019**. [CrossRef] [PubMed]
17. Toledo-Guzmán, M.E.; Bigoni-Ordóñez, G.D.; Ibáñez Hernández, M.; Ortiz-Sánchez, E. Cancer stem cell impact on clinical oncology. *World J. Stem Cells* **2018**, *10*, 183–195. [CrossRef] [PubMed]
18. Oh, J.; Hlatky, L.; Jeong, Y.S.; Kim, D. Therapeutic Effectiveness of Anticancer Phytochemicals on Cancer Stem Cells. *Toxins* **2016**, *8*, 199. [CrossRef] [PubMed]
19. Chen, K.; Huang, Y.H.; Chen, J.L. Understanding and targeting cancer stem cells: Therapeutic implications and challenges. *Acta Pharmacol. Sin.* **2013**, *34*, 732–740. [CrossRef] [PubMed]

20. Taylor, W.F.; Jabbarzadeh, E. The use of natural products to target cancer stem cells. *Am. J. Cancer Res.* **2017**, *7*, 1588–1605. [PubMed]
21. Hu, W.Y.; Shi, G.B.; Lam, H.M.; Hu, D.P.; Ho, S.M.; Madueke, I.C.; Kajdacsy-Balla, A.; Prins, G.S. Estrogen-initiated transformation of prostate epithelium derived from normal human prostate stem-progenitor cells. *Endocrinology* **2011**, *152*, 2150–2163. [CrossRef] [PubMed]
22. Prins, G.S.; Hu, W.Y.; Xie, L.; Shi, G.B.; Hu, D.P.; Birch, L.; Bosland, M.C. Evaluation of Bisphenol A (BPA) Exposures on Prostate Stem Cell Homeostasis and Prostate Cancer Risk in the NCTR-Sprague-Dawley Rat: An NIEHS/FDA CLARITY-BPA Consortium Study. *Environ. Health Perspect.* **2018**, *126*, 117001. [CrossRef] [PubMed]
23. Morath, I.; Hartmann, T.N.; Orian-Rousseau, V. CD44: More than a mere stem cell marker. *Int. J. Biochem. Cell Biol.* **2016**, *81*, 166–173. [CrossRef] [PubMed]
24. Wan, X.; Cheng, C.; Shao, Q.; Lin, Z.; Lu, S.; Chen, Y. CD24 promotes HCC progression via triggering Notch-related EMT and modulation of tumor microenvironment. *Tumour Biol.* **2016**, *37*, 6073–6084. [CrossRef] [PubMed]
25. Kumar, A.; Bhanja, A.; Bhattacharyya, J.; Jaganathan, B.G. Multiple roles of CD90 in cancer. *Tumour Biol.* **2016**, *37*, 11611–11622. [CrossRef] [PubMed]
26. Kim, H.M.; Haraguchi, N.; Ishii, H.; Ohkuma, M.; Okano, M.; Mimori, K.; Eguchi, H.; Yamamoto, H.; Nagano, H.; Sekimoto, M.; et al. Increased CD13 expression reduces reactive oxygen species, promoting survival of liver cancer stem cells via an epithelial-mesenchymal transition-like phenomenon. *Ann. Surg. Oncol.* **2012**, S539–S548. [CrossRef] [PubMed]
27. Nakahata, K.; Uehara, S.; Nishikawa, S.; Kawatsu, M.; Zenitani, M.; Oue, T.; Okuyama, H. Aldehyde Dehydrogenase 1 (ALDH1) Is a Potential Marker for Cancer Stem Cells in Embryonal Rhabdomyosarcoma. *PLoS ONE* **2015**, *10*, e0125454. [CrossRef] [PubMed]
28. Wang, N.; Wang, S.; Li, M.Y.; Hu, B.G.; Liu, L.P.; Yang, S.L.; Yang, S.; Gong, Z.; Lai, P.B.S.; Chen, G.G. Cancer stem cells in hepatocellular carcinoma: An overview and promising therapeutic strategies. *Ther. Adv. Med. Oncol.* **2018**, *10*, 1–25. [CrossRef] [PubMed]
29. Yan, Y.; Zuo, X.; Wei, D. Concise Review: Emerging Role of CD44 in Cancer Stem Cells: A Promising Biomarker and Therapeutic Target. *Stem Cells Transl. Med.* **2015**, *4*, 1033–1043. [CrossRef] [PubMed]
30. Jaggupilli, A.; Elkord, E. Significance of CD44 and CD24 as cancer stem cell markers: An enduring ambiguity. *Clin. Dev. Immunol.* **2012**, 708036. [CrossRef] [PubMed]
31. Li, W.; Ma, H.; Zhang, J.; Zhu, L.; Wang, C.; Yang, Y. Unraveling the roles of CD44/CD24 and ALDH1 as cancer stem cell markers in tumorigenesis and metastasis. *Sci. Rep.* **2017**, *7*, 13856. [CrossRef] [PubMed]
32. Munz, M.; Baeuerle, P.A.; Gires, O. The emerging role of EpCAM in cancer and stem cell signaling. *Cancer Res.* **2009**, *69*, 5627–5629. [CrossRef] [PubMed]
33. Jang, J.W.; Song, Y.; Kim, S.H.; Kim, J.; Seo, H.R. Potential mechanisms of CD133 in cancer stem cells. *Life Sci.* **2017**, *184*, 25–29. [CrossRef] [PubMed]
34. Glumac, P.M.; LeBeau, A.M. The role of CD133 in cancer: A concise review. *Clin. Transl. Med.* **2018**, *7*, 18. [CrossRef] [PubMed]
35. Haraguchi, N.; Ishii, H.; Mimori, K.; Tanaka, F.; Ohkuma, M.; Kim, H.M.; Akita, H.; Takiuchi, D.; Hatano, H.; Nagano, H.; et al. CD13 is a therapeutic target in human liver cancer stem cells. *J. Clin. Investig.* **2010**, *120*, 3326–3339. [CrossRef] [PubMed]
36. Luo, J.; Wang, P.; Wang, R.; Wang, J.; Liu, M.; Xiong, S.; Li, Y.; Cheng, B. The Notch pathway promotes the cancer stem cell characteristics of CD90+ cells in hepatocellular carcinoma. *Oncotarget* **2016**, *7*, 9525–9537. [CrossRef] [PubMed]
37. Shaikh, M.V.; Kala, M.; Nivsarkar, M. CD90 a potential cancer stem cell marker and a therapeutic target. *Cancer Biomark.* **2016**, *16*, 301–307. [CrossRef] [PubMed]
38. Tomita, H.; Tanaka, K.; Tanaka, T.; Hara, A. Aldehyde dehydrogenase 1A1 in stem cells and cancer. *Oncotarget* **2016**, *7*, 11018–11032. [CrossRef] [PubMed]
39. Katoh, M. Canonical and non-canonical WNT signaling in cancer stem cells and their niches: Cellular heterogeneity, omics reprogramming, targeted therapy and tumor plasticity. *Int. J. Oncol.* **2017**, *51*, 1357–1369. [CrossRef] [PubMed]
40. Matsui, W.H. Cancer stem cell signaling pathways. *Medicine* **2016**, *95*, S8–S19. [CrossRef] [PubMed]

41. Koury, J.; Zhong, L.; Hao, J. Targeting Signaling Pathways in Cancer Stem Cells for Cancer Treatment. *Stem Cells Int.* **2017**, 2925869. [CrossRef] [PubMed]
42. Kuşoğlu, A.; Avcı, Ç.B. Cancer stem cells: A brief review of the current status. *Gene* **2019**, *681*, 80–85. [CrossRef]
43. Lee, C.M.; Su, Y.H.; Huynh, T.T.; Lee, W.H.; Chiou, J.F.; Lin, Y.K.; Hsiao, M.; Wu, C.H.; Lin, Y.F.; Wu, A.T.; et al. BlueBerry Isolate, Pterostilbene, Functions as a Potential Anticancer Stem Cell Agent in Suppressing Irradiation-Mediated Enrichment of Hepatoma Stem Cells. *Evid. Based Complement. Alternat. Med.* **2013**, 258425. [CrossRef] [PubMed]
44. Singh, A.; Settleman, J. EMT, cancer stem cells and drug resistance: An emerging axis of evil in the war on cancer. *Oncogene* **2010**, *29*, 4741–4751. [CrossRef] [PubMed]
45. Dandawate, P.; Padhye, S.; Ahmad, A.; Sarkar, F.H. Novel strategies targeting cancer stem cells through phytochemicals and their analogs. *Drug Deliv. Transl. Res.* **2013**, *3*, 165–182. [CrossRef] [PubMed]
46. Venkatesh, V.; Nataraj, R.; Thangaraj, G.S.; Karthikeyan, M.; Gnanasekaran, A.; Kaginelli, S.B.; Kuppanna, G.; Kallappa, C.G.; Basalingappa, K.M. Targeting Notch signalling pathway of cancer stem cells. *Stem Cell Investig.* **2018**, *5*, 5. [CrossRef] [PubMed]
47. Samadani, A.A.; Norollahi, S.E.; Rashidy-Pour, A.; Mansour-Ghanaei, F.; Nemati, S.; Joukar, F.; Afshar, A.M.; Ghazanfari, S.; Safizadeh, M.; Rostami, P.; et al. Cancer signaling pathways with a therapeutic approach: An overview in epigenetic regulations of cancer stem cells. *Biomed. Pharmacother.* **2018**, *108*, 590–599. [CrossRef] [PubMed]
48. Dandawate, P.R.; Subramaniam, D.; Jensen, R.A.; Anant, S. Targeting cancer stem cells and signaling pathways by phytochemicals: Novel approach for breast cancer therapy. *Semin. Cancer Biol.* **2016**, *40*, 192–208. [CrossRef] [PubMed]
49. Du, W.Z.; Feng, Y.; Wang, X.F.; Piao, X.Y.; Cui, Y.Q.; Chen, L.C.; Lei, X.H.; Sun, X.; Liu, X.; Wang, H.B.; et al. Curcumin suppresses malignant glioma cells growth and induces apoptosis by inhibition of SHH/GLI1 signaling pathway in vitro and vivo. *CNS Neurosci. Ther.* **2013**, *19*, 926–936. [CrossRef] [PubMed]
50. Chang, L.; Graham, P.H.; Ni, J.; Hao, J.; Bucci, J.; Cozzi, P.J.; Li, Y. Targeting PI3K/Akt/mTOR signaling pathway in the treatment of prostate cancer radioresistance. *Crit. Rev. Oncol. Hematol.* **2015**, *96*, 507–517. [CrossRef] [PubMed]
51. Suvarna, V.; Murahari, M.; Khan, T.; Chaubey, P.; Sangave, P. Phytochemicals and PI3K Inhibitors in Cancer-An Insight. *Front. Pharmacol.* **2017**, *8*, 916. [CrossRef] [PubMed]
52. Ning, Y.; Feng, W.; Cao, X.; Ren, K.; Quan, M.; Chen, A.; Xu, C.; Qiu, Y.; Cao, J.; Li, X.; et al. Genistein inhibits stemness of SKOV3 cells induced by macrophages co-cultured with ovarian cancer stem-like cells through IL-8/STAT3 axis. *J. Exp. Clin. Cancer Res.* **2019**, *38*, 19. [CrossRef] [PubMed]
53. Banerjee, K.; Resat, H. Constitutive activation of STAT3 in breast cancer cells: A review. *Int. J. Cancer* **2016**, *138*, 2570–2578. [CrossRef] [PubMed]
54. Cafferkey, C.; Chau, I. Novel STAT 3 inhibitors for treating gastric cancer. *Expert Opin. Investig. Drugs* **2016**, *25*, 1023–1031. [CrossRef] [PubMed]
55. He, Y.C.; Zhou, F.L.; Shen, Y.; Liao, D.F.; Cao, D. Apoptotic death of cancer stem cells for cancer therapy. *Int. J. Mol. Sci.* **2014**, *15*, 8335–8351. [CrossRef] [PubMed]
56. Safa, A.R. Resistance to Cell Death and Its Modulation in Cancer Stem Cells. *Crit. Rev. Oncog.* **2016**, *21*, 203–219. [CrossRef] [PubMed]
57. Rinkenbaugh, A.L.; Baldwin, A.S. The NF-κB Pathway and Cancer Stem Cells. *Cells* **2016**, *5*, 16. [CrossRef] [PubMed]
58. Pramanik, K.C.; Makena, M.R.; Bhowmick, K.; Pandey, M.K. Advancement of NF-κB Signaling Pathway: A Novel Target in Pancreatic Cancer. *Int. J. Mol. Sci.* **2018**, *19*, 3890. [CrossRef] [PubMed]
59. Chan, M.M.; Chen, R.2.; Fong, D. Targeting cancer stem cells with dietary phytochemical—Repositioned drug combinations. *Cancer Lett.* **2018**, *433*, 53–64. [CrossRef] [PubMed]
60. Mayne, S.T.; Playdon, M.C.; Rock, C.L. Diet, nutrition, and cancer: Past, present and future. *Nat. Rev. Clin. Oncol.* **2016**, *13*, 504–515. [CrossRef] [PubMed]
61. Mukherjee, S.; Saha, S.; Manna, A.; Mazumdar, M.; Chakraborty, S.; Paul, S.; Das, T. Targeting Cancer Stem Cells by Phytochemicals: A Multimodal Approach to Colorectal Cancer. *Curr. Colorectal. Cancer Rep.* **2014**, *10*, 431–441. [CrossRef]

62. Jaiswal, A.S.; Marlow, B.P.; Gupta, N.; Narayan, S. Beta-catenin-mediated transactivation and cell-cell adhesion pathways are important in curcumin (diferuylmethane)-induced growth arrest and apoptosis in colon cancer cells. *Oncogene* **2002**, *21*, 8414–8427. [CrossRef] [PubMed]
63. Ryu, M.J.; Cho, M.; Song, J.Y.; Yun, Y.S.; Choi, I.W.; Kim, D.E.; Park, B.S.; Oh, S. Natural derivatives of curcumin attenuate the Wnt/beta-catenin pathway through down-regulation of the transcriptional coactivator p300. *Biochem. Biophys. Res. Commun.* **2008**, *377*, 1304–1308. [CrossRef] [PubMed]
64. Wang, Z.; Zhang, Y.; Banerjee, S.; Li, Y.; Sarkar, F.H. Notch-1 down-regulation by curcumin is associated with the inhibition of cell growth and the induction of apoptosis in pancreatic cancer cells. *Cancer* **2006**, *106*, 2503–2513. [CrossRef] [PubMed]
65. Fujiki, H.; Sueoka, E.; Rawangkan, A.; Suganuma, M. Human cancer stem cells are a target for cancer prevention using (-)-epigallocatechin gallate. *J. Cancer Res. Clin. Oncol.* **2017**, *143*, 2401–2412. [CrossRef] [PubMed]
66. Zhu, J.; Jiang, Y.; Yang, X.; Wang, S.; Xie, CH.; Li, X.; Li, Y.; Chen, Y.; Wang, X.; Meng, Y.; et al. Wnt/β-catenin pathway mediates (−)-Epigallocatechin-3-gallate (EGCG) inhibition of lung cancer stem cells. *Biochem. Biophys. Res. Commun.* **2017**, *482*, 15–21. [CrossRef] [PubMed]
67. Lee, S.H.; Nam, H.J.; Kang, H.J.; Kwon, H.W.; Lim, Y.C. Epigallocatechin-3-gallate attenuates head and neck cancer stem cell traits through suppression of Notch pathway. *Eur. J. Cancer* **2013**, *49*, 3210–3218. [CrossRef] [PubMed]
68. Zhang, L.; Wen, X.; Li, M.; Li, S.; Zhao, H. Targeting cancer stem cells and signaling pathways by resveratrol and pterostilbene. *Biofactors* **2018**, *44*, 61–68. [CrossRef] [PubMed]
69. Fu, Y.; Chang, H.; Peng, X.; Bai, Q.; Yi, L.; Zhou, Y.; Zhu, J.; Mi, M. Resveratrol inhibits breast cancer stem-like cells and induces autophagy via suppressing Wnt/β-catenin signaling pathway. *PLoS ONE* **2014**, *9*, e102535. [CrossRef] [PubMed]
70. Cilibrasi, C.; Riva, G.; Romano, G.; Cadamuro, M.; Bazzoni, R.; Butta, V.; Paoletta, L.; Dalprà, L.; Strazzabosco, M.; Lavitrano, M.; et al. Resveratrol Impairs Glioma Stem Cells Proliferation and Motility by Modulating the Wnt Signaling Pathway. *PLoS ONE* **2017**, *12*, e0169854. [CrossRef] [PubMed]
71. Peng, L.; Jiang, D. Resveratrol eliminates cancer stem cells of osteosarcoma by STAT3 pathway inhibition. *PLoS ONE* **2018**, *13*, e0205918. [CrossRef] [PubMed]
72. Mak, K.K.; Wu, A.T.; Lee, W.H.; Chang, T.C.; Chiou, J.F.; Wang, L.S.; Wu, CH.; Huang, C.Y.; Shieh, Y.S.; Chao, T.Y.; et al. Pterostilbene, a bioactive component of blueberries, suppresses the generation of breast cancer stem cells within tumor microenvironment and metastasis via modulating NF-κB/microRNA 448 circuit. *Mol. Nutr. Food Res.* **2013**, *57*, 1123–1134. [CrossRef] [PubMed]
73. Kumar, G.; Farooqui, M.; Rao, C.V. Role of Dietary Cancer-Preventive Phytochemicals in Pancreatic Cancer Stem Cells. *Curr. Pharmacol. Rep.* **2018**, *4*, 326–335. [CrossRef] [PubMed]
74. Fan, P.; Fan, S.; Wang, H.; Mao, J.; Shi, Y.; Ibrahim, M.M.; Ma, W.; Yu, X.; Hou, Z.; Wang, B.; et al. Genistein decreases the breast cancer stem-like cell population through Hedgehog pathway. *Stem Cell Res. Ther.* **2013**, *4*, 146. [CrossRef] [PubMed]
75. Cao, X.; Ren, K.; Song, Z.; Li, D.; Quan, M.; Zheng, Y.; Cao, J.; Zeng, W.; Zou, H. Difluoromethoxyl-5,4′-di-n-octyl genistein inhibits the stem-like characteristics of gastric cancer stem-like cells and reverses the phenotype of epithelial-mesenchymal transition in gastric cancer cells. *Oncol. Rep.* **2016**, *36*, 1157–1165. [CrossRef] [PubMed]
76. Li, Y.; Zhang, T. Targeting cancer stem cells by curcumin and clinical applications. *Cancer Lett.* **2014**, *346*, 197–205. [CrossRef] [PubMed]
77. Chen, Y.; Li, Y.; Wang, X.Q.; Meng, Y.; Zhang, Q.; Zhu, J.Y.; Chen, J.Q.; Cao, W.S.; Wang, X.Q.; Xie, C.F.; et al. Phenethyl isothiocyanate inhibits colorectal cancer stem cells by suppressing Wnt/β-catenin pathway. *Phytother Res.* **2018**, *32*, 2447–2455. [CrossRef] [PubMed]
78. Li, Y.; Domina, A.; Lim, G.; Chang, T.; Zhang, T. Evaluation of curcumin, a natural product in turmeric, on Burkitt lymphoma and acute myeloid leukemia cancer stem cell markers. *Future Oncol.* **2018**, *14*, 2353–2360. [CrossRef] [PubMed]
79. Zhou, Q.; Ye, M.; Lu, Y.; Zhang, H.; Chen, Q.; Huang, S.; Su, S. Curcumin Improves the Tumoricidal Effect of Mitomycin C by Suppressing ABCG2 Expression in Stem Cell-Like Breast Cancer Cells. *PLoS ONE* **2015**, *10*, e0136694. [CrossRef] [PubMed]

80. Sha, J.; Li, J.; Wang, W.; Pan, L.; Cheng, J.; Li, L.; Zhao, H.; Lin, W. Curcumin induces G0/G1 arrest and apoptosis in hormone independent prostate cancer DU-145 cells by down regulating Notch signaling. *Biomed. Pharmacother.* **2016**, *84*, 177–184. [CrossRef] [PubMed]
81. Pistollato, F.; Giampieri, F.; Battino, M. The use of plant-derived bioactive compounds to target cancer stem cells and modulate tumor microenvironment. *Food Chem. Toxicol.* **2015**, *75*, 58–70. [CrossRef] [PubMed]
82. Cheung, K.L.; Kong, A.N. Molecular targets of dietary phenethyl isothiocyanate and sulforaphane for cancer chemoprevention. *AAPS J.* **2010**, *12*, 87–97. [CrossRef] [PubMed]
83. Li, S.H.; Fu, J.; Watkins, D.N.; Srivastava, R.K.; Shankar, S. Sulforaphane regulates self-renewal of pancreatic cancer stem cells through the modulation of Sonic hedgehog-GLI pathway. *Mol. Cell Biochem.* **2013**, *373*, 217–227. [CrossRef] [PubMed]
84. Li, Q.Q.; Xie, Y.K.; Wu, Y.; Li, L.L.; Liu, Y.; Miao, X.B.; Liu, Q.Z.; Yao, K.T.; Xiao, G.H. Sulforaphane inhibits cancer stem-like cell properties and cisplatin resistance through miR-214-mediated downregulation of c-MYC in non-small cell lung cancer. *Oncotarget* **2017**, *8*, 12067–12080. [CrossRef] [PubMed]
85. Castro, N.P.; Rangel, M.C.; Merchant, A.S.; MacKinnon, G.M.; Cuttitta, F.; Salomon, D.S.; Kim, Y.S. Sulforaphane suppresses the growth of triple-negative breast cancer stem-like cells in vitro and in vivo. *Cancer Prev. Res.* **2019**. [CrossRef] [PubMed]
86. Yun, J.H.; Kim, K.A.; Yoo, G.; Kim, S.Y.; Shin, J.M.; Kim, J.H.; Jung, S.H.; Kim, J.; Nho, C.W. Phenethyl isothiocyanate suppresses cancer stem cell properties in vitro and in a xenograft model. *Phytomedicine* **2017**, *30*, 42–49. [CrossRef] [PubMed]
87. Zhang, Q.; Li, X.T.; Chen, Y.; Chen, J.Q.; Zhu, J.Y.; Meng, Y.; Wang, X.Q.; Li, Y.; Geng, S.S.; Xie, C.F.; et al. Wnt/β-catenin signaling mediates the suppressive effects of diallyl trisulfide on colorectal cancer stem cells. *Cancer Chemother. Pharmacol.* **2018**, *81*, 969–977. [CrossRef] [PubMed]
88. Li, X.; Meng, Y.; Xie, C.; Zhu, J.; Wang, X.; Li, Y.; Geng, S.; Wu, J.; Zhong, C.; Li, M. Diallyl Trisulfide inhibits breast cancer stem cells via suppression of Wnt/β-catenin pathway. *J. Cell Biochem.* **2018**, *119*, 4134–4141. [CrossRef] [PubMed]
89. Kapinova, A.; Stefanicka, P.; Kubatka, P.; Zubor, P.; Uramova, S.; Kello, M.; Mojzis, J.; Blahutova, D.; Qaradakhi, T.; Zulli, A.; et al. Are plant-based functional foods better choice against cancer than single phytochemicals? A critical review of current breast cancer research. *Biomed. Pharmacother.* **2017**, *96*, 1465–1477. [CrossRef] [PubMed]
90. Kim, Y.M.; Kim, I.H.; Nam, T.J. Capsosiphon fulvescens glycoprotein inhibits AGS gastric cancer cell proliferation by downregulating Wnt-1 signaling. *Int. J. Oncol.* **2013**, *43*, 1395–1401. [CrossRef] [PubMed]
91. Kubatka, P.; Kello, M.; Kajo, K.; Kruzliak, P.; Výbohová, D.; Mojžiš, J.; Adamkov, M.; Fialová, S.; Veizerová, L.; Zulli, A.; et al. Oregano demonstrates distinct tumour-suppressive effects in the breast carcinoma model. *Eur. J. Nutr.* **2017**, *56*, 1303–1316. [CrossRef] [PubMed]
92. Kubatka, P.; Uramova, S.; Kello, M.; Kajo, K.; Kruzliak, P.; Mojzis, J.; Vybohova, D.; Adamkov, M.; Jasek, K.; Lasabova, Z.; et al. Antineoplastic effects of clove buds (Syzygium aromaticum L.) in the model of breast carcinoma. *J. Cell Mol. Med.* **2017**, *21*, 2837–2851. [CrossRef] [PubMed]
93. Mandal, A.; Bhatia, D.; Bishayee, A. Anti-Inflammatory Mechanism Involved in Pomegranate-Mediated Prevention of Breast Cancer: The Role of NF-κB and Nrf2 Signaling Pathways. *Nutrients* **2017**, *9*, E436. [CrossRef] [PubMed]
94. Mandal, A.; Bishayee, A. Trianthema portulacastrum Linn. displays anti-inflammatory responses during chemically induced rat mammary tumorigenesis through simultaneous and differential regulation of NF-κB and Nrf2 signaling pathways. *Int J. Mol. Sci.* **2015**, *16*, 2426–2445. [CrossRef] [PubMed]
95. Dong, R.; Chen, P.; Chen, Q. Extract of the Medicinal Plant Pao Pereira Inhibits Pancreatic Cancer Stem-Like Cell In Vitro and In Vivo. *Integr. Cancer Ther.* **2018**, *17*, 1204–1215. [CrossRef] [PubMed]
96. Dong, R.; Chen, P.; Chen, Q. Inhibition of pancreatic cancer stem cells by Rauwolfia vomitoria extract. *Oncol. Rep.* **2018**, *40*, 3144–3154. [CrossRef] [PubMed]
97. Zhang, Y.; Chen, S.; Wei, C.; Rankin, G.O.; Ye, X.; Chen, Y.C. Dietary compound proanthocyanidins from Chinese bayberry (Myrica rubra Sieb. et Zucc.) leaves attenuate chemotherapy-resistant ovarian cancer stem cell traits via targeting the Wnt/β-catenin signaling pathway and inducing G1 cell cycle arrest. *Food Funct.* **2018**, *9*, 525–533. [CrossRef] [PubMed]

98. Aravindan, S.; Ramraj, S.K.; Somasundaram, S.T.; Herman, T.S.; Aravindan, N. Polyphenols from marine brown algae target radiotherapy-coordinated EMT and stemness-maintenance in residual pancreatic cancer. *Stem Cell Res. Ther.* **2015**, *6*, 182. [CrossRef] [PubMed]
99. Yen, CH.; Lai, C.C.; Shia, T.H.; Chen, M.; Yu, H.C.; Liu, Y.P.; Chang, F.R. Gynura divaricata attenuates tumor growth and tumor relapse after cisplatin therapy in HCC xenograft model through suppression of cancer stem cell growth and Wnt/β-catenin signalling. *J. Ethnopharmacol.* **2018**, *213*, 366–375. [CrossRef] [PubMed]
100. Reddivari, L.; Charepalli, V.; Radhakrishnan, S.; Vadde, R.; Elias, R.J.; Lambert, J.D.; Vanamala, J.K. Grape compounds suppress colon cancer stem cells in vitro and in a rodent model of colon carcinogenesis. *BMC Complement. Altern. Med.* **2016**, *16*, 278. [CrossRef] [PubMed]
101. Nguyen, A.V.; Martinez, M.; Stamos, M.J.; Moyer, M.P.; Planutis, K.; Hope, C.; Holcombe, R.F. Results of a phase I pilot clinical trial examining the effect of plant-derived resveratrol and grape powder on Wnt pathway target gene expression in colonic mucosa and colon cancer. *Cancer Manag. Res.* **2009**, *1*, 25–37, PMC3004662. [PubMed]
102. Messing, E.; Gee, J.R.; Saltzstein, D.R.; Kim, K.; diSant'Agnese, A.; Kolesar, J.; Harris, L.; Faerber, A.; Havighurst, T.; Young, J.M.; et al. A phase 2 cancer chemoprevention biomarker trial of isoflavone G-2535 (genistein) in presurgical bladder cancer patients. *Cancer Prev. Res.* **2012**, *5*, 621–630. [CrossRef] [PubMed]
103. Nuñez-Sánchez, M.A.; González-Sarrías, A.; García-Villalba, R.; Monedero-Saiz, T.; García-Talavera, N.V.; Gómez-Sánchez, M.B.; Sánchez-Álvarez, C.; García-Albert, A.M.; Rodríguez-Gil, F.J.; Ruiz-Marín, M.; et al. Gene expression changes in colon tissues from colorectal cancer patients following the intake of an ellagitannin-containing pomegranate extract: A randomized clinical trial. *J. Nutr. Biochem.* **2017**, *42*, 126–133. [CrossRef] [PubMed]
104. ClinicalTrials.gov. Available online: https://clinicaltrials.gov/ (accessed on 28 January 2019).

molecules

MDPI

Review

Potential of Zerumbone as an Anti-Cancer Agent

Sosmitha Girisa [1], Bano Shabnam [1], Javadi Monisha [1], Lu Fan [2], Clarissa Esmeralda Halim [2], Frank Arfuso [3], Kwang Seok Ahn [4,*], Gautam Sethi [2,*] and Ajaikumar B. Kunnumakkara [1,*]

[1] Cancer Biology Laboratory, DBT-AIST International Laboratory for Advanced Biomedicine (DAILAB), Department of Biosciences & Bioengineering, Indian Institute of Technology, Guwahati, Assam 781039, India; sosmi176106101@iitg.ac.in (S.G.); bano176106104@iitg.ac.in (B.S.); j.monisha@iitg.ernet.in (J.M.)

[2] Department of Pharmacology, Yong Loo Lin School of Medicine, National University of Singapore, Singapore 117600, Singapore; phcfanl@nus.edu.sg (L.F.); phsceh@nus.edu.sg (C.E.H.)

[3] Stem Cell and Cancer Biology Laboratory, School of Pharmacy and Biomedical Sciences, Curtin Health Innovation Research Institute, Curtin University, Perth, WA 6102, Australia; frank.arfuso@curtin.edu.au

[4] College of Korean Medicine, Kyung Hee University, 24 Kyungheedae-ro, Dongdaemun-gu, Seoul 02447, Korea

* Correspondence: ksahn@khu.ac.kr (K.S.A.); phcgs@nus.edu.sg (G.S.); kunnumakkara@iitg.ac.in or ajai78@gmail.com (A.B.K.); Tel.: +82-2-961-2316 (K.S.A.); +65-6516-3267 (G.S.); +91-361-258-2231 (A.B.K.); Fax: +65-6873-7690 (G.S.); +91-361-258-2249 (A.B.K.)

Academic Editor: Roberto Fabiani
Received: 21 December 2018; Accepted: 16 February 2019; Published: 18 February 2019

Abstract: Cancer is still a major risk factor to public health globally, causing approximately 9.8 million deaths worldwide in 2018. Despite advances in conventional treatment modalities for cancer treatment, there are still few effective therapies available due to the lack of selectivity, adverse side effects, non-specific toxicities, and tumour recurrence. Therefore, there is an immediate need for essential alternative therapeutics, which can prove to be beneficial and safe against cancer. Various phytochemicals from natural sources have been found to exhibit beneficial medicinal properties against various human diseases. Zerumbone is one such compound isolated from *Zingiber zerumbet* Smith that possesses diverse pharmacological properties including those of antioxidant, antibacterial, antipyretic, anti-inflammatory, immunomodulatory, as well as anti-neoplastic. Zerumbone has shown its anti-cancer effects by causing significant suppression of proliferation, survival, angiogenesis, invasion, and metastasis through the molecular modulation of different pathways such as NF-κB, Akt, and IL-6/JAK2/STAT3 (interleukin-6/janus kinase-2/signal transducer and activator of transcription 3) and their downstream target proteins. The current review briefly summarizes the modes of action and therapeutic potential of zerumbone against various cancers.

Keywords: zerumbone; cancer; apoptosis; NF-κB; IL-6/JAK2/STAT3; Akt; FOXO1

1. Introduction

Cancer is a serious health problem globally and is the second leading cause of death [1–5]. The risk factors for cancer mortality may be due to behavioural and environmental factors such diet, exposure to air pollution, use of addictive substances, lack of physical activity, etc. [6]. The recent targeted therapies for cancer are associated with non-specific toxicities, exhibit limited efficacy, and are expensive to use [7]. Also, one of the major drawbacks of anti-cancer drugs has been the lack of selectivity, and thus they can exert adverse effects on the healthy tissues and organs [8]. Furthermore, conventional chemotherapeutics are also associated with the development of chemoresistance [9–12]. Overall, most cancer treatment strategies are associated with side effects, lack of selectivity, toxicity,

and development of chemoresistance, leading to high mortality and poor prognosis [7–13]. Herbs, vegetables, fruits, spices, cereals, pulses, and nuts have been shown to produce a large number of phytochemicals that exert chemopreventive and therapeutic properties against various human ailments [14–29]. Since ancient times, plants and plant-based compounds have been extensively used in tribal and folklore medicine due to their beneficial pharmacological properties and fewer side effects [20,30–32]. One such plant-derived compound is zerumbone (Figure 1), extracted from the traditional plant *Zingiber zerumbet* Smith, which is also known as bitter ginger, shampoo ginger, and pinecone ginger [33–38].

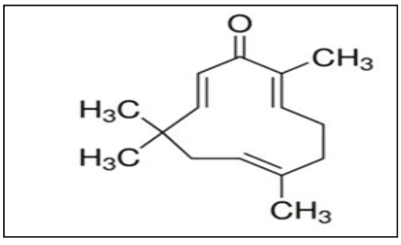

Figure 1. Structure of zerumbone [38].

Traditionally, the rhizomes of *Z. zerumbet* are widely used as a food flavouring agent and appetizer in various cuisines; it is also used in herbal folk medicine and pain relief [37–40]. Zerumbone is known for its biomedical properties such as being antioxidant, antibacterial, antipyretic, antinociceptive, anti-hypersensitive, anti-inflammatory, as well as possessing hepatoprotective, and immunomodulatory activities [16,17,41–44]. Besides the aforementioned properties, zerumbone can also function as an antitumor drug exhibiting its diverse effects on proliferation, angiogenesis, and apoptosis against various cancer cell lines, which has drawn the attention of many researchers [45–47]. Zerumbone (2,6,9,9-tetramethyl-(2*E*,6*E*,10*E*)-cycloundeca-2,6,10-trien-1-one) is a crystalline sesquiterpene compound containing an 11-membered ring with three double bonds at C6, C2, and C10, forming part of a cross-conjugated ketone system that participates in its biological activity [48–51]. A number of prior studies have elaborated upon the potential anti-allergic, immunomodulatory, and anti-cancer properties of zerumbone. The present review summarizes the anti-cancer properties of zerumbone along with its mode of actions and molecular targets in different cancer types.

2. Molecular Targets of Zerumbone against Cancer

It is now well established that cancer arises as a result of dysregulation of multiple cellular pathways. Therefore, multi-targeted compounds have high potential in the prevention and treatment of cancer [2,5,18,26,52–58]. Increasing lines of evidence suggest that zerumbone can act on multiple pathways and can suppress the growth of cancer cells. With regard to this, in melanoma zerumbone treatment downregulated Bcl-2 (B-cell lymphoma 2), upregulated Bax (BCL2 associated X protein), cytochrome c gene-related proteins, and activated caspase-3 [59]. In addition, zerumbone decreased cell viability through the downregulation of cyclin B1, cyclin-dependent kinase (CDK)-1, Cdc25C, and Cdc25B, and induced apoptosis by significantly activating Bax and Bak proteins in breast cancer [60]. Moreover, zerumbone downregulated CXCR4 expression on human-epidermal growth factor receptor-2 (HER2)-overexpressing breast cancer cells by abrogating NF-κB activation which correlated with the arrest of invasion and metastasis induced by CXCL12 expression [61]. In addition, zerumbone could also activate caspase-3 and poly (ADP-ribose) polymerase (PARP) production and reduced Akt phosphorylation, which increased cell death induction in glioblastoma [62]. Further, the treatment of zerumbone on mouse epidermal JB6 cells can induce an increase in NF-E2-related factor 2(Nrf2) nuclear translocation complemented by the upregulation of heme oxygenase-1 (HO-1),

causing Nrf2 to bind directly to the antioxidant response element, and thus exert chemopreventive effects against mouse skin carcinogenesis [63]. In addition, zerumbone inhibited breast cancer and multiple myeloma-induced osteoclast formation through suppression of activated IkappaBalpha (IκBα) kinase (IKK), IκBα phosphorylation, and IκBα degradation, which led to the abrogation of receptor activator of nuclear factor kappa-B ligand (RANKL)-induced NF-κB activation, which serves as a major mediator for bone resorption [64]. Zerumbone could also induce apoptosis in leukemic cells through the initiation of the cleavage of Bid, Bax, and Mcl-1 proteins, loss of the mitochondrial transmembrane potential, and activation of caspase-3 and -9, leading to degradation of PARP [65].

Natural products possess several properties, which enable them to fight against various cancer cell types [34,66]. Zerumbone possesses antiproliferative properties against various cancers such as brain, breast, cervical, colon, liver, lung, pancreas, and skin cancer [3,67]. The reported anti-tumour activities of zerumbone against different malignancies are briefly summarized below.

2.1. Zerumbone and Brain Tumor

Brain tumors are the leading cause of cancer-related death in children [68,69]. The incidence of primary malignant brain tumours is increasing, of which 80% consist of high-grade malignant tumors such as glioblastoma multiforme (GBM) [70]. Prior studies have reported that treatment with zerumbone suppressed FOXO1 and Akt phosphorylation due to inactivation of IKKα while activating caspase-3 protein and PARP, which resulted in decreased cell viability, and induction of apoptosis in GBM cells [62].

2.2. Zerumbone and Breast Cancer

Breast cancer is the most common and highly complex cancer associated with poorest clinical outcome in women worldwide [71–76]. Among the various subtypes, triple-negative breast cancer (TNBC) is the most aggressive form and, occurs in young age pre-menopausal women [77,78]. Triple-negative breast cancer fails to express the estrogen receptor (ER), human-epidermal growth factor receptor-2 (HER2) proteins, and progesterone receptor (PR) [77]. Zerumbone was found to increase the induction of presenilin-1 protein and transcriptional activation of Notch, leading to cleavage of Notch2. In addition, there was a reduction in cleaved Notch1 and Notch4 proteins, which resulted in increased apoptosis and suppression of cellular migration [79]. Zerumbone also decreased the levels of IL-8 and MMP-3 expression through the downregulation of NF-κB activity, which led to reduction in IL-1β-induced cell migration and invasion in TNBC [72,80]. Zerumbone induced G(2)/M cell arrest and Bax/Bak-mediated apoptosis [60]. Zerumbone also inhibited invasion and metastasis in breast cancer by downregulating the expression of CXCR4 [61]. Further, zerumbone suppressed TGF-β1-induced FN, MMP-2, and MMP-9 expression through the decreased phosphorylation of TGF-β1-induced Smad3, and also inhibited Ki67 expression [77].

Further, in mouse xenografts, zerumbone treatment was noted to reduce the tumor growth [60]. In addition, zerumbone decreased breast cancer-associated osteolysis in athymic nude mice with MDA-MB-231 breast cancer [64]. The mice treated with 20 mg/kg of zerumbone were observed to develop significantly smaller tumors than the control group treated with vehicle. Thus, zerumbone mitigated the tumorigenicity by reducing tumor volume and weight, and metastasis in xenograft models of TNBC [77].

2.3. Zerumbone and Colorectal Cancer

Colorectal cancer (CRC) is the third-leading cause of cancer-related deaths after lung and breast cancer [81,82]. Zerumbone inhibited the proliferation of colon cancer cells and thereby induced apoptosis, which might be due to mitochondria transmembrane dysfunction, translocation of phosphatidylserine, and chromatin condensation [83]. Zerumbone downregulated the expression of FLICE-like inhibitory protein (cFLIP); and in the presence of both Bax and p21, stimulated tumor necrosis factor-related apoptosis-inducing ligand (TRAIL) death receptor (DR)4 and

DR5, which intensified TRAIL-induced apoptosis in human HCT116 colon cancer cells, thus resulting in the enhanced anticancer effects of TRAIL [84]. Zerumbone pre-treatment inhibited the expression of radiation-induced DNA repair proteins ataxia-telangiectasia mutated (ATM) and DNA-PKcs through glutathione (GSH) depletion, leading to cell cycle arrest (G2/M) and increase in apoptosis, thus enhancing radiosentitivity of CRC cells [82]. Zerumbone induced IL-1β pathways through the expression of interleukin (IL)-1α, IL-1β, IL-6, and tumor necrosis factor (TNF)-α, which might be associated with the activation of c-Jun N-terminal kinase and extracellular signal-regulated protein kinase [85]. Further, zerumbone treatment on HCT-116 and SW48 cells showed its anti-metastatic potential through the inhibition of Fak/PI3k/NF-κB-uPA pathway [86].

Oral administration of zerumbone at 100, 250, and 500 ppm for the duration of 17 weeks to the mice significantly inhibited the multiplicity and inflammation in colonic adenocarcinomas through the repression of NF-κB and heme oxygenase (HO)-1, which resulted in suppression of the proliferation and induction of apoptosis [87].

2.4. Zerumbone and Cholangiocarcinoma

Cholangiocarcinoma (CCA) is an aggressive and deadly malignant tumor arising in the bile duct epithelial cells [88–90]. It is characterized by a high degree of genetic instability contributing to a heterogeneous malignant phenotype, and this variation is related to the distribution of different risk factors [91,92]. Surgical resection continues to be the best therapeutic approach for patients with CCA. Nevertheless, it is often associated with poor prognosis, and due to lack of early diagnostic evidence, most patients are not suitable for surgery [93]. The inhibition of CDK-2, CDK-5 or EGFR could result in reduction in CCA cell proliferation, and previous reports have revealed the overexpression of CDK-2, CDK-5 or EGFR in CCA. Molecular docking studies have demonstrated that derivatives of zerumbone with the presence of amine, epoxyamine, hydroxylamine, and nitrile groups can exhibit potent anti-cancer activities against CCA cells by interacting with the molecular target EGFR, but not CDK-2, CDK-5, and GSK-3. The derivative with the presence of an amine group has shown higher potency against proliferation of cancer cells through the inhibition of EGFR [49].

2.5. Zerumbone and Gastric Cancer

Gastric cancer is the fourth most common malignant tumor and second main cause of cancer deaths in both sexes worldwide [13,94–98]. Zerumbone could induce apoptosis in gastric cancer cells by blocking the activity of cyclophilin A and subsequently promoting mitochondrial pathway-mediated apoptosis. The mitochondrial pathway caused cyt C release from the mitochondria into the cytoplasm, leading to caspase-3 activation, which acted as an effector molecule for caspase-dependent apoptosis [13]. In addition, zerumbone caused inhibition of cell proliferation and tube formation area of human umbilical vein endothelial cells through the reduction in expression of vascular endothelial growth factor (VEGF) and NF-κB activities, and thereby inhibiting angiogenesis [99].

2.6. Zerumbone and Leukemia

Leukemia is the most common cancer that occurs in the blood forming tissues [5,100]. Zerumbone was reported to reduce the proliferation of leukemic cells by inducing G2/M cell cycle arrest through suppression of cyclin B1/cdk 1 protein along with the phosphorylation of ATM/Chk1/Chk2, followed by apoptosis via initiation of Fas (CD95)/Fas Ligand (CD95L) expression associated with caspase-8 activation [65,101]. Analogous to the abovementioned anti-proliferative effects, the use of a zerumbone-loaded nanostructured lipid carrier (NLC) arrested Jurkat cells in the G2/M phase via inactivation of cyclin B1 protein and activation of intrinsic apoptotic proteins (i.e., caspase-3 and caspase-9), and release of cytochrome c with subsequent cleavage of PARP [102,103]. Zerumbone-NLC also induced activation of the mitochondrial-dependent apoptotic pathway in murine leukemic cells [104]. Zerumbone inhibited K562 chronic myelogenous leukemic cell proliferation and colony formation, with induction of DNA damage and mitochondria mediated apoptosis through

the activation of pro-caspase-3, -9, and PARP cleavage, with an increase in free intracellular Ca^{2+}, ROS, and soluble histone-H2AX (H2A histone family member X) upregulation [105]. Additionally, zerumbone exerted a cytotoxic effect against CEM-ss leukemic cells by producing characteristics of apoptosis such as membrane blebbing, holes, and cytoplasmic extrusions [100].

2.7. Zerumbone and Liver Cancer

Hepatocellular carcinoma (HCC) is one of the most prevalent and highly aggressive liver malignancy [106–114]. Zerumbone has been shown to cause the inhibition of HCC cells proliferation by G2-M cell cycle arrest through the inhibition of PI3K/AKT/mTOR and signal transducer and activator of transcription 3 (STAT3) signalling pathways leading to the induction of apoptosis [115]. Zerumbone also inhibited the proliferation and migration of a liver cancer HepG2 cell line by significantly decreasing the expression of the MMP-9, VEGF, and VEGF receptor proteins in a dose-dependent manner [116]. Further, zerumbone exhibited also induced apoptosis via upregulation of Bax and suppression of Bcl-2 protein expression on HepG2 cells [117]. In line with the above, zerumbone treatment in DEN/AAF (diethylnitrosamine/2-acetylaminofluorene) rat livers induced mitochondria-regulated apoptosis by increasing Bax and decreasing Bcl-2 protein expression, along with a reduction of oxidative stress and an inhibition of proliferation, and thereby minimizing DEN/AAF-induced carcinogenesis [67]. Zerumbone can activate the Nrf2/ARE-dependent detoxification pathway induced by nuclear localization of Nrf2, which can bind to the antioxidant response element of the phase II enzyme genes, thereby suggesting an antioxidant role of zerumbone in neutralizing lipid peroxidation in liver cells to put a stop to cancer [48]. A soluble complex of zerumbone with hydroxypropyl-β-cyclodextrin (HP-β-CD) induced apoptosis and G2/M arrest along with the release of cytochrome c and loss of mitochondrial membrane potential, with a significant increase in caspase 3/7, caspase 9, and caspase 8, and with the depletion of BID that is cleaved by caspase 8 [118].

2.8. Zerumbone and Lung Cancer

Lung cancer is one of the most common malignancies and leading cause of cancer-related death worldwide [119–122]. About 80% of diagnosed lung cancer is non-small cell lung cancer (NSCLC), which ranks top in both incidence and mortality [123,124]. Zerumbone induces apoptosis through loss of mitochondrial membrane potential, release of cytochrome c, caspase-9 and -3 activation, increased expression of p53 and Bax, and increased ROS production, and zerumbone also sensitized NSCLC cells to cisplatin [125].

Further, dietary administration of zerumbone at 250 and 500 ppm to the mice for 21 weeks was found to significantly inhibit the multiplicity of lung cancer in a dose-dependent manner. The suppression of lung carcinogenesis was caused through the reduction of growth, decreased inflammation, and decreased expression of NF-κB and HO-1, thereby causing apoptosis [87].

2.9. Zerumbone and Oral Cancer

Oral cancer is a serious cancer in developing countries and many parts of the globe, with varying incidence rate according to geographic regions [126,127]. It affects approximately 274,000 people worldwide annually and the pattern of use of tobacco products usually marks the frequency of occurrence [128]. Zerumbone treatment inhibited cell proliferation, migration, and invasion in oral squamous cell carcinoma by suppressing the expression of CXCR4, RhoA proteins, and PI3K-mTOR signalling pathway, causing G2/M cell cycle arrest followed by apoptotic activity. The inhibition of the PI3K-mTOR signalling pathway was associated with the suppression of Akt and S6 proteins [129].

2.10. Zerumbone and Cervical and Ovarian Cancer

Cervical cancer ranks as the second most common cause of cancer death among women [130]. Zerumbone along with cisplatin treatment can stimulate apoptosis by arresting cells at the G2/M

phase and decreasing the levels of IL-6 in HeLa and Caov-3 cells [131]. Zerumbone also downregulated the expression of proliferating cellular nuclear antigen, thus revealing its antitumor effect on human cervical cancer cells [132]. Similarly, zerumbone can induce apoptosis by causing regression of cervical intraepithelial neoplasia (CIN) tissues in female Balb/c mice treated with diethylstilbestrol, which showed an effect resembling that of cisplatin, through the modulation of Bax and Bcl-2 genes [130]. Zerumbone showed its cytotoxic property on HeLa cells by increasing cellular caspase-3 levels and producing distinct morphological features of apoptotic death such as nuclear and chromatin condensation, cell shrinkage, membrane blebbing, abnormalities of mitochondrial cristae, multinucleation, and formation of apoptotic bodies [133].

Also, the combination of zerumbone with cisplatin has been shown to cause regression of (CIN) via modulation of the IL-6 level in the serum of female Balb/c mice. Four groups of mice were taken for the treatment along with a group with no treatment from 52 days of age to 60 days of age with four dosages on alternate days. Group 1 mice were treated with 0.9% normal saline for the positive control while group 2 and group 3 mice were administered with 8 mg/kg and 16 mg/kg of zerumbone, respectively. The mice representing group 4 was treated with 10 mg/kg while group 5 was given no treatment to act as a negative control. Both the compounds, at their mentioned effective dosages were able to regress the progression of cancerous cervix tissues [130].

2.11. Zerumbone and Pancreatic Cancer

Pancreatic carcinoma is a common cancer with a gradual increase in incidence rate [134]. Treatment of pancreatic cancer cells with zerumbone inhibited tube formation of human umbilical vein endothelial cells through the suppression of mRNA expression and proteins associated with angiogenic function and NF-κB activity [135]. Further, zerumbone reduced cell viability and induced apoptosis in PANC-1 cells, as evidenced the upregulated expression of p53, p21 protein, and elevated ROS levels [134]. In addition, zerumbone caused downregulation in the expression of CXCR4, which correlated with suppression of CXCL12-induced invasion [61].

2.12. Zerumbone and Prostate Cancer

Prostate cancer is the one of the most common causes of malignancy in males, and is without curative options in the advanced state [136–143]. Pre-treatment of prostate cancer cells with zerumbone significantly decreased the radiation-induced expression of phosphorylated ATM (ataxia telangiectasia-mutated) and suppressed the expression of JAK2 and STAT3, which are involved in DNA damage repair [144]. In addition, zerumbone selectively inhibited the IL-6/JAK2/STAT3 pathway and blocked the prostate cancer-associated genes- cyclin D1, IL-6, COX2 (cytochrome c oxidase), and ETS Variant 1 (ETV1); thereby inducing cytotoxicity through G0/G1 cell cycle arrest and causing apoptosis [145]. Zerumbone also attenuated microtubule assembly and induced endoplasmic reticulum (ER) stress and MMP-2 expression in prostate cancer cells and upregulated the expression of GRP-78 and C/EBP homologous protein (CHOP)/ growth arrest and DNA damage 153 (GADD153). An increase in intracellular Ca^{2+} levels potentially acted as a crosstalk marker between this ER stress and mitochondrial insult, which was associated with the formation of the active calpain I fragment. Zerumbone also induced apoptosis and autophagy through the caspase-dependent pathway and LC3-II formation [43].

2.13. Zerumbone and Renal Cell Carcinoma

Renal cell carcinoma (RCC) is a malignant disease insensitive to conventional treatments, contributing >90% of the most common form of kidney cancer [146,147]. Zerumbone showed its anti-cancer effects by initiating apoptosis through the activation of caspase-3 and caspase-9, leading to cleavage of PARP and downregulation of Gli-1 and Bcl-2 [146]. In addition, zerumbone could induce the expression of tyrosine phosphatase SHP-1(Src homology region 2 domain-containing

phosphatase-1), which has been associated with inhibition of STAT3 activation thereby resulting in the suppression of the gene products that are involved with proliferation, survival, and angiogenesis.

In line with the above, similar abrogation of STAT3 activation was exhibited in tumor growth and tissues upon administration of zerumbone in athymic nu/nu mice with an RCC xenograft. For this, the tumor tissues were treated with vehicle and 50 mg/kg body weight of zerumbone for 6-week duration and substantial inhibition of STAT3 activation was noted [148].

2.14. Zerumbone and Skin Cancer

Skin cancer is the most commonly diagnosed cancer that begins with an abnormal growth in the epidermal layer, and can be classified as melanoma and non-melanoma skin cancer [149]. Pre-treatment with zerumbone at the tumor promotion stage in mice suppressed tumor growth and the mechanism behind its effect might be due to increased expression of xenobiotic-metabolizing enzymes (GSTP1, NQO1) and mRNA levels for manganese superoxide dismutase (MnSOD) and glutathione peroxidase-1 (GPx1). In addition, zerumbone decreased the levels of cyclooxygenase-2 (COX-2) expression, ERK1 phosphorylation, H_2O_2-induced edema formation, and leukocyte infiltration [150].

Further, treatment of epidermal cells with zerumbone in mice enhanced the binding property of Nrf2 to the antioxidant element, which resulted in increased HO-1 activity, thus providing a basis for the reported antioxidant effects of this agent against skin carcinogenesis [63].

3. Cytotoxicity Data

The cytotoxicity data has been analyzed for both the in vitro and in vivo studies. The treatment of zerumbone on various cancers was reported to be effective in various in vitro studies. For the liver cancer, the IC_{50} of zerumbone in HepG2 cells was reported to be 6.20 µg/mL [116]. While the IC_{50} for cervical cancer in Hela cells was reported to be 6.4 µg/mL, and in breast cancer cell lines (MCF-7 and MDA-MB 231) 23.0 µg/mL and 24.3 µg/mL respectively [151]. In case of the in vivo studies, zerumbone suppressed the tumor growth and volume in different cancers with different dosage rates. In line with this, the treatment of zerumbone for a 6-week duration caused tumor growth inhibition in renal cancer model, the dosage was five times a week with 50 mg/kg body weight. The treatment also showed less substantial toxic effects as it did not cause weight loss in treated mice [148] while in cervical cancer models different groups were administered with 4 mg/kg, 8 mg/kg, and 16 mg/kg of zerumbone respectively. No remarkable regression of the CIN lesions was observed with 4 mg/kg dosage as compared to the later dosages. The dosage of 8 mg/kg showed antiproliferative properties while 16 mg/kg showed decreased in CIN lesions [130]. The dosage of zerumbone in breast cancer can also be compared where the mice models were treated with 20 mg/kg of zerumbone which resulted to smaller tumors than the control group treated with vehicle. The weight level of tumor in zerumbone treated mice was lesser with 1.22 ± 0.35 g as compared to the mice treated with vehicle that weighed 2.56 ± 0.68 g [77]. In case of colon and lung cancer studies, the mice models were injected with azoxymethane (10 mg/kg bw), promoted by 1.5% dextran sulphate sodium in drinking water for 7 days to initiate colon tumour while the other models were injected with 4-(methylnitrosamino)-1-(3-pyridyl)-1-butanone (10 micromol/mouse) to induce lung tumor. Both the tumor models were later administered with zerumbone at 100, 250, and 500 ppm for 17 weeks and 21 weeks, respectively, that resulted in inhibition of multiplicity the cancers [87].

4. Limitation and Future Prospects

Various potential studies of zerumbone against different tumor cell lines have been reported. However, most of the reports are mainly confined to in vitro studies. Few in vivo model studies are reported in only few cancers such as breast, colorectal, cervical, lung, renal cell carcinoma, and skin cancers. Also, relevant clinical trials to test the safety and efficacy of zerumbone are not available. The limitations in clinical studies might be due to few in vivo model findings. Further, the pharmacokinetic properties such as solubility, distribution, etc. of the compound should be

analysed properly. A previous study that aimed to enhance the solubility of zerumbone was explored to analyse its interaction with hydroxypropyl-β-cyclodextrin (HPβCD) in aqueous media where it was showed that the solubility of zerumbone substantially increased with an augmentation in the concentration of HPβCD at 20 °C thereby suggesting that this complexation can be used in this drug formulation [50].

Therefore, apart from in vitro and in vivo studies, the pharmacokinetic properties of zerumbone can be investigated and established, and also clinical trial studies can be carried out further to validate its therapeutic application in cancer patients.

5. Conclusions

Despite the advancement in treatment methods, cancer is still one of the deadliest diseases causing havoc to human health. Most of the treatment methods available are less effective and often associated with severe side effects and emergence of chemoresistance. Therefore, it is essential to discover a new alternate, safe, and efficacious treatment method against cancer. Zerumbone, a monocyclic sesquiterpene, isolated from *Z. zerumbet* is a compound that has been reported for its diverse anti-cancer properties mediated by suppression of proliferation, induction of cell cycle arrest, and apoptosis in various cancers such as those of brain, breast, colon, liver, and lung through the modulation of various proteins and signalling pathways (Table 1). With regard to this, various in vitro studies have shown that zerumbone can downregulate the expression CXCR4, activation of NF-κB, and other oncogenic proteins. Additionally, zerumbone can also repress the IL-6/JAK2/STAT3, PI3K/AKT/mTOR pathways, and expression of associated genes such as *cyclin D1*, *IL-6*, *COX2*, and *ETV1*, thus inhibiting proliferation and angiogenic activity by increasing cell cycle arrest and apoptosis. Moreover in preclinical studies, administration of zerumbone in various mouse models was observed to tumor growth and metastasis. However, despite the availability of many pre-clinical studies on the anti-cancer properties of zerumbone, clinical trials with this compound have been rarely reported. Therefore, more preclinical studies would be required to establish clinical results and a better therapeutic potential of zerumbone, to target cancer.

Table 1. Possible role of zerumbone against various cancers.

Cancer	In Vitro/In Vivo	Model	Mechanism of Action	Reference
Breast cancer	In vitro	MDA-MB-231, MDA-MB-468, MDA-MB-361, T-47D	↓CD1d	[152]
	In vitro	MCF7, Hs578T, MDA-MB231	↓IL-1β	[72]
	In vitro	HCC1806	↓TGF-β1	[77]
	In vitro	SKBR3, MDA-MB468	↓CD44, ↓STAT-3	[71]
	In vitro	MCF-7, MDA-MB-231	↓Notch4	[79]
	In vitro	Hs578T, MDA-MB231	↓IL-8, ↓MMP-3	[80]
	In vitro	MDA-MB-231, MCF-7	↑Bax, ↑Bak	[60]
	In vivo	Mouse	↓Tumor growth	[60]
	In vitro	MDA-MB-231, U266	↓NF-κB	[64]
	In vivo	Athymic mice	↓Osteolysis	[64]
Cervical cancer	In vitro	HeLa, H9c2	↑Caspase 3	[8]
	In vivo	female BALB/c mice	↓Neoplasia	[133]
	In vivo	female BALB/c mice	↑apoptosis	[130]
Colon cancer	In vitro	Caco-2, Colo320DM, HT-29	↑IL-6	[85]
	In vitro	HCT116	↓TNF-α	[40]
	In vitro	HCT116	↑DR5, DR4, Caspase-8	[84]
	In vitro	HCT-116, SW-48	↓β-catenin	[153]
	In vitro	SW480	↑caspase 3, ↑caspase 8, ↑caspase 9	[3]
	In vitro	HCT116	↓GSH	[82]
	In vivo	Mice	↓multiplicity of adenomas	[87]
Gastric cancer	In vitro	SGC-7901	↓Bcl-2	[13]
	In vitro	MKN1, MKN28, MKN45, MKN74, NUGC4, AGS	↓NF-κB	[99]
Liver cancer	In vitro	HepG2	↑Bax	[117]
	In vitro	HepG2	↑p27, ↑Cyt-c, ↑caspase-3 & caspase-9	[154]
	In vitro	HepG2	↓VEGF, ↓MMP-9	[116]
	In vitro	HepG2, Hep3B, Sk-Hep-1, SNU-182, SNU-449	↓PI3K/AKT/mTOR, ↓STAT-3	[115]
	In vitro	HepG2	↑Cell cycle arrest	[155]
Leukemia	In vitro	CEM-ss	↑Caspase-3	[100]
Lung Cancer	In vitro	A549	↓FAK/AKT/ROCK	[38]
	In vitro	A549, NCI-H460	↑p53	[125]
	In vivo	Mice	↓Carcinogenesis	[87]
Oral cancer	In vitro	OSCC	↓PI3K-mTOR	[129]
Pancreatic cancer	In vitro	PaCa	↓NF-κB	[135]

Table 1. *Cont.*

Cancer	In Vitro/In Vivo	Model	Mechanism of Action	Reference
	In vitro	PANC-1, SW1990	↑ROS	[134]
Prostate cancer	In vitro	PC3, DU145	↓Phosphorylated ATM	[144]
	In vitro	DU145, PC3	↓JAK2/STAT3	[145]
Renal cell carcinoma	In vitro	786-0,769-P	↓Gli-1/Bcl-2	[146]
	In vivo	Athymic nu/nu mice	↓STAT3, ↓Tumor growth	[148]
Skin cancer	In vitro	CHL-1	↑ROS	[156]
	In vitro	A375	↓Bcl-2	[59]

Author Contributions: S.G., B.S., J.M., A.B.K., and G.S. conceived the project and wrote the article. F.A., L.F., C.E.H., K.S.A. edited the manuscript. G.S., A.B.K., and K.S.A. carried out the overall supervision of work. All authors read and approved the final version of manuscript.

Funding: A.B.K. received funding (DBT/UXEL/2017) from the Department of Biotechnology, Government of India.

Conflicts of Interest: The authors declare no conflicts of interest.

Abbreviations

ATM	Ataxia-telangiectasia mutated
Bcl-2	B-cell lymphoma- 2
Bak	Bcl-2 homologous antagonist/killer
Bax	BCL2-associated X protein
CD1d	Cluster of differentiation 1
CD44	Cluster of differentiation 44
DR	Death receptor
Gli 1	Glioma-associated oncogene 1
GSH	Glutathione
IL-6	Interleukin 6
IL-8	Interleukin 8
IL-1β	Interleukin 1 beta
JAK2	Janus kinase 2
MMP-3	matrix metalloproteinase-3
MMP-9	Matrix metallopeptidase 9
mTOR	Mammalian target of rapamycin
NF-κB	nuclear factor kappa light chain enhancer of activated B cells
OSCC	Oral squamous cell carcinoma
ROCK	Rho-associated protein kinase
ROS	Reactive oxygen species
STAT-3	Signal transducer and activator of transcription 3
TGF-β1	Transforming growth factor beta 1
TNFα	Tumour necrosis factor alpha
VEGF	Vascular endothelial growth factor

References

1. Husain, I.; Ahmad, R.; Chandra, A.; Raza, S.T.; Shukla, Y.; Mahdi, F. Phytochemical characterization and biological activity evaluation of ethanolic extract of Cinnamomum zeylanicum. *J. Ethnopharmacol.* **2018**, *219*, 110–116. [CrossRef] [PubMed]
2. Khwairakpam, A.D.; Bordoloi, D.; Thakur, K.K.; Monisha, J.; Arfuso, F.; Sethi, G.; Mishra, S.; Kumar, A.P.; Kunnumakkara, A.B. Possible use of Punica granatum (Pomegranate) in cancer therapy. *Pharmacol. Res.* **2018**, *133*, 53–64. [CrossRef] [PubMed]
3. Sithara, T.; Dhanya, B.P.; Arun, K.B.; Sini, S.; Dan, M.; Kokkuvayil Vasu, R.; Nisha, P. Zerumbone, a Cyclic Sesquiterpene from *Zingiber zerumbet* Induces Apoptosis, Cell Cycle Arrest, and Antimigratory Effects in SW480 Colorectal Cancer Cells. *J. Agric. Food Chem.* **2018**, *66*, 602–612. [CrossRef] [PubMed]
4. Siegel, R.L.; Miller, K.D.; Jemal, A. Cancer statistics, 2018. *CA Cancer J. Clin.* **2018**, *68*, 7–30. [CrossRef]
5. Ranaware, A.M.; Banik, K.; Deshpande, V.; Padmavathi, G.; Roy, N.K.; Sethi, G.; Fan, L.; Kumar, A.P.; Kunnumakkara, A.B. Magnolol: A Neolignan from the Magnolia Family for the Prevention and Treatment of Cancer. *Int. J. Mol. Sci.* **2018**, *19*, 2362. [CrossRef] [PubMed]
6. Weiderpass, E. Lifestyle and cancer risk. *J. Prev. Med. Public Health = Yebang Uihakhoe Chi* **2010**, *43*, 459–471. [CrossRef] [PubMed]

7. Kunnumakkara, A.B.; Nair, A.S.; Ahn, K.S.; Pandey, M.K.; Yi, Z.; Liu, M.; Aggarwal, B.B. Gossypin, a pentahydroxy glucosyl flavone, inhibits the transforming growth factor β-activated kinase-1-mediated NF-κB activation pathway, leading to potentiation of apoptosis, suppression of invasion, and abrogation of osteoclastogenesis. *Blood* **2007**, *109*, 5112–5121, Erratum in **2013**, *122*, 1327–1328. [CrossRef]
8. Saranya, J.; Dhanya, B.P.; Greeshma, G.; Radhakrishnan, K.V.; Priya, S. Effects of a new synthetic zerumbone pendant derivative (ZPD) on apoptosis induction and anti-migratory effects in human cervical cancer cells. *Chem. Biol. Interact.* **2017**, *278*, 32–39. [CrossRef] [PubMed]
9. Roy, N.K.; Deka, A.; Bordoloi, D.; Mishra, S.; Kumar, A.P.; Sethi, G.; Kunnumakkara, A.B. The potential role of boswellic acids in cancer prevention and treatment. *Cancer Lett.* **2016**, *377*, 74–86. [CrossRef] [PubMed]
10. Monisha, J.; Padmavathi, G.; Roy, N.K.; Deka, A.; Bordoloi, D.; Anip, A.; Kunnumakkara, A.B. NF-κB Blockers Gifted by Mother Nature: Prospectives in Cancer Cell Chemosensitization. *Curr. Pharm. Des.* **2016**, *22*, 4173–4200. [CrossRef] [PubMed]
11. Banik, K.; Harsha, C.; Bordoloi, D.; Lalduhsaki Sailo, B.; Sethi, G.; Leong, H.C.; Arfuso, F.; Mishra, S.; Wang, L.; Kumar, A.P.; et al. Therapeutic potential of gambogic acid, a caged xanthone, to target cancer. *Cancer Lett.* **2018**, *416*, 75–86. [CrossRef] [PubMed]
12. Monisha, J.; Roy, N.K.; Padmavathi, G.; Banik, K.; Bordoloi, D.; Khwairakpam, A.D.; Arfuso, F.; Chinnathambi, A.; Alahmadi, T.A.; Alharbi, S.A.; et al. NGAL is Downregulated in Oral Squamous Cell Carcinoma and Leads to Increased Survival, Proliferation, Migration and Chemoresistance. *Cancers* **2018**, *10*, 228. [CrossRef] [PubMed]
13. Wang, D.; Li, Y.; Cui, P.; Zhao, Q.; Tan, B.B.; Zhang, Z.D.; Liu, Y.; Jia, N. Zerumbone induces gastric cancer cells apoptosis: Involving cyclophilin A. *Biomed. Pharmacother. = Biomed. Pharmacother.* **2016**, *83*, 740–745. [CrossRef]
14. Aggarwal, B.B.; Kunnumakkara, A.B.; Harikumar, K.B.; Tharakan, S.T.; Sung, B.; Anand, P. Potential of spice-derived phytochemicals for cancer prevention. *Planta Med.* **2008**, *74*, 1560–1569. [CrossRef] [PubMed]
15. Sung, B.; Prasad, S.; Yadav, V.R.; Aggarwal, B.B. Cancer cell signaling pathways targeted by spice-derived nutraceuticals. *Nutr. Cancer* **2012**, *64*, 173–197. [CrossRef] [PubMed]
16. Hemn, H.O.; Hazilawati, H.; Noordin, M.M.; Heshu, S.R.; Zuki, A. Influence of Zerumbone Supplementation a Natural Dietary Product from *Zingiber zerumbet* smith on Early-Developed Atherosclerotic Lesions in Cholesterol-Fed Rabbits. *Open Conf. Proc. J.* **2013**, *4*, 61–64. [CrossRef]
17. Ghasemzadeh, A.; Jaafar, H.Z.; Rahmat, A.; Swamy, M.K. Optimization of microwave-assisted extraction of zerumbone from *Zingiber zerumbet* L. rhizome and evaluation of antiproliferative activity of optimized extracts. *Chem. Cent. J.* **2017**, *11*, 5. [CrossRef] [PubMed]
18. Sailo, B.L.; Banik, K.; Padmavathi, G.; Javadi, M.; Bordoloi, D.; Kunnumakkara, A.B. Tocotrienols: The promising analogues of vitamin E for cancer therapeutics. *Pharmacol. Res.* **2018**, *130*, 259–272. [CrossRef]
19. Deorukhkar, A.; Krishnan, S.; Sethi, G.; Aggarwal, B.B. Back to basics: How natural products can provide the basis for new therapeutics. *Expert Opin. Investig. Drugs* **2007**, *16*, 1753–1773. [CrossRef]
20. Yang, S.F.; Weng, C.J.; Sethi, G.; Hu, D.N. Natural bioactives and phytochemicals serve in cancer treatment and prevention. *Evid. Based Complement. Altern. Med.* **2013**, *2013*, 698190. [CrossRef]
21. Tang, C.H.; Sethi, G.; Kuo, P.L. Novel medicines and strategies in cancer treatment and prevention. *BioMed Res. Int.* **2014**, *2014*, 474078. [CrossRef]
22. Hsieh, Y.S.; Yang, S.F.; Sethi, G.; Hu, D.N. Natural bioactives in cancer treatment and prevention. *BioMed Res. Int.* **2015**, *2015*, 182835. [CrossRef] [PubMed]
23. Yarla, N.S.; Bishayee, A.; Sethi, G.; Reddanna, P.; Kalle, A.M.; Dhananjaya, B.L.; Dowluru, K.S.; Chintala, R.; Duddukuri, G.R. Targeting arachidonic acid pathway by natural products for cancer prevention and therapy. *Semin. Cancer Biol.* **2016**, *40–41*, 48–81. [CrossRef] [PubMed]
24. Hasanpourghadi, M.; Looi, C.Y.; Pandurangan, A.K.; Sethi, G.; Wong, W.F.; Mustafa, M.R. Phytometabolites Targeting the Warburg Effect in Cancer Cells: A Mechanistic Review. *Curr. Drug Targets* **2017**, *18*, 1086–1094. [CrossRef] [PubMed]
25. Shanmugam, M.K.; Warrier, S.; Kumar, A.P.; Sethi, G.; Arfuso, F. Potential Role of Natural Compounds as Anti-Angiogenic Agents in Cancer. *Curr. Vasc. Pharmacol.* **2017**, *15*, 503–519. [CrossRef] [PubMed]
26. Kunnumakkara, A.B.; Sailo, B.L.; Banik, K.; Harsha, C.; Prasad, S.; Gupta, S.C.; Bharti, A.C.; Aggarwal, B.B. Chronic diseases, inflammation, and spices: How are they linked? *J. Transl. Med.* **2018**, *16*, 14. [CrossRef] [PubMed]

27. Tewari, D.; Nabavi, S.F.; Nabavi, S.M.; Sureda, A.; Farooqi, A.A.; Atanasov, A.G.; Vacca, R.A.; Sethi, G.; Bishayee, A. Targeting activator protein 1 signaling pathway by bioactive natural agents: Possible therapeutic strategy for cancer prevention and intervention. *Pharmacol. Res.* **2018**, *128*, 366–375. [CrossRef] [PubMed]
28. Kunnumakkara, A.B.; Bordoloi, D.; Harsha, C.; Banik, K.; Gupta, S.C.; Aggarwal, B.B. Curcumin mediates anticancer effects by modulating multiple cell signaling pathways. *Clin. Sci.* **2017**, *131*, 1781–1799. [CrossRef]
29. Kashyap, D.; Sharma, A.; Tuli, H.S.; Sak, K.; Garg, V.K.; Buttar, H.S.; Setzer, W.N.; Sethi, G. Apigenin: A natural bioactive flavone-type molecule with promising therapeutic function. *J. Funct. Foods* **2018**, *48*, 457–471. [CrossRef]
30. Zakaria, Z.A.; Mohamad, A.S.; Chear, C.T.; Wong, Y.Y.; Israf, D.A.; Sulaiman, M.R. Antiinflammatory and antinociceptive activities of *Zingiber zerumbet* methanol extract in experimental model systems. *Med Princ. Pract.* **2010**, *19*, 287–294. [CrossRef]
31. Rajan, I.; Rabindran, R.; Nithya, N.; Lakshmipriya, T.; Jayasree, P.R.; Kumar, P.R. Assessment of cell cycle phase-specific effects of zerumbone on mitotically synchronous surface cultures of Physarum polycephalum. *Protoplasma* **2014**, *251*, 931–941. [CrossRef] [PubMed]
32. Wang, L.; Phan, D.D.; Zhang, J.; Ong, P.S.; Thuya, W.L.; Soo, R.; Wong, A.L.; Yong, W.P.; Lee, S.C.; Ho, P.C.; et al. Anticancer properties of nimbolide and pharmacokinetic considerations to accelerate its development. *Oncotarget* **2016**, *7*, 44790–44802. [CrossRef] [PubMed]
33. Tan, J.W.; Israf, D.A.; Tham, C.L. Major Bioactive Compounds in Essential Oils Extracted From the Rhizomes of *Zingiber zerumbet* (L) Smith: A Mini-Review on the Anti-allergic and Immunomodulatory Properties. *Front. Pharmacol.* **2018**, *9*, 652. [CrossRef] [PubMed]
34. Prasannan, R.; Kalesh, K.A.; Shanmugam, M.K.; Nachiyappan, A.; Ramachandran, L.; Nguyen, A.H.; Kumar, A.P.; Lakshmanan, M.; Ahn, K.S.; Sethi, G. Key cell signaling pathways modulated by zerumbone: Role in the prevention and treatment of cancer. *Biochem. Pharmacol.* **2012**, *84*, 1268–1276. [CrossRef] [PubMed]
35. Kitayama, T. Attractive reactivity of a natural product, zerumbone. *Biosci. Biotechnol. Biochem.* **2011**, *75*, 199–207. [CrossRef] [PubMed]
36. Gupta, S.C.; Kim, J.H.; Prasad, S.; Aggarwal, B.B. Regulation of survival, proliferation, invasion, angiogenesis, and metastasis of tumor cells through modulation of inflammatory pathways by nutraceuticals. *Cancer Metastasis Rev.* **2010**, *29*, 405–434. [CrossRef] [PubMed]
37. Haque, M.A.; Jantan, I.; Arshad, L.; Bukhari, S.N.A. Exploring the immunomodulatory and anticancer properties of zerumbone. *Food Funct.* **2017**, *8*, 3410–3431. [CrossRef] [PubMed]
38. Kang, C.G.; Lee, H.J.; Kim, S.H.; Lee, E.O. Zerumbone Suppresses Osteopontin-Induced Cell Invasion Through Inhibiting the FAK/AKT/ROCK Pathway in Human Non-Small Cell Lung Cancer A549 Cells. *J. Nat. Prod.* **2016**, *79*, 156–160. [CrossRef] [PubMed]
39. Fusi, F.; Durante, M.; Sgaragli, G.; Khanh, P.N.; Son, N.T.; Huong, T.T.; Huong, V.N.; Cuong, N.M. In vitro vasoactivity of zerumbone from *Zingiber zerumbet*. *Planta Med.* **2015**, *81*, 298–304. [CrossRef] [PubMed]
40. Singh, S.P.; Nongalleima, K.; Singh, N.I.; Doley, P.; Singh, C.B.; Singh, T.R.; Sahoo, D. Zerumbone reduces proliferation of HCT116 colon cancer cells by inhibition of TNF-alpha. *Sci. Rep.* **2018**, *8*, 4090. [CrossRef]
41. Rahman, H.S.; Rasedee, A.; How, C.W.; Abdul, A.B.; Zeenathul, N.A.; Othman, H.H.; Saeed, M.I.; Yeap, S.K. Zerumbone-loaded nanostructured lipid carriers: Preparation, characterization, and antileukemic effect. *Int. J. Nanomed.* **2013**, *8*, 2769–2781. [CrossRef] [PubMed]
42. Rahman, H.S.; Rasedee, A.; Yeap, S.K.; Othman, H.H.; Chartrand, M.S.; Namvar, F.; Abdul, A.B.; How, C.W. Biomedical properties of a natural dietary plant metabolite, zerumbone, in cancer therapy and chemoprevention trials. *BioMed Res. Int.* **2014**, *2014*, 920742. [CrossRef] [PubMed]
43. Chan, M.L.; Liang, J.W.; Hsu, L.C.; Chang, W.L.; Lee, S.S.; Guh, J.H. Zerumbone, a ginger sesquiterpene, induces apoptosis and autophagy in human hormone-refractory prostate cancers through tubulin binding and crosstalk between endoplasmic reticulum stress and mitochondrial insult. *Naunyn-Schmiedeberg's Arch. Pharmacol.* **2015**, *388*, 1223–1236. [CrossRef] [PubMed]
44. Singh, Y.P.; Girisa, S.; Banik, K.; Ghosh, S.; Swathi, P.; Deka, M.; Padmavathi, G.; Kotoky, J.; Sethi, G.; Fan, L.; et al. Potential application of zerumbone in the prevention and therapy of chronic human diseases. *J. Funct. Foods* **2019**, *53*, 248–258. [CrossRef]
45. Kirana, C.; McIntosh, G.H.; Record, I.R.; Jones, G.P. Antitumor activity of extract of Zingiber aromaticum and its bioactive sesquiterpenoid zerumbone. *Nutr. Cancer* **2003**, *45*, 218–225. [CrossRef]

46. Kalantari, K.; Moniri, M.; Boroumand Moghaddam, A.; Abdul Rahim, R.; Bin Ariff, A.; Izadiyan, Z.; Mohamad, R. A Review of the Biomedical Applications of Zerumbone and the Techniques for Its Extraction from Ginger Rhizomes. *Molecules* **2017**, *22*, 1645. [CrossRef]
47. Leung, W.S.; Yang, M.L.; Lee, S.S.; Kuo, C.W.; Ho, Y.C.; Huang-Liu, R.; Lin, H.W.; Kuan, Y.H. Protective effect of zerumbone reduces lipopolysaccharide-induced acute lung injury via antioxidative enzymes and Nrf2/HO-1 pathway. *Int. Immunopharmacol.* **2017**, *46*, 194–200. [CrossRef]
48. Nakamura, Y.; Yoshida, C.; Murakami, A.; Ohigashi, H.; Osawa, T.; Uchida, K. Zerumbone, a tropical ginger sesquiterpene, activates phase II drug metabolizing enzymes. *FEBS Lett.* **2004**, *572*, 245–250. [CrossRef]
49. Songsiang, U.; Pitchuanchom, S.; Boonyarat, C.; Hahnvajanawong, C.; Yenjai, C. Cytotoxicity against cholangiocarcinoma cell lines of zerumbone derivatives. *Eur. J. Med. Chem.* **2010**, *45*, 3794–3802. [CrossRef]
50. Eid, E.E.M.; Abdul, A.B.; Suliman, F.E.O.; Sukari, M.A.; Rasedee, A.; Fatah, S.S. Characterization of the inclusion complex of zerumbone with hydroxypropyl-β-cyclodextrin. *Carbohydr. Polym.* **2011**, *83*, 1707–1714. [CrossRef]
51. Kalesh, K.A.; Clulow, J.A.; Tate, E.W. Target profiling of zerumbone using a novel cell-permeable clickable probe and quantitative chemical proteomics. *Chem. Commun.* **2015**, *51*, 5497–5500. [CrossRef] [PubMed]
52. Shanmugam, M.K.; Kannaiyan, R.; Sethi, G. Targeting cell signaling and apoptotic pathways by dietary agents: Role in the prevention and treatment of cancer. *Nutr. Cancer* **2011**, *63*, 161–173. [CrossRef] [PubMed]
53. Aggarwal, B.B.; Sethi, G.; Baladandayuthapani, V.; Krishnan, S.; Shishodia, S. Targeting cell signaling pathways for drug discovery: An old lock needs a new key. *J. Cell. Biochem.* **2007**, *102*, 580–592. [CrossRef] [PubMed]
54. Parikh, N.R.; Mandal, A.; Bhatia, D.; Siveen, K.S.; Sethi, G.; Bishayee, A. Oleanane triterpenoids in the prevention and therapy of breast cancer: Current evidence and future perspectives. *Phytochem. Rev. Proc. Phytochem. Soc. Eur.* **2014**, *13*, 793–810. [CrossRef] [PubMed]
55. Kanchi, M.M.; Shanmugam, M.K.; Rane, G.; Sethi, G.; Kumar, A.P. Tocotrienols: The unsaturated sidekick shifting new paradigms in vitamin E therapeutics. *Drug Discov. Today* **2017**, *22*, 1765–1781. [CrossRef]
56. Ko, J.H.; Sethi, G.; Um, J.Y.; Shanmugam, M.K.; Arfuso, F.; Kumar, A.P.; Bishayee, A.; Ahn, K.S. The Role of Resveratrol in Cancer Therapy. *Int. J. Mol. Sci.* **2017**, *18*, 2589. [CrossRef]
57. Shanmugam, M.K.; Arfuso, F.; Kumar, A.P.; Wang, L.; Goh, B.C.; Ahn, K.S.; Bishayee, A.; Sethi, G. Modulation of diverse oncogenic transcription factors by thymoquinone, an essential oil compound isolated from the seeds of *Nigella sativa* Linn. *Pharmacol. Res.* **2018**, *129*, 357–364. [CrossRef]
58. Sethi, G.; Shanmugam, M.K.; Warrier, S.; Merarchi, M.; Arfuso, F.; Kumar, A.P.; Bishayee, A. Pro-Apoptotic and Anti-Cancer Properties of Diosgenin: A Comprehensive and Critical Review. *Nutrients* **2018**, *10*, 645. [CrossRef] [PubMed]
59. Wang, S.D.; Wang, Z.H.; Yan, H.Q.; Ren, M.Y.; Gao, S.Q.; Zhang, G.Q. Chemotherapeutic effect of Zerumbone on melanoma cells through mitochondria-mediated pathways. *Clin. Exp. Dermatol.* **2016**, *41*, 858–863. [CrossRef]
60. Sehrawat, A.; Arlotti, J.A.; Murakami, A.; Singh, S.V. Zerumbone causes Bax- and Bak-mediated apoptosis in human breast cancer cells and inhibits orthotopic xenograft growth in vivo. *Breast Cancer Res. Treat.* **2012**, *136*, 429–441. [CrossRef]
61. Sung, B.; Jhurani, S.; Ahn, K.S.; Mastuo, Y.; Yi, T.; Guha, S.; Liu, M.; Aggarwal, B.B. Zerumbone down-regulates chemokine receptor CXCR4 expression leading to inhibition of CXCL12-induced invasion of breast and pancreatic tumor cells. *Cancer Res.* **2008**, *68*, 8938–8944. [CrossRef] [PubMed]
62. Weng, H.Y.; Hsu, M.J.; Wang, C.C.; Chen, B.C.; Hong, C.Y.; Chen, M.C.; Chiu, W.T.; Lin, C.H. Zerumbone suppresses IKKalpha, Akt, and FOXO1 activation, resulting in apoptosis of GBM 8401 cells. *J. Biomed. Sci.* **2012**, *19*, 86. [CrossRef]
63. Shin, J.W.; Ohnishi, K.; Murakami, A.; Lee, J.S.; Kundu, J.K.; Na, H.K.; Ohigashi, H.; Surh, Y.J. Zerumbone induces heme oxygenase-1 expression in mouse skin and cultured murine epidermal cells through activation of Nrf2. *Cancer Prev. Res.* **2011**, *4*, 860–870. [CrossRef] [PubMed]
64. Sung, B.; Murakami, A.; Oyajobi, B.O.; Aggarwal, B.B. Zerumbone abolishes RANKL-induced NF-κB activation, inhibits osteoclastogenesis, and suppresses human breast cancer-induced bone loss in athymic nude mice. *Cancer Res.* **2009**, *69*, 1477–1484. [CrossRef]

65. Xian, M.; Ito, K.; Nakazato, T.; Shimizu, T.; Chen, C.K.; Yamato, K.; Murakami, A.; Ohigashi, H.; Ikeda, Y.; Kizaki, M. Zerumbone, a bioactive sesquiterpene, induces G2/M cell cycle arrest and apoptosis in leukemia cells via a Fas- and mitochondria-mediated pathway. *Cancer Sci.* **2007**, *98*, 118–126. [CrossRef]
66. Matsuo, Y.; Takeyama, H. Zerumbone from Ginger (Monoterpenoid). *Enzymes* **2014**, *36*, 87–94. [CrossRef] [PubMed]
67. Taha, M.M.; Abdul, A.B.; Abdullah, R.; Ibrahim, T.A.; Abdelwahab, S.I.; Mohan, S. Potential chemoprevention of diethylnitrosamine-initiated and 2-acetylaminofluorene-promoted hepatocarcinogenesis by zerumbone from the rhizomes of the subtropical ginger (*Zingiber zerumbet*). *Chem. Biol. Interact.* **2010**, *186*, 295–305. [CrossRef] [PubMed]
68. Bousselham, A.; Bouattane, O.; Youssfi, M.; Raihani, A. Brain tumor temperature effect extraction from MRI imaging using bioheat equation. *Procedia Comput. Sci.* **2018**, *127*, 336–343. [CrossRef]
69. Guerreiro Stucklin, A.S.; Ramaswamy, V.; Daniels, C.; Taylor, M.D. Review of molecular classification and treatment implications of pediatric brain tumors. *Curr. Opin. Pediatr.* **2018**, *30*, 3–9. [CrossRef] [PubMed]
70. Kansal, A.R.; Torquato, S.; Harsh, G.I.; Chiocca, E.A.; Deisboeck, T.S. Simulated brain tumor growth dynamics using a three-dimensional cellular automaton. *J. Theor. Biol.* **2000**, *203*, 367–382. [CrossRef] [PubMed]
71. Kim, S.; Kil, W.H.; Lee, J.; Oh, S.J.; Han, J.; Jeon, M.; Jung, T.; Lee, S.K.; Bae, S.Y.; Lee, H.C.; et al. Zerumbone suppresses EGF-induced CD44 expression through the inhibition of STAT3 in breast cancer cells. *Oncol. Rep.* **2014**, *32*, 2666–2672. [CrossRef] [PubMed]
72. Jeon, M.; Han, J.; Nam, S.J.; Lee, J.E.; Kim, S. Elevated IL-1β expression induces invasiveness of triple negative breast cancer cells and is suppressed by zerumbone. *Chem. Biol. Interact.* **2016**, *258*, 126–133. [CrossRef] [PubMed]
73. Wang, C.; Kar, S.; Lai, X.; Cai, W.; Arfuso, F.; Sethi, G.; Lobie, P.E.; Goh, B.C.; Lim, L.H.K.; Hartman, M.; et al. Triple negative breast cancer in Asia: An insider's view. *Cancer Treat. Rev.* **2018**, *62*, 29–38. [CrossRef] [PubMed]
74. Jia, L.Y.; Shanmugam, M.K.; Sethi, G.; Bishayee, A. Potential role of targeted therapies in the treatment of triple-negative breast cancer. *Anti-Cancer Drugs* **2016**, *27*, 147–155. [CrossRef] [PubMed]
75. Bhuvanalakshmi, G.; Basappa; Rangappa, K.S.; Dharmarajan, A.; Sethi, G.; Kumar, A.P.; Warrier, S. Breast Cancer Stem-Like Cells Are Inhibited by Diosgenin, a Steroidal Saponin, by the Attenuation of the Wnt β-Catenin Signaling via the Wnt Antagonist Secreted Frizzled Related Protein-4. *Front. Pharmacol.* **2017**, *8*, 124. [CrossRef] [PubMed]
76. Yuan, Y.; Anbalagan, D.; Lee, L.H.; Samy, R.P.; Shanmugam, M.K.; Kumar, A.P.; Sethi, G.; Lobie, P.E.; Lim, L.H. ANXA1 inhibits miRNA-196a in a negative feedback loop through NF-kB and c-Myc to reduce breast cancer proliferation. *Oncotarget* **2016**, *7*, 27007–27020. [CrossRef] [PubMed]
77. Kim, S.; Lee, J.; Jeon, M.; Lee, J.E.; Nam, S.J. Zerumbone suppresses the motility and tumorigenecity of triple negative breast cancer cells via the inhibition of TGF-β1 signaling pathway. *Oncotarget* **2016**, *7*, 1544–1558. [CrossRef] [PubMed]
78. Thakur, K.K.; Bordoloi, D.; Kunnumakkara, A.B. Alarming Burden of Triple-Negative Breast Cancer in India. *Clin. Breast Cancer* **2018**, *18*, e393–e399. [CrossRef]
79. Sehrawat, A.; Sakao, K.; Singh, S.V. Notch2 activation is protective against anticancer effects of zerumbone in human breast cancer cells. *Breast Cancer Res. Treat.* **2014**, *146*, 543–555. [CrossRef] [PubMed]
80. Han, J.; Bae, S.Y.; Oh, S.J.; Lee, J.; Lee, J.H.; Lee, H.C.; Lee, S.K.; Kil, W.H.; Kim, S.W.; Nam, S.J.; et al. Zerumbone suppresses IL-1β-induced cell migration and invasion by inhibiting IL-8 and MMP-3 expression in human triple-negative breast cancer cells. *Phytother. Res.* **2014**, *28*, 1654–1660. [CrossRef] [PubMed]
81. Aggarwal, B.; Prasad, S.; Sung, B.; Krishnan, S.; Guha, S. Prevention and Treatment of Colorectal Cancer by Natural Agents From Mother Nature. *Curr. Colorectal Cancer Rep.* **2013**, *9*, 37–56. [CrossRef] [PubMed]
82. Deorukhkar, A.; Ahuja, N.; Mercado, A.L.; Diagaradjane, P.; Raju, U.; Patel, N.; Mohindra, P.; Diep, N.; Guha, S.; Krishnan, S. Zerumbone increases oxidative stress in a thiol-dependent ROS-independent manner to increase DNA damage and sensitize colorectal cancer cells to radiation. *Cancer Med.* **2015**, *4*, 278–292. [CrossRef] [PubMed]

83. Murakami, A.; Takahashi, D.; Kinoshita, T.; Koshimizu, K.; Kim, H.W.; Yoshihiro, A.; Nakamura, Y.; Jiwajinda, S.; Terao, J.; Ohigashi, H. Zerumbone, a Southeast Asian ginger sesquiterpene, markedly suppresses free radical generation, proinflammatory protein production, and cancer cell proliferation accompanied by apoptosis: The alpha,β-unsaturated carbonyl group is a prerequisite. *Carcinogenesis* **2002**, *23*, 795–802. [CrossRef]
84. Yodkeeree, S.; Sung, B.; Limtrakul, P.; Aggarwal, B.B. Zerumbone enhances TRAIL-induced apoptosis through the induction of death receptors in human colon cancer cells: Evidence for an essential role of reactive oxygen species. *Cancer Res.* **2009**, *69*, 6581–6589. [CrossRef]
85. Murakami, A.; Miyamoto, M.; Ohigashi, H. Zerumbone, an anti-inflammatory phytochemical, induces expression of proinflammatory cytokine genes in human colon adenocarcinoma cell lines. *Biofactors* **2004**, *21*, 95–101. [CrossRef]
86. Hosseini, N.; Khoshnazar, A.; Saidijam, M.; Azizi Jalilian, F.; Najafi, R.; Mahdavinezhad, A.; Ezati, R.; Sotanian, A.; Amini, R. Zerumbone Suppresses Human Colorectal Cancer Invasion and Metastasis via Modulation of FAk/PI3k/NFκB-uPA Pathway. *Nutr. Cancer* **2019**, 1–13. [CrossRef] [PubMed]
87. Kim, M.; Miyamoto, S.; Yasui, Y.; Oyama, T.; Murakami, A.; Tanaka, T. Zerumbone, a tropical ginger sesquiterpene, inhibits colon and lung carcinogenesis in mice. *Int. J. Cancer* **2009**, *124*, 264–271. [CrossRef] [PubMed]
88. Farooq, M.; Egan, J.B.; McDonald, B.; Markus, H.; Contente-Cuomo, T.; Fernandez-Zapico, M.; Vasmatzis, G.; Braggio, E.; Borad, M.J.; Murtaza, M. Detection of copy number aberrations in cholangiocarcinoma using shallow whole genome sequencing of plasma DNA. *J. Clin. Oncol.* **2018**, *36* (Suppl. 4), 293. [CrossRef]
89. Kitdumrongthum, S.; Metheetrairut, C.; Charoensawan, V.; Ounjai, P.; Janpipatkul, K.; Panvongsa, W.; Weerachayaphorn, J.; Piyachaturawat, P.; Chairoungdua, A. Dysregulated microRNA expression profiles in cholangiocarcinoma cell-derived exosomes. *Life Sci.* **2018**, *210*, 65–75. [CrossRef] [PubMed]
90. Xu, Y.; Yao, Y.; Zhong, X.; Leng, K.; Qin, W.; Qu, L.; Cui, Y.; Jiang, X. Downregulated circular RNA hsa_circ_0001649 regulates proliferation, migration and invasion in cholangiocarcinoma cells. *Biochem. Biophys. Res. Commun.* **2018**, *496*, 455–461. [CrossRef] [PubMed]
91. Shaib, Y.; El-Serag, H.B. The epidemiology of cholangiocarcinoma. *Semin. Liver Dis.* **2004**, *24*, 115–125. [CrossRef] [PubMed]
92. Bozko, P.; Scholta, T.; Bui, K.; Toulany, M.; Rodemann, H.; Malek, N. Notch1-Cyclin E-p27kip1 and RAD17 form a network of proteins which control cellular proliferation and DNA damage response in cholangiocarcinoma. *Z. Gastroenterol.* **2018**, *56*, A4.81. [CrossRef]
93. Qin, W.; Kang, P.; Xu, Y.; Leng, K.; Li, Z.; Huang, L.; Gao, J.; Cui, Y.; Zhong, X. Long non-coding RNA HOTAIR promotes tumorigenesis and forecasts a poor prognosis in cholangiocarcinoma. *Sci. Rep.* **2018**, *8*, 12176. [CrossRef] [PubMed]
94. Li, L.Q.; Pan, D.; Zhang, S.W.; Xie, D.; Zheng, X.L.; Chen, H. Autophagy regulates chemoresistance of gastric cancer stem cells via the Notch signaling pathway. *Eur. Rev. Med. Pharmacol. Sci.* **2018**, *22*, 3402–3407. [CrossRef] [PubMed]
95. Manu, K.A.; Shanmugam, M.K.; Ramachandran, L.; Li, F.; Fong, C.W.; Kumar, A.P.; Tan, P.; Sethi, G. First evidence that gamma-tocotrienol inhibits the growth of human gastric cancer and chemosensitizes it to capecitabine in a xenograft mouse model through the modulation of NF-κB pathway. *Clin. Cancer Res.* **2012**, *18*, 2220–2229. [CrossRef] [PubMed]
96. Manu, K.A.; Shanmugam, M.K.; Li, F.; Chen, L.; Siveen, K.S.; Ahn, K.S.; Kumar, A.P.; Sethi, G. Simvastatin sensitizes human gastric cancer xenograft in nude mice to capecitabine by suppressing nuclear factor-kappa B-regulated gene products. *J. Mol. Med.* **2014**, *92*, 267–276. [CrossRef]
97. Manu, K.A.; Shanmugam, M.K.; Ramachandran, L.; Li, F.; Siveen, K.S.; Chinnathambi, A.; Zayed, M.E.; Alharbi, S.A.; Arfuso, F.; Kumar, A.P.; et al. Isorhamnetin augments the anti-tumor effect of capeciatbine through the negative regulation of NF-κB signaling cascade in gastric cancer. *Cancer Lett.* **2015**, *363*, 28–36. [CrossRef] [PubMed]
98. Ramachandran, L.; Manu, K.A.; Shanmugam, M.K.; Li, F.; Siveen, K.S.; Vali, S.; Kapoor, S.; Abbasi, T.; Surana, R.; Smoot, D.T.; et al. Isorhamnetin inhibits proliferation and invasion and induces apoptosis through the modulation of peroxisome proliferator-activated receptor gamma activation pathway in gastric cancer. *J. Biol. Chem.* **2012**, *287*, 38028–38040. [CrossRef] [PubMed]

99. Tsuboi, K.; Matsuo, Y.; Shamoto, T.; Shibata, T.; Koide, S.; Morimoto, M.; Guha, S.; Sung, B.; Aggarwal, B.B.; Takahashi, H.; et al. Zerumbone inhibits tumor angiogenesis via NF-κB in gastric cancer. *Oncol. Rep.* **2014**, *31*, 57–64. [CrossRef]
100. Abdelwahab, S.I.; Abdul, A.B.; Mohan, S.; Taha, M.M.; Syam, S.; Ibrahim, M.Y.; Mariod, A.A. Zerumbone induces apoptosis in T-acute lymphoblastic leukemia cells. *Leuk. Res.* **2011**, *35*, 268–271. [CrossRef] [PubMed]
101. Huang, G.C.; Chien, T.Y.; Chen, L.G.; Wang, C.C. Antitumor effects of zerumbone from *Zingiber zerumbet* in P-388D1 cells in vitro and in vivo. *Planta Med.* **2005**, *71*, 219–224. [CrossRef] [PubMed]
102. Rahman, H.S.; Rasedee, A.; Abdul, A.B.; Zeenathul, N.A.; Othman, H.H.; Yeap, S.K.; How, C.W.; Hafiza, W.A. Zerumbone-loaded nanostructured lipid carrier induces G2/M cell cycle arrest and apoptosis via mitochondrial pathway in a human lymphoblastic leukemia cell line. *Int. J. Nanomed.* **2014**, *9*, 527–538. [CrossRef]
103. Rahman, H.S.; Rasedee, A.; Chartrand, M.S.; Othman, H.H.; Yeap, S.K.; Namvar, F. Zerumbone induces G2/M cell cycle arrest and apoptosis via mitochondrial pathway in Jurkat cell line. *Nat. Prod. Commun.* **2014**, *9*, 1237–1242. [PubMed]
104. Rahman, H.S.; Rasedee, A.; How, C.W.; Zeenathul, N.A.; Chartrand, M.S.; Yeap, S.K.; Abdul, A.B.; Tan, S.W.; Othman, H.H.; Ajdari, Z.; et al. Antileukemic effect of zerumbone-loaded nanostructured lipid carrier in WEHI-3B cell-induced murine leukemia model. *Int. J. Nanomed.* **2015**, *10*, 1649–1666. [CrossRef] [PubMed]
105. Rajan, I.; Jayasree, P.R.; Kumar, P.R. Zerumbone induces mitochondria-mediated apoptosis via increased calcium, generation of reactive oxygen species and upregulation of soluble histone H2AX in K562 chronic myelogenous leukemia cells. *Tumour Biol.* **2015**, *36*, 8479–8489. [CrossRef] [PubMed]
106. Sethi, G.; Chatterjee, S.; Rajendran, P.; Li, F.; Shanmugam, M.K.; Wong, K.F.; Kumar, A.P.; Senapati, P.; Behera, A.K.; Hui, K.M.; et al. Inhibition of STAT3 dimerization and acetylation by garcinol suppresses the growth of human hepatocellular carcinoma in vitro and in vivo. *Mol. Cancer* **2014**, *13*, 66. [CrossRef] [PubMed]
107. Siveen, K.S.; Ahn, K.S.; Ong, T.H.; Shanmugam, M.K.; Li, F.; Yap, W.N.; Kumar, A.P.; Fong, C.W.; Tergaonkar, V.; Hui, K.M.; et al. Y-tocotrienol inhibits angiogenesis-dependent growth of human hepatocellular carcinoma through abrogation of AKT/mTOR pathway in an orthotopic mouse model. *Oncotarget* **2014**, *5*, 1897–1911. [CrossRef] [PubMed]
108. Swamy, S.G.; Kameshwar, V.H.; Shubha, P.B.; Looi, C.Y.; Shanmugam, M.K.; Arfuso, F.; Dharmarajan, A.; Sethi, G.; Shivananju, N.S.; Bishayee, A. Targeting multiple oncogenic pathways for the treatment of hepatocellular carcinoma. *Target. Oncol.* **2017**, *12*, 1–10. [CrossRef]
109. Dai, X.; Wang, L.; Deivasigamni, A.; Looi, C.Y.; Karthikeyan, C.; Trivedi, P.; Chinnathambi, A.; Alharbi, S.A.; Arfuso, F.; Dharmarajan, A.; et al. A novel benzimidazole derivative, MBIC inhibits tumor growth and promotes apoptosis via activation of ROS-dependent JNK signaling pathway in hepatocellular carcinoma. *Oncotarget* **2017**, *8*, 12831–12842. [CrossRef]
110. Dai, X.; Ahn, K.S.; Wang, L.Z.; Kim, C.; Deivasigamni, A.; Arfuso, F.; Um, J.Y.; Kumar, A.P.; Chang, Y.C.; Kumar, D.; et al. Ascochlorin Enhances the Sensitivity of Doxorubicin Leading to the Reversal of Epithelial-to-Mesenchymal Transition in Hepatocellular Carcinoma. *Mol. Cancer Ther.* **2016**, *15*, 2966–2976. [CrossRef]
111. Dai, X.; Ahn, K.S.; Kim, C.; Siveen, K.S.; Ong, T.H.; Shanmugam, M.K.; Li, F.; Shi, J.; Kumar, A.P.; Wang, L.Z.; et al. Ascochlorin, an isoprenoid antibiotic inhibits growth and invasion of hepatocellular carcinoma by targeting STAT3 signaling cascade through the induction of PIAS3. *Mol. Oncol.* **2015**, *9*, 818–833. [CrossRef] [PubMed]
112. Mastron, J.K.; Siveen, K.S.; Sethi, G.; Bishayee, A. Silymarin and hepatocellular carcinoma: A systematic, comprehensive, and critical review. *Anti-Cancer Drugs* **2015**, *26*, 475–486. [CrossRef] [PubMed]
113. Subramaniam, A.; Loo, S.Y.; Rajendran, P.; Manu, K.A.; Perumal, E.; Li, F.; Shanmugam, M.K.; Siveen, K.S.; Park, J.I.; Ahn, K.S.; et al. An anthraquinone derivative, emodin sensitizes hepatocellular carcinoma cells to TRAIL induced apoptosis through the induction of death receptors and downregulation of cell survival proteins. *Apoptosis* **2013**, *18*, 1175–1187. [CrossRef] [PubMed]
114. Manu, K.A.; Shanmugam, M.K.; Ong, T.H.; Subramaniam, A.; Siveen, K.S.; Perumal, E.; Samy, R.P.; Bist, P.; Lim, L.H.; Kumar, A.P.; et al. Emodin suppresses migration and invasion through the modulation of CXCR4 expression in an orthotopic model of human hepatocellular carcinoma. *PLoS ONE* **2013**, *8*, e57015. [CrossRef] [PubMed]

115. Wani, N.A.; Zhang, B.; Teng, K.Y.; Barajas, J.M.; Motiwala, T.; Hu, P.; Yu, L.; Bruschweiler, R.; Ghoshal, K.; Jacob, S.T. Reprograming of Glucose Metabolism by Zerumbone Suppresses Hepatocarcinogenesis. *Mol. Cancer Res.* **2018**, *16*, 256–268. [CrossRef] [PubMed]
116. Samad, N.A.; Abdul, A.B.; Rahman, H.S.; Rasedee, A.; Tengku Ibrahim, T.A.; Keon, Y.S. Zerumbone Suppresses Angiogenesis in HepG2 Cells through Inhibition of Matrix Metalloproteinase-9, Vascular Endothelial Growth Factor, and Vascular Endothelial Growth Factor Receptor Expressions. *Pharmacogn. Mag.* **2018**, *13* (Suppl. 4), S731–S736. [CrossRef]
117. Sakinah, S.A.; Handayani, S.T.; Hawariah, L.P. Zerumbone induced apoptosis in liver cancer cells via modulation of Bax/Bcl-2 ratio. *Cancer Cell Int.* **2007**, *7*, 4. [CrossRef]
118. Muhammad Nadzri, N.; Abdul, A.B.; Sukari, M.A.; Abdelwahab, S.I.; Eid, E.E.; Mohan, S.; Kamalidehghan, B.; Anasamy, T.; Ng, K.B.; Syam, S.; et al. Inclusion Complex of Zerumbone with Hydroxypropyl-β-Cyclodextrin Induces Apoptosis in Liver Hepatocellular HepG2 Cells via Caspase 8/BID Cleavage Switch and Modulating Bcl2/Bax Ratio. *Evid. Based Complement. Altern. Med.* **2013**, *2013*, 810632. [CrossRef]
119. Lee, J.H.; Kim, C.; Sethi, G.; Ahn, K.S. Brassinin inhibits STAT3 signaling pathway through modulation of PIAS-3 and SOCS-3 expression and sensitizes human lung cancer xenograft in nude mice to paclitaxel. *Oncotarget* **2015**, *6*, 6386–6405. [CrossRef]
120. Ong, P.S.; Wang, L.; Chia, D.M.; Seah, J.Y.; Kong, L.R.; Thuya, W.L.; Chinnathambi, A.; Lau, J.Y.; Wong, A.L.; Yong, W.P.; et al. A novel combinatorial strategy using Seliciclib((R)) and Belinostat((R)) for eradication of non-small cell lung cancer via apoptosis induction and BID activation. *Cancer Lett.* **2016**, *381*, 49–57. [CrossRef]
121. Wang, L.; Syn, N.L.; Subhash, V.V.; Any, Y.; Thuya, W.L.; Cheow, E.S.H.; Kong, L.; Yu, F.; Peethala, P.C.; Wong, A.L.; et al. Pan-HDAC inhibition by panobinostat mediates chemosensitization to carboplatin in non-small cell lung cancer via attenuation of EGFR signaling. *Cancer Lett.* **2018**, *417*, 152–160. [CrossRef] [PubMed]
122. Ko, J.H.; Nam, D.; Um, J.Y.; Jung, S.H.; Sethi, G.; Ahn, K.S. Bergamottin Suppresses Metastasis of Lung Cancer Cells through Abrogation of Diverse Oncogenic Signaling Cascades and Epithelial-to-Mesenchymal Transition. *Molecules* **2018**, *23*, 1601. [CrossRef]
123. Chen, Y.; Ma, Z.; Shen, X.; Li, L.; Zhong, J.; Min, L.S.; Xu, L.; Li, H.; Zhang, J.; Dai, L. Serum Lipidomics Profiling to Identify Biomarkers for Non-Small Cell Lung Cancer. *BioMed Res. Int.* **2018**, *2018*, 5276240. [CrossRef] [PubMed]
124. Pan, Z.; Liu, L.; Nie, W.; Miggin, S.; Qiu, F.; Cao, Y.; Chen, J.; Yang, B.; Zhou, Y.; Lu, J.; et al. Long non-coding RNA AGER-1 functionally upregulates the innate immunity gene AGER and approximates its anti-tumor effect in lung cancer. *Mol. Carcinog.* **2018**, *57*, 305–318. [CrossRef]
125. Hu, Z.; Zeng, Q.; Zhang, B.; Liu, H.; Wang, W. Promotion of p53 expression and reactive oxidative stress production is involved in zerumbone-induced cisplatin sensitization of non-small cell lung cancer cells. *Biochimie* **2014**, *107 Pt B*, 257–262. [CrossRef]
126. Warnakulasuriya, S. Global epidemiology of oral and oropharyngeal cancer. *Oral Oncol.* **2009**, *45*, 309–316. [CrossRef] [PubMed]
127. Khwankong, S.; Sriplung, H.; Kerdpon, D. Knowledge and Health Belief Attitudes of Oral Cancer and Its Screening Among At-Risk Southern Thai Muslims. *J. Cancer Educ.* **2018**, *33*, 615–621. [CrossRef] [PubMed]
128. Proia, N.K.; Paszkiewicz, G.M.; Nasca, M.A.; Franke, G.E.; Pauly, J.L. Smoking and smokeless tobacco-associated human buccal cell mutations and their association with oral cancer—A review. *Cancer Epidemiol. Biomark. Prev.* **2006**, *15*, 1061–1077. [CrossRef] [PubMed]
129. Zainal, N.S.; Gan, C.P.; Lau, B.F.; Yee, P.S.; Tiong, K.H.; Abdul Rahman, Z.A.; Patel, V.; Cheong, S.C. Zerumbone targets the CXCR4-RhoA and PI3K-mTOR signaling axis to reduce motility and proliferation of oral cancer cells. *Phytomedicine* **2018**, *39*, 33–41. [CrossRef] [PubMed]
130. Abdelwahab, S.I.; Abdul, A.B.; Devi, N.; Taha, M.M.; Al-zubairi, A.S.; Mohan, S.; Mariod, A.A. Regression of cervical intraepithelial neoplasia by zerumbone in female Balb/c mice prenatally exposed to diethylstilboestrol: Involvement of mitochondria-regulated apoptosis. *Exp. Toxicol. Pathol.* **2010**, *62*, 461–469. [CrossRef]

131. Abdelwahab, S.I.; Abdul, A.B.; Zain, Z.N.; Hadi, A.H. Zerumbone inhibits interleukin-6 and induces apoptosis and cell cycle arrest in ovarian and cervical cancer cells. *Int. Immunopharmacol.* **2012**, *12*, 594–602. [CrossRef] [PubMed]
132. Abdul, A.B.; Abdelwahab, S.I.; Bin Jalinas, J.; Al-Zubairi, A.S.; Taha, M.M. Combination of zerumbone and cisplatin to treat cervical intraepithelial neoplasia in female BALB/c mice. *Int. J. Gynecol. Cancer* **2009**, *19*, 1004–1010. [CrossRef] [PubMed]
133. Abdel Wahab, S.I.; Abdul, A.B.; Alzubairi, A.S.; Mohamed Elhassan, M.; Mohan, S. In vitro ultramorphological assessment of apoptosis induced by zerumbone on (HeLa). *J. Biomed. Biotechnol.* **2009**, *2009*, 769568. [CrossRef] [PubMed]
134. Zhang, S.; Liu, Q.; Liu, Y.; Qiao, H.; Liu, Y. Zerumbone, a Southeast Asian Ginger Sesquiterpene, Induced Apoptosis of Pancreatic Carcinoma Cells through p53 Signaling Pathway. *Evid. Based Complement. Altern. Med.* **2012**, *2012*, 936030. [CrossRef] [PubMed]
135. Shamoto, T.; Matsuo, Y.; Shibata, T.; Tsuboi, K.; Nagasaki, T.; Takahashi, H.; Funahashi, H.; Okada, Y.; Takeyama, H. Zerumbone inhibits angiogenesis by blocking NF-κB activity in pancreatic cancer. *Pancreas* **2014**, *43*, 396–404. [CrossRef]
136. Lin, C.J.; Lo, U.G.; Hsieh, J.T. The regulatory pathways leading to stem-like cells underlie prostate cancer progression. *Asian J. Androl.* **2018**. [CrossRef]
137. Zainfeld, D.; Goldkorn, A. Liquid Biopsy in Prostate Cancer: Circulating Tumor Cells and Beyond. *Cancer Treat. Res.* **2018**, *175*, 87–104. [CrossRef] [PubMed]
138. Zhang, J.; Ahn, K.S.; Kim, C.; Shanmugam, M.K.; Siveen, K.S.; Arfuso, F.; Samym, R.P.; Deivasigamanim, A.; Lim, L.H.; Wang, L.; et al. Nimbolide-Induced Oxidative Stress Abrogates STAT3 Signaling Cascade and Inhibits Tumor Growth in Transgenic Adenocarcinoma of Mouse Prostate Model. *Antioxid. Redox Signal.* **2016**, *24*, 575–589. [CrossRef] [PubMed]
139. Zhang, J.; Sikka, S.; Siveen, K.S.; Lee, J.H.; Um, J.Y.; Kumar, A.P.; Chinnathambi, A.; Alharbi, S.A.; Basappa; Rangappa, K.S.; et al. Cardamonin represses proliferation, invasion, and causes apoptosis through the modulation of signal transducer and activator of transcription 3 pathway in prostate cancer. *Apoptosis* **2017**, *22*, 158–168. [CrossRef] [PubMed]
140. Lee, J.H.; Kim, C.; Baek, S.H.; Ko, J.H.; Lee, S.G.; Yang, W.M.; Um, J.Y.; Sethi, G.; Ahn, K.S. Capsazepine inhibits JAK/STAT3 signaling, tumor growth, and cell survival in prostate cancer. *Oncotarget* **2017**, *8*, 17700–17711. [CrossRef]
141. Shanmugam, M.K.; Ong, T.H.; Kumar, A.P.; Lun, C.K.; Ho, P.C.; Wong, P.T.; Hui, K.M.; Sethi, G. Ursolic acid inhibits the initiation, progression of prostate cancer and prolongs the survival of TRAMP mice by modulating pro-inflammatory pathways. *PLoS ONE* **2012**, *7*, e32476. [CrossRef] [PubMed]
142. Shanmugam, M.K.; Manu, K.A.; Ong, T.H.; Ramachandran, L.; Surana, R.; Bist, P.; Lim, L.H.; Kumar, A.P.; Hui, K.M.; Sethi, G. Inhibition of CXCR4/CXCL12 signaling axis by ursolic acid leads to suppression of metastasis in transgenic adenocarcinoma of mouse prostate model. *Int. J. Cancer* **2011**, *129*, 1552–1563. [CrossRef] [PubMed]
143. Shanmugam, M.K.; Rajendran, P.; Li, F.; Nema, T.; Vali, S.; Abbasi, T.; Kapoor, S.; Sharma, A.; Kumar, A.P.; Ho, P.C.; et al. Ursolic acid inhibits multiple cell survival pathways leading to suppression of growth of prostate cancer xenograft in nude mice. *J. Mol. Med.* **2011**, *89*, 713–727. [CrossRef] [PubMed]
144. Chiang, P.K.; Tsai, W.K.; Chen, M.; Lin, W.R.; Chow, Y.C.; Lee, C.C.; Hsu, J.M.; Chen, Y.J. Zerumbone Regulates DNA Repair Responding to Ionizing Radiation and Enhances Radiosensitivity of Human Prostatic Cancer Cells. *Integr. Cancer Ther.* **2018**, *17*, 292–298. [CrossRef] [PubMed]
145. Jorvig, J.E.; Chakraborty, A. Zerumbone inhibits growth of hormone refractory prostate cancer cells by inhibiting JAK2/STAT3 pathway and increases paclitaxel sensitivity. *Anti-Cancer Drugs* **2015**, *26*, 160–166. [CrossRef] [PubMed]
146. Sun, Y.; Sheng, Q.; Cheng, Y.; Xu, Y.; Han, Y.; Wang, J.; Shi, L.; Zhao, H.; Du, C. Zerumbone induces apoptosis in human renal cell carcinoma via Gli-1/Bcl-2 pathway. *Die Pharm.* **2013**, *68*, 141–145.
147. Alsaab, H.O.; Sau, S.; Alzhrani, R.M.; Cheriyan, V.T.; Polin, L.A.; Vaishampayan, U.; Rishi, A.K.; Iyer, A.K. Tumor hypoxia directed multimodal nanotherapy for overcoming drug resistance in renal cell carcinoma and reprogramming macrophages. *Biomaterials* **2018**, *183*, 280–294. [CrossRef] [PubMed]

148. Shanmugam, M.K.; Rajendran, P.; Li, F.; Kim, C.; Sikka, S.; Siveen, K.S.; Kumar, A.P.; Ahn, K.S.; Sethi, G. Abrogation of STAT3 signaling cascade by zerumbone inhibits proliferation and induces apoptosis in renal cell carcinoma xenograft mouse model. *Mol. Carcinog.* **2015**, *54*, 971–985. [CrossRef] [PubMed]
149. Henrikson, N.B.; Morrison, C.C.; Blasi, P.R.; Nguyen, M.; Shibuya, K.C.; Patnode, C.D. Behavioral Counseling for Skin Cancer Prevention: Evidence Report and Systematic Review for the US Preventive Services Task Force. *JAMA* **2018**, *319*, 1143–1157. [CrossRef]
150. Murakami, A.; Tanaka, T.; Lee, J.Y.; Surh, Y.J.; Kim, H.W.; Kawabata, K.; Nakamura, Y.; Jiwajinda, S.; Ohigashi, H. Zerumbone, a sesquiterpene in subtropical ginger, suppresses skin tumor initiation and promotion stages in ICR mice. *Int. J. Cancer* **2004**, *110*, 481–490. [CrossRef] [PubMed]
151. Al-Zubairi, A. Anti-proliferative activity of zerumbone against tumour cell lines. *OnLine J. Biol. Sci.* **2018**, *18*, 123–129. [CrossRef]
152. Shyanti, R.K.; Sehrawat, A.; Singh, S.V.; Mishra, J.P.N.; Singh, R.P. Zerumbone modulates CD1d expression and lipid antigen presentation pathway in breast cancer cells. *Toxicol. In Vitro* **2017**, *44*, 74–84. [CrossRef] [PubMed]
153. Dermani, F.K.; Amini, R.; Saidijam, M.; Pourjafar, M.; Saki, S.; Najafi, R. Zerumbone inhibits epithelial-mesenchymal transition and cancer stem cells properties by inhibiting the β-catenin pathway through miR-200c. *J. Cell. Physiol.* **2018**, *233*, 9538–9547. [CrossRef] [PubMed]
154. Lv, T.; Zhang, W.; Han, X. Zerumbone suppresses the potential of growth and metastasis in hepatoma HepG2 cells via the MAPK signaling pathway. *Oncol. Lett.* **2018**, *15*, 7603–7610. [CrossRef] [PubMed]
155. Jegannathan, S.D.; Arul, S.; Dayalan, H. Zerumbone, a Sesquiterpene, Controls Proliferation and Induces Cell Cycle Arrest in Human Laryngeal Carcinoma Cell Line Hep-2. *Nutr. Cancer* **2016**, *68*, 865–872. [CrossRef] [PubMed]
156. Yan, H.; Ren, M.Y.; Wang, Z.X.; Feng, S.J.; Li, S.; Cheng, Y.; Hu, C.X.; Gao, S.Q.; Zhang, G.Q. Zerumbone inhibits melanoma cell proliferation and migration by altering mitochondrial functions. *Oncol. Lett.* **2017**, *13*, 2397–2402. [CrossRef]

molecules

MDPI

Review

Biochemical Basis of Anti-Cancer-Effects of Phloretin—A Natural Dihydrochalcone

Bu Young Choi

Department of Pharmaceutical Science & Engineering, Seowon University, Cheongju, Chungbuk 361-742, Korea; bychoi@seowon.ac.kr; Tel.: +82-043-299-8411

Academic Editor: Roberto Fabiani
Received: 24 December 2018; Accepted: 10 January 2019; Published: 13 January 2019

Abstract: Apple is a rich source of bioactive phytochemicals that help improve health by preventing and/or curing many disease processes, including cancer. One of the apple polyphenols is phloretin [2′,4′,6′-Trihydroxy-3-(4-hydroxyphenyl)-propiophenone], which has been widely investigated for its antioxidant, anti-inflammatory and anti-cancer activities in a wide array of preclinical studies. The efficacy of phloretin in suppressing xenograft tumor growth in athymic nude mice implanted with a variety of human cancer cells, and the ability of the compound to interfere with cancer cells signaling, have made it a promising candidate for anti-cancer drug development. Mechanistically, phloretin has been reported to arrest the growth of tumor cells by blocking cyclins and cyclin-dependent kinases and induce apoptosis by activating mitochondria-mediated cell death. The blockade of the glycolytic pathway via downregulation of GLUT2 mRNA and proteins, and the inhibition of tumor cells migration, also corroborates the anti-cancer effects of phloretin. This review sheds light on the molecular targets of phloretin as a potential anti-cancer and anti-inflammatory natural agent.

Keywords: phloretin; cell proliferation; inflammation; apoptosis; glucose uptake; migration

1. Introduction

Cancer, a heterogenous disease process, still remains a major challenge for human health. Despite the development of a wide variety of anti-cancer therapies such as alkylating agents, various kinase inhibitors, hormone modulators, and very recently introduced immune checkpoint inhibitors, the incidence of and mortality from cancer is still increasing throughout the world. Based on the current trend, unless effective therapeutic interventions are available, a two-fold increase of cancer-related deaths is expected in the next 50 years [1]. A major hurdle to developing anti-cancer therapy is the heterogenous nature of the disease, which often leads to chemotherapy failure or increased resistance to the therapy, thereby allowing recurrence of cancer [2]. Although the neoplastic transformation of cells begins through genetic alterations, such as activation of oncogenes and/or suppression of tumor suppressor genes via chromosomal abrasions, DNA damage, and dysregulation of epigenetic signaling, it has been well documented that various environmental and lifestyle related factors are the major triggers for tumor-inducing genetic and epigenetic changes. Major lifestyle factors that contribute to carcinogenesis include, but are not limited to, consumption of carcinogens from diet, exposure to solar radiation, intake of alcohol, smoking, and lack of physical exercise. Many of these are modifiable factors and thus, cancer can be prevented by adopting an appropriate lifestyle. About half a century ago, the concept cancer prevention was proposed by Michael B. Sporn, who first coined the term "chemoprevention", which refers to the inhibition or reversal of tumorigenic process by non-toxic chemicals [3].

Over the last several decades, the concept of cancer chemoprevention has been matured through extensive research-based proof-of-principle. Although chemoprevention is regarded as intervening

with the pathophysiologic course of tumor development—the initiation, promotion and progression stages [4,5]—based on the clinical perspective, chemoprevention is also classified as either primary, secondary or tertiary prevention of cancer. Any approach directed to prevention of cancer among relatively healthy and at risk groups within a population is termed as primary chemoprevention, while halting the premalignant lesions to complete neoplasia is termed as secondary chemoprevention. The approach of preventing the recurrence of cancer after successful therapy is conceptually termed as tertiary chemoprevention [1,6,7]. Mechanistically, the course of neoplastic transformation of cells can be prevented by intervening with various biochemical processes that become abnormal as a result of DNA damage, and oxidative modifications of proteins and lipids upon exposure to potential carcinogens. These biochemical processes include, but are not limited to, alterations in the activities of enzymes involved in carcinogen metabolism and detoxification, inappropriate amplification of intracellular signaling pathways regulating cell proliferation and apoptosis, tumor angiogenesis, invasion, metastasis, and dysregulation of host immune functions. The key driving forces for all the cancer-related biochemical changes are the persistent oxidative and/or inflammatory stresses imposed on cells or tissues, leading to cellular transformations. Thus, curbing oxidative damage to cellular macromolecules and mitigating inflammatory tissue damage can help prevent tumor development and progression.

A wide array of preclinical and human intervention studies have revealed the potential of various antioxidant and anti-inflammatory phytochemicals to prevent carcinogenesis [2,8]. In fact, many elements of a vegetarian diet, especially fruits and vegetables, contain numerous phytochemicals which can protect cells or tissues from noxious oxidative and inflammation-mediated tissue damage, and hence can prevent the development of tumors. Extensive research has been carried out to explore anti-cancer phytochemicals from fruits and vegetables such as turmeric, broccoli, green tea, grapes, berries, apples, pomegranate, etc. Among those dietary sources, apple is a source of many antioxidant and anti-inflammatory agents. There is a proverb saying that having an apple a day can keep the doctor away. One of the polyphenols present in apple is phloretin [2′,4′,6′-Trihydroxy-3-(4-hydroxyphenyl)-propiophenone], which has received much attention for anti-cancer drug discovery. Being a chalcone compound and having unsaturation and phenolic hydroxyl moieties, phloretin has shown the potential to modify various protein functions, leading to reversal of abnormal signaling and cellular transformation. This review sheds light on the potential of developing phloretin as an anticancer therapy with special focus on its underlying molecular mechanisms.

2. Anti-Inflammatory and Anticancer Effects of Phloretin—Evidence from In Vivo Studies

In addition to its nutritive values, apple (*Malus* spp., Rosaceae) can be used for the prevention and treatment of various diseases. The anti-cancer activity of apple products has been evaluated in a large number of epidemiological and laboratory-based studies [9,10]. For example, a significant reduction in the number and size of polyp in the colon and intestine of *adenomatous polyposis* $(APC)^{min+/+}$ mice has been observed after allowing these animals to drink a polyphenolic extract obtained from apple for 12 weeks [11]. This popular fruit is a rich source of various bioactive chemicals, such as chalcones, flavonoids, procyanidins and terpenoids [9]. One of the bioactive constituents of apple is phloretin [12], which has been widely investigated for its anti-cancer activities. In a pioneering study, Tanaka et al. [13] first demonstrated that phloretin inhibited the neoplastic transformation of BALB/3T3 cells upon exposure to a prototypic tumor promoting agent 12-*O*-tetradecanoyl phorbol-13 acetate (TPA). Subsequent studies have reported that phloretin exhibits antioxidative, anti-inflammatory, antiproliferative and apoptosis inducing properties. In addition, when used alone or in combination with conventional chemotherapy, phloretin can suppress the in vivo growth of xenograft tumors in nude mice [12,14–16]. For example, phloretin significantly reduced the volume and weight of xenograft tumors in severe combined immunodeficiency (SCID) mice inoculated with human hepatocellular carcinoma (HepG2) cells [17]. Phloretin elicited inhibitory

effects on the growth of human lung adenocarcinoma (A549) cell xenograft tumors in nude mice [18] and enhanced the growth inhibitory effect of paclitaxel in HepG2 cell xenograft tumors in SCID mice [15]. Further evidence of in vivo anti-tumor effects of phloretin were reported by Shin et al. [19], who demonstrated that topical application of phloretin significantly reduced the multiplicity of papillomas in 7,12,-dimethylbenz(a)anthracene (DMBA)-initiated and TPA-promoted mouse skin. Oral administration of phloretin also attenuated DMBA-induced buccal pouch carcinogenesis in male Syrian golden hamsters [20]. In healthy human volunteers, topical application of an antioxidant formulation containing vitamin C, ferrulic acid and phloretin suppressed ultra violet (UV) radiation-induced sunburn, thymidine dimer formation, and matrix metalloproteinase-9 (MMP-9) expression in skins [21]. Since exposure to UV radiation is a major cause of skin cancer, this study suggests the potential of phloretin to inhibit UV-induced skin carcinogenesis.

The link between chronic inflammation and cancer has been well documented. Amelioration of colitis, a condition characterized by persistent colonic mucosal inflammation, often progresses to colorectal cancer [22]. Management of colitis with anti-inflammatory therapy reduces the risk colorectal cancer [23]. Administration of phloretin significantly ameliorated trinitrobenzene sulfonic acid (TNBS)-induced colon inflammation and the loss of body weight in rats [24], suggesting the potential of this compound to prevent colorectal carcinogenesis. This has been supported by a recent study demonstrating the effectiveness of phloretin in suppressing the growth of human colorectal cancer (COLO 205) tumor xenografts in Balb/c nude mice [25]. When given intraperitoneally, phloretin inhibited ovalbumin-induced airway inflammation in Balb/C mice [26]. Moreover, intraperitoneal administration of phloretin diminished cigarette smoke (CS)-induced secretion of mucins, infiltration of inflammatory cells and the release of inflammatory cytokines in mouse lungs, and attenuated CS extract-induced expression of MUC5AC and IL-1β in NCI-H292 bronchial epithelial cells, partly by blocking the activation of EGFR, ERK and p38 mitogen-activated protein (MAP) kinase [27]. Thus, it would be interesting to examine whether phloretin can suppress CS-induced lung carcinogenesis. Phloretin was reported to inhibit the xenograft tumor growth of human lung cancer (A549) cells [18] and human breast cancer (MDA-MB-231) cells [28] in Balb/c nude mice.

3. The Biochemistry behind the Anti-Inflammatory and Anti-Cancer Effects of Phloretin

The biochemical mechanisms of anti-inflammatory and anti-cancer effects of phloretin have been widely investigated (Table 1). Phloretin has been shown to scavenge peroxynitrite radicals and inhibit lipid peroxidation, largely due to the presence of 2,6-dihydroxyacetone moiety as the 130 pharmacophore [29]. In another study, Nakamura et al. [12] demonstrated that the presence of a hydroxyl group at 2′-position of all dihydrochalcones, including phloretin, is an essential pharmacophore for the radical scavenging and lipid peroxidation activities. The bond dissociation enthalpies (BDEs) for hydroxyl (-OH) moieties (an indicator of antioxidant activity) of phloretin has recently been examined in a computational modeling study. The authors demonstrated that compared to well-known antioxidants, the BDEs among the four OH groups for phloretin were found to be the lowest, indicating the antioxidant potential of the compound [30]. Phloretin prevented oxidative DNA damage by restoring cellular glutathione (GSH) levels in human colon cancer (Caco-2 and HT-29) cells [31]. Likewise, the elevated cellular GSH level in phloretin-treated rat hepatocytes has been attributed to the induction of γ-glutamyl cysteine ligase (GCL), a rate limiting enzyme in GSH synthesis, via activation of a redox-regulated transcription factor, nuclear factor-erythroid related factor-2 (Nrf2) signaling [32]. These authors also demonstrated that phloretin induced the expression of another Nrf-2-regulated antioxidant enzyme, hemeoxygenase-1 (HO-1), in rat hepatocytes, via the activation of extracellular signal regulated kinase (ERK). By virtue of its antioxidative properties, phloretin attenuates the activation of exogenously exposed carcinogens as well as endogenous accumulation of damaged DNA or proteins, and inhibits the aberrant activation of various kinases and transcription factors involved in inflammatory signaling pathways. The following section will focus on detailing the molecular targets of phloretin as an anti-cancer agent (Figure 1).

Table 1. Anti-inflammatory and anti-cancer activities of phloretin.

Type	Experimental Model	Dose/Concentration	Mechanism of Action	Ref.
Anti-inflammatory	HEK293 cells engineered to either overexpress or deficient in hTLR2	10 or 20 μM	Inhibits the heterodimerization of TLR2/1; reduced the secretion of TNF-α and IL-8	[33]
	Specific pathogen-free male BALB/c mice (6–8 weeks, 22–24 g)	20 mg/kg	Suppressed the mucins secretion, inflammatory cell infiltration and cytokine release in mouse lungs induced by cigarette smoke (CS)	[27]
	OVA-challenged asthmatic mice	5, 10, or 20 mg/kg	Decreased hyperresponsiveness, inflammation, and oxidative responses; reduced ROS, and cytokines production	[26]
	LPS-induced acute lung injury in mice	5 or 20 mg/kg	Suppressed LPS-induced neutrophil infiltration, and reduce the levels of IL-6 and TNF-α in serum and bronchoalveolar lavage fluid; blockade of the NF-κB and MAPK pathways	[34]
	A549 cells	3–100 μM	Inhibited proinflammatory cytokine, COX-2, and ICAM-1 expression; blocked NF-κB and MAPK signaling pathways.	
	TNF-α-stimulated HaCaT human keratinocytes	10, 30, or 100 μM	Decreased the production of IL-6, IL-8, and CCL5; inhibited NF-κB nuclear translocation; suppressed phosphorylation of Akt and MAPK signal.	[36]
	Human THP-1 monocytes	1, 10, or 30 μg/mL	Reduced TNF-α, IL-6 and COX-2 expression	[37]
	Rat basophilic leukemia RBL-2H3 cells	12.5, 25, or 50 μM	Attenuated ROS production, phosphorylation of Akt, ERK1/2, p38 MAP kinase, and JNK	[38]
	LPS-stimulated murine RAW264.7 macrophages	3, 10, 30, or 100 μM	Reduced the levels of NO, PGE2, IL-6, TNF-α, iNOS and COX-2; suppressed nuclear translocation of NF-κB subunit p65 proteins, and decreased phosphorylation of MAPK pathways	
Anti-cancer	Gastric cancer (AGS) cells	IC_{50} 8 μM	Arrested the cell cycle in G2/M phase and decreased the expression of p-JNK and p-p38 MAP kinase	[39]
	Esophageal cancer EC-109 cell lines	60 μg/mL	Apoptosis increased to 225.6 ± 16.0%; increased p53 activity; increased the level of Bax and declined Bcl-2 levels	[40]
	Non-small cell lung cancer (NSCLC): A549, Calu-1, H838 and H520 cells	25, 50 or 75 μg/mL	Suppressed the expression of Bcl-2; increased the protein expression of cleaved-caspase-3 and -9, and deregulated the expression of MMP-2 and -9 on gene and protein levels	[41]
	Human erythroid leukemia K-562 cells	20 μM	Increased the efficacy of HSP70 penetration; increases anti-tumor activity of HSP70 with phloretin combination	[42]
	A549 human lung cancer cell line, Bel 7402 liver cancer cell line, HepG2 human ileocecal cancer cell line, and HT-29 human colon cancer cell line	0–150 mg/mL	Significant positive anti-cancer activities against several human cancer cell lines, IC_{50}: A549 (27 μg/mL), BEL7402 (37 μg/mL, HepG2 (37 μg/mL), HT29 (33 μg/mL)	[43]
	HepG2-xenografted tumor	10 mg/kg phloretin or +1 mg/kg paclitaxel	Reduced tumor growth more than fivefold in the phloretin and paclitaxel-treated mice compared to the paclitaxel only treated mice	[15]

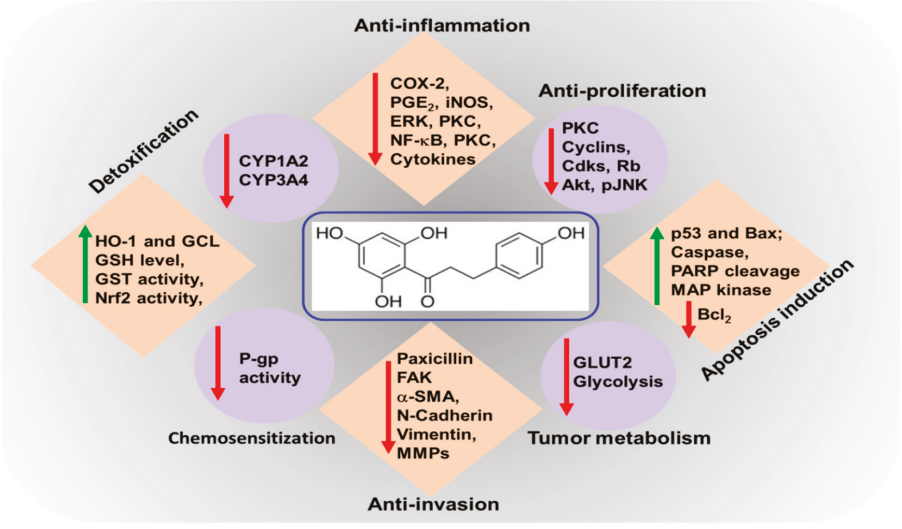

Figure 1. Molecular targets of phloretin as an chemoprevention agent. Anti-inflammation: COX-2 (Cyclooxygenase-2), PGE_2 (Prostaglandin E_2), *i*NOS (Nitric oxide synthases), ERK (extracellular-signal-regulated kinases), PKC (Protein kinase C), NF-kB (nuclear factor kappa-light-chain-enhancer of activated B cells). Anti-proliferation: CDKs (Cyclin-dependent kinases), Rb (Retinoblastoma protein), Akt (protein kinase B), p-JNK (Phospho-c-Jun N-terminal kinases), Apoptosis induction: Bax (Bcl-2-associated X protein), PARP (Poly ADP-ribose polymerase), Bcl_2 (B-cell lymphoma 2). Tumor metabolism: GLUT2 (Glucose transporter 2). Anti-invasion: FAK (focal adhesion kinase), α-SMA (Smooth muscle actin), MMPs (Matrix metalloproteinases). Chemosensitization: P-gp (P-glycoprotein 1). Detoxification: HO-1 (heme oxygenase 1), GCL (Glutamate Cysteine Ligase), GSH (glutathione), GST (Glutathione S-transferases), Nrf2 (Nuclear factor erythroid-related factor-2).

3.1. Inhibitory Effects of Phloretin on Inflammatory Markers

While inflammatory tissue damage is an initial trigger for tumor development, persistent intra-tumoral inflammation contributes to the invasion and metastasis of tumors. The key mediators of inflammation involved in neoplastic transformation of cells include, but are not limited to, inducible nitric oxide synthase (iNOS) and cyclooxygenase-2 (COX-2), and the cellular products catalyzed these enzymes, such as nitric oxide (NO) and prostaglandins (PGs) [22]. Studies have shown that mice harboring transgenic overexpression of *cox-2* in the stomach [44] and skin [45] are highly prone to develop tumors in these organs, whereas genetic ablation of *cox-2* protects mice against gastro-intestinal [46] and skin carcinogenesis [47]. The elevated levels of iNOS and its catabolic product NO have promoted dextran sulfate sodium-induced polyp formation in the colon of APC^{min+} mice as compared to wild type mice [48]. The role of iNOS in skin papillomas has been evident from the inhibition of chemically induced mouse skin tumor development upon treatment with aminoguanidine, which is an iNOS inhibitor [49]. A large number of cytokines, for example, interleukins (IL) and tumor necrosis factor-α (TNFα), and chemokines also act as inflammatory mediators and participate in the tumorigenic process. The burst of inflammatory mediators requires inappropriate amplification of intracellular signaling cascades comprising various kinases and transcription factors. Aberrant activation of MAP kinases, Janus-activated kinase (JAK), and protein kinase B (PKB)/Akt have been implicated in precipitating inflammation and cancer. These upstream kinases transmit activating signals to a variety of redox-sensitive transcription factors, such as nuclear factor-kappaB (NF-κB), activator protein-1 (AP-1), signal transducer and activator of transcription (STAT), which leads to transactivation of genes encoding proteins involved in inflammation and oncogenesis [8,50].

Phloretin exerts anti-cancer effects by curbing inflammatory responses. For instance, phloretin markedly diminished the expression of pro-inflammatory genes by repressing the activation of NF-κB-, IL-8-, and STAT1-dependent signal transduction in human colon cancer (DLD1) cells and other immune cells (T84, MonoMac6, Jurkat) in a concentration-dependent manner [51]. The compound also inhibited TNFα-induced inflammatory responses in human colonic epithelial cells [24]. Shin et al. [19] reported that topical application of phloretin reduced phorbol ester-induced COX-2 expression and skin inflammation in mice by blocking the activation of NF-κB and ERK-mediated signaling. Moreover, pretreatment with phloretin diminished the production of various inflammatory markers, such as NO, PGE_2, IL-6, and TNFα, and attenuated the expression of iNOS and COX-2 in lipopolysaccharide (LPS)-stimulated murine macrophage RAW264.7 cells. According to this study, phloretin blocked nuclear localization of the p65 protein, a component of NF-κB, and negated the phosphorylation in MAP kinases [16]. Phloretin reduced the expression of COX-2 and intracellular adhesion molecule -1 (ICAM-1), and the production of IL-6 in human lung epithelial (A549) cells stimulated with IL-1β by blocking the activation of NF-κB via downregulation of Akt and MAP kinases phosphorylation [35]. Likewise, the secretion of various cytokines and chemokines, such as IL-6, IL-8, and monocyte chemoattractant protein-1(MCP1), and the reduced expression of ICAM-1 in TNF-α-stimulated HaCaT keratinocytes by phloretin, have been attributed to the inactivation of NF-κB and MAP kinases [36]. Huang et al. recently reported that treatment with phloretin attenuated the gene expression of a variety of inflammatory markers, such as COX-2, iNOS, CCL5, MCP1, and ICAM-1 in LPS-treated mouse lung tissue [22,34,36,52,53].

3.2. Modulating Biotransformation of Putative Carcinogens

Cellular transformation is often led by exposure to potential carcinogenic stimuli. While many environmental or dietary factors are non-toxic, some can be turned into potential genotoxic agents once metabolically activated. A rational approach for preventing cells from potential toxic effects of carcinogens is either to block metabolic activation of the apparently nontoxic chemicals or to enhance cellular detoxification pathways to eliminate the noxious chemical entities. A wide array of cytochrome (CYP) P450 enzymes carry out the bioactivation of pro-carcinogens, whereas a series of detoxification enzymes, such as glutathione-*S*-transferase (GST), glucuronyl transferase, sulfotransferase, etc., help in the elimination of metabolically active carcinogens or their reactive intermediates. Phloretin inhibited the biotransformation of aflatoxin B1 (AFB1) to generate AFB1-8,9-epoxide (AFBO), an active metabolite of AFB1, by blocking the activities of CYP1A2 and CYP3A4 enzymes. Moreover, phloretin induced the activity of GST and increased the expression of GSTA3, GSTA4, GSTM1, GSTP1 and GSTT1 via the activation of Nrf2 in alpha mouse liver 12 (AML12) cells [54]. Since metabolically activated AFB1 acts as a potential hepatocarcinogen and causes liver cancer, phloretin may prevent chemically induced liver cancer. Phloretin increased the expression of Nrf2, a redox-regulated transcription factor involved in transactivation of antioxidant and detoxification genes, and upregulated the expression of heme oxygenase-1 (HO-1) in TNFα-stimulated HaCaT keratinocytes [35] and LPS-treated mouse lung tissue [34], suggesting the potential of phloretin to protect against oxidative tissue damage in these organs.

3.3. Antiproliferative and Apoptosis Inducing Effects of Phloretin

There is accumulating evidence suggesting that phloretin arrests the proliferation of tumor cells and induces apoptosis in various human cancer cells, including those of the skin, colon, breast and prostate in culture. The underlying mechanisms of the antiproliferative effects of phloretin appears to be the interference with cell cycle progression via modulation of cyclins and induction of mitochondria-dependent programmed cell death. Park et al. [14] reported that the induction of apoptosis in human colon cancer (HT-29) cells upon treatment with phloretin was associated with increased expression of Bax and release of cytochrome c and Smac/DIABLO in the cytosol, thereby resulting in the cleavage of caspase-8, -9, -7, and -3 and poly(ADP-ribose) polymerase (PARP) [14].

A recent study demonstrated that phloretin induced apoptosis selectively in human gastric cancer cell lines (MGC80-3, BGC-823, SGC-7901, SNU-1, SNU-5, RF-1 and AGS), with IC_{50} values ranging from 8 to 32 μM without affecting the growth of normal gastric epithelial cells [39]. Incubation of AGS cells with phloretin reduced the colony formation in a concentration-dependent manner by arresting cell cycle at the G2/M phase. Moreover, the induction of apoptosis in AGS cells by phloretin was associated with the increase in Bax expression, inhibition of Bcl-2 levels and decrease in the phosphorylation of c-Jun N-terminal kinase (JNK) and p38 MAP kinase [39]. In contrast, the activation of JNK and p38 MAP kinase has been attributed to phloretin-induced caspase-3 cleavage in H-*ras*-transformed human mammary epithelial cells (H-*ras*-MCF-10A) [55]. These authors also reported that phloretin attenuated the proliferation of H-*ras*-MCF-10A cells in a concentration-dependent manner and induced apoptosis via upregulation of p53 and Bax and the cleavage of PARP [55]. Although the induction of apoptosis in B16 melanoma cells by phloretin was associated with the elevated expression of Bax and caspase activation, the compound did not affect the expression of p53 or that of anti-apoptotic proteins Bcl-2 or Bcl-xl [56]. However, according to a recent study phloretin inhibited the expression of Bcl-2 and X-linked inhibitor of apoptosis (XIAP), and activated p53 as the mechanism of apoptosis induction in human esophageal cancer (EC-109) cells [40]. Phloretin arrested cell cycle at the G0/G1 phase and reduced proliferation of human breast cancer (MDA-MB-231) cells in a p53 mutant-dependent manner as evidenced by pre-incubating cells with a p53-specific dominant-negative expression vector [28]. Thus, the effects of phloretin on MAP kinase activation, Bcl-2 expression and p53 induction may be a cell-type specific phenomena.

Kobori et al. reported that phloretin caused apoptosis in human leukemia (HL60) cells, which was associated with decreased protein kinase C (PKC) activity [57]. Various chalcone compounds have been shown to prevent prostate cancer [58]. Phloretin, being a dihydrochalcone, significantly enhanced TNFα-related apoptosis-inducing ligand (TRAIL)-induced apoptosis and cytotoxicity in human prostate cancer (LNCaP) cells [58].

Phloretin attenuated growth and induced apoptosis in a number of lung cancer cells in culture. Treatment of human lung cancer (A549, Calu-1, H838 and H520) cells with phloretin resulted in reduced expression of anti-apoptotic protein Bcl-2 and elevation in the protein expression of cleaved-caspase-3 and -9 [41]. The induction of apoptosis in A549 cells by phloretin was associated with increased levels of Bax, cleavage of caspase-3 and -9, and PARP, and decreased Bcl-2 expression. Mechanistically, phloretin-induced caspase activation was mediated through the induction of p38 MAP kinase and JNK1/2 phosphorylation, as inhibition of these kinases by using specific inhibitors significantly abolished the phloretin-induced caspase activation [18].

The anti-proliferative effects of phloretin are also mediated through the modulation of cyclins and cyclin-dependent kinases (CDKs). According to a recent study, phloretin induced cell cycle arrest at the G0/G1 phase in human glioblastoma cells, at least in part, by increasing the expression of p27 and dampening that of CDK-2, -4, and -6, and cyclin-D, and -E. In addition, the compound suppressed signaling through the PI3K/AKT/mTOR cascades, resulting in reduced cell proliferation. The study also demonstrated that phloretin triggered the mitochondria-mediated cell death via generation of ROS, up-regulation of Bax, Bak and c-PARP, and the inhibition of Bcl-2 [59].

3.4. Blockade of Tumor Cell Migration and Invasion

One of the pathophysiologic features of carcinogenesis is the spreading of localized tumors to distant tissue sites through migration and invasion [60]. Tumor cell migration involves epithelial-mesenchymal transition (EMT) followed by matrix degradation to invade through stromal tissue [61]. While upregulation of N-cadherin and vimentin are known markers of EMT, matrix metalloproteinases (MMPs) are essential molecules that cause matrix degradation [62]. Several studies have demonstrated the ability of phloretin to reduce the migratory potential of various tumors cells, thus blocking tumor progression. Incubation with phloretin diminished migration of human lung epithelial cancer (A549) cells in a concentration-dependent manner, which was associated with

downregulation of NF-κB and MMP-9 expression [18]. Likewise, the inhibition of migration and invasion of non-small cell lung cancer (H838 and H520) cells by phloretin treatment was mediated through suppression of MMP-2 and MMP-9 at both gene and protein levels [41]. According to Wu et al., phloretin treatment diminished the expression of paxillin and α-smooth muscle actin (α-SMA), and decreased the phosphorylation of focal adhesion kinase and Src kinase, thereby slowing down the migration of human breast cancer MDA-MB-231 cells. Although phloretin had no remarkable effect on the expression of E-cadherin in MDA-MB-231 cells, the study showed that the compound upregulated E-cadherin and inhibited N-cadherin and vimentin expression in MDA-MB-231 cells xenograft tumors in nude mice. While a decrease in vimentin level is in agreement, the effect of the compound on cadherin expression failed to support its antimigratory effect [28]. Further studies are required to confirm the effects of phloretin on cadherin levels and its impact on tumor cell migration. Phloretin also attenuated the invasion of human gastric cancer (AGS) cells by blocking the phosphorylation of MAP kinases [39].

3.5. Inhibition of Glucose Uptake by Phloretin

Enhanced glycolysis, a feature of many rapidly growing solid tumors, is associated with elevated expression of glucose transporter proteins (GLUT) and other glycolytic enzymes in neoplastic cells. Treatment with phloretin sensitized human colon cancer (SW620) and leukemia (K562) cells to daunorubicin by reducing the glucose uptake by these cells [63]. Lin et al. [25] reported that elevated levels of GLUT2 mRNA were detected in human colon cancer (COLO 205 and HT29) cells as well as in colorectal cancer tissues. Treatment with phloretin attenuated GLUT2 mRNA and protein expression by blocking hepatocyte nuclear factor 6 (HNF6), which is a transcription factor regulating GLUT2 expression. When compared to normal hepatocytes, the levels of GLUT2 mRNA were found to be five times greater in human hepatoma (HepG2) cells. Phloretin re-sensitized these cells to paclitaxel and induced apoptosis via caspase activation by attenuating GLUT2 expression. Thus, the growth of HepG2 cells xenograft tumors in nude mice markedly diminished by co-treatment with phloretin and paclitaxel, as compared to treatment with paclitaxel alone [15]. Another study has shown that GLUT2 expression is elevated in HepG2 cells and that the siRNA-mediated silencing of GLUT2 induced apoptosis in these cells [17]. While co-treatment of these cells with glucose uptake inhibitor cytochalasin B enhanced phloretin-induced apoptosis, the effect of phloretin was reversed by pretreatment with glucose. These findings suggest that induction of apoptosis in HepG2 cells by phloretin is mediated through inhibition of GLUT2 expression. Likewise, phloretin inhibited the proliferation of rat mammary adenocarcinoma and Fischer bladder cell carcinoma cells and arrested the growth of xenograft tumors of these cells in mice by blocking glucose transmembrane transport [64].

3.6. Phloretin as a Potential Cancer Immunotherapy Agent

The emergence of immunotherapies in recent years is considered a major breakthrough in the development of cancer therapeutics. Reinvigoration of exhausted T cells by blocking immune checkpoint markers, such as cytotoxic T cells antigen-4 (CTLA4), programmed cell death 1 (PD-1) and PD-1 ligand (PDL-1), have recently received Food and Drug Administration approval for the treatment of melanoma, renal cell carcinoma, and non-small cells lung cancer [65]. Although substantial progress has been made in developing cancer immunotherapies, the potential of natural compounds in boosting antitumor immunity is yet to be investigated. A recent study by Zhu et al. [66] reported that phloretin can enhance the tumoricidal effect of γδ T cells on human colon cancer (SW-1116) cells, possibly by stimulating the proliferation of γδ T cells. In another study, phloretin potentiated the anti-cancer effects of intratumorally administered recombinant heat shock protein-70 (HSP70) in B16 mouse melanoma cells, through enhancement of tumor cell sensitivity to cytotoxic lymphocytes by 16%–18% as compared to a treatment with HSP-70 alone. The combined treatment with phloretin and recombinant HSP-70 resulted in B16 melanoma cells xenograft tumor growth and increased the life span of tumor-bearing mice through the activation of innate and adaptive immunity. Authors also demonstrated that rHSP70

was more active in induction of CD8+ cell function and interferon-γ (γIFN) production, but phloretin induced CD56+ cell response [42].

3.7. Phloretin Alleviates Chemotherapy Resistance

A major challenge to the clinical success of curing cancer is the frequent incidence of therapy failure, largely due to the acquisition of resistance by tumor cells to ongoing chemotherapy [67,68]. The biochemical mechanism underlying the development of chemoresistance is the ability of tumor cells to enhance drug efflux, thereby reducing the intracellular drug concentration to a sub-therapeutic level [69]. The overexpression of multidrug resistance proteins (MRP or MDR), for example P-glycoprotein (P-gp), on the cancer cell membrane often facilitates drug efflux and helps tumors to gain chemotherapy resistance [70]. Thus, the blockade of MDR-efflux proteins may help promote the effectiveness of cancer chemotherapy. Co-administration of a wide variety of dietary phytochemicals are shown to sensitize chemoresistant tumor cells in preclinical studies. Nguyen et al. [71] demonstrated that the accumulation of daunomycin and vinblastine in human pancreatic carcinoma Panc-1 cells was significantly increased when the cells were co-treated with phloretin and the effect was mediated through the inhibition of MRP1-mediated drug transport. According to another study, treatment with phloretin reduced the P-gp activity in human MDR1 gene-transfected mouse lymphoma cells (L1210) and human breast cancer cells MDA-MB-231 expressing the MRP1 pump (HTB26) [72]. Moreover, phloretin facilitated cisplatin-induced downregulation of Bcl-2, MMP-2 and -9, and activation of caspase cleavage in NSCLC cells [41], while the compound inhibited cisplatin-induced apoptosis of normal auditory cells [73]. These findings suggest that phloretin not only enhances chemotherapeutic effects of cisplatin, but also prevents the potential side effects of cisplatin in causing auditory damage. Zhou et al. [74] examined the growth inhibitory effect of a combination of atorvastatin, an anti-lipidemic agent, and phloretin on SW620 and HCT116 colon cancer cells. The combination treatment caused a remarkable decrease in cell survival in both cell lines as compared to treatment with an individual compound. The computational analysis of the interaction index between phloretin and atorvastatin appeared to be <1.0, indicating a strong synergistic effect exerted by the compounds. Synergistic anti-cancer effects were revealed by the induction of apoptosis and cell cycle arrest at the G2/M phase, which was associated with reduced expression of cyclin B and elevated expression of phospho-cdc2 and Myt1 [74].

4. Pharmacokinetics and Toxicity Profile of Phloretin

Although the anti-cancer activities of phloretin have been investigated in various cell culture experiments in vitro and animal models in vivo, there have been limited studies on its pharmacokinetics and toxicity profile. In one study, the plasma and urine analysis of phloretin metabolites in rats fed a single meal containing 0.157% phloretin (corresponding to the ingestion of 22 mg of phloretin equivalents) revealed that phloretin was present in plasma primarily as glucuronide and sulphate conjugates, but unconjugated phloretin was also detected. The study also showed that phloretin appeared more rapidly in plasma when rats were fed the aglycone as opposed to its glucoside form. Moreover, the return of plasma phloretin concentration to its baseline after 24 h of the meal indicates the rapid elimination of the compound from the body. The total urinary excretion rate of phloretin was estimated to be 8.5 μmol/24 h, and about 10.4% of the ingested dose was recovered in urine after 24 h of the phloretin-containing meal [75]. Ingestion of polyphenol-rich cloudy apple juice by healthy volunteers followed by ileostomy extract analysis showed that most of the orally administered apple polyphenols are absorbed from, or metabolized in, the small intestine. Both phloretin and its glucuronide conjugates were detected in the ileostomy extract from 2 to 4 h, indicating that most of the apple juice polyphenols, including phloretin, are well absorbed in the small intestine [76]. In contrast, translocation of phloretin and its glucosides through ex vivo pig intestinal smooth muscle remained undetected, suggesting poor absorption of phloretin [77]. A recent study demonstrated the protective effect of a low dose (0.2 to 0.4 mmol/kg body weight) of phloretin against

acetaminophen (AAP)-induced hepatotoxicity in mice, while the compound given intraperitoneally at a dose of 2.4 mmol/kg alone showed 64% lethality [78]. Thus, further studies are warranted to obtain more precise pharmacokinetics parameters, and lethal and sub-acute toxicity for the therapeutic effectiveness of the compound as an anti-cancer agent.

5. Future Perspectives

Despite substantial progress in developing molecular target-based cancer chemotherapeutic agents, including the recently introduced immunotherapies, the clinical success of these therapeutic agents remains limited. The risk of developing resistance, high cost and cancer type-specificity narrow down the utility of these agents for treating millions of cancer patients worldwide. A wide variety of phytochemicals present in our regular foods are shown to prevent or delay the carcinogenesis process. The search for dietary anti-cancer principles and the elucidation of their biochemical mechanisms appears as a rational and active branch of new drug discovery research over this century. The beneficial health effects of plant polyphenols have been well documented. One of the dietary polyphenols is phloretin, which has emerged as a promising anti-cancer agent. While diverse biochemical mechanisms of anti-cancer effects of this apple polyphenol have been explored, exploitation of this molecule for new anti-cancer drug design requires more rigorous studies to address issues like toxicity profile, pharmacokinetics and more elaborate molecular basis of anti-cancer activity.

Funding: This research received no external funding.

Acknowledgments: I wish to thank Joydeb Kumar Kundu for helpful comments on the manuscript.

Conflicts of Interest: The authors declare that no conflict of interest exists.

References

1. Mann, J.R.; Backlund, M.G.; DuBois, R.N. Mechanisms of disease: Inflammatory mediators and cancer prevention. *Nat. Clin. Pract. Oncol.* **2005**, *2*, 202–210. [CrossRef] [PubMed]
2. Baer-Dubowska, W. Cancer chemopreventive agents-drugs for the 21st century? *Acta Pol. Pharm.* **2006**, *63*, 369–373. [PubMed]
3. Sporn, M.B. Approaches to prevention of epithelial cancer during the preneoplastic period. *Cancer Res.* **1976**, *36*, 2699–2702. [PubMed]
4. Moolgavkar, S.H. The multistage theory of carcinogenesis and the age distribution of cancer in man. *J. Natl. Cancer Inst.* **1978**, *61*, 49–52. [CrossRef] [PubMed]
5. Surh, Y.J. Cancer chemoprevention with dietary phytochemicals. *Nat. Rev. Cancer* **2003**, *3*, 768–780. [CrossRef]
6. Tsuda, H.; Ohshima, Y.; Nomoto, H.; Fujita, K.; Matsuda, E.; Iigo, M.; Takasuka, N.; Moore, M.A. Cancer prevention by natural compounds. *Drug Metab. Pharmacokinet.* **2004**, *19*, 245–263. [CrossRef] [PubMed]
7. De Flora, S.; Ferguson, L.R. Overview of mechanisms of cancer chemopreventive agents. *Mutat. Res.* **2005**, *591*, 8–15. [CrossRef]
8. Kundu, J.K.; Surh, Y.J. Breaking the relay in deregulated cellular signal transduction as a rationale for chemoprevention with anti-inflammatory phytochemicals. *Mutat. Res.* **2005**, *591*, 123–146. [CrossRef]
9. Gerhauser, C. Cancer chemopreventive potential of apples, apple juice, and apple components. *Planta Med.* **2008**, *74*, 1608–1624. [CrossRef]
10. Zessner, H.; Pan, L.; Will, F.; Klimo, K.; Knauft, J.; Niewohner, R.; Hummer, W.; Owen, R.; Richling, E.; Frank, N.; et al. Fractionation of polyphenol-enriched apple juice extracts to identify constituents with cancer chemopreventive potential. *Mol. Nutr. Food Res.* **2008**, *52*, S28–S44. [CrossRef]
11. Fini, L.; Piazzi, G.; Daoud, Y.; Selgrad, M.; Maegawa, S.; Garcia, M.; Fogliano, V.; Romano, M.; Graziani, G.; Vitaglione, P.; et al. Chemoprevention of intestinal polyps in ApcMin/+ mice fed with western or balanced diets by drinking annurca apple polyphenol extract. *Cancer Prev. Res.* **2011**, *4*, 907–915. [CrossRef] [PubMed]
12. Nakamura, Y.; Watanabe, S.; Miyake, N.; Kohno, H.; Osawa, T. Dihydrochalcones: Evaluation as novel radical scavenging antioxidants. *J. Agric. Food Chem* **2003**, *51*, 3309–3312. [CrossRef] [PubMed]
13. Tanaka, K.; Ono, T.; Umeda, M. Inhibition of biological actions of 12-*O*-tetradecanoylphorbol-13-acetate by inhibitors of protein kinase C. *Jpn. J. Cancer Res.* **1986**, *77*, 1107–1113. [PubMed]

14. Park, S.Y.; Kim, E.J.; Shin, H.K.; Kwon, D.Y.; Kim, M.S.; Surh, Y.J.; Park, J.H. Induction of apoptosis in HT-29 colon cancer cells by phloretin. *J. Med. Food* **2007**, *10*, 581–586. [CrossRef] [PubMed]
15. Yang, K.C.; Tsai, C.Y.; Wang, Y.J.; Wei, P.L.; Lee, C.H.; Chen, J.H.; Wu, C.H.; Ho, Y.S. Apple polyphenol phloretin potentiates the anti-cancer actions of paclitaxel through induction of apoptosis in human hep G2 cells. *Mol. Carcinog.* **2009**, *48*, 420–431. [CrossRef] [PubMed]
16. Chang, W.T.; Huang, W.C.; Liou, C.J. Evaluation of the anti-inflammatory effects of phloretin and phlorizin in lipopolysaccharide-stimulated mouse macrophages. *Food Chem.* **2012**, *134*, 972–979. [CrossRef] [PubMed]
17. Wu, C.H.; Ho, Y.S.; Tsai, C.Y.; Wang, Y.J.; Tseng, H.; Wei, P.L.; Lee, C.H.; Liu, R.S.; Lin, S.Y. In vitro and in vivo study of phloretin-induced apoptosis in human liver cancer cells involving inhibition of type II glucose transporter. *Int. J. Cancer* **2009**, *124*, 2210–2219. [CrossRef]
18. Min, J.; Huang, K.; Tang, H.; Ding, X.; Qi, C.; Qin, X.; Xu, Z. Phloretin induces apoptosis of non-small cell lung carcinoma A549 cells via JNK1/2 and p38 MAPK pathways. *Oncol. Rep.* **2015**, *34*, 2871–2879. [CrossRef]
19. Shin, J.W.; Kundu, J.K.; Surh, Y.J. Phloretin inhibits phorbol ester-induced tumor promotion and expression of cyclooxygenase-2 in mouse skin: Extracellular signal-regulated kinase and nuclear factor-kappaB as potential targets. *J. Med. Food* **2012**, *15*, 253–257. [CrossRef]
20. Anand, M.A.; Suresh, K. Biochemical profiling and chemopreventive activity of phloretin on 7,12-Dimethylbenz (a) anthracene induced oral carcinogenesis in male golden Syrian hamsters. *Toxicol. Int.* **2014**, *21*, 179–185.
21. Oresajo, C.; Stephens, T.; Hino, P.D.; Law, R.M.; Yatskayer, M.; Foltis, P.; Pillai, S.; Pinnell, S.R. Protective effects of a topical antioxidant mixture containing vitamin C, ferulic acid, and phloretin against ultraviolet-induced photodamage in human skin. *J. Cosmet. Dermatol.* **2008**, *7*, 290–297. [CrossRef] [PubMed]
22. Kundu, J.K.; Surh, Y.J. Emerging avenues linking inflammation and cancer. *Free Radic. Biol. Med.* **2012**, *52*, 2013–2037. [CrossRef] [PubMed]
23. Eaden, J.; Abrams, K.; Ekbom, A.; Jackson, E.; Mayberry, J. Colorectal cancer prevention in ulcerative colitis: A case-control study. *Aliment. Pharmacol. Ther.* **2000**, *14*, 145–153. [CrossRef] [PubMed]
24. Lee, J.H.; Regmi, S.C.; Kim, J.A.; Cho, M.H.; Yun, H.; Lee, C.S.; Lee, J. Apple flavonoid phloretin inhibits Escherichia coli O157:H7 biofilm formation and ameliorates colon inflammation in rats. *Infect. Immun.* **2011**, *79*, 4819–4827. [CrossRef] [PubMed]
25. Lin, S.T.; Tu, S.H.; Yang, P.S.; Hsu, S.P.; Lee, W.H.; Ho, C.T.; Wu, C.H.; Lai, Y.H.; Chen, M.Y.; Chen, L.C. Apple Polyphenol Phloretin Inhibits Colorectal Cancer Cell Growth via Inhibition of the Type 2 Glucose Transporter and Activation of p53-Mediated Signaling. *J. Agric. Food Chem.* **2016**, *64*, 6826–6837. [CrossRef] [PubMed]
26. Huang, W.C.; Fang, L.W.; Liou, C.J. Phloretin Attenuates Allergic Airway Inflammation and Oxidative Stress in Asthmatic Mice. *Front. Immunol.* **2017**, *8*, 134. [CrossRef]
27. Wang, H.; Yang, T.; Wang, T.; Hao, N.; Shen, Y.; Wu, Y.; Yuan, Z.; Chen, L.; Wen, F. Phloretin attenuates mucus hypersecretion and airway inflammation induced by cigarette smoke. *Int. Immunopharmacol.* **2018**, *55*, 112–119. [CrossRef]
28. Wu, K.H.; Ho, C.T.; Chen, Z.F.; Chen, L.C.; Whang-Peng, J.; Lin, T.N.; Ho, Y.S. The apple polyphenol phloretin inhibits breast cancer cell migration and proliferation via inhibition of signals by type 2 glucose transporter. *J. Food Drug Anal.* **2018**, *26*, 221–231. [CrossRef]
29. Rezk, B.M.; Haenen, G.R.; van der Vijgh, W.J.; Bast, A. The antioxidant activity of phloretin: The disclosure of a new antioxidant pharmacophore in flavonoids. *Biochem. Biophys. Res. Commun.* **2002**, *295*, 9–13. [CrossRef]
30. Mendes, R.A.; BLS, E.S.; Takeara, R.; Freitas, R.G.; Brown, A.; de Souza, G.L.C. Probing the antioxidant potential of phloretin and phlorizin through a computational investigation. *J. Mol. Model.* **2018**, *24*, 101. [CrossRef]
31. Schaefer, S.; Baum, M.; Eisenbrand, G.; Dietrich, H.; Will, F.; Janzowski, C. Polyphenolic apple juice extracts and their major constituents reduce oxidative damage in human colon cell lines. *Mol. Nutr. Food Res.* **2006**, *50*, 24–33. [CrossRef] [PubMed]
32. Yang, Y.C.; Lii, C.K.; Lin, A.H.; Yeh, Y.W.; Yao, H.T.; Li, C.C.; Liu, K.L.; Chen, H.W. Induction of glutathione synthesis and heme oxygenase 1 by the flavonoids butein and phloretin is mediated through the ERK/Nrf2 pathway and protects against oxidative stress. *Free Radic. Biol. Med.* **2011**, *51*, 2073–2081. [CrossRef] [PubMed]
33. Kim, J.; Durai, P.; Jeon, D.; Jung, I.D.; Lee, S.J.; Park, Y.M.; Kim, Y. Phloretin as a Potent Natural TLR2/1 Inhibitor Suppresses TLR2-Induced Inflammation. *Nutrients* **2018**, *10*, 868. [CrossRef] [PubMed]

34. Huang, W.C.; Lai, C.L.; Liang, Y.T.; Hung, H.C.; Liu, H.C.; Liou, C.J. Phloretin attenuates LPS-induced acute lung injury in mice via modulation of the NF-kappaB and MAPK pathways. *Int. Immunopharmacol.* **2016**, *40*, 98–105. [CrossRef] [PubMed]
35. Huang, W.C.; Wu, S.J.; Tu, R.S.; Lai, Y.R.; Liou, C.J. Phloretin inhibits interleukin-1beta-induced COX-2 and ICAM-1 expression through inhibition of MAPK, Akt, and NF-kappaB signaling in human lung epithelial cells. *Food Funct.* **2015**, *6*, 1960–1967. [CrossRef] [PubMed]
36. Huang, W.C.; Dai, Y.W.; Peng, H.L.; Kang, C.W.; Kuo, C.Y.; Liou, C.J. Phloretin ameliorates chemokines and ICAM-1 expression via blocking of the NF-kappaB pathway in the TNF-alpha-induced HaCaT human keratinocytes. *Int. Immunopharmacol.* **2015**, *27*, 32–37. [CrossRef]
37. Sekhon-Loodu, S.; Ziaullah; Rupasinghe, H.P. Docosahexaenoic acid ester of phloridzin inhibit lipopolysaccharide-induced inflammation in THP-1 differentiated macrophages. *Int. Immunopharmacol.* **2015**, *25*, 199–206. [CrossRef]
38. Chung, M.J.; Sohng, J.K.; Choi, D.J.; Park, Y.I. Inhibitory effect of phloretin and biochanin A on IgE-mediated allergic responses in rat basophilic leukemia RBL-2H3 cells. *Life Sci.* **2013**, *93*, 401–408. [CrossRef]
39. Xu, M.; Gu, W.; Shen, Z.; Wang, F. Anti-cancer Activity of Phloretin Against Human Gastric Cancer Cell Lines Involves Apoptosis, Cell Cycle Arrest, and Inhibition of Cell Invasion and JNK Signalling Pathway. *Med. Sci. Monit.* **2018**, *24*, 6551–6558. [CrossRef]
40. Duan, H.; Wang, R.; Yan, X.; Liu, H.; Zhang, Y.; Mu, D.; Han, J.; Li, X. Phloretin induces apoptosis of human esophageal cancer via a mitochondria-dependent pathway. *Oncol. Lett.* **2017**, *14*, 6763–6768. [CrossRef]
41. Ma, L.; Wang, R.; Nan, Y.; Li, W.; Wang, Q.; Jin, F. Phloretin exhibits an anti-cancer effect and enhances the anti-cancer ability of cisplatin on non-small cell lung cancer cell lines by regulating expression of apoptotic pathways and matrix metalloproteinases. *Int. J. Oncol.* **2016**, *48*, 843–853. [CrossRef] [PubMed]
42. Abkin, S.V.; Ostroumova, O.S.; Komarova, E.Y.; Meshalkina, D.A.; Shevtsov, M.A.; Margulis, B.A.; Guzhova, I.V. Phloretin increases the anti-tumor efficacy of intratumorally delivered heat-shock protein 70 kDa (HSP70) in a murine model of melanoma. *Cancer Immunol. Immunother.* **2016**, *65*, 83–92. [CrossRef] [PubMed]
43. Qin, X.; Xing, Y.F.; Zhou, Z.; Yao, Y. Dihydrochalcone Compounds Isolated from Crabapple Leaves Showed Anti-cancer Effects on Human Cancer Cell Lines. *Molecules* **2015**, *20*, 21193–21203. [CrossRef] [PubMed]
44. Oshima, H.; Oshima, M.; Inaba, K.; Taketo, M.M. Hyperplastic gastric tumors induced by activated macrophages in COX-2/mPGES-1 transgenic mice. *EMBO J.* **2004**, *23*, 1669–1678. [CrossRef] [PubMed]
45. Muller-Decker, K.; Neufang, G.; Berger, I.; Neumann, M.; Marks, F.; Furstenberger, G. Transgenic cyclooxygenase-2 overexpression sensitizes mouse skin for carcinogenesis. *Proc. Natl. Acad. Sci. USA* **2002**, *99*, 12483–12488. [CrossRef] [PubMed]
46. Oshima, M.; Dinchuk, J.E.; Kargman, S.L.; Oshima, H.; Hancock, B.; Kwong, E.; Trzaskos, J.M.; Evans, J.F.; Taketo, M.M. Suppression of intestinal polyposis in Apc delta716 knockout mice by inhibition of cyclooxygenase 2 (COX-2). *Cell* **1996**, *87*, 803–809. [CrossRef]
47. Tiano, H.F.; Loftin, C.D.; Akunda, J.; Lee, C.A.; Spalding, J.; Sessoms, A.; Dunson, D.B.; Rogan, E.G.; Morham, S.G.; Smart, R.C.; et al. Deficiency of either cyclooxygenase (COX)-1 or COX-2 alters epidermal differentiation and reduces mouse skin tumorigenesis. *Cancer Res.* **2002**, *62*, 3395–3401.
48. Tanaka, T.; Kohno, H.; Suzuki, R.; Hata, K.; Sugie, S.; Niho, N.; Sakano, K.; Takahashi, M.; Wakabayashi, K. Dextran sodium sulfate strongly promotes colorectal carcinogenesis in Apc(Min/+) mice: Inflammatory stimuli by dextran sodium sulfate results in development of multiple colonic neoplasms. *Int. J. Cancer* **2006**, *118*, 25–34. [CrossRef]
49. Chun, K.S.; Cha, H.H.; Shin, J.W.; Na, H.K.; Park, K.K.; Chung, W.Y.; Surh, Y.J. Nitric oxide induces expression of cyclooxygenase-2 in mouse skin through activation of NF-kappaB. *Carcinogenesis* **2004**, *25*, 445–454. [CrossRef]
50. Surh, Y.J.; Kundu, J.K.; Na, H.K.; Lee, J.S. Redox-sensitive transcription factors as prime targets for chemoprevention with anti-inflammatory and antioxidative phytochemicals. *J. Nutr.* **2005**, *135*, 2993S–3001S. [CrossRef]
51. Jung, M.; Triebel, S.; Anke, T.; Richling, E.; Erkel, G. Influence of apple polyphenols on inflammatory gene expression. *Mol. Nutr. Food Res.* **2009**, *53*, 1263–1280. [CrossRef] [PubMed]
52. Alsanea, S.; Gao, M.; Liu, D. Phloretin Prevents High-Fat Diet-Induced Obesity and Improves Metabolic Homeostasis. *AAPS J.* **2017**, *19*, 797–805. [CrossRef] [PubMed]

53. Kim, M.S.; Park, S.H.; Han, S.Y.; Kim, Y.H.; Lee, E.J.; Yoon Park, J.H.; Kang, Y.H. Phloretin suppresses thrombin-mediated leukocyte-platelet-endothelial interactions. *Mol. Nutr. Food Res.* **2014**, *58*, 698–708. [CrossRef] [PubMed]
54. Gao, S.S.; Chen, X.Y.; Zhu, R.Z.; Choi, B.M.; Kim, S.J.; Kim, B.R. Dual effects of phloretin on aflatoxin B1 metabolism: Activation and detoxification of aflatoxin B1. *Biofactors* **2012**, *38*, 34–43. [CrossRef] [PubMed]
55. Kim, M.S.; Kwon, J.Y.; Kang, N.J.; Lee, K.W.; Lee, H.J. Phloretin induces apoptosis in H-Ras MCF10A human breast tumor cells through the activation of p53 via JNK and p38 mitogen-activated protein kinase signaling. *Ann. N. Y. Acad. Sci.* **2009**, *1171*, 479–483. [CrossRef] [PubMed]
56. Kobori, M.; Shinmoto, H.; Tsushida, T.; Shinohara, K. Phloretin-induced apoptosis in B16 melanoma 4A5 cells by inhibition of glucose transmembrane transport. *Cancer Lett.* **1997**, *119*, 207–212. [CrossRef]
57. Kobori, M.; Iwashita, K.; Shinmoto, H.; Tsushida, T. Phloretin-induced apoptosis in B16 melanoma 4A5 cells and HL60 human leukemia cells. *Biosci. Biotechnol. Biochem.* **1999**, *63*, 719–725. [CrossRef] [PubMed]
58. Szliszka, E.; Czuba, Z.P.; Mazur, B.; Paradysz, A.; Krol, W. Chalcones and dihydrochalcones augment TRAIL-mediated apoptosis in prostate cancer cells. *Molecules* **2010**, *15*, 5336–5353. [CrossRef] [PubMed]
59. Liu, Y.; Fan, C.; Pu, L.; Wei, C.; Jin, H.; Teng, Y.; Zhao, M.; Yu, A.C.; Jiang, F.; Shu, J.; et al. Phloretin induces cell cycle arrest and apoptosis of human glioblastoma cells through the generation of reactive oxygen species. *J. Neurooncol.* **2016**, *128*, 217–223. [CrossRef] [PubMed]
60. Yin, M.; Ma, W.; An, L. Cortactin in cancer cell migration and invasion. *Oncotarget* **2017**, *8*, 88232–88243. [CrossRef] [PubMed]
61. Zhang, Z.; Zou, Y.; Liang, M.; Chen, Y.; Luo, Y.; Yang, B.; Liu, F.; Qin, Y.; He, D.; Wang, F.; et al. Suppressor of fused (Sufu) promotes epithelial-mesenchymal transition (EMT) in cervical squamous cell carcinoma. *Oncotarget* **2017**, *8*, 114226–114238. [CrossRef] [PubMed]
62. Cho, S.H.; Park, Y.S.; Kim, H.J.; Kim, C.H.; Lim, S.W.; Huh, J.W.; Lee, J.H.; Kim, H.R. CD44 enhances the epithelial-mesenchymal transition in association with colon cancer invasion. *Int. J. Oncol.* **2012**, *41*, 211–218. [PubMed]
63. Cao, X.; Fang, L.; Gibbs, S.; Huang, Y.; Dai, Z.; Wen, P.; Zheng, X.; Sadee, W.; Sun, D. Glucose uptake inhibitor sensitizes cancer cells to daunorubicin and overcomes drug resistance in hypoxia. *Cancer Chemother. Pharmacol.* **2007**, *59*, 495–505. [CrossRef] [PubMed]
64. Nelson, J.A.; Falk, R.E. The efficacy of phloridzin and phloretin on tumor cell growth. *Anti-Cancer Res.* **1993**, *13*, 2287–2292.
65. Eno, J. Immunotherapy Through the Years. *J. Adv. Pract. Oncol.* **2017**, *8*, 747–753. [PubMed]
66. Zhu, S.P.; Liu, G.; Wu, X.T.; Chen, F.X.; Liu, J.Q.; Zhou, Z.H.; Zhang, J.F.; Fei, S.J. The effect of phloretin on human gammadelta T cells killing colon cancer SW-1116 cells. *Int. Immunopharmacol.* **2013**, *15*, 6–14. [CrossRef] [PubMed]
67. Yang, W.; Ma, J.; Zhou, W.; Zhou, X.; Cao, B.; Zhang, H.; Zhao, Q.; Fan, D.; Hong, L. Molecular mechanisms and clinical implications of miRNAs in drug resistance of esophageal cancer. *Expert Rev. Gastroenterol. Hepatol.* **2017**, *11*, 1151–1163. [CrossRef]
68. Goldstein, L.J. Clinical reversal of drug resistance. *Curr. Probl. Cancer* **1995**, *19*, 65–124. [CrossRef]
69. Bai, X.; Chen, Y.; Hou, X.; Huang, M.; Jin, J. Emerging role of NRF2 in chemoresistance by regulating drug-metabolizing enzymes and efflux transporters. *Drug Metab. Rev.* **2016**, *48*, 541–567. [CrossRef]
70. Xue, X.; Liang, X.J. Overcoming drug efflux-based multidrug resistance in cancer with nanotechnology. *Chin. J. Cancer* **2012**, *31*, 100–109. [CrossRef]
71. Nguyen, H.; Zhang, S.; Morris, M.E. Effect of flavonoids on MRP1-mediated transport in Panc-1 cells. *J. Pharm. Sci.* **2003**, *92*, 250–257. [CrossRef] [PubMed]
72. Molnar, J.; Engi, H.; Hohmann, J.; Molnar, P.; Deli, J.; Wesolowska, O.; Michalak, K.; Wang, Q. Reversal of multidrug resitance by natural substances from plants. *Curr. Top. Med. Chem.* **2010**, *10*, 1757–1768. [PubMed]
73. Choi, B.M.; Chen, X.Y.; Gao, S.S.; Zhu, R.; Kim, B.R. Anti-apoptotic effect of phloretin on cisplatin-induced apoptosis in HEI-OC1 auditory cells. *Pharmacol. Rep.* **2011**, *63*, 708–716. [CrossRef]
74. Zhou, M.; Zheng, J.; Bi, J.; Wu, X.; Lyu, J.; Gao, K. Synergistic inhibition of colon cancer cell growth by a combination of atorvastatin and phloretin. *Oncol. Lett.* **2018**, *15*, 1985–1992. [CrossRef]
75. Adam, A.; Crespy, V.; Levrat-Verny, M.A.; Leenhardt, F.; Leuillet, M.; Demigne, C.; Remesy, C. The bioavailability of ferulic acid is governed primarily by the food matrix rather than its metabolism in intestine and liver in rats. *J. Nutr.* **2002**, *132*, 1962–1968. [CrossRef] [PubMed]

76. Kahle, K.; Kraus, M.; Scheppach, W.; Richling, E. Colonic availability of apple polyphenols–a study in ileostomy subjects. *Mol. Nutr. Food Res.* **2005**, *49*, 1143–1150. [CrossRef] [PubMed]
77. Deusser, H.; Rogoll, D.; Scheppach, W.; Volk, A.; Melcher, R.; Richling, E. Gastrointestinal absorption and metabolism of apple polyphenols ex vivo by the pig intestinal mucosa in the Ussing chamber. *Biotechnol. J.* **2013**, *8*, 363–370. [CrossRef]
78. Geohagen, B.C.; Korsharskyy, B.; Vydyanatha, A.; Nordstroem, L.; LoPachin, R.M. Phloretin cytoprotection and toxicity. *Chem. Biol. Interact.* **2018**, *296*, 117–123. [CrossRef]

MDPI
St. Alban-Anlage 66
4052 Basel
Switzerland
Tel. +41 61 683 77 34
Fax +41 61 302 89 18
www.mdpi.com

Molecules Editorial Office
E-mail: molecules@mdpi.com
www.mdpi.com/journal/molecules

MDPI
St. Alban-Anlage 66
4052 Basel
Switzerland

Tel: +41 61 683 77 34
Fax: +41 61 302 89 18

www.mdpi.com

ISBN 978-3-03943-115-1